# Hydrogen Bonding Phase-Transfer Catalysis: A New Approach to Asymmetric Fluorination

A thesis submitted to the Board of the Faculty of Physical Sciences, in partial fulfilment of the requirements for the degree of Doctor of Philosophy at the University of Oxford.

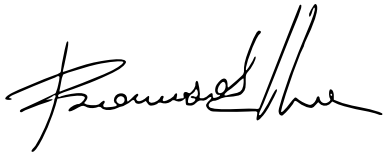



**Francesco Ibba**
Balliol College
University of Oxford
Hilary Term 2020

## Author's Declaration

The work presented in this thesis was conducted under the supervision of Prof. Véronique Gouverneur at the Department of Chemistry, University of Oxford. All of the work is my own, unless otherwise stated, and has not been submitted for any other degree at this or any other university.

Francesco Ibba



# Table of Contents

Abstract ..... v
Acknowledgments ..... vi
Abbreviations and Acronyms ..... viii

**1 Introduction ..... 1**
1.1 Prologue – A Brief Historical Overview ..... 1
1.2 Organofluorine Compounds ..... 3
1.2.1 Fluorine and the C–F Bond ..... 3
1.2.2 Properties and Application of Organofluorine Compounds ..... 4
1.2.2.1 Acidity, Bioavailability and Metabolism Blocking ..... 4
1.2.2.2 Stereoelectronic and Conformational Properties ..... 7
1.2.2.3 Hydrogen Bonding Properties of the C–F Bond ..... 9
1.3 Nucleophilic Fluorine Sources ..... 13
1.3.1 Origin and Occurrence of Fluorine ..... 13
1.3.2 Fluoride Anion and Fluoride Salts ..... 16
1.3.3 Nature's Approach to Fluorination ..... 18
1.3.3.1 Enzymatic Fluorination ..... 18
1.3.3.2 Enzymatic Defluorination ..... 22
1.3.4 Hydrogen Bonding with Fluoride ..... 22
1.3.4.1 Hydrogen Bonded Supramolecular Structure ..... 22
1.3.4.2 Hydrogen Bonded Promoted Nucleophilic Fluorination ..... 23
1.3.4.3 Hydrogen Bonded Fluoride Complexes in Asymmetric Fluorination ..... 28
1.4 Current Approaches to Asymmetric Fluorination ..... 31
1.4.1 Asymmetric Fluorination with Electrophilic Fluorine Reagents ..... 31
1.4.1.1 Transition-Metal Catalysed Asymmetric Electrophilic Fluorination ..... 31
1.4.1.2 Organocatalytic Asymmetric Electrophilic Fluorination ..... 32
1.4.2 Asymmetric Nucleophilic Fluorination ..... 37
1.4.2.1 Transition-Metal Catalysed Asymmetric Nucleophilic Fluorination ..... 37
1.4.2.2 Organocatalytic Asymmetric Nucleophilic Fluorination ..... 39
1.5 References ..... 40

**2 Hydrogen Bonding Mediated Asymmetric Nucleophilic Fluorination ..... 46**
2.1 Introduction ..... 46
2.1.1 Phase-Transfer Catalysis ..... 46
2.1.2 Hydrogen Bonding for Anion Binding Catalysis ..... 50
2.1.3 Hydrogen Bonding Phase-Transfer Catalysis ..... 52
2.2 Results and Discussion ..... 55
2.2.1 Reaction Development: Non-Enantioselective Catalytic System ..... 55
2.2.1.1 Fluoride Source ..... 59
2.2.1.2 Achiral Ureas Catalysts ..... 60
2.2.1.3 Solvents ..... 62
2.2.1.4 Nucleophilicity of Thiourea Catalysts ..... 63
2.2.2 Asymmetric Fluorination with Fluoride Salts ..... 65

2.2.2.1 Solvent Effect ....67
2.2.2.2 Catalyst Screening ....70
2.2.2.3 *N*-Alkylated *bis*-Urea Catalysts ....72
2.2.2.4 Substrate Scope....76
2.2.3 Preliminary Mechanistic Insights ....81
2.2.3.1 Mechanistic Considerations ....81
2.2.3.2 Non-Linear Effect Studies....83
2.2.3.3 Crystal Structure of **4u**:TBAF ....85
2.2.3.4 Transition States Analyses ....88
2.3 Conclusions ....90
2.4 References ....91

**3 Structure and Conformation of *bis*-Urea Catalysts for Hydrogen Bonding Phase-Transfer Catalysis: Insights from NMR Spectroscopy ....94**
3.1 Introduction ....94
3.1.1 NMR Spectroscopy of Hydrogen Bonded Systems ....94
3.1.1.1 Hydrogen Bonding Coupling....94
3.1.2 NMR Studies on Hydrogen Bonding Phase-Transfer Catalysis ....96
3.2 Results and Discussion....98
3.2.1 Catalyst Synthesis....98
3.2.2 Conformational Properties of *bis*-Urea Catalysts ....100
3.2.2.1 BINAM Urea (**4a**) *vs.* iPr BINAM Urea (**4u**) ....100
3.2.2.2 *N*-Alkylated Analogues ....109
3.2.3 Complexation with TBAF....111
3.2.3.1 Binding Studies....111
3.2.3.2 NMR Study of iPr BINAM Urea–TBAF (**4u**:TBAF) in Solution ....117
3.2.3.3 Hydrogen Bonding Coupling of *bis*-Urea:TBAF Complexes....129
3.2.4 Complexation with CsF....134
3.2.4.1 NMR Study of iPr BINAM Urea–CsF Complex (**4u**:CsF) in Solution. ....134
3.2.4.2 Crystal Structure of **4ad**:CsF....141
3.2.4.3 NMR Study of **4y**:CsF in Solution....144
3.2.5 Implication for Catalysis ....148
3.2.5.1 Reactivity and Enantioselectivity of *bis*-Urea Catalysts ....148
3.2.5.2 *Reactivity of iPr BINAM Urea–CsF Complex (**4u**:CsF)....152*
3.3 Conclusions ....154
3.4 References ....157

**4 Experimental ....159**
4.1 Generality and NMR Methods .... 159
4.2 Hydrogen Bonding Mediated Asymmetric Nucleophilic Fluorination .... 162
4.2.1 Catalysts Synthesis and Characterisation.... 162
4.2.1.1 Achiral Catalysts.... 162
4.2.1.2 Chiral Catalysts .... 165
4.2.2 Substrates Synthesis and Characterisation .... 185
4.2.2.1 β-Hydroxy Sulfides.... 185
4.2.2.2 β-Bromo Sulfides .... 195
4.2.3 Products Characterisation .... 206

4.2.4 X-Ray Analyses ..... 220
4.3 Structure and Conformation of *bis*-Urea Catalysts for Hydrogen Bonding Phase-Transfer Catalysis: Insights from NMR Spectroscopy ..... 224
4.3.1 Catalyst Synthesis and Characterisation ..... 224
4.3.2 NMR characterisation of BINAM Urea (**4a**) and iPr BINAM Urea (**4u**) ..... 239
4.3.2.1 BINAM Urea (**4a**) – assignment and copy of NMR spectra ..... 239
4.3.2.2 iPr BINAM Urea (**4u**) – assignment and copy of NMR spectra ..... 244
4.3.2.3 iPr BINAM Urea (**4u**) – spectra in DMSO-$d_6$ and 1,2-DCB-$d_4$ ..... 252
4.3.2.4 iPr BINAM Urea (**4u**) – NOESY ..... 256
4.3.3 Binding Studies ..... 258
4.3.3.1 UV-vis Titrations ..... 258
4.3.3.2 NMR Titrations ..... 263
4.3.4 iPr BINAM Urea–TBAF Complex (**4u**:TBAF) ..... 270
4.3.4.1 Sample Preparation ..... 270
4.3.4.2 Assignment and Copy of NMR Spectra ..... 271
4.3.4.3 Concentration and Variable Temperature Studies ..... 276
4.3.4.4 $^{1}$H-$^{19}$F CLIP-HSQC ..... 278
4.3.4.5 HOESY ..... 279
4.3.4.6 NOESY ..... 281
4.3.4.7 T1 measurements ..... 283
4.3.5 Hydrogen Bonding Coupling of *bis*-Urea–TBAF Complexes ..... 285
4.3.5.1 Sample Preparation ..... 285
4.3.5.2 Copy of NMR Spectra ..... 286
4.3.5.3 $^{1}$H-$^{19}$F CLIP-HSQC ..... 299
4.3.6 iPr BINAM Urea–CsF Complex (**4u**:CsF) ..... 300
4.3.6.1 Sample Preparation ..... 300
4.3.6.2 Variable Temperature Studies ..... 301
4.3.6.3 HSQC ..... 303
4.3.6.4 NOESY and ROESY ..... 306
4.3.6.5 HOESY ..... 308
4.3.6.6 Diffusion Studies ..... 310
4.3.6.7 T1 measurements ..... 312
4.3.7 *(S)-iPrBINAM-N$^{a}$-[3,5-bis(CF$_3$)phenyl]-N$^{b}$-phenyl bis-Urea–CsF Complex (**4y**:CsF)* ..... 314
4.3.7.1 Sample Preparations ..... 314
4.3.7.2 Variable Temperature Studies ..... 315
4.3.7.3 HSQC ..... 316
4.3.7.4 ROESY ..... 319
4.3.7.5 HOESY ..... 321
4.3.7.6 Diffusion studies ..... 322
4.3.8 X-Ray Analyses ..... 324
4.4 References ..... 325

## Abstract

*Chapter 1 – Introduction.* This chapter aims to highlight the importance of enantioselective fluorination in modern organic chemistry. The peculiar and sometimes contradictory properties of fluorine and fluorinated organic molecules are detailed along with examples of their applications in the life sciences. The origin and the chemistry of fluorinating reagents are also discussed, with a particular emphasis on the fluoride anion's uses and challenges in organic synthesis. Lastly, a summary of the current methodologies to access enantiopure fluorinated compounds is presented and discussed.

*Chapter 2 – Hydrogen Bonding Mediated Asymmetric Nucleophilic Fluorination.* The work describes the development of the first protocol for asymmetric nucleophilic fluorination utilising alkali metal fluorides as fluorine source and a newly developed tridentate *bis*-urea organocatalyst. This novel strategy, named Hydrogen Bonding Phase-Transfer Catalysis (HB PTC), embraces the poor solubility of fluoride salts in organic solvents and their tendency to engage in hydrogen bonding to deliver fluorinated molecules in high enantioselectivity.

*Chapter 3 – Structure and Conformation of bis-Urea Catalysts for Hydrogen Bonding Phase-Transfer Catalysis: Insights from NMR Spectroscopy.* A detailed NMR spectroscopic investigation is presented herein in order to unveil the mechanistic details of HB PTC. The work investigates the conformational preferences of *bis*-urea catalysts under relevant reaction conditions and their changes upon binding of fluoride. The characterisation of *bis*-ureas–TBAF and *bis*-ureas–CsF complexes, in solution and in the solid state, provides information about the hydrogen bonding network around fluoride. The detection of scalar coupling across hydrogen-bonding, $^{1h}J_{NH\cdots F^-}$, represents a key parameter to study catalyst-fluoride interactions. NMR data are used to investigate how the structural features of the catalysts influence the outcome of HB PTC fluorinations.

## Acknowledgment

I would first like to thank Prof. Véronique Gouverneur for her support throughout these years, as my PhD supervisor. Véronique not only made the work in this thesis possible, she raised me as a scientist welcoming in her group. Thanks to Dr. John Brown for the invaluable discussion, I am honoured to have met and worked with such an amazing chemist. I also would like to thank Prof. Tim Claridge for his utmost scientific contribution, and Dr. Nader Amin for his help in an uncountable number of occasions.

The warmest thanks goes to the members of the VG group. I had the privilege to meet so many fantastic people and superb scientists, every single one of them taught me something valuable. Particularly, I want to thank Dr. Paolo Ricci, Dr. Lukas Pfeifer and Dr. Enrico Emer, who were the firsts to look after my work, I am grateful for everything I learnt from them. Thanks to Dr. Gabriele Pupo, who was a fundamental contributor to my PhD project, a great scientist and a friend. Thanks to Dr. David Ascough who, together with Gabriele, enormously contributed to the worked described herein. A special thanks to the people I shared the lab with in these years, first and most important Anna Chiara Vicini who helped me going through this four-year long journey.

This thesis is certainly unique since it has been written during a global pandemic, fortunately my housemate Ben Dodds was a precious moral support and a surprisingly good cook. At the same time, I want to thank all my housemates to have made our house such a nice place to live. Thanks to all my friends, the ones that I met in Oxford and the ones that I left in Genova, without them nothing would make much sense.

Finally, thanks to my father for his unconditional support, while also contributing to this thesis with a beautiful artwork featured in the first chapter.

To my mother.

## Abbreviations and Acronyms (*alphabetical)*

| | |
|---|---|
| # | bioavailability |
| 5’-FDA | 5'-fluoro-5'-deoxyadenosine |
| Å | Angstrom, 1 x$10^{-10}$ m |
| AAAS | American Association for the Advancement of Science |
| Ar | aryl |
| BDE | bond dissociation energy |
| BINAM | [1,1'-binaphthalene]- 2,2'-diamine |
| BINAP | 2,2’-bis(diphenylphosphino)-1,1’-binaphthyl |
| Bn | benzyl |
| br | broad, referred to NMR peaks |
| *cf.* | compare with |
| COSY | COrrelated SpectroscopY |
| DBN | 1,8-diazabicycloundec-7-ene |
| DCM | dichloromethane |
| DFB | difluorobenzene |
| DFT | density functional theory |
| DMF | *N,N*-dimethyl formamide |
| DMSO | dimethyl sulfoxide |
| DNP | 2,4-dinitrophenyl |
| DOSY | Diffusion Ordered SpectroscopY |
| e.r. | enantiomeric ratio |
| E2 | bimolecular elimination |
| ee | enantiomeric excess |
| $\varepsilon_r$ | relative permittivity, relative to the vacuum |
| FDA | Food and Drugs Administration |
| FDAS | 5'-fluoro-5'-deoxyadenosine synthase |
| GABA | γ-aminobutyric acid |
| $GABA_A$ | γ -aminobutyric acid receptor A |
| $GABA_{AT}$ | γ -aminobutyric acid aminotransferase |
| $GABA_C$ | γ -aminobutyric acid receptor C |
| $G_z$ | gradient along the z-axis |

| | |
|---|---|
| HB | hydrogen bond |
| HB PTC | Hydrogen Bonding Phase-Transfer Catalysis |
| HBD | hydrogen bond donor |
| HFIP | hexafluoroisopropanol |
| HMBC | Heteronuclear Multiple Bond Correlation |
| HOESY | Heteronuclear nuclear Overhauser Effect SpectroscopY |
| HSQC | Heteronuclear Single Bond Correlation |
| $IC_{50}$ | half maximal inhibitory concentration |
| IR | infra-red |
| IRC | intrinsic reaction coordinate |
| KDR | kinase insert domain receptor, VEGFR-2 |
| LG | leaving group |
| *m*CPBA | *meta*-chloroperoxybenzoic acid |
| MD | molecular dynamics |
| MF | metal fluoride |
| ms | millisecond |
| MTBE | methyl *tert*-butyl ether |
| NFSI | *N*-fluorobenzenesulfonimide |
| NLE | non-linear effect |
| NMR | nuclear magnetic resonance |
| nOe | nuclear Overhauser effect |
| NOESY | Nuclear Overhauser Effect SpectroscopY |
| P-gp | *P*-glycoprotein |
| $PBr_3$ | phosphorus tribromide |
| $Pd_2(dba)_3$ | tris(dibenzylideneacetone)dipalladium |
| PDGFR | platelet-derived growth factor receptors |
| $PhF_6$ | hexafluorobenzene |
| PhMe | toluene |
| p$K_a$ | acid dissociation constant, $-\log_{10}$ |
| PT | phase transfer |
| PTC | phase transfer catalysis |
| r.t. | room temperature |
| ROESY | Rotating frame nuclear Overhauser Effect SpectroscopY |

| | |
|---|---|
| rpm | revolutions per minute |
| SAM | *S*-adenosylmethionine |
| SCXRD | single crystal X-ray diffraction |
| $S_N2$ | bimolecular nucleophilic substitution |
| T | Tesla, unit of magnetic flux |
| TBA | tetrabuthylammonium |
| TBAF | tetrabutylammonium fluoride |
| TFB | trifluorobenzene |
| THF | tetrahydrofurane |
| TLC | thin layer chromatography |
| $\tau_m$ | mixing time |
| TMAF | tetramethylammonium fluoride |
| TMSBr | trimethylsilyl bromide |
| TOCSY | TOtal Correlated SpectroscopY |
| TS | transition state |
| *v.* | *vide*, refer to |
| VDW | Van der Waals |
| VEGFR | vascular endothelial growth factor receptor |
| µL | micro litres |
| µM | micro molar |

# 1. Introduction

## 1.1 Prologue – A Brief Historical Overview

*<< Fluorine leaves nobody indifferent; it inflames emotions, be that affections or aversions. >>*

*Manfred Schlosser*




Figure 1.1: Henry Moissan, artwork.

The fascinating history of fluorine chemistry recounts some of the most important scientific and technological advances of the 20$^{th}$ century. After Henri Moissan's heroic effort to isolate fluorine gas in 1886,[1,2] the study of fluorine chemistry received unprecedented scientific relevance. The first industrial production of fluorochemicals had its origin as part of the Manhattan project, when fluorine found key application in the isotopic enrichment of uranium by centrifugation of $^{235}UF_6/^{238}UF_6$ mixture.[3] The serendipitous discovery of Teflon® and the development of chlorofluorocarbons, widely used refrigerants, boosted the fluorochemical industry to worldwide production. In the 1950s, fluorinated corticosteroids and pyrimidines were the first fluorinated drugs that showed enhanced biological activity compared to their non-fluorinated counterparts, paving the way to the application of fluorinated molecules in the life sciences. Innovation in chemical synthesis followed thereafter, and featured the development of new methodologies and reagents able to access an unprecedented diversity

of fluorinated motifs. Nowadays, fluorine chemistry plays a crucial role in almost every aspect of human life, from energy to materials as well as healthcare and agriculture.[4] The production of fluorinated organic molecules, considered a highly specialised field in the past, is now a vibrant area of research in the chemistry community. A contemporary challenge in organofluorine chemistry is the precise introduction of fluorine in highly functionalized molecules using accessible and easy-to-handle fluorine sources.

## 1.2 Organofluorine Compounds

The discussion below introduces the properties of fluorine and covers the most important effects that fluorine substitution exerts on organic small-molecules. Selected applications of aliphatic fluorinated molecules will serve to illustrate the pivotal role of chiral fluorinated compounds in pharmaceutical and bioorganic chemistry.

### *1.2.1 Fluorine and the C–F bond*

Fluorinated molecules show unusual behaviour when compared with their non-fluorinated analogues; they often possess exceptional physical and chemical properties which make them important tools for a multitude of applications. Numerous examples have shown that the introduction of fluorine into an organic molecule is able to alter its physical-chemical, conformational and pharmacological properties. Not surprisingly, in the last decades, fluorination became an important strategy in drug design.[5] The impact of fluorination on molecular properties can be rationalised by considering the combination of the unique features of the fluorine atom. The small size ($r_{VDW}$ = 1.47 Å), intermediate between hydrogen and oxygen, and its high electronegativity ($\chi_p$ = 3.98) make fluorine an exceptionally electron-dense atom, which translate in low-energy atomic orbitals ($2s_{(F)}$ = -40.1 eV, $2p_{(F)}$ = -18.9 eV)[6] and low polarizability (Table 1.1).[7,8] Carbon and fluorine valence atomic orbitals have similar energies ($2s_{(C)}$ = -19.4 eV *vs*. $2p_{(F)}$ = -18.9 eV) which ensure optimal overlap; the corresponding C–F bond is therefore the strongest known carbon single bond (C–F Bond Dissociation Energy = 115 kcal/mol). Furthermore, the low-lying, antibonding orbital ($\sigma^*$) of the C–F bond is responsible for a variety of stereoelectronic effects which have a great impact on the conformation of fluorinated molecules.[9–11]

Table 1.1: Fundamental properties of selected elements and corresponding carbon bonds.[12]

| X | Electronegativity, $\chi_p$ | Van der Waals radius (Å) | Polarizability $\alpha$ (Å$^3$) | C–X bond length (Å) | C–X BDE (kcal/mol) | C–X dipole moment $\mu$ (D) |
|---|---|---|---|---|---|---|
| H | 2.20 | 1.20 | 0.67 | 1.09 | 98.0 | (0.4) |
| **F** | **3.98** | **1.47** | **0.56** | **1.35** | **115.7** | **1.41** |
| Cl | 3.16 | 1.75 | 2.18 | 1.79 | 77.2 | 1.46 |
| Br | 2.96 | 1.85 | 3.05 | 1.94 | 64.3 | 1.38 |
| I | 2.66 | 1.98 | 4.70 | 2.13 | 50.7 | 1.19 |
| C | 2.55 | 1.70 | 1.76 | 1.53 | 83 | 0.0 |

### *1.2.2 Properties and Applications of Organofluorine Compounds*

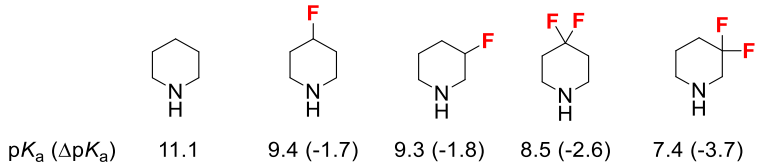
No fluorinated pharmaceuticals were known before the development of fluorinated pyrimidines in 1957;[13] nowadays more than one hundred have been approved for clinical use. Fluorinated drugs represent a significant share of the market; in 2019, among the 35 new small-molecules approved by the FDA, 11 contained at least one fluorine atom and one featured its radioactive isotope $^{18}$F.[14] The indisputable success that fluorinated drugs have had in recent years builds on our fundamental understanding of their properties which, together with a constant growing knowledge of structural biology, allows selective fluorination to be used as a precise tool for the rational design of pharmaceuticals.[15] The small size of fluorine marginally influences the steric volume, being the smallest substitute of hydrogen beside deuterium. Accordingly, fluorine can serve as a bioisostere for proton, OH, $OCH_3$ and carbonyl groups, while the fluorovinyl group has been used to replace amides. However, the different electronic properties of the carbon–fluorine bond result in a radically different physiological behaviour in terms of bioavailability, resistance to metabolism and biochemical interactions.

*1.2.2.1 Acidity, Bioavailability and Metabolism Blocking.* The introduction of a single fluorine atom in a molecule influences its ionization state, stability and reactivity. The single best-known feature of fluorine is perhaps the strong electron-withdrawing inductive effect. Fluorine substitution onto aliphatic carbon chains substantially increases the Brønsted acidity of neighbouring groups (Table 1.2).

Table 1.2: Effect of fluorination on the p$K_a$ of common carboxylic acids, alcohols and amines.[5]

| Carboxylic acid | p$K_a$ | Alcohol | p$K_a$ | Amine | p$K_a$ (conj. acid) |
|---|---|---|---|---|---|
| $CH_3CO_2H$ | 4.8 | $(CH_3)_2CHOH$ | 17.1 | $CH_3CH_2NH_2$ | 10.7 |
| $CH_2FCO_2H$ | 2.6 | $CF_3CH_2OH$ | 12.4 | $CH_2FCH_2NH_2$ | 9.0 |
| $CHF_2CO_2H$ | 1.3 | $(CF_3)_2CHOH$ | 9.3 | $CHF_2CH_2NH_2$ | 7.3 |
| $CF_3CO_2H$ | 0.5 | $(CF_3)_3OH$ | 5.4 | $CF_3CH_2NH_2$ | 5.7 |

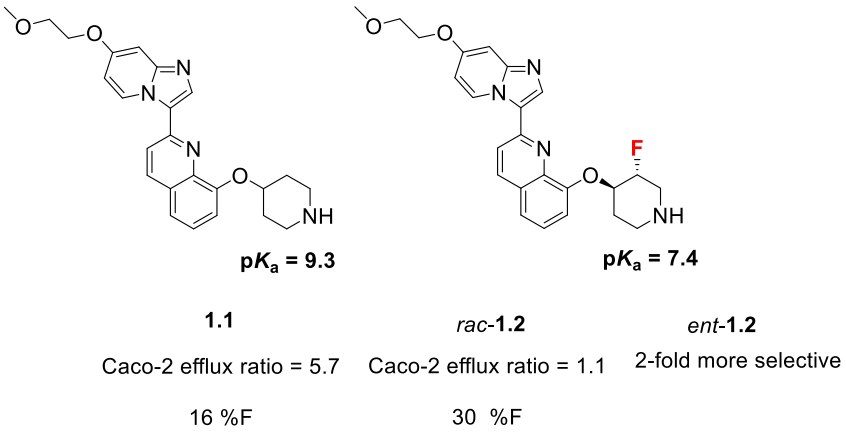
The effect of fluorine on the p$K_a$ of alkylamines is well understood and predictable; every fluorine introduced onto the β-carbon of an amine decreases its basicity by 1.7 p$K_a$ units. The effect is attenuated by carbon homologation, resulting in -0.7 $\Delta$p$K_a$ for γ-fluorine substituents, -0.3 and -0.1 $\Delta$p$K_a$ for substitution at the δ and ε position, respectively.[5] In a similar manner, cyclic amines are influenced by fluorine substitution with additive effects that extend in both directions of the ring, as exemplified by the p$K_a$ variation of the mono and difluorinated piperidines (Scheme 1.1).




Scheme 1.1: Effect of fluorine substitution on the p$K_a$ (conj. acid) of mono and difluorinated piperidines.[5]

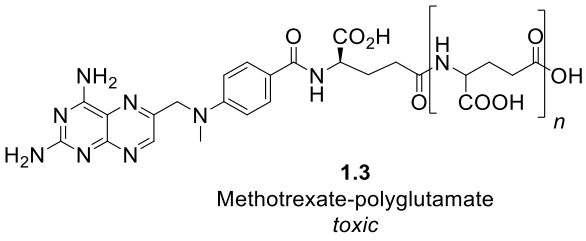
The introduction of fluorine to modulate the p$K_a$ of basic sites is a well-established strategy in medicinal chemistry to improve biodistribution and bioavailability of drug candidates. The piperidine derivative **1.1** (Scheme 1.2), was identified by scientists at Pfizer as a promising lead candidate to selectively inhibit one form of platelet-derived growth factor receptors, PDGFR-$\beta$. Despite good potency ($IC_{50}$ = 3 nM) and selectivity over members of the VEGFR family (10x over KDR), the compound showed poor oral absorption due to extensive *P*-glycoprotein (*P*-gp) mediated intestinal efflux. Selective incorporation of fluorine into the β-position of the piperidine ring, as in *rac*-**1.2**, resulted in a reduced basicity, thus decreasing efflux and substantially improving bioavailability (%F). When the single enantiomers of **1.2**

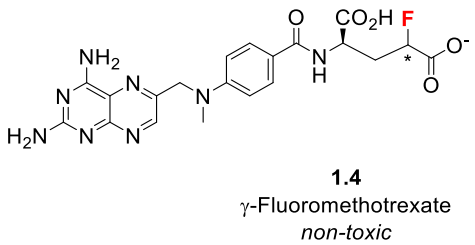
were separated and tested *in vitro*, one was found to be 2-fold more selective than both the racemic mixture and the parent compound **1.1**, thereby advancing to preclinical studies.[16]




Scheme 1.2: Effect of fluorine substitution on bioavailability and substrate selectivity. Stereochemistry of *ent*-**1.2** not assigned.

Lowering the p$K_a$ of acid functionalities can serve to alter metabolic pathways to achieve more favourable toxicological profiles. Methotrexate is a folic acid anti-metabolite widely used for the treatment of cancer and rheumatoid arthritis; unfortunately, the metabolic formation of poly-glutamates **1.3** is responsible for elevated cytotoxicity (Scheme 1.3).

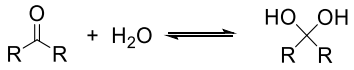



Scheme 1.3: Effect of fluorination on the formation of toxic metabolites of Methotrexate.

γ-Fluoromethotrexate **1.4** was studied as a safer alternative exploiting the inductive effect of fluorine to enhance the acidity of the γ-carboxylic acid, thus impeding the *in vivo* formation of toxic polyglutamylated metabolites.[17]

Fluorination influences the reactivity of neighbouring functional groups. Due to the electron-withdrawing effect of fluorine, α-fluorinated carbonyl compounds are very reactive towards nucleophilic attack, favouring the formation of *gem*-diols in aqueous solution. For example, the perfluorinated analogue of acetone, hexafluoroacetone, is commercialised in its hydrated form as *gem*-diol, which makes it more convenient to transport than the gaseous ketone. This is possible because the equilibrium constant towards hydration greatly favours the hydrated form (Scheme 1.4).



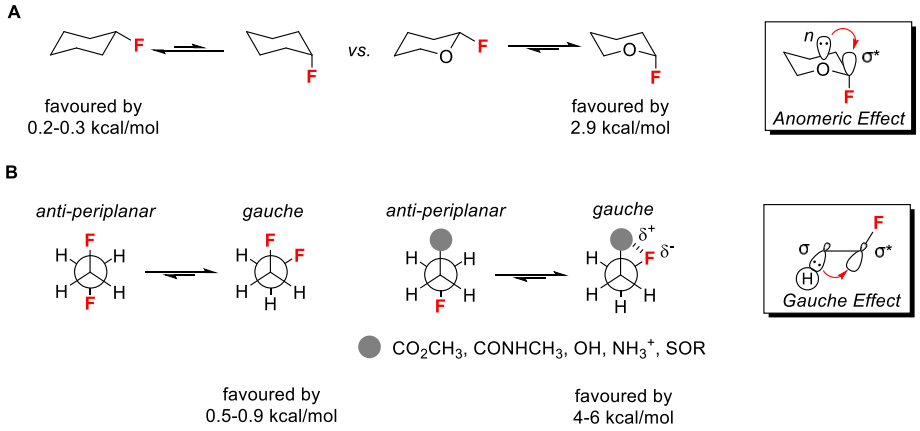

$R = CH_3$, $K_{eq} = 1.4 \times 10^{-3}\ M^{-1}$

$R = CF_3$, $K_{eq} = 1.2 \times 10^{6}\ M^{-1}$

Scheme 1.4: Equilibrium constant for the hydration of acetone and hexafluoroacetone.

*1.2.2.2 Stereoelectronic and Conformational Properties.* Nowadays, it is largely accepted that orbital interaction significantly affects the molecular conformation of fluorinated compounds. In analogy with C–O, the C–F bond has a low-energy σ* orbital, which can accept electron-density from neighbouring bonds, π-systems or lone pairs, when correctly aligned. Thereby, the presence of a fluorine atom can stabilise particular conformations, intermediates or transition states that would not be energetically favourable otherwise. Didactic examples are depicted in Scheme 1.5 that shows how the axial conformer of 2-fluoropyrane is favoured by 2.9 kcal/mol, in contrast with the conformational preference observed for cyclic hydrofluorocarbons (Scheme 1.5 A). In a similar way, the conformational preference for 1,2-

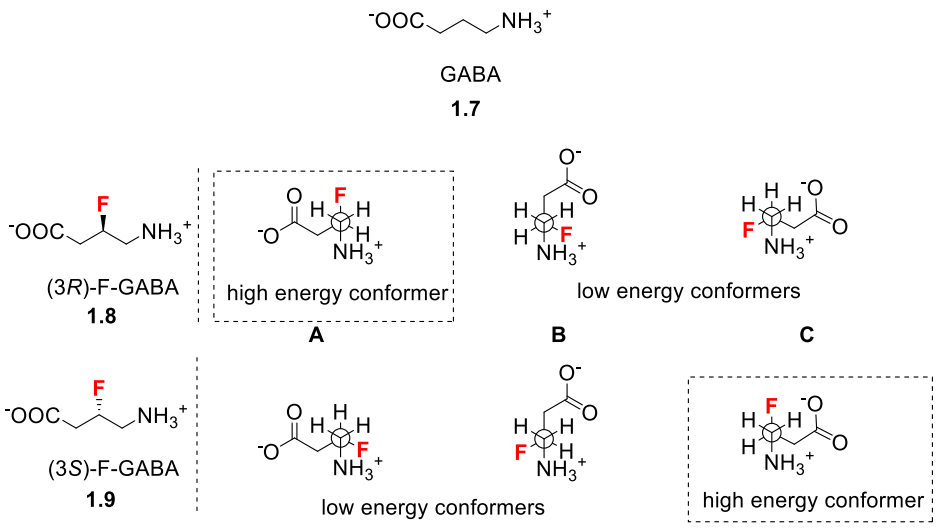
difluoroethane might appear counter-intuitive; the synclinical (gauche, 60 °) disposition of the two fluorines is favoured by around 1 kcal/mol over the antiperiplanar arrangement (anti, 180 °). The gauche conformer is stabilised by two reinforcing hyperconjugative interactions between the electron-rich C–H bonds and the electron-poor C–F bond, $\sigma_{C-H} \rightarrow \sigma^*_{C-F}$. This is not encountered in other 1,2-dihaloethanes which favour the *anti*-geometry, due to the increased steric demand and the lack of stereoelectronic stabilisation. The gauche effect observed in 1,2-difluoroethane can be generalised; substitution of one of the two fluorines with an electron-withdrawing group preserves the gauche preference. In this case, electrostatic interactions play a significant role in addition to the stereoelectronic stabilisation, (Scheme 1.5 B). Applications of this subtle, yet important, effect are widespread in medicinal chemistry, biology, and most recently organocatalysis.[18–21]




Scheme 1.5: Examples of stereoelectronic effects on the conformation of organofluorine compounds.

The predictable conformational preference of fluorinated molecules is a valuable tool to investigate binding of small-molecules to biological targets. One example is the elegant work of O'Hagan and co-workers on fluorinated analogues of γ-aminobutyric acid (GABA, **1.7**). GABA is one of the most important neurotransmitters in mammals, binding an important class of receptors (GABAergic receptors); however, its binding mode proved hard to elucidate.

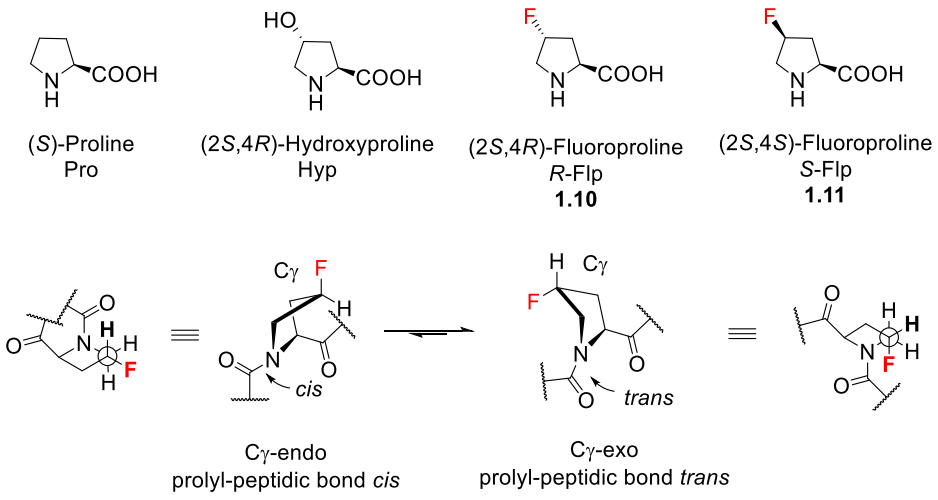
O'Hagan and co-workers synthesised the two enantiomers of 3-fluoro-γ-aminobutyric acid to gain insights into the binding conformation of the natural ligand. (3*R*)-F-GABA **1.8** and (3*S*)-F-GABA **1.9** have three distinct conformers, one conformer of each enantiomer destabilised by the antiperiplanar disposition of fluorine and ammonium group (Scheme 1.6).




Scheme 1.6: Fluorinated analogues of GABA employed as molecular probes.

After extensive experimentation, it was found that the $GABA_A$ receptor was unable to discriminate between the two enantiomers of 3-F-GABA, which were both less active than the parent non-fluorinated γ-amino acid.[22] Based on these observations, the authors concluded that conformation **B** was the active binding mode of the endogenous substrate towards $GABA_A$. When $GABA_{AT}$ and $GABA_C$ were considered, (3*R*)-F-GABA was found to be a better ligand than its enantiomer (10x for $GABA_{AT}$ and 2x for $GABA_C$) thus the bent conformation **C** was proposed as the preferred binding conformation of γ-aminobutyric acid towards $GABA_{AT}$ and $GABA_C$ receptors.[23,24] One example that illustrates the impact of fluorine on organic biomolecules comes from the work of Raines and co-workers on collagen.[25–28] Collagen is the most important structural protein in animals, making 30 % of the whole protein content in humans and three-quarters of human skin weight; its well-established quaternary structure

consists in three parallel protein strands forming a triple-helix. Each polypeptidic chain is composed of a repetitive unit XaaYaaGly, where (*S*)-proline (Pro) and (2*S*,4*R*)-hydroxyproline (Hyp) residues are the main constituents. It was believed that the thermal stability of collagen was due to an intricate hydrogen-bonding network between water molecules interacting with the OH of the hydroxyproline residues. This widely accepted theory was challenged when the proline analogue, (2*S*,4*R*)-fluoroproline (**1.10**), was synthesised and embedded into collagen oligomers, in place of Hyp. The newly generated polypeptidic chain $(ProFlpGly)_n$ was more thermally stable than the natural occurring protein. Since organic fluorine is unable to participate in hydrogen bonding it was concluded that the stability of collagen arises from stereoelectronic effects imparted by electronegative substituents, and not from hydrogen bonding. The stereoselective introduction of a fluorine imparts a strong conformational preference on the proline ring; (4*R*)-Flp stabilises the C$\gamma$-*exo* pucker conformer through a fluorine-amide gauche effect. The C$\gamma$-*exo* pucker conformer favours the formation of polypeptidic chains with a high percentage of *trans* prolyl-peptidic bonds, that are ultimately responsible for the higher thermal stability of collagen. Conversely, the diastereoisomer (4*S*)-Flp (**1.11**), favouring a C$\gamma$-*endo* conformer, leads to a less stable polymer.




Scheme 1.7: Fluorine stereoelectronic effects on the thermal stability of collagen.

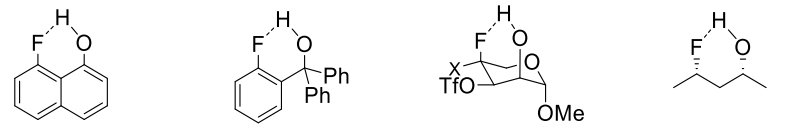
*1.2.2.3 Hydrogen Bonding Properties of the C–F Bond*. As demonstrated by the large number of critical reports on the subject, the capability of the C–F bond to accept hydrogen bonds is rather controversial.[29-30] This ambiguity comes from the very definition of hydrogen bonding. Hydrogen bonds can be categorised depending on their bond energy (Scheme 1.7).[31] *i) Very strong* hydrogen bonds are characterized by substantial covalent character (BDE = 15–40 kcal/mol), short length (1.2–1.5 Å) and linear geometry (∢ X–H···A ~ 180 °), the best example of this category is bifluoride anion ($HF_2^-$), recognised as the strongest HB known;[32] *ii) strong* hydrogen bonds are the most commonly encountered in organic chemistry, and they have a dominant electrostatic character with generally only a modest contribution due to orbital overlap. The hydrogen bond length measures between 1.5 and 2.2 Å with a wider range of geometries (∢ X–H···A = 130–180 °); for many organic chemists this type of HB is representative of the whole category; *iii) weak* hydrogen bonds arise exclusively from weak electrostatic interactions. These hydrogen bonds (HB) do not share electrons and therefore may not be retained *genuine* hydrogen bonds.

| $[F{-}H{\cdots}F]^-$ | C=O···H–O | C–F···H–O |
|---|---|---|
| $R_2P(O){-}OH{\cdots}O{=}PR_3$ | C=O···H–N | O–H···Ph |
| *very strong* | *strong* | *weak* |
| 15–40 kcal/mol | 4–15 kcal/mol | < 4 kcal/mol |
| X–H ~ A–H | A···H > X–H | A···H >> X–H |
| *d*(H···A) = 1.2–1.5 Å | *d*(H···A) = 1.5–2.2 Å | *d*(H···A) = 2.0–3.0 Å |
| ∠(X–H···A) = 175–180 ° | ∠(X–H···A) = 130–180 ° | ∠(X–H···A) = 90–180 ° |

Scheme 1.8: Steiner's classification of hydrogen bonds (X–H = donor, A = acceptor) [27]

Considering the orbital interactions characteristic of a hydrogen bond, $n_A \rightarrow \sigma^*_{XH}$, where $n_A$ represents the electron lone pair of the hydrogen bond acceptor and $\sigma^*_{XH}$ the unfilled antibonding molecular orbital of the hydrogen bond donor, it appears clear that the low–lying

lone pairs of fluorine cannot engage in strong hydrogen bonding. Strikingly, in the crystal structure of ammonium trifluoroacetate ($NH_4^+CF_3COO^-$) there is no contact indicative of NH···F–C interaction, despite four protons and three fluorines in the crystal lattice.[33] Thereby, the carbon-fluorine bond is a very weak hydrogen bond acceptor which engages hydrogen bonding only in the absence of a better acceptor. Nevertheless, several literature contributions reported the experimental observation of intramolecular hydrogen bonds involving the C–F bond, investigated by X-ray or spectroscopic methods (Scheme 1.8).[34-38] NMR spectroscopy is particularly suitable for the study of hydrogen bonds in solution, as deshielding of proton resonances and the detection of scalar coupling across the hydrogen bonds are recognised as evidences of hydrogen bonding (***vd. infra.*** 3*.1.1 NMR Spectroscopy of Hydrogen Bonded System*).




$^{1h}J_{FH}$ = 28.4 Hz — Takemura *et al.*

$^{1h}J_{FH}$ = 9.2 Hz — Takemura *et al.*

$^{1h}J_{FH}$ = 10.5 Hz — Gouverneur *et al.*

$^{1h}J_{FH}$ = 6.6 Hz — Linclau *et al.*

Scheme 1.9: Spectroscopic evidences of C–F···H–O hydrogen bonding.

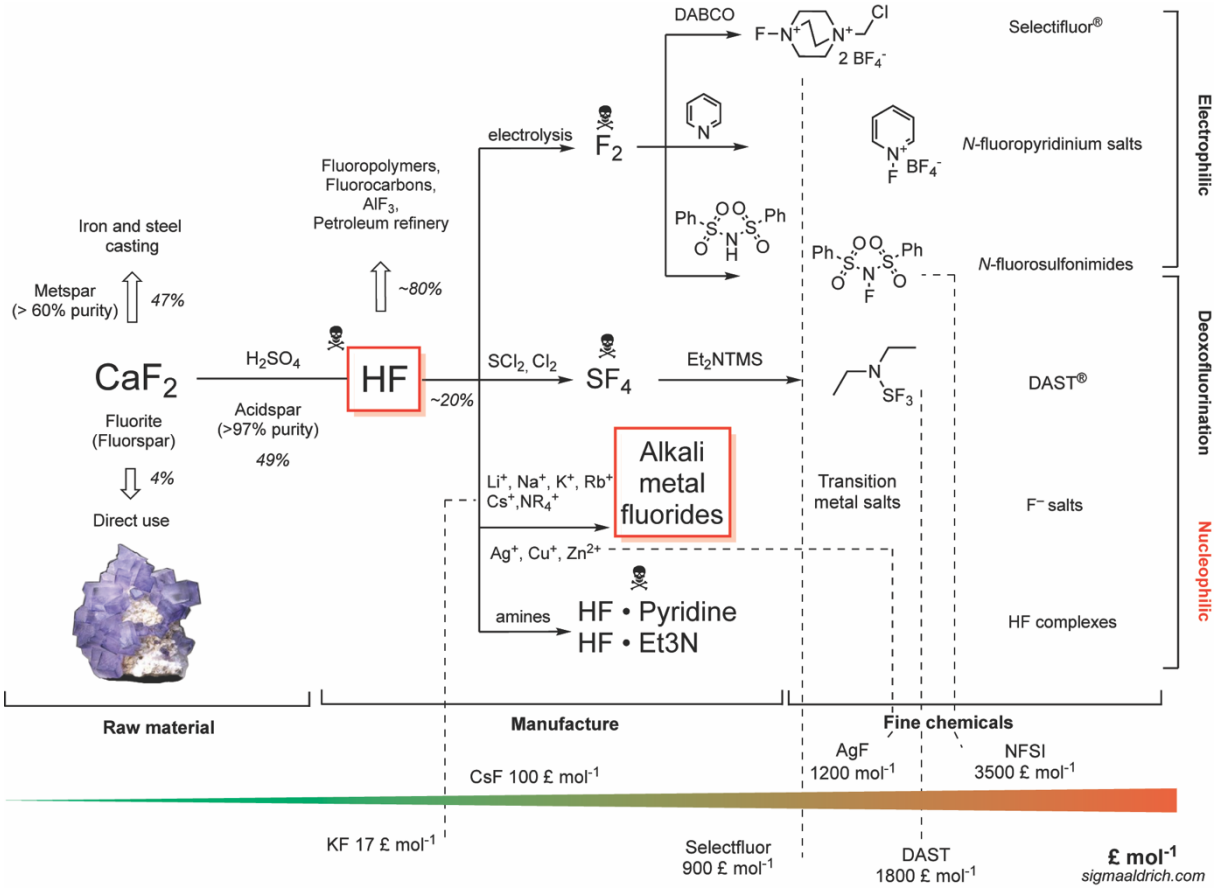
## 1.3 Nucleophilic Fluorine Sources

The tremendous effects that fluorine has on organic molecules have driven the investigation of new fluorination methodologies and reagents; however, despite remarkable advances in the field, little success can be claimed in terms of industrial applicability. Fluorinations on scale still heavily rely on building-block approaches and on the use of toxic reagents such as HF (nucleophilic fluorination), $F_2$ (electrophilic fluorination) or $SF_4$ (deoxyfluorination). While transition-metal catalysed aromatic fluorinations have the potential to be applied on a large scale in the future, enantioselective fluorination is generally not a viable option in an industrial setting. The development of new strategies for asymmetric carbon-fluorine bond formation with inexpensive and easy-to-handle fluorinating reagents would be an appealing synthetic strategy. In the next section, the origin of fluorine and fluorinated reagents are discussed, with an emphasis on nucleophilic fluorine sources.

### *1.3.1 Origin and Occurrence of Fluorine*

The origin of fluorine in the Universe is still uncertain. Perhaps surprisingly, fluorine in the interstellar medium is considered a rare element, being the least abundant nuclide among those with an atomic mass of between 11 and 32.[39] $^{19}F$, the only stable isotope of fluorine, is not present in the main nuclear burning phases of stars. A fascinating hypothesis on fluorine cosmological formation invokes a neutrino reaction. Accordingly, $^{20}Ne$ would react with highly energetic neutrinos, generated from supernovae bursts, to give fluorine nuclei along with the ejection of a proton.[40-41] On Earth, fluorine is the 13$^{th}$ most abundant constituent of the Crust, significantly more abundant than the other halogens (20$^{th}$ Cl, 62$^{nd}$ Br, 64$^{th}$ I). Among the many fluorine-containing ores and minerals, three of them allow, at least in principle, for commercial extraction.[42] Cryolite ($Na_3AlF_6$) was an uncommon mineral with a modest

commercial importance, mined to extinction by the end of the 1980; Fluoroapatite ($Ca_5(PO_4)_3F$), virtually the largest reservoir of fluorine, is not directly exploited for fluorine extraction due to economic costs, however small amount of fluorosilic acid ($H_2SiF_6$) are recovered as a waste product in the production of phosphoric acid; Fluorite (Fluorspar, $CaF_2$), is the source of every single fluorine atom used (Scheme 1.10). In 2018, 5.8 million tonnes of Fluorite were mined with an estimated reserve of around 300 million tonnes, present mainly in Mexico, China and South Africa.[43] Around half of the Fluorspar mined is used for iron and steel smelting processes. The purest fraction, known in this context as Acidspar, is subjected to treatment with sulfuric acid in the process yielding to anhydrous HF, which is, directly or indirectly, the starting material for the preparation of all the fluorinated organic motifs.

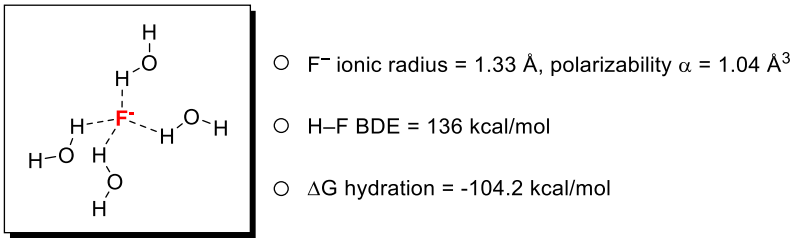



Scheme 1.10: Fluorspar value chain.

While vastly used for the industrial production of fluorocarbons, low molecular weight fluorinated building-blocks, and in the oil industry, anhydrous HF is avoided in research laboratories because it is toxic and hugely corrosive.[44] In 2019, the news reported a disastrous accident in Philadelphia, USA, that resulted in the spillage of 300,000 Kg of HF due to corroded pipes. HF, which is a commonly used acid catalyst in the refinery of low molecular weight hydrocarbons, was released in the atmosphere during a 24-hour long fire. The accident miraculously did not cause any fatality, however the company responsible for the plant filed for bankruptcy.[45] HF is transformed in elemental fluorine gas, $F_2$, by electrolysis in a perfected version of Moissan's process; remarkably a chemical synthesis of $F_2$ has been successfully completed by Karl Christe, in time for the 100-years-celebration of Moissan work.[46] $F_2$ is further reacted to form the many available electrophilic fluorinating reagents of tailored reactivity. Among them, 1-Chloromethyl-4-fluoro-1,4-diazoniabicyclo[2.2.2]octane bis(tetrafluoroborate) (Selectfluor®), *N*-fluoropyridinium salts and *N*-fluorosulfonimides, such as *N*-fluorobenzenesulfonimide (NFSI), found extensive applications in modern organic synthesis. Although the impact of electrophilic fluorinating reagents on organic chemistry has been tremendous and cannot be understated, some clear disadvantages of electrophilic $F^+$ equivalents had emerged. Electrophilic fluorinating reagents are difficult and expensive to synthesize, relying on the production, handling and storage of $F_2$ gas. Their oxidizing properties are sometimes incompatible with highly functionalized substrates. Furthermore, the high molecular weight of these reagents makes them non-ideal in terms of atom economy. On the other hand, nucleophilic sources of fluorine can be both cost-effective and environmentally friendly. This includes sulfur-based reagents employed in deoxyfluorination, HF complexes able to attenuate in some extent HF acidity, and fluoride salts. Among all $F^-$ sources, a

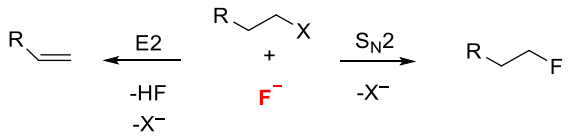
privileged role must be recognized to alkali metal fluoride salts (MF, M = Li, Na, K, Rb, Cs) due to their well-known availability, cost-effectiveness, safety, and low environmental impact.

### *1.3.2 Fluoride Anion and Fluoride Salts*

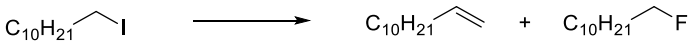



Scheme 1.11: Properties of the fluoride anion.

Fluoride salts are ideal sources of fluorine atoms, but a number of fundamental limitations hamper their use. Fluoride, as the most densely charged monovalent anion (charge density = 24 C/mm$^3$), is an excellent hydrogen bond acceptor, forming strong hydrogen bonds with water, alcohols, amides and generally with every hydrogen bond donor accessible. The high hydration energy of fluoride ($\Delta G_{hydr.}$ = -104.2 kcal/mol) implies the formation of tight hydration shells in aqueous solutions and explains the propensity of most of its salts to be highly hygroscopic. Hydrogen bonding interactions are typically perceived as detrimental for fluoride nucleophilicity, as the formation of hydrogen bonds results in decreased electron density on fluoride. Accordingly, fluoride nucleophilicity in solution is severely diminished by the presence of water or other hydrogen bond donors. Fluoride becomes extremely reactive when protic sources are rigorously excluded; its increased nucleophilicity is then accompanied by greater basicity responsible for extensive side reactivity. This is a general problem for nucleophilic fluorination of aliphatic chains, where E2 product often prevails over the desired $S_N2$ pathway (Scheme 1.12).




X = (pseudo)halide




| | | |
|---|---|---|
| KF/18-crown-6 ($CH_3CN$) | 49 % | 51 % |
| TBAF (THF) | 89 % | 11 % |

Scheme 1.12: Nucleophile–base dichotomy of fluoride anion.[47,48]

Fluoride makes extremely strong ionic bonds with alkali metal cations; the lattice energy increases with decreasing ionic radius of the cation as a consequence of higher charge density (Table 1.3). Solubility in water is inversely proportional with respect to the lattice energy, this makes CsF the weakest crystalline lattice among the alkali metal fluoride series, and the most soluble. The hygroscopicity of alkali metal fluorides also increase with the cation size; CsF is considerably hygroscopic while LiF does not show appreciable accumulation of water.

Table 1.3: Selected properties of fluoride salts.[12]

| Fluoride Salt | Cationic radius (Å) | Cation charge density ($C/mm^3$) | Lattice Energy (kcal/mol) | Solubility (g/100 g $H_2O$) |
|---|---|---|---|---|
| $CaF_2$ | 1.12 | 52 | 634 | 0.0016 |
| LiF | 0.79 | 52 | 251 | 0.134 |
| NaF | 1.02 | 24 | 222 | 4.13 |
| KF | 1.38 | 11 | 198 | 102 |
| RbF | 1.52 | 8 | 190 | 300 |
| CsF | 1.67 | 6 | 181 | 573 |

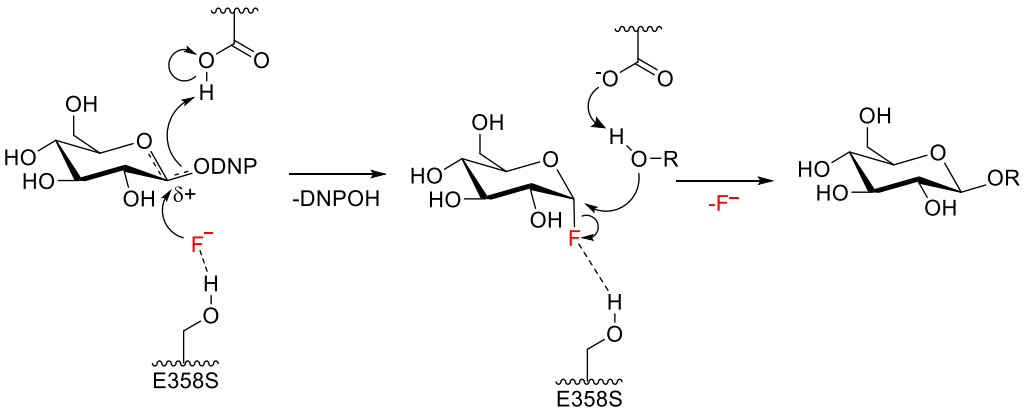
In view of their high lattice energy, alkali metal fluorides are poorly soluble in organic solvents; CsF, at room temperature, is completely solvated only by methanol, which is able to break the ionic lattice through hydrogen bonding. A conventional approach to increase the solubility of alkali metal fluorides in aprotic solvents is the encapsulation of the metallic counter-cation with crown ethers or cryptands, which weakens the ionic interaction resulting in a *free* and

*naked* fluoride anion. The use of organic counter-cations is another viable option to increase solubility of fluoride salts; tetrabutylammonium fluoride (TBAF), the most commonly used tetraalkylammonium salt, is highly soluble in apolar solvents. However, the reduced lattice energy translates in a high hygroscopicity, so that TBAF is commercialized as trihydrate complex; it is considered a poor nucleophile often leading to hydrolysis instead of fluorination. Upon drying, the fluoride in TBAF becomes extremely reactive, triggering Hofmann elimination that ultimately leads to self-decomposition of the salt. Anhydrous TBAF can be generated using the protocol developed by Dimagno,[49] used and stored at low temperature. Alternatively, the use of counter-cation with no β-hydrogen is a possible way to obtain a dry fluoride salt, as for tetramethylammonium fluoride (TMAF). Even though the use of dry TMAF was proven to be useful for selected aromatic fluorination,[50] *naked* fluoride has limited synthetic utility due to its uncontrollable reactivity.[51] The simultaneous control of selectivity and reactivity is an underlying problem of fluoride chemistry. Practical limitations such as solubility and hygroscopicity severely hampered the development of synthetic methodologies. The following paragraphs describe how Nature and synthetic chemists make use of hydrogen bonding interactions to tackle these issues.

### *1.3.3 Nature's Approach to Fluorination*

*1.3.3.1 Enzymatic Fluorination.* One of the most distinctive aspects of fluorine chemistry is the paucity of biochemical pathways capable of producing fluorinated natural products. Despite fluorine being an abundant element, only six discrete fluorinated natural products have been unambiguously identified among the 130,000 characterised to date.[52] Even though reservoirs of Fluorspar are not rare, the solubility in water of $CaF_2$ is extremely low (0.0016 g/100 g $H_2O$), thereby a very low concentration of $F^-$ is available in the biosphere. Moreover, fluoride is poorly reactive in heavily hydrated biological systems, and cannot be oxidised by $H_2O_2$

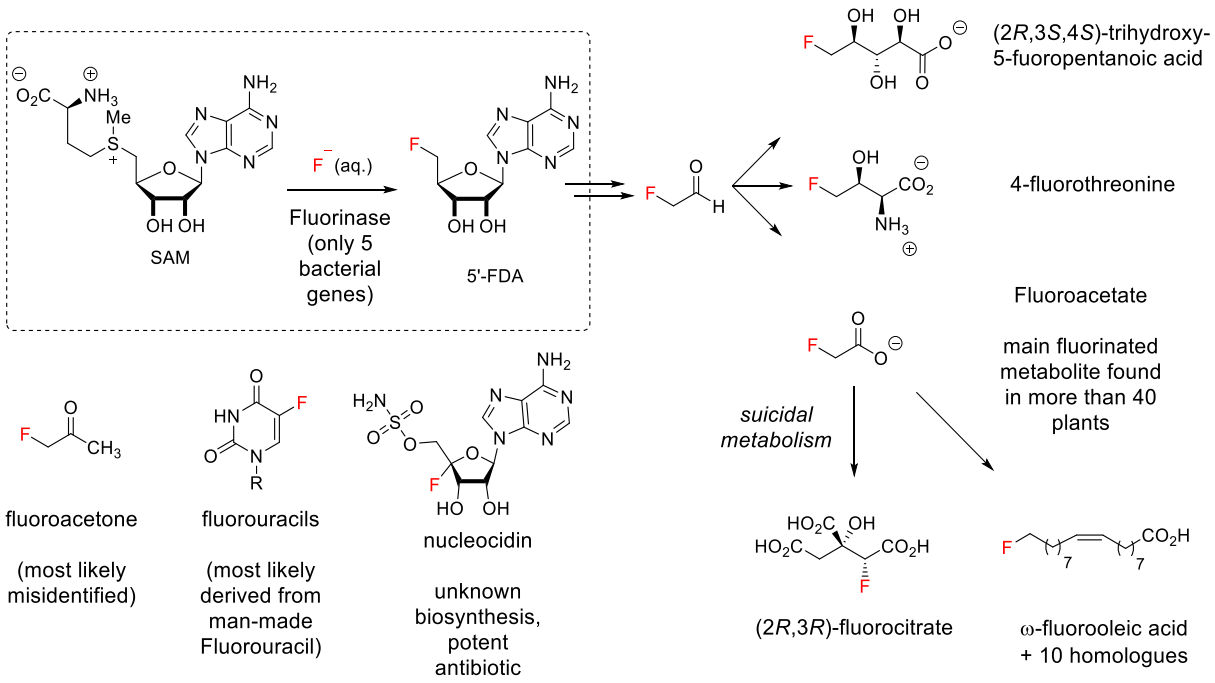
dependent haloperoxidases (standard reduction potential $E^o(F_2)$ = +2.87 V *cf.* $E^o(Cl_2)$ +1.36 V, $E^o(Br_2)$ = +1.06 V), precluding the most common enzymatic halogenation pathways. In 2001, the remarkable discovery that two mutated glycosidases (*Agrobacterium sp*. $\beta$-glucosidase E358S and *Cellulomonas fimi* $\beta$-mannosidase E429A) could form C–F bonds showed for the first time that fluorination was feasible under biological conditions.[53-54] The importance of hydrogen bonding in the stabilization of the fluoride anion was proposed based on the beneficial interaction of one serine residue in the catalytic pocket (Scheme 1.13).




DNP = 2,4-dinitrophenyl

Scheme 1.13: Enzymatic formation of C–F bonds as reported by Withers *et al.*

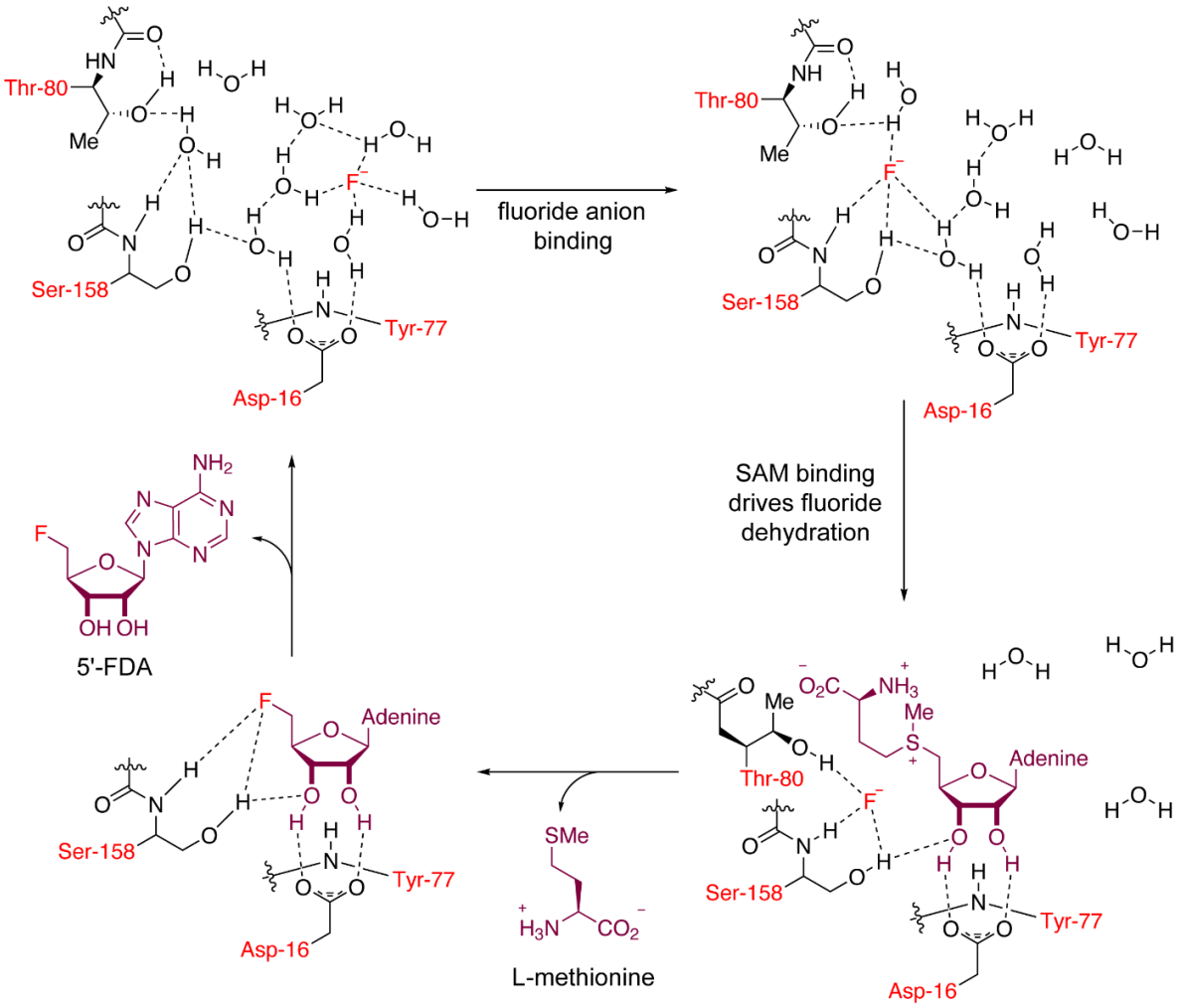
Shortly thereafter, O'Hagan identified and characterised the first natural enzyme capable of forming carbon-fluorine bonds. The enzyme, isolated from strains of the bacterium *Streptomyces cattleya*, catalyses the reaction between $F^-$ and *S*-adenosylmethionine (SAM) to form the primary fluorinated metabolite 5'-fluoro-5'-deoxyadenosine (5'-FDA) and methionine. The enzyme was named 5'-fluoro-5'-deoxyadenosine synthase (FDAS), commonly shortened as *fluorinase*. 5'-FDA is the precursor of the limited number of fluorinated metabolites known, with the notable exception of nucleocidin, the biosynthesis of which being currently unknown (Scheme 1.14).[55]




Scheme 1.14: Fluorinated natural products.

Structural and mechanistic investigations were of fundamental importance to understand how Nature evolved an enzyme capable of performing nucleophilic fluorination in water. 5'-Fluoro-5'-deoxyadenosine synthase is organised in a hexameric structure composed of two trimers; each of the three monomeric subunits counts 299 amino acids, as shown by high-resolution X-ray crystal structures obtained from the protein co-crystallised with SAM and 5'-FDA.[56] Fluorinase exhibits a low turnover ($k_{cat}$ = 0.06 $min^{-1}$) and a low binding affinity for $F^-$ ($K_{m\ F^-}$ = 10 mM, 20 μM SAM); the overall poor efficiency ($k_{cat}/K_m$ = $10^4$ $min^{-1}$ $M^{-1}$) reflects the enormous kinetic cost of the transformation. Fluorine incorporation proceeds with inversion of configuration at carbon 5' of SAM, suggesting a $S_N2$ reaction mechanism, rather uncommon in enzymatic catalysis.[57] To act as a nucleophile, $F^-$ needs to be dehydrated, at least partially, by the enzyme.[58,59] This is favoured by three hydrogen bonds deployed in the enzymatic pocket; these HB interactions involve the amidic NH and the side chain OH from a serine ($Ser_{158}$ residue), and the OH of a threonine side chain ($Thr_{80}$ residue). A complementary theoretical study highlights the electrostatic interaction between the sulfonium ion of SAM

and $F^-$ as an important contribution to the stabilisation of the transition state.[59] Combined mechanistic information led to a plausible pathway for the enzymatic fluorination mediated by fluorinase (Scheme 1.15).[60] *i)* Hydrated fluoride passively diffuses into the enzymatic pocket which binds the halide through bidentate hydrogen bonding with $Serine_{158}$; *ii)* Upon binding of the substrate, SAM, fluoride loses the last molecules of water in exchange for an additional hydrogen bond with $Thr_{80}$, which trap $F^-$ preparing for the nucleophilic substitution;[61] *iii)* $S_N2$ attack by the desolvated fluoride provide 5'-FDA and L-methionine; *iv)* the fluorinated product is released from the enzyme following two subsequent conformational changes.




Scheme 1.15: Mechanism of the fluorinase enzymatic fluorination.

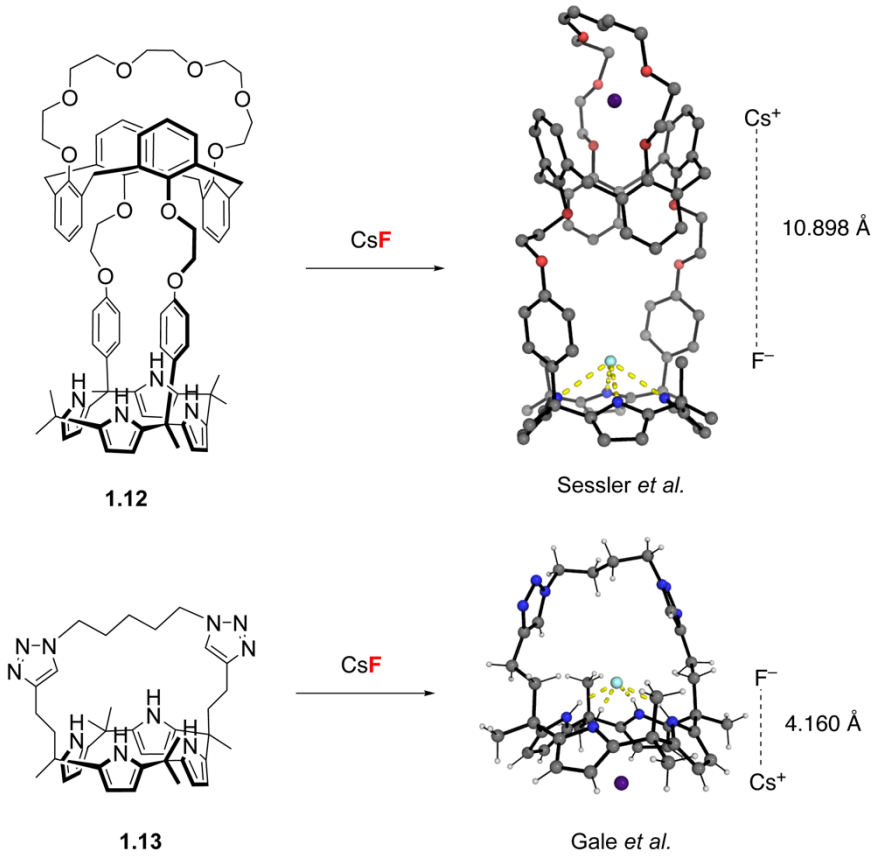
*1.3.3.2 Enzymatic Defluorination.* Fluoroacetate is the most common fluorinated natural product and can be found in more than 40 plants. It is extremely toxic to mammals that metabolise it *in vivo* as fluorocitrate in what has been referred to as *lethal biosynthesis* or *suicidal metabolism,* which leads to the inhibition of the Krebs cycle and death of the organism. Curiously, Nature evolved several biochemical structures to detoxify and remove fluorinated molecules and fluoride ions from the intracellular matrix.[62–65] In a recent example, the molecular steps for enzymatic defluorination of fluoroacetate were disclosed.[66] Fluoroacetate is defluorinated *via* an $S_N2$ attack of one aspartate residue, which displace $F^-$. Strikingly, the enzymatic pocket closely resembles the one of fluorinase, with three key hydrogen bonds ($His_{NH}$, $Trp_{NH}$ and $Tyr_{OH}$) employed to stabilise the fluoride leaving group.

*1.3.4 Hydrogen Bonding with Fluoride*

Hydrogen bonding is a defining feature of fluoride chemistry employed by Nature to synthesise the few known fluorinated natural products. Recently, hydrogen bonding has also been embraced as a way to control the behaviour of fluoride salts in a laboratory context.[67]

*1.3.4.1 Hydrogen Bonded Supramolecular Structures.* The ability of fluoride to engage in hydrogen bonding has been extensively utilised in the design of anion sensors and transporters selective for $F^-$. Commonly used scaffolds for fluoride sensing and recognition include ureas, thioureas and calix[4]pyrroles.[68,69] A remarkable contribution from the Sessler group showed the use of a calix[4]pyrrole capped with a crown ether (**1.12**) as an effective receptor to form a stable complex with CsF by separating the ion pair in a rare example of cation/anion double recognition (Scheme 1.16).[70] Gale and co-workers expanded the scope of calix[4]pyrroles-based artificial receptor to fluoride transport across cellular membranes, in

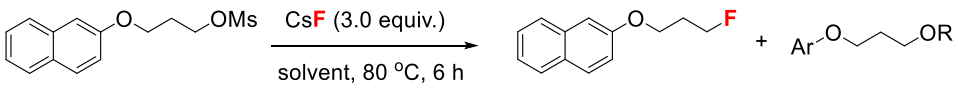
the first example of its kind.[71] The hydrogen bond donor **1.13** shows selectivity for fluoride over chloride and resembles naturally occurring fluoride transporters (Scheme 1.16).




Scheme 1.16: Examples of supramolecular fluoride binding.

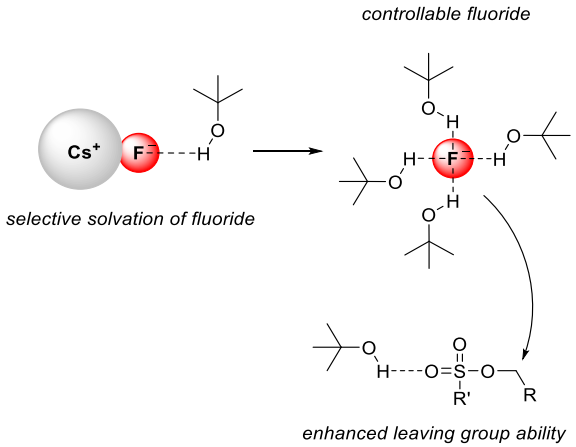
*1.3.4.2 Hydrogen Bonding Promoted Nucleophilic Fluorination.* Kim and co-workers were the first to report that performing fluorinations in bulky aliphatic alcohols, such as *t*-amyl alcohol and *t*-butanol, greatly enhanced rate and selectivity in $S_N2$ fluorination with CsF (Table 1.4).[72,73] The hydrogen bonding ability of the solvent was invoked to explain the favourable reaction profile: alcohol-fluoride hydrogen bonding interactions justify the reduced basicity of $F^-$, while alcohol-sulfonate interactions facilitate the reaction by enhancing leaving group ability (Scheme 1.17).

Table 1.4: $S_N2$ fluorination promoted by hydrogen bonding.



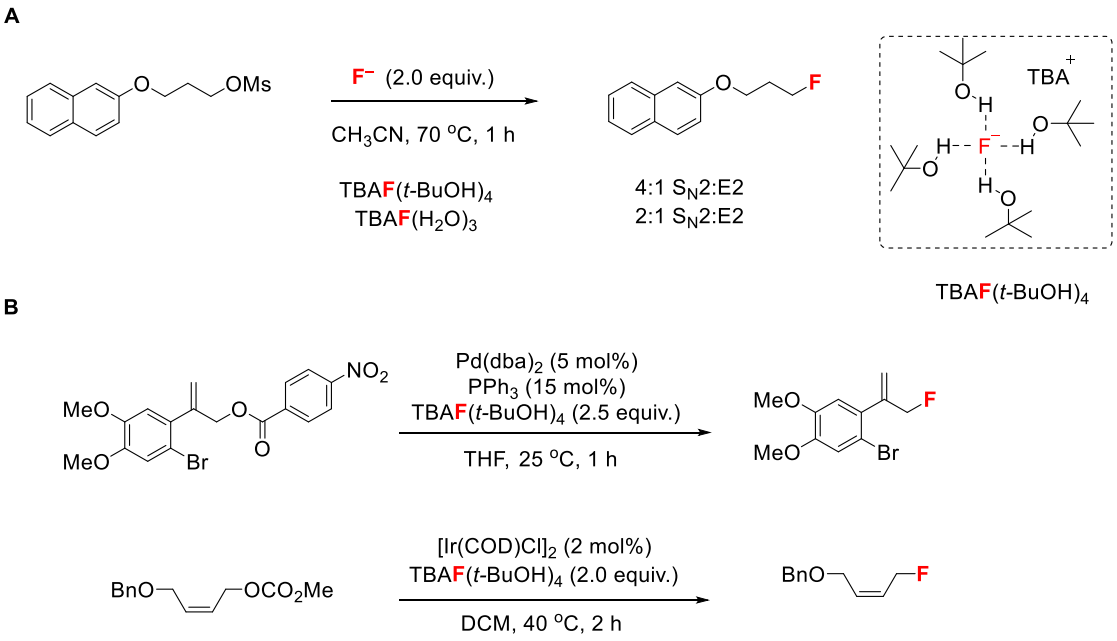

**1.14** **1.15** **1.16**

| Solvent | Starting material (**1.14**) | Product (**1.15**) | Side Product (**1.16**) |
|---|---|---|---|
| *t*-AmylOH | – | 93 | 5 |
| *t*-BuOH | trace | 92 | 7 |
| *n*-BuOH | 4 | 64 | 30 |
| $CH_3CN$ | 91 | 7 | – |
| DMF | 33 | 48 | – |



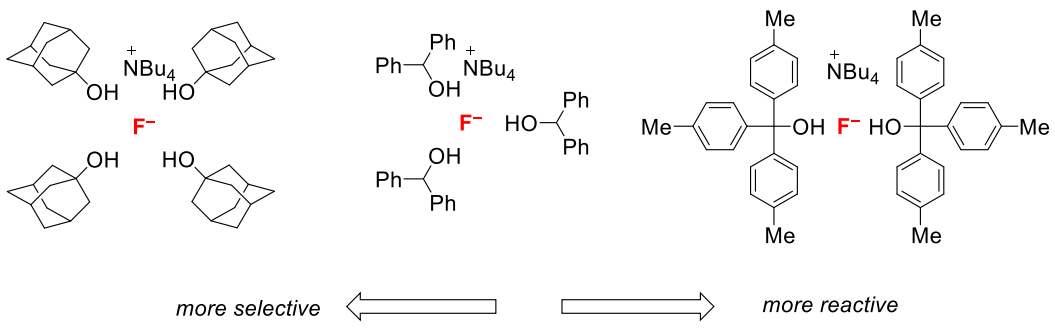

Scheme 1.17: Hydrogen bonding interactions in $S_N2$ fluorination using *t*-BuOH as a solvent

The authors were able to synthesise TBAF(*t*-BuOH)$_4$ complex which was structurally characterised by single crystal X-ray diffraction. The newly generated TBAF complex showed similar reactivity and selectivity compared to the reaction with CsF in *t*-BuOH, and significant improvement with respect to commercial TBAF·3($H_2O$) (Scheme 1.18 A).[74] Remarkably, TBAF(*t*-BuOH)$_4$ is a stable solid that is significantly less hygroscopic than TBAF·3($H_2O$). TBAF(*t*-BuOH)$_4$ has been selected as preferred fluoride source in the palladium and iridium catalysed fluorination of allylic carbonates, published by Gouverneur and co-workers (Scheme 1.18 B). [75,76]



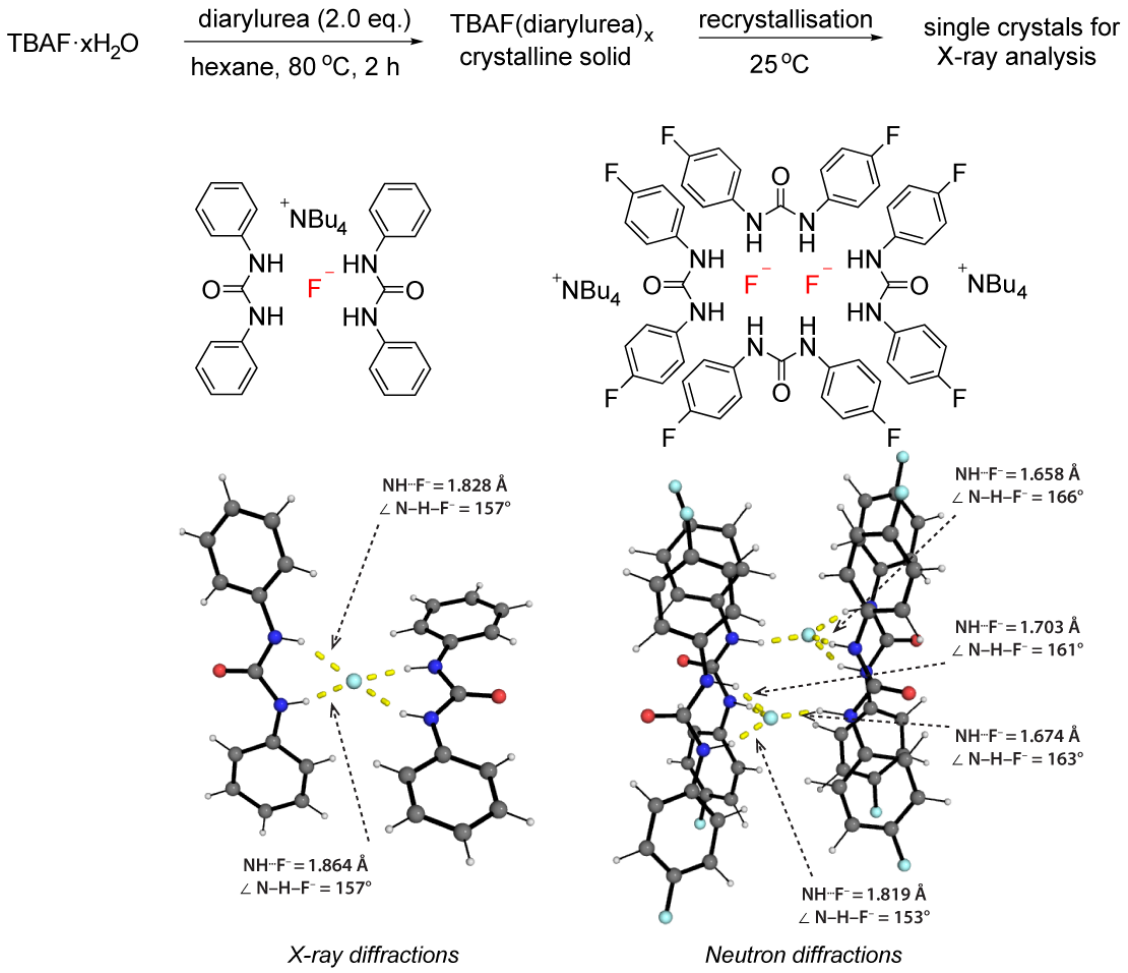

Scheme 1.18: Applications of TBAF(*t*-BuOH)$_4$.

In an effort to systematically study how different hydrogen bond donors affect fluoride chemistry, Gouverneur and co-workers reported a detailed study on a series of alcohols, diols, triols and tetraols complexed with TBAF. The thorough structural characterisation of fourteen new fluoride complexes demonstrates a great variability in the coordination stoichiometry, with smaller alcohols favouring tetracoordinated complexes and bulkier alcohols forming tri- or, even, bis-coordinated fluorides. The hydrogen bonding network around fluoride is crucial to control nucleophilicity and basicity. Generally, higher coordinated $F^-$:complexes display a reduced reaction rate and a more favourable $S_N2$:E2 selectivity (Scheme 1.19).[77]




Scheme 1.19: Reactivity and selectivity trends observed in (ROH)$_n$TBAF complexes.

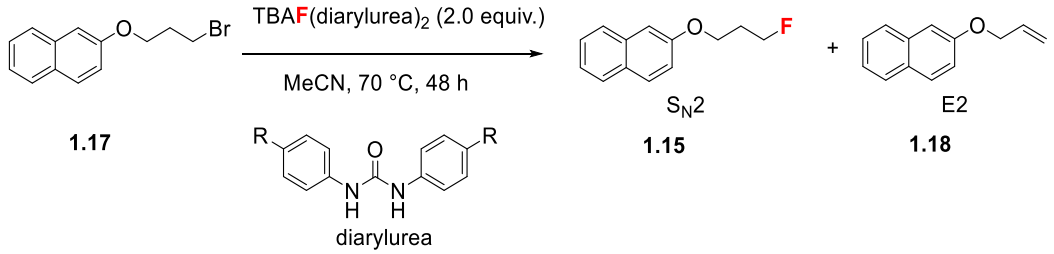
Follow-up investigations focused on the synthesis and characterisation of fluoride complexes with novel hydrogen bond donors, such as diarlyureas.[78] The structural work produced eighteen crystal structures of urea:fluoride complexes. While the majority were obtained from x-ray data, three of them were solved from neutron diffraction patterns, which can more accurately describe hydrogen positioning, locating the nuclei of a molecule instead of its electron-density. Diarylureas tend to co-crystallise with TBAF in a 2:1 arrangement, even though different geometries, such as 4:2 binding mode, were also observed (Scheme 1.20). The novel urea:TBAF complexes were easily prepared and serve as effective fluorinating reagents showing a significantly slower reaction compared with the previously described alcohol complexes and unbound TBAF·3($H_2O$).




Scheme 1.20: Diarylureas–TBAF complexes.

A major advantage of the diarylurea scaffold is the possibility of modulating the acidity of the NH by modifying the electronic character of the aromatic rings, thereby influencing NH hydrogen bonding ability. As a consequence of their stronger hydrogen bonding interactions, electron-poor ureas:TBAF complexes are less reactive than electron-neutral and electron-rich complexes; however, they show higher $S_N2$/E2 selectivity, with 1,3-bis(4-(trifluoromethyl)phenyl)urea accounting for the best $S_N2$/E2 ratio ($S_N2$/E2 = 8.7, R = $CF_3$) (Table 1.5). Even though diarylureas:TBAF show a 2:1 binding mode in the solid state ($U_2F^-$, U = urea), the increased reaction rate upon dilution and binding studies in solution suggested that the reactive species is a 1:1 urea–fluoride ($UF^-$) generated from the dissociation of one urea ligand from $U_2F^-$.

Table 1.5: Reactivity and selectivity of diarylurea:TBAF complexes as stoichiometric reagents.

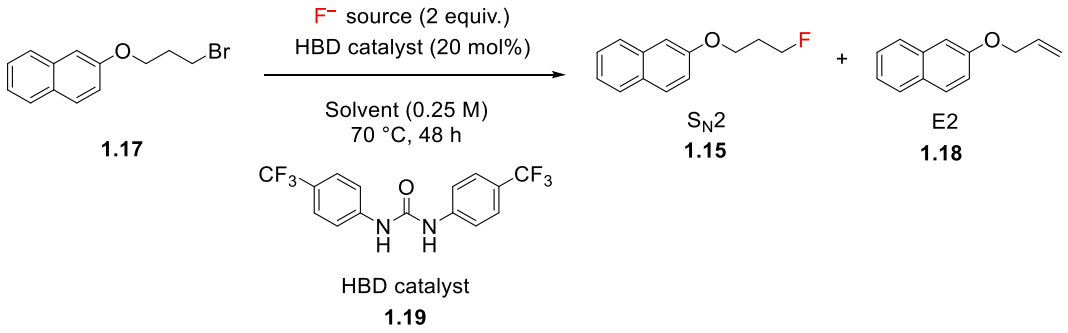



| R | *k* (relative) | **1.15**/**1.18** ($S_N2$/E2) |
|---|---|---|
| 4-OMe | 7.7 | 5.2 |
| 4-Me | 6.0 | 5.7 |
| 4-H | 3.5 | 6.8 |
| 4-F | 3.4 | 7.1 |
| 4-Cl | 3.5 | 6.9 |
| 4-$NO_2$ | 2 | 8.4 |
| **4-$CF_3$** | **1** | **8.7** |
| TBAF($H_2O$)$_3$ | 227 | 1.6 |

While most of the work involved the stoichiometric use of urea:TBAF complexes, selected experiments were conducted using catalytic amounts of 1,3-bis(4-(trifluoromethyl)phenyl)urea **1.19** and various fluoride salts in a $S_N2$ model-reaction (Table 1.6). Interestingly, the urea catalyst showed the ability to influence the outcome of the

transformation, resulting in substantial improvements of both reactivity and selectivity when CsF was reacted in acetonitrile in the presence of 20 mol% of HBD catalyst.

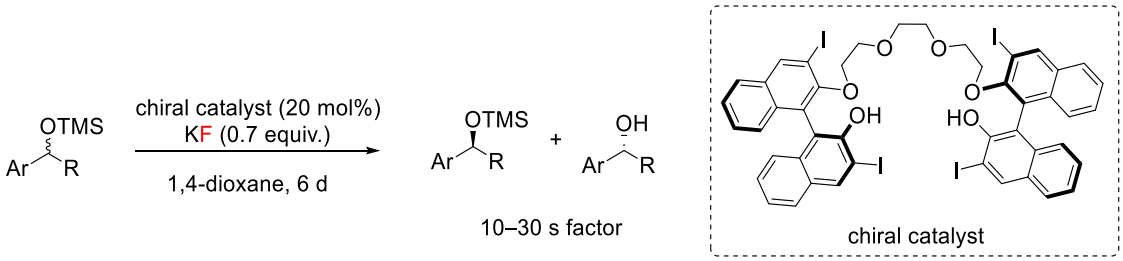
Table 1.6 : Fluorination using diarylureas as HBD catalysts.




**1.17** | $S_N2$ **1.15** | E2 **1.18** | HBD catalyst **1.19**

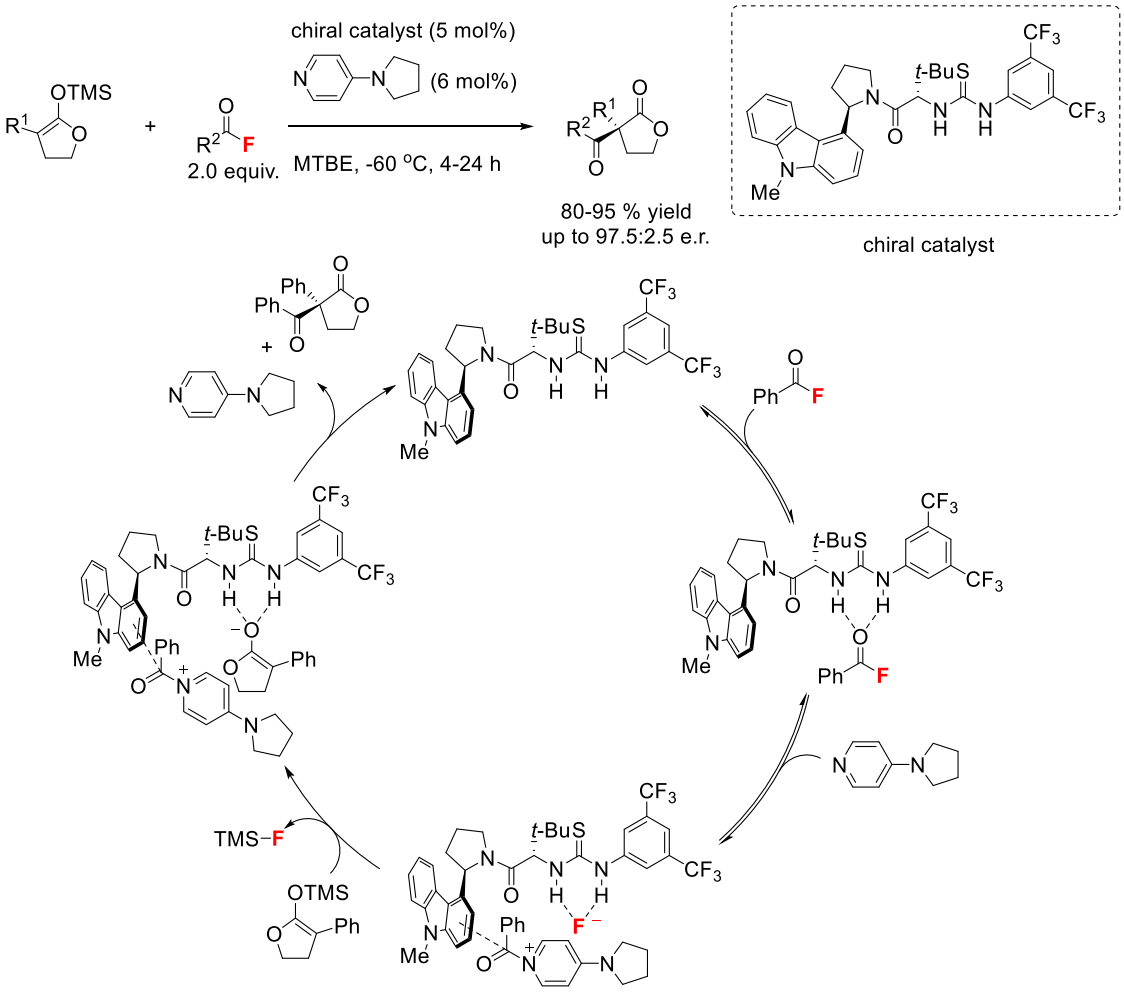
| Catalyst loading | F⁻ source | Solvent | Conversion % | RF % (**1.15**) | Alkene % (**1.18**) |
|---|---|---|---|---|---|
| 20 mol% | CsF | $CH_3CN$ | 68 | 46 | 20 |
| – | CsF | $CH_3CN$ | 24 | 7 | 6 |
| 20 mol% | CsF | DMSO | >95 | 27 | 71 |
| 20 mol% | RbF | $CH_3CN$ | 13 | 12 | trace |
| – | RbF | $CH_3CN$ | 4 | trace | 3 |
| 20 mol% | AgF | $CH_3CN$ | 48 | 43 | 2 |
| – | AgF | $CH_3CN$ | 48 | 43 | 2 |

*1.3.4.3 Hydrogen Bonded Fluoride Complexes in Asymmetric Catalysis.* More recently, the participation of chiral enantiopure hydrogen-bonded fluoride complexes has been suggested as intermediates in asymmetric catalysis. In 2010, Song and collaborators reported the design of a new class of 1,1'-bis-2-naphtol (BINOL)-based polyethers, capable of binding KF and mediating kinetic resolution of secondary silyl ethers *via* a desilylative process (Scheme 1.21).[79] The authors underlined the importance of the halogen substituent in the 3,3'-position, responsible for improved selectivity passing from Cl (*s* = 1.5) to the more polarizable iodine, (*s* = 29). Upon methylation of the two phenol groups the catalyst became inactive, suggesting hydrogen bonding interactions to fluoride. Important insights were obtained from the X-ray crystal structure of the catalyst and KF; the major contribution is likely to originate from the Lewis basic oxygens of the polyglycol chain coordinating the potassium ion, thereby reducing the ionic strength of the $K^+F^-$ interaction.




Scheme 1.21: Desilylative kinetic resolution of silyl ether mediated by a chiral KF complex.

In 2011, Jacobsen and collaborators reported the organocatalytic enantioselective acylation of silyl ketene acetals co-catalysed by chiral thioureas and DMAP analogues.[80] The best results in terms of yield and enantioselectivity were obtained with an acyl fluoride. The rather unusual choice of the acylating agent was rationalised by the multiple role that the catalyst plays in the catalytic cycle (Scheme 1.22).




Scheme 1.22: Enantioselective acylation of silyl ketene acetals involving a chiral HB-fluoride complex.

Firstly, the thiourea catalyst activates the acyl fluoride by coordination to the carbonyl, subsequent acylation of the amino pyridine co-catalyst is mediated by the catalyst in a double fashion: through hydrogen bonding with fluoride and by means of cation-$\pi$ interaction. Desilylation of the silyl ketene acetal gives a hydrogen bonded enolate, prone to undergo the enantiodetermining acylation.

## 1.4 Current Approaches to Asymmetric Fluorination

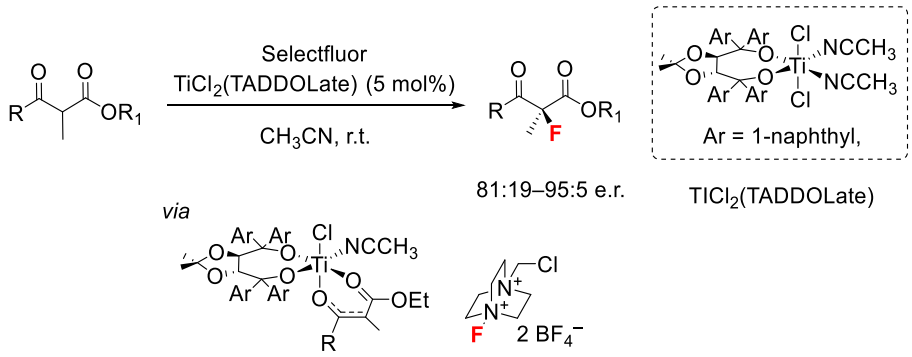
The development of catalytic methodologies allowing for asymmetric fluorination progressed at a significantly slower pace than other enantioselective functionalisations such as C–C, C–N and C–O bond formation.[81] The following section presents a selection of strategies for the catalytic enantioselective introduction of fluorine, using electrophilic and nucleophilic fluorinating reagents. For a comprehensive discussion on modern approaches to enantioselective fluorination, the reader can refer to the many excellent reviews in the literature.[82-85]

### *1.4.1 Asymmetric Fluorination with Electrophilic Fluorine Reagents*

Significant advancements in catalytic electrophilic enantioselective fluorination were possible after the introduction of mild $F^+$ surrogates such as NFSI and Selectfluor®, which paved the way for the development of transition-metal mediated and organocatalytic protocols.

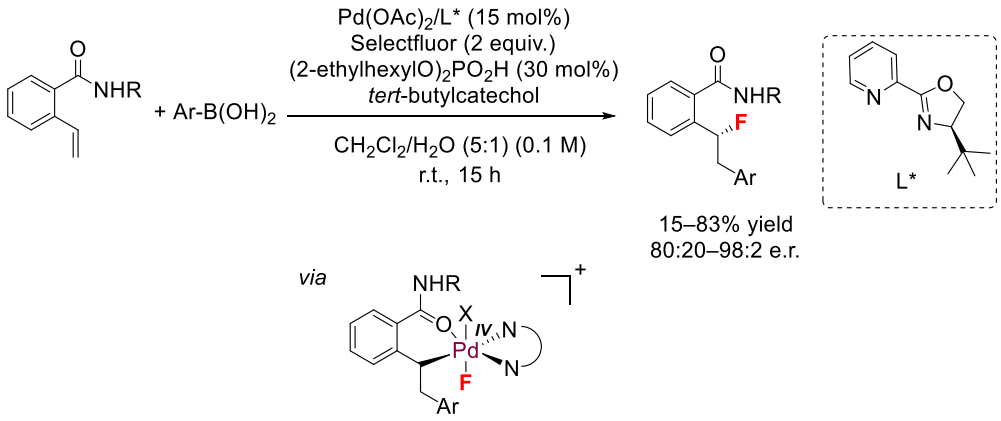
*1.4.1.1 Transition-Metal Catalysed Asymmetric Electrophilic Fluorination.* The first examples of catalytic asymmetric fluorination were enabled by the use of transition-metal based chiral Lewis acids. In 2000, Togni and co-workers reported the enantioselective fluorination of β-keto esters, using Selectfluor® as fluorine source and Ti-TADDOL complex as enantiopure catalyst (Scheme 1.23).[86,87] After Togni's seminal report, several protocols for the enantioselective α-fluorination of bidentate carbonyl compounds such as α-acyl lactams, oxindoles, β-keto phosphonates, α-cyano esters and α-cyano phosphonates appeared in the literature. Even though a wide variety of transition metals/chiral ligands were employed, most notably Pd(II)/BINAP[88] Ni(II)/*bis*-oxazoline[89] and Cu(II)/*bis*-oxazoline,[90] all the reactions are believed to proceed *via* a similar mechanism. Coordination of the substrate to the chiral Lewis

acid favours the formation of a metal enolate which reacts with the $F^+$ reagent and generates the desired enantioenriched product.




Scheme 1.23: The first example of catalytic asymmetric fluorination reported by Togni *et al*.

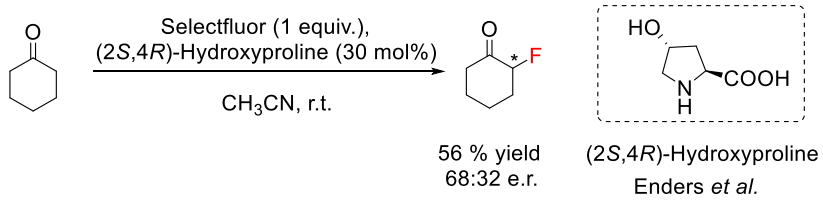
In 2014, Toste and co-workers disclosed a three-component reaction involving Selectfluor®, styrenes and boronic acids to afford enantiopure fluorinated compounds in one of the few examples of transition-metal catalysed asymmetric fluorination not involving α-carbonyl C–F bond formation (Scheme 1.24). The reaction proceeds through a high-valent Pd(IV) intermediate, stabilised by the anchimeric assistance of the proximal amide, which also dictates the observed regioselectivity.[91]




Scheme 1.24: Palladium catalysed enantioselective fluorination of styrenes.

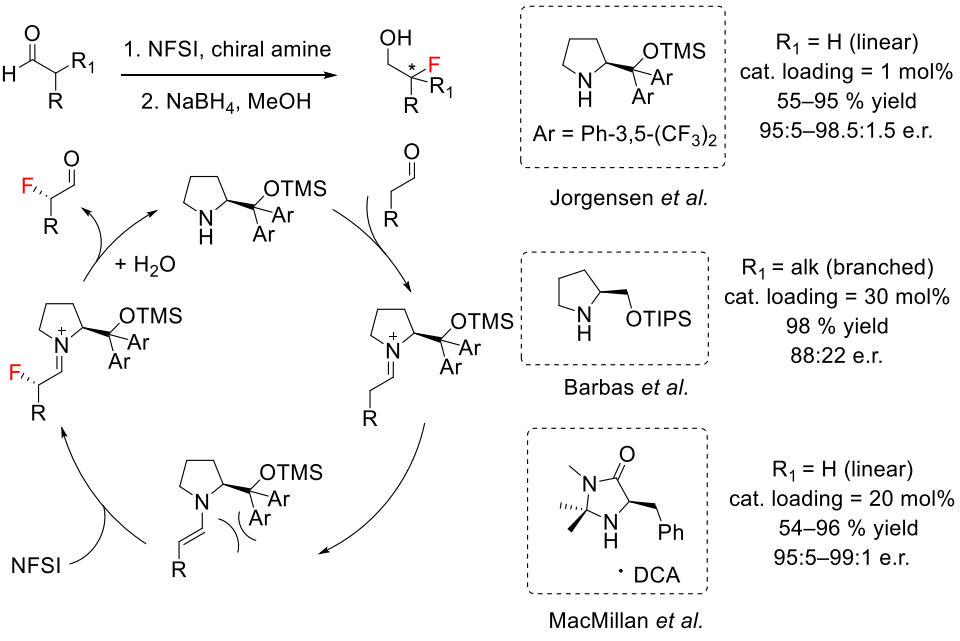
*1.4.1.2 Organocatalytic Asymmetric Electrophilic Fluorination.* The advent of asymmetric enamine catalysis influenced fluorination leading to several reports of enantioselective

electrophilic α-fluorination of aldehydes and ketones catalysed by chiral secondary amines. In 2005, seminal work from Enders and co-workers demonstrated the feasibility of this approach using (*S*)-proline derivatives and Selecfluor® (Scheme 1.25).[92]




Scheme 1.25: The first organocatalytic asymmetric fluorination reported by Enders *et al.*

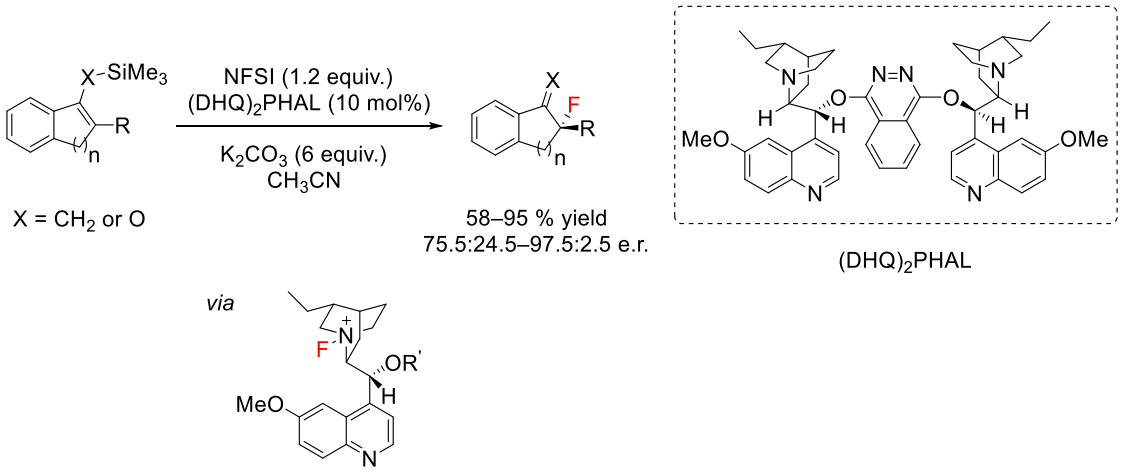
Jørgensen and collaborators employed his popular silylated prolinol catalyst to direct the asymmetric fluorination of aldehydes with NFSI, obtaining excellent yields and enantioselectivities (Scheme 1.26).. The desired fluorinated products were reduced *in situ* to avoid undesired racemization.[93] The choice of NFSI as fluorinating reagents was critical for ensuring improved enantiocontrol compared with the more reactive Selectfluor®, this latter reagent being responsible for non-enantioselective background reactivity.




Scheme 1.26: Application of chiral enamine catalysis to asymmetric fluorination.

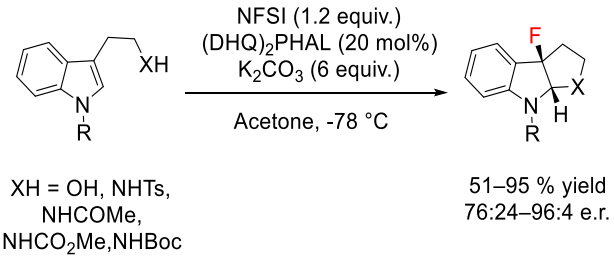
Shortly after, Barbas *et al.* published promising enantioselectivity for the fluorination of α-branched aldehydes using a structurally related catalyst.[94] MacMillan *et al.* reported the use of chiral imidazolidinone dichloroacetate for the fluorination of linear aldehyde achieving excellent yields and enantioselectivities. Most notably, the substrate scope demonstrated wide applicability of this methodology.[95]

In 2008, Shibata and co-workers reported a highly selective, catalytic process using a *bis*-cinchona alkaloid as organocatalyst and NFSI as fluorinating reagent (Scheme 1.27).[96] This work followed prior efforts that established asymmetric fluorinations using stoichiometric enantiopure N–F reagents.



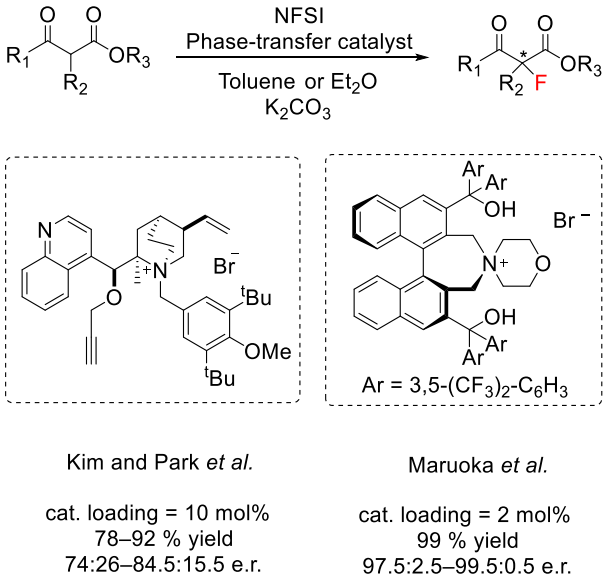

Scheme 1.27: Enantioselective fluorination using cinchona alkaloid dimers as catalysts.

This concept was subsequently exploited by Gouverneur and co-workers in the enantioselective fluorocyclization of prochiral indoles.[97] Notably, this methodology provides fluorinated quaternary centres, a particularly challenging motif to access in high enantioselectivity (Scheme 1.28).




Scheme 1.28: Organocatalytic asymmetric fluoro cyclization.

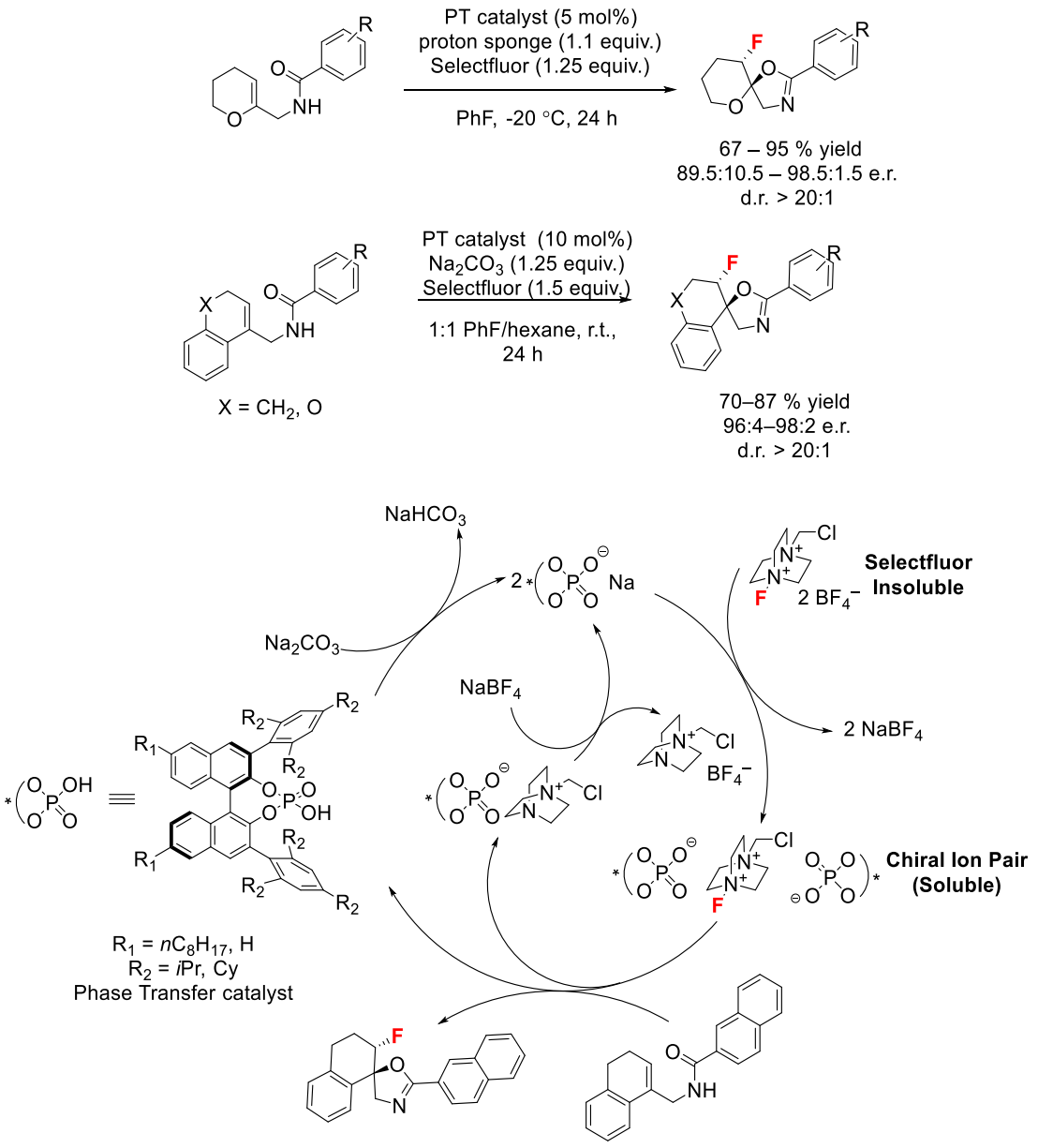
A cationic phase-transfer approach to electrophilic fluorination was introduced by Kim and Park in 2002, and ameliorated by Maruoka in 2010.[98,99] This catalytic mode involves the participation of a chiral ammonium salt capable of transferring an insoluble metal enolate in the organic phase, thereby generating a soluble chiral ammonium enolate equivalent which is intercepted by NFSI (Scheme 1.29).




Scheme 1.29: Cationic asymmetric PTC fluorination.

In 2011, The Toste group reported a conceptually different phase-transfer methodology in which an anionic phase-transfer catalyst was able to directly transport an insoluble fluorinating reagent to achieve highly enantioselective fluorocyclizations of enol ethers, analogous conditions were employed for the fluorocyclization of less electron-rich dihydronaphtalenes and chromenes derivatives (Scheme 1.30).[100] The catalyst is a chiral

phosphoric acid that solubilises Selectlfuor® *via* the formation of a chiral ionic species consisting of two molecules of catalyst for and one molecule of Selectfluor®. This radically different approach was a major advancement in the field and its application was expanded to several appealing substrates, most notably enamides [101] and conjugated dienes.[102]




Scheme 1.30: Anionic asymmetric PTC fluorination.

*1.4.2 Asymmetric Nucleophilic Fluorination*

Asymmetric fluorination using $F^-$ reagents is underdeveloped when compared with asymmetric electrophilic methodologies which benefited from the introduction of $F^+$ reagents of tailored reactivity. Progress in the field of asymmetric nucleophilic fluorination has taken place in the last 10 years with major contributions from the Doyle group.

*1.4.2.1 Transition-Metal Catalysed Asymmetric Nucleophilic Fluorination*. In 2010, following seminal contribution from Bruns and Haufe,[103] Doyle and collaborators disclosed an enantioselective protocol for the ring opening of *meso*-epoxide using a dual-catalytic system composed by a chiral amine and chiral Co(II)(salen) catalyst.[104] The use of a combination of benzoyl fluoride and hexafluoroisopropanol (HFIP) as latent source of HF overcomes the unselective background fluorination and catalyst poisoning observed when HF or its surrogates were employed. However, both a chiral amine, (–)-tetramisol, and a chiral Lewis-acid, (*R*,*R*)-Co(III)(salen)OTs, are required to achieve high yields and enantiomeric ratios (Scheme 1.31).

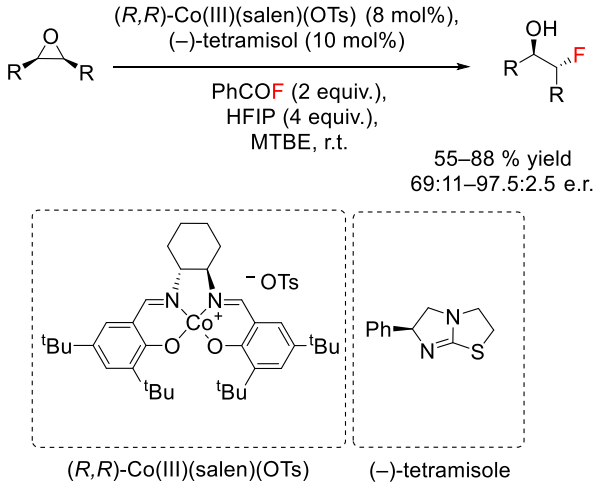
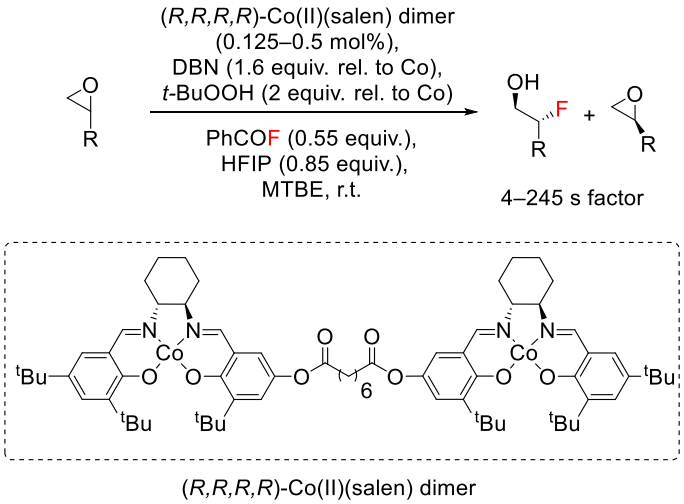


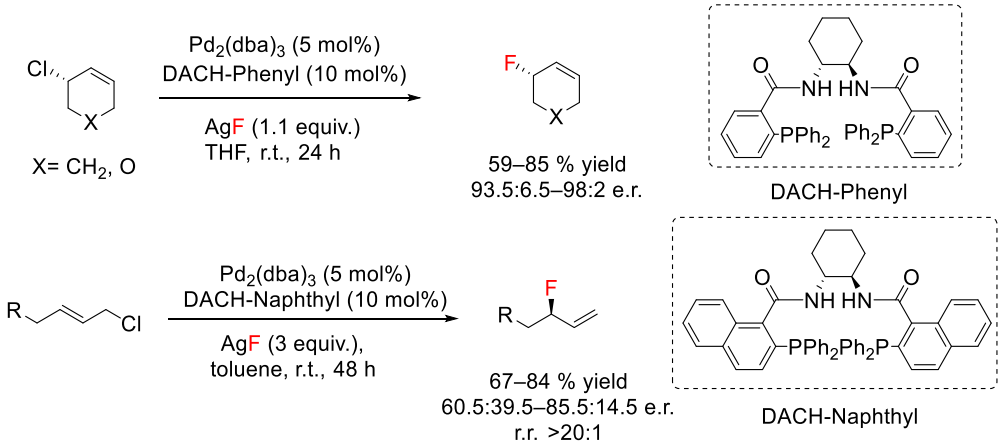

Figure 1.31: Cobalt catalysed asymmetric nucleophilic fluorination of *meso*-epoxides.

Following an elegant mechanistic study,[105] the reaction was improved by developing a dimeric Co(II) catalyst, which provided a significant rate acceleration and allowed efficient kinetic resolution of terminal epoxides (Scheme 1.32). With these new reaction conditions, a non-chiral amine catalyst could be employed.




Scheme 1.32: Cobalt catalysed kinetic resolution of terminal epoxides.

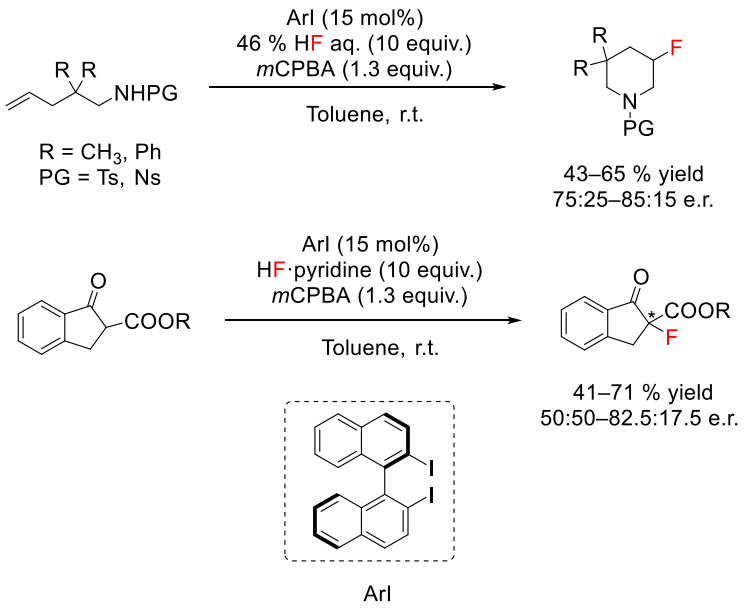
In the same period, the Doyle group reported the nucleophilic fluorination of allyl chlorides, using $Pd_2(dba)_3$ and chiral *bis*-phosphine ligand in combination with AgF, to afford enantiopure allylic fluorides.[106] Tuning of the experimental conditions allowed the authors to access acyclic allylic fluorides in good regioselectivities and moderate enantiomeric ratios. (Scheme 1.33).[107]




Scheme 1.33: Palladium catalysed asymmetric nucleophilic fluorination of allyl chlorides.

An additional example of enantioselective ring-opening was reported by Lautens and collaborators, who disclosed the enantioselective rhodium-catalysed ring-opening of oxabicyclic alkenes with $Et_3N{\cdot}HF$ as the optimal fluoride source.[108]

*1.4.2.2 Organocatalytic Asymmetric Nucleophilic Fluorination.* Before the publication of the work described in this thesis, an early example of organocatalytic asymmetric nucleophilic fluorination appeared in 2014.[109] Shibata and co-workers reported the oxidative nucleophilic fluorination of cyclic α-ketoesters and oxidative nucleophilic fluorocyclisation of γ-aminoalkenes, using chiral iodoarenes, *m*CPBA and aqueous HF (Scheme 1.34).




Scheme 1.34: Enantioselective oxidative nucleophilic fluorination with HF.

The combination of HF, chiral iodoarenes and an oxidant generates *in situ the* electrophilic species $ArIF_2$. Despite this significant conceptual contribution, pioneered by Nevado *et al.*,[110] the enantioselectivity is modest (up to 85:15 e.r.), hazardous HF was used and stoichiometric amount of oxidant were required.

## 1.5 References


(1) Banks, R. E. Isolation of Flourine by Moissan: Setting the Scene. *J. Fluor. Chem.* **1986**, *33* (1–4), 3–26.

(2) Flahaut, J.; Viel, C. The Life and Scientific Work of Henri Moissan. *J. Fluor. Chem.* **1986**, *33* (1–4), 27–43.

(3) Goldwhite, H. The Manhattan Project. *J. Fluor. Chem.* **1986**, *33* (1–4), 109–132.

(4) Harsanyi, A.; Sandford, G. Organofluorine Chemistry: Applications, Sources and Sustainability. *Green Chem.* **2015**, *17* (4), 2081–2086.

(5) Gillis, E. P.; Eastman, K. J.; Hill, M. D.; Donnelly, D. J.; Meanwell, N. A. Applications of Fluorine in Medicinal Chemistry. *J. Med. Chem.* **2015**, *58* (21), 8315–8359.

(6) Fleming, I. *Molecular Orbitals and Organic Chemical Reactions*; John Wiley & Sons, Ltd: Chichester, 2010.

(7) Pauling, L. *The Nature of the Chemical Bond and the Structure of Molecules and Crystals*; Cornell University Press: Ithaca, 1939.

(8) Bondi, A. Van Der Waals Volumes and Radii. *J. Phys. Chem.* **1964**, *68* (3), 441–451.

(9) Kirsch, P. *Modern Fluoroorganic Chemistry*; Wiley-VCH: Weinheim, 2013.

(10) Banks, R. E.; Smart, B. E.; Tatlow, J. C. *Organofluorine Chemistry*; Springer: Boston, 1994.

(11) Uneyama, K. *Organofluorine Chemistry*; Blackwell Publishing: Oxford, 2006.

(12) *CRC Handbook of Chemistry and Physics, 84th Edition*; Lide, D. R., Ed.; CRC Press: Boca Raton, 2003.

(13) Heidelberger, C.; Chaushuri, N. K.; Danneberg, P.; Mooren, D.; Griesbach, L.; Duschinsky, R.; Schnitzer, R. J.; Pleven, E.; Scheiner, J. Fluorinated Pyrimidines, A New Class of Tumour-Inhibitory Compounds. *Nature* **1957**, *179* (4561), 663–666.

(14) New Drug Therapy Approvals 2019, (https://www.fda.gov/drugs)

(15) Müller, K.; Faeh, C.; Diederich, F. Fluorine in Pharmaceuticals: Looking beyond Intuition. *Science* **2007**, *317* (5846), 1881–1886.

(16) Hicken, E. J.; Marmsater, F. P.; Munson, M. C.; Schlachter, S. T.; Robinson, J. E.; Allen, S.; Burgess, L. E.; Delisle, R. K.; Rizzi, J. P.; Topalov, G. T.; et al. Discovery of a Novel Class of Imidazo[1,2-a]Pyridines with Potent PDGFR Activity and Oral Bioavailability. *ACS Med. Chem. Lett.* **2014**, *5* (1), 78–83.

(17) Kokuryo, Y.; Kawata, K.; Nakatani, T.; Kugimiya, A.; Tamura, Y.; Kawada, K.; Matsumoto, M.; Suzuki, R.; Kuwabara, K.; Hori, Y.; et al. Synthesis and Evaluation of Novel Fluorinated Methotrexate Derivatives for Application to Rheumatoid Arthritis Treatment. *J. Med. Chem.* **1997**, *40* (20), 3280–3291.

(18) Hunter, L. The C–F Bond as a Conformational Tool in Organic and Biological Chemistry. *Beilstein J. Org. Chem.* **2010**, *6* (38), 1–14.

(19) Aufiero, M.; Gilmour, R. Informing Molecular Design by Stereoelectronic Theory: The Fluorine Gauche Effect in Catalysis. *Acc. Chem. Res.* **2018**, *51* (7), 1701–1710.

(20) Zimmer, L. E.; Sparr, C.; Gilmour, R. Fluorine Conformational Effects in Organocatalysis: An Emerging Strategy for Molecular Design. *Angew. Chem. Int. Ed.* **2011**, *50* (50), 11860–11871.

(21) Cahard, D.; Bizet, V. The Influence of Fluorine in Asymmetric Catalysis. *Chem. Soc. Rev.* **2014**, *43* (1), 135–147.

(22) Deniau, G.; Slawin, A. M. Z.; Lebl, T.; Chorki, F.; Issberner, J. P.; van Mourik, T.; Heygate, J. M.; Lambert, J. J.; Etherington, L.-A.; Sillar, K. T.; et al. Synthesis, Conformation and Biological Evaluation of the Enantiomers of 3-Fluoro-γ-Aminobutyric Acid ((*R*)- and (*S*)-3F-GABA): An Analogue of the Neurotransmitter GABA. *ChemBioChem* **2007**, *8* (18), 2265–2274.

(23) Clift, M. D.; Ji, H.; Deniau, G. P.; O'Hagan, D.; Silverman, R. B. Enantiomers of 4-Amino-3-Fluorobutanoic Acid as Substrates for γ-Aminobutyric Acid Aminotransferase. Conformational Probes for GABA Binding. *Biochemistry* **2007**, *46* (48), 13819–13828.

(24) Yamamoto, I.; Deniau, G. P.; Gavande, N.; Chebib, M.; Johnston, G. A. R.; O'Hagan, D. Agonist Responses of (*R*)- and (*S*)-3-Fluoro-γ-Aminobutyric Acids Suggest an Enantiomeric Fold for GABA Binding to $GABA_C$ Receptors. *Chem. Commun.* **2011**, *47*, 7956–7958..

(25) DeRider, M. L.; Wilkens, S. J.; Waddell, M. J.; Bretscher, L. E.; Weinhold, F.; Raines, R. T.; Markley, J. L. Collagen Stability: Insights from NMR Spectroscopic and Hybrid Density Functional Computational Investigations of the Effect of Electronegative Substituents on Prolyl Ring Conformations. *J. Am. Chem. Soc.* **2002**, *124* (11), 2497–2505.

(26) Bretscher, L. E.; Jenkins, C. L.; Taylor, K. M.; DeRider, M. L.; Raines, R. T. Conformational Stability of Collagen Relies on a Stereoelectronic Effect. *J. Am. Chem. Soc.* **2001**, *123* (4), 777–778.

(27) Holmgren, S. K.; Taylor, K. M.; Bretscher, L. E.; Raines, R. T. Code for Collagen's Stability Deciphered. *Nature* **1998**, *392* (6677), 666–667.

(28) Jenkins, C. L.; Raines, R. T. Insights on the Conformational Stability of Collagen. *Nat. Prod. Rep.* **2002**, *19* (1), 49–59.

(29) Howard, J. A. K.; Hoy, V. J.; O'Hagan, D.; Smith, G. T. How Good Is Fluorine as a Hydrogen Bond Acceptor? *Tetrahedron* **1996**, *52* (38), 12613–12622.

(30) Dunitz, J. D.; Taylor, R. Organic Fluorine Hardly Ever Accepts Hydrogen Bonds. *Chem. Eur. J.* **1997**, *3* (I), 89–98.

(31) Desiraju, G.; Steiner, T. *The Weak Hydrogen Bond: In Structural Chemistry and Biology*; Oxford University Press: Oxford, 2001.

(32) Emsley, J. Very Strong Hydrogen Bonding. *Chem. Soc. Rev.* **1980**, *9* (1), 91.

(33) Dunitz, J. D. Organic Fluorine: Odd Man Out. *ChemBioChem* **2004**, *5* (5), 614–621.

(34) Takemura, H.; Kaneko, M.; Sako, K.; Iwanaga, T. The Intramolecular C–F···HO Hydrogen Bond of 2-Fluorophenyldiphenylmethanol. *New J. Chem.* **2009**, *33* (10), 2004.

(35) Takemura, H.; Kotoku, M.; Yasutake, M.; Shinmyozu, T. 9-Fluoro-18-Hydroxy-[3.3]Metacyclophane: Synthesis and Estimation of a C–F···H–O Hydrogen Bond. *Eur. J. Org. Chem.* **2004**, *2004* (9), 2019–2024.

(36) Linclau, B.; Peron, F.; Bogdan, E.; Wells, N.; Wang, Z.; Compain, G.; Fontenelle, C. Q.; Galland, N.; Le Questel, J. Y.; Graton, J. Intramolecular OH...Fluorine Hydrogen Bonding in Saturated, Acyclic Fluorohydrins: The γ-Fluoropropanol Motif. *Chem. Eur. J.* **2015**, *21* (49), 17808–17816.

(37) Giuffredi, G. T.; Gouverneur, V.; Bernet, B. Intramolecular $OH^{\cdots}FC$ Hydrogen Bonding in Fluorinated Carbohydrates: CHF Is a Better Hydrogen Bond Acceptor than $CF_2$. *Angew. Chem. Int. Ed.* **2013**, *52* (40), 10524–10528.

(38) Mishra, S.; Suryaprakash, N. Intramolecular Hydrogen Bonding Involving Organic Fluorine: NMR Investigations Corroborated by DFT-Based Theoretical Calculations. *Molecules* **2017**, *22* (3), 423.

(39) Clayton, D. *Handbook of Isotopes in the Cosmos: Hydrogen to Gallium*; Cambridge University Press: Cambridge, 2007.

(40) Renda, A.; Fenner, Y.; Gibson, B. K.; Karakas, A. I.; Lattanzio, J. C.; Campbell, S.; Chieffi, A.; Cunha, K.; Smith, V. V. On the Origin of Fluorine in the Milky Way. *Mon. Not. R. Astron. Soc.* **2004**, *354* (2), 575–580.

(41) Pilachowski, C. A.; Pace, C. The Abundance of Fluorine in Normal G and K Stars of the Galactic Thin Disk. *Astron. J.* **2015**, *150* (3), 66.

(42) Villalba, G.; Ayres, R. U.; Schroder, H. Accounting for Fluorine. *J. Ind. Ecol.* **2007**, *11* (1), 85–101.

(43) U.S. Geological Survey. *Mineral Commodity Summaries: Fluorspar*; 2019.

(44) Özcan, M.; Allahbeickaraghi, A.; Dündar, M. Possible Hazardous Effects of Hydrofluoric Acid and Recommendations for Treatment Approach: A Review. *Clin. Oral Investig.* **2012**, *16* (1), 15–23.

(45) Kearney, L. Old, Corroded Pipe Led to Philadelphia Refinery Fire: Chemical Safety Board. *Reuters.com*. 2019.

(46) Christe, K. O. Chemical Synthesis of Elemental Fluorine. *Inorg. Chem.* **1986**, *25* (21), 3721–3722.

(47) Lee, J.-W.; Oliveira, M. T.; Jang, H. Bin; Lee, S.; Chi, D. Y.; Kim, D. W.; Song, C. E. Hydrogen-Bond Promoted Nucleophilic Fluorination: Concept, Mechanism and Applications in Positron Emission Tomography. *Chem. Soc. Rev.* **2016**, *45* (17), 4638–4650.

(48) Schwesinger, R.; Link, R.; Wenzl, P.; Kossek, S. Anhydrous Phosphazenium Fluorides as Sources for Extremely Reactive Fluoride Ions in Solution. *Chem. Eur. J.* **2005**, *12* (2), 438–445.

(49) Sun, H.; DiMagno, S. G. Anhydrous Tetrabutylammonium Fluoride. *J. Am. Chem. Soc.* **2005**, *127* (7), 2050–2051.

(50) Schimler, S. D.; Ryan, S. J.; Bland, D. C.; Anderson, J. E.; Sanford, M. S. Anhydrous Tetramethylammonium Fluoride for Room-Temperature SNAr Fluorination. *J. Org. Chem.* **2015**, *80* (24), 12137–12145.

(51) Christe, K. O.; Wilson, W. W. Reaction of the Fluoride Anion with Acetonitrile. Chloroform and Methylene Chloride. *J. Fluor. Chem.* **1990**, *47* (1), 117–120.

(52) Chan, K. K. J.; O'Hagan, D. The Rare Fluorinated Natural Products and Biotechnological Prospects for Fluorine Enzymology. In *Methods in Enzymology*; Academic Press Inc., 2012.

(53) Nashiru, O.; Zechel, D. L.; Stoll, D.; Mohammadzadeh, T.; Warren, R. A. J.; Withers, S. G. -Mannosynthase: Synthesis of -Mannosides with a Mutant -Mannosidase. *Angew. Chem. Int. Ed.* **2001**, *40* (2), 417–420.

(54) Zechel, D. L.; Reid, S. P.; Nashiru, O.; Mayer, C.; Stoll, D.; Jakeman, D. L.; Warren, R. A. J.; Withers, S. G. Enzymatic Synthesis of Carbon-Fluorine Bonds. *J. Am. Chem. Soc.* **2001**, *123* (18), 4350–4351.

(55) O'Hagan, D.; Schaffrath, C.; Cobb, S. L.; Hamilton, J. T. G.; Murphy, C. D. Biosynthesis of an Organofluorine Molecule. *Nature* **2002**, *416* (6878), 279–279.

(56) Dong, C.; Huang, F.; Deng, H.; Schaffrath, C.; Spencer, J. B.; O'Hagan, D.; Naismith, J. H. Crystal Structure and Mechanism of a Bacterial Fluorinating Enzyme. *Nature* **2004**, *427* (6974), 561–565.

(57) Cadicamo, C. D.; Courtieu, J.; Deng, H.; Meddour, A.; O'Hagan, D. Enzymatic Fluorination in Streptomyces Cattleya Takes Place with an Inversion of Configuration Consistent with an $S_N2$ Reaction Mechanism. *ChemBioChem* **2004**, *5* (5), 685–690.

(58) Lohman, D. C.; Edwards, D. R.; Wolfenden, R. Catalysis by Desolvation: The Catalytic Prowess of SAM-Dependent Halide-Alkylating Enzymes. *J. Am. Chem. Soc.* **2013**, *135* (39), 14473–14475.

(59) Vincent, M. A.; Hillier, I. H. The Solvated Fluoride Anion Can Be a Good Nucleophile. *Chem. Commun.* **2005**, No. 47, 5902.

(60) Zhu, X.; Robinson, D. A.; McEwan, A. R.; O'Hagan, D.; Naismith, J. H. Mechanism of Enzymatic Fluorination in *Streptomyces Cattleya*. *J. Am. Chem. Soc.* **2007**, *129* (47), 14597–14604.

(61) Senn, H. M.; O'Hagan, D.; Thiel, W. Insight into Enzymatic C−F Bond Formation from QM and QM/MM Calculations. *J. Am. Chem. Soc.* **2005**, *127* (39), 13643–13655.

(62) Baker, J. L.; Sudarsan, N.; Weinberg, Z.; Roth, A.; Stockbridge, R. B.; Breaker, R. R. Widespread Genetic Switches and Toxicity Resistance Proteins for Fluoride. *Science* **2012**, *335* (6065), 233–235.

(63) Stockbridge, R. B.; Kolmakova-Partensky, L.; Shane, T.; Koide, A.; Koide, S.; Miller, C.; Newstead, S. Crystal Structures of a Double-Barrelled Fluoride Ion Channel. *Nature* **2015**, *525* (7570), 548–551.

(64) Stockbridge, R. B.; Robertson, J. L.; Kolmakova-Partensky, L.; Miller, C. A Family of Fluoride-Specific Ion Channels with Dual-Topology Architecture. *Elife* **2013**, *2013* (2), 1–14.

(65) Stockbridge, R. B.; Lim, H. H.; Otten, R.; Williams, C.; Shane, T.; Weinberg, Z.; Miller, C. Fluoride Resistance and Transport by Riboswitch-Controlled CLC Antiporters. *Proc. Natl. Acad. Sci. U.S.A.* **2012**, *109* (38), 15289–15294.

(66) Chan, P. W. Y.; Yakunin, A. F.; Edwards, E. A.; Pai, E. F. Mapping the Reaction Coordinates of Enzymatic Defluorination. *J. Am. Chem. Soc.* **2011**, *133* (19), 7461–7468.

(67) Liang, S.; Hammond, G. B.; Xu, B. Hydrogen Bonding: Regulator for Nucleophilic Fluorination. *Chem. Eur. J.* **2017**, *23* (71), 17850–17861.

(68) Cametti, M.; Rissanen, K. Recognition and Sensing of Fluoride Anion. *Chem. Commun.* **2009**, No. 20, 2809.

(69) Busschaert, N.; Caltagirone, C.; Van Rossom, W.; Gale, P. A. Applications of Supramolecular Anion Recognition. *Chem. Rev.* **2015**, *115* (15), 8038–8155.

(70) Sessler, J. L.; Kim, S. K.; Gross, D. E.; Lee, C.-H.; Kim, J. S.; Lynch, V. M. Crown-6-Calix[4]Arene-Capped Calix[4]Pyrrole: An Ion-Pair Receptor for Solvent-Separated CsF Ions. *J. Am. Chem. Soc.* **2008**, *130*, 13162–13166.

(71) Clarke, H. J.; Howe, E. N. W.; Wu, X.; Sommer, F.; Yano, M.; Light, M. E.; Kubik, S.; Gale, P. A. Transmembrane Fluoride Transport: Direct Measurement and Selectivity Studies. *J. Am. Chem. Soc.* **2016**, *138* (50), 16515–16522.

(72) Kim, D. W.; Jeong; Lim, S. T.; Sohn, M.-H.; Katzenellenbogen, J. A.; Chi, D. Y. Facile Nucleophilic Fluorination Reactions Using Tert -Alcohols as a Reaction Medium: Significantly Enhanced Reactivity of Alkali Metal Fluorides and Improved Selectivity. *J. Org. Chem.* **2008**, *73* (3), 957–962.

(73) Kim, D. W.; Ahn, D. S.; Oh, Y. H.; Lee, S.; Kil, H. S.; Oh, S. J.; Lee, S. J.; Kim, J. S.; Ryu, J. S.; Moon, D. H.; et al. A New Class of $S_N2$ Reactions Catalyzed by Protic Solvents: Facile Fluorination for Isotopic Labeling of Diagnostic Molecules. *J. Am. Chem. Soc.* **2006**, *128* (50), 16394–16397.

(74) Kim, D. W.; Jeong, H.-J.; Lim, S. T.; Sohn, M.-H. Tetrabutylammonium Tetra( Tert -Butyl Alcohol)-Coordinated Fluoride as a Facile Fluoride Source. *Angew. Chem. Int. Ed.* **2008**, *47* (44), 8404–8406.

(75) Hollingworth, C.; Hazari, A.; Hopkinson, M. N.; Tredwell, M.; Benedetto, E.; Huiban, M.; Gee, A. D.; Brown, J. M.; Gouverneur, V. Palladium-Catalyzed Allylic Fluorination. *Angew. Chem. Int. Ed.* **2011**, *50* (11), 2613–2617.

(76) Benedetto, E.; Tredwell, M.; Hollingworth, C.; Khotavivattana, T.; Brown, J. M.; Gouverneur, V. Regio- and Stereoretentive Synthesis of Branched, Linear (E)- and (Z)-Allyl Fluorides from Allyl Carbonates under Ir-Catalysis. *Chem. Sci.* **2013**, *4* (1), 89–96.

(77) Engle, K. M.; Pfeifer, L.; Pidgeon, G. W.; Giuffredi, G. T.; Thompson, A. L.; Paton, R. S.; Brown, J. M.; Gouverneur, V. Coordination Diversity in Hydrogen-Bonded Homoleptic Fluoride–Alcohol Complexes Modulates Reactivity. *Chem. Sci.* **2015**, *6* (9), 5293–5302.

(78) Pfeifer, L.; Engle, K. M.; Pidgeon, G. W.; Sparkes, H. A.; Thompson, A. L.; Brown, J. M.; Gouverneur, V. Hydrogen-Bonded Homoleptic Fluoride-Diarylurea Complexes: Structure, Reactivity, and Coordinating Power. *J. Am. Chem. Soc.* **2016**, *138* (40), 13314–1325.

(79) Yan, H.; Jang, H. Bin; Lee, J.-W.; Kim, H. K.; Lee, S. W.; Yang, J. W.; Song, C. E. A Chiral-Anion Generator: Application to Catalytic Desilylative Kinetic Resolution of Silyl-Protected Secondary Alcohols. *Angew. Chem. Int. Ed.* **2010**, *49* (47), 8915–8917.

(80) Birrell, J. A.; Desrosiers, J.-N.; Jacobsen, E. N. Enantioselective Acylation of Silyl Ketene Acetals through Fluoride Anion-Binding Catalysis. *J. Am. Chem. Soc.* **2011**, *133* (35), 13872–13875.

(81) Ibrahim, H.; Togni, A. Enantioselective Halogenation Reactions. *Chem. Commun.* **2004**, *4* (10), 1147.

(82) Yang, X.; Wu, T.; Phipps, R. J.; Toste, F. D. Advances in Catalytic Enantioselective Fluorination , Mono - , Di - , and Trifluoromethylation , and Trifluoromethylthiolation Reactions. *Chem. Rev.* **2015**, *115*, 826–870.

(83) Taylor, S. D.; Kotoris, C. C.; Hum, G. Recent Advances in Electrophilic Fluorination. *Tetrahedron* **1999**, *55* (43), 12431–12477.

(84) Ma, J. A.; Cahard, D. Asymmetric Fluorination, Trifluoromethylation, and Perfluoroalkylation Reactions. *Chem. Rev.* **2004**, *104* (12), 6119–6146.

(85) Champagne, P. A.; Desroches, J.; Hamel, J. D.; Vandamme, M.; Paquin, J. F. Monofluorination of Organic Compounds: 10 Years of Innovation. *Chem. Rev.* **2015**, *115* (17), 9073–9174.

(86) Hintermann, L.; Togni, A. Catalytic Enantioselective Fluorination of β-Ketoesters. *Angew. Chem. Int. Ed.* **2000**, *39* (23), 4359–4362.

(87) Hintermann, L.; Perseghini, M.; Togni, A. Development of the Titanium–TADDOLate-Catalyzed Asymmetric Fluorination of β-Ketoesters. *Beilstein J. Org. Chem.* **2011**, *7*, 1421–1435.

(88) Hamashima, Y.; Yagi, K.; Takano, H.; Tamás, L.; Sodeoka, M. An Efficient Enantioselective Fluorination of

Various β-Ketoesters Catalyzed by Chiral Palladium Complexes. *J. Am. Chem. Soc.* **2002**, *124* (49), 14530–14531.

(89) Shibata, N.; Ishimaru, T.; Nagai, T.; Kohno, J.; Toru, T. First Enantio-Flexible Fluorination Reaction Using Metal-Bis(Oxazoline) Complexes. *Synlett* **2004**, *10*, 1703–1706.

(90) Ma, J. A.; Cahard, D. Copper(II) Triflate-Bis(Oxazoline)-Catalysed Enantioselective Electrophilic Fluorination of β-Ketoesters. *Tetrahedron Asymmetry* **2004**, *15* (6), 1007–1011.

(91) Talbot, E. P. A.; Fernandes, T. D. A.; McKenna, J. M.; Toste, F. D. Asymmetric Palladium-Catalyzed Directed Intermolecular Fluoroarylation of Styrenes. *J. Am. Chem. Soc.* **2014**, *136* (11), 4101–4104.

(92) Enders, D.; Hüttl, M. Direct Organocatalytic α-Fluorination of Aldehydes and Ketones. *Synlett* **2005**, *2005* (06), 0991–0993.

(93) Marigo, M.; Fielenbach, D.; Braunton, A.; Kjærsgaard, A.; Jørgensen, K. A. Enantioselective Formation of Stereogenic Carbon - Fluorine Centers by a Simple Catalytic Method. *Angew. Chem. Int. Ed.* **2005**, *44* (24), 3703–3706.

(94) Steiner, D. D.; Mase, N.; Barbas, C. F. Direct Asymmetric α-Fluorination of Aldehydes. *Angew. Chem. Int. Ed.* **2005**, *44* (24), 3706–3710.

(95) Beeson, T. D.; MacMillan, D. W. C. Enantioselective Organocatalytic α-Fluorination of Aldehydes. *J. Am. Chem. Soc.* **2005**, *127* (24), 8826–8828.

(96) Ishimaru, T.; Shibata, N.; Horikawa, T.; Yasuda, N.; Nakamura, S.; Toru, T.; Shiro, M. Cinchona Alkaloid Catalyzed Enantioselective Fluorination of Allyl Silanes, Silyl Enol Ethers, and Oxindoles. *Angew. Chem. Int. Ed.* **2008**, *47* (22), 4157–4161.

(97) Lozano, O.; Blessley, G.; Martinez del Campo, T.; Thompson, A. L.; Giuffredi, G. T.; Bettati, M.; Walker, M.; Borman, R.; Gouverneur, V. Organocatalyzed Enantioselective Fluorocyclizations. *Angew. Chem. Int. Ed.* **2011**, *50* (35), 8105–8109.

(98) Kim, D. Y.; Park, E. J. Catalytic Enantioselective Fluorination of β-Keto Esters by Phase-Transfer Catalysis Using Chiral Quaternary Ammonium Salts. *Org. Lett.* **2002**, *4* (4), 545–547.

(99) Wang, X.; Lan, Q.; Shirakawa, S.; Maruoka, K. Chiral Bifunctional Phase Transfer Catalysts for Asymmetric Fluorination of β-Keto Esters. *Chem. Commun.* **2010**, *46* (2), 321–323.

(100) Rauniyar, V.; Lackner, A. D.; Hamilton, G. L.; Toste, F. D. Asymmetric Electrophilic Fluorination Using an Anionic Chiral Phase-Transfer Catalyst. *Science* **2011**, *334* (6063), 1681–1684.

(101) Honjo, T.; Phipps, R. J.; Rauniyar, V.; Toste, F. D. A Doubly Axially Chiral Phosphoric Acid Catalyst for the Asymmetric Tandem Oxyfluorination of Enamides. *Angew. Chem. Int. Ed.* **2012**, *51* (38), 9684–9688.

(102) Phipps, R. J.; Hiramatsu, K.; Toste, F. D. Asymmetric Fluorination of Enamides: Access to α-Fluoroimines Using an Anionic Chiral Phase-Transfer Catalyst. *J. Am. Chem. Soc.* **2012**, *134* (20), 8376–8379.

(103) Bruns, S.; Haufe, G. Enantioselective Introduction of Fluoride into Organic Compounds: First Asymmetric Ring Opening of Epoxides by Hydrofluorinating Reagents. *J. Fluor. Chem.* **2000**, *104* (2), 247–254.

(104) Kalow, J. A.; Doyle, A. G. Enantioselective Ring Opening of Epoxides by Fluoride Anion Promoted by a Cooperative Dual-Catalyst System. *J. Am. Chem. Soc.* **2010**, *132* (10), 3268–3269.

(105) Kalow, J. A.; Doyle, A. G. Mechanistic Investigations of Cooperative Catalysis in the Enantioselective Fluorination of Epoxides. *J. Am. Chem. Soc.* **2011**, *133* (40), 16001–16012.

(106) Katcher, M. H.; Doyle, A. G. Palladium-Catalyzed Asymmetric Synthesis of Allylic Fluorides. *J. Am. Chem. Soc.* **2010**, *132* (49), 17402–17404.

(107) Katcher, M. H.; Sha, A.; Doyle, A. G. Palladium-Catalyzed Regio- and Enantioselective Fluorination of Acyclic Allylic Halides. *J. Am. Chem. Soc.* **2011**, *133* (40), 15902–15905.

(108) Zhu, J.; Tsui, G. C.; Lautens, M. Rhodium-Catalyzed Enantioselective Nucleophilic Fluorination: Ring Opening of Oxabicyclic Alkenes. *Angew. Chem. Int. Ed.* **2012**, *51* (49), 12353–12356.

(109) Suzuki, S.; Kamo, T.; Fukushi, K.; Hiramatsu, T.; Tokunaga, E.; Dohi, T.; Kita, Y.; Shibata, N. Iodoarene-Catalyzed Fluorination and Aminofluorination by an Ar-I/HF·pyridine/mCPBA System. *Chem. Sci.* **2014**, *5*

(7), 2754–2760.

(110) Kong, W.; Feige, P.; De Haro, T.; Nevado, C. Regio- and Enantioselective Aminofluorination of Alkenes. *Angew. Chem. Int. Ed.* **2013**, *52* (9), 2469–2473.

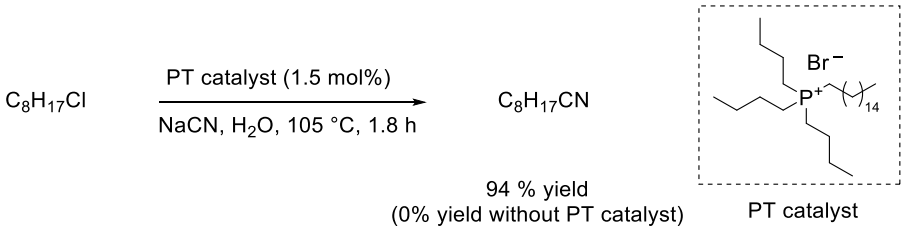
# 2. Hydrogen Bonding Mediated Asymmetric Nucleophilic Fluorination

The work described in this chapter was carried out in collaboration with Dr. Gabriele Pupo and Dr. David Ascough. Dr. Gabriele Pupo performed the synthesis of molecules **2b–2c**, **4b**–**4e**, **4g**–**4j**, **4m**–**4n** described herein. Dr. David Ascough carried out all the computational work. The contribution of each author is clearly stated in the original manuscript *Asymmetric nucleophilic fluorination under hydrogen bonding phase- transfer catalysis*, G. Pupo*, F. Ibba*, D. M. H. Ascough*, A. C. Vicini, P. Ricci, K. E. Christensen, L. Pfeifer, J. R. Morphy, J. M. Brown, R. S. Paton, V. Gouverneur, *Science* **2018**, *360*, 638–642.[1] The work was adapted with permission from AAAS©.

## 2.1 Introduction

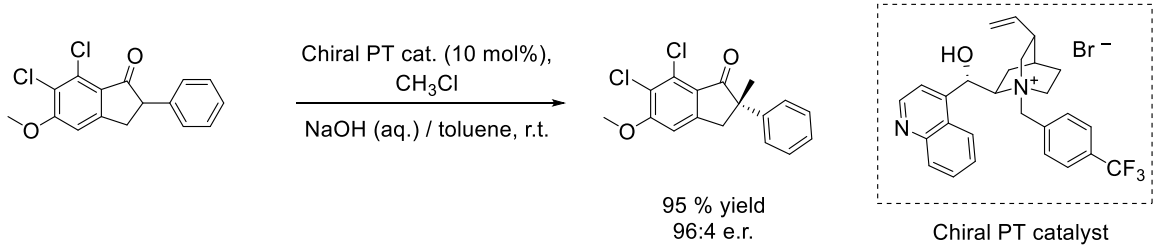
### *2.1.1 Phase Transfer Catalysis*

Phase-transfer catalysis (PTC) is a powerful strategy in organic chemistry as it enables transformations with reagents present in different phases by addition of a catalytic amount of a phase transfer (PT) agent. The phase-transfer catalyst is required to transport a species across the interface, into a phase in which it would not be otherwise soluble, so that the reaction can occur. The concept was established in 1971 by Charles Starks showing that the reaction of neat 1-chlorooctane with aqueous sodium cyanide took place only in the presence of quaternary ammonium or phosphonium salts, capable of shuttling cyanide anions from the aqueous to the organic phase (Scheme 2.1).[2,3] In the following decades, PTC has attracted increasing interest as it combines mild reaction conditions, simple experimental protocols, inexpensive reagents, and it is amenable to large-scale preparations.[4]




Scheme 2.1: Stark's cyanation of alkyl chlorides under phase-transfer catalysis.

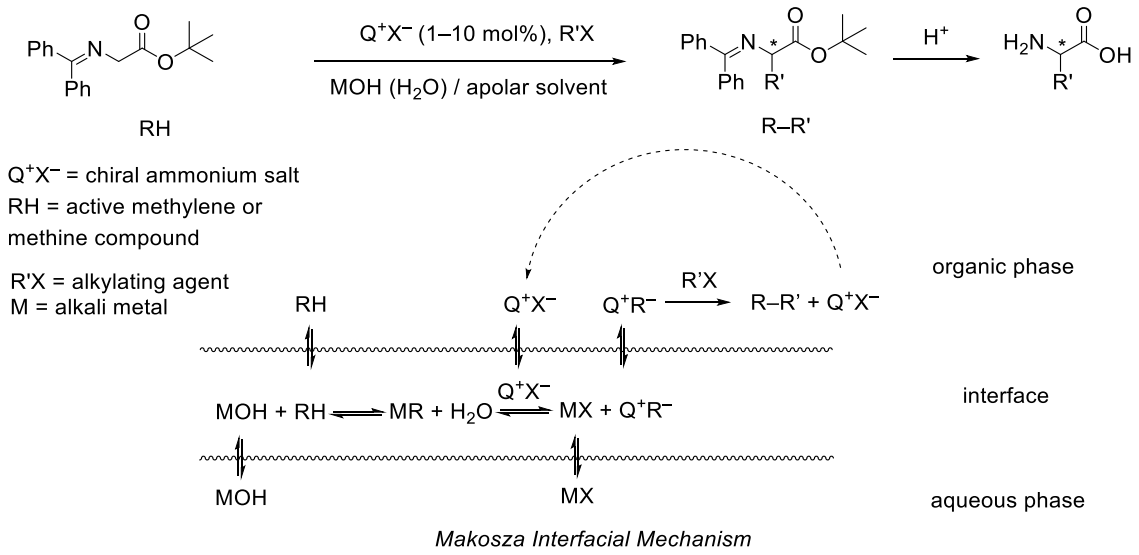
The principle of phase-transfer catalysis has been applied to asymmetric synthesis, with pioneering studies introducing alkaloids salts as enantioselective catalysts.[5-8] In 1984, Merck (MSD) scientists reported a highly enantioselective synthesis of Indacrinone using a novel *N*-benzylcinchoninium salt derivative as efficient PT catalyst (Scheme 2.2).[9] Since then, asymmetric phase-transfer catalysis has been largely dominated by the use of chiral nonracemic quaternary ammonium salts.[10-11]




Scheme 2.2: Asymmetric phase-transfer catalysis.

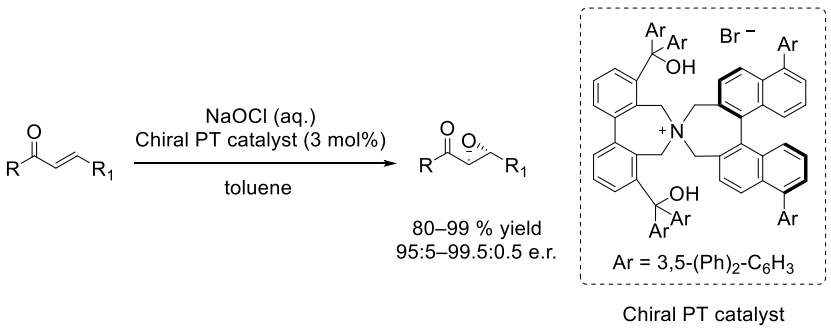
One of the most popular applications of asymmetric PTC is the synthesis of unnatural amino acids by alkylation of $\alpha$-imino esters, followed by hydrolysis of the resulting enantioenriched product (Scheme 2.3). Archetypical reactions under asymmetric phase-transfer catalysis, employing highly lipophilic catalysts, are likely to follow the interfacial mechanism postulated by Makozsa (Scheme 2.3).[12] Formation of an organic carbanion (MR) from an inorganic base (MOH) and an active methylene (or methine) compound (RH) occurs at the interface between aqueous and organic phase. The intervention of a chiral ammonium salt (QX) extracts the carbanion species from the interfacial area into the organic phase to allow the reaction with

an electrophile, typically an alkylating agent (RX). After the reaction takes place, the regenerated chiral ammonium catalyst (QX) can enter another catalytic cycle.



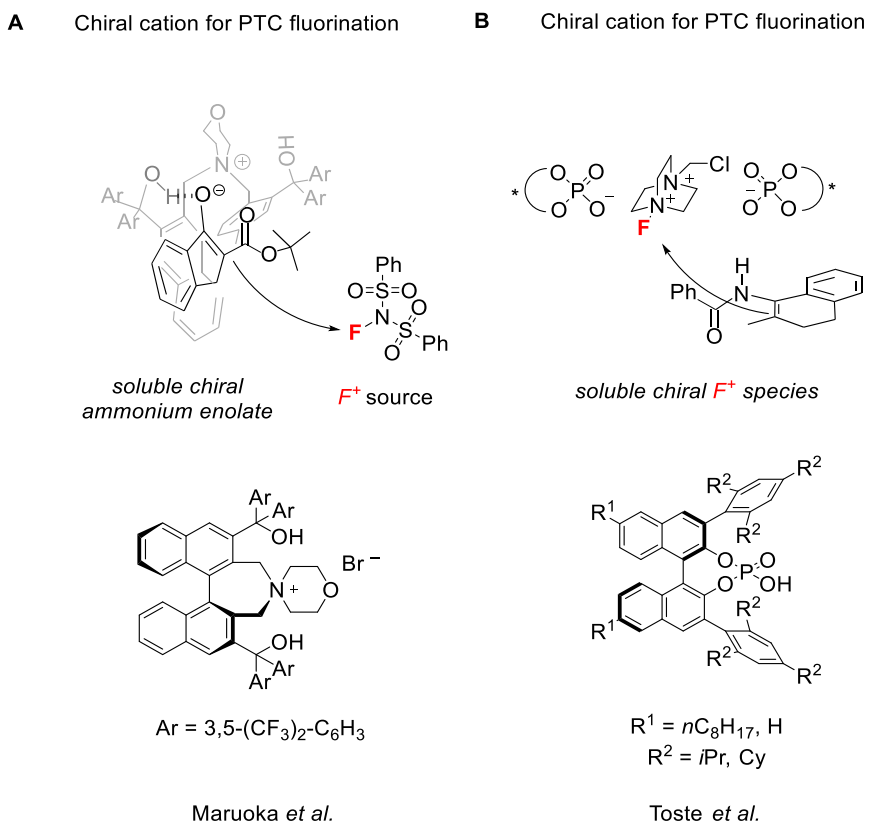

Scheme 2.3: Asymmetric synthesis of unnatural amino acids *via* PTC and proposed interfacial mechanism.

In another prominent category of asymmetric reactions under phase-transfer catalysis, the catalyst interacts directly with the reactant, often a nucleophile supplied as an aqueous solution or as inorganic salt. The reactant is transferred across the phases by the PT catalyst, also in this case an interfacial mechanism has been postulated. One of the most notable application of this methodology has been reported for the asymmetric epoxidation of enones using a chiral ammonium salt and an aqueous solution of sodium hypochlorite as the oxidant (Scheme 2.4).[13]




Scheme 2.4: Asymmetric epoxidation *via* PTC

Asymmetric PTC has been applied to fluorination using $F^+$ reagents; as previously discussed (*v. 1.4.1.2 Organocatalytic Asymmetric Electrophilic Fluorination*) two distinct approaches have been developed. The use of chiral ammonium salts is a valuable method to form highly enantioenriched fluorinated β-keto esters. With this approach, the source of chirality is embedded with the prochiral nucleophilic substrate, which benefits from non-covalent stabilization as well as ion-pairing with the catalyst (Scheme 2.5 A). In a charge inverted process, the use of chiral phosphates enables asymmetric fluorinations via solid-liquid phase-transfer of the insoluble salt Selectfluor®. In this case, the PT catalyst interacts primarily with the fluorinating reagent, generating *in situ* a soluble chiral $F^+$ species. The slow release of $F^+$ reagent in the organic phase is crucial for achieving high level of enantioselectivity (Scheme 2.5 B).



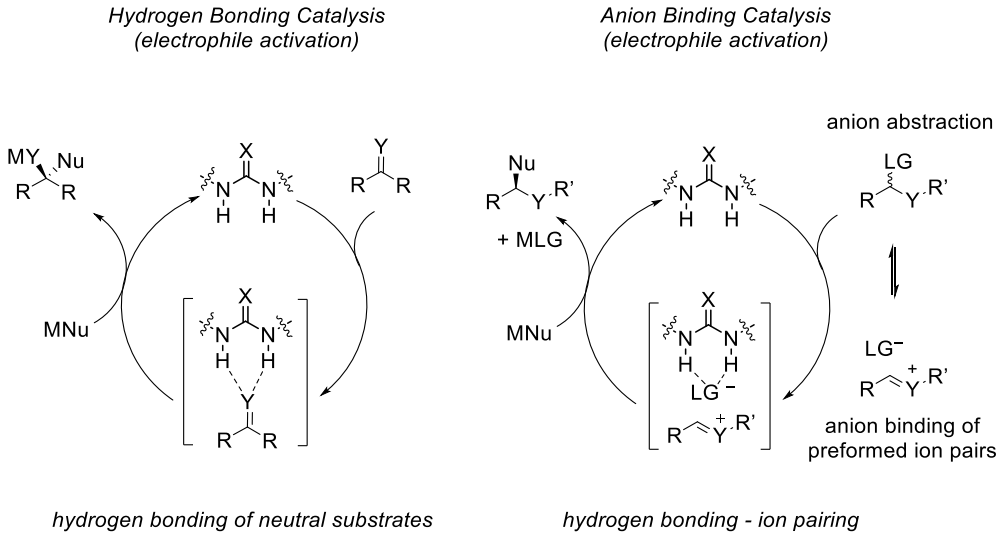

Scheme 2.5: Electrophilic fluorination *via* asymmetric PTC.

Phase-transfer agents enabling nucleophilic, rather than electrophilic fluorination, have been extensively investigated, with the most common approach to enhance metal fluorides' reactivity in organic solvents by complexation of the metal cation by crown ethers or by lipophilic quaternary ammonium salts.[14] The use of chiral quaternary ammonium fluorides, either generated *in situ* via PTC or as preformed chiral catalyst, is a viable strategy in asymmetric catalysis for the formation of C–C bonds;[15] this includes taking advantage of the formation of strong F–Si bonds to activate nucleophilic functionality, one example being the enantioselective organocatalytic Mukayama-type aldol addition.[16] Enantioselective reactions using fluoride as a *chiral base* have also been reported.[17] However, solubilisation of fluoride salts using chiral phase-transfer catalysts never resulted in fruitful enantioselective protocol for C–F bond formation. This is likely due to the difficulties in controlling the reactivity of a *naked* fluoride species generated *via* these methods

### *2.1.2 Hydrogen Bonding for Anion Binding Catalysis*

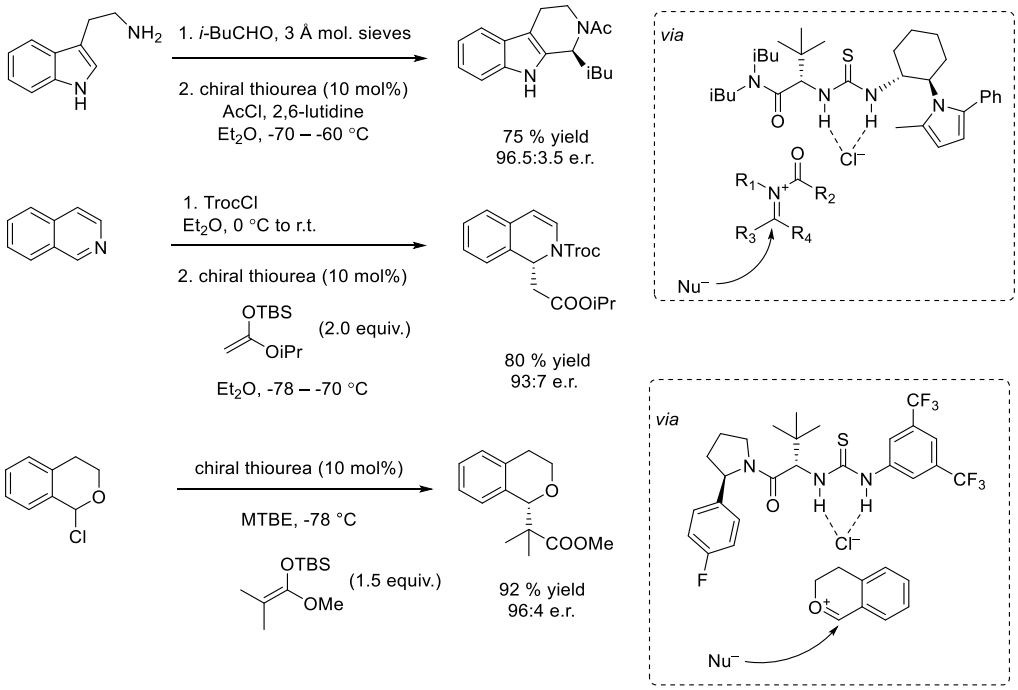
In the past decade, dual hydrogen bond donors (HBD) have emerged as privileged functionalities in asymmetric organocatalysis, furnishing a mild, stable and user-friendly alternative to Lewis-acids for electrophile activation.[18-19] The first examples of the use of chiral HBD embraced hydrogen bonding for the direct activation of neutral functionalities possessing a Lewis basic handle such as carbonyls, imines and nitro olefins, enabling highly enantioselective additions of nucleophiles.[20] More recently, the chemistry of HBDs have expanded to take advantage of the well-known anion binding propensity of ureas, thioureas and squaramides. In anion-binding catalysis, the enantiopure HBD catalyst binds the anionic component of an ion pair, generating a highly reactive cationic species in a chiral environment; this scenario enables control over enantioselectivity of the subsequent addition of an external nucleophile *via* electrostatic and non-covalent interactions. The ionic pair can be pre-formed

(anion binding catalysis), generated by intervention of the HBD catalyst (anion abstraction catalysis)[21] or can be derived by addition of a Brønsted or Lewis acid co-catalyst (Scheme 2.6).[22, 23] The generation of a prochiral ionic electrophile, in a chiral environment dictated by the HBD is the common feature for all these enantioselective catalytic transformations.




Scheme 2.6: Hydrogen bonding and anion binding catalysis for electrophile activation.

This approach enabled a range of enantioselective reactions involving heteroatom-stabilised cation including: acyl-Pictet-Spengler,[24] acyl-Mannich [25] and addition to oxocarbenium ions (Scheme 2.7).[26] Chiral thioureas show high enantioinduction by forming hydrogen bonding with the chloride counter-cation of the electrophilic acyl-iminium or oxacarbenium ion. The choice of the solvent is crucial to ensure good enantioselectivity, with apolar solvents such as ethers preferred for their ability to generate tight ion pairs. Reactions are generally carried out at low temperature (-60 – -78 °C) to limit decomposition of the highly reactive intermediate and to tame non-selective background reactivity.




Scheme 2.7: Chiral thiourea catalyzed addition to cationic electrophiles *via* anion binding catalysis.

A unique example of hydrogen bonding anion-binding catalysis involving fluoride is the enantioselective acylation of silyl ketene acetals reported by Jacobsen and co-workers (*v. 1.3.4.3 Hydrogen Bonded Fluoride Complexes in Asymmetric Fluorination*). However, no examples of asymmetric C–F bond formation mediated by a HB–fluoride have been reported in the literature.

### *2.1.3 Hydrogen Bonding Phase-Transfer Catalysis*

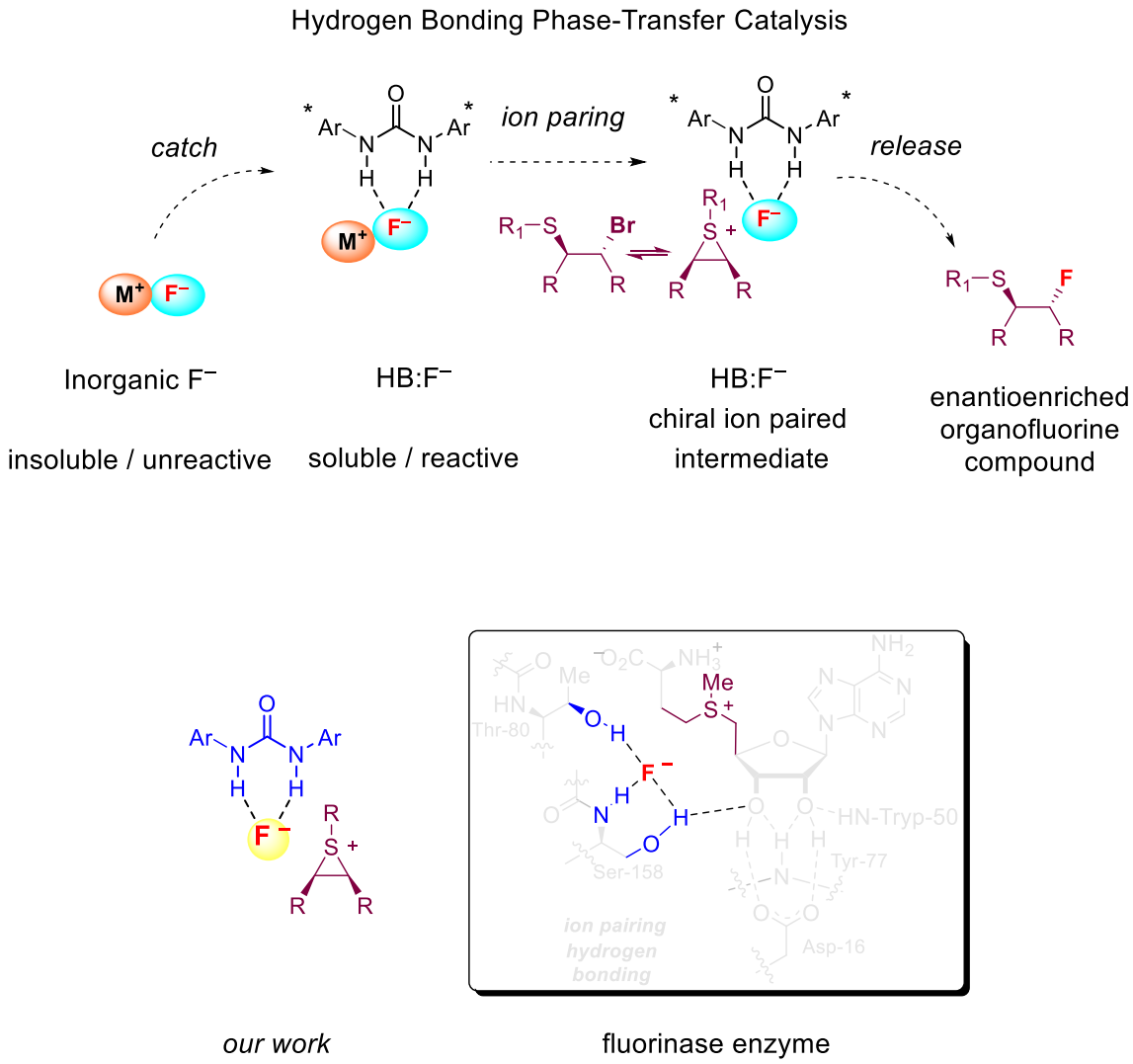
Our aim was to develop new catalytic methods for asymmetric fluorination employing alkali metal fluorides, in order to do so several fundamental challenges had to be addressed: *i)* fluoride reactivity is difficult to tame, resulting in a highly nucleophilic and basic anion when present in organic solvents, while being unreactive in aqueous or protic media; *ii)* alkali metal fluorides are poorly soluble in organic solvents which limits their applicability. Conventional phase-transfer approaches fails to provide selective fluorination due to the generation of *naked* fluoride, incompatible with enantioselective synthesis; *iii)* The design of a novel chiral

organocatalyst is required to control the stereoselective outcome of nucleophilic fluorination reactions.

We reasoned that hydrogen bonding would be suitable to modulate fluoride reactivity and selectivity. Specifically, we envisioned a two-step *catch and release* mechanism in which $F^-$ is bound to a suitable HBD, imparting the desired reactivity and (enantio)selectivity, and subsequently delivered to the reaction partner with concomitant release of the HBD. Fluoride hydrogen bonding is well-documented in supramolecular anion recognition (*catch*) but the reactivity of HB-fluoride species (*release*) has been investigated only recently and has never been employed to control enantioselectivity. Additionally, hydrogen bonded fluoride species are intrinsically less reactive than unbound fluoride, so the enantioselectivity of the process may be undermined by dominant non-selective background fluorinations. In order to overcome these conceptual limitations, we thought to combine the concept of hydrogen bonding with phase-transfer catalysis as a new catalytic approach to nucleophilic fluorination. In our working hypothesis, a chiral neutral hydrogen bond donor could serve as a solid-liquid phase-transfer catalyst to transport an insoluble alkali metal fluoride into organic solvents. The H-bonded fluoride complex would become soluble and capable of mediating fluorination of suitable organic electrophiles. With this manifold, coined Hydrogen Bonding Phase-Transfer Catalysis (HB PTC), the insolubility of metal alkali fluorides and their tendency to engage in hydrogen bonding, normally perceived as limiting factors, would be beneficial enabling precise release of ‘‘*chiral fluoride’’*.

Building on our previous reports on the effect of HB on fluoride reactivity, we speculated that aromatic ureas were the appropriate candidates to form reactive fluoride complexes in apolar solvents. The choice of the reaction partner was also of fundamental importance; we drew inspiration from the natural occurring fluorinase enzyme, that forms C($sp^3$)–F bonds *via*

nucleophilic attack to a positively charged sulfonium leaving group. The electrostatic ion pairing between $R_3S^+$ and $F^-$ significantly contributes to fluoride stabilisation, and helps directing the nucleophilic fluorination. We therefore selected β-bromo sulfides as substrates for fluorination, as they readily form highly reactive episulfonium ions *in situ*.[27] Additionally, *meso*-episulfonium ions are prochiral electrophiles which may undergo desymmetrization to give enantioenriched β-substituted sulfides.[28-29] We envisaged that ion pairing between the episulfonium ion and the chiral HB:$F^-$ complex would favour enantioselective formation of C–F bonds.

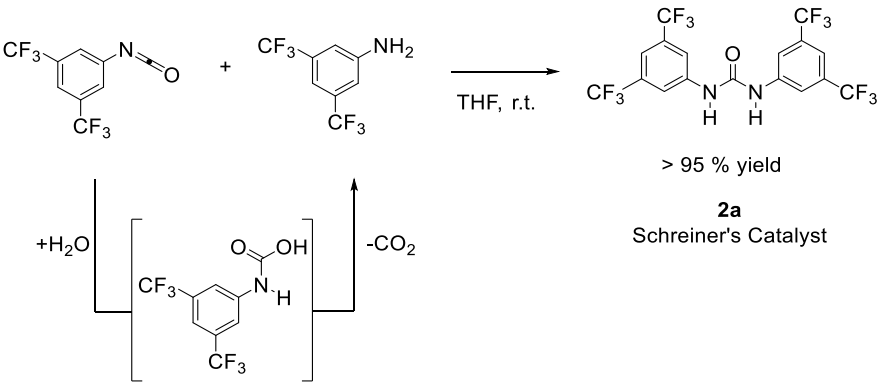



Scheme 2.8: Hydrogen Bonding Phase-Transfer Catalysis (HB PTC).

## 2.2 Results and Discussion

### *2.2.1 Reaction development: non-enantioselective catalytic system*

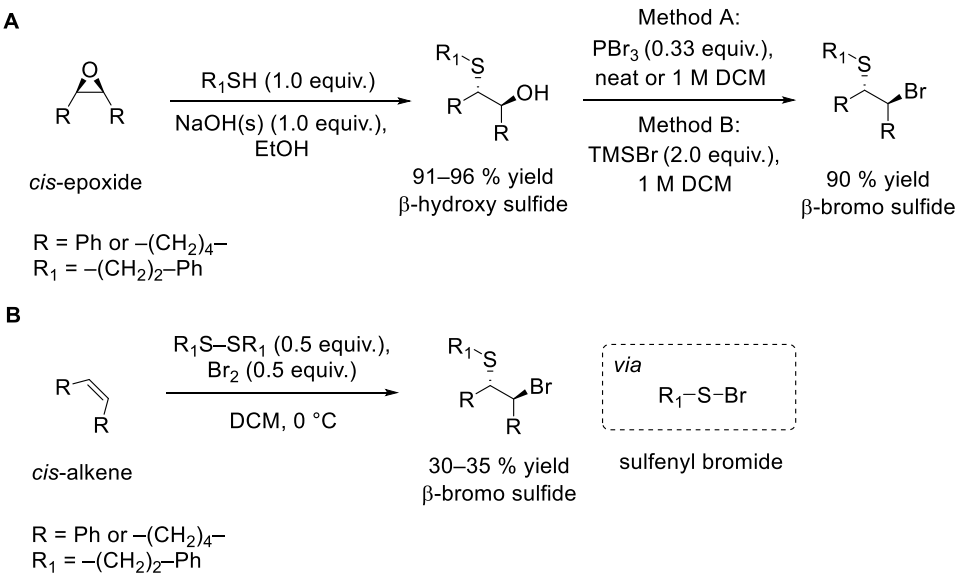
Initially, we sought to demonstrate the feasibility of our concept by establishing a non-enantioselective catalytic system using achiral hydrogen bond donors. For preliminary screening, we selected 1,3-bis(3,5-bis(trifluoromethyl)phenyl)urea (**2a**), known as Schreiner's catalyst, who pioneered the use of HBD catalysts in organic synthesis.[30-32] Urea **2a** can be easily prepared in quantitative yields by addition of 3,5-bis(trifluoromethyl) isocyanate to 3,5-bis(trifluoromethyl)aniline. The Schreiner's catalyst is spontaneously formed when 3,5-bis(trifluoromethyl) isocyanate is not stored under strictly inert atmosphere. In this case, adventitious presence of water triggers hydrolysis of the highly reactive isocyanate, followed by decarboxylation of the carbamic acid intermediate, to yield an equivalent amount of 3,5-bis(trifluoromethyl)aniline that reacts with a second molecule of 3,5-bis(trifluoromethyl) isocyanate to give **2a** (Scheme 2.9).




Scheme 2.9: Synthesis of Schreiner's catalyst **2a**

Schreiner's catalyst is insoluble in apolar hydrocarbons, due to its propensity to self-aggregate in solution, and only moderately soluble in chlorinated solvents. On the contrary, Lewis-basic solvents such as THF, $Et_2O$ or EtOAc solubilise **2a** by disrupting the formation of multimeric structures by hydrogen bonding with the urea.

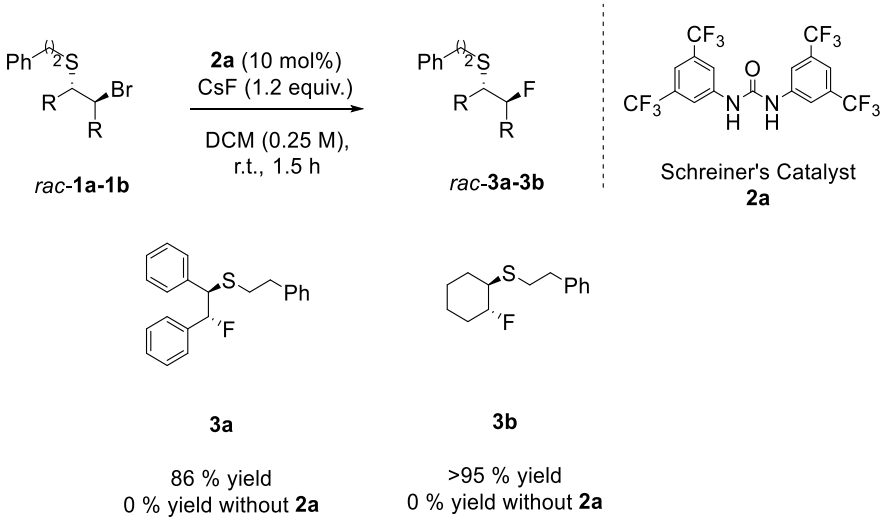
Racemic β-bromo sulfides, selected as starting materials, were conveniently prepared from the corresponding *cis*-epoxides *via* thiolate ring opening followed by bromination using either phosphorus tribromide ($PBr_3$) or trimethylsilyl bromide (TMSBr) as brominating reagents (Scheme 2.10 A). The opening of an epoxide occurs with inversion of configuration while bromination of the β-hydroxy sulfide results in retention of configuration; thereby the process affords exclusively β-bromo sulfides with the substituents in a syn orientation. An alternative synthetic route involved the one-step addition of sulfenyl halides (R–S–X, X = Cl or Br) to the corresponding *cis*-alkene (Scheme 2.10 B). The sulfenyl halides were generated *in situ* by treating a disulfide with $Br_2$, a process known as Zincke disulfide cleavage.[33] The reaction is believed to pass through an episulfonium intermediate in polar solvents while a σ-sulfurane intermediate has been postulated for apolar solvents. Both mechanisms are stereospecific, thus leading to *syn* β-bromo sulfides from *cis*-alkenes.[34-35]




Scheme 2.10: Synthesis of β-bromo sulfides by epoxide opening-bromination sequence (A) or by addition of sulfenyl bromides to *cis*-alkenes (B).

With an achiral HBD and our substrates in hand, we proceeded to investigate the HB PTC fluorination of β-bromo sulfides. No product was observed when **1a** or **1b** were treated with

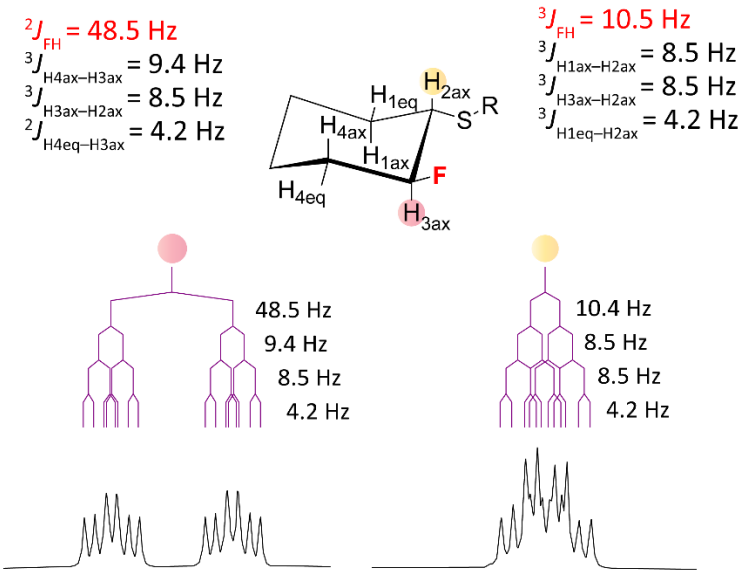
1.2 equivalents of CsF in dichloromethane for 24 hours at room temperature, conversely, fluorination took place in the presence of 10 mol% of Schreiner's catalyst **2a**, affording the desired products after 1.5 hour (Scheme 2.11). Over the course of the reaction, the precipitation of a white solid was ascribed to the formation of CsBr as a side product. Stilbene-derived fluorinated sulfide **3a** and cyclohexyl-derived **3b** were obtained in excellent yields; **3b** was purified by removing the catalyst and CsBr by filtration, while **3a** required chromatographic purification.




Scheme 2.11: Fluorination of **1a** and **1b** with CsF and achiral HBD **2a**.

The products were characterised by $^{1}H$ and $^{19}F$ NMR spectroscopy. Distinctive patterns for β-fluoro sulfides **3a** and **3b** are the $^{19}F$ NMR signals at -172 and -169 ppm respectively, and the characteristic $^{1}H$ NMR resonances at 5.7 and 4.4 ppm, showing large geminal coupling to fluorine, $^{2}J_{FH}$ = 46 Hz (**3a**) and $^{2}J_{FH}$ = 48 Hz (**3b**). The analysis of the vicinal coupling constants ($^{3}J$) can provide detailed information about the geometrical disposition of the two atoms involved in the scalar-coupling. Both HH and HF $^{3}J$ have been extensively used to establish the stereochemical relationship among substituents; this method is particularly well-suited for six-membered rings which offer a favourable system to study. According to the Karplus

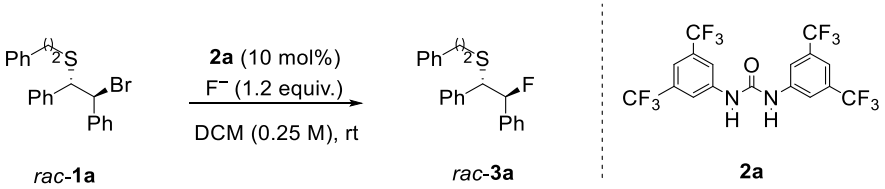
relationship, axial-axial $^3J$ are much larger in magnitude ($^3J_{H(ax)H(ax)}$ ~ 10 Hz, $^3J_{F(ax)H(ax)}$ ~ 50 Hz) than both equatorial-equatorial and equatorial-axial $^3J$ ($^3J_{H(eq/ax)H(eq)}$ ~ 4 Hz, $^3J_{F(eq/ax)H(eq)}$ ~ 20 Hz). In the six-membered product **3b** analysis of $^3J_{HH}$ reveals that proton H(3) (geminal to fluorine) shows two large couplings of 9.5 and 8.5 Hz, and one small coupling of 4 Hz. Similarly, proton H(2) (geminal to sulfur) shows three $^3J_{HH}$ with magnitude of 8.5, 8.5 and 4 Hz. This is consistent with each protons having two $^3J_{H(ax)H(ax)}$ and one $^3J_{H(ax)H(eq)}$, thus indicating a *trans* configuration of sulfur and fluorine, both situated in equatorial positions (Scheme 2.12). For the stilbene-derived product **3a** the conformational analysis is considerably more complicated, however the large $^3J_{HH}$ of 7.5 Hz and the small $^3J_{FH}$ of 13.6 Hz suggest a conformation analogous to **3b.** Net retention of configuration was also inferred by comparison of the $^1$H NMR data with literature precedents of structurally related compounds.[28]




Scheme 2.12: Analysis of the $^3J$ coupling constants of **3b.**

*2.2.1.1 Fluoride Source.* The effect of different $F^-$ sources was evaluated. Substrate **1a** underwent fluorination using KF and catalyst **2a**, albeit with a substantial decrease in yield compared to CsF (Entry 1–3, Table 2.1). NaF and LiF, having significantly higher lattice energies (KF = 198, NaF, 222, LiF, 254 kcal/mol *cf*. CsF = 181 kcal/mol), were not competent fluoride sources for this reaction (Entry 4–5, Table 2.1). Substrate **1b** showed no reactivity with KF, NaF or LiF (Entry 2–4, Table 2.2). As expected, the use of $CaF_2$ did not lead to fluorinated product using either substrates **1a** or **1b** (Entry 6, Table 2.1; Entry 5, Table 2.2). Employing a soluble source of fluoride, such as tetrabutylammonium fluoride (TBAF·$3H_2O$), resulted in low yields together with copious amount of alcohol side-product, derived from water acting as a nucleophile in place of fluoride (Entry 7, Table 2.1; Entry 6, Table 2.2). In this case, the addition of catalyst **2a** was not beneficial, resulting in a slightly reduced yield. This observation indicates that complexation with HBD, under homogeneous conditions, slows down the fluorination process (Entry 8, Table 2.1).

Table 2.1: Screening of fluoride sources with **1a**.

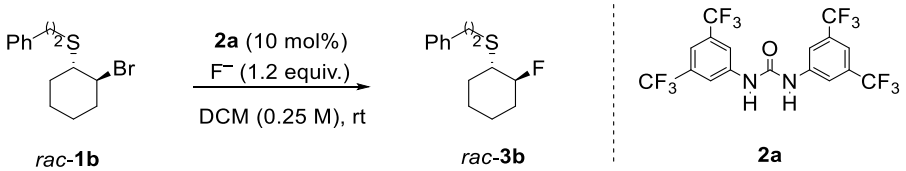



*rac*-**1a** *rac*-**3a** **2a**

| Entry | $F^-$ source | Catalyst | Cat. loading (mol%) | Time (h) | Yield (%)[a] |
|---|---|---|---|---|---|
| 1 | CsF | **2a** | 10 | 1.5 | 86 |
| 2 | KF | **2a** | 10 | 24 | 55 |
| 3 | KF | **2a** | 10 | 1.5 | 21 |
| 4 | NaF | **2a** | 10 | 1.5 | no reaction |
| 5 | LiF | **2a** | 10 | 1.5 | no reaction |
| 6 | $CaF_2$ | **2a** | 10 | 1.5 | no reaction |
| 7[b] | TBAF | – | – | 1.5 | 37 |
| 8[b] | TBAF | **2a** | 10 | 1.5 | 24 |

General conditions: 0.05 mmol substrate, 0.06 fluoride source, stirring at 1200 rpm. [a]Determined by $^{19}F$ NMR using 4-fluoroanisole as internal standard; [b]25 % of β-hydroxy sulfide observed by NMR.

Table 2.2: Screening of fluoride sources with **1b**.



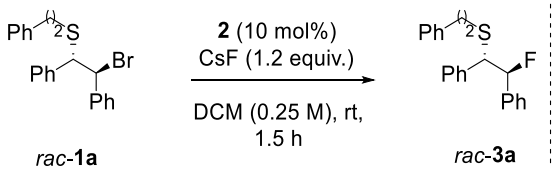

*rac*-**1b** *rac*-**3b** **2a**

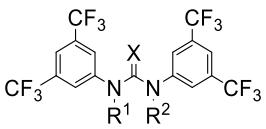
| Entry | $F^-$ source | Catalyst | Cat. loading (mol%) | Time (h) | Yield (%)[a] |
|---|---|---|---|---|---|
| **1** | CsF | **2a** | 10 | 1.5 | >95 |
| 2 | KF | **2a** | 10 | 1.5 | trace |
| 3 | NaF | **2a** | 10 | 1.5 | no reaction |
| 4 | LiF | **2a** | 10 | 1.5 | no reaction |
| 5 | $CaF_2$ | **2a** | 10 | 1.5 | no reaction |
| 6[b] | TBAF | – | – | 1.5 | 45 |

General conditions: 0.05 mmol substrate, 0.06 fluoride source, stirring at 1200 rpm. [a] Determined by $^{19}F$ NMR using 4-fluoroanisole as internal standard; [b] 33 % of the corresponding alcohol observed by NMR

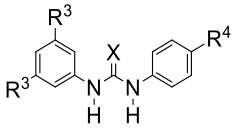
*2.2.1.2 Achiral Urea Catalysts.* Catalyst **2a** retained catalytic activity when the loading was reduced to 5 mol% affording **3a** in 64 % yield after 24 hours, however further lowering to 0.5 mol% proved detrimental (Entry 1–3 Table 2.3). Different achiral ureas and thioureas were evaluated for the fluorination of **1a** and **1b** in DCM using cesium fluoride. No reaction ocurred using a mono or di- *N*-methylated analogue of **2a** (Entry 4–5, Table 2.3). The acidity of the NH groups of the catalyst is highly important; indeed, the more electron-rich 1-(3,5-bis(trifluoromethyl)phenyl)-3-(4-methoxyphenyl)urea **2e** (Entry 6, Table 2.3) and diphenyl urea **2f** (Entry 7, Table 2.3; Entry 2, Table 2.4) gave low yields. These results indicate the requirement for an effective NH···$F^-$ interaction for achieving sufficient reactivity. Surprisingly, thioureas **2d** and **2g** (Entry 8–9, Table 2.3; Entry 3–4, Table 2.4) resulted in no product formation for both substrates tested (*v. 2.2.1.4 Nucleophilicity of Thiourea HBD*).

Table 2.3: Screening of achiral catalysts with **1a**.




**2a** X = O, $R^1 = R^2$ = H
**2b** X = O, $R^1$ = $CH_3$, $R^2$ = H
**2c** X = O, $R^1 = R^2 = CH_3$
**2d** X = S, $R^1 = R^2$ = H

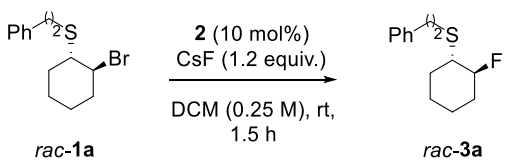


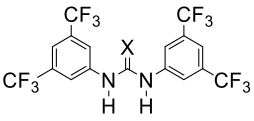

**2e** X = O, $R^3 = CF_3$, $R^4 = OCH_3$
**2f** X = O, $R^3 = R^4$ = H
**2g** X = S, $R^3 = R^4$ = H

| Entry | Catalyst | Cat. loading (mol%) | Time (h) | Yield (%)[a] |
|---|---|---|---|---|
| 1 | **2a** | 10 | 1.5 | 86 |
| 2 | **2a** | 5 | 24 | 64 |
| 3 | **2a** | 0.5 | 24 | 6 |
| 4 | **2b** | 10 | 1.5 | no reaction |
| 5 | **2c** | 10 | 1.5 | no reaction |
| 6 | **2e** | 10 | 1.5 | 20 |
| 7 | **2f** | 10 | 1.5 | 5 |
| 8 | **2d** | 10 | 1.5 | no reaction |
| 9 | **2g** | 10 | 1.5 | no reaction |

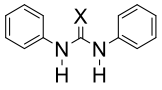
General conditions: 0.05 mmol substrate, 0.06 fluoride source, stirring at 1200 rpm. [a] Determined by $^{19}F$ NMR using 4-fluoroanisole as internal standard.

Table 2.4: Screening of achiral catalysts with **1b**.




**2a** X = O
**2d** X = S



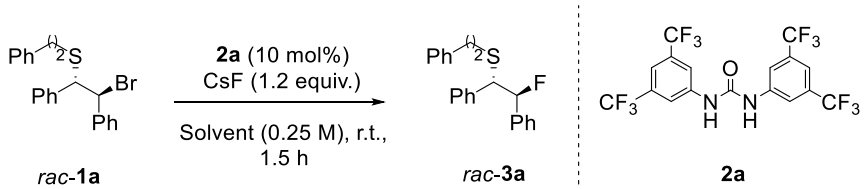

**2f** X = O,
**2g** X = S

| Entry | $F^-$ source | Catalyst | Cat. loading (mol %) | Time (h) | Yield (%)[a] |
|---|---|---|---|---|---|
| 1 | CsF | **2a** | 10 | 1.5 | > 95 |
| 2 | CsF | **2f** | 10 | 1.5 | 15 |
| 3 | CsF | **2d** | 10 | 1.5 | no reaction |
| 4 | CsF | **2g** | 10 | 1.5 | no reaction |

General conditions: 0.05 mmol substrate, stirring at 1200 rpm. [a] Determined by $^{19}F$ NMR using 4-fluoroanisole as internal standard.

*2.2.1.3 Solvents.* The reaction carried out without catalyst **2a** using dichloromethane, toluene or acetonitrile as a solvent, gave only traces of product (< 5% for **1a**, Entry 2, 4 and 6, Table 2.5) or no reaction (0 % for **2a**, Entry 2, 4 and 6, Table 2.6), suggesting that the concentration of soluble fluoride in the organic phase is negligible in the absence of a suitable HBD catalyst. By adding Schreiner's catalyst **2a**, dichloromethane and acetonitrile afforded the desired product in satisfactory yields for both substrates (Entry 1 and 5, Table 2.5; Entry 1 and 5, Table 2.6). Toluene afforded low yields (33%, **1a**, Entry 3 Table 2.5; 23% **2a,** Entry 3 Table 2.6) presumably due to the limited solubility of **2a** in apolar solvents. Dimethylformamide, capable of binding metal cations and thereby solubilising alkali metal salts, gave low yields in both the catalysed and uncatalysed reaction (Entry 7–8, Table 2.5; Entry 7–8, Table 2.6). Accordingly, methanol, capable of solubilising CsF via hydrogen bonding, did not discriminate between catalysed and uncatalysed pathway while also competing as a nucleophile in the reaction (Entry 9–10, Table 2.5; Entry 9–10, Table 2.6).

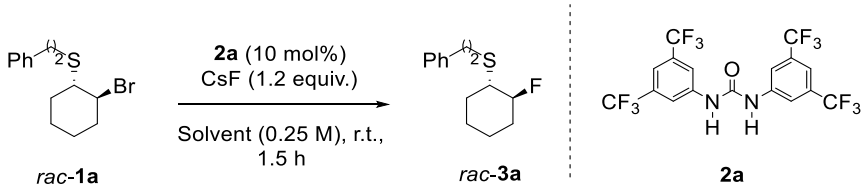
Table 2.5: Screening of solvents with **1a**




| Entry | Solvent | Catalyst | Cat. loading (mol%) | Yield (%)[a] |
|---|---|---|---|---|
| 1 | DCM | **2a** | 10 | 86 |
| 2 | DCM | – | – | no reaction |
| 3 | PhMe | **2a** | 10 | 33 |
| 4 | PhMe | – | – | < 5 |
| 5 | $CH_3CN$ | **2a** | 10 | 72 |
| 6 | $CH_3CN$ | – | – | < 5 |
| 7 | DMF | **2a** | 10 | 10 |
| 8 | DMF | – | – | 9 |
| 9[b] | MeOH | **2a** | 10 | 10 |
| 10[b] | MeOH | – | – | 10 |

General conditions: 0.05 mmol substrate, stirring at 1200 rpm. [a] Determined by $^{19}F$ NMR using 4-fluoroanisole as internal standard, [b] The major product detected by $^{1}H$ NMR was the methyl ether derived from MeOH attack of the episulfonium ion.

Table 2.6: Screening of solvents with **1b**.

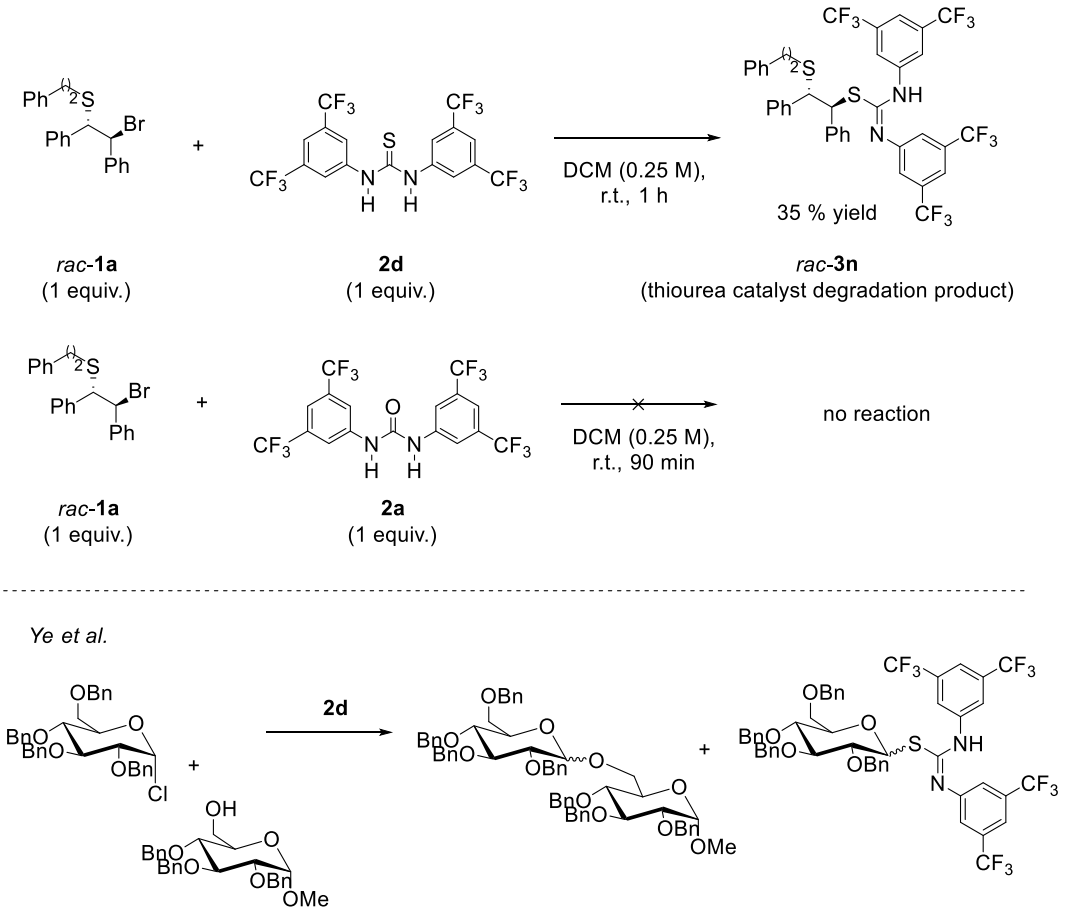



| Entry | Solvent | Catalyst | Cat. loading (mol%) | Yield (%)[a] |
|---|---|---|---|---|
| 1 | DCM | **2a** | 10 | >95 |
| 2 | DCM | – | – | no reaction |
| 3 | PhMe | **2a** | 10 | 23 |
| 4 | PhMe | – | – | no reaction |
| 5 [b] | $CH_3CN$ | **2a** | 10 | 88 |
| 6 | $CH_3CN$ | – | – | no reaction |
| 7 | DMF | **2a** | 10 | 36 |
| 8 | DMF | – | – | 33 |
| 9 [b, c] | MeOH | **2a** | 10 | 14 |
| 10 [c] | MeOH | – | – | no reaction |

General conditions: 0.05 mmol substrate, stirring at 1200 rpm. [a] Determined by $^{19}F$ NMR using 4-fluoroanisole as internal standard; [b] 18 hours reaction; [c] the major product detected by $^{1}H$ NMR was the methyl ether derived from MeOH attack of the episulfonium ion

*2.2.1.4 Nucleophilicity of Thiourea HBD.* Acidity is a widely used guiding principle for the design of hydrogen bond donor catalysts. Following this principle, thioureas are regarded as *better* or *stronger* HBD catalysts in hydrogen bonding and anion binding catalysis. However, this notion has been challenged by showing equal or greater catalytic activity for ureas over their thioureas analogues in several occasions.[36] Spectroscopic studies also showed that ureas are better anion binder than thioureas.[37] In asymmetric anion binding catalysis, thioureas generally give marginally better or equal results than ureas in terms of reactivity and enantioselectivity; thioureas are ultimately preferred for their better solubility in a wide range of solvents. In the design of our catalytic system, considerations about the acidity of the catalyst played an important role; an ideal HB PTC catalyst has to be acidic enough to strongly bind fluoride from the solid state and thus to ensure the occurrence of the phase-transfer event (*catch*), but not so strongly as to impede the subsequent fluoride delivery (*release*). In addition, strongly acidic HBD could lead to protonation of $F^-$ with concomitant release of HF

and $HF_2^-$, potentially triggering unselective fluorination. We have shown that modulation of the acidity of achiral aromatic ureas impacts the yield of our reaction, with the more acidic Schreiner's catalyst **2a** ($pK_{a\,(DMSO)}$ = 13.8; [38]86 % yield of **1a**, >95 % yield of **1b**) performing better than diphenyl urea **2f** ($pK_{a\,(DMSO)}$ = 18.7; 5 % yield of **1a**, 15 % yield of **1b**). However, Schreiners' thiourea **2d** ($pK_{a\,(DMSO)}$ = 8.5) and diphenyl thiourea **2g** ($pK_{a\,(DMSO)}$ = 13.4) were both unable to catalyse the fluorination of **1a** and **1b**. This initially surprising result was later ascribed to the competitive formation of a covalent adduct between the substrate and the thiourea catalyst. Compound **3n** was isolated and fully characterised from the reaction of **1a** and a stoichiometric amount of thiourea **2d**; in contrast, urea **2a**, did not react with **1a** (Scheme 2.13)**.** Recently, Ye *et al.* reported the stereoselective addition of nucleophiles to glycosyl halides *via* anion binding catalysis.[39]



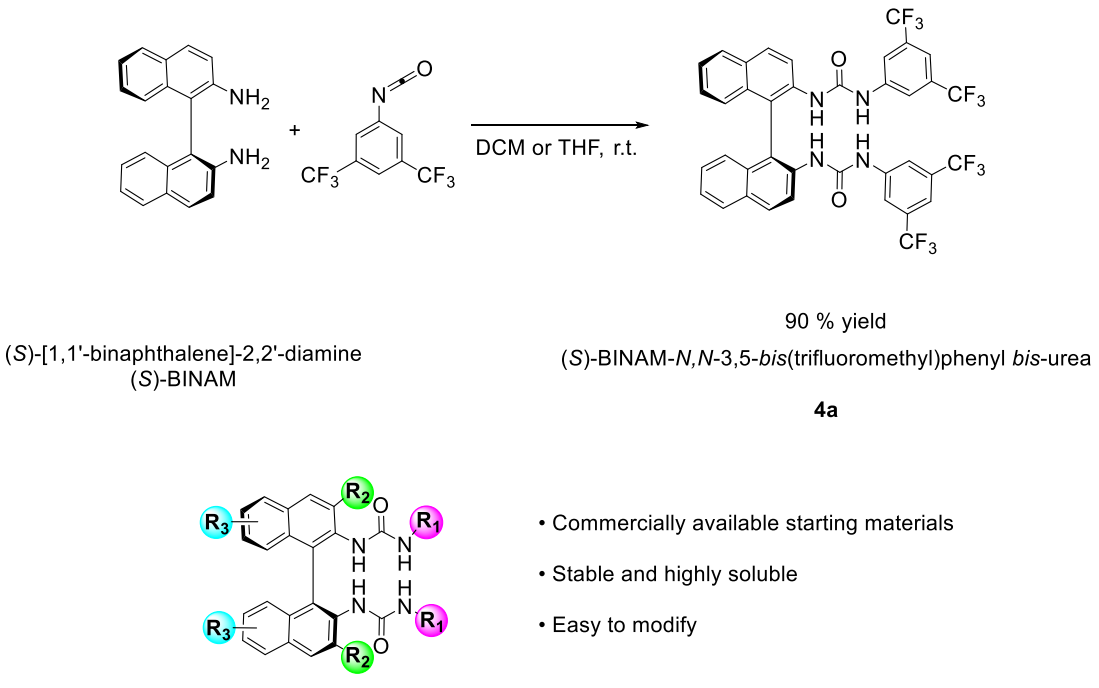

Scheme 2.13: Undesired reactivity as nucleophile of thiourea catalysts.

They noticed that, when Schreiner's thiourea was used, a covalent adduct derived from the nucleophilic addition of the thiourea to the strongly electrophilic oxocarbenium intermediate was observed together with the formation of the desired disaccharide. Jacobsen and collaborators also noticed the formation of catalyst–substrate adducts during anion binding reactions catalysed by thioureas. They hypothesised that chiral thioureas could act as nucleophilic catalysts, as opposed to HBD, in specific circumstances.[37] In our case, **3n** was stable and did not undergo fluorination if subjected to the reaction conditions, thus excluding the possibility of its involvement as an active intermediate.

*2.2.2 Asymmetric Fluorination with Fluoride Salts*

This solid-liquid phase-transfer manifold has advantages over the use of soluble fluoride sources not least because it generates reactive fluoride at controllable low concentration and offers the potential of inducing asymmetry with a chiral nonracemic urea catalyst. We focused our attention on axially chiral $C_2$-symmetric ureas, derived from BINAM ([1,1'-binaphthalene]-2,2'-diamine). This scaffold can be easily tuned through structural modification, it is commercially accessible in both enantiomeric forms, and the extended binaphthyl backbone ensures good solubility in a wide range of solvents. The *S* enantiomer of BINAM was employed for this study. Catalyst **4a** was conveniently synthesised in high yields from commercially available (*S*)-BINAM and 3,5-(trifluoromethyl)phenyl isocyanate; the reaction was carried out under rigorously anhydrous conditions and a careful purification was required to ensure that Schreiner's catalyst **2a** was not present in the final compound, as potentially capable to mediate competitive non-enantioselective fluorination (Scheme 2.14). The addition of methanol upon completion of the reaction was found to facilitate the subsequent purification by quenching unreacted 3,5-bis(trifluoromethyl)phenyl isocyanate, thereby impeding the adventitious formation of **2a**. Purity is most conveniently assessed by careful inspection of the

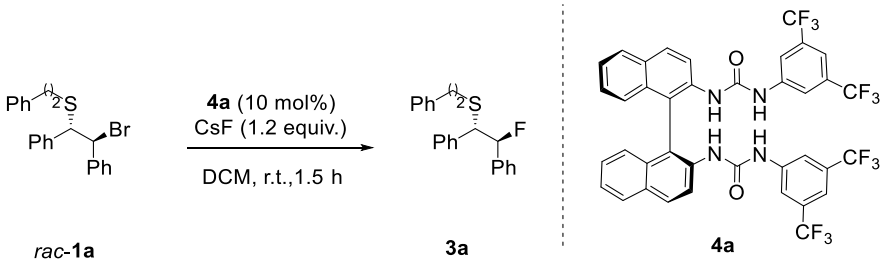
trifluoromethyl region of the $^{19}F$ NMR spectrum ($\delta$ $CF_3$ **2a** = -62.96 ppm *vs.* $\delta$ $CF_3$ **4a** -63.22, $CDCl_3$).




Scheme 2.14: Synthesis of (*S*)-BINAM Urea catalyst **4a.**

Substrate **1a** underwent fluorination with CsF and **4a** in dichloromethane at room temperature affording **3a** after 1.5 hours in >95 % yield and a promising enantiomeric ratio (e.r.) of 82:18 (Entry 1, Table 2.7). The reaction carried out using a batch of CsF subjected to a careful drying procedure (72 h at 150 °C under high vacuum) and dry solvents gave an identical result to the use of commercially available CsF (Entry 1–2, Table 2.7), therefore suggesting that traces of water do not interfere with the HB PTC process. Changes in the concentration affect the reactivity, with a reduced yield of 62 % observed when the reaction was carried out at higher dilution (0.1 M) and 90 % yield when the reaction was concentrated at 0.5 M, however no effect on enantioselectivity was noticed (Entry 3–4, Table 2.7)

Table 2.7: Asymmetric fluorination of **1a** using **4a** as HBD catalyst.




| Entry | CsF (equiv.) | Concentration (M) | Yield (%) [a] | e.r.[b] |
|---|---|---|---|---|
| 1 | 1.2 | 0.25 | >95 (75) [c] | 82:18 |
| 2[d] | 1.2 [e] | 0.25 | >95 | 82:18 |
| 3 | 1.2 | 0.5 | 90 | 82:18 |
| 4 | 1.2 | 0.1 | 62 | 82:18 |

General conditions: Substrate (0.05 mmol), catalyst (0.005 mmol) and CsF (0.06 mmol) in 200 µL of DCM stirred at 1200 rpm; reference racemic mixtures for HPLC analysis were obtained by stirring the corresponding bromide starting material with 1.2 equiv of AgF in $CH_3CN$ (0.25 M) for 1 h; [a]determined by $^{19}F$ NMR using 4-fluoroanisole as internal standard; [b] e.r. was determined by HPLC analysis using a chiral stationary phase; [c] yield of isolated product on a 0.25 mmol scale; [d] flame dried CsF was used.

*2.2.2.1 Solvent Effect.* The stability of an ion pair in solution is largely dictated by the electric properties of the solvent; as a consequence, reactions involving ionic reagents or intermediates are greatly dependent on the solvent used. The strength of an electrostatic interaction is inversely proportional with the polarity of the medium. Thus, ionic interactions are stronger in apolar solvents, able to promote the formation of contact ion-pairs, and weaker in polar solvents, which favours solvent-shared or solvent separated ion-pairs. In hydrogen bonding catalysis involving ionic intermediates higher enantioselectivity is generally observed with ethers or apolar aromatic solvents. With the aim of improving the selectivity of our transformation, the effect of different solvents on the enantioselectivity was therefore investigated (Figure 2.1 and Table 2.8). Non-polar solvents ($\varepsilon_r < 4$) of different classes such as cyclohexane, $CCl_4$, $Et_2O$ and MTBE were detrimental for reactivity affording only trace amount of product (Entry 2–5, Table 2.8). Similarly, apolar aromatic solvents such as benzene, hexafluorobenzene, 1,4-difluorobenzene, 1,3,5-trifluorobenzene provided very low yields (Entry 7–10, Table 2.8). Chloroform ($\varepsilon_r = 4.8$) afforded **3a** in 36 % yield with an 81.5:18.5 e.r.

(Entry 6, Table 2.8). Fluorobenzene and 1,3-difluorobenzne ($\varepsilon_r \sim 5$) similarly to chloroform afforded a low yield of 33 % and 29 %, however higher enantioselectivities were obtained, with an enantiomeric ratio of 83:17 and of 86:14, respectively (Entry 11–12, Table 2.8). 1,2-Difluorobenzene (1,2-DFB), one of the more polar aromatic solvent known ($\varepsilon_r$ = 13.4), afforded excellent reactivity (>95 % yield) while retaining the improved enantioselectivity of 86:14 e.r. (Entry 13, Table 2.7). Ethyl acetate, despite having intermediate polarity ($\varepsilon_r$ = 6.1), did not lead to product (Entry 14, Table 2.7). In this case, catalyst deactivation due to hydrogen bonding with the solvent is a likely scenario; as **4a:**EtOAc adducts can indeed be detected in $^1$H NMR and proved surprisingly stable to evaporation under reduced pressure and silica gel column chromatography. The highly polar and Lewis-basic solvent nitromethane affords a moderate yield of 40 % and poor enantiocontrol with 74:26 e.r. (Entry 15, Table 2.7). This observation suggests that solvent with high dielectric constant may be unsuitable to achieve high enantiocontrol in HB PTC, however also in this case catalyst-solvent interactions cannot be ruled out.

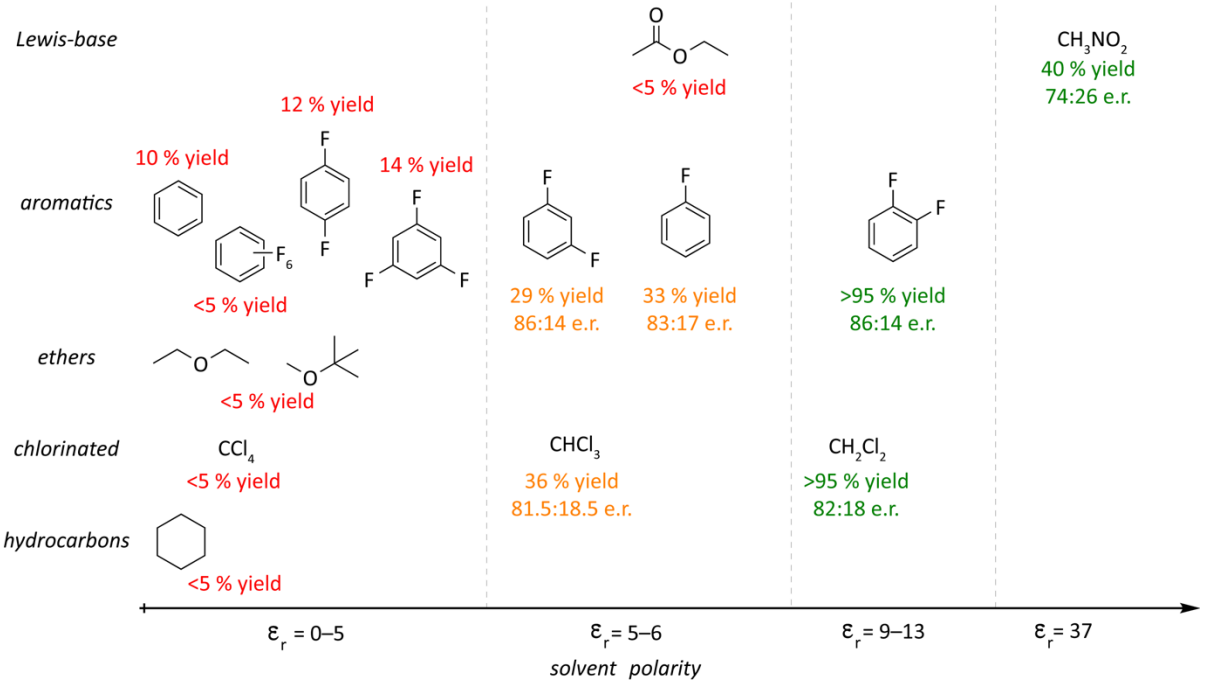
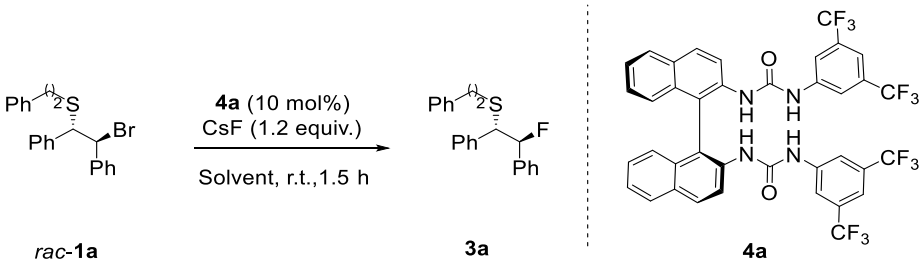



Figure 2.1: Reactivity and enantioselectivity of HB PTC fluorination in solvents of different polarity.

Table 2.8: Screening of solvents with **1a** using **4a** as chiral HBD catalyst.




| Entry | Solvent | CsF (equiv.) | Time (h) | Yield (%) [a] | e.r.[b] | $\varepsilon_r$[c] |
|---|---|---|---|---|---|---|
| 1 | DCM | 1.2 | 1.5 | >95 | 82:18 | 8.9 |
| 2 | Cyclohexane | 1.2 | 1.5 | <5 | – | 2.2 |
| 3 | $CCl_4$ | 1.2 | 4 | <5 | – | 2.2 |
| 4 | $Et_2O$ | 1.2 | 1.5 | <5 | – | 3.9 |
| 5 | MTBE | 1.2 | 1.5 | <5 | – | – |
| 6 | $CHCl_3$ | 1.2 | 1.5 | 36 | 81.5:18.5 | 4.8 |
| 7 | Benzene | 1.2 | 1.5 | 10 | – | 2.3 |
| 8 | $PhF_6$ | 1.2 | 1.5 | < 5 | – | 2.0 |
| 9 | 1,4-DFB | 1.2 | 1.5 | 12 | – | – |
| 10 | 1,3,5-TFB | 1.2 | 1.5 | 14 | 80:20 | – |
| 11 | PhF | 1.2 | 1.5 | 33 | 83:17 | 5.5 |
| 12 | 1,3-DFB | 1.2 | 1.5 | 29 | 86:14 | 5.0 |
| 13 | 1,2-DFB | 1.2 | 1.5 | >95 | 86:14 | 13.4 |
| 14 | EtOAc | 1.2 | 1.5 | < 5 | – | 6.1 |
| 15 | $CH_3NO_2$ | 1.2 | 1.5 | 40 | 74:26 | 37.3 |

General conditions: Substrate (0.05 mmol), catalyst (0.005 mmol) and CsF (0.06 mmol) in 200 µL of solvent stirred at 1200 rpm for the indicated time; reference racemic mixtures for HPLC analysis were obtained by stirring the corresponding bromide starting material with 1.2 equiv of AgF in $CH_3CN$ (0.25 M) for 1h; [a] determined by $^{19}F$ NMR using 4-fluoroanisole as internal standard; [b] e.r. was determined by HPLC analysis using a chiral stationary phase; [c] relative permittivity (dielectric constant).[40] MTBE = methyl *tert*-butyl ether; DFB = difluorobenzene; TBF = trifluorobenzene.

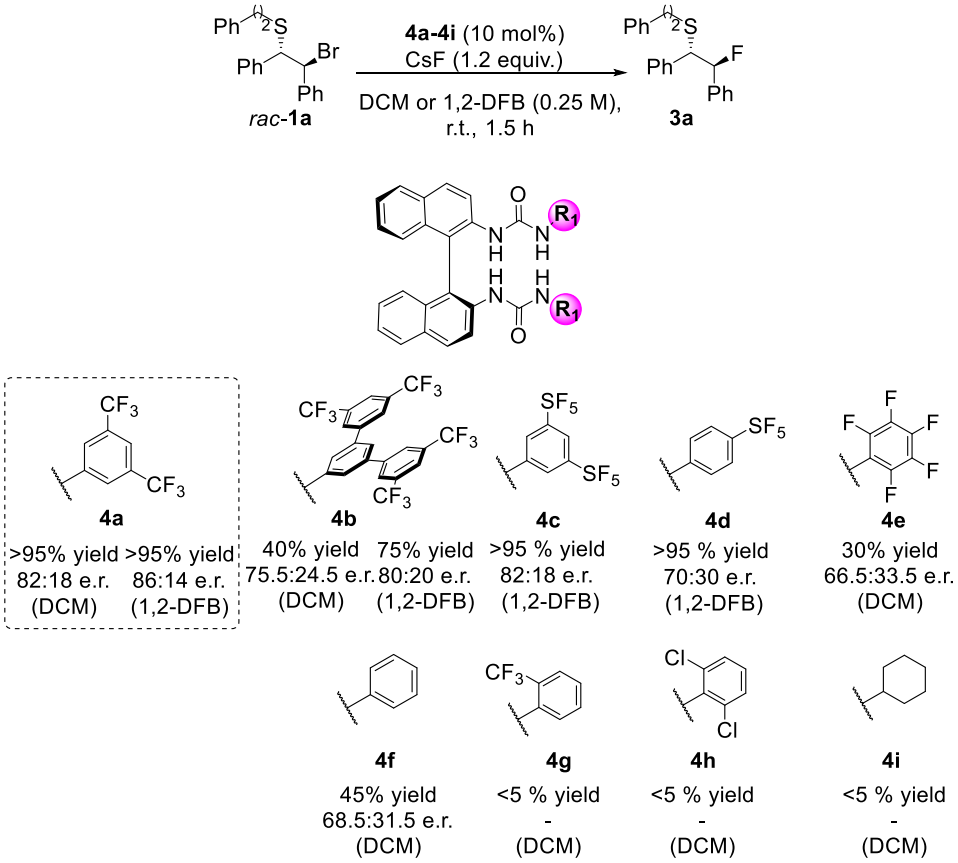
It is worth pointing out that apolar solvents are ineffective reaction media under HB PTC conditions, while generally preferred for hydrogen bonding catalysis. This may be connected to the effect of solvent polarity on the solid-liquid phase-transfer process. In this regard, the polarity of the organic phase has been recognised to influence the rate of PTC.[3] Additionally, in the case of apolar hydrocarbons, such as cyclohexane and benzene, or apolar fluorocarbons, such as hexafluorobenzene, the scarce solubility of the catalyst may play a role in the observed low reactivity. Overall, best results in terms of reactivity are achieved using polar chlorinated solvents and polar fluorinated aromatics. The enantioselectivity is higher in polar fluorinated

aromatic solvents, with 1,2-difluorobenzene (1,2-DFB) ensuring optimal reactivity and improved enantiocontrol compared to DCM.

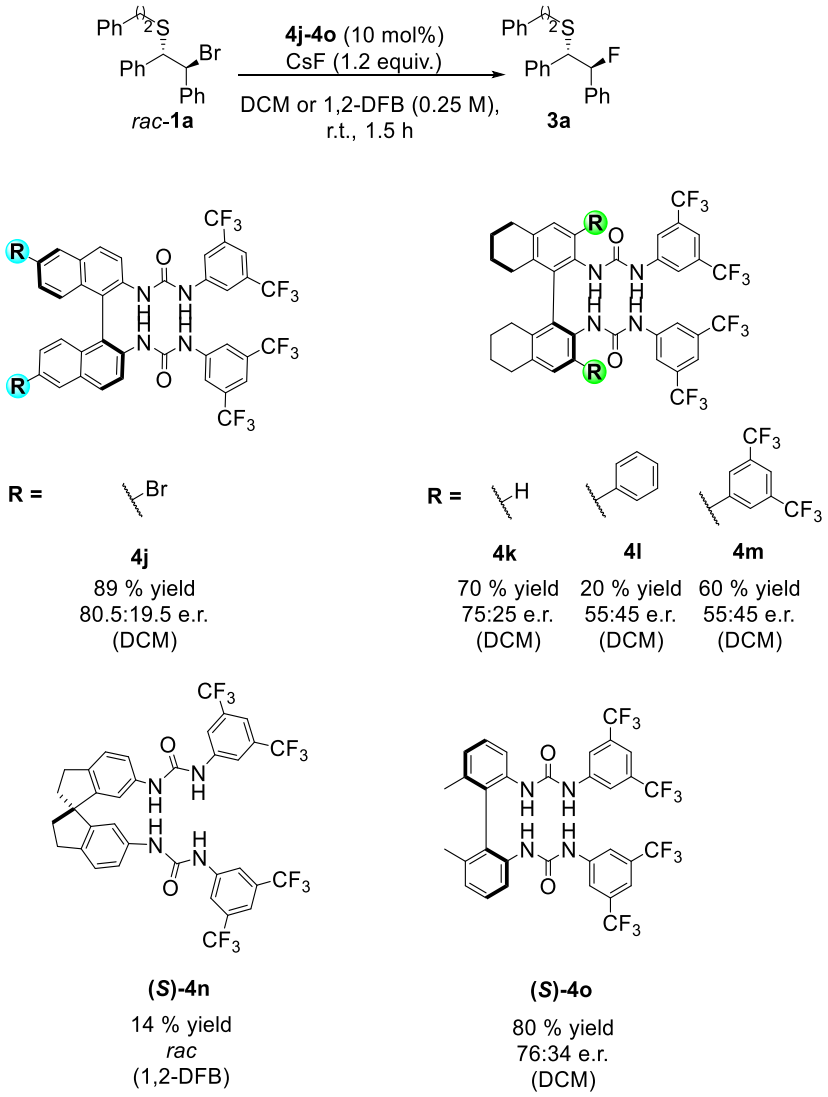
*2.2.2.2 Catalyst Screening.* Catalysts **4b–i** presenting differently substituted rings instead of the 3,5-(trifluoromethyl)phenyl groups were evaluated (Scheme 2.15). Catalyst **4b** featuring 3,5-bis((3,5-trifluoromethyl)phenyl)phenyl substituents, and **4c**, presenting 3,5-pentafluorosulfanyl substitution, furnished the product in slightly lower enantioselectivities (**4b** 80:20 e.r., **4c** 82:18 e.r. *cf.* **4a** 86:14 e.r.), while *para*-substituted **4d**, bearing 4-(pentafluorosulfanyl)phenyl groups, led to a substantial decrease of enantiocontrol (**4d** 75:35 e.r.). Catalysts **4e** and **4f**, featuring phenyl or perfluorophenyl rings resulted in low reactivity (**4e** 45 % yield; **4f** 29% yield) and low enantioselectivity (**4e** 68.5:31.5 e.r.; **4f** 66.5:35.5 e.r.). Catalysts having *ortho*-substituted aromatic rings, such as **4g** and **4h**, or cyclohexyl rings in place of aromatic groups (**4i**) resulted in no product formation.

Catalysts with modification at the BINAM backbone, **4j–4m**, were synthesised and tested (Scheme 2.16). Bromination at the 6,6'-positions of the binaphthyl rings was achieved by treatment of the protected BINAM *bis*-acetamide with $Br_2$ followed by deprotection and urea coupling (**4j**). To access 3,3' functionalised catalysts, partial hydrogenation of the BINAM aromatic rings was required to avoid competitive reaction at the more reactive 6,6' positions, subsequent bromination (or iodination) and Pd-catalysed cross coupling afforded 3,3' substituted **4l-4m**. The use of **4j** resulted in no improved enantiocontrol, compared with **4a**, despite a good yield (**4j**, 89 % yield, 80.5:19.5 e.r.). Saturation of the backbone and modification at the 3,3' position, as in catalyst **4k–m**, were detrimental for both reactivity and enantioselectivity. Finally, *bis*-ureas with structurally different backbones **4n–4o** were evaluated. Spiroindane-derived *bis*-urea **4n** was poorly reactive and afforded a racemic mixture while *bis*-tolyl-derived *bis*-urea **4o** gave low enantioselectivity despite good reactivity.

From these data, we can conclude that all the catalysts tested performed worse than **4a**; the 3,5-substitution pattern and the electron-withdrawing nature of the groups on the aromatic rings appear critical to ensure efficient catalysis. Variation of the binaphthyl backbone led to diminished selectivity. This is evident for catalysts substituted in 3,3' and for backbones different from the BINAM scaffold, suggesting that an extended conjugated system on the catalyst is important for enantioselectivity.



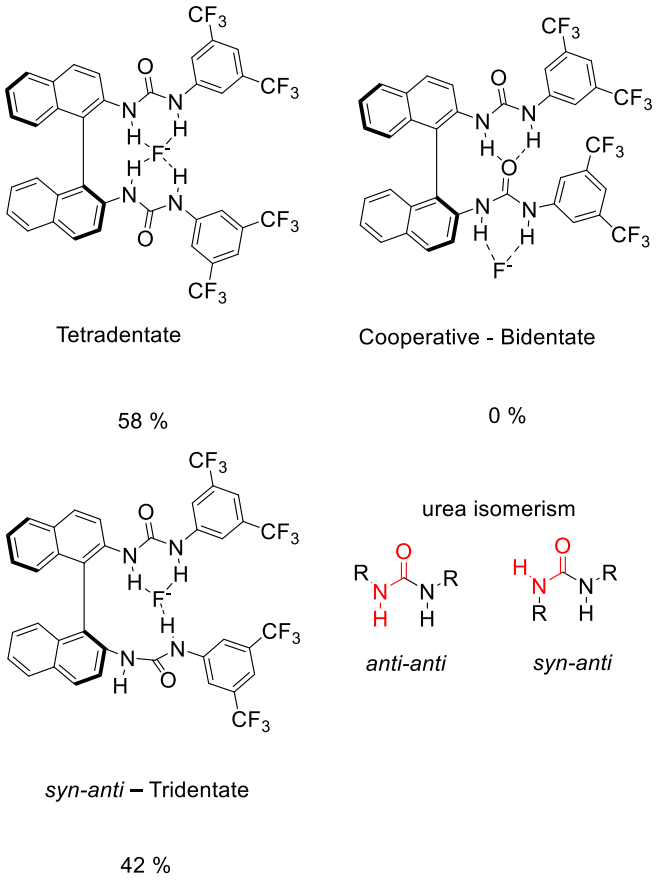

Scheme 2.15: Screening of chiral *bis*-urea **4a–4i**; 1,2-DFB = 1,2-difluorobenzene.



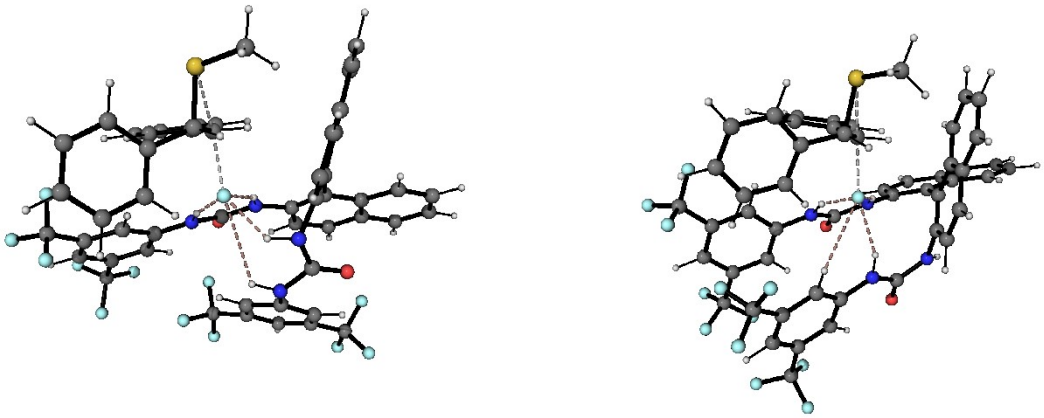

Scheme 2.16: Screening of chiral *bis*-urea **4j–4o**; 1,2-DFB = 1,2-difluorobenzene.

*2.2.2.3 N-Alkylated bis-Urea Catalysts.* The presence of two urea motifs within **4a** and the paucity of information about the conformation and the binding mode of the catalyst, urged us to question whether all four H-bond interactions were effectively required for reactivity and enantioselectivity. Molecular dynamics (MD) simulations of **4a**:CsF, sampled at 373 K, showed that no bidentate cooperative binding mode was operative; 58 % of the population displayed tetradentate binding, and surprisingly 42 % showed tridentate binding to fluoride, where one urea underwent conformational change from the *anti-anti* to the *syn-anti* urea isomer (Scheme 2.17). Plausible transition states (TS) involving tetradentate and tridentate

binding were optimised using DFT calculations finding that the syn-anti conformer, displaying tridentate binding mode, was energetically favoured by 24 kJ/mol compared with the tetradentate TS (Scheme 2.18).



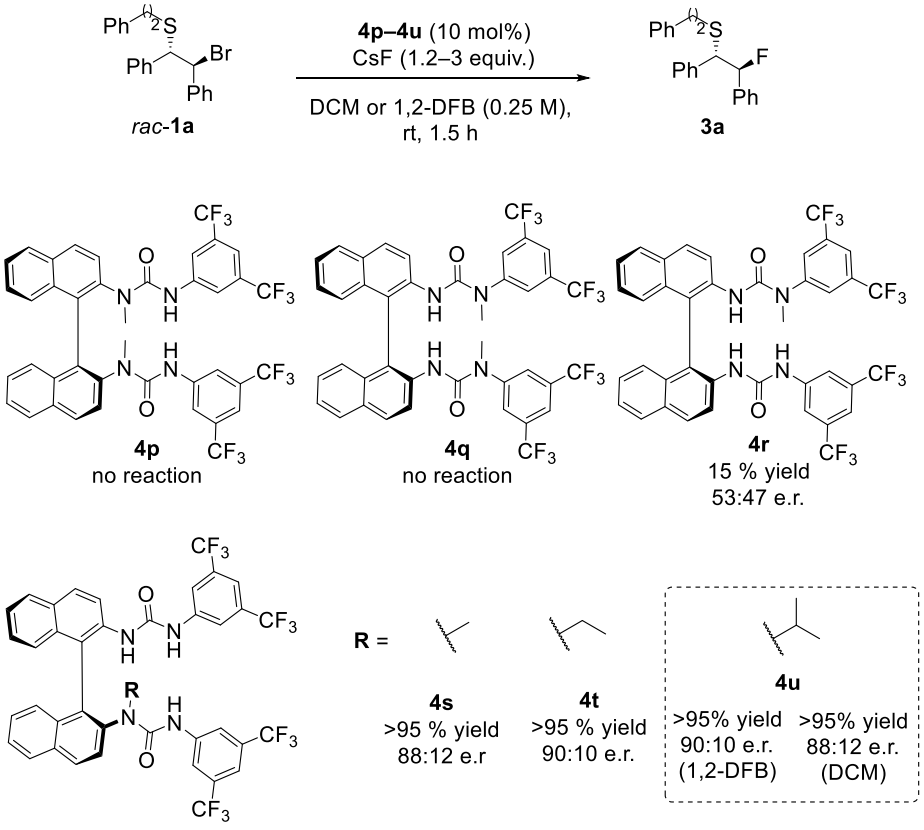

Scheme 2.17: Molecular dynamic simulations of **4a**:CsF (373 K). Computational work performed by Dr. David Ascough.



TS **4a**:F⁻ tetradentate TS **4a**:F⁻ tridentate

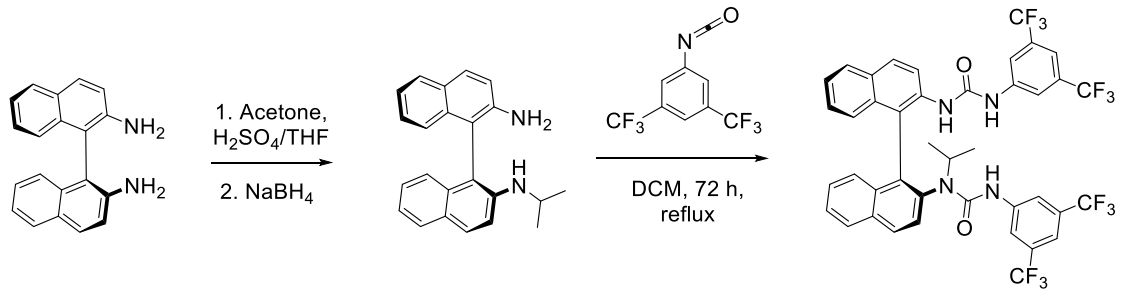
Scheme 2.18: DFT optimization, at def2-SVP(TZVPPD) level, of the TS including β-bromo sulfide and **4a**:F⁻ displaying a tetradentate and a tridentate binding mode. Computational work performed by Dr. David Ascough. Adapted with permission form reference 1.

In light of these considerations, we synthesised two dimethylated (**4p**–**4q**) and two monomethylated (**4r**–**4s**) analogues of **4a** to evaluate how the removal of specific hydrogen bonding sites would impact the reaction outcome (Scheme 2.19). The synthesis was performed by reacting the corresponding dimethylated BINAM or monomethylated 3,5-bis(trifluoromethyl) aniline with triphosgene. The fluorination of **1a** carried out with dimethylated **4p** or **4q** resulted in no product formation; **4r** monomethylated on one NH adjacent to the 3,5-substituted aryl ring, gave poor yield and enantiocontrol. When monomethylated catalyst **4s** was synthesised and tested, it was found to enhance enantioselectivity to 88:12 e.r., while retaining excellent reactivity (>95 % yield). The replacement of the *N*-methyl group with a larger alkyl (**4t–u**), afforded **3a** in >95% yield with an enantiomeric ratio of 90:10.




Scheme 2.19: Screening of *N*-alkylated *bis*-ureas.

Final optimization was carried out with *N*-isopropylated *bis*-urea **4u**, synthesized from *N*-isopropylated binaphthyl aniline **5e** (Scheme 2.22).




(*S*)-BINAM

(*S*)-iPr BINAM

57 % yield

**5e**

(*S*)-iPr BINAM Urea

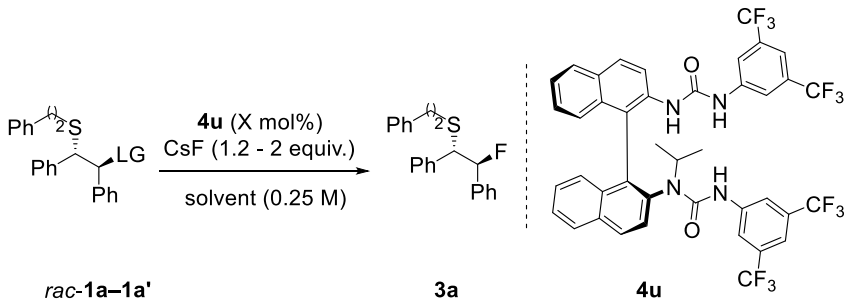
91 % yield

**4u**

Scheme 2.20: Synthesis of (*S*)-iPr BINAM Urea catalyst **4u.**

The chlorinated analogue of **1a** showed the same level of enantioselectivity, albeit with a reduced reactivity (Entry 1–2, Table 2.9). The catalyst loading could be reduced to 2 mol% with only a modest decrease in yield, however when 0.1 mol% of **4u** was used the reaction did not yield detectable product (Entry 3–5, Table 2.9). Importantly, deliberate addition of water (up to 1 equivalent) had no significant effect on the transformation, while the addition of 10 equivalents of $H_2O$ severely impacts the yield, although the enantioselectivity was largely preserved (Entry 6–7, Table 2.9). In agreement with what observed using catalyst **4a**, apolar solvents, such as hexafluorobenzene, were detrimental for the reaction and resulted in trace amount of product (Entry 8, Table 2.9). Highly polar $CH_3CN$ provided a moderate yield of 69 % and enantiomeric ratio of 85:15 (Entry 9, Table 2.9). Fluorinated aromatic solvent of intermediate polarity, such as fluorobenzene and 1,3-difluorobenzene, provided excellent enantioselectivity (90:10 e.r) albeit with moderate yields of 67 % and 50 % respectively (Entry 10–11, Table 2.9). 1,2-Difluorobenzene was consistently the best solvent choice for both reactivity and enantioselectivity. Finally, lowering of the temperature to -30 °C afforded the product in 90 % yield over 72 hours and 95.5:4.5 enantiomeric ratio (Entry 12, Table 2.9).

Table 2.9: Final optimization using **4u.**

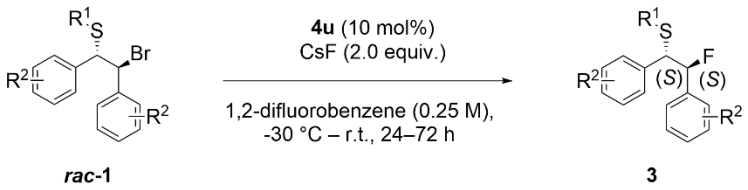


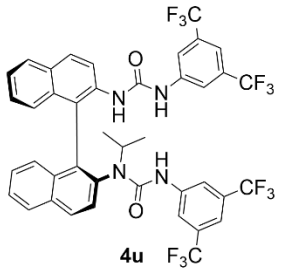

*rac*-**1a–1a'** **3a** **4u**

| Entry | Cat. loading (mol%) | LG | Solvent | Temp. (°C) | Time (h) | $H_2O$ (equiv.) | Yield (%) [a] | e.r.[b] |
|---|---|---|---|---|---|---|---|---|
| 1 | 10 | Br | DCM | r.t. | 1.5 | – | >95 | 88:12 |
| 2 | 10 | Cl | DCM | r.t. | 6 | – | 90 | 88:12 |
| 3 | 10 | Br | 1,2-DFB | r.t. | 1.5 | – | >95 | 90:10 |
| 4 | 2 | Br | 1,2-DFB | r.t. | 1.5 | – | 78 | 90:10 |
| 5 | 0.1 | Br | 1,2-DFB | r.t. | 48 | – | <5 | – |
| 6 | 10 | Br | 1,2-DFB | r.t. | 1.5 | $H_2O$ (1.1) | >95 | 89.5:9.5 |
| 7 | 10 | Br | 1,2-DFB | r.t. | 1.5 | $H_2O$ (10) | 26 | 89.5:9.5 |
| 8 | 10 | Br | $PhF_6$ | r.t. | 1.5 | – | <5 | – |
| 9 | 10 | Br | $CH_3CN$ | r.t. | 1.5 | – | 69 | 85:15 |
| 10 | 10 | Br | PhF | r.t. | 1.5 | – | 67 | 90:10 |
| 11 | 10 | Br | 1,3-DFB | r.t. | 1.5 | – | 50 | 90:10 |
| 12 | 10 | Br | 1,2-DFB | -30 | 72 | – | 90 (83) [c] | 95.5:4.5 |

General conditions: substrate (0.05 mmol, 1 equiv.), catalyst (2–10 mol%) and CsF (1.2 or 2 equiv.) in 200 µL of 1,2-difluorobenzene (0.25 M) stirred at 1200 rpm for the indicated time at the indicated temperature; [a] determined by $^{19}F$ NMR using 4-fluoroanisole as internal standard; [b] e.r. was determined by HPLC analysis using a chiral stationary phase; [c] In parenthesis, the isolated yield on a 0.2 mmol scale is shown.

*2.2.2.4 Substrate Scope.* The scope of the HB PTC fluorination was investigated with catalyst (*S*)-**4u** under the optimized reaction conditions (Scheme 2.21). Stilbene-derived β-bromo sulfides featuring electron-donating and electron-withdrawing substituents in *meta* and *para* positions of the aromatic backbone afforded the desired products in high yields and enantioselectivities; *meta*-substituted substrates (**3c–3g**) provided slightly higher yields and enantioselectivities compared to *para*-substituted sulfides **3h–3k**. The substituent on the sulfur can be modified, with the phenyl-ethyl motif affording the products with the highest enantioselectivity. The yields of the isolated products after purification are consistently lower than what measured by analysis of the crude mixture by NMR, thus suggesting that β-fluoro sulfides undergo decomposition upon chromatographic purification.



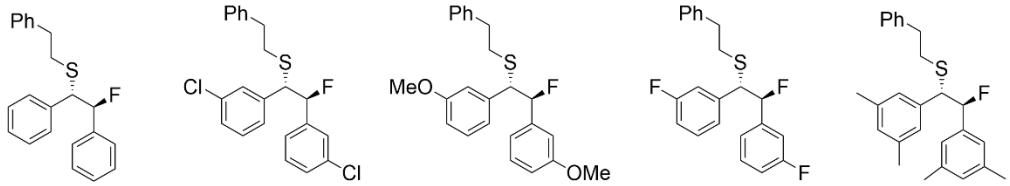
**4u**

**(*S*)-iPrBINAM Urea**

*Gouverneur Fluorination Catalyst*

Merck KGaA - 904805

CAS# 22227157-06-2



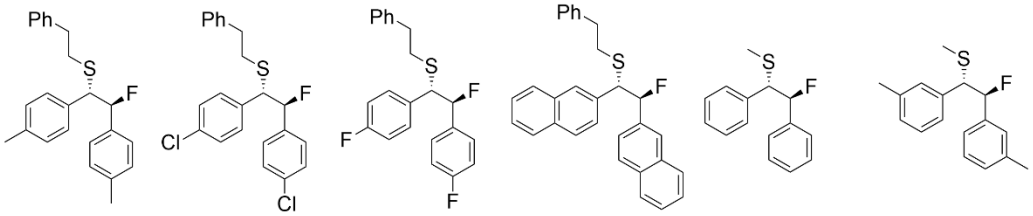
**3a**
83% yield
95.5:4.5 e.r.
(–30 °C)

**3c**
98% yield
97:3 e.r.
(rt)

**3e**
89% yield
96:4 e.r.
(0 °C)

**3f**
75% yield
94:6 e.r.
(rt)

**3g**
73% yield
96.5:3.5 e.r.
(rt)



**3h**
60% yield
91:9 e.r.
(–30 °C)

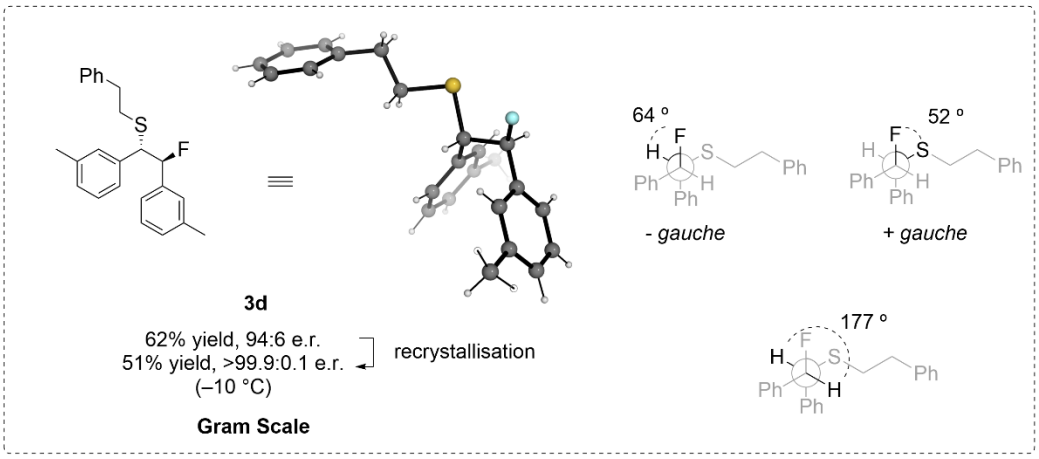
**3i**
53% yield
93:7 e.r.
(0 °C)

**3j**
58% yield
94:6 e.r.
(0 °C)

**3k**
61% yield
95.5:4.5 e.r.
(rt)

**3l**
72% yield
91:9 e.r.
(–30 °C)

**3m**
87% yield
92.5:7.5 e.r.
(–10 °C)




**3d**

62% yield, 94:6 e.r.
51% yield, >99.9:0.1 e.r.
(–10 °C)

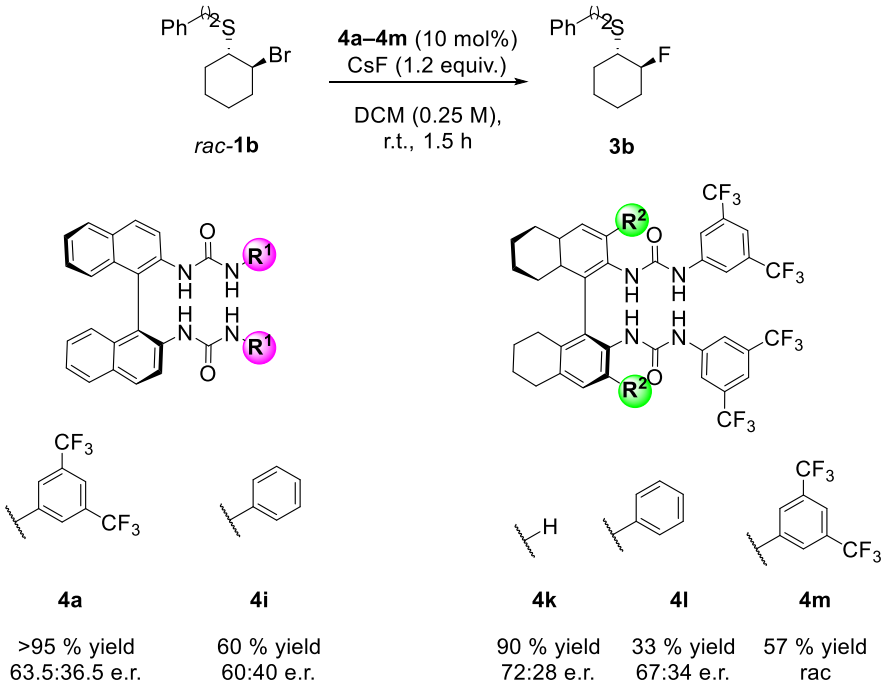
recrystallisation

**Gram Scale**

Scheme 2.21: Evaluation of the substrate scope for substrate **1a**–**1m.**

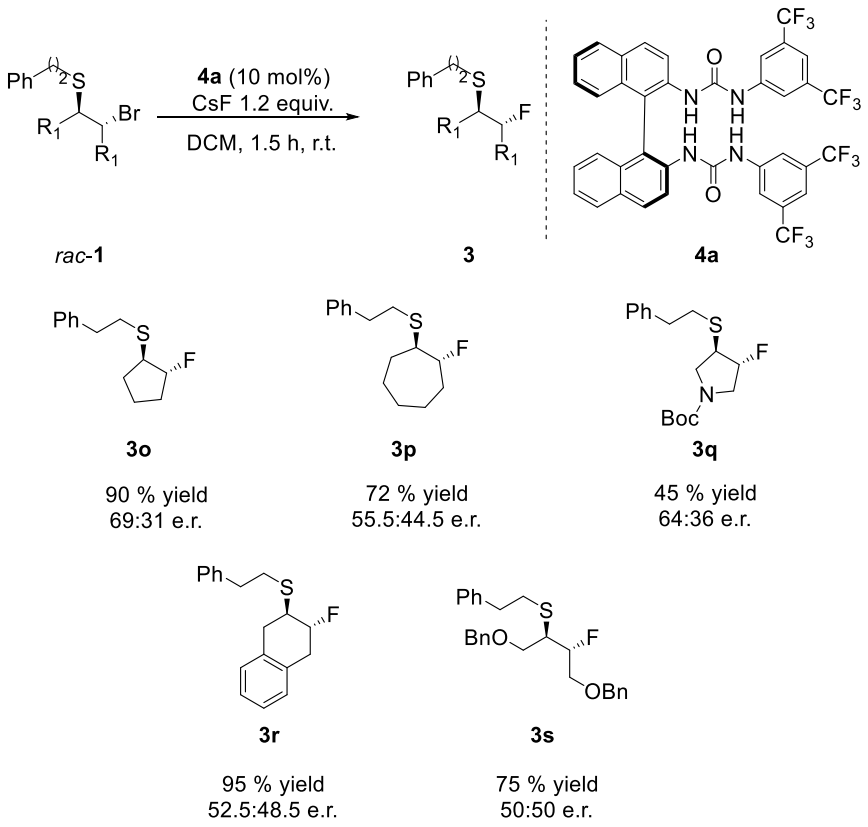
A gram quantity of **1d** underwent fluorination affording **3d** in 62 % overall yield and 94:6 enantiomeric ratio; the product was recrystallised from hexane to obtain a single enantiomer of **3d** (>99.9:0.1 e.r.) in 51 % yield. X-ray quality crystals were obtained from **3d** and analysed by single crystal X-ray diffraction; this allowed to assign the absolute configuration (*S*,*S*) to the fluorinated products. The solid-state structure of **3d** (Scheme 2.21, bottom) also provides useful information about the conformation of β-fluoro sulfides. As previously discussed (*v. 1.2.2.2 Stereoelectronic and Conformational Properties*), the X–$C_\alpha$–$C_\beta$–F motif (X = electron-withdrawing group) imparts a precise conformational preference in which F and X are disposed in a *syn-clinical* arrangement (gauche effect); this effect, common for oxygen and nitrogen substituents, has recently been extended to include sulfur containing groups.[41] This is confirmed in the solid state structure of **3d**, where the sulfur and fluorine are positioned in a gauche arrangement, with a dihedral angle (Φ) of 52 °.

The fluorination of cyclic bromo sulfide **1b** was also investigated using *bis*-urea **4a**, **4i** and **4k–4l** (Scheme 2.24). Despite a good reactivity, the enantioselectivity of the transformation is substantially lower than what observed for *cis*-stilbene derived substrate**s**. Catalyst **4a** and **4i** give poor enantiocontrol with an enantiomeric ratio of 63.5:36.5 and of 60:40 respectively (*cf.* 82:18 and 68.5:31.5 for **1a** with **4a** and **4i** respectively). In contrast to stilbene derived substrates, *bis*-urea **4k**, featuring saturated rings on the BINAM backbone, proved to be a better catalyst affording an improved enantiomeric ratio of 72:28. Substitution of the 3,3' positions is detrimental leading to a decreased enantiocontrol (67:34 e.r, **4l**) or to a racemic mixture (**4k**).




Scheme 2.22: Chiral catalysts screening with **1b** and chiral *bis*-urea catalysts.

The fluorination of cyclic bromo sulfides **1o–1r** or of the linear analogue **1s,** was carried out with catalyst **4a** (Scheme 2.23). Similarly to six-membered ring **1b**, the reaction provided the fluorinated products **3o–3r** in good yields, however a very poor enantioselectivity was observed. Five-membered sulfide **3o** was obtained in an enantiomeric ratio of 69:31; similarly, the *N*-Boc pyrrolidine derivative **3q** afforded low enantioselectivity with e.r. of 64:36. The seven-membered ring **3p**, the benzo-fused derivative **3r** and the linear substrate **3s** afforded racemic products. These results suggest that expansion of the scope to include β-bromo sulfides **1b** and **1o-1s** will require the design of a novel catalyst for HB PTC.

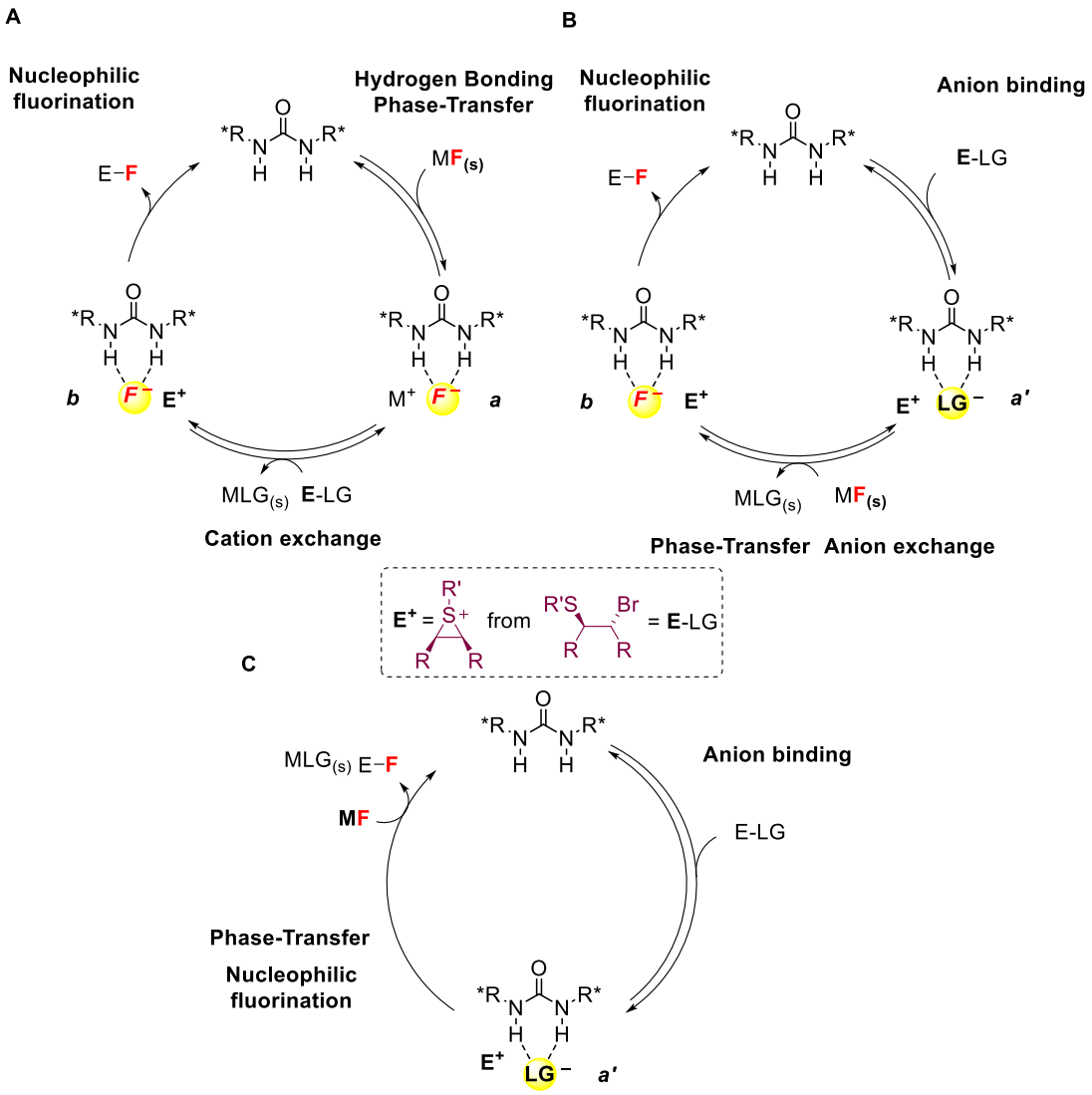



Scheme 2.23: Evaluation of the substrate scope with substrate **1o**–**1s** and catalyst **4a**.

*2.2.3 Preliminary Mechanistic Insights*

*2.2.3.1 Mechanistic Considerations.* We envisage a catalytic system consisting of three fundamental steps: *i)* Formation of a soluble, hydrogen bonded catalyst-fluoride complex; *ii)* formation of a reactive hydrogen bonded ion-pair with an electrophilic substrate and concomitant precipitation of CsBr; *iii)* collapse of the ion-paired intermediate generating the fluorinated product and allowing the urea catalyst to enter another catalytic cycle. Two catalytic cycles were hypothesised. The HBD catalyst can interact firstly with CsF by forming a *bis*-urea–CsF complex (Scheme 2.24 A, ***a***), subsequent cation exchange with the episulfonium ion leads to the formation of the key ion-paired intermediate (***b***) and insoluble CsBr. In an alternative scenario the HBD catalyst can interact directly with the episulfonium bromide, by forming a urea-bromide intermediate (Scheme 2.24 B, ***a'***), this complex is then responsible for anion exchange leading to the reactive ion pair ***b***. In both mechanistic hypotheses, the hydrogen bonded ion pair ***b*** leads to irreversible formation of the fluorinated product. Both catalytic cycles are plausible and can contribute to the formation of the pre-reaction complex ***b,*** however in the absence of a thorough kinetic investigation, discriminating between the two pathways is not trivial. Formation of an episulfonium bromide from a β-bromo sulfide can occur spontaneously or be mediated by the HBD following an anion abstraction pathway. This was investigated computationally by calculating the Gibbs free energy required for both the catalysed pathway (anion abstraction) and the uncatalyzed formation of episulfonium halide (auto ionisation). The system investigated included β-bromo sulfide **1l** and Schreiner's catalyst **2a**. The barriers for the formation of the episulfonium ion with or without urea assistance are very close in energy resulting in the uncatalyzed pathway favoured by 10 kJ/mol. The energetic requirement for the auto-ionization is 90 kJ/mol, suggesting that this could readily occur at room temperature ($k_{TST}$ = 1 x $10^{-3}$ $s^{-1}$, 298 K, computational work carried out by Dr. David

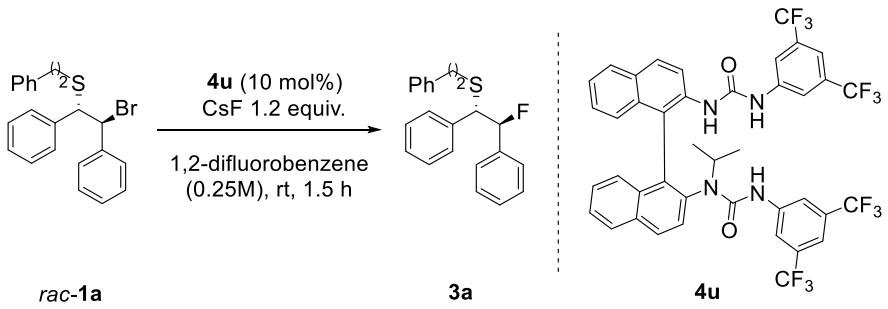
Ascough). An additional mechanistic proposal can be envisioned by taking into consideration the anion binding manifold pioneered by Jacobsen (Scheme 2.24 C). This would require the formation of a urea-bromide reactive ion pair (***a'***) undergoing direct fluorination from CsF. This hypothesis seems unlikely in light of the poor solubility of cesium fluoride under the reaction conditions, suggested by the fact that the reaction does not take place in the absence of catalyst. The experimental observation that a different leaving group (Cl *vs*. Br) result in identical enantioselectivity also strongly advocates against this scenario.




Scheme 2.24: Mechanistic hypotheses for HB PTC fluorination.

*2.2.3.2 Non-Linear Effect Studies.* Studying the relationship between the enantioselectivity of a reaction and the enantiopurity of the catalyst is a common method to gather mechanistic information. Specifically, a nonlinear relationship is often associated with the presence of multiple chiral species in the transition state.[42] Six mixtures of **4u**, with enantiopurity varying between 50.5:49.5 and 99.9:0.1 e.r., were prepared by mixing (*S*)-**4u** and (*R*)-**4u** in different proportions. The enantiopurity of each scalemic mixture was measured by comparing the optical rotation with the one recorded for an enantiopure sample of **4u**. Fluorination of **1a** was carried out with each scalemic mixture and the enantioselectivity measured. For this purpose, the enantiopurity of both product and catalyst is expressed in enantiomeric excess (ee = $|\chi(R) - \chi(S)|$%, $\chi$ = molar fraction) as conventional for these analyses. We found that the enantioselectivity of the process linearly correlates with the enantiopurity of the catalyst, thus strongly suggesting that only one molecule of **4u** is present in the relevant enantiodetermining transition state (Table 2.10).

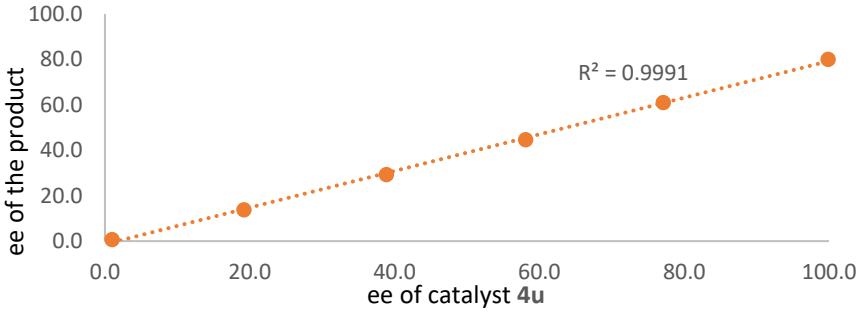
Table 2.10: Non-linear effect studies of catalyst **4u**.




*rac*-**1a** **3a** **4u**

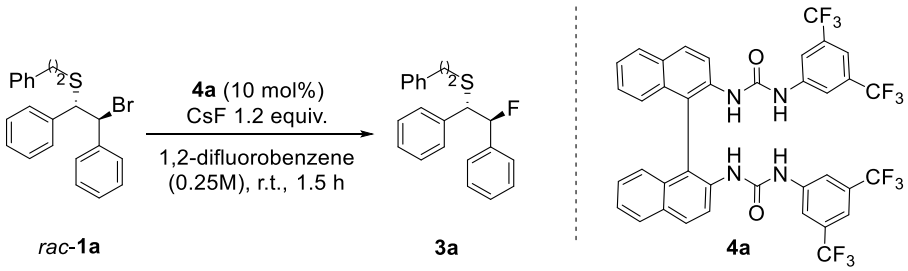
| Entry | ee of catalyst **4u** | ee of product **3a** [a] |
|---|---|---|
| 1 | 1.0 | 0.6 |
| 2 | 19.2 | 13.7 |
| 3 | 38.9 | 29.2 |
| 4 | 58.1 | 44.6 |
| 5 | 77.2 | 61.0 |
| 6 | 99.9 | 80.0 |

[a] The ee of the product was determined by HLPC analysis using a chiral stationary phase at 254 nm; ee = enantiomeric excess = $|\chi(R) - \chi(S)|$%, $\chi$ = molar fraction



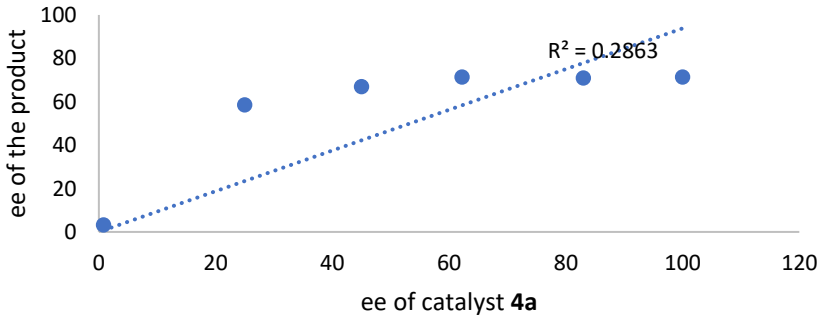

The same study was carried out with the non-alkylated catalyst **4a** (Table 2.11). In this case, a prominent positive non-linear effect (+NLE) was observed.

Table 2.11: Nonlinear effect studies for catalyst **4a**.




| Entry | ee of catalyst **4a** [a] | ee of product **3a** [b] |
|---|---|---|
| 1 | 0.8 | 3.2 |
| 2 | 25 | 58.6 |
| 3 | 45 | 67 |
| 4 | 62.2 | 71.4 |
| 5 | 83 | 71.4 |
| 6 | 99.99 | 71.4 |

[a] (*rac*) and (*S*) mixtures of **4a** were premixed in a ratio between 100:0 and 0:100, respectively; [b] The ee of the catalyst was determined by HLPC analysis using a chiral stationary phase at 254 nm HPLC [†] The ee of the product was determined by HLPC analysis using a chiral stationary phase at 254 nm ee = enantiomeric excess = $|\chi(R) - \chi(S)|$%, $\chi$ = molar fraction



However, an appreciable difference in solubility between the scalemic catalyst mixtures and the enantiopure **4a** was also noticed. This was evident from the different reactivity that (*S*)-BINAM and (*rac*)-BINAM have towards 3,5-bis(trifluoromethyl)phenyl isocyanate in dichloromethane (0.4 M). While enantiopure BINAM reacts over the course of 12 hours, resulting in a clear solution and a mildly exothermic reaction, *rac*-BINAM, under the same conditions, affords an instantaneous precipitate and significant evolution of heat. Racemic **4a** was recovered in quantitative yield by filtration after only 10 minutes. The lower solubility of racemic **4a** can be rationalised through the formation of insoluble heterochiral dimers, (*R*/*S*)-**4a**. Therefore, the presence of a positive non-linear effect may not imply multiple species in the enantio-determining step in this particular case. Interestingly, the same enantioselectivity can be achieved when non-enantiopure (> 50% ee) **4a** is used, since the minor enantiomer of **4a** is scavenged by precipitation of the heterochiral dimer. This phenomenon, generally referred to as self-disproportionation of the enantiomers or optical self-purification, has been object of extensive investigation with implications on the origin of optically pure biomolecules.[43]

*2.2.3.3 Crystal Structure of **4u**:TBAF.* Since the formation of a *bis*-urea-fluoride complex is key in our mechanistic proposal, we focused our efforts to elucidate the structure of **4u**:F at an atomic level. The vigorous reflux of **4u** and tetrabutylammonium fluoride (TBAF·3$H_2O$) in hexane provided a solid complex subsequently recrystallized from slow evaporation of a mixture of diethyl ether and hexane, to afford crystals suitable for single-crystal X-ray diffraction. **4u**:TBAF, in the solid state shows a 1:1 binding mode with the three NH bound to fluoride (Figure 2.2). The isopropyl group points towards the binaphthyl scaffold showing that the *N*-isopropylated urea adopts a *syn*-*anti* conformation to better accommodate fluoride. The large counter-cation is located in proximity of the catalytic pocket, and notably, no

molecules of water are observed in the crystal lattice. The angle between the two ureas and $F^-$ (C–F–C, Figure 2.1) measures 69 °, with the alkylated urea twisted out of the plane described by the adjacent naphthyl ring by 60 °, while the bidentate urea is twisted by 30 °. The dihedral angle between the two naphthyl rings of the BINAM scaffold measures 74 °. The high quality of the crystal generated strong diffraction data; therefore, the individual positions of the hydrogen atoms were revealed in the Fourier difference map, hence relevant internuclear distances and angles describing hydrogen bonding to fluoride could be reliably measured and compared (Table 2.12). It is worth noticing that measuring the position of H-atoms by X-ray diffraction is intrinsically problematic since the electron density of a hydrogen atom, bound to electronegative atoms, generally does not coincide with its centre of mass. Therefore, the absolute H···A distances (A = HB acceptor) measured from X-ray diffraction must be considered with great care, while relative measurements within the crystal structure are accurate. In **4u**:TBAF, the two NH adjacent to the 3,5-bis-(trifluoromethyl)phenyl groups, NH(a) and NH(b), display the shortest hydrogen bonds. The distances measured from the heteroatom are very similar (**N**H(a)···**F**$^-$ = 2.661 Å; **N**H(b)-**F**$^-$ = 2.668 Å), while the hydrogen bond lengths indicate that N**H**(a)···**F**$^-$ is 0.02 Å shorter than N**H**(b)···**F**$^-$. NH(c), proximal to the BINAM scaffold, displays the longest HB (N**H**(c)···**F**$^-$ = 1.922 Å). The three NH···F$^-$ present a similar hydrogen bond angle (∠ N–H–F) of 154 ° for NH(a), 155 ° for NH(b), and 152 ° for NH(c). A fourth short-contact is present between the *ortho* aromatic proton adjacent to the alkylated urea and fluoride, CH(d)···F$^-$. The angle C–H–F significantly deviates from linearity (∠ C–H–F = 129 °) and interatomic distances are substantially longer than the one measured for NH···F$^-$ (C**H**(d)···**F**$^-$ = 2.359 Å). This interaction, although presumably weak, is believed to be important, since *ortho*-substituted *bis*-ureas are not competent catalysts (< 5 % yield with **4g** and **4h**, Scheme 2.15).

The participation of *ortho*-aromatic protons as additional binding sites is favoured by the increased acidity derived by the vicinal trifluoromethyl groups.[40]

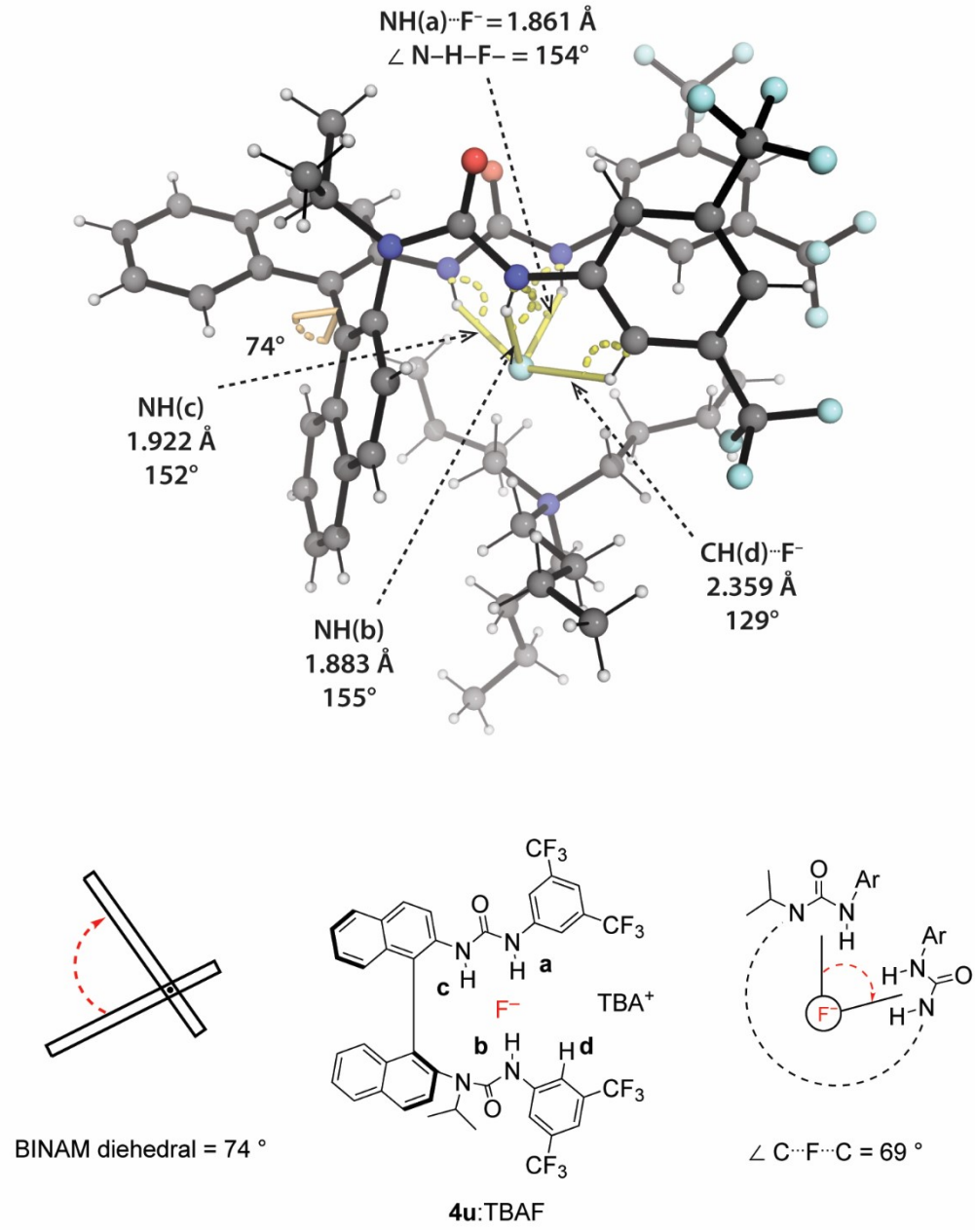



Figure 2.2: X-ray structure of **4u**:TBAF. SCXRD data acquired and solved by Dr. K Chirstensen.

Table 2. 12: Relevant internuclear distances and angles of **4u**:TBAF; D = HB donor, A = HB acceptor.

| DH···A | *d* D–H [Å] | *d* D–A [Å] | *d* H···A [Å] | ∠ X –H–F [°] |
|---|---|---|---|---|
| NH(a)···F⁻ | 0.870 | 2.661 | 1.861 | 154 |
| NH(b)···F⁻ | 0.833 | 2.668 | 1.883 | 155 |
| NH(c)···F⁻ | 0.840 | 2.691 | 1.922 | 152 |
| CH(d)···F⁻ | 0.963 | 3.058 | 2.359 | 129 |

*2.2.3.4 Transition States Analyses.* The low energies transition states (TS) leading to the major and minor enantiomer of **3k** (S-$R_1$ = S–$CH_3$) with *N*-isopropylated catalyst **4u**, were optimised using DFT calculations to gain insights into the origin of enantioselectivity in HB PTC. The first striking observation is that the computed structures of both major and minor TS are remarkably similar to the crystal structure of **4u**:TBAF determined by X-ray crystallography, with the substrate in the TS that occupies the position of the cation (tetrabutylammonium) in the crystal structure (Figure 2.3).

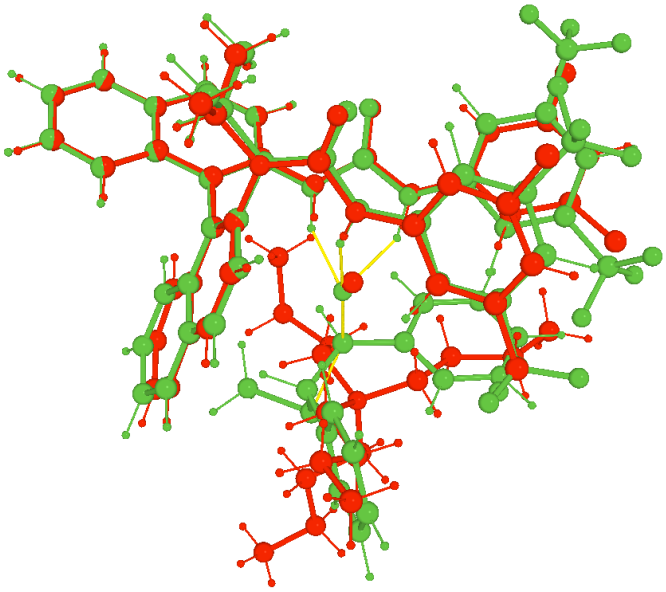


Figure 2.3: Overlay of the X-ray crystal structure of **4u**:TBAF (red) and the major TS computed using DFT calculation. Computational work performed by Dr. David Ascough. Adapted with permission form reference 1.

In both TS the catalyst interacts with the substrate *via* non-covalent interactions which are key to determine the observed selectivity. A cation-π interaction occurs between the episulfonium ion and one of the naphthyl rings of the BINAM scaffold; additionally, a CH-π interaction between the *ortho* aromatic proton of the catalyst and one phenyl ring of the substrate, substantially contribute to the stabilisation of the transition state. In both TS the catalyst displays intramolecular π–π stacking between the two 3,5-substituted aryl rings

(Figure 2.4). Catalyst–substrate noncovalent interactions are similar in the two competing transition states, however, a shorter distance for the crucial cation-π interaction is observed in the major TS. This is ultimately responsible for the energetic difference ($\Delta\Delta G^{\ddagger}$) and consequently for the observed enantioselectivity. The low enantioselectivity measured for substrates **1b** and **1o–1s**, which do not possess the aromatic groups featured in the stilbene-derived substrates, can be ascribed to a reduced stabilization in the transition states caused by the absence of cation-π and CH- π non-covalent interactions.

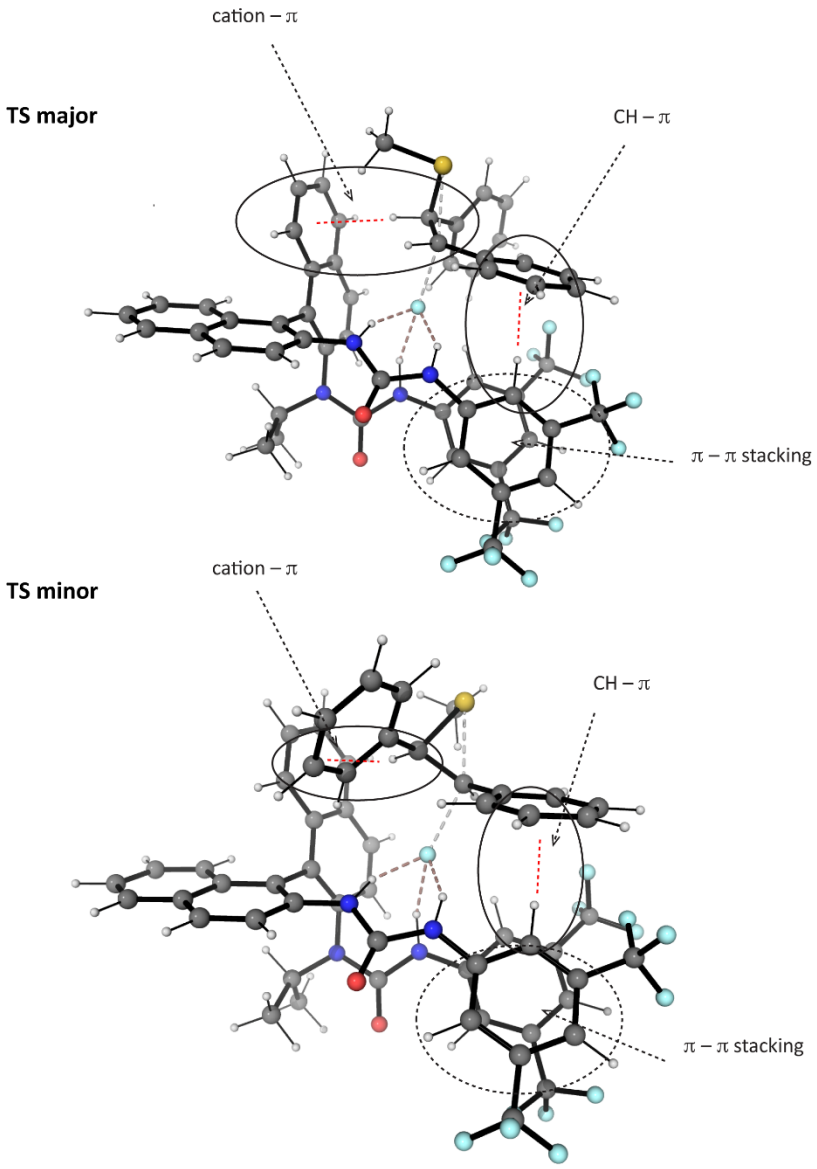



Figure 2.4: Major and minor TS computed using DFT calculation. Computational work performed by Dr. David Ascough. Adapted with permission form reference 1.

## 2.3 Conclusions

Herein, we described the developed of the first catalytic protocol for asymmetric fluorination using alkali metal fluorides as a safe, economical, easy-to-use and readily available source of fluorine. In a conceptually novel catalytic manifold, hydrogen bonding is employed to modulate the reactivity and enantioselectivity of fluoride salts while also regulating their solubility in organic solvents. This approach is distinct from previous examples of hydrogen bonding anion-binding catalysis, as the catalyst-bound anion is itself the nucleophile for fluorination. To overcome the inherently faster uncatalysed racemic pathway, the poor solubility of alkali metal fluorides in organic solvents was used as an expedient to limit the presence of unbound fluoride in solution. The design of a novel class of chiral *N*-alkylated bis-ureas was crucial for the success of the methodology. Employing Hydrogen Bonding Phase-Transfer Catalysis we were able to access β-fluoro sulfides in high yields and enantioselectivities with an operationally simple and cost-effective protocol. We aim in the future to expand the scope of HB PTC allowing selective fluorination of a wide range of substrates. In addition, the industrial applications of this methodology is an appealing outlook, in view of the simplicity of the protocol and of the value of fluorinated compounds across medicinal chemistry.

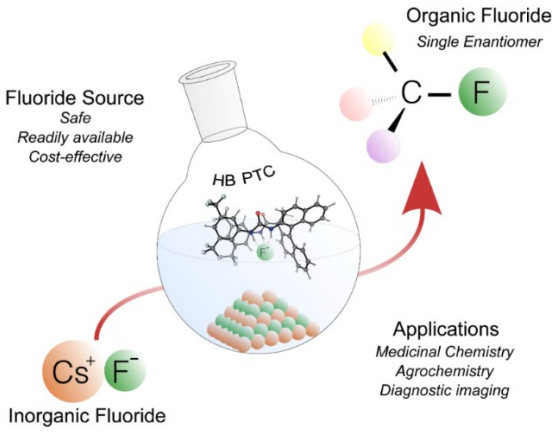



Figure 2.5: Hydrogen Bonding Phase-transfer Catalysis

## 2.4 References


(1) Pupo, G.; Ibba, F.; Ascough, D. M. H.; Vicini, A. C.; Ricci, P.; Christensen, K. E.; Pfeifer, L.; Morphy, J. R.; Brown, J. M.; Paton, R. S.; et al. Asymmetric Nucleophilic Fluorination under Hydrogen Bonding Phase-Transfer Catalysis. *Science* **2018**, *360*, 638–642.

(2) Starks, C. M. Phase-Transfer Catalysis. I. Heterogeneous Reactions Involving Anion Transfer by Quaternary Ammonium and Phosphonium Salts. *J. Am. Chem. Soc.* **1971**, *93* (1), 195–199.

(3) Starks, C. M.; Liotta, C. L.; Halpern, M. *Phase-Transfer Catalysis: Fundamentals, Applications and Industrial Perspectives.*; Chapman & Hall: London, 1994.

(4) *Handbook of Phase Transfer Catalysis*; Sasson, Y., Neumann, R., Eds.; Springer Netherlands: Dordrecht, 1997.

(5) Fiaud, J. C. Asymmetric Alkylation Reaction by Means of a Chiral Phase Transfer Catalyst. *Tetrahedron Lett.* **1975**, *16* (40), 3495–3496.

(6) Helder, R.; Hummelen, J. C.; Laane, R. W. P. M.; Wiering, J. S.; Wynberg, H. Catalytic Asymmetric Induction in Oxidation Reactions. The Synthesis of Optically Active Epoxides. *Tetrahedron Lett.* **1976**, *17* (21), 1831–1834.

(7) Colonna, S.; Re, A.; Wynberg, H. Asymmetric Induction in the Michael Reaction by Means of Chiral Phase-Transfer Catalysts Derived from Cinchona and Ephedra Alkaloids. *J. Chem. Soc. Perkin Trans. 1* **1981**, 547.

(8) Juliá, S.; Ginebreda, A. Asymmetric Induction by Phase-Transfer Catalysis Using Chiral Catalysts. Synthesis of 1,2-Dichloroalkanes and Acetylcyanohydrins. *Tetrahedron Lett.* **1979**, *20* (23), 2171–2174.

(9) Dolling, U. H.; Davis, P.; Grabowski, E. J. J. Efficient Catalytic Asymmetric Alkylations. 1. Enantioselective Synthesis of (+)-Indacrinone via Chiral Phase-Transfer Catalysis. *J. Am. Chem. Soc.* **1984**, *106* (2), 446–447.

(10) Maruoka, K. *Asymmetric Phase Transfer Catalysis*; Wiley-VCH: Weinheim, 2008.

(11) Shirakawa, S.; Maruoka, K. Recent Developments in Asymmetric Phase-Transfer Reactions. *Angew. Chem. Int. Ed.* **2013**, *52* (16), 4312–4348.

(12) Makosza, M. Reactions of Organic Anions. XI. Catalytic Alkylation of Indene. *Tetrahedron Lett.* **1966**, *7* (38), 4621–4624.

(13) Ooi, T.; Ohara, D.; Tamura, M.; Maruoka, K. Design of New Chiral Phase-Transfer Catalysts with Dual Functions for Highly Enantioselective Epoxidation of α,β-Unsaturated Ketones. *J. Am. Chem. Soc.* **2004**, *126* (22), 6844–6845.

(14) Liotta, C. L.; Harris, H. P. The Chemistry of “Naked” Anions. I. Reactions of the 18-Crown-6 Complex of Potassium Fluoride with Organic Substrates in Aprotic Organic Solvents. *J. Am. Chem. Soc.* **1974**, *96* (7), 2250–2252.

(15) Ooi, T.; Maruoka, K. Asymmetric Organocatalysis of Structurally Well-Defined Chiral Quaternary Ammonium Fluorides. *Acc. Chem. Res.* **2004**, *37* (8), 526–533.

(16) Ooi, T.; Doda, K.; Maruoka, K. Distinct Advantage of the in Situ Generation of Quaternary Ammonium Fluorides under Phase-Transfer Conditions toward Catalytic Asymmetric Synthesis. *Org. Lett.* **2001**, *3* (9), 1273–1276.

(17) Corey, E. J.; Zhang, F. Y. Re- and Si-Face-Selective Nitroaldol Reactions Catalyzed by a Rigid Chiral Quaternary Ammonium Salt: A Highly Stereoselective Synthesis of the HIV Protease Inhibitor Amprenavir (Vertex 478). *Angew. Chem. Int. Ed.* **1999**, *38* (13–14), 1931–1934.

(18) Doyle, A. G.; Jacobsen, E. N. Small-Molecule H-Bond Donors in Asymmetric Catalysis. *Chem. Rev.* **2007**, *107* (12), 5713–5743.

(19) Mattson, A. E. Tricks for Noncovalent Catalysis. *Science* **2017**, *358* (6364), 720.

(20) Pihko, P. Introduction. In *Hydrogen Bonding in Organic Synthesis*; John Wiley & Sons, Ltd, 2009.

(21) Ford, D. D.; Lehnherr, D.; Kennedy, C. R.; Jacobsen, E. N. Anion-Abstraction Catalysis: The Cooperative Mechanism of α-Chloroether Activation by Dual Hydrogen-Bond Donors. *ACS Catal.* **2016**, *6* (7), 4616–4620.

(22) Banik, S. M.; Levina, A.; Hyde, A. M.; Jacobsen, E. N. Lewis Acid Enhancement by Hydrogen-Bond Donors for Asymmetric Catalysis. *Science* **2017**, *358* (6364), 761–764.

(23) Xu, H.; Zuend, S. J.; Woll, M. G.; Tao, Y.; Jacobsen, E. N. Asymmetric Cooperative Catalysis of Strong Bronsted Acid-Promoted Reactions Using Chiral Ureas. *Science* **2010**, *327* (5968), 986–990.

(24) Taylor, M. S.; Jacobsen, E. N. Highly Enantioselective Catalytic Acyl-Pictet-Spengler Reactions. *J. Am. Chem. Soc.* **2004**, *126* (34), 10558–10559.

(25) Taylor, M. S.; Tokunaga, N.; Jacobsen, E. N. Enantioselective Thiourea-Catalyzed Acyl-Mannich Reactions of Isoquinolines. *Angew. Chem. Int. Ed.* **2005**, *44* (41), 6700–6704.

(26) Reisman, S. E.; Doyle, A. G.; Jacobsen, E. N. Enantioselective Thiourea-Catalyzed Additions to Oxocarbenium Ions. *J. Am. Chem. Soc.* **2008**, *130* (23), 7198–7199.

(27) Smit, W. A.; Zefirov, N. S.; Bodrikov, I. V.; Krimer, M. Z. Episulfonium Ions: Myth and Reality. *Acc. Chem. Res.* **1979**, *12* (8), 282–288.

(28) Lin, S.; Jacobsen, E. N. Thiourea-Catalysed Ring Opening of Episulfonium Ions with Indole Derivatives by Means of Stabilizing Non-Covalent Interactions. *Nat. Chem.* **2012**, *4* (10), 817–824.

(29) Hamilton, G. L.; Kanai, T.; Toste, F. D. Chiral Anion-Mediated Asymmetric Ring Opening of meso-Aziridinium and Episulfonium Ions. *J. Am. Chem. Soc.* **2008**, *130* (45), 14984–14986.

(30) Schreiner, P. R.; Wittkopp, A. H-Bonding Additives Act like Lewis Acid Catalysts. *Org. Lett.* **2002**, *4* (2), 217–220.

(31) Kotke, M.; Schreiner, P. R. Acid-Free, Organocatalytic Acetalization. *Tetrahedron* **2006**, *62* (2–3), 434–439.

(32) Zhang, Z.; Schreiner, P. R. (Thio)Urea Organocatalysis - What Can Be Learnt from Anion Recognition? *Chem. Soc. Rev.* **2009**, *38* (4), 1187–1198.

(33) Wang, Z. Zincke Disulfide Cleavage. *Compr. Org. Name React. Reagents* **2010**, No. 2, 3163–3167.

(34) Owsley, D. C.; Helmkamp, G. K.; Rettig, M. F. Episulfonium Salts. II. Detection of an Unusual Intermediate in the Reaction of a Stable Episulfonium Salt with Chloride Ion. *J. Am. Chem. Soc.* **1969**, *91* (19), 5239–5242.

(35) Kharasch, N.; Buess, C. M. Derivatives of Sulfenic Acids. II. Characterization of Olefins with 2,4-Dinitrobenzenesulfenyl Chloride. *J. Am. Chem. Soc.* **1949**, *71* (8), 2724–2728.

(36) Walvoord, R. R.; Huynh, P. N. H.; Kozlowski, M. C. Quantification of Electrophilic Activation by Hydrogen-Bonding Organocatalysts. *J. Am. Chem. Soc.* **2014**, *136* (45), 16055–16065.

(37) Rötheli, A. R. A Mechanistic Approach towards Highly Efficient Anion-Binding Catalysts, Harvard University, 2016.

(38) Jakab, G.; Tancon, C.; Zhang, Z.; Lippert, K. M.; Schreiner, P. R. (Thio)Urea Organocatalyst Equilibrium Acidities in DMSO. *Org. Lett.* **2012**, *14* (7), 1724–1727.

(39) Sun, L.; Wu, X.; Xiong, D. C.; Ye, X. S. Stereoselective Koenigs–Knorr Glycosylation Catalyzed by Urea. *Angew. Chem. Int. Ed.* **2016**, *55* (28), 8041–8044.

(40) *CRC Handbook of Chemistry and Physics, 84th Edition*; Lide, D. R., Ed.; CRC Press: Boca Raton, 2003.

(41) Santschi, N.; Thiehoff, C.; Holland, M. C.; Daniliuc, C. G.; Houk, K. N.; Gilmour, R. The Sulfur-Fluorine Gauche Effect in Coinage-Metal Complexes: Augmenting Conformational Equilibria by Complexation. *Organometallics* **2016**, *35* (17), 3040–3044.

(42) Satyanarayana, T.; Abraham, S.; Kagan, H. B. Nonlinear Effects in Asymmetric Catalysis. *Angew. Chem.*

*Int. Ed.* **2009**, *48* (3), 456–494.

(43) Soloshonok, V. A.; Ueki, H.; Yasumoto, M.; Mekala, S.; Hirschi, J. S.; Singleton, D. A. Phenomenon of Optical Self-Purification of Chiral Non-Racemic Compounds. *J. Am. Chem. Soc.* **2007**, *129* (40), 12112–12113.

(44) Lippert, K. M.; Hof, K.; Gerbig, D.; Ley, D.; Hausmann, H.; Guenther, S.; Schreiner, P. R. Hydrogen-Bonding Thiourea Organocatalysts: The Privileged 3,5-Bis(Trifluoromethyl)Phenyl Group. *Eur. J. Org. Chem.* **2012**, No. 30, 5919–5927.

# 3. Structure and Conformation of *bis*-Urea Catalysts for Hydrogen Bonding Phase-Transfer Catalysis: Insights from NMR Spectroscopy

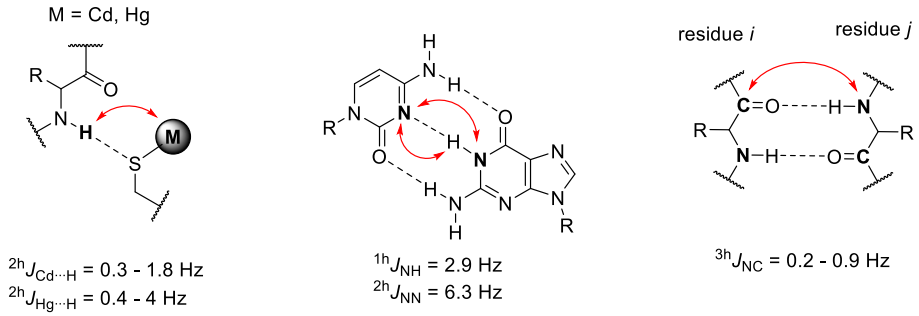
## 3.1 Introduction

### *3.1.1 NMR Spectroscopy of Hydrogen Bonded Systems*

Since its inception in 1945, NMR spectroscopy has been extensively used in deriving information about hydrogen bonding and hydrogen bonded species in solution. The presence of a hydrogen bond is usually detected by observing the variation in the chemical shift of all the nuclei involved in the H-bond. Protons always display shift to higher frequency (deshielding) when engaged in hydrogen bonding, as a consequence of the reorganization on the local electronic environment. Alongside chemical shifts, a number of other NMR observables can be related to the presence of hydrogen bonds; these include primary and secondary isotopic shifts, $^{1}H/^{2}H$ exchange rates and relaxation effects.[1] More recently, direct evidence for the presence of hydrogen bonds was found by the observation of scalar coupling between NMR active nuclei present on each side of the hydrogen bridge.[2,3]

*3.1.1.1 Hydrogen Bond Coupling.* Until the end of the 1990s, the notion of scalar *J*-coupling was almost entirely associated with sharing of electrons through covalent bonds. Nowadays, it is universally accepted that the coupling information can also be transmitted across hydrogen bonds. The designations $^{nh}J_{AB}$ (also $^{hn}J_{AB}$) is found in the modern literature to indicate spin-spin coupling between nuclei A and B across the hydrogen bond. The superscript *h* emphasises the participation of at least one hydrogen bond to the coupling mechanism. Pioneering contributions from Bax *et al.* reported the two-bonds hydrogen bonding couplings (HBC) $^{2h}J_{^{133}Cd-^{1}H}$ and $^{2h}J_{^{199}Hg-^{1}H}$ in metal-substituted rubredoxin, where amide protons are

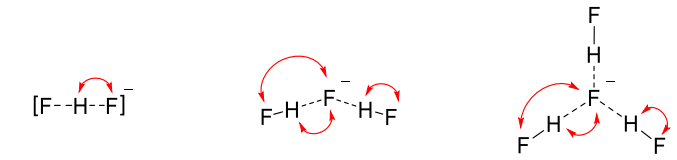
hydrogen bonded to a sulfur of a cysteine bound to a metal.[4] The magnitude of this coupling was between 0.3 Hz and 4 Hz for the cadmium substituted protein and between 0.4 Hz and 4 Hz for the mercury substituted one (Scheme 3.1). In 1998, Dingley and Grzesiek were the first to recognise the potential of HBC as a tool for the structural determination of biomolecules.[5] In their work, Watson-Crick base pairs were successfully characterised through the detection of inter-nucleotide hydrogen bond coupling, $^{2h}J_{NN}$, which measured 6–11 Hz and $^{1h}J_{NH}$ of 1–3 Hz (Scheme 3.1).[6] More recently, detection of HBC in proteins evolved as a valuable tool in biomolecule NMR.[7] The detection of inter-residual $^{3h}J_{NC}$ in protein backbones was extensively used to study protein secondary structure and conformational behaviour. A large number of empirical observations and theoretical studies on H-bond coupling indicate that this parameter is determined by the spatial arrangement of the donor and acceptor groups, depending exponentially on both distance and geometry of the hydrogen bond interaction.[8] In addition, a similar coupling mechanism to conventional *covalent* scalar coupling seems to be operative for HBC, sparking the debate about the covalency of hydrogen bonds.




Scheme 3.1: Example of hydrogen bonding coupling (HBC) in biomolecules.

For HBC to be detected, three conditions have to be met: *i)* at least one nucleus involved in the HB has to have quantum spin number of 1/2, most commonly encountered for $^{1}H$, $^{13}C$, $^{15}N$, $^{19}F$ and $^{31}P$. *ii)* The hydrogen bond has to be intermediate or strong. *iii)* The hydrogen bonding network must be rigid. This last condition is often verified for bio-macromolecules,

held together by multiple hydrogen bonds but it is far less common in small-molecules.[9] However, observations of hydrogen bond coupling have been reported for small-molecules. Some examples were presented in the introductory chapter (*v. 1.2.2.3 Hydrogen bonding properties of the C–F bond*) discussing the C–F···H–O hydrogen bond which, in some cases, displays $^{1h}J_{FH}$ with values between 5 and 30 Hz. Shenderovich and Limbach studied $^{1h}J_{FH}$ in the strongly bound clusters generated by $F^-$ and HF, $[F(HF)_n]^-$, in liquefied freon mixtures ($CDF_3/CDClF_2$) at low temperature (100 – 150 K).[10] The work reported values of $^{1h}J_{FH}$ largely dependent on the geometry of the complex. The linear $[F{\cdots}H{\cdots}F]^-$ showed $^{1h}J_{FH}$ of 124 Hz, the dimeric $[F(HF)_2]^-$ of 24 Hz, while the tricoordinate fluoride adduct, $[F(HF)_3]^-$, presented a $^{1h}J_{FH}$ of 41 Hz (Scheme 3.2). Few examples of particularly stable anion-receptors were reported in the literature showing HBC with fluoride, often measured at low temperature, however no additional information was derived from these values.[11–15]




$^{1h}J_{FH}$ = 124 Hz

$^{1}J_{FH}$ = 354 Hz
$^{2h}J_{FF}$ = 146 Hz
$^{1h}J_{FH}$ = 24 Hz

$^{1}J_{FH}$ = 430 Hz
$^{2h}J_{FF}$ = 92 Hz
$^{1h}J_{FH}$ = 41 Hz

Scheme 3.2: NMR characterisation of hydrogen bonded clusters between $F^-$ and HF

### 3.1.2 NMR Studies on Hydrogen Bonding Phase Transfer Catalysis

The fundamental discovery that chiral *bis*-ureas can serve as catalysts for asymmetric fluorination *via* hydrogen bonding to fluoride has been described in the previous chapter. In the development of Hydrogen Bonding Phase-Transfer Catalysis a novel class of phase-transfer catalysts was disclosed. To achieve the desired reactivity and selectivity we tuned a BINAM derived *bis*-urea, finding that alkylation of a specific nitrogen was important to ensure

good enantiocontrol. Although initial insights were gained with structural studies in the solid state complemented by DFT calculations, detailed information in solution was unknown.

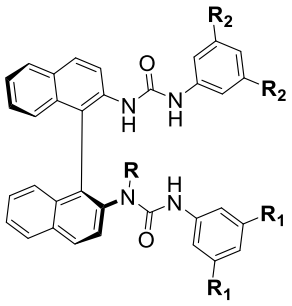
We reasoned that NMR spectroscopy would have been an excellent technique to explore our catalytic system in solution. A detailed spectroscopic investigation is presented, aiming at unveiling the conformational preferences of *bis*-urea catalysts in solution, their ability to coordinate fluoride anions and which structural features influence their reactivity and enantioselectivity in HB PTC.

## 3.2 Results and Discussion

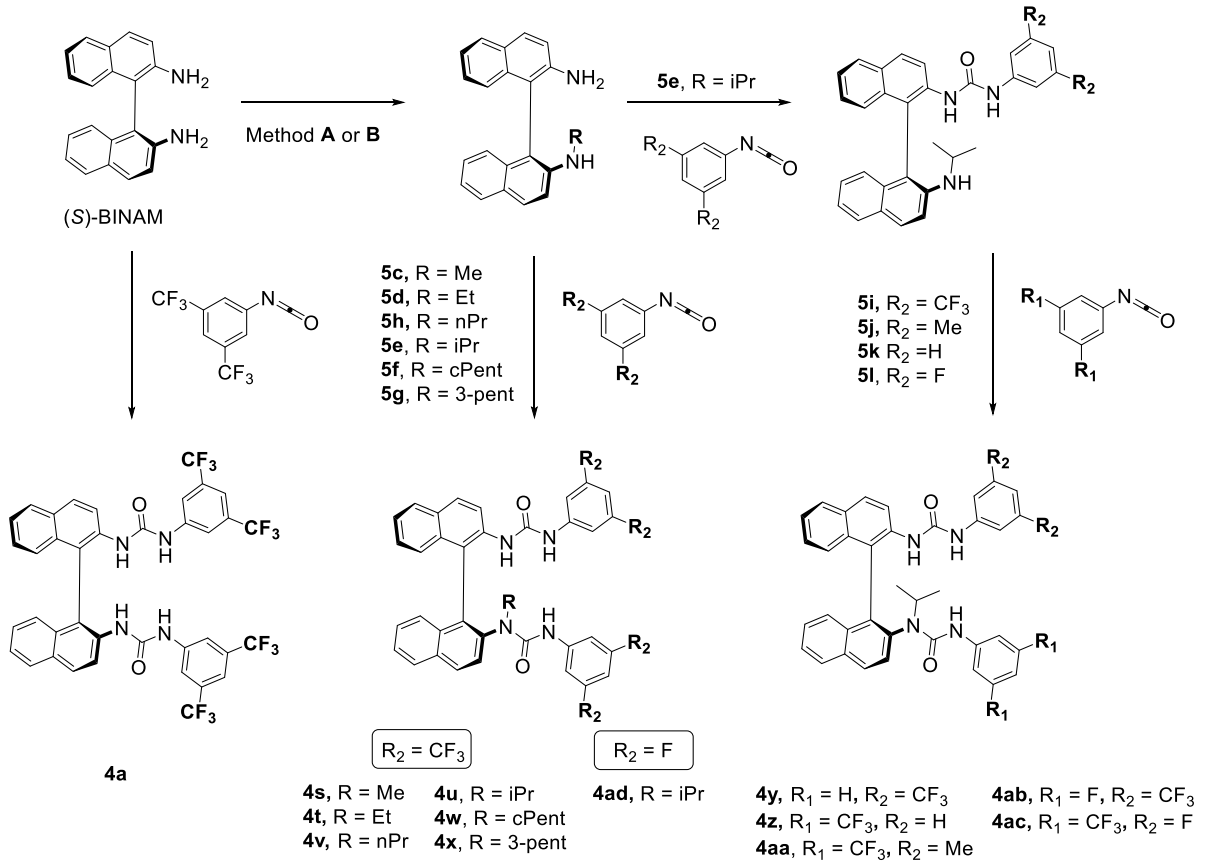
### *3.2.1 Catalyst Synthesis*

We selected and synthesised a library of thirteen BINAM *bis*-ureas to study how rational modifications of the catalyst impact their conformation, the conformation of the corresponding fluoride complexes, and how this affects catalytic performance. Alongside non-alkylated BINAM *bis*-urea (**4a**, R = H, $R_1 = R_2 = CF_3$), and isopropylated **4u** (R = iPr, $R_1 = R_2 = CF_3$), five alkylated analogues **4s** (R = Me), **4t** (R = Et), **4v** (R = nPr,), **4w** (R = cyclopentyl) **4x** (R = 3-pentyl), bearing the 3,5-bis(trifluoromethyl) phenyl groups ($R_1 = R_2 = CF_3$) and six isopropylated (R = iPr) analogues bearing differently substituted phenyl rings **4y** ($R_1$ = H, $R_2 = CF_3$), **4z** ($R_1 = CF_3$, $R_2$ = H), **4aa** ($R_1 = CF_3$, $R_2$ = Me), **4ab** ($R_1$ = F, $R_2 = CF_3$) **4ac** ($R_1 = CF_3$, $R_2$ = F), **4ad** ($R_1 = R_2$ = F) were investigated (Table 3.1).

Table 3.1: General structure of *bis*-urea catalysts investigated in this study.




| Catalyst | R | $R_1$ | $R_2$ |
|---|---|---|---|
| **4a** (BINAM Urea) | H | $CF_3$ | $CF_3$ |
| **4u** (iPr BINAM Urea) | iPr | $CF_3$ | $CF_3$ |
| **4s** | Me | $CF_3$ | $CF_3$ |
| **4t** | Et | $CF_3$ | $CF_3$ |
| **4v** | nPr | $CF_3$ | $CF_3$ |
| **4w** | cPentyl | $CF_3$ | $CF_3$ |
| **4x** | 3-pentyl | $CF_3$ | $CF_3$ |
| **4y** | iPr | H | $CF_3$ |
| **4z** | iPr | $CF_3$ | H |
| **4aa** | iPr | $CF_3$ | Me |
| **4ab** | iPr | F | $CF_3$ |
| **4ac** | iPr | $CF_3$ | F |
| **4ad** | iPr | F | F |




Scheme 3.3: Synthesis of *bis*-urea catalysts. Method A = reductive amination; Method B = three-step sequence a) amidation b) alkylation c) hydrolysis. See Experimental for details.

The synthesis of catalysts with a different *N*-alkyl group followed the procedure described for *N*-isopropylated **4u** (*v. 2.2.2.3 N-Alkylated bis-Urea Catalysts*). The corresponding *N*-alkylated BINAM **5c**–**5g** were reacted with 3,5-bis(trifluoromethyl)phenyl isocyanate to generate **4s**–**4x** or with 3,5-difluorophenyl isocyanate to obtain **4ad**. The non-alkylated amino group ($NH_2$) was invariably more reactive than its alkylated counterpart (NHR). The reactivity of NHR depends critically on the nature of the R substituent. Accordingly, the synthesis of *bis*-ureas featuring bulky or electron-withdrawing groups on the nitrogen, such as R = Ph, R = 2-adamanthly or R = $CF_3CH_2$ proved unsuccessful. Catalysts **4y**–**4ac** required the formation of the *mono*-urea **5i**–**5l** and a second addition of isocyanate to obtain the desired product.

*3.2.2 Conformational properties of bis-urea catalysts*

At the onset of our investigation, we sought to gain insights into the ground state conformation of the *bis*-urea catalysts in solution. The optimal solvents used successfully for fluorination under HB PTC included 1,2-difluorobenzene, chloroform or dichloromethane. Spectra were recorded in DCM-$d_2$ because of its non-coordinating nature, its optimal chemical shift dispersion, and favourable temperature range. When possible, the standard concentration was set to 25 mM to mimic the reaction conditions.

*3.2.2.1 BINAM Urea (**4a**) vs. iPr BINAM Urea (**4u**).* To study whether *N*-alkylation can impart structural and conformational changes to the catalyst, a collection of NMR data for the non-alkylated BINAM Urea **4a** and for the isopropylated analogue **4u** were acquired and their spectroscopic features compared. The $^{1}H$ and $^{13}C$ NMR spectra of **4a** in DCM-$d_2$ show uniformly sharp peaks (Figure 3.1). The protons belonging to the binaphthyl moieties are progressively more shielded moving away from the urea group, H(3) to H(8), while the protons of the 3,5-bis(trifluoromethyl)phenyl ring are ascribed to the sharp singlets at 7.6 and 7.4 ppm. NH are recorded at 7.1 and 6.7 ppm; discrimination between the two pairs was accomplished by $^{1}H$-$^{13}C$ HMBC and $^{1}H$-$^{15}N$ HMBC resulting in more deshielded NH(a/b) compared to NH(c/d) This is consistent with their electronic properties, since the acidity of NH(a/b) is enhanced by the 3,5-bis(trifluoromethyl)phenyl substituents.

$^{1}H$ NMR spectra measured between 2 and 64 mM shows that **4a** displays significant chemical shift variations upon increased concentration (Figure 3.2). Protons bound to carbons experience shielding ($\Delta\delta$ H(11) = -211 ppb), while NH are deshielded ($\Delta\delta$ NH(c/d) = +227 ppb); a behaviour consistent with intermolecular aggregation.

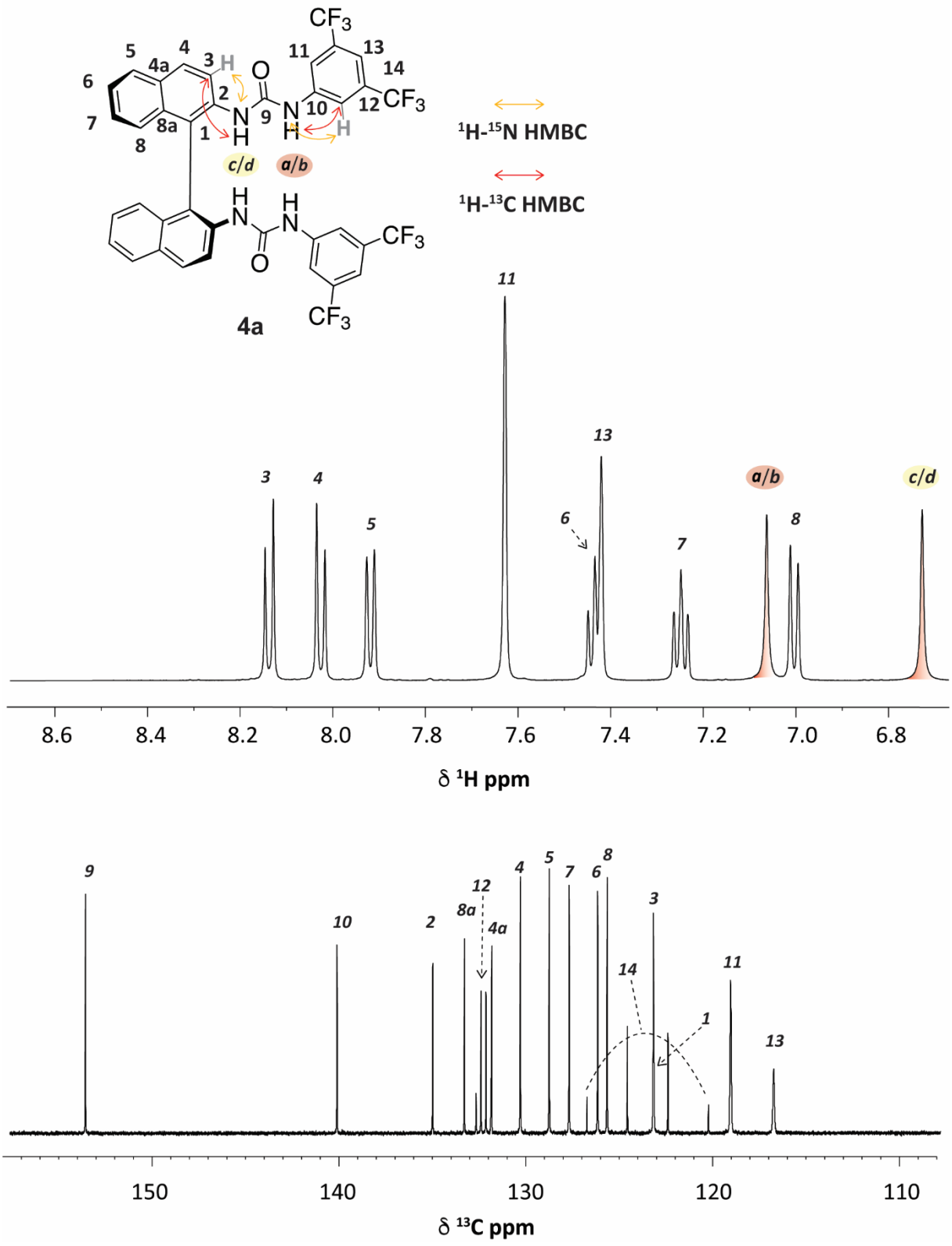



Figure 3.1: $^{1}H$ NMR (DCM-$d_2$, 25 mM, 298 K) and $^{13}C$ NMR (DCM-$d_2$, 40 mM, 298 K), spectra of **4a** see Experimental for details.

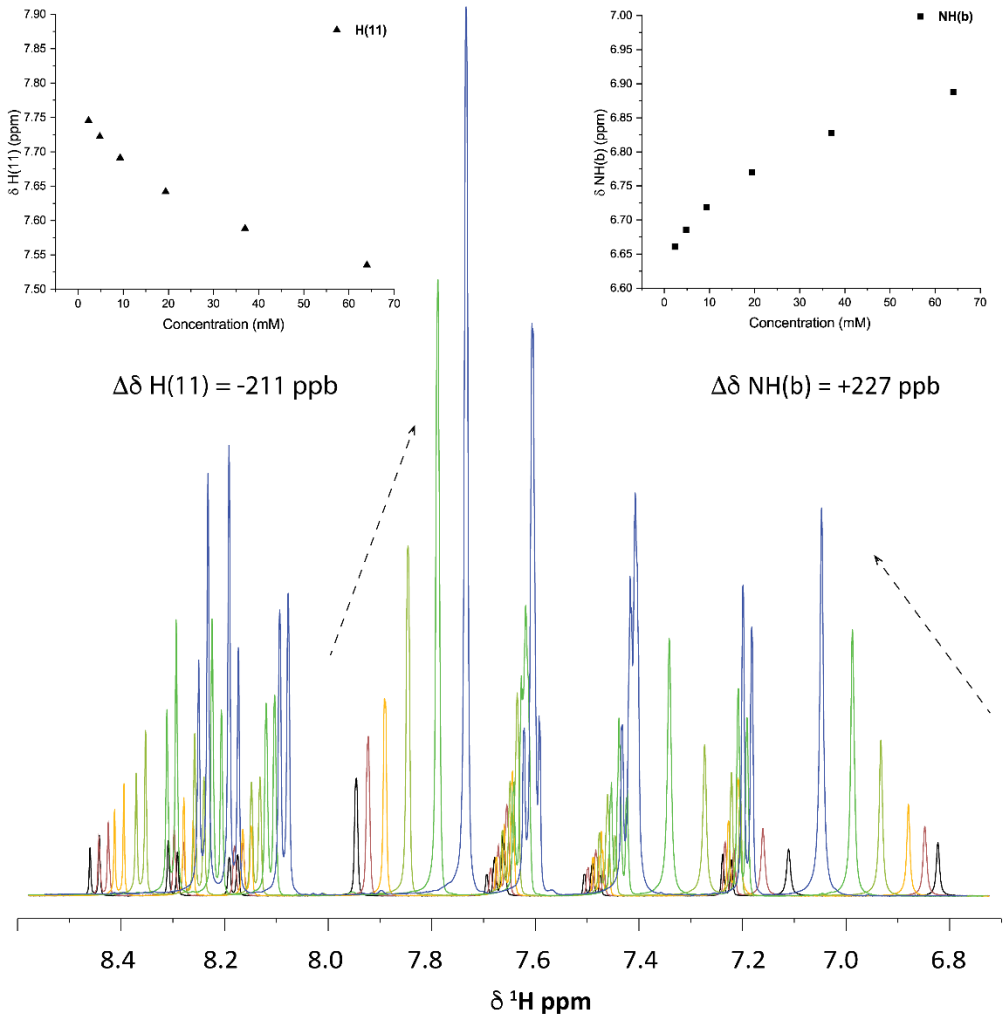



Figure 3.2: Stacked $^{1}$H NMR of **4a** 2–64 mM (DCM-$d_2$, 298 K).

Isopropylated **4u** does not possess the $C_2$-symmetry axis present in **4a**, a feature that complicates the interpretation of the NMR spectra. A combination of mono- and two-dimensional NMR experiments were used in the assignment of **4u** (Figure 3.3). Specifically, $^{1}$H-$^{13}$C HMBC, $^{1}$H-$^{15}$N HMBC and $^{1}$H-$^{15}$N HSQC were employed to discriminate between the two non-symmetric halves of the molecule. Key correlations connected the isopropyl C–H proton with the adjacent carbonyl, $^{3}J$ H(16) ⇔ C(9), and with the naphthyl ring, $^{3}J$ H(16) ⇔ C(2), $^{3}J$ C(2) ⇔ H(4); this allowed to differentiate between the two naphthyl rings. Similarly, $^{1}$H-$^{13}$C HMBC cross-peaks $^{2}J$ C(9') ⇔ NH(a), $^{3}J$ NH(a) ⇔ H(11') were used to distinguish between the

two 3,5-(trifluoromethyl)phenyl rings. With this information, $^{1}$H-$^{1}$H COSY and $^{1}$H-$^{13}$C HSQC sequences allowed for the unambiguous assignment of the remaining protons and C-H carbons. Finally, quaternary carbons were assigned using $^{1}$H-$^{13}$C HMBC.

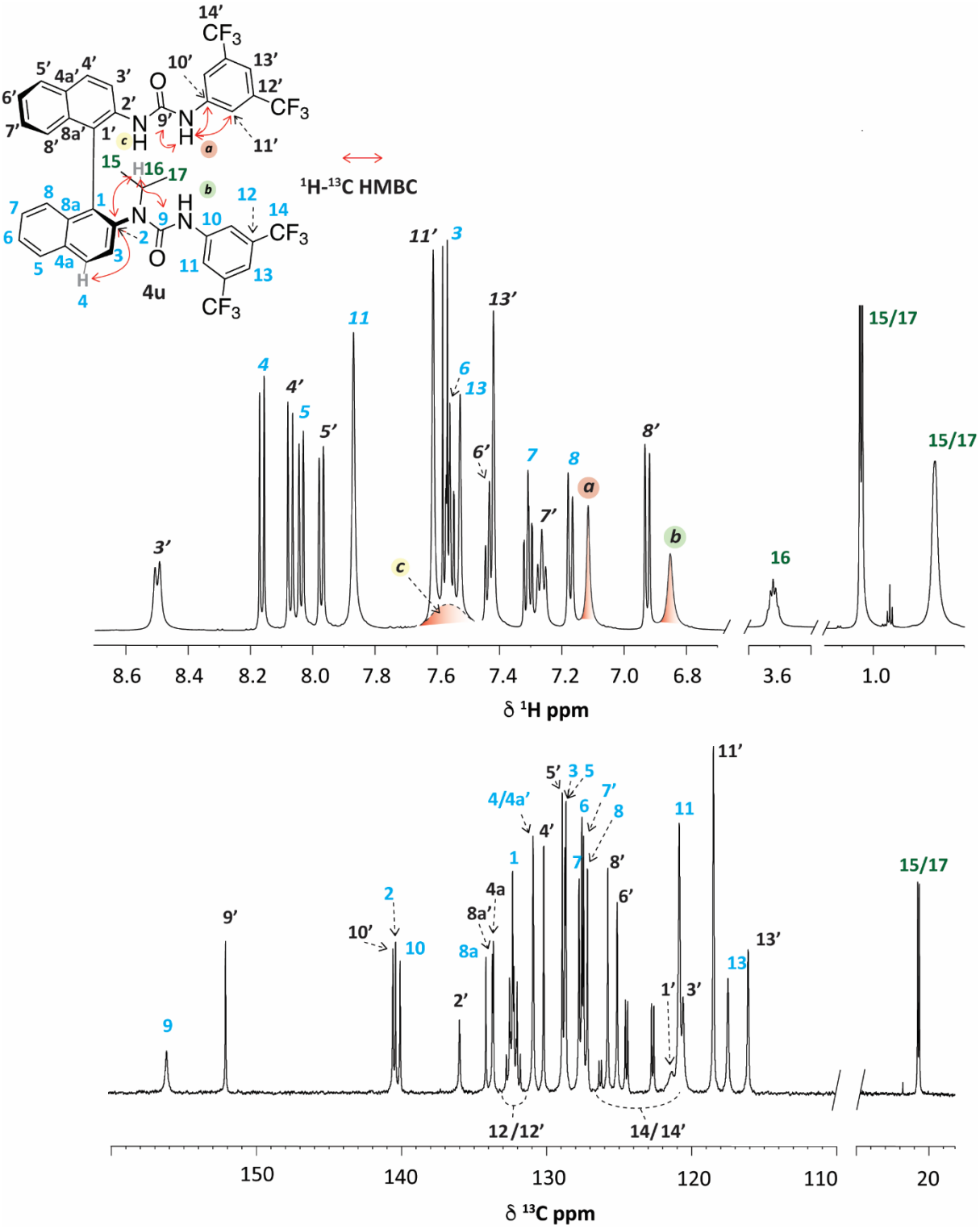



Figure 3.3: $^{1}$H and $^{13}$C NMR spectra of **4u** (DCM-$d_2$, 25 mM, 298 K), see Experimental for details.

The $^{1}H$ and $^{13}C$ NMR spectra of **4u** are informative because of the unexpected chemical shifts and the broad lines of several signals. Proton H(3') and H(3), both positioned on the naphthyl ring *ortho* to the ureas, experience a substantially different shielding (8.47 *vs.* 7.56 ppm). This is likely due to the relative orientation of the adjacent carbonyl, which can affect chemical shifts by means of anisotropic electron currents; protons laying on the plane of the urea will be deshielded, while protons outside of the plane will be shielded. Consequently, the alkylated urea is approximately orthogonal to the adjacent naphthyl ring ($\delta$ H(3) = 7.56 ppm), and H(3') is approximately co-planar with the bidentate urea ($\delta$ H(3') = 8.47 ppm). Similarly, for the isopropyl group the three H(15), more shielded than protons H(17), presumably fall above the aromatic ring current of one of the naphthyl rings, which exerts a shielding effect.

The resonances assigned to NH(a) and NH(b) appear at 7.1 and at 6.9 ppm respectively. The presence of NH(c) can be inferred from the observation of characteristic NOESY and $^{1}H$-$^{15}N$ HSQC cross peaks ($\delta$ NH(c) = 7.6 ppm) but its signal was not directly observed in DCM-$d_2$. The detection of NH(c) is problematic because, in addition to the severely broad lines (> 70 Hz), it overlaps with multiple peaks in a variety of common deuterated solvents (DCM-$d_2$, $CDCl_3$, THF-$d_8$, $CD_3CN$, DMSO-$d_6$, $CH_3OD$). NH(c) was however directly observed when the sample was recorded in 1,2-dichlorobenzene-$d_4$ at 318 K (Figure 3.4). The substantial deshielding of NH(c) is unexpected, being the least electron-deficient NH proton. When $^{1}H$ NMR was recorded in DMSO-$d_6$,[16] NH(a) and NH(b) displayed substantial deshielding compared to the proton spectra in DCM-$d_2$ (+1.5 and +0.8 ppm respectively), presumably due to hydrogen bonding with the Lewis basic oxygen of the solvent, while NH(c) remained relatively unaffected (+0.2 ppm). These observations suggest the existence of an intramolecular hydrogen bond. This involves NH(c) and the opposite carbonyl, C(9)=O, itself presenting a more deshielded and significantly broaden $^{13}C$ signal.

Although the spectra of **4u** show a single set of signals, certain resonances show extensive line broadening in both proton and carbon NMR. The linewidth ($\upsilon_{1/2}$ = half-height linewidth of a peak) is an important spectroscopic observable, directly related to the transverse relaxation rate $R_2$ ($R_2 = 1/T_2 \sim \pi\,\upsilon_{1/2}$ Hz) and hence informative about the dynamic behaviour of a molecule in solution. The broad linewidths therefore suggest that **4u** undergoes dynamic conformational exchange in the NMR time-scale. The signal broadening occurs for protons and carbons proximal to the intramolecular hydrogen bond site, H(3'), C(3'), C(2'), C(1'), C(9), suggesting the presence of a slow-intermediate equilibrium, compared to the NMR time-scale, in which the NH(c)···O=C(9) hydrogen bond is continuously elongating and shortening. This leads to a time-dependent equilibrium between what we refer to as a *folded* conformation, in which the intramolecular HB is prominent and an *open* conformation with no HB interaction.

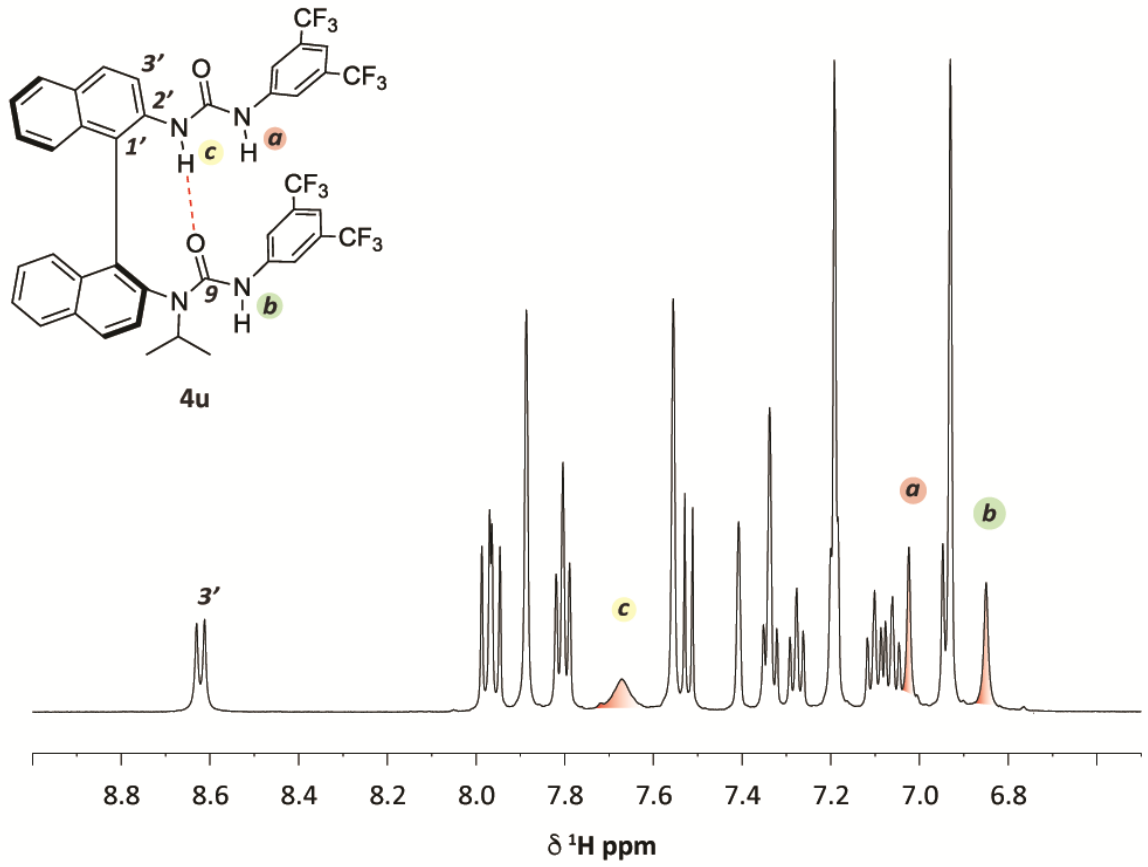



Figure 3.4: $^1$H NMR spectra of **4u** (1,2-dichlorobenzene-$d_4$, 25 mM, 318 K), aromatic region.

$^{1}$H NMR of **4u** were also recorded between 0.5 and 60 mM to study possible aggregation at increasing concentration. Differently from what was observed for non-alkylated **4a**, **4u** shows negligible variations upon concentration changes, thus advocating against intermolecular interactions (Figure 3.5).

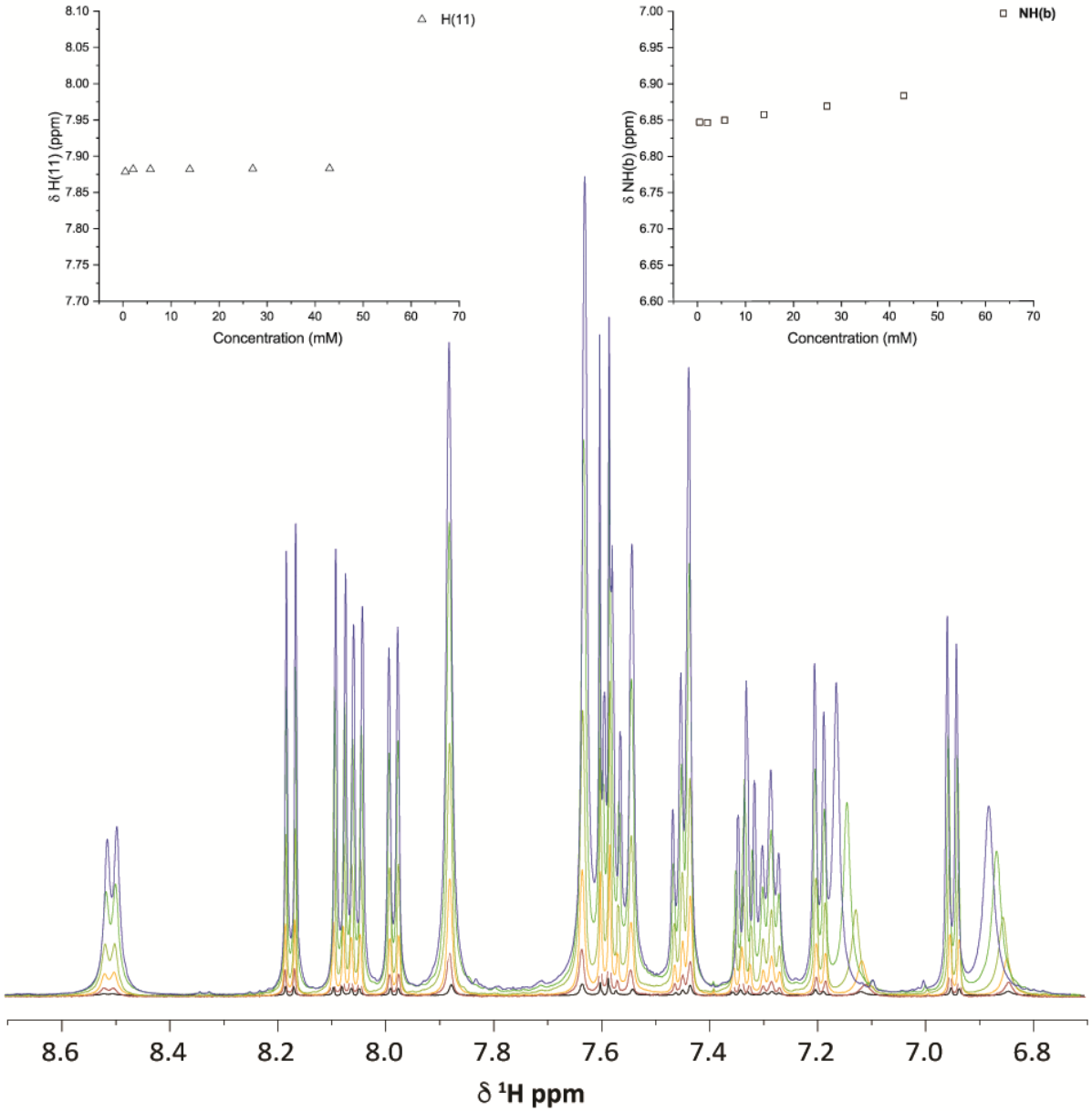



Figure 3.5: Stacked $^{1}$H NMR of **4u** between 0.5–45 mM (DCM-$d_2$, 298 K).

Analyses of through-space correlations by means of high-resolution NOESY allowed us to propose a three-dimensional model of **4u** in DCM-$d_2$ (Figure 3.6–3.7). A strong nOe correlation

is detected between the protons belonging to the isopropyl group, H(15), H(16), H(17), and NH(b) indicating that these groups are proximal and pointing in the same direction (anti-anti urea isomer). An nOe between the isopropyl group and proton 8', together with the NH(a) ⇔ H(11) correlation, suggests that the isopropyl group is projecting towards the opposite naphthyl ring, and alludes to an almost perpendicular disposition of the ureas. Despite our efforts, attempts to obtain an X-ray quality crystal of **4u** resulted in crystallisation into very fine needles that were unsuitable for single crystal X-ray crystallography.

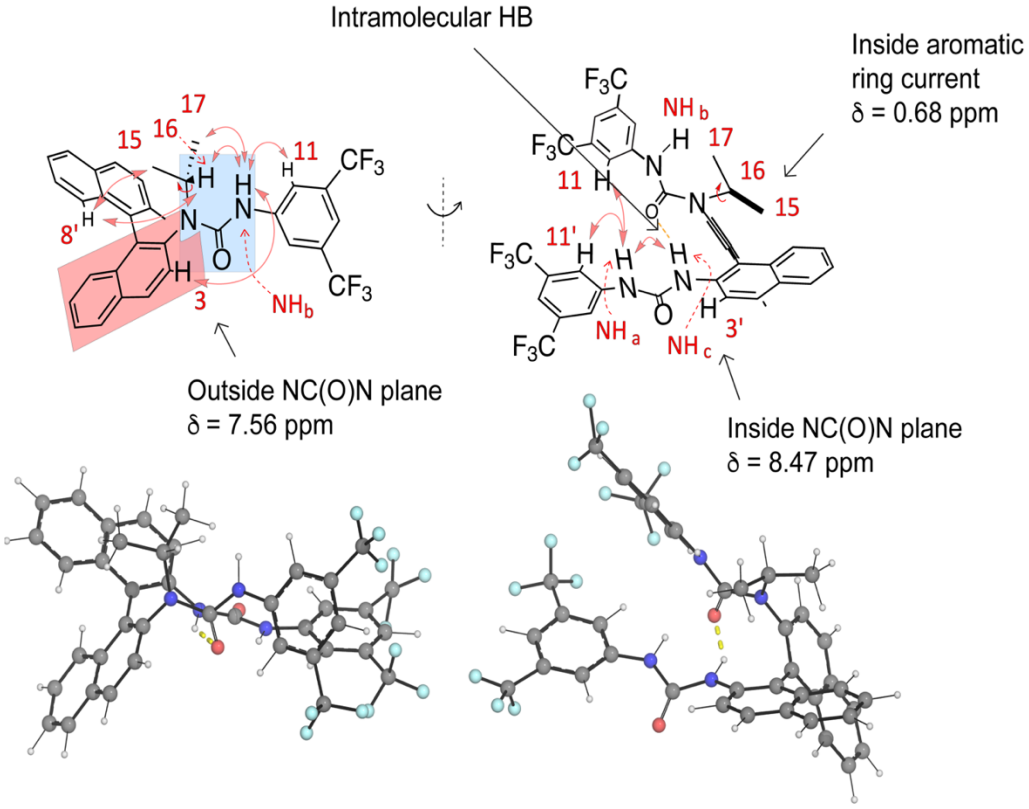



Figure 3.6: 3D Model accounting for the nOe correlation of **4u**.

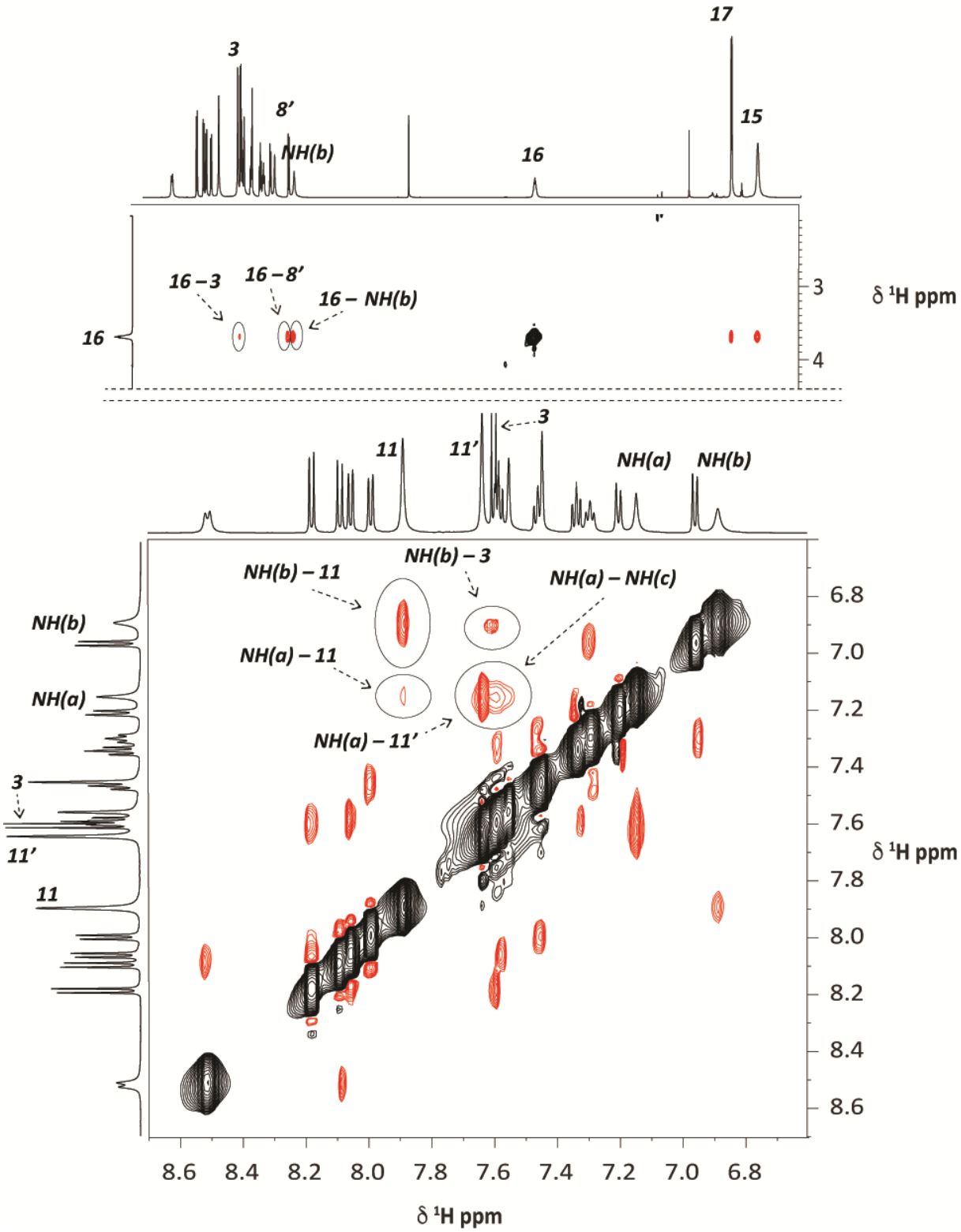



Figure 3.7: $^{1}$H NOESY spectrum of **4u** (600 MHz, DCM-$d_2$, 25mM, 298 K), see Experimental for details.

*3.2.2.2 N-Alkylated Analogues.* ***N***-alkylated BINAM *bis*-urea derivatives featuring and identical BINAM motif but various *N*-alkyl substituents and electronic patterns for the two aryl rings were analysed by NMR spectroscopy in DCM-$d_2$. The spectra of the *N*-alkylated analogues **4s-4x** show strong similarity with the ones of the *N*-isopropyl derivative **4u**. Specifically, all the *N*-alkylated *bis*-ureas with 3,5-bis(trifluoromehtly)phenyl substituents show one particularly deshielded ortho proton, H(3'), presenting broad lines; NH(c) is always the most deshielded among the three NH and is severely broadened on the baseline; the carbonyl belonging to the alkylated urea, C(9), is significantly broader and more deshielded than the one belonging to the non-alkylated urea, C(9'). This suggests a common conformational behaviour among the alkylated catalysts featuring two 3,5-bis(trifluoromethyl)phenyl groups.

Notably, when the aryl ring proximal to the alkylated urea is a phenyl (**4y**), less electron-deficient than 3,5-bis(trifluoromethyl)phenyl, an additional hydrogen bonding interaction NH(a)···O=C is observed (Figure 3.8, top). This confers conformational rigidity to the system which translates to sharp proton and carbon resonances, consistent with the increased Lewis basicity of the carbonyl. On the other hand, when the aromatic ring adjacent to the non-alkylated urea is substituted with a less electron-poor ring such as in **4z**, $^{1}$H and $^{13}$C NMR spectra are remarkably broader, thus suggesting a less dynamically stable structure arising from a weaker intramolecular hydrogen bond (Figure 3.8, bottom).

Taken together, these results demonstrate that alkylation of one BINAM nitrogen influences profoundly the conformational behaviour of the catalyst in solution. The presence of a single *N*-alkyl group leads to an equilibrating conformational state, triggered by the formation of an intramolecular NH···O=C hydrogen bond. This is in contrast to non-alkylated BINAM **4a,** that shows no intramolecular interactions with sharp lines in the observed NMR spectra. In this

case, the two ureas are believed to freely rotate in solution. This study also reveals that $^{1}H$ and $^{19}F$ NMR chemical shifts of **4a** are greatly dependent on concentration, an indicator of aggregation arising from intermolecular hydrogen bonding between the urea groups. The observation that the chemical shifts of **4u** do not vary upon increased concentration suggests that the *N*-isopropyl group of catalyst **4u** discourages aggregation at high concentration.

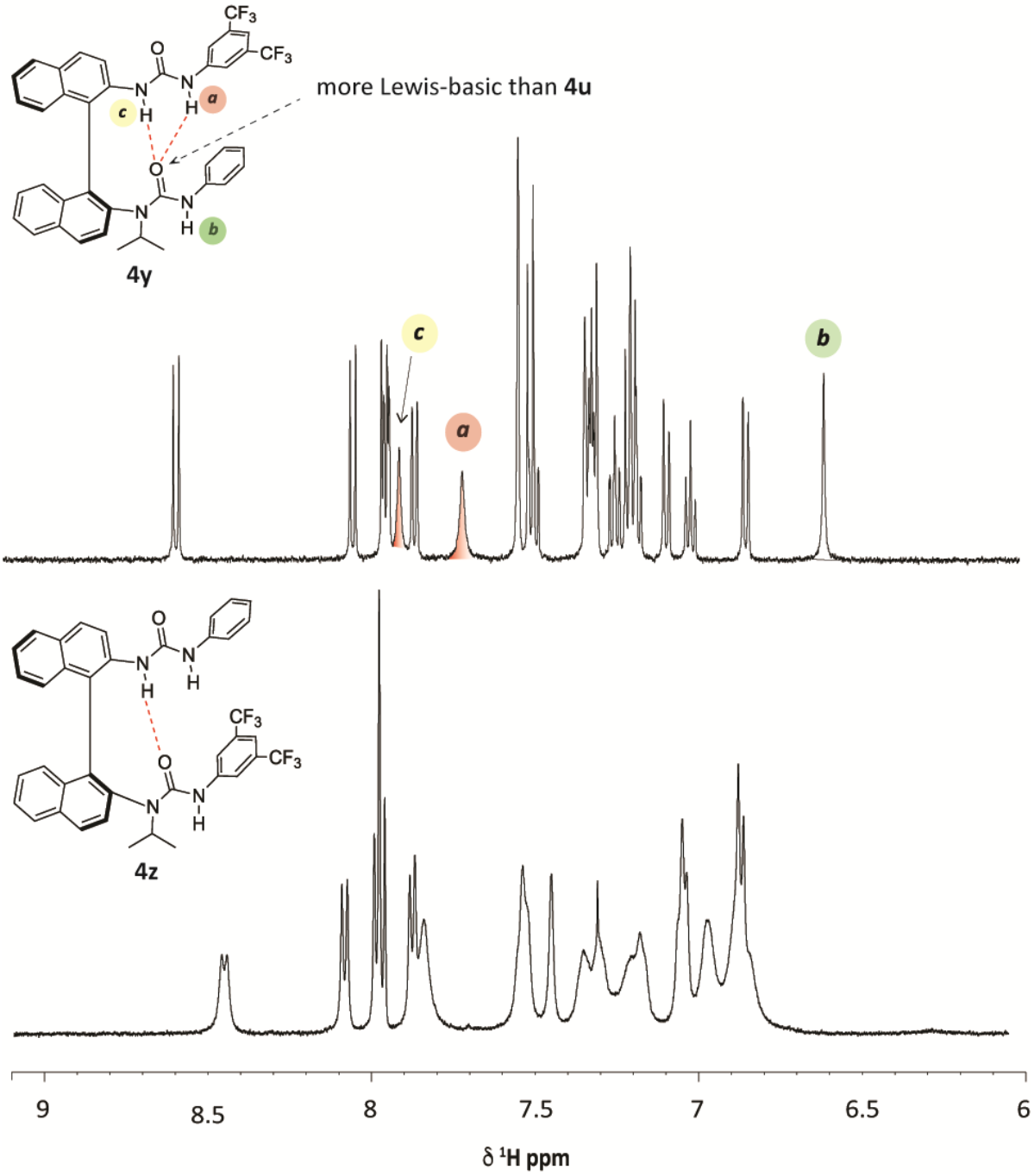



Figure 3.8: $^{1}H$ NMR of **4y** (top) and **4z** (bottom) (DCM-$d_2$, 25 mM, 298 K).

### 3.2.3 Complexation with TBAF

The formation of a hydrogen bonded *bis*-urea-fluoride complex is the cornerstone of successful fluorination with metal alkali fluoride under HB PTC. The X-ray structure of **4u** co-crystallised with tetrabutylammonium fluoride (TBAF·3$H_2O$) provided undisputable evidence in the solid state that fluoride is hold in position by three hydrogen bond contacts within the catalyst (***v.*** *2.2.3.3 Crystal Structure of* ***4u****:TBAF*). However, information on the formation and stability of such complexes in solution is missing.

*3.2.3.1 Binding studies.* The binding affinity of catalyst **4a** and **4u** towards fluoride was studied by UV-vis and NMR spectroscopy to gain information on how non-alkylated and alkylated catalysts compare in terms of fluoride binding properties in solution. Adding an increasing amount of ligand to a receptor, while monitoring the variation of a certain physical property, is a well-established method to gain quantitative information about the binding affinity and stoichiometry of the system in question.[17,18] Since the binding event alters the electronic properties of a species, techniques such as NMR, UV-vis or fluorescence spectroscopy are viable methods to monitor complexation in solution. A series of UV-vis titrations were performed at micromolar concentration of *bis*-urea (5 μM) in dichloromethane. A TBAF solution was prepared in spectrophotometric grade dichloromethane by dissolving commercial TBAF·3$H_2O$. The exact concentration of fluoride was determined by $^{19}F$ NMR of an aliquot dissolved in DCM-$d_2$, using 4-fluoroanisole as standard for quantification. Upon addition of increasing amount of TBAF (0–10 equivalents) to a solution of **4a** or **4u**, the UV-vis spectrum showed bathochromic shift with the build-up of a new maximum of absorption ($\lambda_{max}$) at 273– 275 nm. Plotting the absorbance at $\lambda_{max}$ versus the concentration of added fluoride results in the titration profiles shown in Figure 3.9. The binding constant can be calculated from these data *via* non-linear least-square regression using a dedicated software[19]

(Table 3.2). Both 1:1 and 2:1 binding mode were considered, with 1:1 giving consistently better fitting results. A 1:1 binding was also presumed from the observation of clean isosbestic points, since one isosbestic point usually indicates the presence of only two species contributing to the absorption.

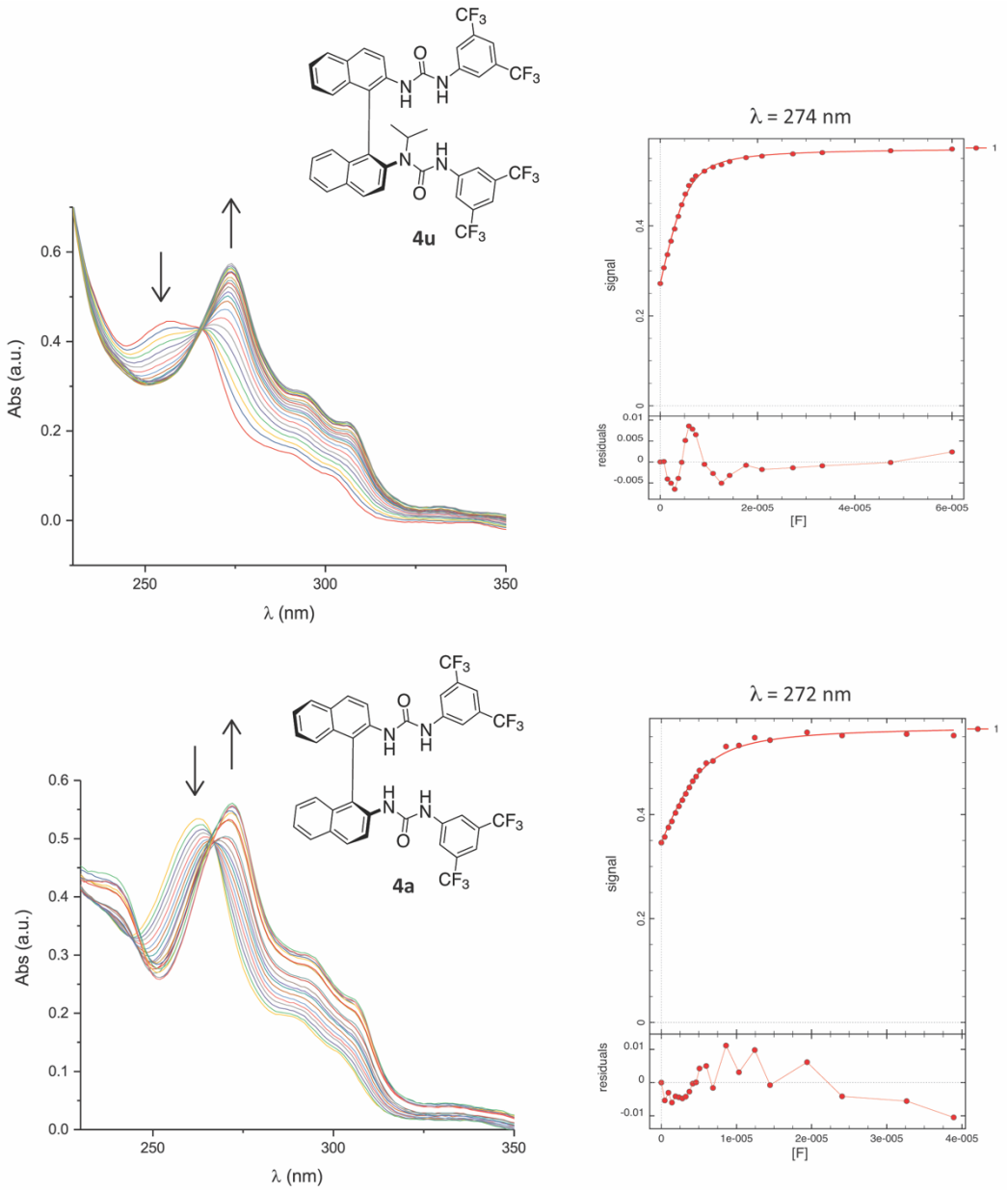
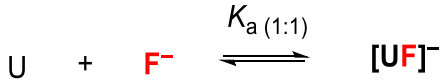



Figure 3.9: Stacked UV-vis spectra recorded for the titration of **4u** (5.4 μM, top) and **4a** (5.0 μM, bottom) with TBAF·3$H_2O$ (0.19 mM) in DCM at 298 K. On the right, titration profiles at the $\lambda_{max}$ (red dots) and fitting function (red lines). Corresponding residual plots are shown below the graphs. See Experimental for details.

The calculated association constants ($K_a$ ~ $10^6$ $M^{-1}$) denote strong binding affinity of both catalysts to fluoride, with **4u** having a marginally higher $K_a$ than **4a**. These values are comparable with the ones found in the literature for fluoride binding receptors that shows $K_a$ typically in the $10^5$–$10^7$ range.[20]

Table 3.2: Association constant ($K_a$), log($K_a$), and corresponding free energies, ΔG, for the formation of 1:1 *bis*-urea:TBAF complex. $K_a$ are calculated by non-linear regression using DynaFit and expressed as average of two independent set of experiments.




| Catalyst | $K_{a\,(1:1)}$ ($M^{-1}$) | log($K_{a,\,1:1}$) | ΔG $_{(1:1)}$ (kJ/mol) |
|---|---|---|---|
| **4a** | 0.80 ± 0.09 x $10^6$ | 5.90 ± 0.05 | -34.0 ± 0.3 |
| **4u** | 1.05 ± 0.02 x $10^6$ | 6.02 ± 0.01 | -34.30 ± 0.04 |

Spectrophotometric techniques, such as UV-vis, are optimal to measure strong binding ($K_a$ > $10^5$), however, the extent of structural information that can be retrieved from a UV-vis spectrum is generally rather limited. On the other hand, NMR titrations can be informative not only on the binding affinity of a complex, but also on the structure and conformation of such systems.[21] NMR titrations were performed at millimolar concentration (3 mM) in DCM-$d_2$. After addition of TBAF (0–1 equivalent) to **4a**, major line broadening occurred in $^1$H NMR, indicating an ongoing *on-off* equilibrium. Sharp lines were gradually recovered approaching 1 equivalent of added fluoride. Noticeable changes in $^1$H and $^{19}$F chemical shifts were observed between 0 and 1 equivalents, after which the chemical shift of all resonances became invariant (Figure 3.10). Over the course of the titration, all the proton signals were shielded between 0 and 0.5 equivalents of fluoride and deshielded between 0.5 and 1.0, before reaching plateau at > 1 equivalent. A signal assigned to the NH pair NH(a/b) appeared in $^1$H NMR at 13.5 ppm after 1 equivalent of fluoride is added, while NH(c/d) was recorded at 7.6 ppm. The overall large deshielding of the NH, and the sharp plateau after 1 equivalent denotes strong binding to fluoride.

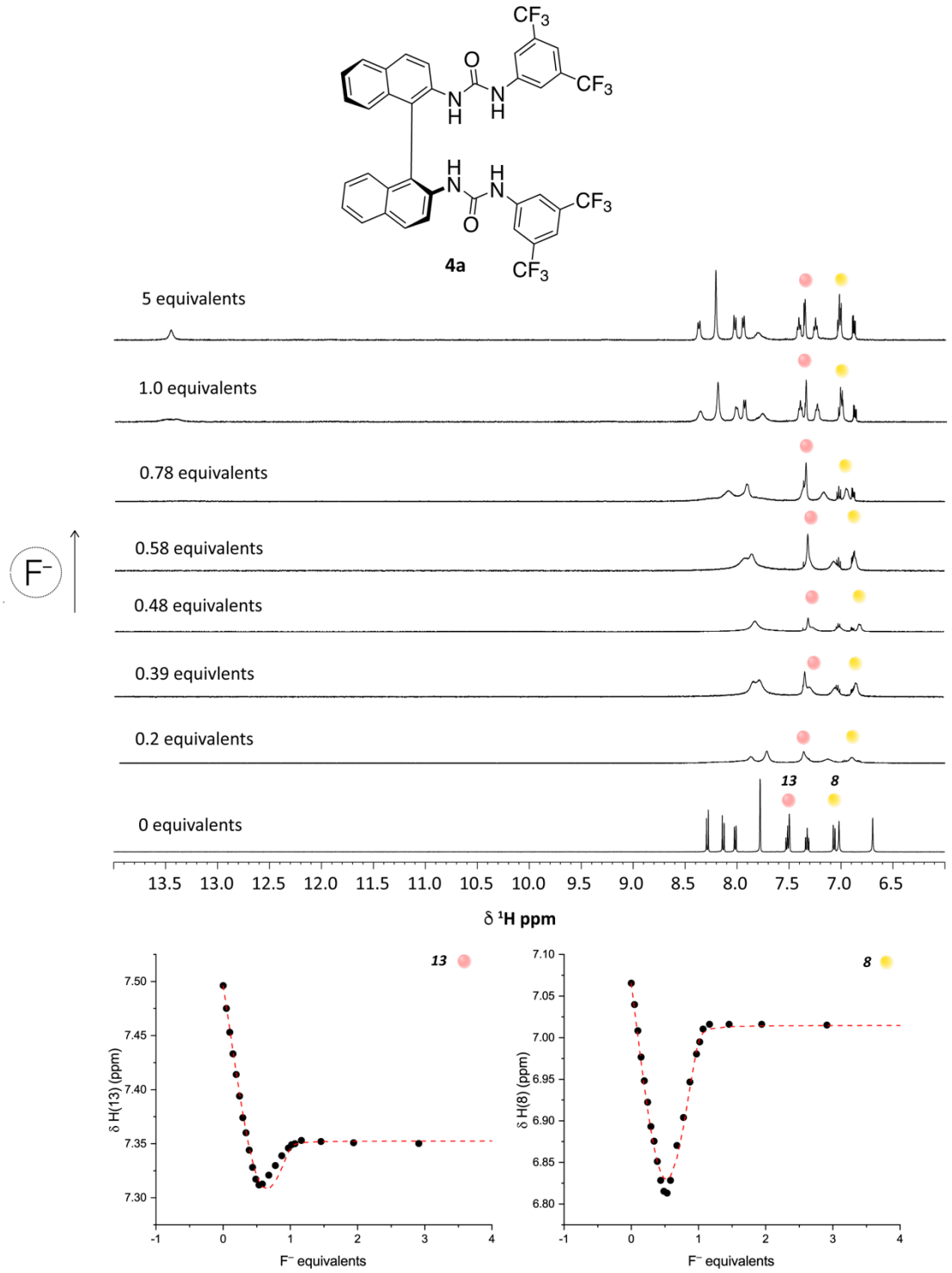



Figure 3.10: Stacked $^{1}$H NMR spectra for the titration of **4a** (2.3 mM) with TBAF·3H2O (55 mM) in DCM-$d_2$ at 298 K (top). Titration profiles of H(13) and H(8) between 0 and 5 equivalents of fluoride, black spot indicates the experimental data while the red dashed line indicate the fitted model used to calculated $K_a$ (bottom). See Experimental for details.

Addition of TBAF to **4u**, also led to line broadening, before quantitative binding was reached (Figure 3.11–3.12). At 1 equivalent of added fluoride the three NH appeared in $^{1}$H NMR, deshielded by ~ 5 ppm with respect to unbound **4u**. Also in this case, two distinct trends could be distinguished, one between 0–0.5 equivalents of added fluoride and one from 0.5–1, before a plateau was reached.

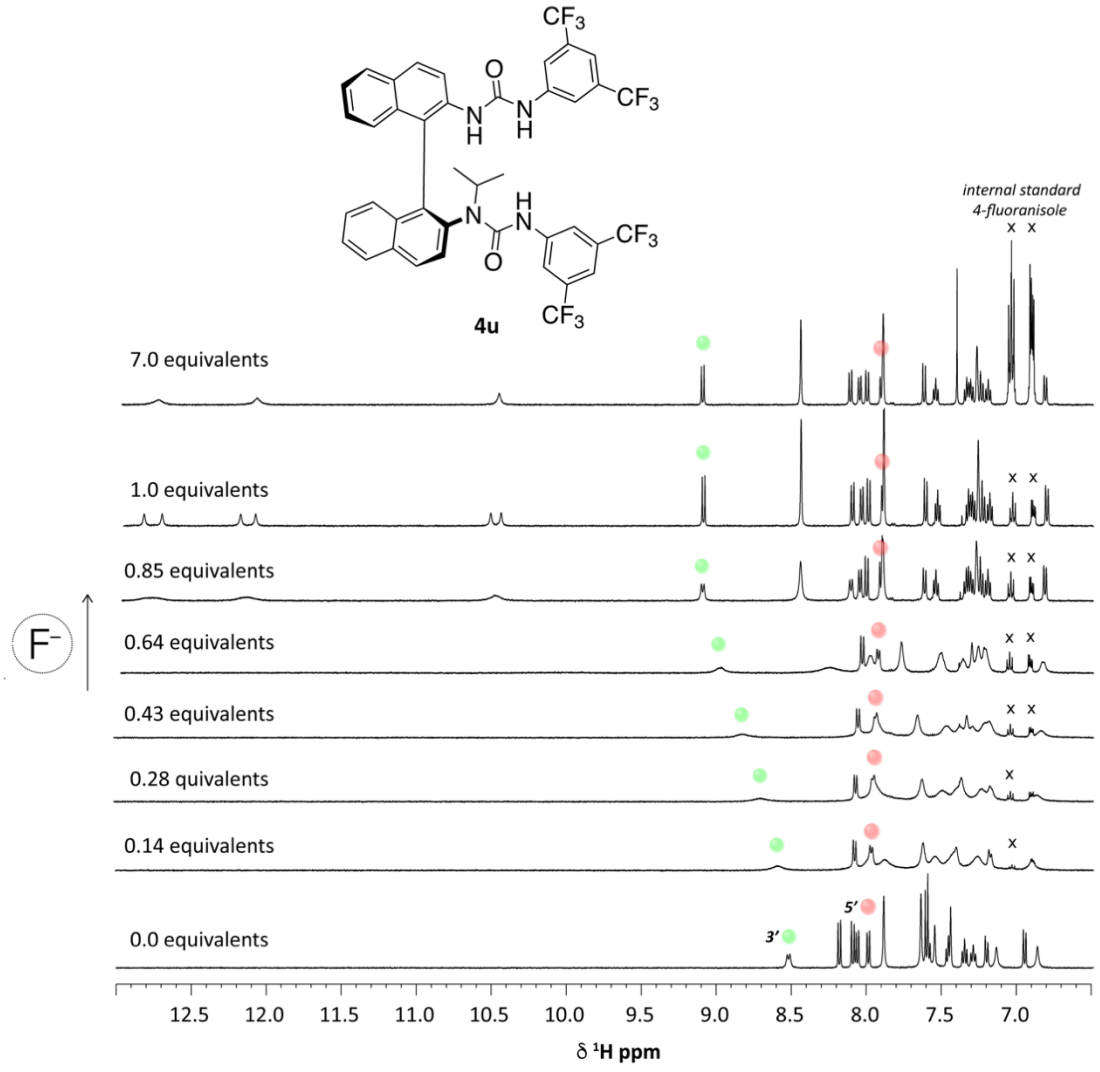



Figure 3.11: Stacked $^{1}$H NMR spectra for the titration of **4u** (3.0 mM) with TBAF·3H$_2$O (54 mM) in DCM-d$_2$ at 298 K (top).

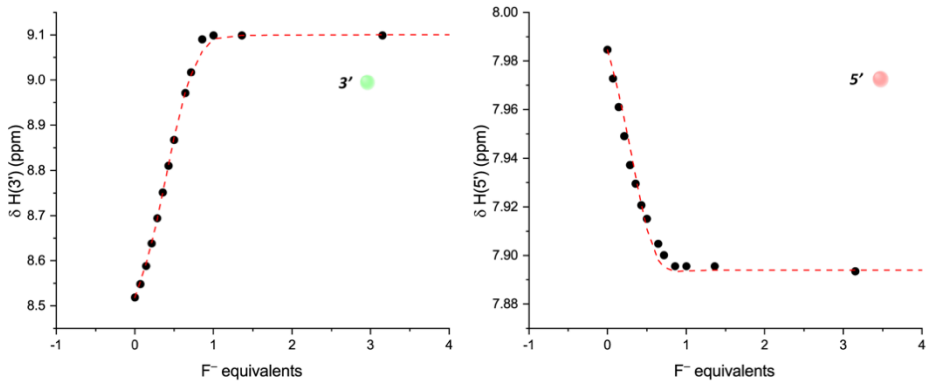



Figure 3.12: Titration profiles of H(3') and H(5') between 0 and 5 equivalents of fluoride, black spot indicates the experimental data while the red dashed line indicate the fitted model used to calculated $K_a$ (bottom). See Experimental for details.

The titration profile of both catalysts **4a** and **4u** clearly reflects a scenario more complicated than a simple 1:1 complexation. This is due to the formation of dimeric species, or higher coordinated fluorides at low concentration of $F^-$, which equilibrate with the more stable $[UF]^-$ (U = **4a** or **4u**) complex over the course of the titration ($K_{1:1} >> K_{2:1}$). The chemical shift variation of diagnostic resonances, H(13) and H(8) for **4a** and H(3') and H(5') for **4u**, was plotted against the concentration of added fluoride and the data analysed with a dedicated software.[19] Initial attempts to fit the NMR titration data to a 1:1 binding mode resulted in a poor fit and non-meaningful data. Conversely, when a 2:1 binding mode was considered, and the $K_a$ 1:1 determined from UV-vis titration included in the calculation, good agreement to the experimental data was found. This allowed the calculation of a 2:1 binding constant and corresponding binding energies for **4a** and **4u** (Table 3.3)

Table 3.3: Association constant ($K_a$), log($K_a$), and corresponding free energies, ΔG, for the formation of 2:1 *bis*-urea:TBAF complex. $K_a$ are calculated by non-linear regression using DynaFit and expressed as average of two independent set of experiments.

$$[UF]^- + U \overset{K_{a\ (2:1)}}{\rightleftharpoons} [U_2F]^-$$

| Catalyst | $K_{a\ (2:1)}$ ($M^{-1}$) | log($K_{a,2:1}$) | $\Delta G_{(2:1)}$ (kJ/mol) |
|---|---|---|---|
| **4a** | 600 ± 120 | 2.80 ± 0.08 | -16.0 ± 0.5 |
| **4u** | 3000 ± 800 | 3.50 ± 0.12 | -20.0 ± 0.7 |

NMR titrations of **4a** and **4u** with TBAF reveal that *bis*-urea catalysts present a 2:1 complexation equilibrium involving two molecules of urea binding one fluoride. The corresponding association constants, $K_{a\ (2:1)}$, are three order of magnitude smaller than the ones measured for 1:1 complexes using UV-vis, with **4a** showing reduced binding affinity compared to **4u**. The combined binding information indicates that a 2:1 $[U_2F]^-$ complex (U = **4a** or **4u**) is present in solution at significant concentrations between 0 to 0.5 equivalents of fluoride. The $[UF]^-$ 1:1 adduct dominates the equilibria at higher concentration of fluoride, being the only species formed when 1 equivalent of fluoride is present in solution.

*3.2.3.2 NMR Study of iPr BINAM Urea–TBAF (4u:TBAF) in Solution.* As demonstrated by the binding studies, addition of one equivalent of a tetrabutylammonium fluoride (TBAF·$3H_2O$) in DCM-$d_2$ to **4u** leads to quantitative formation of a 1:1 *bis*-urea–fluoride complex. **4u**:TBAF can be generated inside a sealed NMR tube and stored for months without noticeable degradation. The thorough inspection of the NMR spectra of this complex reveals to be important in deriving information about its structure in solution.

$^1$H resonances of **4u**:TBAF were conveniently identified following the titration profiles of **4u** or assigned *ex-novo* by using standard 2D-experiments. The three NH were distinguished on the basis of their nOe correlations. In particular, NH(a) ⇔ NH(c), NH(a) ⇔ H(11') and NH(b) ⇔ H(11) were used in the assignment. Compared to the unbound *bis*-urea, **4u**:TBAF shows substantial deshielding of the three NH ($\Delta\delta_{NH}$ ~ +5 ppm). H(11), H(11') and H(3') also display prominent deshielding. At the same time, H(13) and H(13'), located on the 3,5-(trifluoromethyl)phenyl group, as well as H(6'), H(7') and H(8'), belonging to one naphthyl ring, display noticeable shielding. The sharp lines in the $^1$H NMR spectrum of **4u**:TBAF are consistent with a rigid and dynamically stable adduct with fluoride (Figure 3.13).

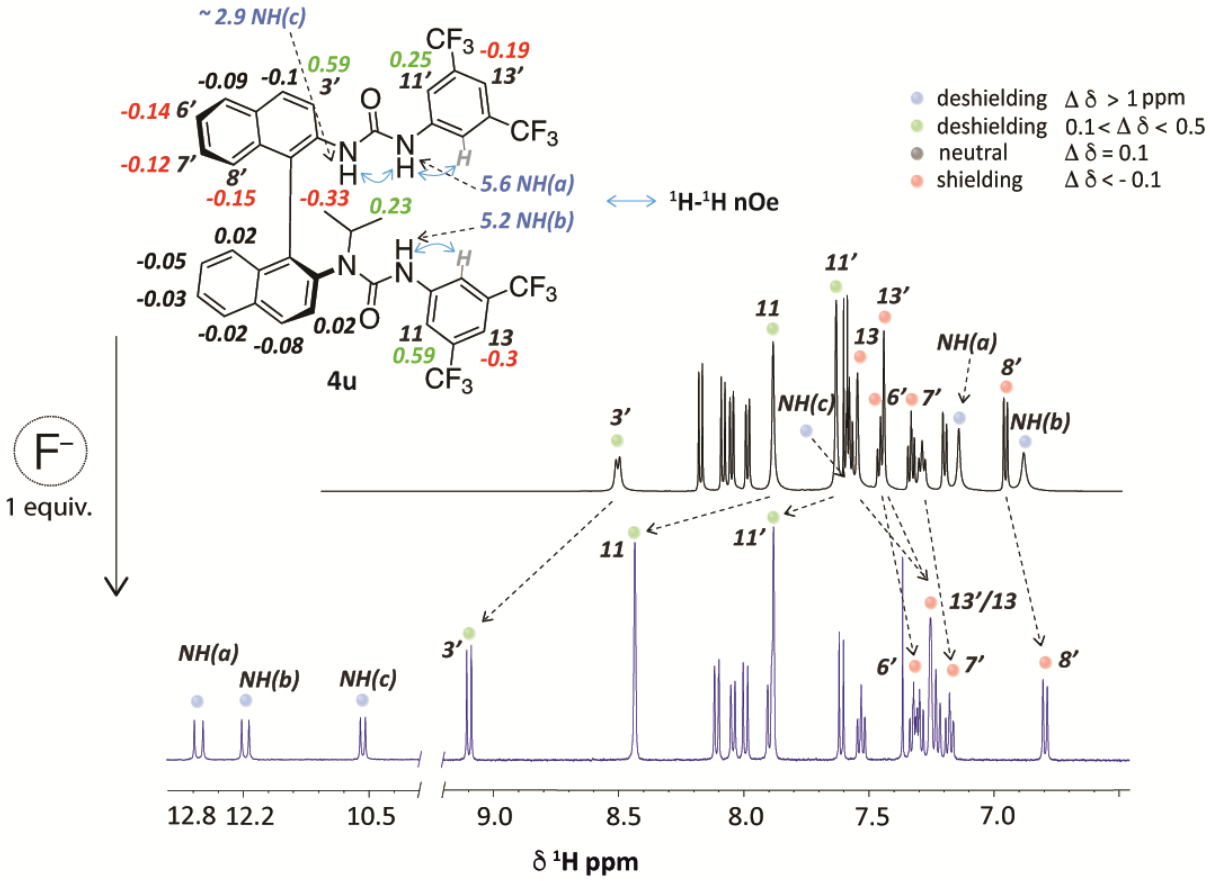



Figure 3.13: δ $^{1}$H NMR variations of **4u** upon $F^-$ complexation. **4u:**TBAF was generated by addition of a one equivalent of TBAF·3$H_2O$ (DCM-$d_2$ solution of known concentration) to **4u** (3 mM in DCM-$d_2$) and measured at 298 K. See Experimental for details.

Alongside considerable deshielding, each NH appears as a doublet in $^{1}$H NMR spectrum, and the $F^-$ signal appears as a doublet of doublet of doublet (ddd) in $^{19}$F NMR. When $^{1}$H NMR was acquired with fluorine decoupling, the three NH collapsed into singlets; accordingly, the splitting of the fluoride peak disappeared when $^{19}$F NMR was acquired with proton decoupling. The multiplicity of NH and $F^-$ represents a case of scalar coupling which develops across hydrogen bonds. Such couplings provide an unambiguous proof of the direct hydrogen bonding interactions between NH and $F^-$ for the complex in solution and provides a quantitative measure of their strength. To the best of our knowledge, this represents the first example of multiple resonances displaying hydrogen bond couplings with $F^-$. As widely demonstrated by the work carried out on biomolecules (*v.* *3.1.1.1 Hydrogen Bond Coupling*),

the presence of HBC opens the possibility of measuring correlation spectra, usually limited to covalently linked nuclei, across the hydrogen bridge. The Clean In Phase-HSQC (CLIP-HSQC) sequence was introduced for the optimal measurement of multiple one-bond constants.[22] We thought to apply this method for the observation of $^{1h}J_{NH\cdots F^-}$ by tailoring the CLIP-HSQC sequence for $^{1}H$-$^{19}F$ detection across HB (Figure 3.14). With this experiment, the four nuclei involved in the hydrogen bonding network of **4u:**TBAF can be observed in a single experiment; $^{1}H$ chemical shifts are reported on the horizontal axis, $^{19}F$ chemical shift on the vertical axis and, the magnitude of $^{1h}J_{NH\cdots F^-}$ is obtained measuring the cross-peak distances.

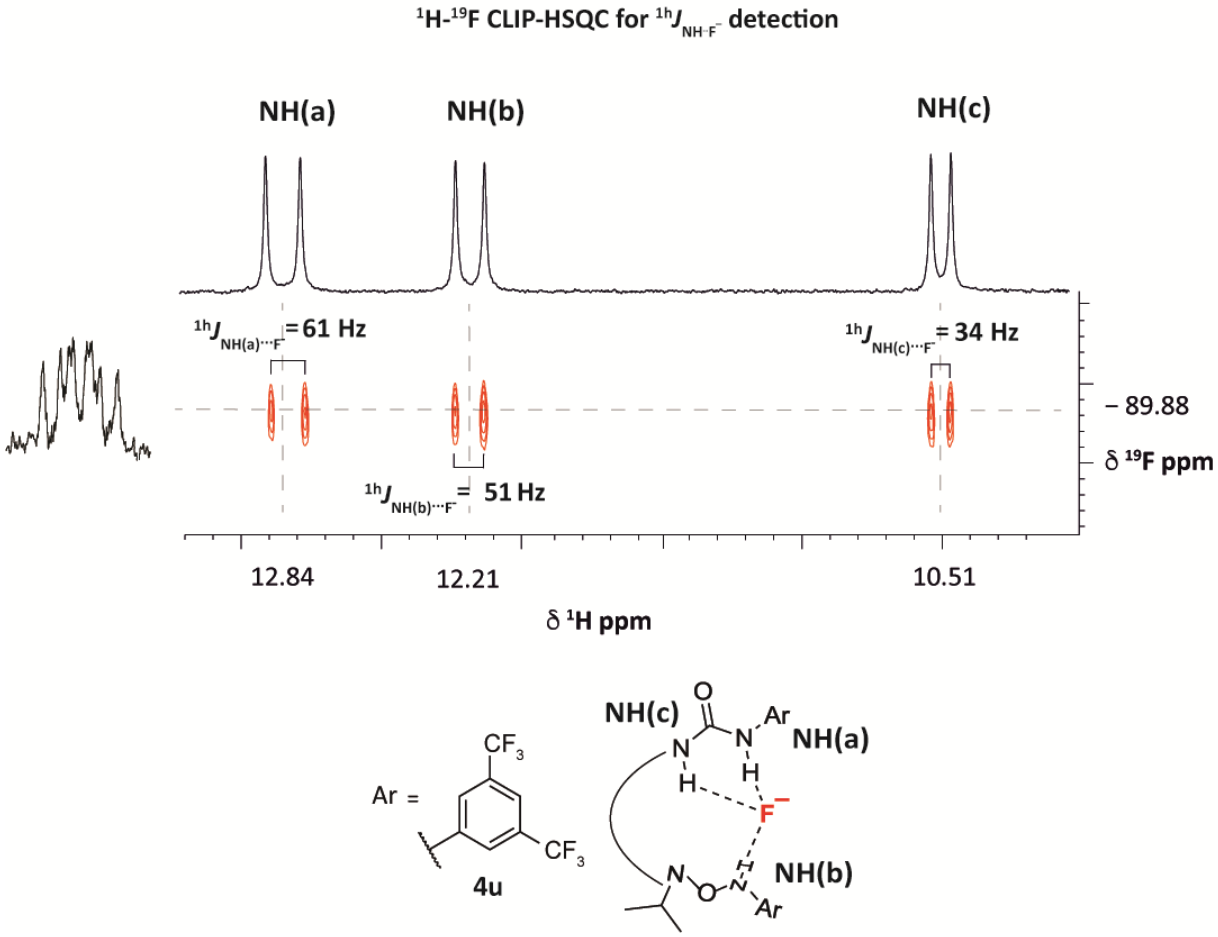


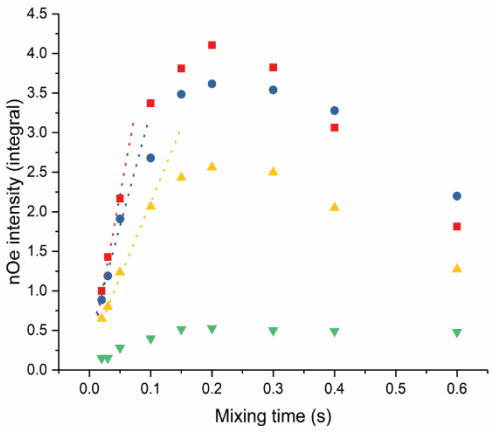

Figure 3.14: $^{1}H$-$^{19}F$ CLIP-HSQC of **4u:**TBAF (500 MHz, DCM-$d_2$, 3 mM, 298 K)

The three hydrogen bond coupling constants measured for **4u**:TBAF are $^{1h}J_{NH(a)\cdots F^-}$ = 61 Hz, $^{1h}J_{NH(b)\cdots F^-}$ = 51 Hz and $^{1h}J_{NH(c)\cdots F^-}$ = 34 Hz. These values are larger in magnitude compared to the

ones reported in the literature for supramolecular fluoride-binder receptors. Interestingly, the averaged values of $^{1h}J_{NH\cdots F^-}$ for **4u**:TBAF is similar to the one reported by Shenderovich *et al.* for the tricoordinate $(HF)_3$:$F^-$ that showed HBC of 41 Hz. NH chemical shifts correlate with the magnitude of the coupling constant, with the most deshielded being NH(a), $\delta$ NH(a) = 12.84 ppm, followed by NH(b), $\delta$ NH(b) = 12.21 and NH(c), $\delta$ NH(c) = 10.51 ppm. The peak of $F^-$ is measured at -90 ppm, deshielded compared to the unbound TBAF·$3H_2O$ in DCM-$d_2$, which resonates at -118 ppm. The longitudinal relaxation time constant ($T_1$) is one of the spectroscopic observables expected to vary upon formation of a hydrogen bonded complex, since $T_1$ depends on the motions of the molecule in solution and hence on its size. Accordingly $T_1$, measured *via* inversion recovery experiments (magnet field strength = 11.7 T), decreases upon fluoride binding passing from 1.43 seconds of TBAF·$3H_2O$ to 0.31 seconds for **4u**:TBAF, consistent with the formation of a larger molecular complex.

The coupling information provided by the $^{1h}J$ splitting is sensitive to the chemical exchange processes occurring in the sample that exchange NH protons with protons from water. **4u**:TBAF recorded at higher concentrations (10–25 mM) shows identical chemical shifts and multiplicity pattern for protons bound to carbons, but the NH present themselves as broad singlets. This is consistent with a faster rate of exchange at higher concentrations, leading to exchange decoupling of the H–F interaction. $^{1h}J$ splitting thereby need to be measured at sufficiently low concentration (~ 1-3 mM) to obtain reliable data. The fact that **4u**:TBAF does not undergo chemical exchange at 3 mM, considering the heavily hydrated sample derived by TBAF·$\underline{3H_2O}$, is a qualitative indication that the hydrogen bonding network is strong. A reduced proton exchange rate is generally ascribed to strong HB interactions, since the rate of the chemical exchange process itself depends on the HB strength, involving necessarily breaking of the hydrogen bond in the exchange mechanism.

The coupling constant $^{1h}J$ of each individual NH inversely correlates with H···F intranuclear distances measured from the solid state structure of **4u**:TBAF, with NH(a)···F$^-$ being the shortest contact with fluoride. To demonstrate the relationship between $^{1h}J_{NH\cdots F^-}$ and hydrogen bond distances in solution, and to compare H···F in solution with the measured value in the solid state, the nOe developed between fluoride and NH was studied by means of $^1$H-$^{19}$F heteronuclear Overhauser effect spectroscopy (HOESY). The intensity of the nuclear Overhauser effect is proportional to the internuclear distance ($\propto r^{-6}$), if the isolated spin-pair approximation (initial rate approximation) is valid and the molecule is assumed to tumble rapidly and isotropically in solution. Within the initial rate approximation, the intensity of the nOe grows linearly with the mixing time ($\tau_m$); this is only valid for $\tau_m$ significantly shorter than $T_1$. A collection of 1D-HOESY experiments was performed varying the mixing time between 10 and 600 ms, and nOe build-up curves were used to calculate the relative length between NH and F$^-$ (Figure 3.15). Absolute distance determination was prevented because **4u** does not have a suitable H-F correlation corresponding to a known distance to be used as internal reference (the distance between aromatic protons and the fluorine of a trifluoromethyl group cannot be reliably determined due to the intrinsic rotation of the $CF_3$ group). The distance of each NH to fluoride increased in the following order: NH(a) < NH(b) < NH(c), with NH(b)···F$^-$ being only 2 % longer than NH(a)···F$^-$ and NH(c)···F$^-$ 12 % longer. This corroborates the notion that $^{1h}J_{NH\cdots F^-}$ corresponds to the measure of the H···F hydrogen bond, with larger $^{1h}J$ value corresponding to shorter HB. A fourth nOe correlation between the *ortho* protons H(11) and fluoride is observed, although of smaller magnitude. The pattern of fluoride correlations that emerges from HOESY data appears confirming what was observed in the solid state, with relative distances to fluoride: NH(a)~NH(b)>NH(c)>>CH(11). X-ray data shows an identical trend, albeit with shorter relative distances.

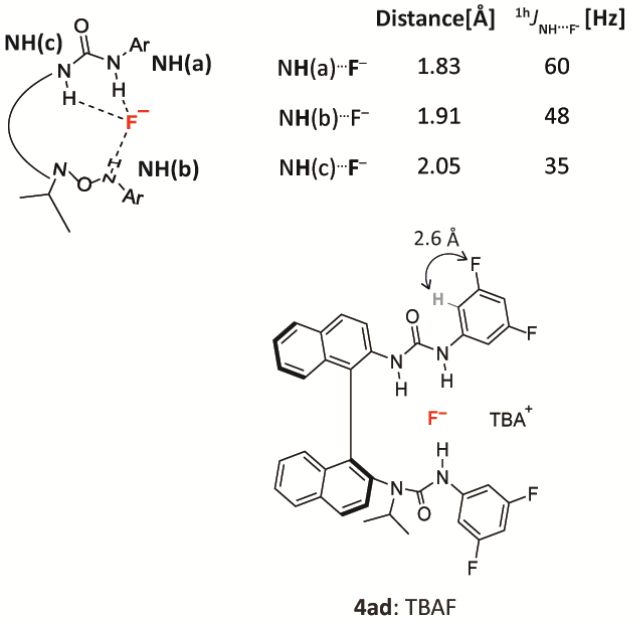



H–F distance relative to H(a)–F⁻ = 1.00

| | NMR (HOESY) | X-ray |
|---|---|---|
| NH(a) – F⁻ | 1.00 | 1.00 |
| NH(b) – F⁻ | 1.02 | 1.01 |
| NH(c) – F⁻ | 1.12 | 1.07 |
| CH(11) – F⁻ | 1.54 | 1.23 |

Figure 3.15: nOe build up curves and relative distances H···F⁻ calculated from HOESY and compared with X-ray data; (DCM-$d_2$, 10 mM, 298 K, $\tau_m$ = 10–600 ms). See Experimental for details.

Since catalyst **4u** does not possess a suitable F-H reference, catalyst **4ad** with 3,5-difluoro phenyl substituents in place of 3,5-bis(trifluoromethyl)phenyl groups was studied. The distance between a proton and the vicinal fluorine in an aromatic ring is known from neutron diffraction data to be 2.59 Å.[23] The calculated distances in **4ad**:TBAF are: N**H**(a)···**F**⁻ = 1.83 Å, N**H**(b)···**F**⁻ = 1.91 Å and N**H**(c)···**F**⁻ = 2.05 Å, inversely proportional to the size of the HB coupling constants $^{1h}J_{NH(a)\cdots F^-}$ = 60 Hz, $^{1h}J_{NH(b)\cdots F^-}$ = 48 Hz, $^{1h}J_{NH(c)\cdots F^-}$ = 35 Hz (Figure 3.16).




| | Distance[Å] | $^{1h}J_{NH\cdots F^-}$ [Hz] |
|---|---|---|
| NH(a)···F⁻ | 1.83 | 60 |
| NH(b)···F⁻ | 1.91 | 48 |
| NH(c)···F⁻ | 2.05 | 35 |




**4ad**: TBAF

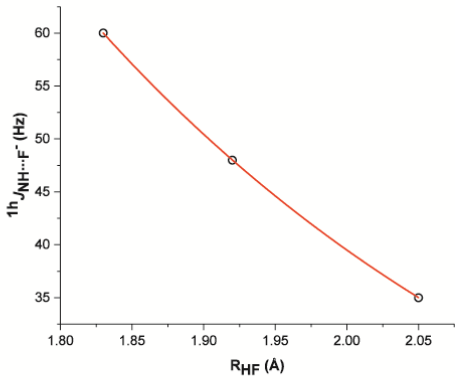



Figure 3.16: Quantitative $^{1}$H-$^{19}$F HOESY of **4ad**:TBAF (DCM-$d_2$, 3 mM, 298 K, $\tau_m$ = 30). See Experimental for details.

Similarly to the heteronuclear $^{1}H$-$^{19}F$ nOe, homonuclear NOESY provided useful quantitative information. NOESY cross-peak volumes of **4u**:TBAF were converted into absolute lengths by calibration with the vicinal protons H(3')–H(4') distance, know from literature and neutron diffraction data to be 2.46 Å.[23] Such data allowed for a quantitative mapping analysis of inter-proton distances of **4u**:TBAF (Figure 3.17–3.18). Key correlation H(16) ⇔ H(8') indicates that the isopropyl group point with the CH to the opposite binaphthyl ring with a measured distance between the two proton of 2.6 Å. NH(b) shows two nOe with H(11) and NH(c) measuring 2.7 and 2.5 Å respectively. The two NH belonging to the same urea display the strongest measured nOe, NH(a) ⇔ NH(c), corresponding to 2.0 Å. NH(a) also presents strong correlation with the adjacent *ortho* aromatic proton H(11') (NH(a)⇔H(11') = 2.7 Å) and with the opposite *ortho* proton, NH(a) ⇔ H(11), corresponding to 3.4 Å. The correlations between the two urea groups on the opposite side of the molecule, suggest that the three NH point towards the centre of the catalytic pocket occupied by fluoride. Additionally, the strong deshielding of H(3') upon formation of the fluoride complex is ascribed to a stronger anisotropic deshielding from the carbonyl, indicating an enhanced coplanarity between H(3') and the adjacent urea in respect to **4u**.

Compared to the conformational preference of the unbound catalyst, this analysis suggests that the addition of fluoride induces *syn-anti* isomerization of the *N*-isopropyl urea motif and concomitant rotation of the isopropyl group around the N-CH bond. This conformational change allows **4u** to participate in three hydrogen bonds to $F^{-}$. The distances measured by NMR are remarkably similar to the ones obtained from the X-rays structure, corroborating precisely the structural features of **4u**:TBAF in the solid state.

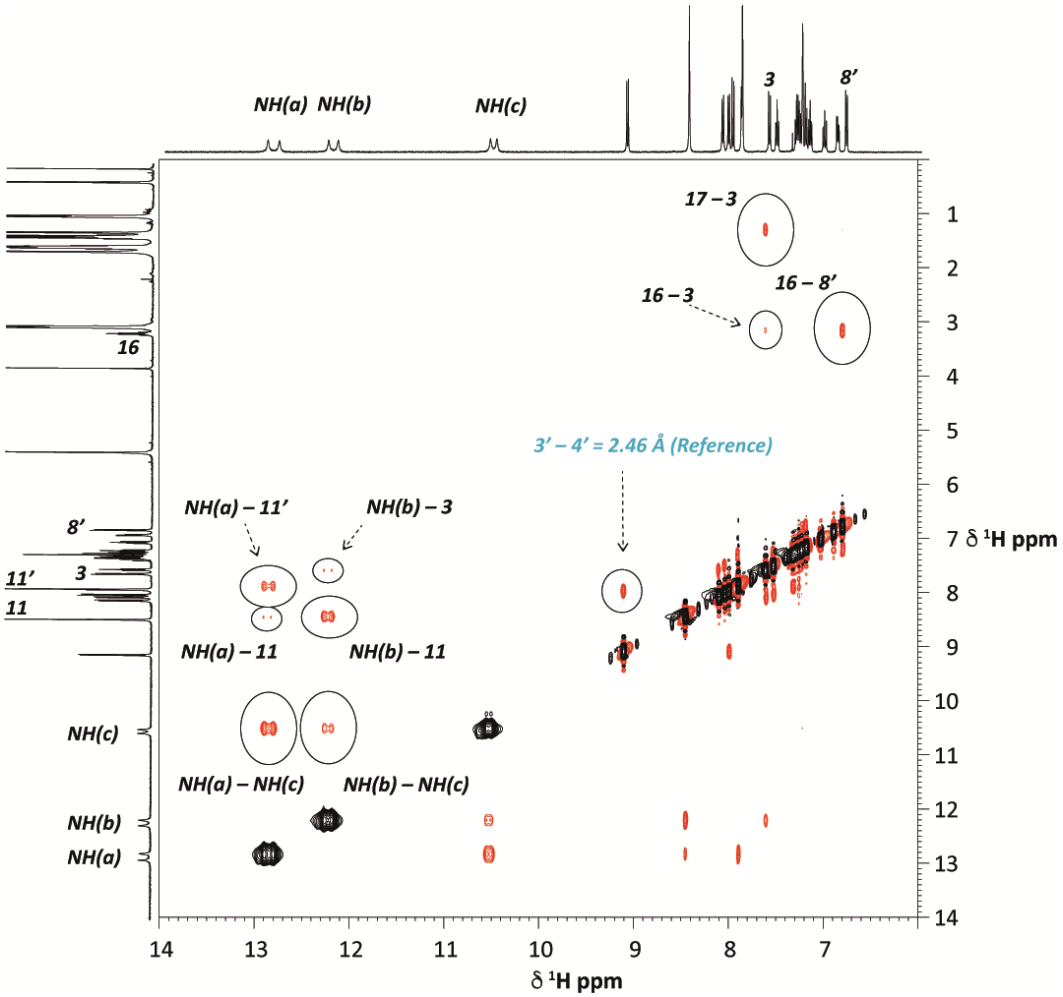
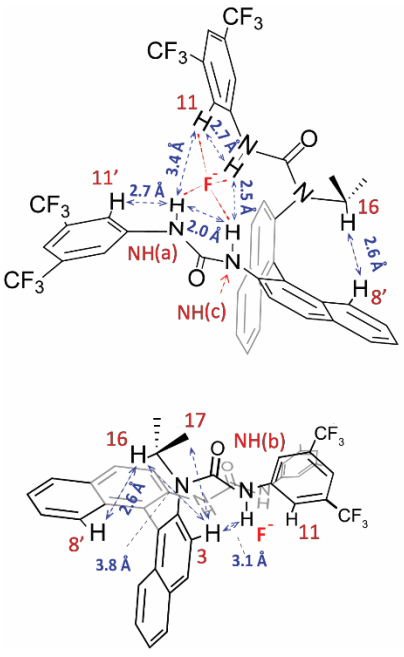



Figure 3.17: $^{1}$H NOESY spectrum of **4u**:TBAF (600 MHz, DCM-$d_2$, 3 mM, 298 K). See Experimental for details.




| Correlation | Distances [Å] | |
|---|---|---|
| | NMR | X-ray |
| NH(a) – NH(c) | 2.0 | 2.1 |
| NH(b) – NH(c) | 2.5 | 2.5 |
| NH(a) – 11 | 3.4 | 3.1 |
| NH(a) – 11′ | 2.7 | 2.3 |
| NH(b) – 11 | 2.7 | 2.3 |
| NH(b) – 3 | 3.1 | 2.8 |
| 3 – 16 | 3.8 | 3.7 |
| 16 – 8′ | 2.6 | 2.8 |

Figure 3.18: 3D model of **4u**:TBAF and internuclear distances calculated from NOESY and compared with the X-ray structure.

The study of the effect that isotopic substitution has on a hydrogen bonded system has been recognised as a valuable method to investigate HB properties.[24,25] In an attempt to develop a deuterated version of the *bis*-urea **4u**, where the three NH groups are replaced by deuterium, **4u** was refluxed in $CD_3OH$ for 72 hours and subsequently evaporated to dryness. **4u** underwent 80 % deuterium incorporation, as estimated by the relative integration of the residuals NH peaks. However, the isotopic exchange did not lead to a single deuterated species, but to a mixture of deuterated **4u**, as denoted by the presence of multiple carbonyl signals in $^{13}C$ NMR. Deutero-**4u** was found to exchange deuterium for protons either in solution or when stored as a solid. When one equivalent of TBAF in DCM-$d_2$, is added to a $^{2}H$-enriched sample of **4u** (40 % deuterium incorporation) an interesting new scenario is observed. Alongside each NH of **4u**:TBAF, two other signals are present in $^{1}H$ NMR. Each set of signals presents HBC with fluoride, as demonstrated by $^{1}H\{^{19}F\}$ NMR (fluorine decoupled $^{1}H$ NMR) which leads to nine NH singlets (Figure 3.19 A). These represent a mixture of four species: **4u**:TBAF and the three *mono*-*N*-deuterated isotopomers, themselves complexed with $F^-$. Other three signals are visible in $^{1}H\{^{19}F\}$ NMR (Figure 3.19 A, marked with an x), although of much reduced intensity. These may be related to three double deuterated analogues. The mono-*N*-deuterated species are bound to fluoride by two hydrogen bonds, $NH\cdots F^-$, and one deuterium bond, $ND\cdots F^-$. Each species has a different deuteration site, $ND_{a/b/c}$. Remarkably, the same distribution of deuterated species is observed in samples of **4u**:TBAF which did not have sources of deuterium other than the solvent, DCM-$d_2$ (Figure 3.19 B). This implies that fluoride catalyses deuterium exchange between DCM-$d_2$ and the catalyst–fluoride complex. A similar deuterium exchange behaviour is reported in the literature for fluoride complexes in DMSO-$d_6$ solution.[15]

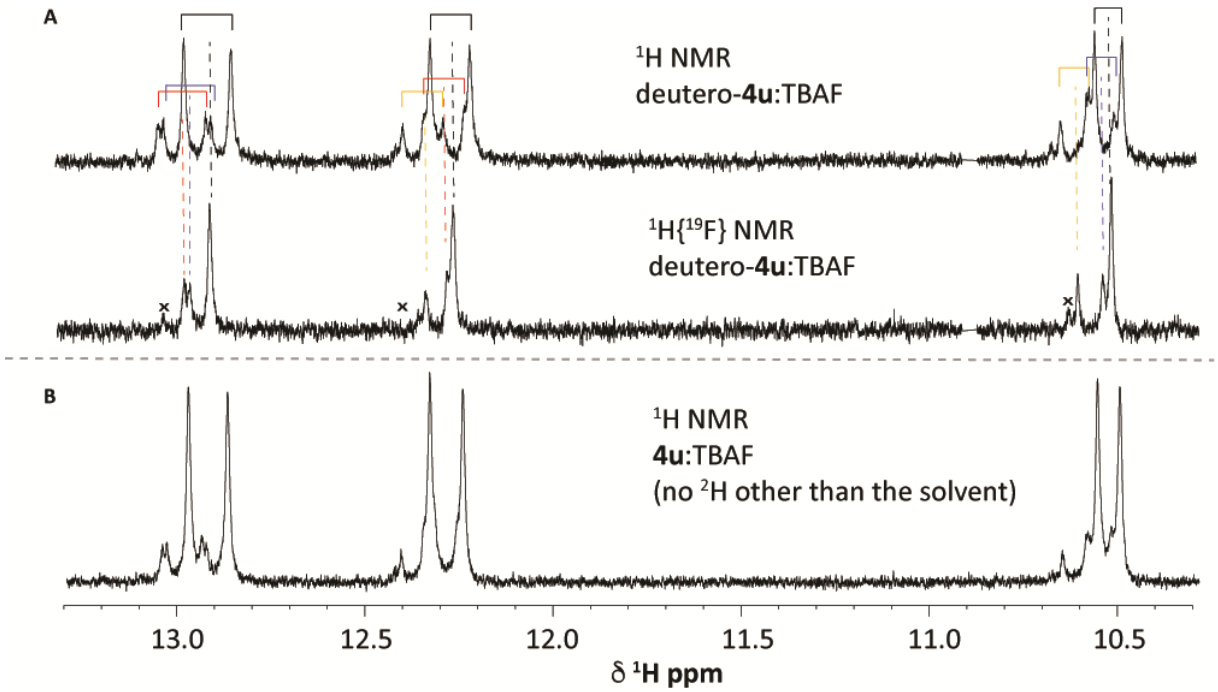



Figure 3.19: (A) $^{1}$H NMR (top) and $^{1}$H{$^{19}$F} NMR (bottom) of $^{2}$H-enriched (40 %) **4u**:TBAF complex (DCM-$d_2$, 3 mM, 298 K), x indicate the presence of additional signals potentially related to *bis*-deuterated complexes.(B) $^{1}$H NMR of **4u**:TBAF showing the presence of the same isotopic pattern of the deuterated isotopomers.

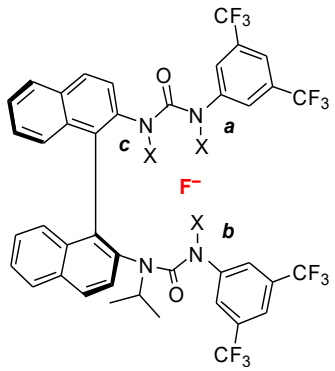
The presence of deuterated complexes in **4u**:TBAF is only noticeable when the TBAF solution in DCM-$d_2$ is more concentrated than 0.1 M, suggesting that fluoride is likely to promote exchange of deuterium between DCM-$d_2$ and the water present in the solution of TBAF, which eventually will exchange with the NH of the catalyst-fluoride complex, until an equilibrium is reached (eq 3.1).

$$F^-(xH_2O) + CD_2Cl_2 \rightleftharpoons F^-(xHDO) + CHDCl_2 \qquad (eq\ 3.1)$$

Using the $^{1}$H-$^{19}$F CLIP-HSQC experiment (Figure 3.20) it is possible to resolve the four species and to measure the corresponding NMR parameters for each NH and for $F^-$ (Table 3.4). The NH signals belonging to the deuterated complexes are slightly deshielded with larger $^{1h}J_{NH\cdots F^-}$ than the non-deuterated **4u**:TBAF, thus suggesting that the deuterium bond is weaker than its proton homologues, leading to an increased interaction of the two other hydrogen bonds as a consequence of the geometrical reorganization of the hydrogen bonding network. The

relative strength of proton and deuterium HB has been discussed in the literature, suggesting that deuterium bonds are stronger than proton bonds when bridged to neutral molecule, while the opposite is observe in the presence of charged species.[26] The three possible secondary isotope shifts on fluoride shielding are defined as $^{1h}\Delta\delta F_{ND(a/b/c)} = |\delta F_{NH}| - |\delta F_{ND(a/b/c)}|$, where $\delta F_{NH}$ is the fluoride chemical shift of the proton complex and $\delta F_{ND(a/b/c)}$ the fluoride chemical shift of the complex where NH(a), NH(b) or NH(c) are deuterated. The isotope shifts ($^{1h}\Delta\delta F_{ND(a)}$ = -0.71 ppm; $^{1h}\Delta\delta F_{ND(b)}$ = -0.75 ppm; $^{1h}\Delta\delta F_{ND(c)}$ = -0.59 ppm) show that fluoride is more shielded when bound in the *N*-deuterated complex and that NH/D(b) is the isotopic substitution that most influences fluoride chemical shift. This suggests that shielding of fluoride is connected with a reduced strength of the hydrogen bonding network and interestingly shows that NH(b) is the major contributor to fluoride chemical shift.

Table 3.4: NMR parameters for **4u**:TBAF and deuterated analogues; $^{1h}\Delta\delta\,^{19}F_{ND}$ = secondary isotopic shift on fluoride chemical shift.




| NX(a) | NX(b) | NX(c) | $^{1h}J_{NH(a)\cdots F^-}$ [Hz] | $^{1h}J_{NH(b)\cdots F^-}$ [Hz] | $^{1h}J_{NH(c)\cdots F^-}$ [Hz] | $\delta^1H_{NH(a)}$ [ppm] | $\delta^1H_{NH(b)}$ [ppm] | $\delta^1H_{NH(c)}$ [ppm] | $\delta^{19}F$ [ppm] | $^{1h}\Delta\delta F_{ND}$ [ppm] |
|---|---|---|---|---|---|---|---|---|---|---|
| H | H | H | 61 | 51 | 34 | 12.82 | 12.20 | 10.51 | -89.88 | – |
| H | H | D | 60 | 52 | – | 12.89 | 12.21 | – | -90.47 | -0.59 |
| D | H | H | – | 52 | 35 | – | 12.27 | 10.60 | -90.59 | -0.71 |
| H | D | H | 62 | – | 34 | 12.88 | – | 10.53 | -90.63 | -0.75 |

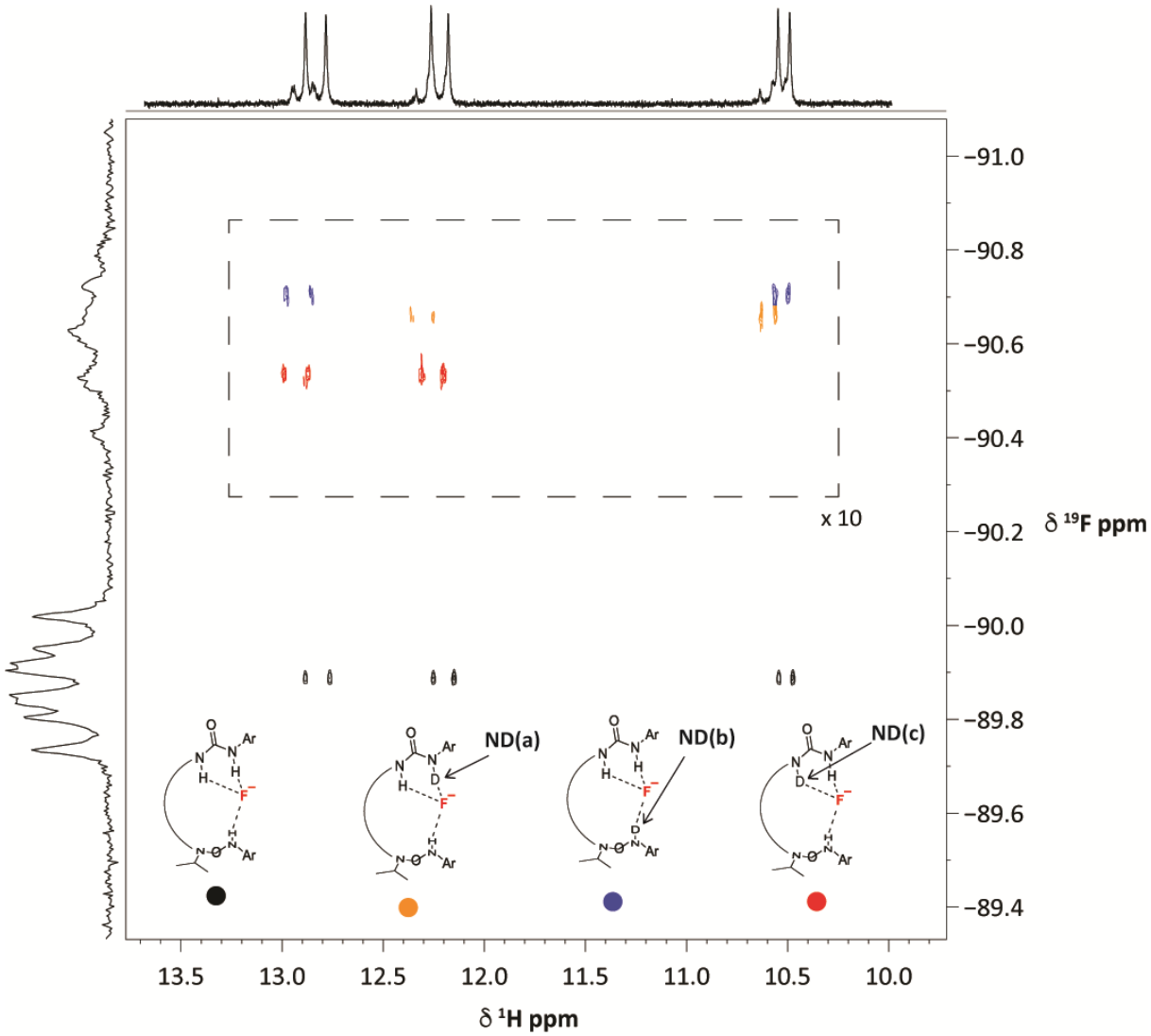



Figure 3.20: $^{1}$H-$^{19}$F CLIP-HSQC of **4u**:TBAF showing $^{1h}J_{NH\cdots F}$ of monodeuterated species (inset, magnified x10) (DCM-$d_2$, 3 mM, 298 K).

*3.2.3.3 Hydrogen Bonding Coupling of bis-Urea TBAF Complexes.* With a robust NMR experiment correlating $^{1h}J_{NH\cdots F^-}$ and internuclear distances in place, we studied how fluoride positioned itself inside the catalytic pocket of a range of different BINAM-derived *bis*-urea catalysts. Thirteen fluoride complexes were formed by addition of 1 equivalent of TBAF to a DCM-$d_2$ solution of the appropriate *bis*-urea (3 mM), and their $^{1h}J_{NH\cdots F^-}$ measured. For every catalyst–fluoride complex $^1$H, $^{19}$F NMR and CLIP-HSQC were recorded at 273 K, to ensure that no proton exchange between catalyst and water was occurring during the analysis. A NOESY experiment was also ran in parallel to help assigning key signals.

Non-alkylated BINAM Urea complexed with TBAF (**4a**:TBAF) at the standard 3 mM concentration, does not present HBC. However, when **4a**:TBAF is recorded at sub-millimolar concentration (0.58 mM) HBC is observed for the pair of symmetrical NH adjacent to the 3,5-bis(trifluoromethyl)phenyl rings, with $^{1h}J_{NH\cdots F^-}$ = 65 Hz and $\Delta\delta_{NH(a/b)}$ = 6 ppm with respect to the unbound **4a**. The fluoride is detected at -86 ppm as a triplet, denoting the presence of a bidentate fluoride complex (Figure 3.21). The pair of NH adjacent to the BINAM backbone, is only slightly shifted downfield upon fluoride binding $\Delta\delta_{NH(c/d)}$ = 1 ppm. Additionally, it appears clear from the number of proton signals that the $C_2$-symmetry is conserved in the complex. These observations suggest that **4a**:TBAF forms a symmetric bidentate complex in which the fluoride is positioned towards the exterior of the catalyst pocket, bound to the two NH(a/b). Participation of the *ortho* aromatic protons H(11) cannot be excluded, however the low concentration of the sample precluded further investigation.

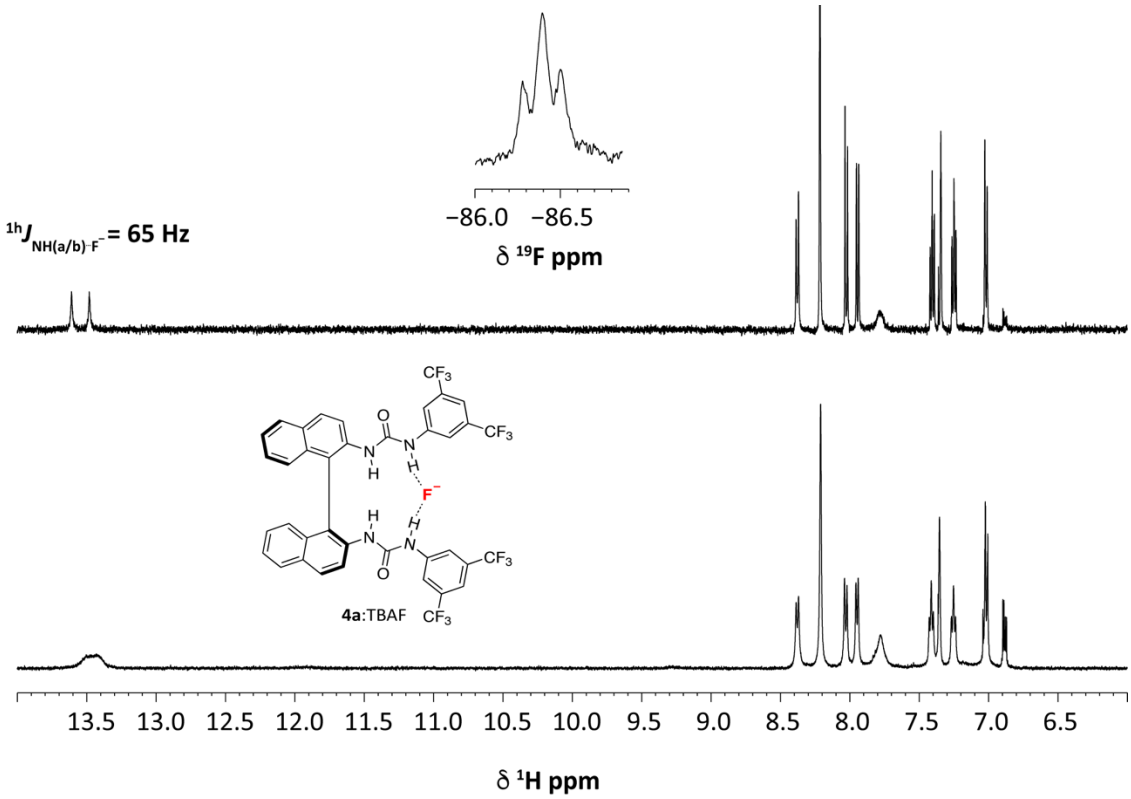
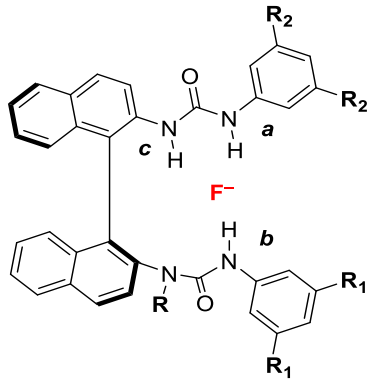



Figure 3.21: $^{1}$H NMR of **4a**:TBAF 2.8 mM (bottom) and 0.58 mM (top) (DCM-$d_2$, 298 K).

Catalysts **4s–4x,** *N*-alkylated with different hydrocarbon chains, display $^{1h}J_{NH\cdots F^-}$ value between 59–61 Hz for NH(a), 48–54 Hz for NH(b) and 33–34 Hz for NH(c) with no substantial changes compared to the *N*-isopropylated model complex **4u:**TBAF (Entry 3–7, Table 3.5). NH(b)···F$^-$ appears to be the most variable interaction, displaying a variation of 6 Hz in $^{1h}J_{NH\cdots F^-}$ within the series. A second set of *bis*-urea–fluoride was prepared where the *N*-alkyl group was fixed (R = iPr) and the 3,5-substituted aromatic rings were modified. These catalysts present different electronic properties; electron-poor rings increase the acidity of the adjacent NH and as a consequence enhance its hydrogen bonding ability; conversely, electron-rich aromatic rings decrease the acidity of the adjacent NH, weakening its relative NH···F$^-$ interaction. Catalyst **4y** ($R_1$ = H, $R_2$ = $CF_3$) and **4ab** ($R_1$ = F, $R_2$ = $CF_3$) were specifically designed to have a weaker NH(b), they indeed present a smaller $^{1h}J_{NH(b)\cdots F^-}$ of 39 Hz and 44 Hz respectively, indicating a reduced degree of interaction between NH(b) and fluoride (Entry 8 and 11, Table 3.5).

An opposite scenario was studied for **4z** ($R_1$ = $CF_3$, $R_2$ = H), **4aa** ($R_1$ = $CF_3$, $R_2$ = Me) and **4ac** ($R_1$ = $CF_3$, $R_2$ = F), weakening NH(a) in favour of NH(b). In this case, while $^{1h}J_{NH(b)\cdots F^-}$ increases its value, it never significantly overcomes that of $^{1h}J_{NH(a)\cdots F^-}$, with **4aa** being the only example studied where $^{1h}J_{NH(b)\cdots F^-}$ is larger in magnitude than $^{1h}J_{NH(a)\cdots F^-}$, although the values are only marginally different (Entry 9, 10 and 12, Table 3.5). This suggests that in **4z** and **4aa**, fluoride is equally shared between NH(a) and NH(b), even if the electronic character of the rings would be in favour of NH(b). Catalyst **4ad** ($R_1$ = $R_2$ = F) presents similar $^{1h}J$ than **4u** for NH(a) and NH(c) but a more pronounced variation in NH(b), which is reduced by 4 Hz (Entry 13, Table 3.5).

Table 3.5: HBC constants $^{1h}J$ and $^{19}F$ chemical shifts of fluoride of *bis*-urea–fluoride complexes.




| Entry | Catalyst | R | $R_1$ | $R_2$ | $^{1h}J_{NH(a)\cdots F^-}$ [Hz] | $^{1h}J_{NH(b)\cdots F^-}$ [Hz] | $^{1h}J_{NH(c)\cdots F^-}$ [Hz] | $\delta$ $^{19}F$ [ppm] |
|---|---|---|---|---|---|---|---|---|
| 1 | **4u** | iPr | $CF_3$ | | 60 | 50 | 33 | -90.53 |
| 2[a] | **4a** | H | $CF_3$ | | 65 | – | – | -86.4 |
| 3 | **4s** | Me | $CF_3$ | | 60 | 54 | 34 | -89.41 |
| 4 | **4t** | Et | $CF_3$ | | 61 | 54 | 34 | -88.64 |
| 5 | **4v** | nPr | $CF_3$ | | 60 | 53 | 33 | -88.79 |
| 6 | **4w** | CyPent | $CF_3$ | | 59 | 48 | 34 | -91.33 |
| 7 | **4x** | 3-Pent | $CF_3$ | | 61 | 52 | 34 | -89.20 |
| 8 | **4y** | iPr | H | $CF_3$ | 63 | 39 | 34 | -93.87 |
| 9 | **4z** | iPr | $CF_3$ | H | 53 | 52 | 33 | -90.15 |
| 10 | **4aa** | iPr | $CF_3$ | Me | 52 | 53 | 34 | -89.79 |
| 11 | **4ab** | iPr | F | $CF_3$ | 60 | 44 | 33 | -91.59 |
| 12 | **4ac** | iPr | $CF_3$ | F | 59 | 51 | 33 | -90.95 |
| 13 | **4ad** | iPr | F | | 59 | 46 | 34 | -91.17 |

The fluoride complexes were generated by addition of one equivalent of TBAF·3H2O (DCM-$d_2$ solution of known concentration) to the *bis*-urea (3 mM in DCM-$d_2$) and measured at 273 K; [a] measured at 0.58 mM, 273 K. See Experimental for a full set of spectra for each complex.

It appears from these data that a different alkylation of the catalyst does not significantly affect fluoride positioning. However, the *N*-alkyl group is required to have a more stable hydrogen bonding network allowing three NH to participate in the binding of fluoride. This aspect is emphasised by the behaviour of **4a**:TBAF, which displays a bidentate binding towards fluoride. **4a**:TBAF presents a higher rate of exchange with water, evidencing coupling only at sub-millimolar concentration. This suggests an overall less dynamically stable bonding due to the presence of only two HB, although of significant strength judging from the large value of $^{1h}J_{NH(a)\cdots F^-}$ of 65 Hz. NH(a) provides almost in every case the dominant hydrogen bonding interaction, even when specifically designed to be weaker; this might be due to a more favourable geometrical arrangement in solution. NH(b) is the hydrogen bond that varies the most within the catalyst tested. NH(c) provides always the weakest contribution settling its *J*-value around 33-34 Hz, however, it must be taken into account that the set of catalysts studied did not allow for a systematic variation of the electronic properties of NH(c).

The chemical shifts of NH(a) and NH(b) linearly correlate with the corresponding $^{1h}J$ coupling constants, with bigger couplings corresponding to more deshielded protons (Figure 3.22). This is typically observed for hydrogen bond couplings, even though the theoretical treatment of nuclear shielding and spin-spin coupling are not rigorously connected.

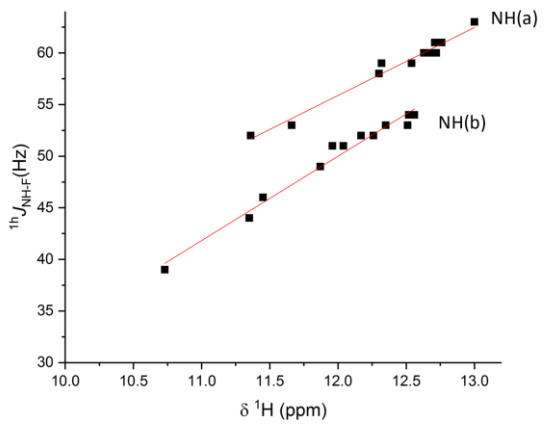



Figure 3.22: Correlation between chemical shifts and $^{1h}J$; NH(a) $R^2$ = 0.9729, NH(b) $R^2$ = 0.9765

Catalyst binding substantially affects fluoride chemical shift. The fluoride complexes investigated in this study display chemical shift varying between -86 and -94 ppm. As previously noted for **4u**:TBAF this results in an overall deshielding effect of around 30 ppm in respect to unbound TBAF in DCM-$d_2$. While fluoride chemical shifts are notoriously difficult to rationalise[27], in this case it appears that stronger hydrogen bonds inevitably result in a more deshielded fluoride. Interestingly, the value of $^{1h}J_{NH(b)\cdots F^-}$ linearly correlates with $F^-$ chemical shift, with bigger *J*-coupling corresponding to a more deshielded $F^-$ (Figure 3.23). This also appears to match the observation from isotopic exchange experiments with deuterium, which suggested that NH(b) has the greatest influence on the chemical shift of fluoride.

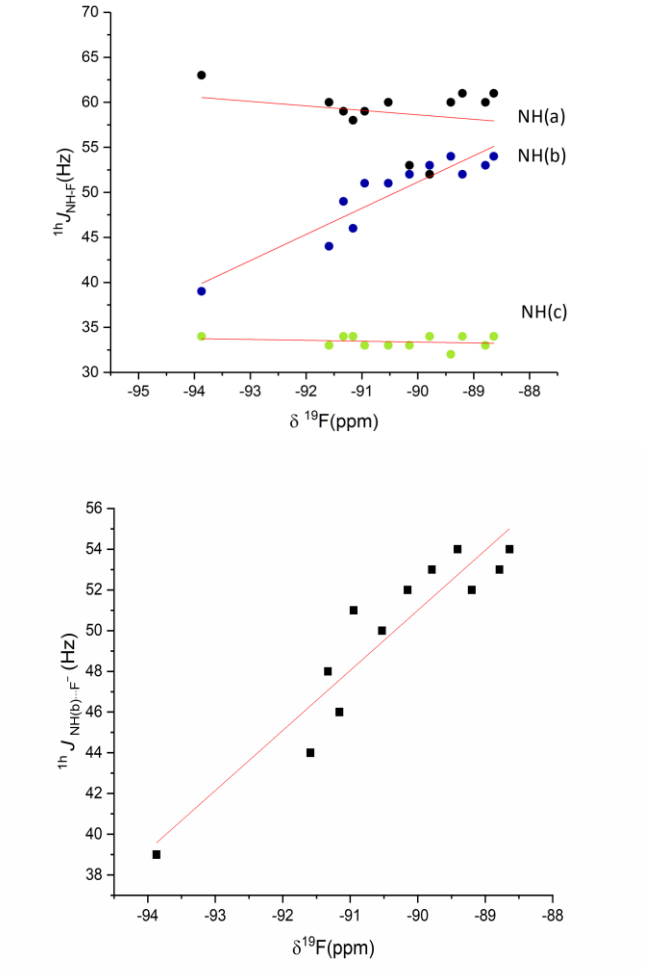



Figure 3.23: Correlation between $^{19}$F chemical shifts and $^{1h}J$ coupling constants for the three NH (top). Detail of the linear correlation between $^{1h}J_{NH(b)\cdots F^-}$ and fluoride chemical shift, $R^2$ = 0.8803 (bottom).

*3.2.4 Complexation with CsF*

Up to this point, we focused our studies on fluoride complexes obtained using tetrabutylammonium fluoride (TBAF) as fluoride source. TBAF is a widely employed source of $F^-$ in organic chemistry, because it ensures excellent solubility in apolar solvents. In our case, **4u**:TBAF proved to be a good model to study *bis*-urea–fluoride binding and complexation in solution and in the solid state. However, fluorinations under HB PTC are carried out with alkali metal fluorides, and they require the formation of a soluble *bis*-urea:CsF adduct as a reaction intermediate. Hence the observation and spectroscopic characterization of the catalyst-CsF complex would provide valuable information on HB PTC.

*3.2.4.1 NMR Study of iPr BINAM Urea–CsF Complex (**4u**:CsF) in Solution.*

Since the solubility of CsF in organic solvents is very limited, a different approach from the one used to generate TBAF complexes was required. The *bis*-urea catalyst (25 mM) was stirred in DCM-$d_2$ with an excess of CsF (50 equivalents) and the filtrate collected in an NMR tube; alternatively, the complex was directly generated inside a sealed NMR tube by sonication of the catalyst and CsF (50 equivalents) in DCM-$d_2$. The two approaches furnished the same NMR data, however the sample prepared filtering out cesium fluoride underwent degradation overtime, showing precipitation of an unidentified white solid within 6 hours. On the other hand, the complex generated inside the sealed NMR tube, with an excess of CsF, is stable at room temperature for months without visible sign of degradation.

$^1$H NMR of **4u**:CsF, at room temperature, shows extensive line broadening indicating that several species equilibrate in solution. $^1$H NMR, carried out at low temperature (293–243 K), reveal three sets of signals; a major species (green circles) and two minor ones (pink circles) having signals of equal intensity (Figure 3.24 A). This is evident for the diagnostic H(16),

ascribed to the isopropyl C–H, indicating that **4u** shows itself in three different chemical environments. The presence of seven NH signals exhibiting $^{1h}J$ coupling also denotes the presence of multiple species in solution. These species are in mutual exchange, as revealed by the negative sign of ROESY cross-peaks (Figure 3.24 B).

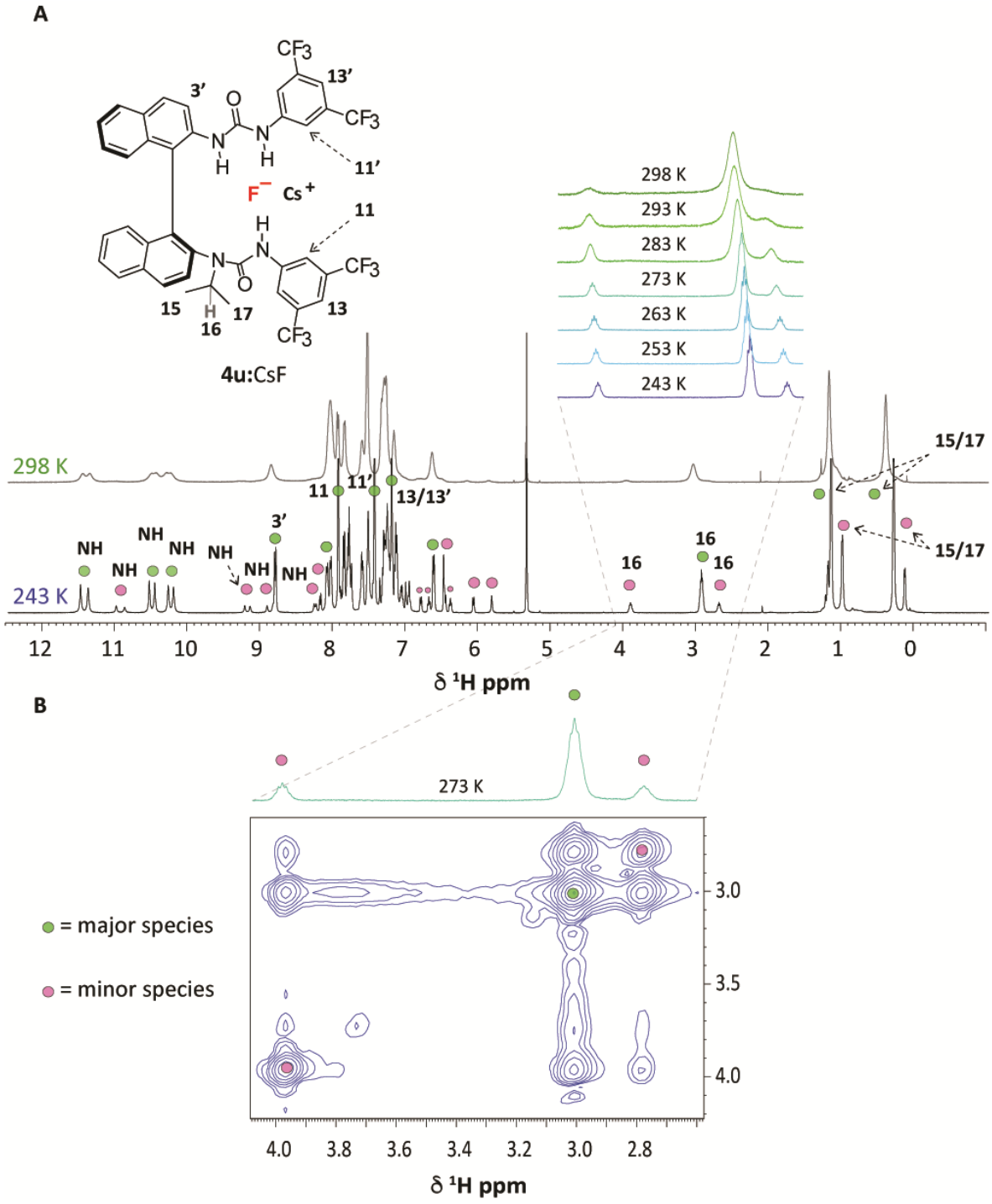



Figure 3.24: A) $^{1}$H NMR of **4u**:CsF (DCM-$d_2$, 25 mM) recorded at 298 K (overlaid, grey line) and 243 K (black line); B) detail of ROESY spectrum recorded at 273 K showing chemical exchange peaks.

The sign of the cross-peaks in ROESY is indicative of a dipolar interaction (nOe) when the cross-peaks have opposite phase to the one of the diagonal, the latter being negative by convention. In contrast, cross-peaks with the same phase of the diagonal indicate a species undergoing an exchange process. In this study, ROESY was used preferentially over NOESY since the latter was unable to differentiate between nOe and exchange processes, both phenomena showing negative cross-peaks for these species at low temperature. This is commonly encountered for slowly tumbling species, such as large (MW > 1000) molecular entities measured below room temperature or in viscous media. This observation also denotes that our system is in the slow-intermediate NMR exchange regime. $^{19}$F NMR between 298 and 243 K shows two signals ascribable to fluorides, a major signal resonating at -65 ppm and a minor at -96 (Figure 3.25). $T_1$ was determined by inversion recovery experiments for both fluoride resonances at room temperature (magnet field strength 11.7 T). The major species shows a $T_1$ of 145 ms while the minor one of just 5 ms. These values are substantially shorter than both **4u**:TBAF (313 ms) and unbound TBAF (1430 ms). This suggests a significantly slower tumbling in solution for the minor species, presumably connected with a larger molecular complex.

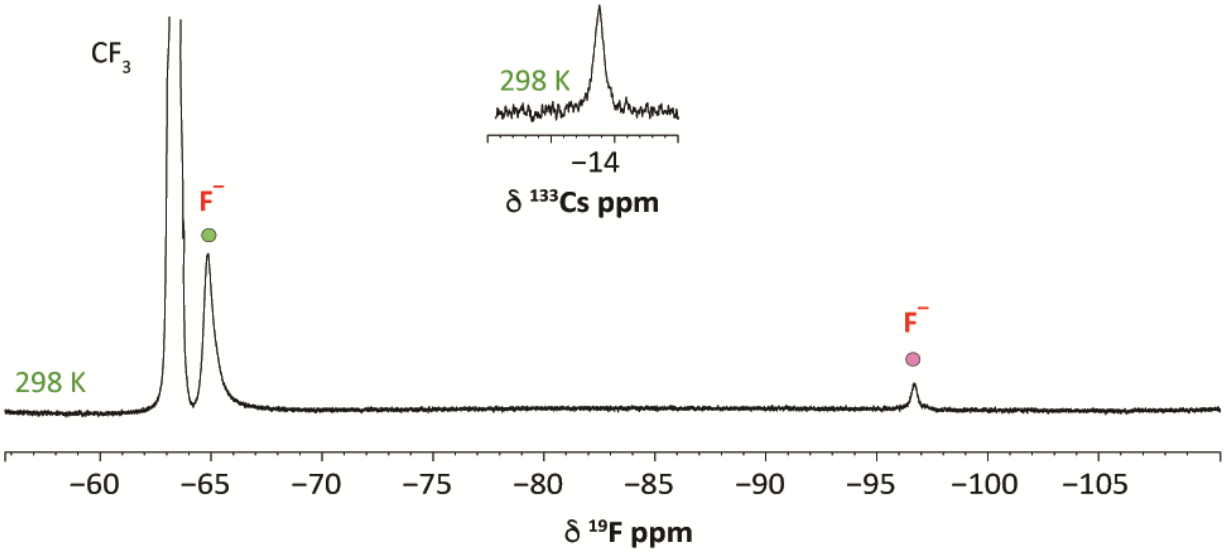



Figure 3.25: $^{19}$F NMR and $^{133}$Cs NMR (inset) of **4u**:CsF (DCM-$d_2$, 25 mM, 298 K).

$^{133}$Cs NMR shows one significantly wide peak (Figure 3.25, inset), broadened both from its quadrupolar moment and from the dynamic averaging of multiple species. The $^{133}$Cs signal is recorded at -14 ppm at room temperature and shows deshielding and severe line broadening with the lowering of the temperature.

Proton diffusion experiments ($^{1}$H DOSY) carried out at 243 K reveals that the three sets of peaks belong to only two species, as already inferred from $^{19}$F NMR. The minor species (pink circle) has a lower diffusion coefficient ($D$ = 1.9 x $10^{-10}$ $m^2s^{-1}$) denoting a larger (slower) molecular complex, while the major species (green circle) displays faster diffusion ($D$ = 2.4 x $10^{-10}$ $m^2s^{-1}$). These data are consistent with the presence in solution of a 1:1 complex Cs[U:F] (U= **4u**) as major species, and a non-symmetrical 2:1 complex incorporating two molecules of urea for every molecule of cesium fluoride, Cs[$U_2$:F], as the minor species (Figure 3.26). The two complexes are in equilibrium with a ratio Cs[U:F]/ Cs[$U_2$:F] of 85:15, as estimated by the relative integration of the fluoride peaks at room temperature.

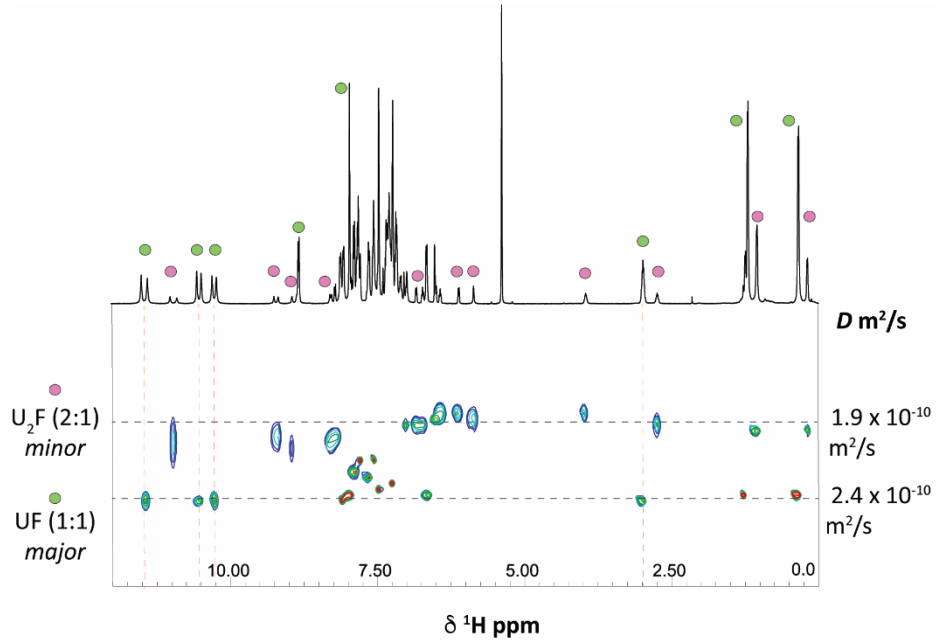



Figure 3.26: $^{1}$H DOSY pseudo-2D spectra of **4u**:CsF (DCM-$d_2$, 25 mM, 243 K). See Experimental for details.

In analogy with **4u**:TBAF, the three NH belonging to the 1:1 Cs[**4u**:F] complex were assigned based on nOe correlations. The relative shielding of NH protons measured at 243 K, matches the one found for **4u**:TBAF, with NH(a) being the most deshielded (δ NH(a) = 11.46 ppm), followed by NH(b) (δ NH(b) = 10.52 ppm), and NH(c) (δ NH(c) = 10.26 ppm). Cs[**4u**:F] displays $^{1h}J_{NH\cdots F^-}$ splitting of 52 Hz for NH(a), 37 Hz for NH(b) and 34 Hz for NH(c). This contrasts with **4u**:TBAF that shows 61 Hz for NH(a), 51 Hz for NH(b) and 34 Hz for NH(c). $^{1h}J_{NH\cdots F^-}$ for NH(a) and NH(b) are diminished, compared to the complex having $TBA^+$ as counter-ion. NH(b) shows the biggest decrement with a coupling constant reduced by 14 Hz. $^1$H-$^{19}$F CLIP-HSQC was used for the identification of the NH belonging to both species of **4u**:CsF (Figure 3.27–3.28). At 273 K only the cross-peaks referred to the $NH\cdots F^-$ of Cs[**4u**:F] are visible, while at 243 K only those belonging to Cs[(**4u**)$_2$:F], this is ascribed to the different linewidths at different temperatures showed by the two species.

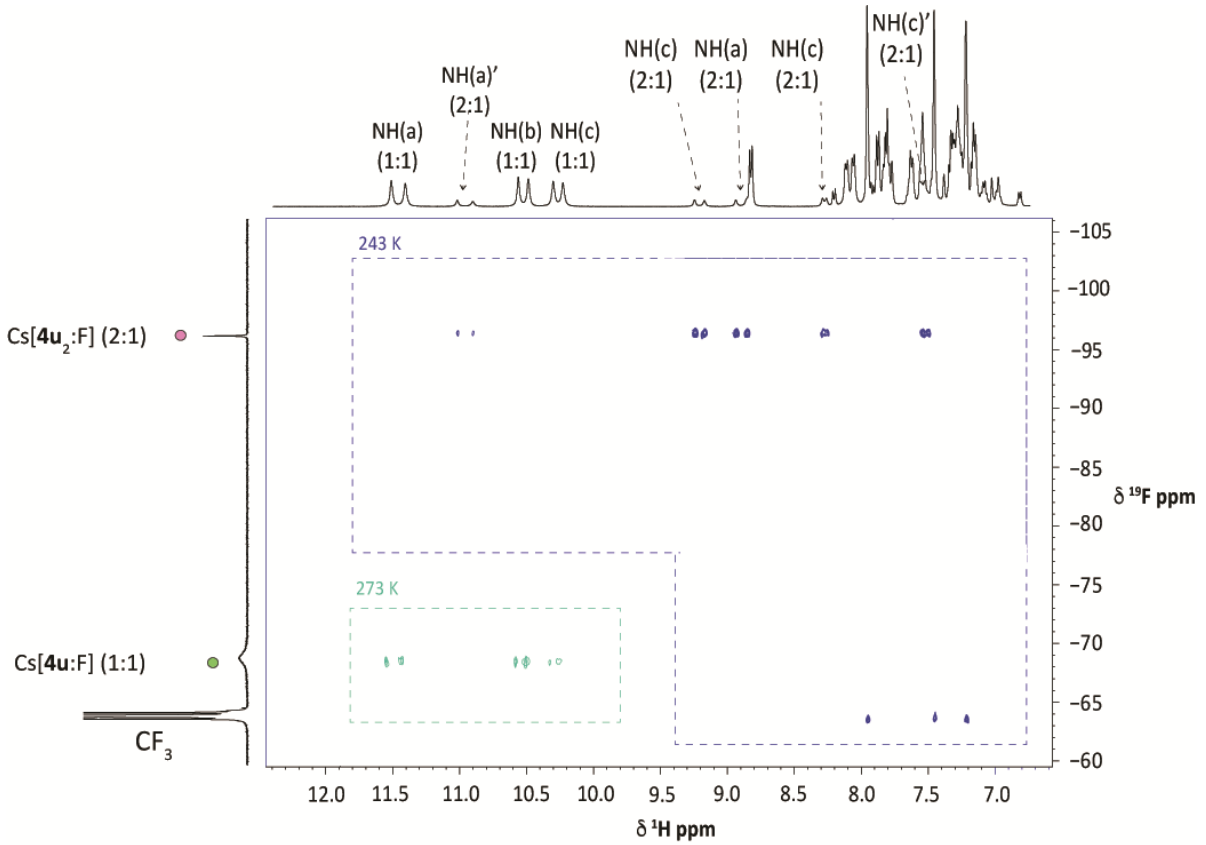



Figure 3.27 Stacked $^1$H-$^{19}$F CLIP-HSQC of **4u**:CsF measured at 273 K (azure) and 243 K (blue), (DCM-$d_2$, 25 mM).

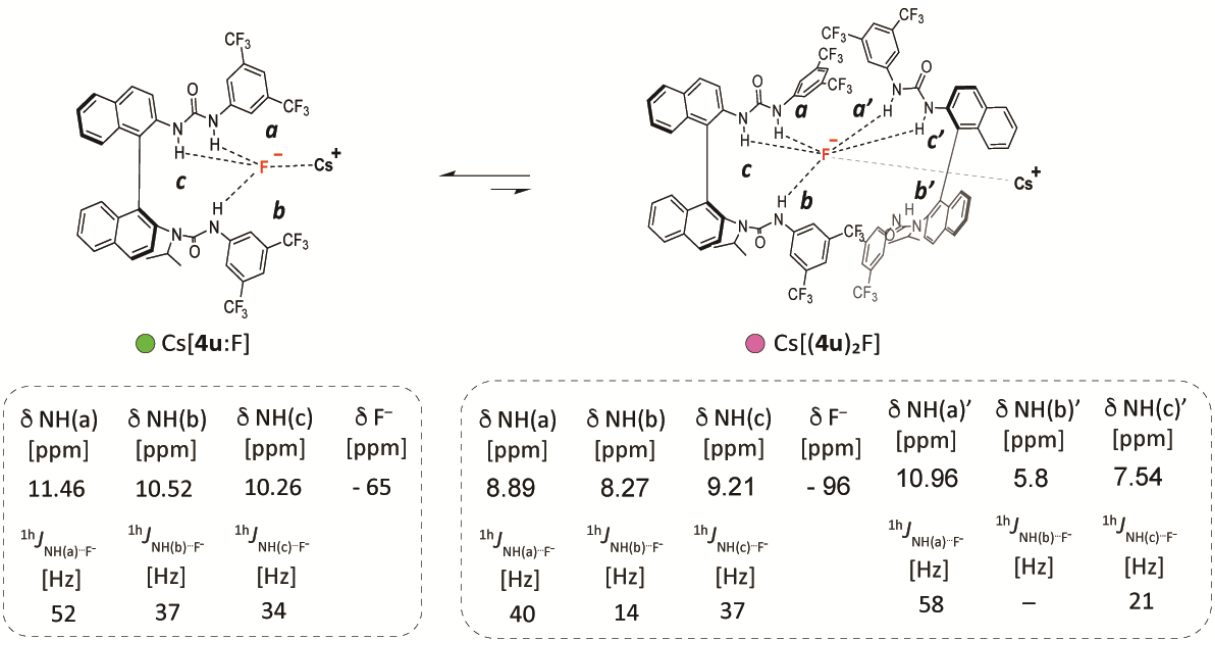



Figure 3.28: NMR parameters measured for 1:1 **4u**:CsF, (Cs[UF], and for 2:1 4u:CsF, Cs[U2F].

The 2:1 Cs[(**4u**)$_2$:F] complex shows five NH···F correlation in $^{1}$H-$^{19}$F CLIP-HSQC. The assignment of these signals was accomplished using NOESY and ROESY experiments (Figure 3.29). NOESY experiments measured at 273 K using a short mixing time ($\tau_m$ = 80 ms), showed predominantly exchange processes which are dominant over nOe effects. This was used to relate the NH already assigned for the 1:1 complex Cs[**4u**:F], to the ones of Cs[**4u**$_2$:F]; ROESY cross-peaks were then employed to distinguish between the two triads NH(a), NH(b), NH(c) and NH(a)', NH(b)', NH(c)' belonging to the 2:1 complex. In Cs[(**4u**)$_2$F], one molecule of **4u** exhibits a tridentate binding ($^{1h}J_{NH(a)\cdots F^-}$ = 40 Hz, $^{1h}J_{NH(b)\cdots F^-}$ = 14 Hz, $^{1h}J_{NH(c)\cdots F^-}$ = 37 Hz,) while the other molecule binds only with the non-alkylated urea ($^{1h}J_{NH(a)'\cdots F^-}$ = 58 Hz, $^{1h}J_{NH(c)'\cdots F^-}$ = 21 Hz). NH(b)' does not interact with fluoride and is substantially shielded, resonating at 5.8 ppm.

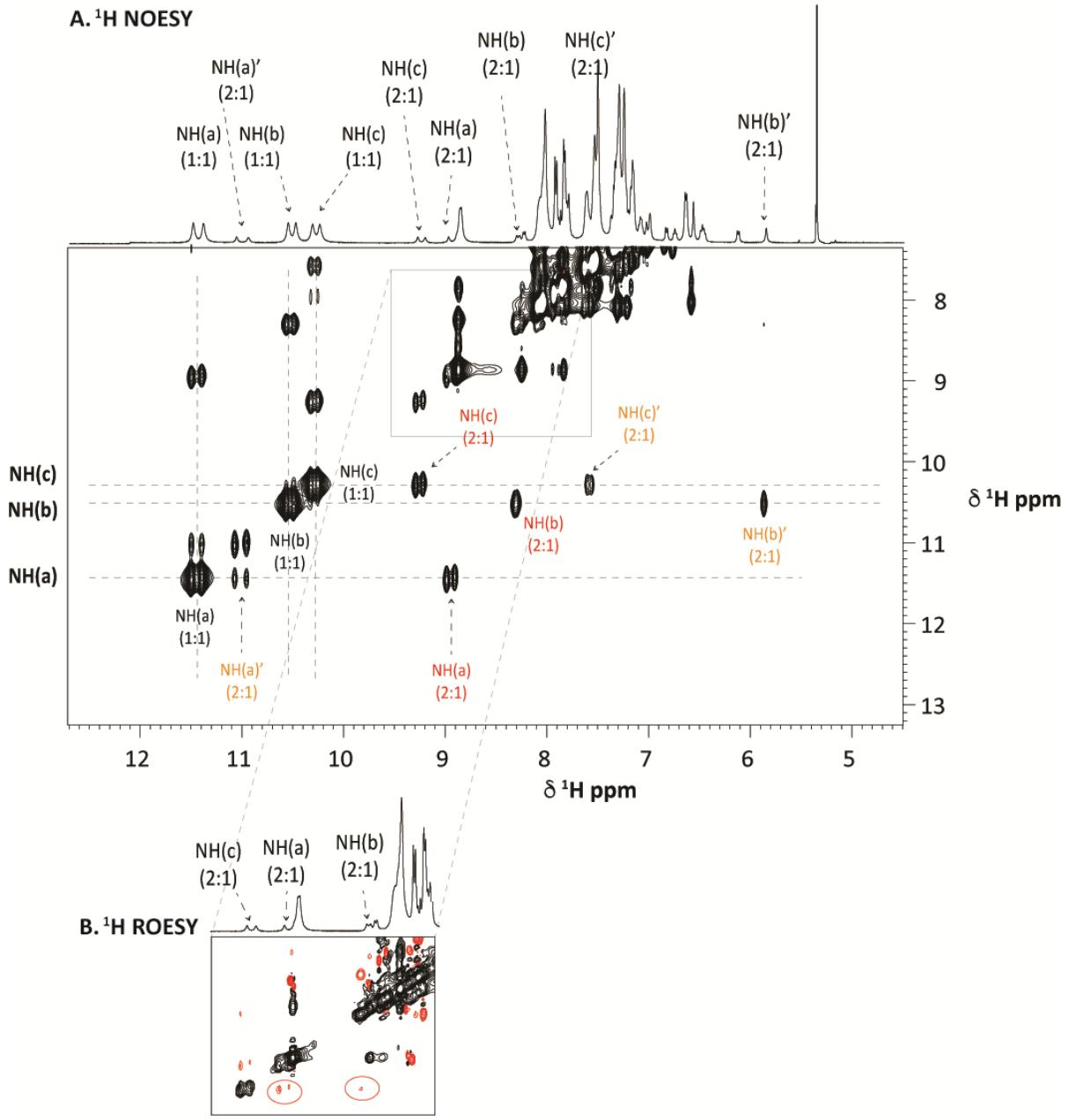



Figure 3.29: A) $^{1}$H NOESY of **4u**:CsF (DCM-$d_2$, 25 mM, 273 K, $\tau_m$ = 80 ms); B) detail of $^{1}$H ROESY of **4u**:CsF (DCM-$d_2$, 25 mM, 243 K, p15 = 100ms)

Taken together these data indicate that the complexation of **4u** with CsF leads to an equilibrium between a 1:1 and a 2:1 complex. Cs[**4u**:F] binds fluoride with three NH···F$^-$ hydrogen bonds. The interaction of the two strongest HB, NH(a)···F$^-$ and NH(b)···F$^-$, is diminished in the CsF complex with respect to **4u**:TBAF. This is more prominent for NH(b) that presents a small $^{1h}J$ comparable with NH(c) ($^{1h}J_{NH(b)\cdots F^-}$ = 37 Hz, $^{1h}J_{NH(c)\cdots F^-}$ = 34 Hz). The overall conformation of the catalyst complex is related to the one observed in **4u**:TBAF, judging by

the similarity in the NMR data. Cs[(**4u**)$_2$F] is a 2:1 complex that binds fluoride with five NH···F$^-$ contacts from two molecules of **4u**. In this case, NH(b)···F$^-$ is the weakest contributor to the HB network, displaying in one molecule of **4u** constituting the complex a small $^{1h}J$ of 14 Hz while no NH(b)···F$^-$ is detected by NMR for the other *bis*-urea . One striking detail of **4u**:CsF is that the two F$^-$ resonances strongly differ in their chemical shift. In Cs[U$_2$:F], F$^-$ appears at -96 ppm, while in Cs[U:F] the fluoride chemical shift is measured at -65 ppm. This large difference can account for the Cs$^+$ counter-cation effect. In the case of the 2:1 complex Cs[U$_2$:F], the fluoride at -96 ppm does not interact significantly with Cs$^+$, while in Cs[U:F] the anomalous value of -65 ppm is consistent with the proximity of Cs$^+$, which forms in DCM solution a tight ion pair with F$^-$.

*3.2.4.2 Crystal Structure of **4ad**:CsF.* Unfortunately, attempts to obtain a crystal suitable for X-ray diffraction of **4u**:CsF ultimately failed, however the serendipitous crystallization of the fluorinated analogue **4ad** in the presence of CsF allowed us to study the solid-state structure of the corresponding complex. **4ad**:CsF in the solid state forms columnar superstructures where Cs$^+$ is bridged between F$^-$ and the two carbonyls of a second *bis*-urea (Figure 3.30). Considering a single asymmetric unit cell, the complex shows a 1:1 binding mode to fluoride, hydrogen bonded by the three NH. The structure of the BINAM scaffold is similar to the one of **4u**:TBAF in the solid state, with a slightly wider BINAM dihedral angle of 79 ° (*cf.* **4u**:TBAF BINAM dihedral angle = 74 °); the angle between the two ureas and fluoride in this case is of 65 °, reduced with respect to the X-ray structure of **4u**:TBAF (*cf.* **4u**:TBAF ∠ C–F–C = 69 °). Relevant HB parameters are reported in Table 3.6. Remarkably, NH(b)···F$^-$ shows the longest HB (N**H**(b)-**F**$^-$ = 2.096 Å) distance and smallest N–H–F angle (∠ N–H–F = 144 °) compared to NH(a) and NH(c). This is ascribed to a prominent cation–π interaction observed from Cs$^+$ to one naphthyl ring, capable to effectively positions fluoride towards the bidentate urea,

weakening the NH(b) contribution. $Cs^+$ is bound to $F^-$ in the solid state, with a Cs–F distance of 2.74 Å, 0.05 Å longer than the distance in the CsF lattice (2.69 Å).[28] Comparing these data with the H···$F^-$ distances of **4ad**:TBAF in DCM-$d_2$ determined by NMR (Table 3.6) it results an elongation of H(b) ···$F^-$ in the solid state compared to the TBAF complex in solution and a concomitant shortening of H(c) ···$F^-$. H(a) ···$F^-$ displays the same HB distance in solution and in the solid state, within error margin.

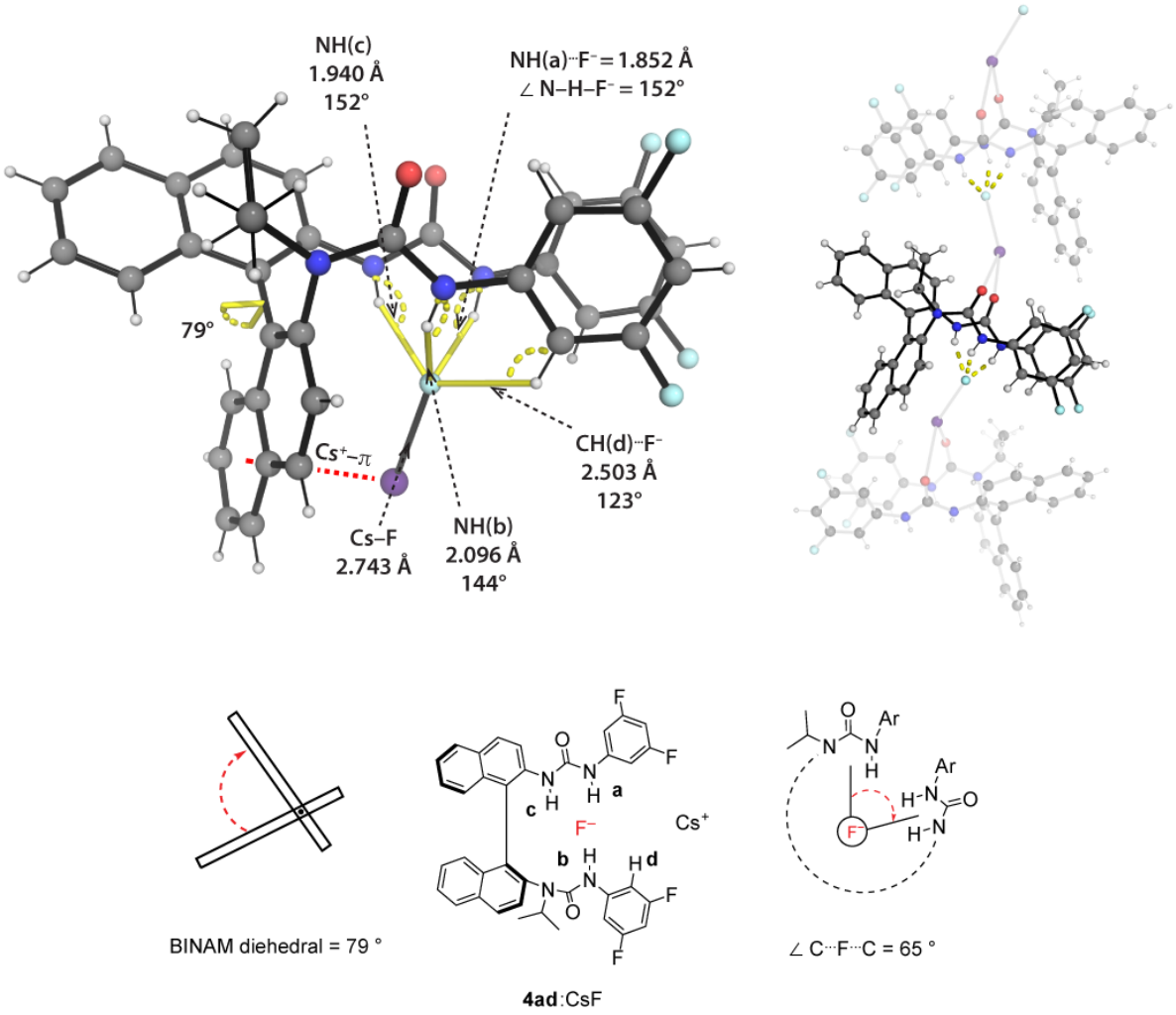



Figure 3.30: X-ray structure of **4ad**:CsF. SCXRD data acquired and solved by Dr. G. Pupo.

From these insights combined with NMR data, it appears that the presence of $Cs^+$ in place of $TBA^+$ does not substantially modify the overall structure of the catalyst–fluoride complex, however, the interaction of $Cs^+$ with the BINAM scaffold effectively weaken the NH(b)···$F^-$ contribution.

Table 3.6*:* Relevant internuclear distances and angles of **4ad**:CsF; D = HB donor, A = HB acceptor. [a] Determined by NMR from HOESY experiments.

| DH···A | *d* D–H [Å] | *d* D–A [Å] | *d* H···A [Å] | *d* H···A [Å] NMR [a] | ∠ X –H–F [°] |
|---|---|---|---|---|---|
| NH(a)···$F^-$ | 0.856 | 2.640 | 1.852 | 1.83 | 152 |
| NH(b)···$F^-$ | 0.855 | 2.834 | 2.096 | 1.91 | 144 |
| NH(c)···$F^-$ | 0.861 | 2.730 | 1.940 | 2.05 | 152 |
| CH(d)···$F^-$ | 0.930 | 3.111 | 2.503 | – | 123 |

*3.2.4.3 NMR Study of **4y**:CsF in Solution.* The weakening effect that the $Cs^+$ counter-cation displays on NH(b)···$F^-$ prompted us to investigate the CsF complex of *bis*-urea **4y** which presents a phenyl ring adjacent to the isopropylated urea in place of the 3,5-bis(trifluoromethyl)phenyl group. This is an interesting example, since **4y**:TBAF already showed a reduced NH(b)···$F^-$ interaction, as demonstrated by the small $^{1h}J_{NH(b)\cdots F^-}$ value of 39 Hz. Similarly to **4u**:CsF, the complex was generated inside a sealed NMR tube by sonication of **4y** (25 mM) and CsF (50 equivalents.) in DCM-$d_2$. Also in this case, analyses of proton signals required lowering of the temperature to slow down the equilibration of multiple species.$^1$H NMR at 243 K shows two sets of signals, while $^{19}$F NMR presents a single fluoride peak resonating at -99.5 ppm (Figure 3.31).

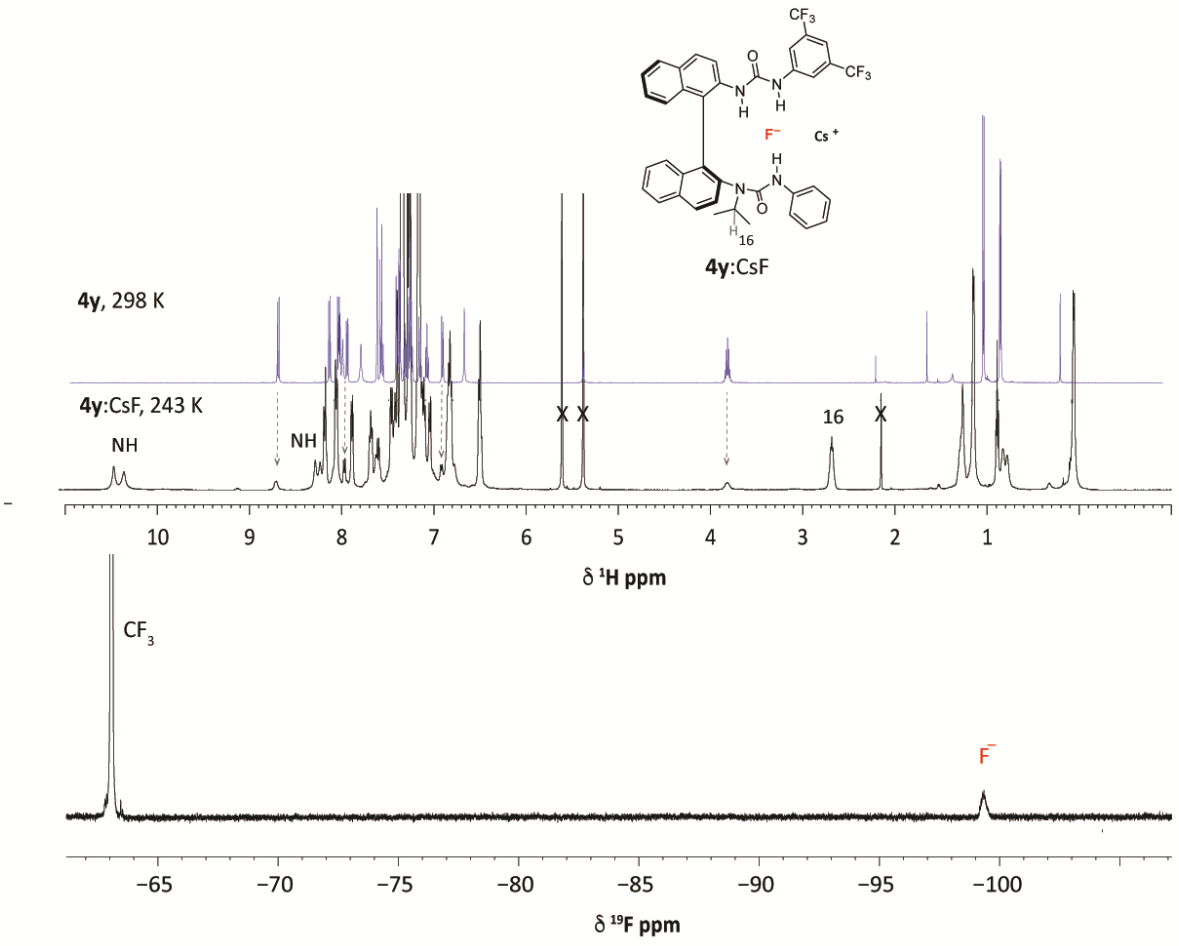



Figure 3.31: $^1$H NMR and $^{19}$F NMR of **4y**:CsF (DCM-$d_2$,25 mM, 243 K), overlaid $^1$H NMR of **4y** (DCM-$d_2$,m25 mM, 298 K).

The major species in $^{1}$H NMR presents two visible signals corresponding to NH groups deshielded at 11.4 ppm and at 8.3 ppm, while also displaying HBC coupling with fluoride. The third NH is not observed and is presumably submerged into the aromatic region. The minor species accounts for the unbound *bis*-urea, since its proton peaks match the ones of **4y** independently measured in DCM-$d_2$ at 298 K (Figure 3.31, overlaid spectrum). Accordingly, diffusion measurements ($^{1}$H DOSY) carried out on **4y**:CsF at 243 K indicate a slower diffusion for the major species ($D_{\mathbf{4y}:CsF}$ = 1.2 x $10^{-10}$) compared to the minor component (**4y**), which as expected shows a substantially larger diffusion coefficient ($D$ = 3.3 x $10^{-10}$, Figure 3.32 A).

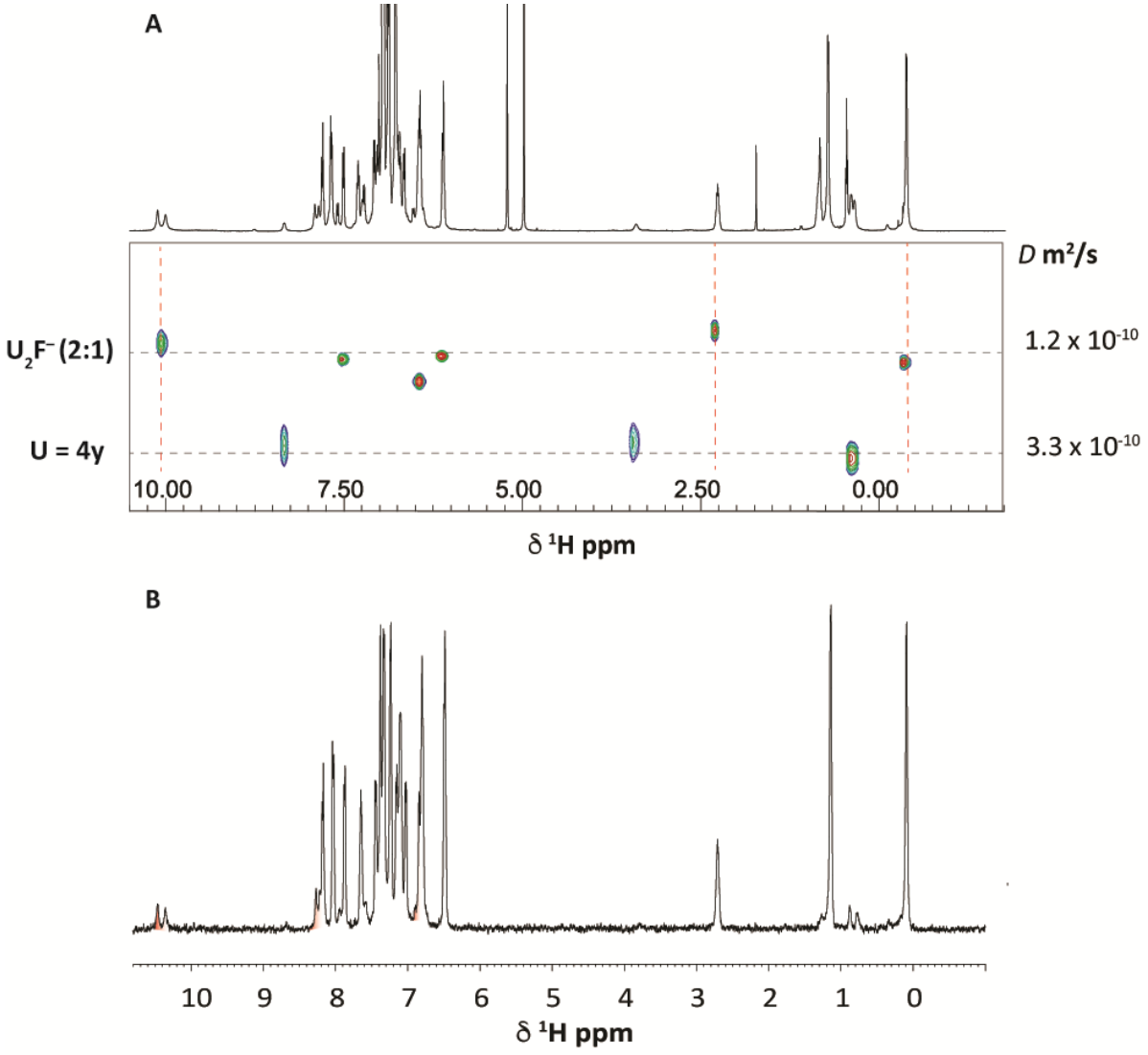



Figure 3.32: A) $^{1}$H DOSY pseudo-2D spectra of **4y**:CsF (DCM-$d_2$,25 mM, 243 K); B) 1D DOSY of **4y**:CsF acquire using $G_z$ = 90%. See Experimental for details.

$^{1}$H NMR of **4y**:CsF was acquired by using a 1D DOSY sequence, which effectively removes from the spectrum the signals belonging to **4y** as well as solvent peaks; this is possible since the self-diffusion of **4y**:CsF and **4y** is sufficiently different (Figure 3.32 B). The diffusion coefficient of **4y**:CsF is similar to the one measured for Cs[**4u**$_2$:F] at the same temperature and concentration ($D_{\mathbf{4y}:CsF}$ = 1.2 x $10^{-10}$ *cf.* $D_{2:1,\ \mathbf{4u}:CsF}$ = 1.9 x $10^{-10}$ , 243 K, 25 mM). Additionally, the fluoride peak of **4y**:CsF resonates at similar frequency compared to Cs[**4u**$_2$:F] ($\delta\,^{19}F_{\mathbf{4y}:CsF}$ = -99.5 ppm *cf.* $\delta\,^{19}F_{2:1,\ \mathbf{4u}:CsF}$ = -96 ppm). These observations suggest that **4y**:CsF in solution forms a 2:1 complex with CsF, differently from **4u**:CsF the NMR spectra of **4y**:CsF are consistent with a symmetric adduct.

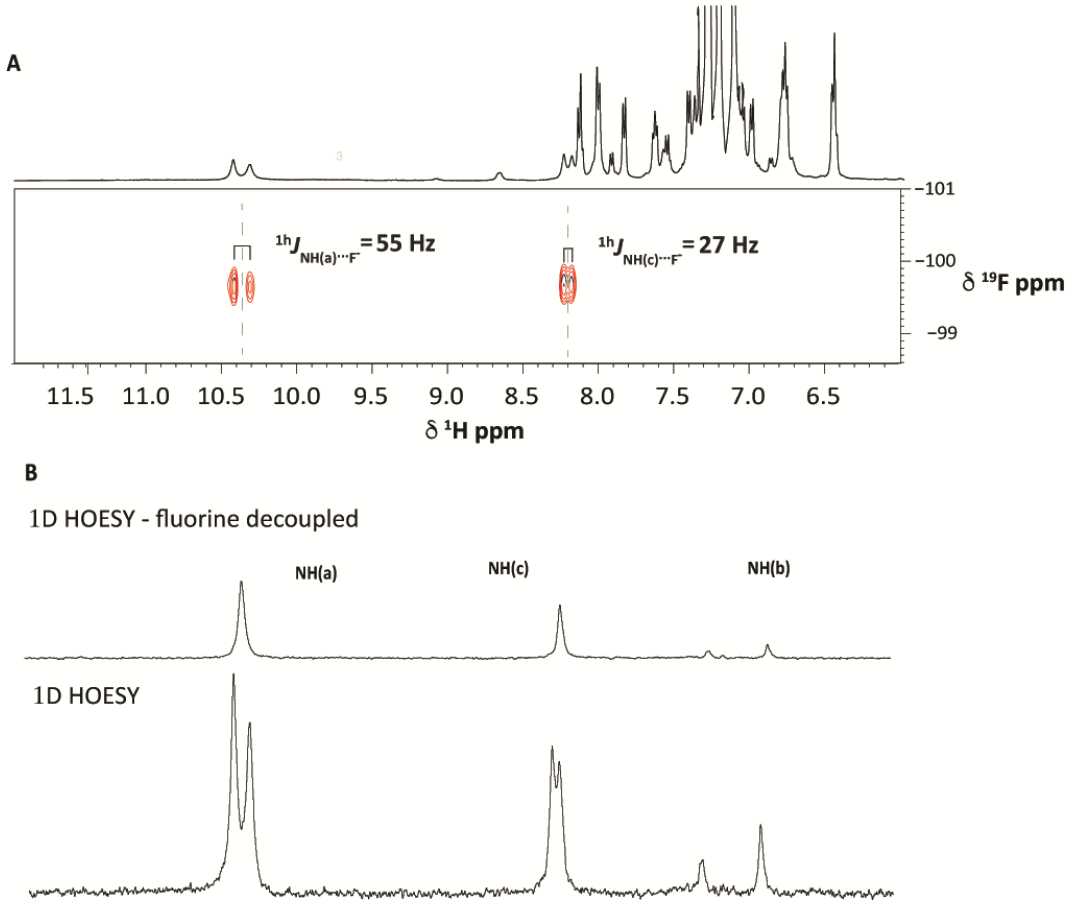



Figure 3.33: A) $^{1}$H-$^{19}$F CLIP-HSQC of **4y**:CsF (DCM-d$_2$,25 mM, 243 K); B) $^{1}$H-$^{19}$F HOESY with proton decoupling during acquisition (top) and $^{1}$H-$^{19}$F HOESY showing HBC with fluoride (bottom, DCM-d$_2$, 25 mM, 243 K).

The assignment of the NH resonances, achieved using ROESY, reveals that the doublet at 10.4 ppm corresponds to NH(a), while the resonance at 8.2 ppm is ascribed to NH(c). $^{1}$H-$^{19}$F CLIP-HSQC and $^{1}$H-$^{19}$F HOESY confirm that NH(a) and NH(c) show hydrogen bonding coupling with fluoride, with constants of 55 Hz, $^{1h}J_{NH(a)\cdots F^-}$, and of $^{27}$ Hz ,$^{1h}J_{NH(c)\cdots F^-}$ (Figure 3.33). NH(b) is detected at 6.8 ppm; the absence of HBC and the peak of low intensity measured by HOESY indicate that NH(b) does not form a hydrogen bond interaction with fluoride.

These data indicate that **4y**, engineered to have a weak NH(b)$\cdots F^-$, binds CsF exclusively *via* the bidentate urea, employing hydrogen bonds from NH(a) and NH(c). The NMR data of **4y**:CsF are consistent with a 2:1 complex, however further insights into the conformation of the complex are limited by the presence of a symmetry element that generates a single set of resonances in $^{1}$H NMR. In contrast, **4y**:TBAF showed tridentate binding with $^{1h}J$ values of 63 Hz for NH(a), 39 Hz for NH(b) and 34 Hz for NH(c). This corroborates the hypothesis that the presence of $Cs^+$ in place of $TBA^+$ reduces the NH$\cdots F^-$ hydrogen bonding interactions with a more prominent effect on NH(b) $\cdots F^-$.

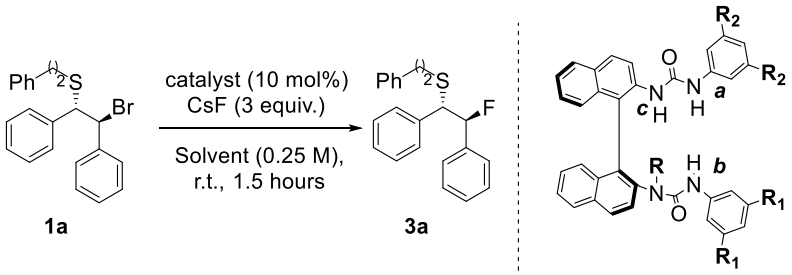
*3.2.5 Implication for Catalysis*

The NMR spectroscopic analyses revealed important details about catalysts' structure allowing investigations on the binding mode of *bis*-ureas with TBAF, and ultimately demonstrating the formation of a *bis*-urea–CsF complex that was characterised in solution. Preliminary mechanistic studies (*v.* 2.2.3 Preliminary mechanistic insights) have shown that a 1:1 catalyst–fluoride complex participates in the enantiodetermining transition state of fluorinations under HB PTC; the conformation of the fluoride complex in the TS is closely related to the one that the *bis*-urea–fluoride complex adopts in the solid state and in solution. The structure and conformation of the *bis*-urea fluoride intermediate is thus key for the stereochemical outcome of the reaction.

*3.2.5.1 Reactivity and Enantioselectivity of bis-Urea Catalysts.* The catalytic performance of our set of catalysts was evaluated versus a model reaction using **1a** in DCM or 1,2-DFB, at room temperature for 1.5 hours (Table 3.7). Initially, reactivity and enantioselectivity of catalysts having different *N*-alkyl groups, **4s**–**4x** and of the non-alkylated *bis*-urea **4a** (Entry 2–7, Table 3.7) were measured and compared. Catalysts **4a**–**4x** provided an excellent yield (>95%), presumably derived from the presence of the 3,5-bis-(trifluoromethyl)phenyl substituents on the ureas which ensures strong binding with fluoride ($K_{a\ 1:1}$ = 0.8 x $10^6$ $M^{-1}$ for **4a** and $K_{a\ 1:1}$ =1.05 x $10^6$ $M^{-1}$ for **4u**) and thus an effective phase-transfer. BINAM urea (**4a**), lacking *N*-alkylation, was less enantioselective than all its alkylated analogues (Entry 2, 86:14 e.r.). For catalysts **4t**–**4w** the difference in enantioselectivity was very small (89.5:10.5–90:10 e.r.); Notably *N*-methylated catalyst **4s** performed worse than the other alkylated *bis*-ureas tested, providing an enantiomeric ratio of 88:12. Conversely, *N*-(3-pentyl) catalysts **4x** provided the best enantioselectivity (Entry 7, 91:9 e.r.). The small variation in enantioselectivity of catalyst with different *N*-alkyl groups suggests that the structure of the alkyl does not play a prominent

role in the enantiodetermining transition states. This is corroborated by NMR conformational analyses, X-ray structures and DFT calculation which indicate that the *N*-alkyl substituent points towards the exterior of the catalytic pocket. However, the presence of an *N*-alkyl substituent is important for enantioselectivity, since invariably *N*-alkylated bis-urea display higher level of enantioselectivity than **4a**. NMR data showed that *N*-alkylated catalysts form tridentate *bis*-urea–fluoride complexes while **4a,** lacking *N*-substituents, display a bidentate binding with fluoride.

Table 3.7: Evaluation of catalytic performance of *bis*-urea catalysts **4a–4ad**.




| | | | | | 1,2-DFB | | DCM | |
|---|---|---|---|---|---|---|---|---|
| Entry | Catalyst | R | $R_1$ | $R_2$ | Yield [a] % | e.r. [b] | Yield [a] % | e.r. [b] |
| 1 | **4u** | iPr | $CF_3$ | | >95 | 90:10 | >95 | 88:12 |
| 2 | **4a** | H | $CF_3$ | | >95 | 86:14 | >95 | 82:18 |
| 3 | **4s** | Me | $CF_3$ | | >95 | 88:12 | >95 | 83.5:16.5 |
| 4 | **4t** | Et | $CF_3$ | | >95 | 90:10 | >95 | 87.5:12.5 |
| 5 | **4v** | nPr | $CF_3$ | | >95 | 89.5:10.5 | >95 | 88:12 |
| 6 | **4w** | cPent | $CF_3$ | | >95 | 89:11 | >95 | 87.5:12.5 |
| 7 | **4x** | 3-Pent | $CF_3$ | | >95 | 91:9 | >95 | 89.5:10.5 |
| 8 | **4y** | iPr | H | $CF_3$ | 18 | 76.5:23.5 | 36 | 77:23 |
| 9 | **4z** | iPr | $CF_3$ | H | 75 | 86.5:13.5 | 85 | 84:16 |
| 10 | **4aa** | iPr | $CF_3$ | Me | 48 | 87.5:12.5 | 80 | 84.5:15.5 |
| 11 | **4ab** | iPr | F | $CF_3$ | 68 | 81:19 | 18 | 79:21 |
| 12 | **4ac** | iPr | $CF_3$ | F | >95 | 88.5:11.5 | >95 | 86:14 |
| 13 | **4ad** | iPr | F | | >95 | 72:28 | >95 | 74:26 |

General conditions: substrate (0.05 mmol), catalyst (0.005 mmol) and CsF (0.06 mmol) in 200 µL of solvent stirred at 1200 rpm for the indicated time; [a] Determined by $^{19}F$ NMR using 4-fluoroanisole as internal standard; [b] e.r. was determined by HPLC analysis using a chiral stationary phase; [c] **4u**:CsF was generated by sonicating **4u** and CsF (50 equiv.) in DCM-$d_2$ (25 mM) for 2 hours. 1,2-DFB = 1,2-difluorobenzene

Reactivity and enantioselectivity of a second set of catalysts having differently substituted aromatic rings were subsequently assessed (Entry 8–13, Table 3.7). When the aryl proximal to the alkylated urea is a phenyl (**4y**, $R_1$ = H, $R_2$ = $CF_3$) both reactivity and selectivity decrease drastically (Entry 8, 18 % yield, 76.5:23 e.r.). Conversely, when phenyl is installed proximal to the bidentate urea (**4z**, $R_1$ = $CF_3$, $R_2$ = H) only a moderate decrease in both yield an enantioselectivity is observed (Entry 9, 75 % yield, 86.5:13.5 e.r.). When the 3,5-bis(methyl)phenyl group is introduced (**4aa**, $R_1$ = $CF_3$, $R_2$ = $CH_3$), slightly better enantioselectivity is measured albeit with a lower yield (Entry 10, 48 % yield, 87.5:12.5 e.r.). Fluorinated analogue **4ab,** bearing fluorine in place of trifluoromethyl on the aromatic ring adjacent to the alkylated urea ($R_1$ = F, $R_2$ = $CF_3$), provides better results than **4y** (Entry 11, 68 % yield, 81:19 e.r.); however, fluorine substitution on the aryl ring adjacent to the bidentate urea **4ac** ($R_1$ = $CF_3$, $R_2$ = F) provides significantly improved reactivity and enantioselectivity (Entry 12, >95 % yield, 88.5:11.5 e.r.), comparable with the benchmark **4u** (*cf.* Entry 1, >95 % yield, 90:10 e.r). Substitution of the trifluoromethyl groups on both aromatic rings, with fluorine (**4ad**, $R_1$, $R_2$ = F) is severely detrimental for enantioselectivity while displaying good reactivity (Entry 13, >95 % yield, 72:28 e.r.).

Catalyst modifications affecting the electronic properties of the aromatic ring proximal to the alkylated urea ($R_1$ substitution), have a much more pronounced effect than modification of the ring proximal to the bidentate urea ($R_2$ substitution), the latter consistently resulting in better yields and enantioselectivities. The NMR data of the corresponding catalyst–TBAF complexes indicate that *bis*-urea having larger $^{1h}J_{NH(b)\cdots F^-}$, thus stronger $NH_{(b)}\cdots F^-$ contribution, correlate with better reaction outcome, thereby suggesting that $NH(b)\cdots F^-$ is a key interaction for achieving high yield and enantioselectivity in HB PTC. This is evident for catalyst **4y** ($R_1$ = H, $R_2$ = $CF_3$) which displays low reactivity and selectivity, together with a small $^{1h}J_{NH(b)\cdots F^-}$ value

when complexed with TBAF, while the NH(b)···$F^-$ interaction is absent in **4y**:CsF. Catalyst **4ad** contrasts with these observations, showing excellent reactivity and particularly low enantiocontrol while having $^{1h}J_{NH(b)\cdots F^-}$ of 46 Hz in the corresponding TBAF complex. In this specific case, the intermediate involved in the relevant enantiodetermining TS may be significantly different from what observed in solution and in the solid state.

The particularly important role that NH(b) has on the selectivity of *bis*-urea catalysts in HB PTC is corroborated by DFT calculations. The evolution of the reaction along the intrinsic reaction coordinate (IRC) showed that the three NH···$F^-$ hydrogen bonds elongate during fluoride delivery to the episulfonium ion, as a consequence of charge neutralisation; however the elongation of NH(b)···$F^-$ occurs significantly faster compared with the H-bonds belonging to the bidentate urea, NH(a) and NH(c) (Figure 3.34).

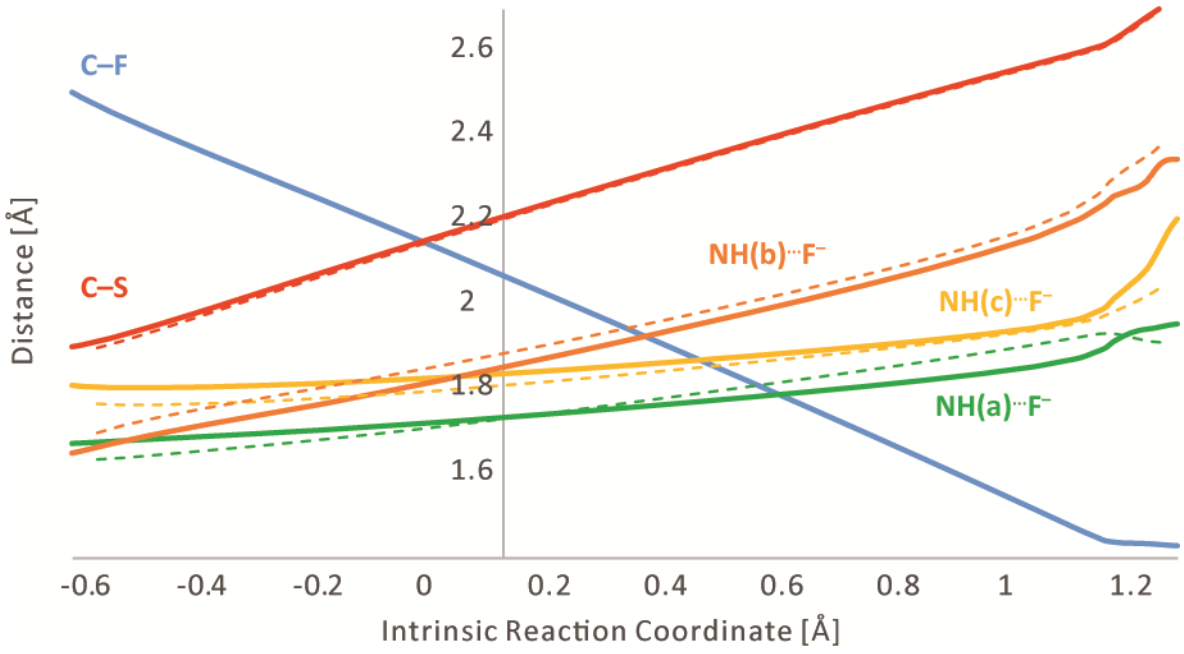



Figure 3. 34: Changes in bond distances over the intrinsic reaction coordinate. The intrinsic reaction coordinate is defined as C–S – C–F. Computational work carried out by Dr. David Ascough. Adapted with permission form reference 1.

These observations suggest that *bis*-urea catalysts displaying a weak NH(b)···$F^-$ hydrogen bond when binding with fluoride, may present a bidentate *bis*-urea–fluoride in the TS, with consequent reduction of enantioselectivity.

From these data we can conclude that a tridentate binding of fluoride is important to ensure a good outcome in HB PTC fluorinations. Fluoride needs to interact with all three NH binding site to ensure the reaction to proceed in good yields and enantioselectivities, however NH(b) showed to be critical for the stereochemical outcome of the transformation.

*3.2.5.2 Reactivity of iPr BINAM Urea–CsF complex (**4u**:CsF).* Finally, to indubitably prove the participation of a *bis*-urea–CsF complex in HB PTC fluorinations, *in situ* generated **4u**:CsF was tested. **4u**:CsF was obtained by sonication of **4u** and CsF in DCM-$d_2$ (25 mM), and subsequently, β-bromo sulfide **1a** (2 equivalents) was added to the NMR tube as a solid and the sample briefly agitated. This resulted in the instantaneous formation of a noticeable precipitate ascribed to CsBr; $^1$H and $^{19}$F NMR evidenced that product **3a** was formed. The enantiomeric ratio was of 86.5:13.5, in agreement with the enantioselectivity measured for the catalytic reaction (*cf.* 88:12, Entry 1-2 Table 3.7). This observation demonstrates that **4u**:CsF, formed and characterised *in situ*, is effective in the enantioselective fluorination of **1a**. Moreover, this supports the proposed mechanistic hypothesis which involves the formation of a *bis*-urea–CsF complex as a key intermediate for the fluorination of episulfonium ions. However, the complex formed by sonicating **4u** and CsF in the NMR tube may not be fully representative of what occurs in a catalytic reaction, where kinetic parameters come into play. In particular, the formation of a 2:1 catalyst–fluoride complex in catalytic conditions will be dependent on the lifetime of the 1:1 UF complex, so on the relative rate between UF formation (phase-transfer) and fluoride delivery (fluorination step). This may explain the slight

discrepancy in the observed enantioselectivity between catalytic reaction and the reaction using **4u**:CsF.

## 3.3 Conclusions

We described a detailed NMR spectroscopic investigation which unveiled important information about the structure and conformation in solution of BINAM-derived *bis*-ureas in their ground-state and when complexed with fluoride.

The study showed that *N*-alkylated ureas under conditions relevant to catalysis in terms of solvent (DCM) and concentration (25 mM), exist in solution as equilibrating structures held together by the presence of an intramolecular, time-dependent hydrogen bond, NH(c)···O=C. The stability of this interaction is dependent on the electronic properties of the substituents on the catalyst. In contrast, the non-alkylated *bis*-urea **4a** showed no intramolecular interactions, while presenting evidence of intermolecular aggregation at high concentrations. Titration experiments demonstrated that BINAM urea **4a** and *N*-isopropylated **4u** strongly bind fluoride, with the formation of a 2:1 $[U_2F]^-$ complex (U = **4a** or **4u**) at low concentration of TBAF ($K_{a\ 2:1}$ **4a** = 600 ± 120 $M^{-1}$, $K_{a\ 2:1}$ **4u** = 3000 ± 820 $M^{-1}$), and a more stable 1:1 $[UF]^-$ complex dominant at high concentration of TBAF ($K_{a\ 1:1}$ **4a** = 0.80 ± 0.09 x $10^6$ $M^{-1}$, $K_{a\ 1:1}$ **4u** = 1.05 ± 0.02 x $10^6$ $M^{-1}$). The conformation in solution of the 1:1 complex **4u**:TBAF was studied by means of quantitative NOESY and compared to the one of the unbound catalyst; upon formation of the fluoride complex, the *N*-isopropylated *bis*-urea undergoes a substantial conformational change with the isomerisation of the alkylated urea from an anti-anti to an syn-anti arrangement. The catalyst engages in three hydrogen bonds with fluoride, resulting in a rigid and dynamically stable conformer, remarkably similar to the conformation in the solid state. The hydrogen bonding network around fluoride was investigated by analysing the hydrogen bonding coupling constants $^{1h}J_{NH\cdots F^-}$, using $^1$H-$^{19}$F CLIP-HSQC experiments, and by studying the heteronuclear $^1$H-$^{19}$F nOe, using HOESY. It was found that the three NH

participate to the hydrogen bonding displaying different degree of interaction; NH(a)···$F^-$ is the strongest HB ($^{1h}J_{NH(a)...F^-}$,= 61 Hz), followed by NH(b)···$F^-$ ($^{1h}J_{NH(b)...F^-}$,= 51 Hz) and by NH(c)···$F^-$ ($^{1h}J_{NH(c)...F^-}$,= 34 Hz).

The detection of HBC between NH and $F^-$ was used to determine fluoride positioning in the catalytic pocket of a set of *bis*-urea catalysts modified with various *N*-alkyl groups and with substituents having different electronic properties. The data showed that all the *N*-alkylated *bis*-ureas present tridentate binding with fluoride, NH(a) being the dominant contributor to the HB network, while NH(b) showed to significantly vary in catalysts with different electronic characters. In contrast, the non-alkylated *bis*-urea **4a** displayed bidentate binding with fluoride.

The complexes of **4u** with CsF were characterised in solution. Low-temperature NMR experiments showed that **4u**:CsF presents a 1:1 complex $[UF]^-$ as main species, in equilibrium with a 2:1 $[U_2F]^-$ complex (85:15 at 298 K). The structure and conformation of the 1:1 Cs[U:F] adduct is related to the one of **4u**:TBAF, however the presence of $Cs^+$ as counter-ion is responsible for a weakening effect on all the NH···$F^-$ interactions, presumably due to a $Cs^+$-π interaction with the catalyst backbone. The effect is more relevant for NH(b) which showed a substantial reduction in HB interaction. Finally, NMR data were reconnected with the reaction outcome by assessing the reactivity and selectivity of the set of catalysts on a model HB PTC fluorination. The data showed the importance of having a strong tridentate *bis*-urea–fluoride binding, with NH(b)···$F^-$ being a critical interaction to ensure good control over enantioselectivity. With these data in hand, we can substantiate our proposed catalytic cycle with the new findings (Figure 3.35).

In conclusion, the present studies suggest that fine-tuning of tridentate bis-urea allows for control of fluoride microenvironment, which in turn dictates reactivity and selectivity of fluorination with alkali metal fluoride salts. The information gained with this study is relevant both from a fundamental perspective, expanding the understanding of fluoride reactivity and binding in solution, and practically, allowing the rational design of new catalysts for HB PTC.

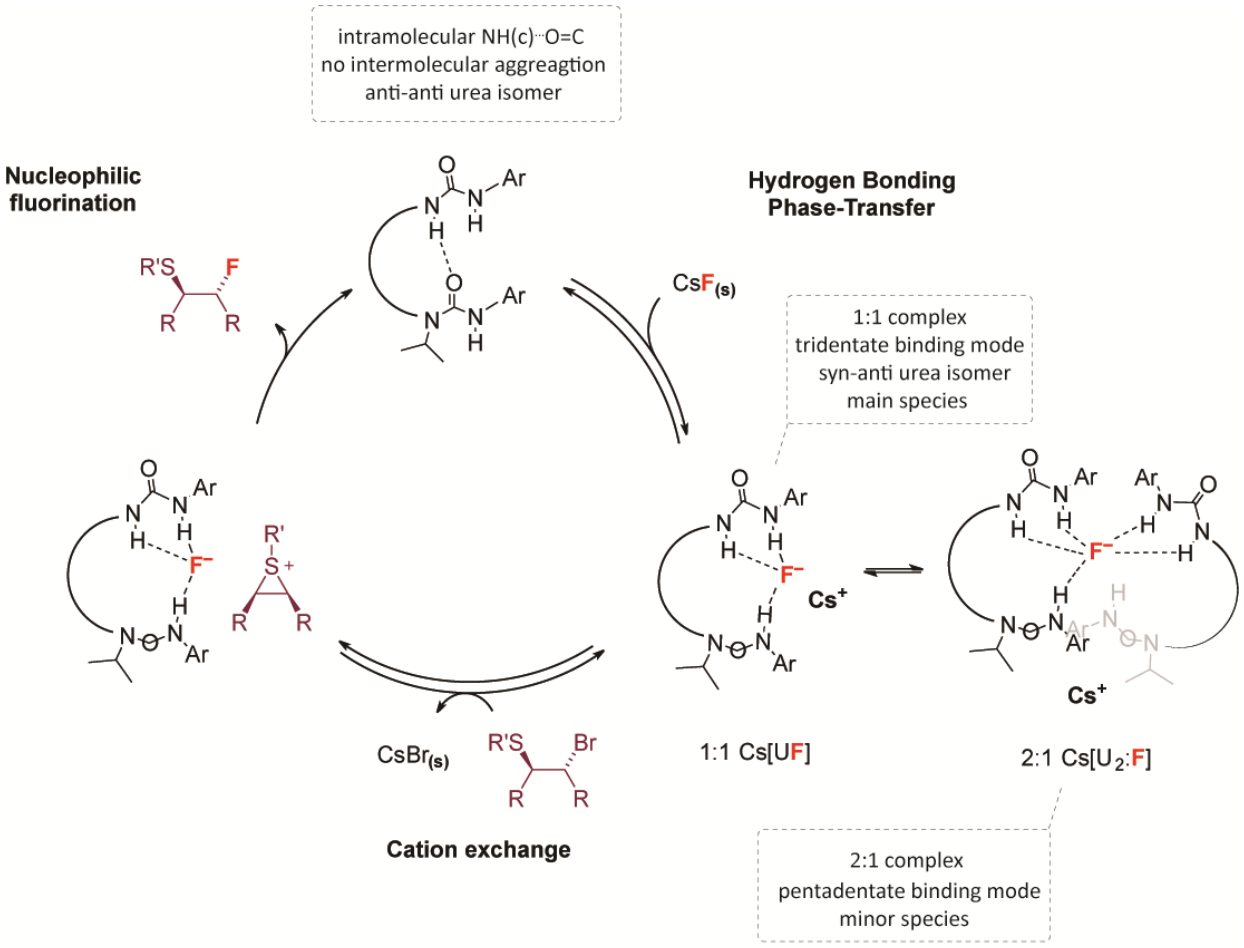



Figure 3.35: Proposed catalytic cycle for HB PTC fluorination substantiated in light of the new spectroscopic evidences.

## 3.4 References


(1) Becker, E. D. Hydrogen Bonding. In *Encyclopedia of Nuclear Magnetic Resonance*; John Wiley & Sons, Ltd: New York, 1996.

(2) Grzesiek, S.; Cordier, F.; Dingley, A. J. Scalar Couplings across Hydrogen Bonds. *Methods Enzymol.* **2001**, *338*, 111–133.

(3) Dingley, A. J.; Cordier, F.; Grzesiek, S. An Introduction to Hydrogen Bond Scalar Couplings. *Concepts Magn. Reson.* **2001**, *13* (2), 103–127.

(4) Blake, P. R.; Lee, B.; Summers, M. F.; Adams, M. W. W.; Park, J. B.; Zhou, Z. H.; Bax, A. Quantitative Measurement of Small Through-Hydrogen-Bond and 'through-Space' $^{1}H$-$^{113}Cd$ and $^{1}H$-$^{199}Hg$ J Couplings in Metal-Substituted Rubredoxin from Pyrococcus Furiosus. *J. Biomol. NMR* **1992**, *2* (5), 527–533.

(5) Grzesiek, S.; Cordier, F.; Jaravine, V.; Barfield, M. Insights into Biomolecular Hydrogen Bonds from Hydrogen Bond Scalar Couplings. *Prog. Nucl. Magn. Reson. Spectrosc.* **2004**, *45* (3–4), 275–300.

(6) Dingley, A. J.; Grzesiek, S. Direct Observation of Hydrogen Bonds in Nucleic Acid Base Pairs by Internucleotide $^{2}J_{(NN)}$ Couplings. *J. Am. Chem. Soc.* **1998**, *120* (33), 8293–8297.

(7) Nisius, L.; Grzesiek, S. Key Stabilizing Elements of Protein Structure Identified through Pressure and Temperature Perturbation of Its Hydrogen Bond Network. *Nat. Chem.* **2012**, *4* (9), 711–717.

(8) Scheurer, C.; Brüschweiler, R. Quantum-Chemical Characterization of Nuclear Spin-Spin Couplings across Hydrogen Bonds. *J. Am. Chem. Soc.* **1999**, *121* (37), 8661–8662.

(9) Alkorta, I.; Elguero, J.; Denisov, G. S. A Review with Comprehensive Data on Experimental Indirect Scalar NMR Spin-Spin Coupling Constants across Hydrogen Bonds. *Magn. Reson. Chem.* **2008**, *46* (7), 599–624.

(10) Shenderovich, I. G.; Smirnov, S. N.; Denisov, G. S.; Gindin, V. A.; Golubev, N. S.; Dunger, A.; Reibke, R.; Kirpekar, S.; Malkina, O. L.; Limbach, H.-H. Nuclear Magnetic Resonance of Hydrogen Bonded Clusters between $F^-$ and $(HF)_n$: Experiment and Theory. *Ber. Bunsenges. Phys. Chem.* **1998**, *102* (3), 422–428.

(11) Gale, P. A.; Sessler, J. L.; Kral, V. Calixpyrroles. *Chem. Commun.* **1998**, *0*, 1–8.

(12) Clarke, H. J.; Howe, E. N. W.; Wu, X.; Sommer, F.; Yano, M.; Light, M. E.; Kubik, S.; Gale, P. A. Transmembrane Fluoride Transport: Direct Measurement and Selectivity Studies. *J. Am. Chem. Soc.* **2016**, *138* (50), 16515–16522.

(13) Woods, C. J.; Camiolo, S.; Light, M. E.; Coles, S. J.; Hursthouse, M. B.; King, M. A.; Gale, P. A.; Essex, J. W. Fluoride-Selective Binding in a New Deep Cavity Calix[4]Pyrrole: Experiment and Theory. *J. Am. Chem. Soc.* **2002**, *124* (29), 8644–8652.

(14) Kang, S. O.; Day, V. W.; Bowman-James, K. Fluoride: Solution- and Solid-State Structural Binding Probe. *J. Org. Chem.* **2010**, *75* (2), 277–283.

(15) Kang, S. O.; VanderVelde, D.; Powell, D.; Bowman-James, K. Fluoride-Facilitated Deuterium Exchange from DMSO-$d_6$ to Polyamide-Based Cryptands. *J. Am. Chem. Soc.* **2004**, *126* (39), 12272–12273.

(16) Semetey, V.; Hemmerlin, C.; Didierjean, C.; Schaffner, A. P.; Giner, A. G.; Aubry, A.; Briand, J. P.; Marraud, M.; Guichard, G. Unexpected Stability of the Urea Cis-Trans Isomer in Urea-Containing Model Pseudopeptides. *Org. Lett.* **2001**, *3* (24), 3843–3845.

(17) Brynn Hibbert, D.; Thordarson, P. The Death of the Job Plot, Transparency, Open Science and Online Tools, Uncertainty Estimation Methods and Other Developments in Supramolecular Chemistry Data Analysis. *Chem. Commun.* **2016**, *52* (87), 12792–12805.

(18) Thordarson, P. Determining Association Constants from Titration Experiments in Supramolecular Chemistry. *Chem. Soc. Rev.* **2011**, *40* (3), 1305–1323.

(19) Kuzmič, P. Program DYNAFIT for the Analysis of Enzyme Kinetic Data: Application to HIV Proteinase. *Anal. Biochem.* **1996**, *237* (2), 260–273.

(20) Cametti, M.; Rissanen, K. Recognition and Sensing of Fluoride Anion. *Chem. Commun.* **2009**, *20*, 2809.

(21) Fielding, L. Determination of Association Constants ($K_{(a)}$) from Solution NMR Data. *Tetrahedron* **2000**, *56* (34), 6151–6170.

(22) Enthart, A.; Freudenberger, J. C.; Furrer, J.; Kessler, H.; Luy, B. The CLIP/CLAP-HSQC: Pure Absorptive Spectra for the Measurement of One-Bond Couplings. *J. Magn. Reson.* **2008**, *192* (2), 314–322.

(23) Pfeifer, L.; Engle, K. M.; Pidgeon, G. W.; Sparkes, H. A.; Thompson, A. L.; Brown, J. M.; Gouverneur, V. Hydrogen-Bonded Homoleptic Fluoride-Diarylurea Complexes: Structure, Reactivity, and Coordinating Power. *J. Am. Chem. Soc.* **2016**, *138* (40), 13314–13325.

(24) Golubev, N.; Denisov, G.; Limbach, H.-H. Hydrogen Bond Isotope Effects Studied by NMR. In *Isotope Effects In Chemistry and Biology*; CRC Press, 2005.

(25) Smirnov, S. N.; Golubev, N. S.; Denisov, G. S.; Benedict, H.; Schah-Mohammedi, P.; Limbach, H. H. Hydrogen/Deuterium Isotope Effects on the NMR Chemical Shifts and Geometries of Intermolecular Low-Barrier Hydrogen-Bonded Complexes. *J. Am. Chem. Soc.* **1996**, *118* (17), 4094–4101.

(26) Scheiner, S.; Čuma, M. Relative Stability of Hydrogen and Deuterium Bonds. *J. Am. Chem. Soc.* **1996**, *118* (6), 1511–1521.

(27) Gerken, M.; Boatz, J. .; Kornath, A.; Haiges, R.; Schneider, S.; Schroer, T.; Christe, K. . The NMR Shifts Are Not a Measure for the Nakedness of the Fluoride Anion. *J. Fluor. Chem.* **2002**, *116* (1), 49–58.

(28) Zhu, Q.; Oganov, A. R.; Zeng, Q. Formation of Stoichiometric $CsF_n$ Compounds. *Sci. Rep.* **2015**, *5*, 3–8.

# 4 Experimental

## 4.1 Generality and NMR Methods

Unless otherwise stated, all reagents were purchased from commercial suppliers (Sigma-Aldrich, Alfa Aesar, Fluorochem or Apollo Scientific) and used without further purification. Unless otherwise stated, solvents were used without prior drying or degassing. Reactions requiring anhydrous conditions are clearly stated and were conducted after flame-drying of the appropriate reaction flask and under an inert atmosphere of nitrogen or argon. Reactions were monitored by thin layer chromatography (TLC) on silica gel pre-coated aluminium sheets (Merck Silica Gel 60 $F_{254}$). Visualization was accomplished by irradiation with UV light at 254 nm, and/or phosphomolybdic acid (PMA) stain, and/or Cerium Ammonium Molybdate (CAM) stain, and/or $KMnO_4$ stain. Column chromatography was performed on Merck silica gel (60, particle size 0.040-0.063 mm). Optical rotations were measured on an Autopol L 2000 (Schmidt-Haensh) at 589 nm, 25 °C. Data are reported as: $[\alpha]_{\mathrm{D}}^{\mathrm{T}}$ concentration (c in g/100 mL), and solvent. The absolute configuration was determined by X-ray analysis. Low temperature single crystal X-ray diffraction data were collected using a (Rigaku) Oxford Diffraction SuperNova A diffractometer. Full crystallographic data for **4u**:TBAF and **3d** have been deposited with the Cambridge Crystallographic Data Centre (CCDC 1812187-88). UV-Vis spectra were recorded using a PG instruments T60 UV/Vis or a Shimadzu UV-2600 UV-Vis spectrophotometer. High resolution mass spectra were determined on a Thermo Exactive mass spectrometer using electrospray ionization (ESI) or atmospheric pressure chemical ionization (APCI) or on an Agilent 7200 Q-TOF spectrometer equipped with a direct insertion probe supplied by Scientific Instrument Manufacturer (SIM) GmbH using electron ionization (EI – 20eV). β-bromo sulfides were found to be unstable under a variety of MS ionization

methods (CI, EI, ESI) and therefore no HRMS could be obtained for them; this is clearly stated in the single experiment. Infrared spectra were recorded as the neat compound or in solution using a Bruker Tensor 27 FT-IR spectrometer. Absorptions are reported in wavenumber ($cm^{-1}$). Melting points of solids were measured on non-recrystallised samples, using a Griffin apparatus and are uncorrected. All enantiomeric ratios were determined on spectroscopically pure compounds (after purification) by HPLC analysis on a Shimadzu *i*-Prominence LC-2030 (PDA detector) employing a chiral stationary phase column and an eluent mixture specified in the individual experiment (HPLC traces analysis), by comparing the samples with the appropriate racemic mixtures.

NMR spectra were recorded on AVIII HD 500 equipped with a 5 mm TBO probe or AVIII HD 600 equipped with a 5mm BB-F/$^{1}$H Prodigy $N_2$ cryoprobe. The spectra were acquired at 298 K or at low temperature using a BCU II fridge unit assembled on AVIII HD 500. Deuterated solvents were purchased from Euroisotops® and used without further purification. DCM-$d_2$ was stored at 4 ˚C over 3 Å molecular sieves, under nitrogen atmosphere. $CDCl_3$ was stored at room temperature over 3 Å molecular sieves. DMSO-$d_6$ was stored at room temperature over 3 Å molecular sieves. Spectra were processed with TopSpin 3.6.2, spectral data are reported as follows: chemical shift (multiplicity [singlet (s), doublet (d), triplet (t), quartet (q), pentet (p), septet (sept), multiplet (m), doublet of doublets (dd), doublet of doublet of doublets (ddd), doublet of triplet of doublets (dtd), doublet of triplets (dt), triplet of doublets (td), etc., coupling constant, relative integration for $^{1}$H only). $^{1}$H resonances are referenced to solvent residual peaks (DCM-$d_2$ 5.32 ppm; $CDCl_3$ 7.26 ppm; DMSO-$d_6$ 2.50 ppm). $^{13}$C-NMR spectra were recorded with protons fully decoupled and referenced to the solvent peak (DCM-$d_2$ 53.84 ppm; $CDCl_3$ 77.16 ppm; DMSO-$d_6$ 45.40 ppm). $^{19}$F NMR spectra are referenced relative to $CFCl_3$ using the Bruker internal referencing procedure (edlock). Non-standard pulse sequences and

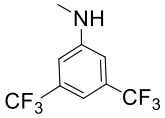
acquisition parameters are clearly stated in the text according to the following naming convention. NS = number of scans, DS = number of dummy scans, TD = time domain points [pt], SI = zero filling, SW = spectral window [ppm], o1p = spectrum offset, centre of spectrum [ppm].

## 4.2 Hydrogen Bonding Mediated Asymmetric Nucleophilic Fluorination

### *4.2.1 Catalysts Synthesis and Characterisation*

#### *4.2.1.1 Achiral Catalysts*

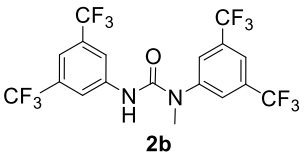
*N*-methyl-3,5-bis(trifluoromethyl)aniline (**5a**)



**5a**

In a flame-dried Schlenk flask under inert atmosphere, 3,5-bis(trifluoromethyl)aniline (6.4 mmol, 1.0 ml, 1 equiv.) was dissolved in dry DCM (0.4 M, 15 ml). The mixture was cooled to 0 ° with an ice bath and trifluoroacetic anhydride (19 mmol, 2.7 ml, 3 equiv.) was added dropwise. The solution was allowed to warm to room temperature and stirred for 20 minutes. The solvent and the excess of trifluoroacetic anhydride were distilled off and the residue was dissolved in acetone (0.4 M, 15 ml). $K_2CO_3$ (13 mmol, 1.8 g, 2 equiv.) and methyl iodide (19 mmol, 1.2 ml, 3 equiv.) were added and the mixture was refluxed for 2 hours. The precipitate was filtered off and the filtrate was first evaporated under reduced pressure and then was dissolved in methanol:$H_2O$ (8:2, 30 ml). $K_2CO_3$ (6.4 mmol, 0.9 g, 1 equiv.) was added and the mixture stirred for 1 hour at room temperature. The methanol was evaporated, and the residue was washed with water and brine. After anhydrification with $MgSO_4$ and filtration, the volatiles were evaporated under reduced pressure to yield the desired compound as a yellow oil (85 % yield, 1.2 g). **$^1$H NMR** (600 MHz, $CDCl_3$) $\delta$ = 7.15 (s, 1H), 6.92 (s, 2H), 4.16 (br s, 1H), 2.90 (s, *J* = 5.1 Hz, 3H), **$^{19}$F NMR** (565 MHz, $CDCl_3$) $\delta$ = -63.24 (s), **$^{13}$C NMR** (151 MHz, $CDCl_3$) $\delta$ = 149.86, 132.54 (q, *J* = 32.5 Hz), 123.80 (q, *J* = 274.1 Hz), 111.55 (br s), 110.14 (br m), 30.47. Spectroscopic data are in agreement with those previously reported.[1]

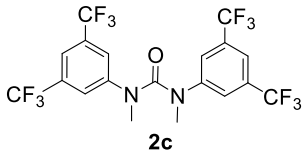
1,3-bis(3,5-bis(trifluoromethyl)phenyl)-1-methylurea (**2b**) – *synthesised by Dr. G. Pupo*



**2b**

In a flame-dried Schlenk under inert atmosphere, *N*-methyl-3,5-bis(trifluoromethyl)aniline (**5a**) (0.411 mmol, 100 mg, 1 equiv.) was dissolved in dry DCM (0.4 M). 3,5-bis(trifluoromethyl)phenyl isocyanate (71 µL, 0.411 mmol, 1 equiv.) was added dropwise and the solution was stirred overnight. After dilution with hexane (1 mL), the crude was filtered and the white solid was washed (2 x 5 mL) with a hexane:DCM mixture (8:2) to yield the desired compound as a white solid (68 % yield, 140 mg). **$^{1}$H NMR** (400 MHz, $CDCl_3$) $\delta$ = 7.89 (s, 1H), 7.82 (br s, 4H), 7.56 (s, 1H), 6.43 (s, 1H), 3.45 (s, 3H), **$^{19}$F NMR** (376 MHz, $CDCl_3$) $\delta$ = -62.9 (s), –63.0 (s), **$^{13}$C NMR** (126 MHz, $CDCl_3$) $\delta$ = 153.0, 144.1, 139.5, 134.0 (q, *J* = 34.2 Hz), 132.4 (q, *J* = 34.2 Hz), 127.3 (d, *J* = 3.0 Hz), 123.0 (q, *J* = 273.5 Hz), 122.5 (q, *J* = 274.5 Hz), 121.5 (m), 119.5 (d, *J* = 3.4 Hz), 117.1 (q, *J* = 3.7 Hz), 37.8; **IR** (liquid film) *v* = 3333, 3129, 1658, 1550, 1372, 1124, 1108, 937, 911, 887, 844, 757, 727, 701, 682, 657, 617 $cm^{-1}$; **mp** 166–167 °C; **HRMS** (APCI+) m/z calculated for $C_{18}H_{11}ON_2F_{12}$ $(M+H)^+$ 499.06743, found 499.06623.

1,3-bis(3,5-bis(trifluoromethyl)phenyl)-1,3-dimethylurea (**2c**) – *synthesised by Dr. G. Pupo*

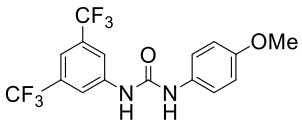


**2c**

In a flame-dried Schlenk under inert atmosphere, NaH (66 % in mineral oil, 1.5 mmol, 37 mg, 2.5 equiv.) was added to a solution of 1,3-bis(3,5-bis(trifluoromethyl)phenyl)urea (300 mg, 0.6 mmol, 1 equiv.) in THF (0.2 M). The reaction was stirred 30 minutes at room temperature after which methyl iodide (84 µL, 1.4 mmol, 2.2 equiv.) was added and the mixture warmed up to 50 °C. The reaction mixture was diluted with water (3 mL) and the crude extracted with DCM. After anhydrification with $MgSO_4$ and filtration, the volatiles were evaporated under reduced pressure to yield the desired compound as a white solid (85 % yield, 1.2 g). **$^{1}$H NMR** (600 MHz,

$CDCl_3$) $\delta$ = 7.43 (s, 2H), 7.16 (s, 4H), 3.34 (s, 6H), **$^{19}$F NMR** (565 MHz, $CDCl_3$) $\delta$ = -63.54 (s), **$^{13}$C NMR** (151 MHz, $CDCl_3$) $\delta$ = 159.06, 146.32, 132.92 (q, *J* = 32.5 Hz), 125.64, 122.61 (q, *J* = 274.1 Hz), 119.04, 39.13. Spectroscopic data are in agreement with those previously reported.[2]

1-(3,5-bis(trifluoromethyl)phenyl)-3-(4-methoxyphenyl)urea (**2e**)



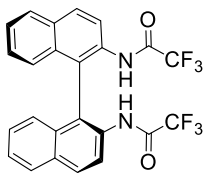
**2e**

In a flame-dried Schlenk under inert atmosphere, *p*-anisidine (123 mg, 1.0 mmol, 1 equiv.) was dissolved in dry DCM (0.4 M). 3,5-bis(trifluoromethyl)phenyl isocyanate (172 µL, 1.0 mmol, 1 equiv.) was added dropwise and the solution was stirred overnight. After dilution with hexane (1 mL), the crude was filtered and the white solid was washed (2 x 5 mL) with hexane to yield the desired compound as a white solid (85 % yield, 300 mg). **$^{1}$H NMR** (500 MHz, $CDCl_3$) $\delta$ = 9.31 (br s, 1H), 8.78 (br s, 1H), 8.13 (s, 2H), 7.61 (s, 1H), 7.38 (d, *J* = 9.0 Hz, 2H), 6.89 (d, *J* = 9.0 Hz, 2H), 3.73 (s, 3H), **$^{19}$F NMR** (470 MHz, $CDCl_3$) $\delta$ = -61.7 (s), **$^{13}$C NMR** (126 MHz, $CDCl_3$) $\delta$ = 155.5, 153.0, 142.6, 131.1 (q, *J* = 32.7 Hz), 123.8 (q, *J* = 272.2 Hz), 121.4, 118.3 (d, *J* = 3.9 Hz), 114.5 (m), 114.4, 55.7; **IR** (liquid film) *v* = 3342, 3123, 1702, 1654, 1573, 1527, 1513, 1473, 1443, 1385, 1300, 1273, 1249, 1228, 1170, 1129, 1054, 1030, 951, 909, 884, 790, 704, 680, 621 $cm^{-1}$; **mp** 178–179 °C; **HRMS** (ESI+) m/z calculated for $C_{16}H_{13}O_2N_2F_6$ $(M+H)^+$ 379.08757, found 379.08754.

*4.2.1.2 Chiral Catalysts*

General procedure for the synthesis of *N*-alkylated 1,1'-binaphthyl-2,2'-diamines (**General Procedure A**). A round-bottom flask was charged with *N*,*N*'-([1,1'-binaphthalene]-2,2'-diyl)bis(2,2,2-trifluoroacetamide) **5b** (1 equiv.), $K_2CO_3$ (2 equiv.) and the appropriate alkyl iodide (1.05 equiv.) in acetone (0.25 M). After stirring at reflux for 18–36 h, the solvent was removed under reduced pressure and the crude mixture was re-dissolved in a 4:1 EtOH:$H_2O$ mixture (0.25 M). 10 equiv. of KOH were added, and the reaction was stirred at 70 °C for 12 h. The mixture was then cooled to room temperature and EtOAc was added. The phases were separated, and the aqueous phase extracted three times with EtOAc. The combined organic phases were then washed with brine. After anhydrification with $MgSO_4$ and filtration, the solvents were evaporated under reduced pressure and the crude product was purified by column chromatography (hexane:DCM or hexane:$Et_2O$ as eluent) to afford the desired products as white solids.

(*S*)-*N*,*N*'-([1,1'-binaphthalene]-2,2'-diyl)bis(2,2,2-trifluoroacetamide) (**5b**)

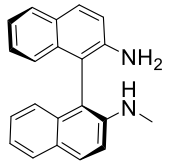


**5b**

A flame-dried two-neck round-bottom flask equipped with a magnetic stirrer was charged with (*S*)-1,1'-binaphthyl-2,2'-diamine (2.0 g, 7 mmol, 1 equiv.) under a flow of nitrogen. 14 mL of DCM (0.5 M) were added followed by trifluoroacetic anhydride (5.8 mL, 42 mmol, 6 equiv.) at 0 °C. The solution was allowed to warm to room temperature and stirred for 20 min. The volatiles were then carefully evaporated to afford the desired product without any further purification. White solid, 3.30 g, 99 % yield. **$^1$H NMR** (500 MHz, $CDCl_3$) $\delta$ = 8.21 (d, *J* = 9.0 Hz, 2H), 8.17 (d, *J* = 9.0 Hz, 2H), 8.03 (d, *J* = 8.2 Hz, 2H), 7.73 (br s, 2H), 7.59 (t, *J* = 7.6 Hz, 2H), 7.41 (t, *J* = 7.6 Hz, 2H), 7.16 (d, *J* = 8.5 Hz, 2H), **$^{19}$F NMR** (470 MHz, $CDCl_3$) $\delta$ = -76.3 (s), **$^{13}$C NMR** (126 MHz, $CDCl_3$) $\delta$ = 155.6 (q, *J* = 37.9 Hz), 132.3, 131.8, 131.7, 130.9, 128.7, 128.2, 127.0, 124.7, 123.9, 121.8, 114.3 (q, *J* =

289.1 Hz); **IR** (liquid film) *v* = 3259, 1705, 1530, 1509, 1337, 1266, 1236, 1191, 1161, 933, 910, 864, 812, 765, 741, 717, 649 $cm^{-1}$; **mp** 179–180 °C; **HRMS** (ESI+) m/z calculated for $C_{24}H_{15}O_2N_2F_6$ $(M+H)^+$ 477.1032, found 477.1033; $[\boldsymbol{\alpha}]_{\mathbf{D}}^{\mathbf{25}}$ = -100.1 (c 0.5, $CHCl_3$).

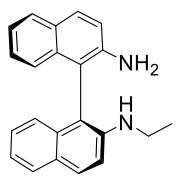
(*S*)-*N*$^2$-methyl-[1,1'-binaphthalene]-2,2'-diamine (**5c**)



**5c**

*N*-methylated aniline **5c** was synthesised according to the General Procedure A by employing 2.0 g (4.20 mmol) of **5b** and 274 µL (4.41 mmol) of methyl iodide and stirring for 18 h. **Purification** column chromatography, hexane:$Et_2O$ (90:10 to 80:20). White solid, 1.0 g, 80 % yield. **$^1$H NMR** (400 MHz, $CDCl_3$) $\delta$ = 7.84 (d, *J* = 8.9 Hz, 1H), 7.77–7.70 (m, 3H), 7.22–7.04 (m, 6H), 6.99–6.91 (m, 2H), 3.65 (s, 2H), 2.77 (s, 3H), 1.48 (br s, 1H), **$^{13}$C NMR** (126 MHz, $CDCl_3$) $\delta$ = 144.9, 142.8, 133.9, 133.4, 129.8, 129.6, 128.5, 128.2, 128.1, 127.8, 126.9, 126.8, 124.0, 123.7, 122.5, 122.1, 118.4, 113.6, 112.5, 112.3, 31.4; **IR** (liquid film) *v* = 3349, 2813, 1616, 1594, 1508, 1494, 1470, 1420, 1381, 1337, 1300, 1280, 1247, 1212, 1168, 1153, 1022, 951, 912, 811, 773, 748 $cm^{-1}$; **mp** 177–178 °C; **HRMS** (ESI+) m/z calculated for $C_{21}H_{19}N_2$ $(M+H)^+$ 299.1542, found 299.1538; $[\boldsymbol{\alpha}]_{\mathbf{D}}^{\mathbf{25}}$ = -144.8 (c 1.0, $CHCl_3$).

(*S*)-*N*$^2$-ethyl-[1,1'-binaphthalene]-2,2'-diamine (**5d**)

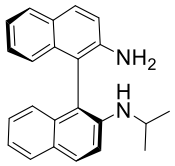


**5d**

*N*-ethylated aniline **5d** was synthesized according to the General Procedure A by employing 700 mg (1.47 mmol) of **5b** and 124 µL (1.54 mmol) of methyl iodide and stirring for 36 h. **Purification** column chromatography, hexane:DCM (70:30 to 50:50). White solid, 330 mg, 72 % yield. **$^1$H NMR** (400 MHz, $CDCl_3$) $\delta$ = 7.79 (d, *J* = 9.1 Hz, 1H), 7.67–7.74 (m, 3H), 7.20–7.03 (m, 6H), 6.98–6.94 (m, 1H), 6.93–6.80 (m, 1H), 6.56 (s br, 3H), 3.16 (q, *J* = 7.1 Hz, 2H), 0.95 (t, *J* = 7.1 Hz, 3H), **$^{13}$C NMR** (126 MHz, $CDCl_3$) $\delta$ = 144.4, 143.0, 134.0, 133.6, 129.6, 129.5, 128.5, 128.2, 128.1, 127.7, 126.8, 126.7, 124.0, 123.8, 122.4, 121.9, 118.3, 114.3, 112.5, 112.4, 38.7, 15.2; **IR** (liquid film) *v* = 3435,

3370, 3348, 2964, 1614, 1596, 1567, 1508, 1494, 1470, 1427, 1378, 1349, 1334, 1304, 1280, 1259, 1246, 1213, 1166, 1144, 1066, 1023, 964, 928, 860, 821, 810, 773, 755, 748, 683 $cm^{-1}$; **mp** 159–160 °C; **HRMS** (ESI+) m/z calculated for $C_{22}H_{21}N_2$ $(M+H)^+$ 313.1699, found 313.1699; $[\alpha]_D^{25}$ = -170.4 (c 1.0, $CHCl_3$).

(*S*)-*N*$^2$-*isopropyl-[1,1'-binaphthalene]-2,2'-diamine* (***5e***)



**5e**

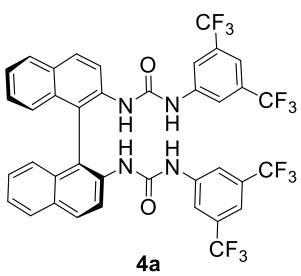
*N*-isopropylated aniline **5e** was synthesized according to a slightly modified protocol from a previously published one.[3] In a round-bottom flask equipped with a magnetic stirrer, acetone (361 µL, 4.92 mmol, 1.4 equiv.) was dissolved in THF (0.25M, 14 mL) and a 20 % aqueous solution of $H_2SO_4$ (7 mL, 2 $mL/mmol_{substrate}$) was added. After stirring for 30 min, (*S*)-1,1′-binaphthyl-2,2′-diamine (1.0 g, 3.52 mmol, 1 equiv.) was added. After 5 min of stirring, the solution was cooled to 0 °C and $NaBH_4$ (1.3 g, 70.0 mmol, 10 equiv.) was carefully added in portions. The mixture was stirred for 1 hour at room temperature, then quenched with 1 M KOH and diluted with EtOAc. The phases were separated and the aqueous phase extracted three times with EtOAc. The combined organic phases were then washed with brine. After anhydrification with $MgSO_4$ and filtration, the solvents were evaporated under reduced pressure and the crude product was purified by column chromatography (hexane:EtOAc = 95:5 to 90:10) to afford the desired product as a white solid (660 mg, 57% yield). **$^1$H NMR** (500 MHz, DMSO-$d_6$) $\delta$ = 7.90 (d, *J* = 9.0 Hz, 1H), 7.75–782 (m, 3H), 7.34 (d, *J* = 9.0 Hz, 1H), 7.24 (d, *J* = 8.8 Hz, 1H), 7.17–7.07 (m, 4H), 6.76 (dd, *J* = 8.2, 0.8 Hz, 1H), 6.73 (dd, *J* = 8.1, 0.8 Hz , 1H), 4.67 (s, 2H), 3.84–3.75 (m, 1H), 3.40 (s, 1H), 1.01 (d, *J* = 6.3 Hz, 3H), 0.91 (d, *J* = 6.3 Hz, 3H), **$^{13}$C NMR** (126 MHz, DMSO-$d_6$) $\delta$ = 144.8, 144.2, 134.1, 133.8, 129.5, 129.4, 128.6, 128.5, 127.7, 127.7, 126.7, 123.9, 123.4, 121.9, 121.7, 118.9, 115.9, 113.2, 109.8, 44.4, 23.6, 23.5; **IR** (liquid film) *v* = 3462, 3368, 2969, 1611, 1591, 1508, 1490, 1461, 1424, 1382, 1349, 1316, 1287, 1245, 1212, 1168, 1145, 1123, 1029, 958, 909, 821,

809, 772, 747, 687, 621 $cm^{-1}$; **mp** 165–166 °C; **HRMS** (APCI+) m/z calculated for $C_{23}H_{23}N_2$ $(M+H)^+$327.1855, found. Spectroscopic data are in agreement with those previously reported.[3]

General procedure for the synthesis of *bis*-urea catalysts (**General Procedure B**). In a flame-dried Schlenk under inert atmosphere, the appropriate *bis*-aniline (1 equiv.) was dissolved in dry DCM (0.4 M) and the appropriate isocyanate (2 equiv.) was added dropwise. The mixture was stirred at room temperature or at reflux for the indicated time. After removal of the solvent under reduced pressure, the crude mixture was directly purified by column chromatography to afford the desired product.

General procedure for the synthesis of *bis*-urea catalysts (**General Procedure C**). In a flame-dried two-neck flask under inert atmosphere, triphosgene (0.7 equiv.) was dissolved in DCM (5 mL). To this solution, a 0.2 M solution of the appropriate *bis*-aniline (2 equiv.) in DCM was added at 0 °C. Then dry $NEt_3$ (4 equiv.) was added dropwise at 0 °C and the reaction mixture was allowed to stir at room temperature for 2 h under a flow of nitrogen. (*S*)-(–)-1,1'-binaphthyl-2,2'-diamine or the appropriate aniline (1 equiv.) was then added and the reaction stirred at room temperature for 24 h (until TLC showed no further conversion). The reaction was then quenched by addition of water and the aqueous phase was extracted with DCM three times. The combined organic layers were washed with brine, dried over $MgSO_4$ and evaporated *in vacuo*. The crude mixture was then purified by column chromatography.

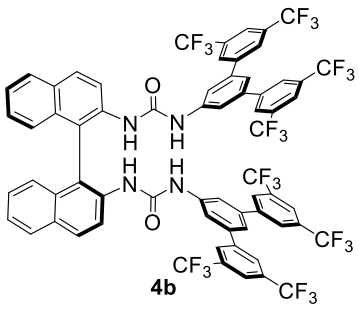
(*S*)-1,1'-([1,1'-binaphthalene]-2,2'-diyl)bis(3-(3,5-bis(trifluoromethyl)phenyl)urea) (**4a**)




Catalyst **4a** was prepared according to the General Procedure B by employing (*S*)-1,1'-binaphthyl-2,2'-diamine (1.64 g, 5.8 mmol, 1 equiv.) and 3,5-bis(trifluoromethyl)phenyl isocyanate (11.5 mmol, 2.0 ml, 2 equiv.), stirred overnight at room temperature. **Purification**

column chromatography, 1st hexane:EtOAc (100:0 to 90:10), 2nd pentane:DCM (50:50 to 0:100). White solid, 4 g, 87 % yield. Full NMR characterisation and assignment tables are presented along with copy of the spectra (*v. 4.3.2.1 BINAM Urea (**4a**) – assignment and copy of NMR spectra)*. The compound is known in the literature and its spectroscopic data are in agreement with those previously reported.[4]

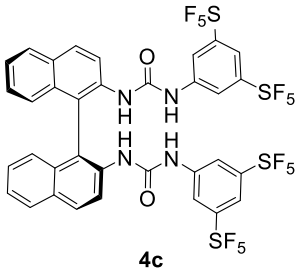
1,1'-([1,1'-binaphthalene]-2,2'-diyl)bis(3-(3,3'',5,5''-tetrakis(trifluoromethyl)-[1,1':3',1''-terphenyl]-5'-yl)urea) (**4b**) – *synthesised by Dr. G. Pupo*



**4b**

Catalyst **4b** was prepared according to the General Procedure C by employing aniline 3,3'',5,5''-tetrakis(trifluoromethyl)-[1,1':3',1''-terphenyl]-5'-amine (4.36 g, 8.45 mmol, 2 equiv.) and (*S*)-(–)-1,1'- binaphthyl-2,2'-diamine (1.2 g, 4.22 mmol, 1 equiv.). **Purification** column chromatography, pentane:DCM (80:20 to 0:100). White solid, 4.23 g, 73 % yield. **$^1$H NMR** (400 MHz, DMSO-$d_6$) $\delta$ = 9.33 (br s, 2H), 8.43 (d, *J* = 9.1 Hz, 2H), 8.14 (d, *J* = 9.1 Hz, 2H), 8.10 (s, 8H), 8.04 (d, *J* = 8.3 Hz, 2H), 7.99 (s, 4H), 7.64 (s, 4H), 7.61 (s, 2H), 7.52 (s, 2H), 7.44 (t, *J* = 7.4 Hz, 2H), 7.28 (t, *J* = 8.0 Hz, 2H), 6.84 (d, *J* = 8.6 Hz, 2H), **$^{19}$F NMR** (376 MHz, DMSO-$d_6$) $\delta$ = -61.4 (s), **$^{13}$C NMR** (101 MHz, DMSO-$d_6$) $\delta$ = 153.0, 142.2, 141.0, 138.2, 136.2, 132.9, 130.8 (q, *J* = 33.0 Hz), 130.3, 128.9, 128.2, 127.3, 126.7, 124.8, 124.6, 123.1 (q, *J* = 272.8 Hz), 122.8, 121.1, 119.6, 119.4, 117.2; **IR** (liquid film) *v* =3361, 1691, 1599, 1569, 1505, 1428, 1396, 1367, 1278, 1220, 1177, 1131, 1107, 900, 866, 844, 824, 747, 705, 682, 638 cm$^{-1}$; **mp** not determined (decomposition at T >200–220 °C); **HRMS** (APCI+) m/z calculated for $C_{66}H_{35}O_2N_4F_{24}$ $[M+H]^+$ 1371.2371, found 1371.2368; $[\boldsymbol{\alpha}]_{\mathbf{D}}^{\mathbf{25}}$ = -96.7 (c 0.5, $CHCl_3$).

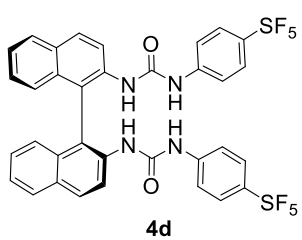
(*S*)-1,1'-([1,1'-binaphthalene]-2,2'-diyl)bis(3-(3,5-bis(pentafluoro-λ$^6$-sulfaneyl)phenyl)urea) (**4c**) – *synthesised by Dr. G. Pupo*



**4c**

Catalyst **4c** was prepared according to the General Procedure C by employing (*S*)-1,1'-binaphthyl-2,2'-diamine (100 mg, 0.4 mmol, 1 equiv.) and 3,5-bis(pentafluorosulfanyl)aniline (0.8 mmol, 276 mg, 2 equiv.), stirred overnight at room temperature. **Purification** the solid was filtered and washed with cold hexane. White solid, 163 mg, 41 % yield. **$^1$H NMR** (400 MHz, $CDCl_3$) $\delta$ = 8.22 (d, *J* = 8.9, 2H), 8.03 (d, *J* = 9.0 Hz, 2H), 7.93 (d, *J* = 8.2 Hz, 2H), 7.84 (d, *J* = 1.9 Hz, 4H), 7.69 (s, 2H), 7.67–7.59 (br m, 2H), 7.46 (t, *J* = 8.0, 2H), 7.28 (t, *J* = 8.0, 2H), 7.02 (d, *J* = 8.5 Hz, 2H), 6.81 (s, 2H), **$^{19}$F NMR** (376 MHz, $CDCl_3$) $\delta$ = 81.61 (p, *J* = 150.4 Hz, 4F), 62.55 (d, *J* = 150.5 Hz, 16F), **$^{13}$C NMR** (101 MHz, $CDCl_3$) $\delta$ = 153.75 (p, *J* = 19.3 Hz), 153.10, 134.62, 132.96, 131.31, 130.13, 128.50, 127.75, 126.04, 125.31, 122.35, 121.86, 119.19, 119.14, 118.19; **IR** (solid) *v* = 3322, 3118, 1662, 1597, 1550, 1504, 1460, 1429, 1325, 1280, 1251, 1217, 1139, 959, 838, 747, 725, 681, 657 cm$^{-1}$; **mp** 175–179 °C; **HRMS** (APCI+) m/z calculated for $C_{34}H_{23}F_{20}N_4O_2S_4$ $(M+H)^+$ 1027.03790, found 1027.03699; $[\boldsymbol{\alpha}]_{\mathbf{D}}^{\mathbf{25}}$ = -87.8 (c 0.5, $CHCl_3$).

(*S*)-1,1'-([1,1'-binaphthalene]-2,2'-diyl)bis(3-(4-(pentafluoro-l6-sulfaneyl)phenyl)urea) (**4d**) – *synthesised by Dr. G. Pupo*

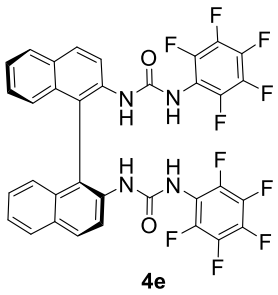


**4d**

Catalyst **4d** was prepared according to the General Procedure C by employing (*S*)-1,1'-binaphthyl-2,2'-diamine (0.4 mmol, 100 mg, 1 equiv.) and 4-pentafluorosulfanyl aniline (0.8 mmol, 175 mg, 2 equiv.), stirred overnight at room temperature. **Purification** column chromatography, DCM:$Et_2O$ (100:0 to 80:20). White solid, 150 mg, 51 % yield. **$^1$H NMR** (400 MHz, $CDCl_3$) $\delta$ = 8.00 (d, *J* = 9.0 Hz, 2H), 7.94 (d, *J* = 9.0 Hz, 2H), 7.88–7.82 (m, 2H), 7.40 (ddd, *J*

= 8.2, 6.9, 1.2 Hz, 2H), 7.38–7.32 (m, 4H), 7.23 (s, 2H), 7.19 (ddd, *J* = 8.3, 6.8, 1.3 Hz, 2H), 6.97 (dd, *J* = 8.4, 1.1 Hz, 2H), 6.89 (d, *J* = 8.8 Hz, 4H), 6.83 (s, 2H), **$^{19}$F NMR** (377 MHz, $CDCl_3$) $\delta$ = 85.15 (p, *J* = 151.7 Hz, 2F), 63.46 (d, *J* = 150.5 Hz, 8F), **$^{13}$C NMR** (101 MHz, $CDCl_3$) $\delta$ = 153.46, 148.67 (p, *J* = 20 Hz), 140.55, 134.80, 132.90, 131.30, 129.93, 128.49, 127.58, 126.95, 125.95, 125.27, 122.87, 122.59, 118.84; **IR** (solid) *v* = 3322, 1666, 1596, 1499, 1427, 1247, 1192, 1102, 832, 746, 670 cm$^{-1}$; **mp** 180–188 °C; **HRMS** (APCI+) m/z calculated for $C_{34}H_{25}F_{10}N_4O_2S_2$ $(M+H)^+$ 775.12538, found 775.12448; $[\alpha]_D^{25}$ = -123.1 (c 0.5, $CHCl_3$).

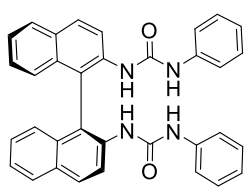
(*S*)-1,1'-([1,1'-binaphthalene]-2,2'-diyl)bis(3-(perfluorophenyl)urea) (**4e**) – *synthesised by Dr. G. Pupo*



**4e**

Catalyst **4e** was prepared according to the General Procedure B by employing (*S*)-1,1′-binaphthyl-2,2′-diamine (284 mg, 1.0 mmol, 1 equiv.) and pefluorophenyl isocyanate, stirred overnight at room temperature. **Purification**: the solid was filtered and washed with cold hexane. White solid, 611 mg, 87 % yield. **$^{1}$H NMR** (400 MHz, $CDCl_3$) $\delta$ = 8.11 (d, *J* = 9.0 Hz, 2H), 7.94 (d, *J* = 9.0 Hz, 2H), 7.88 (dt, *J* = 8.2, 0.9 Hz, 2H), 7.42 (ddd, *J* = 8.1, 6.8, 1.2 Hz, 2H), 7.21 (ddd, *J* = 8.3, 6.8, 1.3 Hz, 2H), 6.95 (dd, *J* = 8.5, 1.1 Hz, 2H), 6.70 (s, 2H), 6.37 (s, 2H), **$^{19}$F NMR** (377 MHz, $CDCl_3$) $\delta$ = -146.29 (d, *J* = 17.1 Hz), -156.83 (t, *J* = 21.6 Hz), -161.73 – -162.90 (m), **$^{13}$C NMR** (101 MHz, $CDCl_3$) $\delta$ = 153.20, 143.21 (d, *J* = 255 Hz), 139.99 (d, *J* = 240.3 Hz), 137.77 (d, *J* = 250.16 Hz), 134.81, 132.66, 131.24, 129.97, 128.38, 127.47, 125.80, 125.18, 122.31, 122.01, 119.99 (t, *J* = 16.4 Hz); **IR** (solid) *v* = 3260, 1704, 1650, 1600, 1523, 1503, 1463, 1429, 1335, 1270, 1217, 1056, 1009, 981, 867, 814, 774, 747, 695, 641 cm$^{-1}$; **mp** 162–164 °C; **HRMS** (APCI+) m/z calculated for $C_{34}H_{17}F_{10}N_4O_2$ $(M+H)^+$ 703.11863, found 703.11804; $[\alpha]_D^{25}$ = -51.5 (c 0.2, $CHCl_3$).

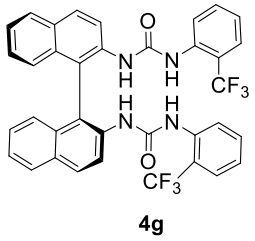
(*S*)-1,1'-([1,1'-binaphthalene]-2,2'-diyl)bis(3-phenylurea) (**4f**)



**4f**

Catalyst **4f** was prepared according to the General Procedure B by employing (*S*)-1,1′-binaphthyl-2,2′-diamine (2 mmol, 580 mg, 1 equiv.) and phenyl isocyanate, stirred for 30 hours at room temperature. **Purification** column chromatography, hexane:$Et_2O$ (100:0 to 90:10). White solid, 900 mg, 86 % yield. **$^1$H NMR** (500 MHz, DMSO-$d_6$) $\delta$ = 9.04 (s, 2H), 8.59 (d, *J* = 9.1 Hz, 2H), 8.10 (d, *J* = 9.2 Hz, 2H), 7.98 (dd, *J* = 8.2, 1.3 Hz, 2H), 7.42 (s, 2H), 7.38 (ddd, *J* = 8.1, 6.8, 1.2 Hz, 2H), 7.32–7.26 (m, 4H), 7.23 (ddd, *J* = 8.3, 6.8, 1.3 Hz, 2H), 7.21–7.13 (m, 4H), 6.90 (t, *J* = 7.4, 2H), 6.79 (d, *J* = 8.5 Hz, 2H), **$^{13}$C NMR** (126 MHz, DMSO-$d_6$) [overlapping signals] $\delta$ = 152.58, 139.41, 137.02, 132.66, 130.03, 128.98, 128.77, 128.22, 126.76, 124.39, 124.22, 121.94, 121.35, 118.29. Spectroscopic data are in agreement with those previously reported.[5]

(*S*)-1,1'-([1,1'-binaphthalene]-2,2'-diyl)bis(3-(2-(trifluoromethyl)phenyl)urea) (**4g**) – *synthesised by Dr. G. Pupo*

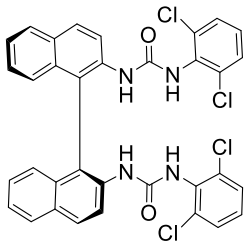


**4g**

Catalyst **4g** was prepared according to the General Procedure B by employing (*S*)-1,1′-binaphthyl-2,2′-diamine (1.0 mmol, 284 mg, 1 equiv.) and 2-(trifluoromethyl)phenyl isocyanate stirred for 72 h at room temperature. **Purification**: column chromatography, DCM:$Et_2O$ (100:0 to 80:20). White solid, 580 mg, 88 % yield. **$^1$H NMR** (400 MHz, $CDCl_3$) $\delta$ = 8.23 (d, *J* = 9.0 Hz, 2H), 7.93 (d, *J* = 9.0 Hz, 2H), 7.84 (dd, *J* = 8.3, 1.2 Hz, 2H), 7.39 (m, 4H), 7.21 (t, *J* = 7.6 Hz, 2H), 7.18–7.02 (m, 6H), 6.98 (dd, *J* = 8.5, 1.1 Hz, 2H), 6.64 (br s, 2H), 6.62 (br s, 2H), **$^{19}$F NMR** (377 MHz, $CDCl_3$) $\delta$ = -61.29 (s), **$^{13}$C NMR** (101 MHz, $CDCl_3$) $\delta$ = 153.36, 135.13, 134.57, 132.70, 132.41, 130.91, 129.72, 128.19, 127.23, 126.48, 126.21 (q, *J* = 5.4 Hz), 125.31, 125.25, 124.85, 123.43 (q, *J* = 273.2 Hz), 123.19 (q, *J* = 29.9 Hz), 121.79, 120.95; **IR** (solid) *v* = 2922, 1670, 1590, 1505,

1457, 1427, 1319, 1271, 1170, 1112, 1035, 767, 652 $cm^{-1}$; **mp** 127–135 °C; **HRMS** (APCI+) m/z calculated for $C_{36}H_{25}F_6N_4O_2$ $(M+H)^+$ 659.18762, found 659.18676 $[\alpha]_D^{25}$ = -118.3 (c 0.5, $CHCl_3$).

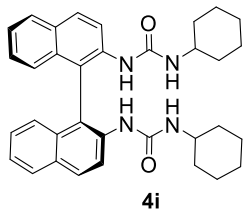
(*S*)-1,1'-([1,1'-binaphthalene]-2,2'-diyl)bis(3-(2,6-dichlorophenyl)urea) (**4h**) – *synthesised by Dr. G. Pupo*



**4h**

Catalyst **4h** was prepared according to the General Procedure B by employing (*S*)-1,1′-binaphthyl-2,2′-diamine (284 mg, 1.0 mmol, 1 equiv.) and 2,6-dichlorophenyl isocyanate, stirred overnight at room temperature. **Purification**: column chromatography, DCM:$Et_2O$ (80:20). White solid, 428 mg, 65 % yield. **$^1$H NMR** (400 MHz, $CDCl_3$) $\delta$ = 8.46 (d, *J* = 9.1 Hz, 2H), 7.85 (d, *J* = 9.1 Hz, 2H), 7.78 (d, *J* = 8.1 Hz, 2H), 7.34 (ddd, *J* = 8.1, 6.8, 1.2 Hz, 2H), 7.17 (ddd, *J* = 8.3, 6.8, 1.3 Hz, 2H), 7.05 – 6.97 (m, 4H), 6.95 (d, *J* = 8.4, 2H), 6.92 (t, *J* = 8.8, 2H), 6.24 (s, 2H), 6.20 (s, 2H), **$^{13}$C NMR** (101 MHz, $CDCl_3$) $\delta$ = 152.85, 135.72, 134.47, 132.24, 131.09, 130.54, 129.99, 128.83, 128.48, 128.23, 127.35, 125.07, 124.73, 120.30, 118.32; **IR** (solid) *v* = 3375, 3206, 1681, 1594, 1580, 1498, 1427, 1336, 1294, 1196, 1151, 1103, 864, 814, 781, 745, 699, 644 $cm^{-1}$; **mp** 165–166 °C; **HRMS** (APCI+) m/z calculated for $C_{34}H_{23}Cl_4N_4O_2$ $(M+H)^+$ 659.05696, found 659.05655; $[\alpha]_D^{25}$ = -66.1 (c 0.3, $CHCl_3$).

(*S*)-1,1'-([1,1'-binaphthalene]-2,2'-diyl)bis(3-cyclohexylurea) (**4i**) – *synthesised by Dr. G. Pupo*

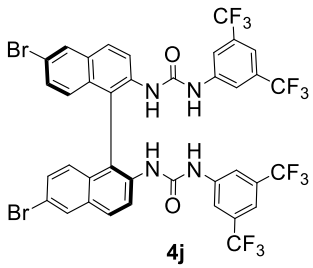


**4i**

Catalyst **4i** was prepared according to the General Procedure B by employing (*S*)-1,1′-binaphthyl-2,2′-diamine (284 mg, 1.0 mmol, 1 equiv.) and cyclohexyl isocyanate, stirred for 72 hours at room temperature. **Purification** column chromatography, hexane:DCM:$Et_2O$ (50:50:0 to 0:100:0 to 0:95:5). White solid, 65 % yield. **$^1$H NMR** (400 MHz, $CDCl_3$) $\delta$ = 8.39 (d, *J* = 9.0 Hz, 2H), 7.98 (d, *J* = 9.1 Hz, 2H), 7.89 (d, *J* = 9.1 Hz, 2H), 7.38 (ddd, *J* = 8.1, 6.8, 1.2 Hz, 2H), 7.21 (ddd, *J* = 8.2, 6.8, 1.3 Hz, 2H),

6.98 (d, *J* = 8.4 Hz, 2H), 6.11 (s, 2H), 4.55 (d, *J* = 7.8 Hz, 2H), 3.27 (s, 2H), 2.18 – 1.48 (m, 10H), 1.35 – 0.66 (m, 10H), **$^{13}$C NMR** (101 MHz, $CDCl_3$) *δ* = 155.15, 136.55, 133.03, 130.62, 129.71, 128.29, 127.09, 125.32, 124.89, 121.78, 119.19, 49.51, 33.53, 25.56, 24.96. Spectroscopic data are in agreement with those previously reported.[5]

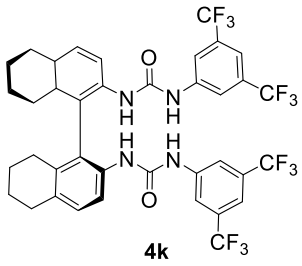
(*S*)-1,1'-(6,6'-dibromo-[1,1'-binaphthalene]-2,2'-diyl)bis(3-(3,5-bis(trifluoromethyl)phenyl)urea) (**4j**) – *synthesised by Dr. G. Pupo*



**4j**

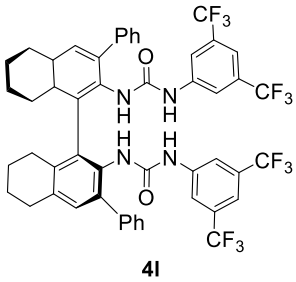
Catalyst **4j** was prepared according to the General Procedure B by employing 6,6'-dibromo-[1,1'-binaphthalene]-2,2'-diamine (442 mg, 1.0 mmol, 1 equiv.) and 3,5-bis(trifluoromethyl)phenyl isocyanate, stirred for 24 hours at room temperature. **Purification** column chromatography, hexane:DCM (70:30). White solid, 618 mg, 45 % yield. **$^{1}$H NMR** (400 MHz, DMSO-$d_6$) *δ* = 9.56 (br s, 2H), 8.42 (d, *J* = 9.1 Hz, 2H), 8.34 (d, *J* = 2.1 Hz, 2H), 8.15 (d, *J* = 9.1 Hz, 2H), 7.82 (s, 4H), 7.62 (br s, 2H), 7.50 (s, 2H), 7.44 (dd, *J* = 9.0, 2.1 Hz, 2H), 6.76 (d, *J* = 9.0 Hz, 2H), **$^{19}$F NMR** (376 MHz, DMSO-$d_6$) *δ* = -57.19 (s), **$^{13}$C NMR** (101 MHz, DMSO-$d_6$) *δ* = 152.40, 141.22, 136.43, 131.70, 131.25, 130.60 (q, *J* = 34.2 Hz) 130.11, 129.97, 128.62, 126.81, 123.61, 123.19 (q, *J* = 273.2 Hz) 119.38, 118.07, 117.40, 114.41; **IR** (solid) *ν* = 3359, 1674, 1572, 1476, 1387, 1334, 1274, 1191, 1170, 1128, 953, 928, 879, 816, 702, 682, 641 $cm^{-1}$; **mp** 180–183 °C; **HRMS** (APCI+) m/z calculated for $C_{38}H_{21}O_2N_4{}^{79}Br_2F_{12}$ $(M+H)^+$ 950.98342, found 950.98218; $[\alpha]_D^{25}$ = -128.1 (c 0.5, $CHCl_3$).

1,1'-(4a,5,5',6,6',7,7',8,8a,8'-decahydro-[1,1'-binaphthalene]-2,2'-diyl)bis(3-(3,5bis(trifluoromethyl)phenyl)urea) (**4k**)


**4k**

Catalyst **4k** was prepared according to the General Procedure B by employing (*S*)-4a,5,5',6,6',7,7',8,8a,8'-decahydro-[1,1'-binaphthalene]-2,2'-diamine (0.08 mmol, 24 mg, 1 equiv.) and 3,5-bis(trifluoromethyl)phenyl isocyanate, stirred for 24 hours at room temperature. **Purification** column chromatography, hexane:DCM (80:20 to 70:30). White solid, 40 mg, 62 % yield. **$^{1}$H NMR** (400 MHz, $CDCl_3$) $\delta$ = 7.49 (s, 4H), 7.65 (d, *J* = 8.8 Hz, 2H), 7.41 (s, 2H), 7.36 (br s, 2H), 7.16 (d, *J* = 8.4, 2H), 6.38 (s, 2H), 2.89 – 2.70 (m, 4H), 2.21–2.07 (m, 4H), 179–1.56 (m, 8H), **$^{19}$F NMR** (377 MHz, $CDCl_3$) $\delta$ = -63.21 (s), **$^{13}$C NMR** (101 MHz, $CDCl_3$) $\delta$ = 153.42, 139.96, 136.62, 135.19, 132.90, 132.27 (q, *J* = 32.7 Hz), 130.14, 128.10, 123.14 (q, *J* = 273.2 Hz), 120.88, 118.65, 116.36, 29.60, 27.54, 23.08, 22.79. Spectroscopic data are in agreement with those previously reported.[4]

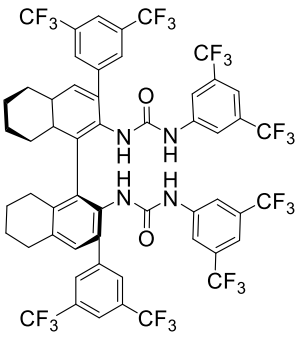
1,1'-(3,3'-diphenyl-4a,5,5',6,6',7,7',8,8a,8'-decahydro-[1,1'-binaphthalene]-2,2'-diyl)bis(3-(3,5-bis(trifluoromethyl)phenyl)urea) (**4l**)


**4l**

Catalyst **4l** was prepared according to the General Procedure B by employing (*S*)-3,3'-diphenyl-4a,5,5',6,6',7,7',8,8a,8'-decahydro-[1,1'-binaphthalene]-2,2'-diamine (0.11 mmol, 50 mg, 1 equiv.) and 3,5-bis(trifluoromethyl)phenyl isocyanate, stirred for 24 hours at room temperature. **Purification** column chromatography, hexane:DCM (30:70 to 0:100). White solid, 52 mg, 50 % yield. **$^{1}$H NMR** (500 MHz, $CDCl_3$) $\delta$ = 7.43–7.37 (m, 4H), 7.34–7.28 (m, 10H), 7.25–7.20 (m, 4H), 6.37 (s, 2H), 6.20 (br s, 2H), 2.89 (t, *J* = 6.3 Hz, 4H), 2.34–2.18 (m, 4H), 2.01–1.68 (m, 8H), **$^{19}$F NMR** (470 MHz, $CDCl_3$) $\delta$ = -63.20 (s), **$^{13}$C NMR** (126 MHz, $CDCl_3$) $\delta$ = 153.13,

139.37, 139.03, 138.35, 137.11, 136.25, 135.90, 132.82 (q, *J* = 33.8 Hz), 131.80, 128.83 (2C), 128.55 (2C), 127.78, 123.12 (q, *J* = 273.1 Hz) 119.36, 116.52, 29.84, 27.82, 23.09, 22.76. Spectroscopic data are in agreement with those previously reported. [4]

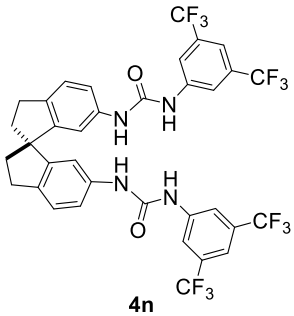
1,1'-(3,3'-bis(3,5-bis(trifluoromethyl)phenyl)-4a,5,5',6,6',7,7',8,8a,8'-decahydro-[1,1'-binaphthalene]-2,2'-diyl)bis(3-(3,5-bis(trifluoromethyl)phenyl)urea) (**4m**) – *synthesised by Dr. G. Pupo*



**4m**

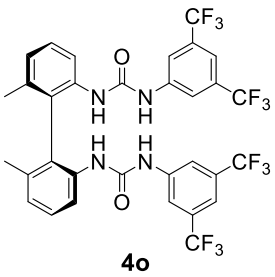
Catalyst **4m** was prepared according to the General Procedure B by employing (*S*)-3,3'-[3,5-bis(trifluoromethyl)phenyl]-1,1'-binaphthyl-2,2'-diamine (0.22 mmol, 160 mg, 1 equiv.) and 3,5-bis(trifluoromethyl)phenyl isocyanate stirred for 24 hours at room temperature. **Purification** column chromatography, hexane:EtOAc (98:2 to 90:10). White solid, 246 mg, 90 % yield. **$^1$H NMR** (500 MHz, $CDCl_3$) $\delta$ = 7.86 (s, 4H), 7.77 (s, 2H), 7.52 (s, 4H), 7.49 (s, 2H), 7.21 (s, 2H), 6.55 (br s, 2H), 6.46 (s, 2H), 2.96–2.80 (m, 4H), 2.26–2.37 (m, 2H), 2.25–2.16 (m, 2H), 1.85–1.66 (m, 8H), **$^{19}$F NMR** (470 MHz, $CDCl_3$) $\delta$ = –63.1 (s, 12F), –63.3 (s, 12F), **$^{13}$C NMR** (126 MHz, $CDCl_3$) $\delta$ = 153.5, 141.6, 139.1, 138.6, 137.1, 135.7, 132.3 (q, *J* = 33.8 Hz), 131.6 (q, *J* = 33.8 Hz), 130.8, 129.1, 128.8, 123.2 (q, *J* = 272.5 Hz), 122.9 (q, *J* = 272.9 Hz), 121.0, 119.2, 117.0, 29.7, 27.6, 22.8, 22.5; **IR** (liquid film) *v* = 2963, 1655, 1621, 1569, 1472, 1384, 1275, 1172, 1126, 942, 899, 882, 845, 703, 681 $cm^{-1}$; **mp** 161–162 °C; **HRMS** (APCI+) m/z calculated for $C_{54}H_{35}O_2N_4F_{24}$ $(M+H)^+$ 1227.2376, found 1227.2356; $[\alpha]_D^{25}$ = +219.2 (c 0.4, $CHCl_3$).

(*S*)-1,1'-(2,2',3,3'-tetrahydro-1,1'-spirobi[indene]-6,6'-diyl)bis(3-(3,5-bis(trifluoromethyl)phenyl)urea) (**4n**) – *synthesised by Dr. G. Pupo*


**4n**

Catalyst **4n** was prepared according to the General Procedure B by employing (*S*)-2,2',3,3'-tetrahydro-1,1'-spirobi[indene]-6,6'-diamine (0.4 mmol, 100 mg, 1 equiv.) and 3,5-bis(trifluoromethyl)phenyl isocyanate, stirred overnight at room temperature. **Purification** column chromatography, hexane:EtOAc (95:5 to 80:20). White solid, 199 mg, 70 % yield. **$^1$H NMR** (400 MHz, DMSO-$d_6$) $\delta$ = 9.05 (s, 2H), 7.86 (s, 4H), 7.54 (s, 2H), 7.13 (s, 2H), 7.11–6.98 (m, 6H), 3.05 (br s, 4H), 2.27 (br s, 4H), **$^{19}$F NMR** (377 MHz, DMSO-$d_6$) $\delta$ = -61.87 (s, 12F), **$^{13}$C NMR** (101 MHz, DMSO-$d_6$) $\delta$ = 152.77, 144.67, 141.93, 141.03, 133.51, 130.45 (q, *J* = 34.61 Hz), 127.41, 125.90 (q, *J* = 273.2 Hz), 124.35, 121.99, 118.05, 113.95, 59.26, 38.46, 30.82; **IR** (solid) *v* = 3275, 1654, 1565, 1471, 1447, 1384, 1275, 1175, 1126, 944, 883, 848, 766, 701, 681 cm$^{-1}$; **mp** 135–138 °C; **HRMS** (APCI+) m/z calculated for $C_{35}H_{25}F_{12}N_4O_2$ $(M+H)^+$ 761.17804, found 761.17688; $[\alpha]_D^{25}$ = -120.9 (c 0.5, $CHCl_3$).

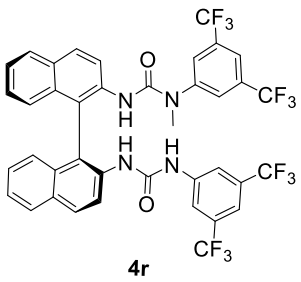
(*S*)-1,1'-(6,6'-dimethyl-[1,1'-biphenyl]-2,2'-diyl)bis(3-(3,5-bis(trifluoromethyl)phenyl)urea) (**4o**) – *synthesised by Dr. L. Pfeifer*


**4o**

Catalyst **4o** was prepared according to the General Procedure A by employing (*S*)-6,6'-dimethyl-[1,1'-biphenyl]-2,2'-diamine (0.24 mmol, 50 mg, 1 equiv.) and 3,5-bis(trifluoromethyl)phenyl isocyanate, stirred overnight at room temperature. **Purification**: column chromatography, hexane:EtOAc (90:10 to 70:30). White solid, 170 mg, 95 % yield. **$^1$H NMR** (600 MHz, $CDCl_3$) $\delta$ = 7.72 (d, *J* = 8.2 Hz, 2H), 7.62 (s, 4H), 7.43 (s, 2H), 7.36 (br s, 2H), 7.33 (t, *J* = 7.9 Hz, 2H), 7.14 (d, *J* = 7.9 Hz, 2H), 6.58 (br s, 2H), 1.94 (s, 6H), **$^{19}$F NMR** (565 MHz, $CDCl_3$)

$\delta$ = -63.24 (s), **$^{13}$C NMR** (151 MHz, $CDCl_3$) $\delta$ = 153.35, 139.64, 138.17, 135.52, 132.41 (q, *J* = 33.3 Hz), 129.34 (2C), 128.50, 127.35, 123.11 (q, *J* = 269.8 Hz), 119.06, 116.78, 19.88; **IR** (solid) *v* = 3324, 3117, 1657, 1541, 1468, 1444, 1384, 1275, 1248, 1174, 1127, 934, 883, 851, 766, 701, 660, 681 $cm^{-1}$; **mp** 139–141°C; **HRMS** (APCI+) m/z calculated for $C_{32}H_{23}F_{12}N_4O_2$ $(M+H)^+$ 723.1624, found 723.1619; $[\boldsymbol{\alpha}]_{\mathbf{D}}^{\mathbf{25}}$ = +23.5 (c 0.4, $CHCl_3$).

(*S*)-1-(3,5-bis(trifluoromethyl)phenyl)-3-(2'-(3-(3,5-bis(trifluoromethyl)phenyl)ureido)-[1,1'-binaphthalen]-2-yl)-1-methylurea (**4r**)

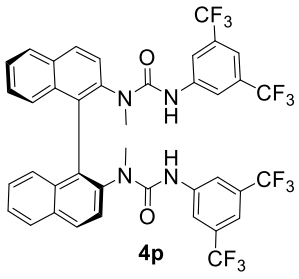


**4r**

In a flame-dried Schlenk under a flow of nitrogen, triphosgene (40.0 mg, 0.135 mmol, 0.5 equiv.) was dissolved in DCE (1 mL). A 0.2 M solution of *N*-methyl-3,5-bis(trifluoromethyl)aniline (**5a**) (72 mg, 0.3 mmol, 1.1 equiv.) in DCE (1.7 mL) was slowly added at 0 °C. Dry $NEt_3$ (150 µL, 1.1 mmol, 4 equiv.) was then added dropwise at the same temperature. After stirring for 2 hours at r.t., 1-(2'-amino-[1,1'-binaphthalen]-2-yl)-3-(3,5-bis(trifluoromethyl)phenyl)urea (145 mg, 0.27 mmol, 1 equiv.) was added in one portion as a solid. The reaction was then refluxed for 24 hours until full consumption of the starting material. The mixture was then cooled to r.t. and quenched with water. The phases were separated, and the aqueous phase extracted three times with DCM. The combined organic phases were then washed with brine. After anhydrification with $MgSO_4$ and filtration, the solvents were evaporated under reduced pressure and the crude product was purified by column chromatography, 1$^{st}$ pentane:$Et_2O$ (100:0 to 80:20), 2$^{nd}$ (pentane:DCM = 70:30) to afford the desired product as a white solid (75 mg, 34% yield).**$^{1}$H NMR** (500 MHz, $CDCl_3$) $\delta$ = 8.53 (d, *J* = 9.1 Hz, 1H), 8.16 (d, *J* = 8.9 Hz, 1H), 7.98 (d, *J* = 8.9 Hz, 1H), 7.96–7.91 (m, 2H), 7.83–7.80 (m, 2H), 7.75 (s, 2H), 7.53 (s br, 1H), 7.48–7.44 (m, 1H), 7.42 (s br, 1H), 7.36–7.27 (m, 4H), 7.16–7.08 (m, 2H), 6.80–6.75 (2H), 5.70 (s, 1H), 3.10 (s, 3H), **$^{19}$F NMR** (470 MHz, $CDCl_3$) $\delta$ = -62.9

(s, 6F), –63.0 (s, 6F), **$^{13}$C NMR** (126 MHz, $CDCl_3$) [overlapping signals], $\delta$ = 155.6, 152.1, 143.3, 140.0, 135.3, 134.8, 133.2 (q, *J* = 34.3 Hz), 132.8, 132.2 (q, *J* = 33.4 Hz), 132.1, 131.7, 130.2, 130.1, 129.9, 128.5, 128.4, 127.7, 127.4, 127.3, 127.2, 126.3, 125.7, 125.0, 124.1, 123.9, 123.3 (q, *J* = 273.6 Hz), 122.4 (q, *J* = 273.0 Hz), 121.5 (m), 120.8, 120.1, 118.5, 118.1 (m), 115.9, 37.4; **IR** (liquid film) *v* = 3326, 3062, 2987, 1693, 1660, 1620, 1598, 1575, 1522, 1501, 1474, 1429, 1383, 1324, 1275, 1174, 1129, 1057, 1027, 1011, 950, 900, 882, 847, 819, 774, 746, 724, 703, 681, 620 cm$^{-1}$; **mp** 134–135 °C; **HRMS** (APCI+) m/z calculated for $C_{39}H_{25}O_2N_4F_{12}Na$ $(M+H)^+$ 809.1780, found 809.1762; $[\alpha]_D^{25}$= -58.1 (c 0.3, $CHCl_3$).

(*S*)-1,1'-([1,1'-binaphthalene]-2,2'-diyl)bis(3-(3,5-bis(trifluoromethyl)phenyl)-1-methylurea) (**4p**)

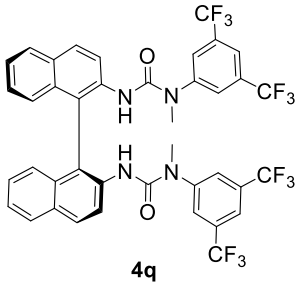


**4p**

Catalyst **4p** was prepared according to the General Procedure B by employing (*S*)-*N*$^2$,*N*$^{2'}$-dimethyl-[1,1'-binaphthalene]-2,2'-diamine (75 mg, 0.24 mmol, 1 equiv.) and 3,5-bis(trifluoromethyl)phenyl isocyanate (15 µL, 0.5 mmol, 3 equiv.). **Purification** column chromatography, pentane:$Et_2O$ (100:0 to 80:20 gradient). White solid, 172 mg, 87 % yield. Spectroscopic analysis of this compound is highly challenging due to the presence of multiple interconverting rotamers and aggregates. $^1$H NMR spectra were dependant on sample concentration and only showed non-assignable very broad signals even at high temperatures (up to 90 °C). $^1$H NMR and $^{19}$F NMR could be recorded in a diluted solution of DMSO-$d_6$ (2 mg/mL) at 418 K (1 main species observed). Due to instrument limitations at these high temperatures, $^{13}$C NMR could not be acquired. **$^1$H NMR** (500 MHz, DMSO-$d_6$, 418 K) $\delta$ = 7.92 (d, *J* = 9.0 Hz, 2H), 7.80–7.77 (m, 2H), 7.30 (d, *J* = 9.0, 2H), 7.17–7.07 (m, 8H), 7.00 (s br, 2H), 6.79 (d, *J* = 8.4 Hz, 2H), 5.74 (s br, 2H), 2.79 (s, 3H), 2.78 (s, 3H) **$^{19}$F NMR** (470 MHz, DMSO-$d_6$, 120 °C) $\delta$ = –62.1 (s); **IR** (liquid film) *v* = 3422, 1665, 1619, 1595, 1536, 1472, 1440, 1387, 1347,

1312, 1276, 1169, 1127, 1001, 937, 880, 844, 821, 753, 733, 700, 682, 647, 615 $cm^{-1}$; **mp** 155–156 °C; **HRMS** (ESI+) m/z calculated for $C_{40}H_{27}O_2N_4F_{12}$ $(M+H)^+$ 823.1915, found 823.1937; $[\alpha]_D^{25}$ = -288.7 (c 1.0, $CHCl_3$).

(*S*)-1,1'-([1,1'-binaphthalene]-2,2'-diyl)bis(3-(3,5-bis(trifluoromethyl)phenyl)-3-methylurea) (**4q**)

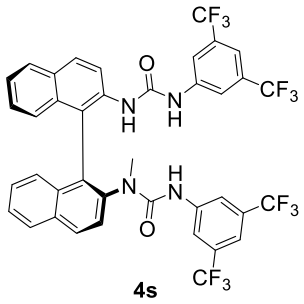


**4q**

In a flame-dried Schlenk under a flow of nitrogen, triphosgene (103.5 mg, 0.35 mmol, 0.7 equiv) was dissolved in 0.5 mL of DCM. A 0.5 M solution of *N*-methyl-3,5-bis(trifluoromethyl)aniline (**5a**) (243 mg, 1 mmol, 2 equiv.) in DCM (2 mL) was slowly added at 0 °C. Dry $NEt_3$ (278 µL, 2 mmol, 4 equiv.) was then added dropwise at the same temperature. After stirring for 2 hours at r.t., (*S*)-1,1'-binaphthyl-2,2'-diamine (142 mg, 0.5 mmol, 1 equiv.) was added in one portion as a solid. The reaction was then refluxed for 36 hours until full consumption of the starting material. The mixture was then cooled to r.t. and quenched with water. The phases were separated and the aqueous phase extracted three times with DCM. The combined organic phases were then washed with brine. After anhydrification with $MgSO_4$ and filtration, the solvents were evaporated under reduced pressure and the crude product was purified by column chromatography (hexane:$Et_2O$ 100:0 to 80:20) to afford the desired product as a white solid (218 mg, 53 % yield). **$^1$H NMR** (500 MHz, $CDCl_3$) $\delta$ = 8.23 (d, *J* = 9.0 Hz, 2H), 7.83 (d, *J* = 8.1 Hz, 2H), 7.74 (d, *J* = 8.1 Hz, 2H), 7.51 (s, 2H), 7.34–7.30 (m, 6H), 7.16–7.12 (m, 2H), 6.83 (d, *J* = 8.4 Hz, 2H), 5.66 (s, 2H), 3.06 (s, 6H), **$^{19}$F NMR** (470 MHz, $CDCl_3$) $\delta$ = -62.7 (s), **$^{13}$C NMR** (126 MHz, $CDCl_3$) [overlapping signals] $\delta$ = 153.6, 143.5, 135.3, 132.8 (q, *J* = 34.1 Hz), 131.5, 130.2, 129.6, 128.1, 127.3 (2C), 125.1, 124.0, 122.5 (q, *J* = 273.6 Hz), 121.0, 120.9 (sept, *J* = 3.5 Hz), 119.1, 37.0; **IR** (liquid film) *v* = 3395, 1690, 1620, 1597, 1499, 1469, 1431,

1383, 1313, 1275, 1254, 1176, 1135, 1105, 1026, 1008, 965, 900, 847, 818, 774, 746, 705, 692, 682 $cm^{-1}$; **mp** 152–153 °C; **HRMS** (APCI+) m/z calculated for $C_{40}H_{27}O_2N_4F_{12}$ $(M+H)^+$ 823.1915, found 823.1936; $[\alpha]_D^{25}$ -121.8 (c 1.0, $CHCl_3$).

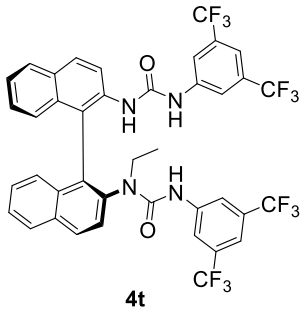
(*S*)-3-(3,5-bis(trifluoromethyl)phenyl)-1-(2'-(3-(3,5-bis(trifluoromethyl)phenyl)ureido)-[1,1'-binaphthalen]-2-yl)-1-methylurea (**4s**)



**4s**

Catalyst **4s** was prepared according to the General Procedure B by employing (*S*)-*N*-methylated *bis*-aniline **5c** (0.33 mmol, 100 mg, 1 equiv.) and 3,5-bis(trifluoromethyl)phenyl isocyanate, stirred 72 hours at reflux. **Purification** column chromatography, hexane:$Et_2O$ (80:20 to 60:40). White solid, 180 mg, 68 % yield. **$^1$H NMR** (400 MHz, $CDCl_3$) $\delta$ = 8.50 (d, *J* = 8.7 Hz, 1H), 8.13 (d, *J* = 8.7 Hz, 1H), 7.91 (t, *J* = 9.2 Hz, 2H), 7.91 (d, *J* = 8.1 Hz, 1H), 7.80 (s, 2H), 7.64 (s, 2H), 7.60–7.37 (m, 6H), 7.32–7.22 (m, 2H), 7.12 (s br, 1H), 7.10 (d, *J* = 8.5 Hz, 1H), 6.93 (d, *J* = 8.5 Hz, 1H), 6.80 (s br, 1H), 2.89 (s, 3H), **$^{19}$F NMR** (376 MHz, $CDCl_3$) $\delta$ = -63.2 (s), -63.3 (s), **$^{13}$C NMR** (101 MHz, $CDCl_3$) [overlapping signals] $\delta$ = 156.0, 151.7, 139.9, 139.9, 139.2, 135.4, 133.5, 133.2, 133.0, 132.3 (q, *J* = 32.9 Hz), 132.0 (q, *J* = 32.9 Hz), 131.1, 131.0, 130.2, 129.8, 128.5, 128.3, 127.6, 127.3, 127.2, 126.5, 126.3, 125.0, 124.7, 123.1 (q, *J* = 272.9 Hz), 122.8 (q, *J* = 272.9 Hz), 120.1, 119.8, 118.11, 117.4, 115.9, 37.1; **IR** (liquid film) *v* = 3326, 3064, 1654, 1621, 1600, 1538, 1505, 1473, 1443, 1386, 1358, 1340, 1317, 1276, 1173, 1127, 1058, 1001, 949, 881, 844, 823, 776, 750, 725, 700, 682 $cm^{-1}$; **mp** 156–157 °C; **HRMS** (APCI+) m/z calculated for $C_{39}H_{25}O_2N_4F_{12}$ $(M+H)^+$ 809.1773, found 809.1780; $[\boldsymbol{\alpha}]_{\mathbf{D}}^{\mathbf{25}}$ = -81.5 (c 1.0, $CHCl_3$).

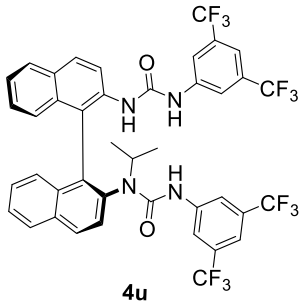
(*S*)-3-(3,5-bis(trifluoromethyl)phenyl)-1-(2'-(3-(3,5-bis(trifluoromethyl)phenyl)ureido)-[1,1'-binaphthalen]-2-yl)-1-ethylurea (**4t**)



**4t**

Catalyst **4t** was prepared according to the General Procedure B by employing (*S*)-*N*-ethylated *bis*-aniline **5d** (0.48 mmol, 150 mg, 1 equiv.) and 3,5-bis(trifluoromethyl)phenyl isocyanate, stirred 72 hours at reflux. **Purification** column chromatography, 1st pentane:DCM (80:20 to 0:100 gradient), 2nd pentane:EtOAc (95:5 to 80:20 gradient). White solid, 257.0 mg, 65 % yield. **$^1$H NMR** (400 MHz, $CDCl_3$) $\delta$ = 8.49 (d, *J* = 7.9 Hz, 1H), 8.13 (d, *J* = 8.7 Hz, 1H), 8.02–7.96 (m, 2H), 7.92 (d, *J* = 8.3 Hz, 1H), 7.83 (br s, 2H), 7.63 (s, 2H), 7.55–7.96 (m, 4H), 7.43–7.36 (m, 2H), 7.30–7.22 (m, 2H), 7.14 (s br, 1H), 7.08 (d, *J* = 8.3 Hz, 1H), 6.90 (d, *J* = 8.7 Hz, 2H), 3.30–3.18 (m, 1H), 3.18–3.03 (br s, 1H), 1.00 (d, *J* = 7.2 Hz, 3H), **$^{19}$F NMR** (376 MHz, $CDCl_3$) $\delta$ = -63.2 (s, 6F), –63.3 (s, 6F), **$^{13}$C NMR** (101 MHz, $CDCl_3$) [overlapping signals] $\delta$ = 155.7, 151.7, 139.8, 139.3, 138.7, 135.4, 133.6, 133.2, 130.0, 132.4 (q, *J* = 33.2 Hz), 132.0 (q, *J* = 33.6 Hz), 131.4, 130.7, 130.2, 129.8, 128.6, 128.2, 127.7, 127.6, 127.3, 127.2, 126.6, 124.9, 124.7, 123.0 (q, *J* = 272.2 Hz), 122.9 (q, *J* = 272.0 Hz), 122.3, 120.1 119.9, 118.1, 117.4, 115.8 (m), 44.5, 13.2; **IR** (liquid film) *v* = 3338, 3064, 1644, 1600, 1505, 1473, 1440, 1385, 1371, 1340, 1275, 1174, 1125, 1060, 1033, 1015, 1000, 968, 948, 880, 845, 823, 810, 787, 774, 749, 724, 700, 681 $cm^{-1}$; **mp** 141–142 °C; **HRMS** (APCI+) m/z calculated for $C_{40}H_{27}O_2N_4F_{12}$ $(M+H)^+$ 823.1937, found 823.1916; $[\boldsymbol{\alpha}]_{\mathbf{D}}^{\mathbf{25}}$ = -81.5 (c 1.0, $CHCl_3$).

(*S*)-3-(3,5-bis(trifluoromethyl)phenyl)-1-(2'-(3-(3,5-bis(trifluoromethyl)phenyl)ureido)-[1,1'-binaphthalen]-2-yl)-1-isopropylurea (**4u**)



**4u**

Catalyst **4u** was prepared according to the General Procedure B by employing *N*-isopropylated *bis*-aniline (**5e** (3.22 mmol, 1.0 g, 1 equiv.) and 3,5-bis(trifluoromethyl)phenyl isocyanate, stirred 72 hours at reflux. **Purification:** column chromatography, hexane:EtOAc (90:10 to 80:20 gradient). White solid, 2.4 g, 91 % yield. **$^{1}$H NMR** (500 MHz, $CDCl_3$) $\delta$ = 8.53 (d, *J* = 8.9 Hz, 1H), 8.15 (d, *J* = 8.9 Hz, 1H), 8.01 (d, *J* = 9.1 Hz, 1H), 7.99 (d, *J* = 8.1 Hz, 1H), 7.92 (d, *J* = 8.1 Hz, 1H), 7.80 (s, 2H), 7.60 (s, 2H), 7.56–7.48 (m, 4H), 7.42–7.38 (m, 2H), 7.32–7.28 (m, 1H), 7.26–7.21 (m, 1H), 7.17 (d, *J* = 8.4 Hz, 1H), 7.12 (s, 1H), 6.89 (d, *J* = 8.4 Hz, 1H), 6.79 (br s, 1H), 3.65 (sept, *J* = 7.0 Hz, 1H), 1.04 (d, *J* = 7.0 Hz, 3H), 0.67 (s br, 3H), **$^{19}$F NMR** (470 MHz, $CDCl_3$) [overlapping signals] $\delta$ = -63.2 (s), **$^{13}$C NMR** (126 MHz, $CDCl_3$) [overlapping signals] $\delta$ = 155.9, 151.8, 139.9, 139.8, 139.3, 135.6, 133.7, 133.2, 133.1, 132.3 (q, *J* = 33.5 Hz), 131.9 (q, *J* = 33.5 Hz), 131.8, 130.7, 130.3, 129.9, 128.5, 128.2, 127.9, 127.5, 127.3, 127.2, 127.1, 126.9, 125.2, 124.6, 123.1 (q, *J* = 273.0 Hz), 122.9 (q, *J* = 273.0 Hz), 120.2, 119.9, 118.1, 117.4, 115.8, 53.2, 20.9, 20.6, **IR** (liquid film) ν = 3328, 3064, 2929, 1687, 1637, 1621, 1602, 1540, 1506, 1473, 1439, 1385, 1338, 1276, 1175, 1127, 1060, 1035, 948, 930, 882, 843, 820, 785, 775, 749, 725, 700, 683, 634 cm$^{-1}$; **mp** 139–140 °C; **HRMS** (APCI+) m/z calculated for $C_{41}H_{29}O_2N_4F_{12}$ $(M+H)^+$ 837.2093, found 837.2077; $[\boldsymbol{\alpha}]_{\mathbf{D}}^{\mathbf{25}}$ = -49.9 (c 1.0, $CHCl_3$). Full assignment tables are presented along with copy of the spectra (*v. 4.3.2.2 iPr BINAM Urea (**4u**) – assignment and copy of NMR spectra*).

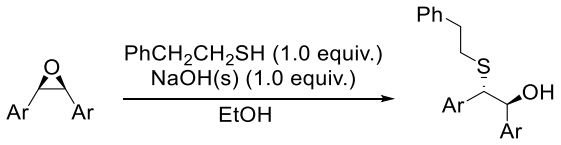
The opposite enantiomer (*R*)-**4u** ($[\alpha]_{\mathrm{D}}^{25^{\circ}\mathrm{C}}$ +50.2 ° (c = 1.0, $CHCl_3$)) was prepared following the same protocol starting from 650 mg (1.99 mmol) of (*R*)-**5e** (1.440 g, 86% yield).

**4u:**TBAF complex was synthesized according to literature procedure[6]: **4u** (100 mg, 0.12 mmol, 1 equiv.) and TBAF·$3H_2O$ (31 mg, 0.12 mmol, 1 equiv.) were refluxed in hexane (0.04 M, 3 mL) for 2 h. The resulting suspension was filtered and the solid dried *in vacuo* affording the desired complex. X-ray quality crystals were obtained by recrystallization layering hexane into a saturated solution of **4u**:TBAF in $Et_2O$.

Single Crystal Data for **4u**:TBAF $C_{57}H_{64}F_{13}N_5O_2$, Mr =1098.14. 150 K – orthorhombic, P21 21 21, a = 10.22990(10) Å, b = 21.55920(10) Å, c = 25.00480(10) Å, V = 5514.77(6) Å, Data/restraints/parameters – 11531/456/751, Flack = 0.000(16) for 5144 Friedel pairs and Hooft = -0.007(16) for 5049 Friedel pairs, P2(correct) > 99.9999%, P3(correct) > 99.9999%, Rint = 0.046, Final R1 = 0.0511, wR2 = 0.1451 (I>2σ(I)).

*4.2.2 Substrates Synthesis and Characterisation*

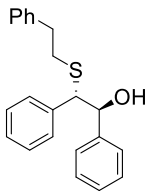
*4.2.2.1 β-Hydroxy Sulfides*




*rac*-**6a–6s**

General procedure for the synthesis of β-hydroxy sulfides (**General Procedure D**): The appropriate *cis*-epoxide (1.0 equiv.) was dissolved in EtOH (0.1 M) in a round-bottom flask and $NaOH_{(S)}$ (1.0 equiv.), 2-phenylethane-1-thiol (1.0 equiv.) were added to the solution at room temperature. The reaction mixture was either stirred overnight at room temperature or reflux for the indicated time (monitored by TLC using hexane:DCM = 80:20 as eluent). When TLC analysis showed no further conversion, the solvent was removed *in vacuo*. To the crude mixture residue was then added $Et_2O$ and water, the layers were partitioned, and the aqueous phase was extracted three times with $Et_2O$. The organic phases were combined, dried over $MgSO_4$, filtered and concentrated *in vacuo* to afford the crude product. The crude products were then purified by flash column chromatography (hexane/$Et_2O$) to afford pure β-hydroxy sulfides.

*rac*-2-(phenethylthio)-1,2-diphenylethan-1-ol (**6a**)

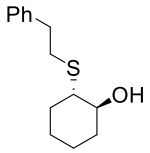



*rac*-**6a**

Alcohol **6a** was prepared according to the General Procedure D using *cis*-stilbene oxide (10.2 mmol, 2.00 g) and by stirring the reaction mixture at reflux for 2 h. **Purification** column chromatography, hexane:$Et_2O$ (100:0 to 80:20). The product was obtained as a yellow oil, 3.19 g, 91 % yield. **$^1$H NMR** (500 MHz, $CDCl_3$) $\delta$ = 7.32–7.26 (m, 2H), 7.25–7.17 (m, 7H), 7.16–7.12 (m, 4H), 7.12–7.08 (m, 2H), 4.86 (dd, *J* = 8.5, 2.7 Hz, 1H), 4.03 (d, *J* = 8.5 Hz, 1H), 3.17 (d, *J* = 2.7 Hz, 1H), 2.87–2.78 (m, 2H),

2.76–2.62 (m, 2H), **$^{13}$C NMR** (126 MHz, $CDCl_3$) $\delta$ = 141.1, 140.3, 139.6, 128.7, 128.6, 128.6, 128.4, 128.1, 127.8, 127.4, 126.8, 126.5, 77.4, 60.4, 36.3, 33.4; **IR** (liquid film) *v* = 3433, 3061, 3027, 2917, 1602, 1494, 1453, 1191, 1044, 1030, 756, 730 $cm^{-1}$; **HRMS** (ESI+) m/z calculated for $C_{22}H_{22}ONaS$ $(M+Na)^+$ 357.1284, found 357.1285.

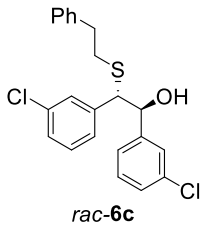
*rac*-2-(phenethylthio)cyclohexan-1-ol (**6b**)



*rac*-**6b**

Alcohol **6b** was prepared according to the General Procedure D using cyclohexene oxide (10 mmol, 0.98 g), and by stirring the reaction mixture at reflux for 4 h. **Purification** column chromatography, hexane:$Et_2O$ (100:0 to 70:30). The product was obtained as a colourless oil, 2.3 g, 96 % yield. **$^1$H NMR** (400 MHz, $CDCl_3$) $\delta$ = 7.34–7.27 (m, 2H), 7.27 – 7.17 (m, 3H), 3.29 (td, *J* = 8.7, 4.5, Hz, 1H), 2.98 – 2.76 (m, 5H), 2.39 (ddd, *J* = 12.2, 9.9, 4.0 Hz, 1H), 2.20–1.99 (m, 2H), 1.85 – 1.65 (m, 2H), 1.53 – 1.37 (m, 1H), 1.37 – 1.17 (m, 3H), **$^{13}$C NMR** (100 MHz, $CDCl_3$) $\delta$ = 140.4, 128.6, 128.6, 126.6, 72.3, 53.8, 36.9, 34.0, 33.1, 31.5, 26.5, 24.6; **IR** (liquid film) *v* = 3444, 2930, 2856, 1496, 1448, 1272, 1068, 1037, 963, 733, 697 $cm^{-1}$; **HRMS** (ESI+) *m/z* calculated for $C_{14}H_{21}OS$ $[M+H]^+$ 237.1308, found 237.1310.

*rac*-1,2-bis(3-chlorophenyl)-2-(phenethylthio)ethan-1-ol (**6c**)

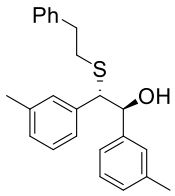


*rac*-**6c**

Alcohol **6c** was prepared according to the General Procedure D from the corresponding epoxide (8.1 mmol, 2.1 g) and by stirring the reaction mixture at reflux for 2 h. **Purification** column chromatography, hexane:$Et_2O$ (100:0 to 80:20). The product was obtained as a yellow oil, 2.9 g, 89 % yield. **$^1$H NMR** (500 MHz, $CDCl_3$) $\delta$ = 7.32–7.21 (m, 3H), 7.20–7.07 (m, 8H), 6.93 (dt, *J* = 7.5, 1.5 Hz, 1H), 6.88 (dt, *J* = 7.7, 1.4 Hz, 1H), 4.73 (d, *J* = 8.3 Hz, 1H), 3.83 (d, *J* = 8.3 Hz, 1H), 3.11 (s br, 1H), 2.81 (t, *J* = 7.5 Hz, 2H), 2.75–2.65 (m, 2H), **$^{13}$C NMR** (126 MHz, $CDCl_3$) [overlapping signals] $\delta$ =

142.7, 141.5, 140.0, 134.4, 134.2, 129.7, 129.4, 128.7, 128.7, 128.2 127.9, 126.9, 126.8, 126.7, 125.1, 76.7, 59.8, 36.3, 33.6; **IR** (liquid film) *v* = 3439, 3027, 2919, 1595, 1496, 1430, 1191, 1098, 1079, 884, 786, 771, 747, 696 $cm^{-1}$; **HRMS** (ESI+) m/z calculated for $C_{22}H_{20}O_{35}Cl_2NaS$ $(M+Na)^+$ 425.0504, found 425.0504.

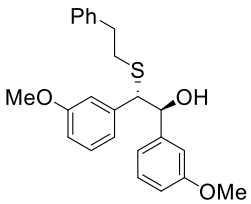
*rac*-2-(phenethylthio)-1,2-di-m-tolylethan-1-ol (**6d**)



*rac*-**6d**

Alcohol **6d** was prepared according to the General Procedure D from the corresponding epoxide (11.6 mmol, 2.6 g) and by stirring the reaction mixture at reflux for 2 h. **Purification** column chromatography, hexane:$Et_2O$ (100:0 to 80:20 gradient). The product was obtained as a yellow oil, 2.7 g, 60 % yield. **$^1$H NMR** (400 MHz, $CDCl_3$) $\delta$ = 7.24–7.12 (m, 3H), 7.08–7.00 (m, 4H), 6.98–6.83 (m, 6H), 4.77 (d, *J* = 8.1 Hz, 1H), 3.94 (d, *J* = 8.1 Hz, 1H), 3.02 (s br, 1H), 2.78–2.70 (m, 2H), 2.68–2.55 (m, 2H), 2.23 (s, 3H), 2.22 (s, 3H), **$^{13}$C NMR** (101 MHz, $CDCl_3$) $\delta$ = 141.1, 140.4, 139.6, 138.0, 137.7, 129.4, 128.6, 128.6, 128.5, 128.2, 128.2, 127.9, 127.4, 126.5, 125.8, 124.0, 77.2, 60.1, 36.3, 33.4, 21.5, 21.5; **IR** (liquid film) *v* = 3442, 3026, 2918, 1605, 1489, 1454, 1378, 1152, 1044, 780, 729, 698 $cm^{-1}$; **HRMS** (ESI+) m/z calculated for $C_{24}H_{26}ONaS$ $(M+Na)^+$ 385.1597, found 385.1598.

*rac*-1,2-bis(3-methoxyphenyl)-2-(phenethylthio)ethan-1-ol (**6e**)

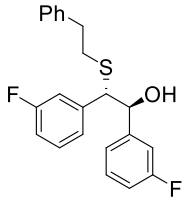


*rac*-**6e**

Alcohol **6e** was prepared according to the General Procedure D from the corresponding epoxide (8.3 mmol, 2.1 g) and by stirring the reaction mixture at reflux for 3 h. **Purification** column chromatography, hexane:$Et_2O$ (100:0 to 70:30 gradient). The product was obtained as a yellow oil, 2.9 g, 88 % yield. **$^1$H NMR** (400 MHz, $CDCl_3$) $\delta$ = 7.25–7.18 (m, 2H), 7.17–7.11 (m, 1H), 7.10–7.00 (m, 4H), 6.71–6.60 (m, 6H), 4.75 (dd, *J* = 8.3, 2.8 Hz, 1H), 3.91 (d, *J* = 8.3 Hz, 1H), 3.66 (s, 3H), 3.64 (s, 3H), 3.05 (d, *J* = 2.8 Hz, 1H), 2.78–2.72 (m, 2H), 2.68–2.58 (m, 2H), **$^{13}$C NMR**

(101 MHz, $CDCl_3$) $\delta$ = 159.6, 159.4, 142.7, 141.2, 140.3, 129.3, 129.1, 128.7, 128.6, 126.5, 121.2, 119.2, 114.3, 113.7, 113.0, 112.1, 77.2, 60.2, 55.3, 55.3, 36.3, 33.5; **IR** (liquid film) $\nu$ = 3455, 3026, 2536, 2835, 1599, 1585, 1489, 1454, 1259, 1150, 1042, 779, 732, 697 $cm^{-1}$; **HRMS** (ESI+) m/z calculated for $C_{24}H_{26}O_3NaS$ $(M+Na)^+$ 417.1495, found 417.1491.

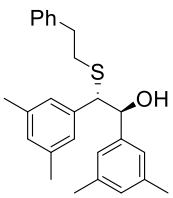
*rac*-1,2-bis(3-fluorophenyl)-2-(phenethylthio)ethan-1-ol (**6f**)



*rac*-**6f**

Alcohol **6f** was prepared according to the General Procedure D from the corresponding epoxide (12.6 mmol, 2.9 g) and by stirring the reaction mixture at reflux for 2 h. **Purification** column chromatography, hexane:$Et_2O$ (100:0 to 80:20 gradient). The product was obtained as a yellow oil, 3.98 g, 85 % yield. **$^1$H NMR** (400 MHz, $CDCl_3$) $\delta$ = 7.24–7.12 (m, 3H), 7.11–6.99 (m, 4H), 6.86–6.68 (m, 6H), 4.68 (d, *J* = 8.5, 1H), 3.80 (d, *J* = 8.4 Hz, 1H), 3.05 (s br, 1H), 2.74 (t, *J* = 7.3 Hz, 2H), 2.67–2.53 (m, 2H), **$^{19}$F NMR** (376 MHz, $CDCl_3$) $\delta$ = -112.7 (td, *J* = 9.0, 5.7 Hz), -113.0 (td, *J* = 9.3, 5.9 Hz), **$^{13}$C NMR** (101 MHz, $CDCl_3$) [overlapping signals] $\delta$ = 162.7 (d, *J* = 246.2 Hz), 162.7 (d, *J* = 246.2 Hz), 143.4 (d, *J* = 7.3 Hz), 142.0 (d, *J* = 7.3 Hz), 140.0, 130.0 (d, *J* = 8.3 Hz), 129.6 (d, *J* = 8.2 Hz), 128.6, 124.4 (d, *J* = 2.9 Hz), 122.5 (d, *J* = 2.9 Hz), 115.5 (d, *J* = 22.0 Hz), 114.9 (d, *J* = 21.1 Hz), 114.6 (d, *J* = 21.1 Hz), 113.6 (d, *J* = 22.2 Hz), 77.3 (d, *J* = 1.8 Hz), 59.9 (d, *J* = 1.8 Hz), 36.2, 33.5; **IR** (liquid film) $\nu$ = 3432, 3028, 2918, 1613, 1589, 1487, 1448, 1254, 1160, 1045, 877, 782, 734, 694 $cm^{-1}$, **HRMS** (ESI+) m/z calculated for $C_{22}H_{20}OF_2NaS$ $(M+Na)^+$ 393.1095, found 393.1095.

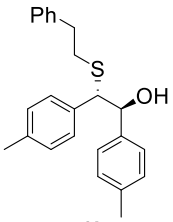
*rac*-1,2-bis(3,5-dimethylphenyl)-2-(phenethylthio)ethan-1-ol (**6g**)



*rac*-**6g**

Alcohol **6g** was prepared according to the General Procedure D from the corresponding epoxide (12.4 mmol, 3.2 g) and by stirring the reaction mixture overnight at room temperature. **Purification** column chromatography, pentane:$Et_2O$ (100:0 to 80:20 gradient). The product was obtained as a yellow oil, 982 mg, 20 % yield (unoptimized). **$^1$H NMR** (400 MHz, $CDCl_3$) $\delta$ = 7.25–7.20 (m 2H), 7.19–7.13 (m, 1H), 7.06–7.00 (m, 2H), 6.82–6.78 (m, 2H), 6.78 (s, 4H), 4.77 (dd, *J* = 7.3, 3.4 Hz, 1H), 3.94 (d, *J* = 7.3 Hz, 1H), 2.98 (d, *J* = 3.5 Hz, 1H), 2.79–2.70 (m, 2H), 2.66–2.53 (m, 2H), 2.21 (s, 6H), 2.20 (s, 6H), **$^{13}$C NMR** (101 MHz, $CDCl_3$) $\delta$ = 141.3, 140.5, 139.7, 137.7, 137.4, 129.3, 129.1, 128.6, 128.5, 126.5, 126.4, 124.5, 76.8, 59.8, 36.3, 33.5, 21.4 (2C); **IR** (liquid film) *v* = 3435, 3025, 2916, 1603, 1454, 1376, 1279, 1155, 1038, 852, 735, 697 $cm^{-1}$; **HRMS** (ESI+) m/z calculated for $C_{26}H_{30}ONaS$ $(M+Na)^+$ 413.1910, found 413.1910.

*rac*-2-(phenethylthio)-1,2-di-p-tolylethan-1-ol (**6h**)

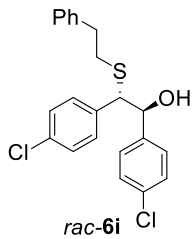


*rac*-**6h**

Alcohol **6h** was prepared according to the General Procedure D from the corresponding epoxide (12.7 mmol, 2.85 g) and by stirring the reaction mixture overnight at room temperature. **Purification** column chromatography, hexane:$Et_2O$ (100:0 to 80:20 gradient). The product was obtained as a yellow oil, 2.99 g, 65 % yield. **$^1$H NMR** (400 MHz, $CDCl_3$) $\delta$ = 7.33–7.27 (m, 2H), 7.26–7.21 (m, 1H), 7.14–7.09 (m, 2H), 7.09–7.01 (m, 8H), 4.86 (dd, *J* = 8.4, 2.8 Hz, 1H), 4.04 (d, *J* = 8.4 Hz, 1H), 3.11 (d, *J* = 2.8 Hz, 1H), 2.87–2.78 (m, 2H), 2.75–2.61 (m, 2H), 2.31 (s, 3H), 2.31 (s, 3H), **$^{13}$C NMR** (101 MHz, $CDCl_3$) $\delta$ = 140.5, 138.3, 137.3, 136.9, 136.6, 129.1, 128.8, 128.7, 128.6 (2C), 126.8, 126.5, 77.0, 59.8, 36.3, 33.3, 21.3, 21.2; **IR** (liquid film) *v* = 3447, 3025, 2920, 2860, 1901,

1604, 1512, 1454, 1179, 1041, 814, 737, 698 $cm^{-1}$; **mp** 68–69 °C; **HRMS** (ESI+) m/z calculated for $C_{24}H_{26}ONaS$ $(M+Na)^+$ 385.1597, found 385.1594.

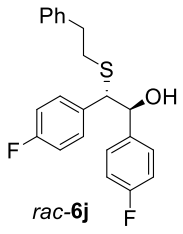
*rac*-1,2-bis(4-chlorophenyl)-2-(phenethylthio)ethan-1-ol (**6i**)



*rac*-**6i**

Alcohol **6i** was prepared according to the General Procedure D from the corresponding epoxide (7.2 mmol, 1.9 g) and by stirring the reaction mixture at reflux for 2 h. **Purification** column chromatography, hexane:$Et_2O$ (100:0 to 80:20 gradient). The product was obtained as a yellow oil, 2.63 g, 92 % yield. **$^1$H NMR** (400 MHz, $CDCl_3$) $\delta$ = 7.23–7.17 (m, 7H), 7.15–7.09 (m, 2H), 7.06–6.99 (m, 4H), 4.65 (dd, *J* = 8.6, 2.5 Hz, 1H), 3.79 (d, *J* = 8.6 Hz, 1H), 3.10 (d, *J* = 2.5 Hz, 1H), 2.74 (t, *J* = 7.3 Hz, 2H), 2.64–2.55 (m, 2H), **$^{13}$C NMR** (101 MHz, $CDCl_3$) [overlapping signals] $\delta$ = 140.0, 139.2, 137.8, 133.6, 133.3, 130.0, 128.7,128.7, 128.4, 128.2, 126.7, 76.7, 59.7, 36.2, 33.4; **IR** (liquid film) *v* = 3432, 3027, 2916, 1901, 1596, 1489, 1454, 1407, 1180, 1089, 1014, 834, 747, 697 $cm^{-1}$; **HRMS** (ESI+) m/z calculated for $C_{22}H_{20}OCl_2NaS$ $(M+Na)^+$ 425.0504, found 425.0505.

*rac*-1,2-bis(4-fluorophenyl)-2-(phenethylthio)ethan-1-ol (**6j**)

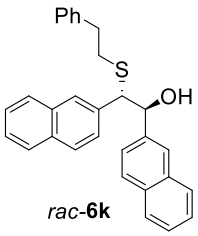


*rac*-**6j**

Alcohol **6j** was prepared according to the General Procedure D from the corresponding epoxide (5.16 mmol, 1.2 g) and by stirring the reaction mixture at reflux for 2 h. **Purification** column chromatography, hexane:$Et_2O$ (100:0 to 80:20 gradient). The product was obtained as a yellow oil, 800 mg, 60 % yield. **$^1$H NMR** (400 MHz, $CDCl_3$) $\delta$ = 7.31–7.19 (m, 3H), 7.11–7.07 (m, 2H), 7.05–6.99 (m, 4H), 6.92–6.84 (m, 4H), 4.73 (d, *J* = 8.8 Hz, 1H), 3.88 (d, *J* = 8.8 Hz, 1H), 3.09 (s br, 1H), 2.81 (t, *J* = 7.3 Hz, 2H), 2.74–2.62 (m, 2H), **$^{19}$F NMR** (376 MHz, CDCl3) $\delta$ = -114.2– -114.3 (m), -114.5–-114.6 (m), **$^{13}$C NMR** (101 MHz, $CDCl_3$) $\delta$ = 164.4 (d, *J* = 246.6 Hz), 162.0 (d, *J* = 245.7 Hz), 140.1, 135.5 (d, *J* = 3.7 Hz), 135.2 (d, *J* = 3.7 Hz), 130.2 (d, *J* = 8.1 Hz), 128.7, 128.5, 128.4 (d, *J* = 8.1 Hz), 126.6,

115.4 (d, *J* = 21.4 Hz), 115.1 (d, *J* = 21.5 Hz), 77.0, 59.7, 36.2, 33.4; **IR** (liquid film) *v* = 3433, 2919, 1603, 1507, 1221, 1157, 1095, 832, 804, 746, 698 $cm^{-1}$; **HRMS** (ESI+) m/z calculated for $C_{22}H_{20}OF_2NaS$ $(M+Na)^+$ 393.1095, found 393.1095.

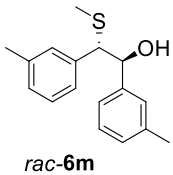
*rac*-1,2-di(naphthalen-2-yl)-2-(phenethylthio)ethan-1-ol (**6k**)



*rac*-**6k**

Alcohol **6k** was prepared according to the General Procedure D from the corresponding epoxide (2.87 mmol, 850 mg) and by stirring the reaction mixture at reflux for 5 hours. **Purification** column chromatography, hexane:$Et_2O$ (100:0 to 80:20 gradient). The product was obtained as a white solid, 1.13 g, 91 % yield. **$^1$H NMR** (500 MHz, $CDCl_3$) $\delta$ = 7.79–7.62 (m, 7H), 7.54 (s, 1H), 7.46–7.35 (m, 5H), 7.30–7.16 (m, 4H), 7.07–7.01 (m, 2H), 5.16 (d, *J* = 8.3 Hz, 1H), 4.30 (d, *J* = 8.3 Hz, 1H), 3.28 (br s, 1H), 2.87–2.76 (m, 2H), 2.75–2.61 (m, 2H), **$^{13}$C NMR** (126 MHz, $CDCl_3$) [overlapping signals] $\delta$ = 140.2, 138.6, 137.0, 133.1, 133.1, 132.8, 128.7, 128.6, 128.3, 128.1, 127.9, 127.9, 127.7, 127.7, 127.7, 126.5, 126.5, 126.2, 126.1, 126.0, 126.0, 126.0, 124.6, 77.1, 60.3, 36.3, 33.4; **IR** (liquid film) *v* = 3427, 3056, 3025, 2916,1631, 1508, 1496, 1454, 1364, 1271, 1048, 906, 820, 747, 698 $cm^{-1}$; **mp** 48–52 °C, **HRMS** (ESI+) m/z calculated for $C_{30}H_{26}ONaS$ $(M+Na)^+$ 457.1597, found 457.1597.

*rac*-2-(methylthio)-1,2-di-m-tolylethan-1-ol (**6m**)

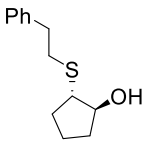


*rac*-**6m**

The corresponding epoxide (4.4 mmol, 1.0 g, 1.0 equiv.) and sodium methane thiolate (2.0 equiv.) were dissolved in EtOH (0.1 M) in a round-bottom flask at room temperature. The mixture was then refluxed until TLC analysis showed no further conversion (hexane:DCM = 80:20 as eluent). The reaction vessel was then cooled to room temperature and the solvent was removed *in vacuo*. The residue was then treated with $Et_2O$ and water, the layers were partitioned and the aqueous phase was extracted three

times with $Et_2O$. The organic phases were combined, dried over $MgSO_4$, filtered and concentrated *in vacuo*. The crude product was then purified by flash column chromatography (hexane:$Et_2O$ 100:0 to 80:20 gradient), to afford **6m** as a yellow oil (1.0 g, 83 % yield). **$^1$H NMR** (500 MHz, $CDCl_3$) $\delta$ = 7.09 (q, *J* = 7.6 Hz, 2H), 7.04–6.92 (m, 6H), 4.87 (d, *J* = 8.1 Hz, 1H), 3.94 (d, *J* = 8.1 Hz, 1H), 3.08 (br s, 1H), 2.27 (s, 3H), 2.26 (s, 3H), 1.97 (s, 3H), **$^{13}$C NMR** (126 MHz, $CDCl_3$) $\delta$ = 141.1, 139.1, 138.0, 137.7, 129.4, 128.6, 128.2, 128.0, 127.4, 125.8, 124.0, 76.6, 61.4, 21.5, 14.9; **IR** (liquid film) *v* = 3421, 3023, 2916, 1606, 1488, 1436, 1044, 778, 732, 699 $cm^{-1}$; **HRMS** (ESI+) m/z calculated for $C_{17}H_{20}ONaS$ $(M+Na)^+$ 295.1127, found 295.1127.

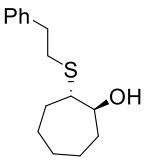
*rac*-2-(phenethylthio)cyclopentan-1-ol (**6o**)



*rac*-**6o**

Alcohol **6o** was prepared according to the General Procedure D using cyclopentene oxide (10 mmol, 0.84 g) and by stirring the reaction mixture at reflux for 2 hours. **Purification** column chromatography, hexane:$Et_2O$ (100:0 to 80:20 gradient). The product was obtained as a colourless oil, 2.4 g, 99% yield. **$^1$H NMR** (400 MHz, $CDCl_3$) $\delta$ = 7.38–7.29 (m, 2H), 7.29–7.19 (m, 3H), 4.06 (q, *J* = 6.0 Hz, 1H), 3.12–2.75 (m, 5H), 2.32–2.13 (m, 1H), 2.07 (ddt, *J* = 13.0, 8.6, 6.5 Hz, 1H), 1.93 – 1.66 (m, 3H), 1.65 – 1.52 (m, 2H), **$^{13}$C NMR** (100 MHz, $CDCl_3$) $\delta$ = 140.6, 128.5, 128.5, 126.4, 79.0, 52.3, 36.6, 33.3, 33.1, 31.4, 21.6; **IR** (liquid film) *v* = 3377, 3026, 2918, 2955, 1496, 1453, 1134, 1073, 1030, 981, 908, 732, 697 $cm^{-1}$; **HRMS** (ESI+) m/z calculated for $C_{13}H_{18}ONaS$ $[M+Na]^+$ 245.0971, found 245.0972.

*rac*-2-(phenethylthio)cycloheptan-1-ol (**6p**)

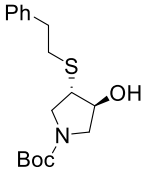


*rac*-**6p**

Alcohol **6p** was prepared according to the General Procedure D using cycloheptene oxide (10 mmol, 1.1 g) and by stirring the reaction mixture at reflux for 2 hours. **Purification** column chromatography, hexane:$Et_2O$ (100:0 to 80:20 gradient). The product was obtained as a colourless oil in 23 % yield. **$^1$H NMR** (400 MHz,

$CDCl_3$) $\delta$ = 7.34–7.27 (m, 2H), 7.25–7.18 (m, 3H), 3.45 (tdd, *J* = 7.9, 3.6, 1.3 Hz, 1H), 2.96–2.77 (m, 5H), 2.55 (td, *J* = 9.6, 3.1 Hz, 1H), 2.09–1.90 (m, 2H), 1.82–1.37 (m, 8H); **$^{13}$C NMR** (100 MHz, $CDCl_3$) $\delta$ = 140.5, 128.7, 128.6, 126.6, 74.8, 56.3, 36.6, 33.8, 32.3, 31.8, 27.5, 26.2, 22.1; **IR** (liquid film) *v* = 3446, 3027, 2927, 2857, 1497, 1454, 1281, 1030, 697; **HRMS** (ESI+) *m/z* calculated for $C_{15}H_{22}ONaS$ $[M+Na]^+$ 273.1284, found 273.1285.

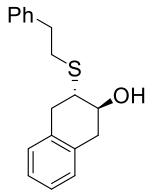
*tert*-butyl-*rac*-3-hydroxy-4-(phenethylthio)pyrrolidine-1-carboxylate (**6q**)



*rac*-**6q**

Alcohol **6q** was prepared according to the General Procedure D using tert-butyl 6-oxa-3-azabicyclo[3.1.0]hexane-3-carboxylate (5.3 mmol, 0.98 g) and by stirring the reaction mixture at reflux for 4 hours. **Purification** column chromatography, hexane:$Et_2O$ (100:0 to 50:50). The product was obtained as a colourless oil, 1.65 g, 90 % yield. **$^1$H NMR** (500 MHz, $CDCl_3$) $\delta$ = 7.33 (t, *J* = 7.5 Hz, 2H), 7.28–7.23 (m, 3H), 4.21–4.13 (m, 1H), 3.90–3.68 (m, 2H), 3.41–3.24 (m, 2H), 3.17–3.10 (m, 1H), 2.97–2.84 (m, 4H), 2.42 (d, *J* = 27.3 Hz, 1H), 1.49 (s, 9H), **$^{13}$C NMR** (126 MHz, $CDCl_3$) $\delta$ = 154.4, 140.0, 128.6, 128.5, 126.7, 79.8, 75.2 (74.6 rotamer), 52.1 (51.8 rotamer), 50.4 (49.9 rotamer), 49.9, (49.4 rotamer), 36.4, 33.2, (33.1 rotamer), 28.5; **IR** (liquid film) *v* = 3400, 2975, 2932, 2883, 1695, 1665, 1454, 1414, 1366, 1161, 1114, 1075, 875, 768, 732, 698 $cm^{-1}$; **HRMS** (ESI+) *m*/z calculated for $C_{17}H_{25}NO_3NaS$ $[M+Na]^+$ 346.1447, found 346.1440.

*rac*-3-(phenethylthio)-1,2,3,4-tetrahydronaphthalen-2-ol (**6r**)

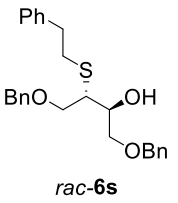


*rac*-**6r**

Alcohol **6r** was prepared according to the General Procedure D using 1*a*,2,7,7*a*-tetrahydronaphtho[2,3-*b*]oxirene. The product was purified by recrystallisation from 20:1 pentane:$Et_2O$ to afford a white crystalline solid in 75 % yield. **$^1$H NMR** (400 MHz, $CDCl_3$) $\delta$ = 7.36–7.28 (m, 2H), 7.27–7.20 (m, 3H), 7.17–7.05 (m, 4H), 3.82 (td, *J* = 9.7, 5.5 Hz, 1H), 3.27 (td, *J* = 15.5, 14.7, 5.0 Hz, 2H), 3.06–2.80 (m, 8H), **$^{13}$C NMR**

(100 MHz, $CDCl_3$) $\delta$ = 140.2, 134.7, 134.2, 129.3, 128.7, 128.6, 128.3, 126.7, 126.5, 126.3, 69.7, 50.2, 37.3, 36.8, 36.3, 32.4; **IR** (liquid film) $v$ = 3433, 2980, 2904, 1495, 1453, 1434, 1385, 1273, 1153, 1110, 1066, 951, 744, 698; **mp** 55–57 ˚C; **HRMS** (ESI+) m/z calculated for $C_{18}H_{21}OS$ $[M+H]^+$ 285.1308, found 285.1309.

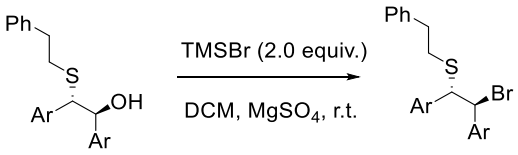
*rac*-1,4-bis(benzyloxy)-3-(phenethylthio)butan-2-ol (**6s**)



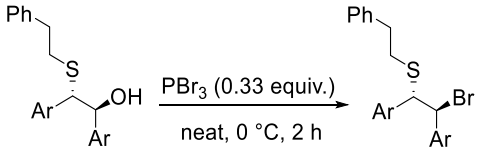
*rac*-**6s**

Alcohol **6s** was prepared according to the General Procedure D using 1,4-bis(benzyloxy)butane oxide. The product was obtained as a bright yellow oil in 86 % yield. **$^1$H NMR** (400 MHz, $CDCl_3$) $\delta$ = 7.43 – 7.10 (m, 15H), 4.58 – 4.49 (m, 4H), 4.19 – 4.11 (m, 1H), 3.86 – 3.64 (m, 2H), 3.62 (d, 5.8 Hz, 2H), 3.01 (ddd, $J$ = 7.1, 4.9, 3.6 Hz, 1H), 2.90 – 2.78 (m, 4H), 2.73 (s, 1H), **$^{13}$C NMR** (100 MHz, $CDCl_3$) $\delta$ = 140.4, 138.1, 137.9, 128.6, 128.6, 128.6, 128.5, 128.0, 127.9, 127.8, 127.1, 126.5, 73.6, 73.5, 72.0, 71.8, 70.6, 48.8, 36.8, 33.9. **IR** (liquid film) $v$ = 3448, 3028, 2861, 1496, 1453, 1362, 1098, 1028, 736, 697; **HRMS** (ESI+) m/z calculated for $C_{26}H_{30}O_3NaS$ $[M+Na]^+$ 445.1808, found 445.1805.

*4.2.2.2 β-Bromo Sulfides*



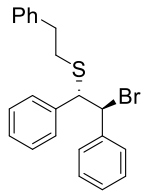

General procedure for the synthesis of β-bromo sulfides with TMSBr (**General Procedure E**). The employed protocol followed a slightly modified literature procedure.[7] In a vial equipped with a magnetic stirring bar, the appropriate β-hydroxy sulfide was dissolved in DCM (1.0 M), and anhydrous $MgSO_4$ was added (500 mg/mmol), followed by dropwise addition of TMSBr (2 equiv.). After stirring at r.t. for 1 h, the crude mixture was filtered over celite and the solvent was evaporated *in vacuo* to afford the desired compounds without any further purification (96–99% purity).




General procedure for the synthesis of β-bromo sulfides with $PBr_3$ (**General Procedure F**). In a flame-dried round-bottom flask equipped with a magnetic stirring bar and under inert atmosphere, the appropriate β-hydroxy sulfide (1.0 equiv., neat for liquid alcohols, 1 M DCM solution for solids) was cooled to 0 °C in an ice-bath and $PBr_3$ (0.33 equiv.) was added dropwise. The solution was then stirred at this temperature for 2 h. After this time, the reaction was quenched by the addition of ice-cold water and diluted with cold $Et_2O$. The layers were partitioned and the aqueous phase was extracted three times with $Et_2O$. The organic phases were combined, dried over $Na_2SO_4$, filtered and concentrated *in vacuo* to afford the desired bromide without any further purification (96–99% purity).

N.B. β-bromo sulfides starting materials were unstable on silica gel and proved to be unstable for MS analysis with a variety of ionization methods (HRMS of the molecular ion was therefore not recorded). To prevent any decomposition, β-bromo sulfides were always stored in the fridge.

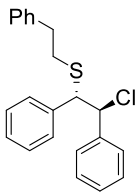
*rac*-2-bromo-1,2-diphenylethyl(phenethyl)sulfane (**1a**)



*rac*-**1a**

Bromide **1a** was prepared from *cis*-stilbene according to a modified literature procedure.[8] In a flame-dried round-bottom flask filled with argon and equipped with a magnetic stirring bar, bis(phenylethyl) disulfide (3 mmol, 814 mg, 1.0 equiv.) was dissolved in 7 ml of anhydrous DCM. The solution was cooled to 0 °C and a solution of $Br_2$ (6 ml, 0.5 M in DCM, 3 mmol, 1.0 equiv.) was added dropwise. The solution was stirred at 0 °C for 2 hours protected from light, forming an orange-yellow solution. After this time, *cis*-stilbene (1 ml, 6 mmol, 2.0 equiv.) was added neat at 0 °C and stirring was continued at the same temperature. Once the orange-yellow colour had disappeared (approx. 1 h), the crude mixture was evaporated to dryness and the residue was stirred in hexane:$Et_2O$ (20:1) to afford a solid which was then recrystallized in hexane:$Et_2O$ (20:1) to afford **1a** as a white solid (800 mg, 33 % yield). **$^1$H NMR** (400 MHz, $CDCl_3$) $\delta$ = 7.27–7.04 (m, 15H), 5.24 (d, *J* = 9.0 Hz, 1H), 4.48 (d, *J* = 9.0 Hz, 1H), 2.89–2.73 (m, 2H), 2.60–2.53 (m, 2H); **$^{13}$C NMR** (100 MHz, $CDCl_3$) $\delta$ = 140.3, 139.6, 138.5, 128.9, 128.5, 128.5, 128.4, 128.3, 128.3 128.2, 127.8, 126.3, 58.1, 58.0, 36.0, 33.6; **mp** 64–65 °C; **IR** (liquid film) *v* = 3657, 2980, 2888, 1473, 1462, 1383, 1252, 1152, 1073, 955, 695 $cm^{-1}$; **HRMS** (APCI+) m/z calculated for $C_{22}H_{21}S$ $(M\text{-}Br)^+$ 317.1358, found 317.1355.

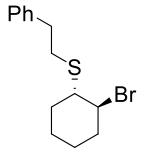
*rac*-2-chloro-1,2-(diphenylethyl)(phenethyl)sulfane (**1a'**)



*rac*-**1a'**

Chloride **1a'** was prepared according to a reported procedure.[9] Alcohol **6a** (500 mg, 1.45 mmol) was dissolved in anhydrous DCM (7.2 ml) under inert atmosphere and the solution was cooled to 0 °C. At this temperature, anhydrous *N*,*N*-dimethylformamide (5 mol%) and thionyl chloride (160 µL, 2.18 mmol, 1.5 equiv.) were sequentially added and the reaction mixture was stirred for 30 min at 0 °C. The volatiles were then evaporated *in vacuo* to afford **1a'** as a pale yellow solid (400 mg, 79 % yield). **$^1$H NMR** (500 MHz, $CDCl_3$) $\delta$ = 7.30–7.04 (m, 15H), 5.19 (d, *J* = 8.4 Hz, 1H), 4.39 (d, *J* = 8.4 Hz, 1H), 2.89–2.73 (m, 2H), 2.59 (t, *J* = 7.9 Hz, 2H), **$^{13}$C NMR** (126 MHz, $CDCl_3$) $\delta$ = 140.5, 139.1, 138.5, 129.1, 128.6, 128.6, 128.4, 128.3, 128.1, 128.0, 127.8, 126.5, 67.0, 58.7, 36.2, 33.6, ; **mp** 58-60 °C; **IR** (liquid film) *v* = 3061, 3028, 2918, 2850, 1602, 1494, 1453, 1074, 1030, 748, 698 $cm^{-1}$; **HRMS** (EI) m/z calculated for $C_{22}H_{20}S$ $(M\text{-}HCl)^{+\cdot}$ 316.1276, found 316.1276.

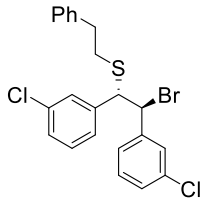
*rac*-2-bromocyclohexyl(phenethyl)sulfane (**1b**)



*rac*-**1b**

Bromide **1b** was prepared according to the General Procedure F by employing alcohol **6b** (4.2 mmol, 1.0 g) as starting material. The product was obtained as a colourless oil, 1.1 g, 90 % yield. **$^1$H NMR** (400 MHz, $CDCl_3$) δ 7.32–7.01 (m, 5H), 4.22 (q, *J* = 3.0 Hz, 1H), 3.01–2.88 (m, 1H), 2.82 (q, *J* = 2.5 Hz, 4H), 2.25 (m, 2H), 1.87–1.74 (m, 1H), 1.48–1.72 (m, 3H), 1.29–1.42 (m, 2H), **$^{13}$C NMR** (100 MHz, $CDCl_3$) $\delta$ = 140.4, 128.6, 126.5, 57.2, 50.6, 36.5, 34.0, 33.6, 30.4, 23.4, 23.3; **IR** (liquid film) *v* = 3026, 2933, 2856, 1603, 1496, 1444, 1259, 1180, 1072, 1030, 1000, 980, 905, 862, 822, 733, 696, 663 $cm^{-1}$ .

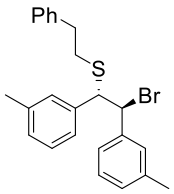
*rac*-2-bromo-1,2-bis(3-chlorophenyl)ethyl(phenethyl)sulfane (**1c**)



*rac*-**1c**

Bromide **1c** was prepared according to the General Procedure F by employing alcohol **6c** (3.4 mmol, 1.4 g) as starting material. The product was obtained as a yellow solid, 1.4 g, 89 % yield. **$^1$H NMR** (500 MHz, $CDCl_3$) $\delta$ = 7.32–7.23 (m, 3H), 7.21–7.09 (m, 8H), 7.01 (ddt, *J* = 24.9, 7.6, 1.5 Hz, 2H), 5.12 (d, *J* = 8.2 Hz, 1H), 4.28 (d, *J* = 8.2 Hz, 1H), 2.92–2.81 (m, 2H), 2.67–2.57 (m, 2H), **$^{13}$C NMR** (126 MHz, $CDCl_3$) [overlapping signals] $\delta$ = 140.9, 140.4, 140.1, 134.2, 134.0, 129.5, 129.4, 128.9, 128.7, 128.6, 128.6, 128.1, 127.2, 126.6, 126.5, 57.5, 56.1, 36.1, 33.7; **mp** 86–88 °C; **IR** (liquid film) *v* = 3063, 3026, 2955, 2933, 1571, 1475, 1430, 1077, 885, 863, 795, 712, 689 $cm^{-1}$.

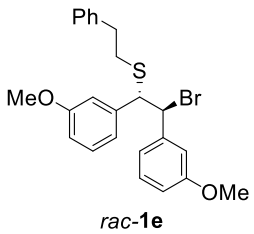
*rac*-2-bromo-1,2-di-*m*-tolylethyl(phenethyl)sulfane (**1d**)



*rac*-**1d**

Bromide **1d** was prepared according to the General Procedure F by employing alcohol **6d** (3.5 mmol, 1.5 g) as starting material. The product was obtained as a brown solid, 1.4 g, 94 % yield. **$^1$H NMR** (500 MHz, $CDCl_3$) $\delta$ = 7.29–7.20 (m, 3H), 7.13–7.05 (m, 4H), 7.09–6.90 (m, 6H), 5.24 (d, *J* = 8.7 Hz, 1H), 4.45 (d, *J* = 8.7 Hz, 1H), 2.85-2.75 (m, 2H), 2.58 (t, *J* = 7.9 Hz, 2H), 2.26 (s, 6H), **$^{13}$C NMR** (126 MHz, $CDCl_3$) $\delta$ = 140.4, 139.5, 138.5, 137.7, 137.6, 129.5, 129.0, 129.0, 128.5, 128.4, 128.4, 128.0, 127.9, 126.3, 126.0, 125.3, 58.4, 58.0, 36.1, 33.6, 21.3, 21.3; **mp** 56–58 °C; **IR** (liquid film) *v* = 3023, 2917, 2851, 1603, 1585, 1488, 1451, 1408, 1374, 1313, 1254, 1226, 1213, 1165, 1156, 1097, 1029, 997, 961, 902, 888,823, 791, 784, 763, 749, 736, 700 $cm^{-1}$.

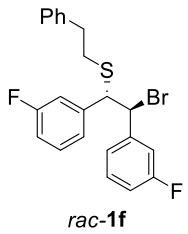
*rac*-2-bromo-1,2-bis(3-methoxyphenyl)ethyl(phenethyl)sulfane (**1e**)



*rac*-**1e**

Bromide **1e** was prepared according to the General Procedure E by employing alcohol **6e** (2.9 mmol, 1.2 g) as starting material. The product was obtained as a brown oil, 835 mg, 63 % yield.**$^{1}$H NMR** (400 MHz, $CDCl_3$) $\delta$ = 7.30–7.16 (m, 4H), 7.13–7.06 (m, 3H), 6.78 (d, *J* = 7.8 Hz, 1H), 6.75–6.67 (m, 5H), 5.19 (d, *J* = 8.8 Hz, 1H), 4.40 (d, *J* = 8.8 Hz, 1H), 3.70 (s, 3H), 3.69 (s, 3H), 2.89–2.69 (m, 2H), 2.64–2.49 (m, 2H), **$^{13}$C NMR** (101 MHz, $CDCl_3$) $\delta$ = 159.3, 159.1, 140.9, 140.3, 140.1, 129.1, 129.1, 128.6, 128.4, 126.3, 121.4, 120.6, 114.3, 114.0, 113.9, 113.3, 58.1, 57.9, 55.2, 55.2, 36.0, 33.6; **IR** (liquid film) *v* = 3059, 3025, 3001, 2935, 2834, 1598, 1584, 1489, 1464, 1260, 1148, 1044 870, 776, 742, 732, 696 $cm^{-1}$.

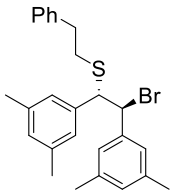
*rac*-2-bromo-1,2-bis(3-fluorophenyl)ethyl(phenethyl)sulfane (**1f**)



*rac*-**1f**

Bromide **1f** was prepared according to the General Procedure E by employing alcohol **6f** (1.3 mmol, 500 mg) as starting material, and by stirring the reaction for 6 hours in the presence of 4 equiv. of TMSBr. The product was obtained as a brown oil, 350 mg, 62 % yield. **$^{1}$H NMR** (500 MHz, $CDCl_3$) $\delta$ = 7.31–7.20 (m, 3H), 7.20–7.10 (m, 4H), 6.95–6.87 (m, 6H), 5.14 (d, *J* = 8.7 Hz, 1H), 4.34 (d, *J* = 8.7 Hz, 1H), 2.88–2.76 (m, 2H), 2.60 (m, 2H), **$^{19}$F NMR** (470 MHz, $CDCl_3$) $\delta$ = -112.4– -112.5 (m), **$^{13}$C NMR** (126 MHz, $CDCl_3$) $\delta$ = 162.5 (d, *J* = 246.9 Hz), 162.3 (d, *J* = 246.8 Hz), 141.5 (d, *J* = 7.4 Hz), 141.0 (d, *J* = 7.0 Hz), 140.0, 129.7 (d, *J* = 8.3 Hz), 129.7 (d, *J* = 8.2 Hz), 128.6, 128.53, 126.5, 124.6 (d, *J* = 2.9 Hz), 123.9 (d, *J* = 3.1 Hz), 115.6 (d, *J* = 22.3 Hz), 115.5 (d, *J* = 21.0 Hz), 115.3 (d, *J* = 22.6 Hz), 114.9 (d, *J* = 21.3 Hz), 57.6 (d, *J* = 1.8 Hz), 56.2 (d, *J* = 2.0 Hz), 36.0, 33.6; **IR** (liquid film) *v* = 3062, 3027, 2917, 2849, 1613, 1589, 1523, 1487, 1447, 1254, 1138, 953, 878, 782, 737, 709, 696 $cm^{-1}$.

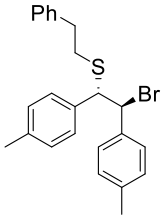
*rac*-2-bromo-1,2-bis(3,5-dimethylphenyl)ethyl(phenethyl)sulfane (**1g**)



*rac*-**1g**

Bromide **1g** was prepared according to General procedure E by employing alcohol **6g** (1.2 mmol, 460 mg) as starting material. The product was obtained as a yellow solid, 300 mg, 60 % yield. **$^1$H NMR** (400 MHz, $CDCl_3$) $\delta$ = 7.28–7.18 (m, 3H), 7.09–7.06 (m, 2H), 6.81 (s, 2H), 6.79 (d, *J* = 3.3 Hz, 2H), 6.74 (s, 2H), 5.20 (d, *J* = 8.2 Hz, 1H), 4.38 (d, *J* = 8.2 Hz, 1H), 2.88–2.68 (m, 2H), 2.62–2.50 (m, 2H), 2.22 (s, 12H), **$^{13}$C NMR** (101 MHz, $CDCl_3$) $\delta$ = 140.5, 139.3, 138.4, 137.4, 137.4, 129.9, 129.2, 128.5, 128.4, 126.8, 126.3, 126.2, 58.7, 57.7, 36.1, 33.7, 21.2, 21.1; **mp** 101–103 °C; **IR** (liquid film) *v* = 3023, 2916, 2856, 1599, 1495, 1453, 1374, 1159, 997, 850, 793, 769, 753, 734, 720, 695, 632 $cm^{-1}$.

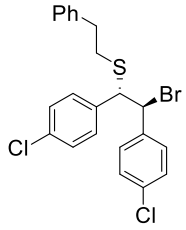
*rac*-2-bromo-1,2-di-*p*-tolylethyl(phenethyl)sulfane (**1h**)



*rac*-**1h**

Bromide **1h** was prepared according to the General Procedure F by employing alcohol **6h** (3.3 mmol, 1.2 g) as starting material. The product was obtained as a brown solid, 0.8 g, 57 % yield. **$^1$H NMR** (400 MHz, $CDCl_3$) $\delta$ = 7.32–7.18 (m, 3H), 7.11–6.97 (m, 10H), 5.26 (d, *J* = 8.9 Hz, 1H), 4.47 (d, *J* = 8.9 Hz, 1H), 2.89–2.73 (m, 2H), 2.58–2.52 (m, 2H), 2.28 (s, 6H), **$^{13}$C NMR** (101 MHz, $CDCl_3$) $\delta$ = 140.4, 138.0, 137.2, 136.7, 135.5, 128.9, 128.8, 128.7, 128.5, 128.4, 128.1, 126.3, 58.4, 57.7, 36.1, 33.6, 21.2, 21.1; **mp** 67–69 °C; **IR** (liquid film) *v* = 3051, 2954, 2854, 1603, 1513, 1496, 1478, 1446, 1412, 1376, 1323, 1298, 1270, 1229, 1199, 1184, 1163, 1111, 1070, 1040, 1021, 970, 912, 868, 784, 764, 738, 722, 707, 696 $cm^{-1}$.

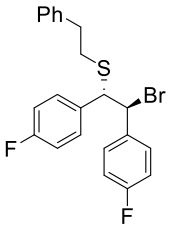
*rac*-2-bromo-1,2-bis(4-chlorophenyl)ethyl(phenethyl)sulfane (**1i**)



*rac*-**1i**

Bromide **1i** was prepared according to the General Procedure E by employing alcohol **6i** (1.2 mmol, 500 mg) as starting material, and by stirring the reaction for 6 h in the presence of 4 equiv. of TMSBr. The product was obtained as a brown oil, 380 mg, 75 % yield. **$^{1}$H NMR** (400 MHz, $CDCl_3$) $\delta$ = 7.30–6.99 (m, 13H), 5.13 (d, *J* = 8.3 Hz, 1H), 4.31 (d, *J* = 8.2 Hz, 1H), 2.80 (dd, *J* = 8.4, 5.6 Hz, 2H), 2.56 (t, *J* = 7.7 Hz, 2H), **$^{13}$C NMR** (101 MHz, $CDCl_3$) $\delta$ = 140.0, 137.4, 136.6, 134.2, 133.6, 130.3, 129.7, 128.5, 128.5, 128.4, 128.3, 126.5, 57.3, 56.3, 36.0, 33.6; **IR** (liquid film) *v* = 3084, 3062, 3026, 2918, 2849, 1650, 1456, 1406, 1315, 1029, 826, 764, 742, 623 $cm^{-1}$.

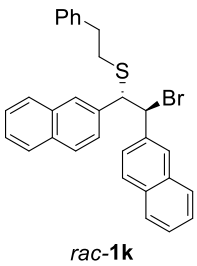
*rac*-2-bromo-1,2-bis(4-fluorophenyl)ethyl(phenethyl)sulfane (**1j**)



*rac*-**1j**

Bromide **1j** was prepared according to the General Procedure F by employing alcohol **6j** (3.2 mmol, 1.2 mg) as starting material. The product was obtained as a brown solid, 800 mg, 60 % yield. **$^{1}$H NMR** (500 MHz, $CDCl_3$) $\delta$ = 7.45–7.30 (m, 3H), 7.25–7.13 (m, 6H), 6.99 (q, *J* = 8.6 Hz, 4H), 5.28 (d, *J* = 8.4 Hz, 1H), 4.47 (d, *J* = 8.4 Hz, 1H), 2.92 (td, *J* = 7.5, 4.6 Hz, 2H), 2.68 (t, *J* = 8.0 Hz, 2H), **$^{19}$F NMR** (470 MHz, $CDCl_3$) $\delta$ = -112.8 (ddd, *J* = 13.7, 8.6, 5.3 Hz), -113.7 (ddd, *J* = 14.1, 8.9, 5.2 Hz), **$^{13}$C NMR** (126 MHz, $CDCl_3$) $\delta$ = 162.3 (d, *J* = 248.1 Hz), 162.0 (d, *J* = 247.3 Hz), 140.1, 135.0 (d, *J* = 3.3 Hz), 133.9 (d, *J* = 3.3 Hz), 130.6 (d, *J* = 8.1 Hz), 130.1 (d, *J* = 8.4 Hz), 128.6, 128.5, 126.5, 115.2 (d, *J* = 17.8 Hz), 115.0 (d, *J* = 18.1 Hz), 57.5, 56.8, 36.0, 33.7; **mp** 54–56 °C; **IR** (liquid film) *v* = 3062, 3024, 2958, 2925, 1601, 1508, 1240, 1220, 1158, 1147, 1072, 1031, 835, 802, 767, 727, 647 $cm^{-1}$.

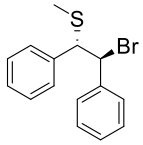
*rac*-2-bromo-1,2-di(naphthalen-2-yl)ethyl(phenethyl)sulfane (**1k**)



*rac*-**1k**

Bromide **1k** was prepared according to the General Procedure E by employing alcohol **6k** (0.9 mmol, 390 mg) as starting material. The product was obtained as a brown solid, 400 mg, 89% yield. **$^1$H NMR** (400 MHz, $CDCl_3$) $\delta$ = 7.76–7.62 (m, 6H), 7.60 (s, 1H), 7.52 (s, 1H), 7.44–7.34 (m, 6H), 7.25–7.17 (m, 3H), 7.03 (d, *J* = 6.3 Hz, 2H), 5.57 (d, *J* = 8.9 Hz, 1H), 4.75 (d, *J* = 8.9 Hz, 1H), 2.91–2.73 (m, 2H), 2.56 (t, *J* = 7.7 Hz, 2H), **$^{13}$C NMR** (101 MHz, $CDCl_3$) $\delta$ = 140.2, 136.7, 135.8, 132.9, 132.8, 132.8, 132.6, 128.6, 128.4, 128.3, 128.2, 128.1, 128.1, 127.8, 127.6, 127.6, 127.4, 126.4, 126.3, 126.2, 126.2, 126.1, 125.9, 125.7, 58.2, 58.0, 36.1, 33.6; **mp** 35–37 °C; **IR** (liquid film) *v* = 3056, 2917, 1700, 1507, 1496, 1453, 1366, 1271, 1156, 1123, 1073, 1218, 960, 893, 859, 816, 796, 745, 697, 622 $cm^{-1}$.

*rac*-2-bromo-1,2-diphenylethyl(methyl)sulfane (**1l**)

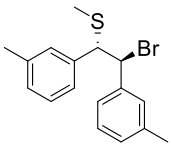


*rac*-**1l**

In a flame-dried argon filled round-bottom flask equipped with a magnetic stirring bar, dimethyl disulfide (5.5 mmol, 0.49 ml, 1.1 equiv.) was dissolved in anhydrous DCM (15 mL). The solution was cooled to 0 °C and a solution of $Br_2$ (10 ml, 0.5 M in DCM, 5 mmol, 1.0 equiv.) was added dropwise. The solution was stirred at 0 °C for 2 hours protected from light. After this time, *cis*-stilbene (1.7 ml, 10 mmol, 2.0 equiv) was added neat at 0 °C and stirring was continued at the same temperature. Once the orange/yellow colour had disappeared (~1 h), the crude mixture was evaporated to dryness and the residue stirred in hexane:$Et_2O$ (20:1) to afford a solid that was then recrystallized in hexane:$Et_2O$ (20:1) to afford **1l** as a white solid (1.2 g, 40 % yield). **$^1$H NMR** (500 MHz, $CDCl_3$) $\delta$ = 7.24–7.14 (m, 10H), 5.29 (d, *J* = 9.1 Hz, 1H), 4.43 (d, *J* = 9.1 Hz, 1H), 1.91(s, 3H), **$^{13}$C NMR** (126 MHz, $CDCl_3$) [overlapping signals] $\delta$ = 139.6, 138.3, 128.7, 128.3, 128.2, 128.1, 127.6, 60.0,

58.0, 15.5; **mp** 58–59 °C; **IR** (liquid film) *v* = 3735, 3649, 2981, 2888, 1456, 1382, 1252, 1151, 1073, 955, 695, 689 $cm^{-1}$.

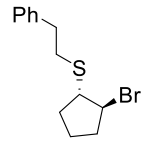
*rac*-2-bromo-1,2-di-(*m*-tolylethyl)(methyl)sulfane (**1m**)



*rac*-**1m**

Bromide **1m** was prepared according to the General Procedure F by employing alcohol **6m** (3.7 mmol, 1.0 g) as starting material. The product was obtained as a brown solid, 1.0 g, 80 % yield. **$^1$H NMR** (500 MHz, $CDCl_3$) $\delta$ = 7.11–7.02 (m, 4H), 7.00–6.91 (m, 4H), 5.28 (d, *J* = 8.8 Hz, 1H), 4.39 (d, *J* = 8.8 Hz, 1H), 2.25 (s, 6H), 1.92 (s, 3H), **$^{13}$C NMR** (126 MHz, $CDCl_3$) $\delta$ = 139.6, 138.3, 137.8, 137.7, 129.4, 129.0, 129.0, 128.3, 127.9, 127.9, 125.9, 125.3, 59.6, 58.3, 21.4, 21.3, 15.6; **mp** 79–80 °C; **IR** (liquid film) *v* = 3007, 2961, 2921, 1601, 1585, 1173, 1154, 1089, 1064, 1039, 998, 814, 701, 669 $cm^{-1}$.

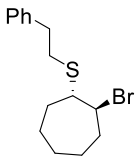
*rac*-2-bromocyclopentyl(phenethyl)sulfane (**1o**)



*rac*-**1o**

Bromide **1o** was prepared according to General Procedure F by employing alcohol **6o** (4.5 mmol, 1.0 g). The product was obtained as a colourless oil, 1.1 g, 89 % yield. **$^1$H NMR** (400 MHz, $CDCl_3$) $\delta$ = 7.27–7.04 (m, 5H), 4.24 (dt, *J* = 5.6, 2.7 Hz, 1H), 3.46–3.34 (m, 1H), 2.94–2.61 (m, 4H), 2.39– 2.11 (m, 2H), 2.05–1.92 (m, 1H), 1.91–1.77 (m, 1H), 1.77– 1.60 (m, 1H), 1.57–1.40 (m, 1H), **$^{13}$C NMR** (100 MHz, $CDCl_3$) $\delta$ = 140.3, 128.6, 128.5, 126.5, 57.7, 53.7, 36.2, 35.6, 34.0, 31.2, 22.7; **IR** (liquid film) *v* =3026, 2954, 1603, 1495, 1453, 1313, 1167, 1029, 907, 720, 696, 620 $cm^{-1}$.

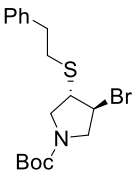
*rac*-2-bromocycloheptyl(phenethyl)sulfane (**1p**)



*rac*-**1p**

Bromide **1p** was prepared according to General Proedure F by employing alcohol **6p** (1.9 mmol, 1.0 g) as starting material. The product was obtained as a colourless oil, 282 mg, 90% yield. **$^1$H NMR** (400 MHz, $CDCl_3$) $\delta$ = 7.37–7.31 (m, 2H), 7.30-7.22 (m, 3H), 4.56 (td, *J* = 5.4, 3.1 Hz, 1H), 3.35 (ddd, *J* = 7.5, 4.9, 2.8 Hz, 1H), 2.99–2.82 (m, 4H), 2.31–2.17 (m, 2H), 2.17–2.05 (m, 1H), 1.92–1.49 (m, 7H). **$^{13}$C NMR** (100 MHz, $CDCl_3$) $\delta$ = 140.5, 128.6, 128.6, 126.6, 60.9, 54.5, 36.5, 34.7, 33.9, 30.4, 27.7, 24.1, 23.5; **IR** (liquid film) *v* = 2928, 2858, 1496, 1454, 734, 720, 697, 669, 658 cm$^{-1}$.

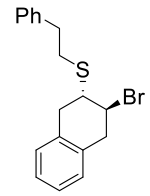
*ert*-butyl-*rac*-3-bromo-4-(phenethylthio)pyrrolidine-1-carboxylate (**1q**)



*rac*-**1q**

Bromide **1q** was prepared according to General Procedure F by employing alcohol **6q** (3.0 mmol, 1.0 g) as starting material. The product was obtained as a white crystalline solid, 620 mg, 54 % yield.**$^1$H NMR** (500 MHz, $CDCl_3$) δ =7.32 (t, *J* = 7.5 Hz, 2H), 7.27 – 7.18 (m, 3H), 4.25 (dd, *J* = 5.0, 2.5 Hz, 1H), 4.12 – 3.88 (m, 2H), 3.82 – 3.64 (m, 1H), 3.53 – 3.29 (m, 2H), 3.01 – 2.83 (m, 4H), 1.47 (s, 9H); **$^{13}$C NMR** (126 MHz, $CDCl_3$) δ = 154.3, 139.8, 128.8, 128.6, 126.8, 80.2, 53.8 (53.4 rotamer), 52.0 (51.2 rotamer), 50.8 (50.5 rotamer), 50.3 (50.1 rotamer); **mp** 69 ˚C; **IR** (liquid film) v 2980, 1932, 2885, 1697, 1476, 1455, 1396, 1366, 1347, 1252, 1161, 1113 cm$^{-1}$.

*rac*-3-bromo-1,2,3,4-tetrahydronaphthalen-2-yl)(phenethyl)sulfane (**1r**) – *synthesised by Richard Surgenor*

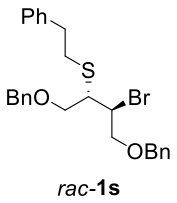


*rac*-**1r**

Bromide **1r** was prepared according to General Procedure F by employing alcohol **6r** as starting material. The product was obtained as a yellow oil in 94 % yield.**$^1$H NMR** (400 MHz, $CDCl_3$) $\delta$ = 7.38 – 7.31 (m, 2H), 7.30– 7.21 (m, 3H), 7.21–7.15 (m, 2H), 7.14–7.06 (m, 2H), 4.65 (dd, *J* = 9.2, 4.8 Hz, 1H), 3.85 (dd, *J* = 17.9,

4.6 Hz, 1H), 3.67 (dd, *J* = 17.4, 5.7 Hz, 1H), 3.46 (d, *J* = 9.2, 5.0 Hz, 1H), 3.23 (dd, *J* = 17.9, 3.9 Hz, 1H), 3.00 – 2.89 (m, 5H); **$^{13}$C NMR** (100 MHz, $CDCl_3$) $\delta$ =140.2, 132.5, 132.1, 129.1, 129.0, 128.7, 128.6, 126.7, 126.5, 51.4, 46.2, 36.4, 35.5, 33.7, 32.7; **IR** (liquid film) *v* = 3024, 2922, 1603, 1496, 1453, 1424, 1260, 1211, 1166, 1106, 1030, 955, 929, 859, 743 $cm^{-1}$.

*rac*-1,4-bis(benzyloxy)-3-bromobutan-2-yl(phenethyl)sulfane (**1s**) – *synthesised by Richard Surgenor*



*rac*-**1s**

Bromide **1s** was prepared according to General Procedure F by employing alcohol **6s** as starting material. The product was was purified by flash chromatography (10:1 pentane:$Et_2O$) to afford the product as a yellow oil in 86 % yield. **$^{1}$H NMR** (400 MHz, $CDCl_3$) $\delta$ = 7.38–7.23 (m, 12H), 7.22 – 7.08 (m, 3H), 4.70 (ddd, *J* = 8.7, 5.7, 2.2 Hz, 1H), 4.59–4.47 (m, 4), 4.04 (dd, *J* = 9.9, 8.8 Hz, 1H), 3.79 (dd, *J* = 9.9, 5.7 Hz, 1H), 3.73 – 3.64 (m, 2H), 3.28 (ddd, *J* = 8.6, 6.3, 2.2 Hz, 1H), 2.88–2.70 (m, 4H), **$^{13}$C NMR** (100 MHz, $CDCl_3$) $\delta$ = 140.3, 130.1, 137.8, 128.61, 128.60, 128.6, 128.6, 127.9, 127.9, 127.9, 73.4, 73.3, 72.1, 71.7, 52.9, 48.2, 37.0, 34.0; **IR** (liquid film) *v* = 3649, 2981, 2888, 1473, 1456, 1383, 1252, 1151, 1074, 954, 696, 669 $cm^{-1}$.

*4.2.3 Products Characterisation*

Procedure for Substrate Scope and Gram-Scale Reaction *(General Procedure G).*

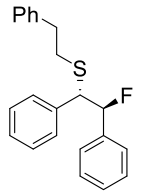
In a screw-cap vial equipped with a magnetic stirring bar were sequentially added the appropriate substrate **1** (1 equiv.), the catalyst (10 mol%), CsF (2 equiv.)* and 1,2-difluorobenzene (0.25 M), pre-cooled at the same temperature as the reaction). The vial was sealed, and the reaction mixture was stirred at 1200 rpm at the appropriate temperature for 24–72 h. The crude mixture was then filtered through a small plug of silica (and eluted with cold DCM), evaporated to dryness under reduced pressure and directly purified by column chromatography (pentane:$Et_2O$ or pentane:DCM mixtures as eluent).

Procedure for Reaction Optimisation *(General Procedure H).*

In a screw-cap vial equipped with a magnetic stirring bar were sequentially added the appropriate substrate **1** (0.05 mmol, 1 equiv.), the catalyst (10 mol%), CsF (1.2–3 equiv.) and the appropriate solvent (0.25 M), pre-cooled at the same temperature as the reaction). The vial was sealed and the reaction mixture was stirred at 1200 rpm at the appropriate temperature for 1.5–72 h. The crude mixture was then filtered through a small plug of silica (and eluted with cold DCM), evaporated to dryness, dissolved in $CDCl_3$ and analysed by $^1H$ and $^{19}F$ NMR (4-fluoroanisole as internal standard). An aliquot of reaction mixtures. After quenching, was purified by preparative TLC (hexane:$Et_2O$ 30:1) and analysed by HPLC to assess the enantiopurity of the product.

* The CsF employed was freshly ground prior to the reaction and used without any additional drying (Sigma-Aldrich, CsF 99.9% trace metal basis).

((1*S*,2*S*)-2-fluoro-1,2-diphenylethyl)(phenethyl)sulfane (**3a**)

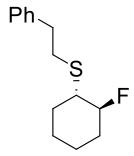


**3a**

Product **3a** was prepared according to the General Procedure G by employing 0.2 mmol of substrate (79.5 mg) and the reaction was stirred at -30 °C for 72 h. **Purification** column chromatography, pentane:$Et_2O$ (100:0 to 99:1 gradient). White solid, 55.0 mg, 83 % yield, e.r. = 95.5:4.5. **$^1$H NMR** (400 MHz, $CDCl_3$) $\delta$ = 7.30–7.19 (m, 9H), 7.17–7.14 (m, 2H), 7.11–7.09 (m, 4H), 5.67 (dd, *J* = 46.3, 7.5 Hz, 1H), 4.22 (dd, *J* = 13.6, 7.5 Hz, 1H), 2.88–2.62 (m, 4H), **$^{19}$F NMR** (376 MHz, $CDCl_3$) $\delta$ = -172.6 (dd, *J* = 46.3, 13.6 Hz), **$^{13}$C NMR** (101 MHz, $CDCl_3$) $\delta$ = 140.5, 137.8 (d, *J* = 4.8 Hz), 137.6 (d, *J* = 21.1 Hz), 129.1, 128.7, 128.6 (d, *J* = 2.4 Hz), 128.5, 128.5, 128.1, 127.8, 126.4 (d, *J* = 7.0 Hz), 126.4, 97.1 (d, *J* = 180.3 Hz), 56.4 (d, *J* = 23.9 Hz), 36.5, 33.4; **mp** 34–36 °C; **IR** (liquid film) *v* = 3029, 2922, 1602, 1495, 1453, 1211, 1049, 1030, 998, 755, 732, 697, 627 $cm^{-1}$; **HRMS** (EI) m/z calculated for $C_{22}H_{20}S$ $(M\text{-}HF)^{+\cdot}$ 316.128, found 316.1281; $[\boldsymbol{\alpha}]_{\mathbf{D}}^{\mathbf{25}}$ = +104.7 (c 1.0, $CHCl_3$, e.r. = 95.5:4.5); **HPLC** DAICEL CHIRALPAK® IC-3, heptane:EtOH = 99.75:0.25, 1 ml/min, $t_1$ = 5.8 (major), $t_2$ = 6.8 (minor).

The opposite enantiomer (*1R,2R*)-**3a** ($[\alpha]_D^{25}$ –97.2 ; c 1.0, $CHCl_3$, e.r. = 95:5) was prepared following the same protocol using (*R*)-**4u** as catalyst (81% yield, e.r. = 95:5).

2-(fluorocyclohexyl)(phenethyl)sulfane (**3b**)

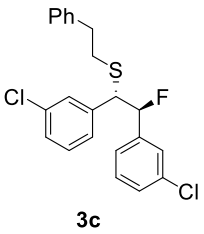


**3b**

Product **3b** was prepared according to the General Procedure H using catalyst **4k**, the reaction was performed in DCM for 1.5 h, at room temperture. **Purification** column chromatography, eluent = pentane:$Et_2O$ (100:0 to 99:1 gradient). Colourless oil, 90 % yield, e.r. = 72:28. **$^1$H NMR** (400 MHz, $CDCl_3$) $\delta$ = 7.22-7.36 (m, 5H), 4.43 (dddd, *J* = 48.5, 9.5, 8.5, 4.2 Hz, 1H), 3.04–2.88 (m, 4H), 2.77 (dtd, *J* = 10.4, 8.5, 4.2 Hz, 1H), 2.23 – 2.01 (m, 2H), 1.86–1.64 (m, 2H), 1.64 – 1.47 (m, 1H), 1.48–1.24 (m, 3H), **$^{19}$F NMR** (376.5

MHz, $CDCl_3$) $\delta$ = -169.7 (d, *J* = 48.0 Hz); **IR** (liquid film) *v* = 3062, 3026, 2855, 1603, 1496, 1447, 1278, 1135, 1080, 1031, 734, 697 $cm^{-1}$, **$^{13}$C NMR** (100 MHz, $CDCl_3$) $\delta$ = 140.6, 128.6, 128.6, 126.5, 96.2 (d, *J* = 176.3 Hz), 48.0 (d, *J* = 18.2 Hz), 36.7, 33.6, 31.7 (d, *J* = 19.5 Hz), 30.9, 24.7, 23.1 (d, *J* = 9.2 Hz); **HRMS** (EI) m/z calculated for $C_{14}H_{19}FS^{+\cdot}$ 238.1186, found 238.1183; **HPLC** Chiralpack Daicel ID-3 heptane:iPrOH 95.5:0.5, 1ml/min, $t_1$: 6.6 min, $t_2$: 8.6 min.

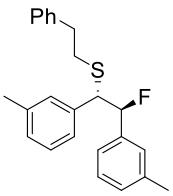
((1*S*,2*S*)-1,2-bis(3-chlorophenyl)-2-fluoroethyl)(phenethyl)sulfane (**3c**)



**3c**

Product **3c** was prepared according to the General Procedure G by employing 0.2 mmol of substrate (93.2 mg) and the reaction was stirred at r.t. for 72 h. **Purification** column chromatography, pentane:$Et_2O$ (100:0 to 99:1 gradient). White solid, 79.4 mg, 98 % yield, e.r. = 97:3. **$^{1}$H NMR** (500 MHz, $CDCl_3$) $\delta$ = 7.34–7.09 (m, 11H), 7.02 (d, *J* = 7.6 Hz, 1H), 6.95 (d, *J* = 7.7 Hz, 1H), 5.62 (dd, *J* = 46.0, 6.6 Hz, 1H), 4.08 (dd, *J* = 15.6, 6.6 Hz, 1H), 2.88–2.78 (m, 2H), 2.79–2.63 (m, 2H), **$^{19}$F NMR** (470 MHz, $CDCl_3$) $\delta$ = -174.9 (dd, *J* = 46.0, 15.5 Hz), **$^{13}$C NMR** (126 MHz, $CDCl_3$) $\delta$ = 140.1, 139.6 (d, *J* = 3.7 Hz), 139.0 (d, *J* = 21.3 Hz), 134.3, 134.1, 129.7, 129.3, 129.0, 128.8 (d, *J* = 1.2 Hz), 128.6, 128.5, 128.1, 127.2, 126.5, 126.3 (d, *J* = 7.6 Hz), 124.4 (d, *J* = 7.1 Hz), 95.5 (d, *J* = 182.9 Hz), 55.5 (d, *J* = 24.0 Hz), 36.2, 33.3 (d, *J* = 1.8 Hz); **mp:** 44–45 °C; **IR** (liquid film) *v* = 3062, 3027, 2918, 2849, 1595, 1573, 1495, 1476, 1453, 1430, 1209, 1188, 1098, 1080, 1051, 999, 882, 785, 773, 746, 694 $cm^{-1}$; **HRMS** (EI) m/z calculated for $C_{22}H_{18}Cl_2S$ $(M\text{-}HF)^{+\cdot}$ 384.0501, found 384.0501; $[\boldsymbol{\alpha}]_{\mathbf{D}}^{\mathbf{25}}$ = +83.4 (c 1.0, $CHCl_3$, e.r. = 97:3); **HPLC** DAICEL CHIRALPAK® IB-3, heptane:EtOH 99.9:0.1, 1 ml/min, $t_1$: 14.5 min (minor), $t_2$: 15.8 min (major).

((1S,2S)-2-fluoro-1,2-di-*m*-tolylethyl)(phenethyl)sulfane (**3d**)

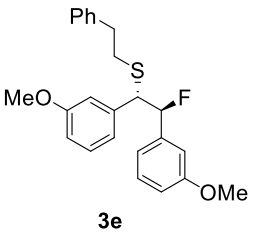


**3d**

Product **3d** was prepared according to the General Procedure G by employing 0.2 mmol of substrate (85 mg) and the reaction was stirred at -30 °C for 72 h. **Purification** column chromatography, pentane:$Et_2O$ (100:0 to 99:1 gradient). White solid, 50 mg , 69 % yield, e.r. = 97:3. **Gram scale** Product **3d** was prepared according to the General Procedure G by employing 2.35 mmol of substrate (1 g) and the reaction was stirred at -10 °C for 72 h; **Purification** column chromatography, pentane:$Et_2O$ (100:0 to 99:1, 25:75 to recover the catalyst). White solid, 531 mg , 62 % yield, e.r. = 94:6; 99% recovered catalyst. After recrystallisation from hexane (82% yield), e.r. > 99.9:0.1. **$^1$H NMR** (500 MHz, $CDCl_3$) $\delta$ = 7.34–7.20 (m, 3H), 7.19–6.88 (m, 10H), 5.66 (dd, *J* = 46.5, 7.2 Hz, 1H), 4.19 (dd, *J* = 14.5, 7.2 Hz, 1H), 2.92–2.76 (m, 2H), 2.71 (m, 2H), 2.31 (s, 3H), 2.31 (s, 3H), **$^{19}$F NMR** (470 MHz, $CDCl_3$) $\delta$ = -173.4 (dd, *J* = 46.4, 14.5 Hz), **$^{13}$C NMR** (126 MHz, $CDCl_3$) [overlapping signals] $\delta$ = 140.5, 138.0, 137.8 (*J* = 4.3 Hz), 137.6, 137.6 (*J* = 20.7 Hz), 129.5, 129.2, 129.1, 128.5, 128.4, 128.2, 127.8, 126.9, (*J* = 6.8 Hz), 126.3, 126.0, 123.4 (*J* = 6.9 Hz), 97.0 (*J* = 180.0 Hz), 56.2 (*J* = 23.7 Hz), 36.2, 33.3 (*J* = 2.1 Hz), 21.4; **mp:** 84–86 °C; **IR** (liquid film) *v* = 3026, 2920, 1605, 1494, 1453, 1378, 1312, 1281, 1158, 1094, 1052, 999, 908, 883, 781, 731, 697, 636, 611 $cm^{-1}$; **HRMS** (EI) m/z calculated for $C_{24}H_{24}S$ $(M\text{-}HF)^{+\cdot}$ 344.1593, found 344.1587; $[\alpha]_D^{25}$ = +86.1 (c 1.0, $CHCl_3$, e.r. = 97:3); **HPLC** DAICEL CHIRALPAK® IC-3, heptane:EtOH 99.75:0.25, 1 ml/min, $t_1$: 4.4 min (major), $t_2$: 5.2 min (minor).

Single Crystal Data for **3d** $C_{24}H_{25}FS$, Mr = 364.53. 150 K – monoclinic, P21, a = 11.4021(3) Å, b = 7.21710(10) Å, c = 12.6576(3) Å, V = 987.66(4) Å, Data/restraints/parameters – 4088/1/236, Flack = 0.011(12) for 1862 Friedel pairs and Hooft = 0.012(3) for 1855 Friedel pairs, P2(correct) > 99.9999%, P3(correct), Rint = 0.033, Final R1 = 0.0318, wR2 = 0.0841 (I>2σ(I)).

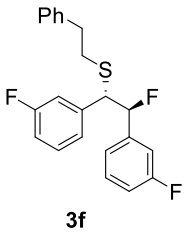
((1*S*,2*S*)-2-fluoro-1,2-bis(3-methoxyphenyl)ethyl)(phenethyl)sulfane (**3e**)



**3e**

Product **3e** was prepared according to the General Procedure G by employing 0.2 mmol of substrate (91.5 mg) and the reaction was stirred at 0 °C for 72 h. **Purification** column chromatography, pentane:$Et_2O$ (100:0 to 80:20 gradient). Colourless oil, 70.5 mg, 89 % yield, e.r. = 96:4. **$^1$H NMR** (500 MHz, $CDCl_3$) $\delta$ = 7.32–7.09 (m, 7H), 6.84–6.64 (m, 6H), 5.66 (dd, *J* = 46.4, 7.2 Hz, 1H), 4.18 (dd, *J* = 14.1, 7.2 Hz, 1H), 3.75 (s, 3H), 3.73 (s, 3H), 2.89–2.77 (m, 2H), 2.76–2.68 (m, 2H), **$^{19}$F NMR** (470 MHz, $CDCl_3$) $\delta$ = -173.1 (dd, *J* = 46.4, 14.1 Hz), **$^{13}$C NMR** (126 MHz, $CDCl_3$) [overlapping signals] $\delta$ = 159.5, 159.2, 140.4, 139.3 (d, *J* = 4.3 Hz), 139.0 (d, *J* = 21.0 Hz), 129.3, 129.0, 128.5, 128.4, 126.3, 121.4, 118.6 (d, *J* = 7.0 Hz), 114.3 (d, *J* = 2.9 Hz), 114.3, 113.4, 111.6 (d, *J* = 7.5 Hz), 96.7 (d, *J* = 181.0 Hz), 56.2 (d, *J* = 23.8 Hz), 55.2, 36.2, 33.3 (d, *J* = 2.0 Hz); **IR** (liquid film) *v* = 3060, 3026, 2935, 2835, 1600, 1585, 1490, 1464, 1453, 1434, 1319, 1261, 1153, 1042, 995, 874, 780, 734, 696 $cm^{-1}$; **HRMS** (EI) m/z calculated for $C_{24}H_{25}FO_2S$ $(M)^{+\cdot}$ 396.1554, found 396.1561; $[\alpha]_D^{25}$ = +74.0 (c 1.0, $CHCl_3$, e.r. = 96:4); **HPLC** DAICEL CHIRALPAK® IF-3, Heptane:EtOH 99.5:0.5, 1 ml/min, $t_1$: 10.7 min (major), $t_2$: 12.3 min (minor).

((1*S*,2*S*)-2-fluoro-1,2-bis(3-fluorophenyl)ethyl)(phenethyl)sulfane (**3f**)

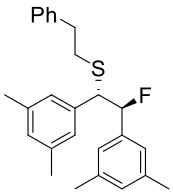


**3f**

Product **3f** was prepared according to the General Procedure G by employing 0.2 mmol of substrate (86.6 mg) and the reaction was stirred at r.t. for 72 h. **Purification** column chromatography, pentane:$Et_2O$ (100:0 to 99:1 gradient). Colourless liquid, 56 mg, 75 % yield, e.r. = 94:6. **$^1$H NMR** (500 MHz, $CDCl_3$) $\delta$ = 7.33–7.18 (m, 5H), 7.12 (dd, *J* = 7.0, 1.7 Hz, 2H), 7.03–6.81 (m, 6H), 5.64 (dd, *J* = 46.1, 6.9 Hz, 1H), 4.12 (dd, *J* = 14.8, 6.9 Hz, 1H), 2.88–2.82 (m, 2H), 2.78–2.64 (m, 2H), **$^{19}$F NMR** (470 MHz, $CDCl_3$) $\delta$ = -112.4 – -112.5 (m, 1F), -112.6–-112.7 (m, 1F), -173.8 (dd, *J* = 46.0,

14.8 Hz, 1F), **$^{13}$C NMR** (126 MHz, $CDCl_3$) $\delta$ = 162.8 (d, *J* = 246.5 Hz), 162.5 (d, *J* = 247.0 Hz), 140.2, 140.1 (dd, *J* = 8.0, 4.3 Hz), 139.7 (dd, *J* = 21.4, 7.1 Hz), 130.1 (d, *J* = 8.0 Hz), 129.8 (d, *J* = 8.0 Hz), 128.7, 128.6, 126.6, 124.7 (d, *J* = 2.0 Hz), 122.0 (dd, *J* = 7.3, *J* = 3.2 Hz), 116.0 (d, *J* = 22.3 Hz), 115.7 (d, *J* = 21.4 Hz), 115.0 (d, *J* = 20.7 Hz), 113.4 (dd, *J* = 22.6, 8.2 Hz), 95.8 (d, *J* = 186.0 Hz), 55.7 (d, *J* = 23.9 Hz), 36.3, 33.4 (d, *J* = 1.9 Hz); **IR** (liquid film) *v* = 3064, 3026, 2920, 2850, 1614, 1591, 1488, 1449, 1257, 1142, 1075, 1051, 1004, 955, 919, 878, 784, 738, 696 $cm^{-1}$; **HRMS** (EI) m/z calculated for $C_{22}H_{18}F_2S$ $(M\text{-}HF)^{+\cdot}$ 352.1092, found 352.1087; $[\boldsymbol{\alpha}]_{\mathbf{D}}^{\mathbf{25}}$ = +91.4 (c 0.5, $CHCl_3$, e.r. = 94:6); **HPLC** DAICEL CHIRALPAK® IB-3, heptane:EtOH 99.75:0.25, 1 ml/min, $t_1$: 6.9 min (minor), $t_2$: 7.6 min (major).

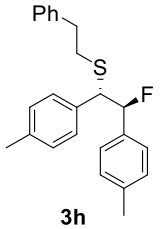
((1*S*,2*S*)-1,2-bis(3,5-dimethylphenyl)-2-fluoroethyl)(phenethyl)sulfane (**3g**)



**3g**

Product **3g** was prepared according to the general Procedure G by employing 0.2 mmol of substrate (90.6 mg) and the reaction was stirred at r.t. for 24 hours. **Purification** column chromatography, pentane:$Et_2O$ (100:0 to 99:1 gradient). Colourless oil, 57 mg, 73 % yield, e.r. = 96.5:3.5. **$^{1}$H NMR** (500 MHz, $CDCl_3$) $\delta$ = 7.30–7.25 (m, 3H), 7.24–7.19 (m, 1H), 7.10 (d, *J* = 7.9 Hz, 1H), 6.91 (s, 1H), 6.87 (s, 1H), 6.81 (s, 2H), 6.77 (s, 2H), 5.63 (dd, *J* = 46.6, 6.7 Hz, 1H), 4.13 (dd, *J* = 16.0, 6.7 Hz, 1H), 2.87–2.74 (m, 2H), 2.74–2.57 (m, 2H), 2.27 (s, 12H), **$^{19}$F NMR** (470 MHz, $CDCl_3$) $\delta$ = -174.6 (dd, *J* = 46.5, 16.1 Hz), **$^{13}$C NMR** (126 MHz, $CDCl_3$) $\delta$ = 140.7, 138.1 (d, *J* = 4.0 Hz), 137.9, 137.8 (d, *J* = 20.2 Hz), 137.5, 130.1 (d, *J* = 1.7 Hz), 129.4, 128.7, 128.5, 126.8, 126.4, 124.2 (d, *J* = 7.1 Hz), 97.0 (d, *J* = 179.8 Hz), 56.2 (d, *J* = 23.4 Hz), 36.4, 33.5 (d, *J* = 2.2 Hz), 21.4, 21.3; **IR** (liquid film) *v* = 3025, 2917, 2860, 1605, 1495, 1454, 1377, 1227, 1161, 1030. 920, 853, 799, 745, 698 $cm^{-1}$; **HRMS** (EI) m/z calculated for $C_{26}H_{28}S$ $(M\text{-}HF)^{+\cdot}$ 372.1906, found 372.1912; $[\boldsymbol{\alpha}]_{\mathbf{D}}^{\mathbf{25}}$ = +84.5 (c 0.5, $CHCl_3$, e.r. = 96.5:3.5); **HPLC** DAICEL CHIRALPAK® ID-3, heptane:EtOH 99.8:0.2, 1 ml/min, $t_1$: 4.7 min (minor), $t_2$: 5.4 min (major).

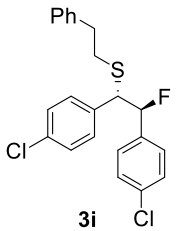
((1*S*,2*S*)-2-fluoro-1,2-di-*p*-tolylethyl)(phenethyl)sulfane (**3h**)



**3h**

Product **3h** was prepared according to the General Procedure G by employing 0.2 mmol of substrate (85 mg) and the reaction was stirred at -30 °C for 72 h. **Purification** column chromatography, pentane:$Et_2O$ (100:0 to 99:1 gradient). White solid, 44 mg , 60 % yield, e.r. = 91:9. **$^1$H NMR** (400 MHz, $CDCl_3$) $\delta$ = 7.31–7.14 (m, 3H), 7.12–6.95 (m, 10H), 5.62 (dd, *J* = 46.3, 7.6 Hz, 1H), 4.19 (dd, *J* = 13.3, 7.6 Hz, 1H), 2.84–2.73 (m, 2H), 2.72–2.60 (m, 2H), 2.29 (s, 3H), 2.29 (s, 3H), **$^{19}$F NMR** (376 MHz, $CDCl_3$) $\delta$ = -171.0 (dd, *J* = 46.3, 13.2 Hz); **$^{13}$C NMR** (101 MHz, $CDCl_3$) $\delta$ = 140.6, 138.3 (d, *J* = 1.9 Hz), 137.4, 134.8 (d, *J* = 21.3 Hz), 134.8 (d, *J* = 5.3 Hz), 129.2, 128.9, 128.8, 128.7, 128.5, 126.4 (d, *J* = 6.7 Hz), 126.3, 97.1 (d, *J* = 179.1 Hz), 56.0 (d, *J* = 24.0 Hz), 36.4, 33.4 (d, *J* = 2.3 Hz), 21.3, 21.2; **mp** 60–62 °C; **IR** (liquid film) *v* = 3027, 2945, 2869, 1602, 1514, 1496, 1448, 1074, 946, 908, 816, 738, 718, 702 $cm^{-1}$; **HRMS** (EI) m/z calculated for $C_{24}H_{24}S$ $(M\text{-}HF)^{+\cdot}$ 344.1593, found 344.1595; $[\alpha]_D^{25}$ = +85.0 (c 0.5, $CHCl_3$, e.r. = 91:9); **HPLC** DAICEL CHIRALPAK® IF-3, heptane:EtOH 99.8:0.2, 1 ml/min, $t_1$: 9.4 min (minor), $t_2$: 10.1 min (major).

((1*S*,2*S*)-1,2-bis(4-chlorophenyl)-2-fluoroethyl)(phenethyl)sulfane (**3i**)

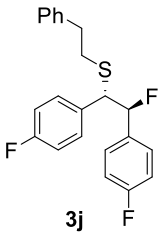


**3i**

Product **3i** was prepared according to the General Procedure G by employing 0.2 mmol of substrate (93.2 mg) and the reaction was stirred at 0 °C for 72 h. **Purification** column chromatography, pentane:$Et_2O$ (100:0 to 99:1 gradient). White solid, 40.0 mg, 53 % yield, e.r. = 93:7. **$^1$H NMR** (400 MHz, $CDCl_3$) $\delta$ = 7.32–7.15 (m, 7H), 7.10–7.05 (m, 2H), 7.02 (d, *J* = 8.4 Hz, 2H), 6.97 (d, *J* = 8.4 Hz, 2H), 5.58 (dd, *J* = 45.8, 7.0 Hz, 1H), 4.09 (dd, *J* = 13.8, 7.0 Hz, 1H), 2.90–2.76 (m, 2H), 2.73–2.56 (m, 2H), **$^{19}$F NMR** (376 MHz, $CDCl_3$) $\delta$ = -172.4 (dd, *J* = 45.9, 13.9 Hz, 1F), **$^{13}$C NMR** (101 MHz, $CDCl_3$) $\delta$ = 140.2, 135.9 (d, *J* = 4.0 Hz), 135.6 (d, *J* = 21.4 Hz), 134.7 (d, *J* = 1.9 Hz), 133.8, 130.4, 128.7, 128.7, 128.6, 128.4, 127.8 (d, *J* = 6.9 Hz), 126.6, 95.9 (d, *J* = 181.7 Hz), 55.4 (d, *J* = 24.4 Hz),

36.2, 33.4 (d, *J* = 1.8 Hz); **mp** 68-70 °C; **IR** (liquid film) *v* = 3062, 3027, 2922, 2850, 1601, 1491, 1453, 1408, 1276, 1209, 1179, 1091, 1052, 1014, 862, 836, 822, 771, 748, 720, 698 $cm^{-1}$; **HRMS** (EI) m/z calculated for $C_{22}H_{18}Cl_2S$ $(M\text{-}HF)^{+\cdot}$ 384.0501, found 384.0499; $[\alpha]_D^{25}$ = +83.7 (c 0.5, $CHCl_3$, e.r. = 93:7); **HPLC** DAICEL CHIRALPAK® IC-3, heptane:EtOH 99.9:0.1, 1 ml/min, $t_1$: 8.1 min (minor), $t_2$: 9.3 min (major).

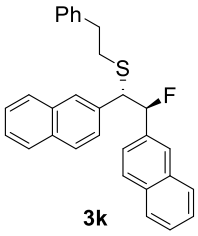
((1S,2S)-1,2-bis(4-fluorophenyl)-2-fluoroethyl)(phenethyl)sulfane (**3j**)



**3j**

Product **3j** was prepared according to the General Procedure G by employing 0.2 mmol of substrate (86.7 mg) and the reaction was stirred at 0 °C for 72 h. **Purification**: column chromatography, pentane:$Et_2O$ (100:0 to 99:1 gradient). Colourless oil, 43.2 mg, 58 % yield, e.r. = 94:6. **$^1$H NMR** (400 MHz, $CDCl_3$) *δ* = 7.30–7.19 (m, 3H), 7.14–6.99 (m, 6H), 6.98–6.89 (m, 4H), 5.60 (dd, *J* = 45.8, 7.3 Hz, 1H), 4.15 (dd, *J* = 13.2, 7.3 Hz, 1H), 2.90–2.78 (m, 2H), 2.75–2.65 (m, 2H), **$^{19}$F NMR** (470 MHz, $CDCl_3$) *δ* = -112.0– -114.0 (m, 1F), -112.6–-112.7 (m, 1F), -170.3 (dd, *J* = 46.7, 11.2 Hz, 1F), **$^{13}$C NMR** (101 MHz, $CDCl_3$) *δ* =162.7 (dd, *J* = 247.0, 1.9 Hz), 162.1 (d, *J* = 247.0 Hz), 140.2, 133.1 (d, *J* = 3.4 Hz), 133.0 (dd, *J* = 18 Hz, *J* = 3.2 Hz), 130.6 (d, *J* = 8.1 Hz), 128.5, 128.5, 128.1 (t, *J* = 7.1 Hz), 126.4, 115.3 (d, *J* = 21.5 Hz), 115.0 (d, *J* = 21.5 Hz), 96.1 (d, *J* = 181.2 Hz), 55.3 (d, *J* = 24.8 Hz), 36.2, 33.3 (d, *J* = 2.0 Hz); **IR** (liquid film) *v* = 3063, 3028, 2922, 2851, 1604, 1508, 1454, 1417, 1298, 1224, 1158, 1096, 1052, 1013, 937, 834, 806, 749, 722, 698 $cm^{-1}$; **HRMS** (EI) m/z calculated for $C_{22}H_{18}F_2S$ $(M\text{-}HF)^{+\cdot}$ 352.1092, found 352.1094; $[\alpha]_D^{25}$ = +65.2 (c 0.5, $CHCl_3$, e.r. = 94:6); **HPLC** DAICEL CHIRALPAK® IC-3, heptane:EtOH 99.9:0.1, 1ml/min, $t_1$: 12.5 min (major), $t_2$: 15.0 min (minor).

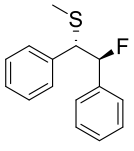
((1*S*,2*S*)-2-fluoro-1,2-di(naphthalen-2-yl)ethyl)(phenethyl)sulfane (**3k**)



**3k**

Product **3k** was prepared according to the General Procedure G by employing 0.05 mmol of substrate (25.0 mg) and the reaction was stirred at r.t. for 24 hours. **Purification** preparative TLC, pentane:DCM (80:20). White solid, 13.2 mg, 61 % yield, e.r. = 95.5:4.5. **$^1$H NMR** (500 MHz, $CDCl_3$) $\delta$ = 7.82–7.69 (m, 6H), 7.66 (s, 1H), 7.60 (s, 1H), 7.50–7.43 (m, 4H), 7.38 (dd, *J* = 8.5, 1.8 Hz, 1H), 7.26–7.17 (m, 4H), 7.10–7.02 (m, 2H), 5.98 (dd, *J* = 46.1, 7.1 Hz, 1H), 4.50 (dd, *J* = 14.4, 7.2 Hz, 1H), 2.92–2.76 (m, 2H), 2.76–2.63 (m, 2H), **$^{19}$F NMR** (470 MHz, $CDCl_3$) $\delta$ = -172.3 (dd, J = 46.0, 14.2 Hz, 1F), **$^{13}$C NMR** (126 MHz, $CDCl_3$) [overlapping signals] $\delta$ = 139.3, 134.2 (d, *J* = 4.1 Hz), 134.0, 133.9 (d, *J* = 20.5 Hz), 132.2, 132.0, 131.7, 127.5, 127.4, 127.3, 127.1, 127.0, 126.8 (d, *J* = 3.6 Hz), 126.6 (d, *J* = 4.2 Hz), 125.5, 125.3 (d, *J* = 3.3 Hz), 125.2 (d, *J* = 3.0 Hz), 125.0, 124.9 (d, *J* = 8.0 Hz), 122.7 (d, *J* = 5.9 Hz), 95.8 (d, *J* = 180.4 Hz), 55.3 (d, *J* = 23.9 Hz), 35.2, 32.2 (d, *J* = 1.9 Hz); **mp** 105–106 °C; **IR** (liquid film) *v* = 3057, 3025, 2919, 2850, 1601, 1508, 1496, 1453, 1368, 1331, 1270, 1188, 1143, 1124, 1053, 1018, 950, 896, 860, 819, 805, 748, 697 cm-1; **HRMS** (EI) m/z calculated for $C_{30}H_{24}S$ $(M\text{-}HF)^{+\cdot}$ 416.1593, found 416.1605; $[\boldsymbol{\alpha}]_{\mathbf{D}}^{\mathbf{25}}$ = +59.5 (c 0.4, $CHCl_3$, e.r. = 95.5:4.5); **HPLC** DAICEL CHIRALPAK® IB-3, heptane:EtOH 99.85:0.15, 1ml/min, $t_1$: 26.2 min (major), $t_2$: 30.2 min (minor).

(1*S,2S*)-(2-fluoro-1,2-diphenylethyl)(methyl)sulfane (**3l**)

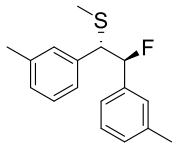


**3l**

Product **3l** was prepared according to the General Procedure G by employing 0.2 mmol of substrate (49.6 mg) and the reaction was stirred at -30 °C for 72 h. **Purification** column chromatography, pentane:$Et_2O$ (100:0 to 99:1 gradient). Colourless oil, 35.5 mg, 72 % yield, e.r. = 91:9. **$^1$H NMR** (400 MHz, $CDCl_3$) $\delta$ = 7.19–7.11 (m, 6H), 7.09 (dd, *J* = 7.5, 2.0 Hz, 2H), 7.07–7.02 (m, 2H), 5.62 (dd, *J* = 46.3, 7.4 Hz, 1H), 4.07 (dd, *J*

= 13.9, 7.4 Hz, 1H), 1.93 (d, *J* = 0.8 Hz, 3H), **$^{19}$F NMR** (376.5 MHz, $CDCl_3$) $\delta$ = -173.2 (dd, *J* = 46.4, 13.9 Hz), **$^{13}$C NMR** (101 MHz, $CDCl_3$) $\delta$ = 137.8 (d, *J* = 16.5 Hz), 137.6, 129.0, 128.6 (d, *J* = 1.5 Hz), 128.5, 128.2, 127.8, 126.4 (d, *J* = 7.1 Hz), 97.1 (d, *J* = 180.2 Hz), 58.1 (d, *J* = 23.8 Hz), 15.5; **IR** (liquid film) *v* = 3031, 2918, 1493, 1453, 1212, 1075, 1051, 998, 916, 756, 737, 696, 627 $cm^{-1}$; **HRMS** (EI) m/z calculated for $C_{15}H_{15}FS$ $(M)^{+\cdot}$ 246.0873, found 246.0878; $[\boldsymbol{\alpha}]_{\mathbf{D}}^{\mathbf{25}}$ = +74.1 (c 0.5, $CHCl_3$, e.r. = 91:9); **HPLC** DAICEL Chiralpack IC-3, Heptane:EtOH 99.9:0.1, 1 ml/min, $t_1$: 8.0 min (major), $t_2$: 9.1 min (minor).

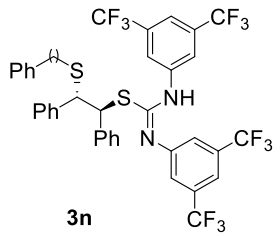
((1*S*,2*S*)-2-fluoro-1,2-di-*m*-tolylethyl)(methyl)sulfane (**3m**)



**3m**

Product **3m** was prepared according to the General Procedure G by employing 0.2 mmol of substrate (67.0 mg) and the reaction was stirred at -10 ° for 72 h. **Purification** column chromatography, pentane:$Et_2O$ (100:0 to 99:1 gradient). Colourless liquid, 43.2 mg , 87 % yield, e.r. = 92.5:7.5. **$^{1}$H NMR** (500 MHz, $CDCl_3$) $\delta$ = 7.21–6.86 (m, 8H), 5.69 (dd, *J* = 46.4, 7.0 Hz, 1H), 4.10 (dd, *J* = 15.0, 7.1 Hz, 1H), 2.29 (s, 6H), 2.01 (s, 3H), **$^{19}$F NMR** (470 MHz, $CDCl_3$) $\delta$ = -174.1 (dd, J = 46.6, 14.9 Hz), **$^{13}$C NMR** (126 MHz, $CDCl_3$) [overlapping signals] $\delta$ = 138.0, 137.7 (d, *J* = 12.0 Hz), 137.6, 137.6 (d, *J* = 3.8 Hz), 129.5, 129.2 (d, *J* = 1.8 Hz), 128.2, 127.8, 126.9 (d, *J* = 6.8 Hz), 126.0, 123.4 (d, *J* = 7.0 Hz), 96.9 (d, *J* = 179.8 Hz), 57.9 (d, *J* = 23.7 Hz), 21.4, 15.4 (d, *J* = 2.6 Hz); **IR** (liquid film) *v* = 3025, 2918, 2864, 1607, 1590, 1488, 1437, 1379, 1313, 1247, 1191, 1159, 1094, 1056, 999, 883, 780, 735, 700 $cm^{-1}$; **HRMS** (EI) m/z calculated for $C_{17}H_{19}FS$ $(M)^{+\cdot}$ 274.1186, found 274.1181; $[\boldsymbol{\alpha}]_{\mathbf{D}}^{\mathbf{25}}$ = +63.7 (c 1.0, $CHCl_3$, e.r. = 92.5:7.5); **HPLC** DAICEL Chiralpack IC-3, heptane:EtOH 99.75:0.25, 1 ml/min, $t_1$: 3.9 min (major), $t_2$: 4.3 min (minor).

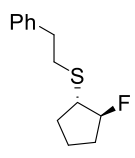
*rac*-2-(phenethylthio)-1,2-diphenylethyl-N,N'-bis(3,5-bis(trifluoromethyl)phenyl)carbamimidothioate (**3n**)



**3n**

The thiourea degradation product **3n** was prepared by dissolving β-bromo sulfide **1a** (0.2 mmol, 79.5 mg, 1 equiv.) and thiourea **2d** (0.2 mmol, 100.0 mg, 1 equiv.) in DCM (0.25 M). After stirring for 1 hour, the solvent was removed *in vacuo* and the crude product was purified by column chromatography (pentane:DCM, 95:5 to 85:15 gradient) to afford a dense sticky oil (57.2 mg, 0.07 mmol, 35 % yield). **$^{1}$H NMR** (500 MHz, DMSO-$d_6$) $\delta$ = 10.09 (s, 1H), 8.06 (s br, 2H), 7.78 (s br, 1H), 7.64 (s br, 1H), 7.20–7.09 (m, 9H), 7.08–7.01 (m, 4H), 7.00–6.94 (m, 4H), 5.29 (d, *J* = 11.0 Hz, 1H), 4.40 (d, *J* = 11.0 Hz, 1H), 2.72–2.56 (m, 2H), 2.50–2.38 (m, 2H), ), **$^{19}$F NMR** (470 MHz, $CDCl_3$) $\delta$ = –61.3 (s, 6F), -61.7 (s, 6F), **$^{13}$C NMR** (126 MHz, DMSO-$d_6$) [overlapping signals] $\delta$ = 151.0, 150.8, 142.3, 140.7, 140.2, 139.7, 131.2 (q, *J* = 32.6 Hz), 131.1 (q, *J* = 32.6 Hz), 128.9, 128.8, 128.6, 128.4, 128.0, 127.9, 127.6, 126.5, 123.7 (q, *J* = 272.7 Hz), 123.6 (q, *J* = 272.7 Hz), 122.8, 119.7, 116.6, 115.9, 56.6, 53.4, 35.4, 32.9; **IR** (liquid film) *v* = 2989, 2883, 1632, 1603, 1532, 1470, 1455, 1433, 1372, 1277, 1173, 1134, 1107, 1030, 970, 885, 847, 721, 700, 683, 668, 642, 616, 606 $cm^{-1}$; **HRMS** (ESI+) m/z calculated for $C_{39}H_{29}N_2F_{12}S_2$ $(M+H)^+$ 817.15751, found 817.15729.

2-(fluorocyclopentyl)(phenethyl)sulfane (**3o**)

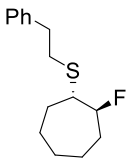


**3o**

Product **3o** was prepared according to the General Procedure H using catalyst **4a**, the reaction was performed in DCM for 1.5 hours at room temperature. Colourless oil, 90 % yield, e.r. = 69:31. **$^{1}$H NMR** (400 MHz, $CDCl_3$) $\delta$ = 7.27–7.19 (m, 2H), 7.18–7.10 (m, 3H), 4.88 (ddt, *J* = 53.7, 4.6, 2.1 Hz, 1H), 3.17 (dddt, *J* = 21.3, 7.6, 5.8, 1.7 Hz, 1H), 2.94–2.66 (m, 4H), 2.24–2.07 (m, 1H), 2.05–1.76 (m, 2H), 1.75–1.65 (m, 2H), 1.48–

1.37 (m, 1H), **$^{19}$F NMR** (376.5 MHz, $CDCl_3$) $\delta$ = -165.2 (dddd, *J* = 53.9, 34.6, 24.0, 21.3 Hz), **$^{13}$C NMR** (100 MHz, $CDCl_3$) $\delta$ = 140.5, 128.6, 128.6, 126.5, 101.0 (d, *J* = 180.2 Hz), 49.4 (d, *J* = 23.0 Hz), 36.3, 33.8, 31.8 (d, *J* = 21.4 Hz), 31.2, 22.6; **IR** (liquid film) *v* = 3026, 2954, 2869, 1603, 1496, 1453, 1340, 1225, 1075, 1043, 1031, 968, 908, 733, 697 $cm^{-1}$; **HPLC** Chiralpack Daicel IA $CH_3CN/H_2O$ 50:50, 1ml/min, $t_1$: 30.7 min, $t_2$: 32.4 min.

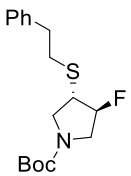
2-(fluorocycloheptyl)(phenethyl)sulfane (**3p**)



**3p**

Product **3p** was prepared according to General Procedure H using catalyst **4a**, the reaction was performed in DCM for 90 min at room temperature. Colourless oil, 72 % yield, e.r. = 55.5:45.5. **$^{1}$H NMR** (400 MHz, $CDCl_3$) $\delta$ = 7.33 – 7.27 (m, 2H), 7.25 – 7.18 (m, 3H), 4.68 (dtd, *J* = 47.0, 6.6, 3.3 Hz, 1H), 3.07 – 2.82 (m, 5H), 2.03 – 1.36 (m, 10H); **$^{19}$F NMR** (376.5 MHz, $CDCl_3$) δ -161.9 (dddd, *J* = 46.5, 31.7, 17.7, 12.6 Hz); **$^{13}$ C NMR** (100 MHz, $CDCl_3$) $\delta$ = 140.7, 128.6, 128.6, 126.5, 98.6 (d, *J*= 172.4 Hz), 50.4 (d, *J* = 22.7 Hz), 36.5, 33.6 (d, *J* = 2.2 Hz), 32.8 (d, *J* = 21.8 Hz), 30.5 (d, *J* = 6.3 Hz), 28.7, 26.2, 21.5 (d, *J* = 7.1 Hz); **IR** (liquid film) *v* = 3734, 3709, 3649, 3629, 1717, 1653, 1456, 669, 651 $cm^{-1}$; **HPLC** Chiralpack Daicel IF-3 Heptane/iPrOH 99:1, 1ml/min, $t_1$: 3.6 min, $t_2$: 3.9 min.

*tert*-butyl-3-fluoro-4-(phenethylthio)pyrrolidine-1-carboxylate (**3q**)

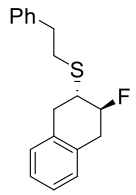


**3q**

Product **3q** was prepared according to General Procedure H using catalyst **4a**, the reaction was performed in DCM for 18 hours at room temperature. White solid, 45 % yield, e.r. = 64:36. **$^{1}$H NMR** (500 MHz, $CDCl_3$) $\delta$ = 7.34 (t, *J* = 7.4 Hz, 2H), 7.28 – 7.21 (m, 3H), 4.97 (dd, *J* = 53, 4.0 Hz, 1H), 3.96 – 3.32 (m, 5H), 3.02 – 2.80 (m, 4H), 1.49 (s, 9H), **$^{19}$F{$^{1}$H} NMR** (470 MHz, $CDCl_3$) δ -169.5, -169.9, **$^{13}$C NMR** (126 MHz, $CDCl_3$) $\delta$ = 154.2, 139.7, 128.6, 128.5, 126.7, 95.8 (d, *J* = 185.4 Hz), (95.1, d, *J* = 185.4 Hz, rotamer), 79.9, 50.6 (d, *J* = 22.9 Hz), (50.1, d, *J* = 22.9 Hz, rotamer), 50.0, (49.5 rotamer), 47.5 (d, *J* = 22.1 Hz), (46.7, d, *J* =

22.1 Hz, rotamer) 36.1, 33.40, (33.4 rotamer), 28.5; **mp** 79 ˚C; **IR** (solid) *v* = 2980, 2890, 1686, 1474, 1453, 1403, 1370, 1355, 1347 $cm^{-1}$; **HPLC** Chiralpack Daicel IC-3 Heptane/iPrOH 95:5, 1ml/min, $t_1$: 9.1 min, $t_2$: 9.7 min.

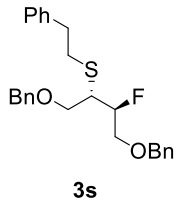
(3-fluoro-1,2,3,4-tetrahydronaphthalen-2-yl)(phenethyl)sulfane: (**3r**)



**3r**

Product **3r** was prepared according to General Procedure H using catalyst **4a**, the reaction was performed in DCM for 1.5 hours at room temperature. Colourless oil, 95 % yield, e.r. = 52.5:47.5.**$^1$H NMR** (400 MHz, $CDCl_3$) $\delta$ = 7.28 – 7.20 (m, 2H), 7.20 – 7.13 (m, 3H), 7.12 – 7.06 (m, 2H), 7.06 – 6.98 (m, 2H), 4.85 (dtd, *J* = 49.5, 6.8, 5.0 Hz, 1H), 3.33 – 3.14 (m, 3H), 3.00 (dd, *J* = 17.4, 6.5 Hz, 1H), 2.95 – 2.82 (m, 4H), 2.76 (dd, *J* = 16.0, 7.2 Hz, 1H); **$^{19}$F NMR** (376.5 MHz, $CDCl_3$) δ -172.4 (m); **$^{13}$C NMR** (100 MHz, $CDCl_3$) $\delta$ = 140.4, 133.7, 132.5, 132.4, 129.1, 128.6, 128.5, 126.7, 126.6, 126.6, 92.6 (d, *J*= 176.6 Hz), 44.2 (d, *J*= 19.7 Hz), 36.6, 34.2 (d, *J*= 22.5 Hz), 33.7, 33.4 (d, *J*= 4.9 Hz); **IR** (liquid film) *v* = 2980, 2921, 2852, 1603, 1495, 1453, 1381, 1261, 1154, 1074, 964, 785, 743, 697 $cm^{-1}$; **HPLC** Chiralpack Daicel IA MeCN/$H_2O$ 60:40, 1ml/min, $t_1$: 22.6 min, $t_2$: 24.4 min.

(1,4-bis(benzyloxy)-3-fluorobutan-2-yl)(phenethyl)sulfane (**3s**)



**3s**

Product **3s** was prepared according to *General Procedure H* using catalyst **4a**, the reaction was performed in DCM for 18 hours at room temperature. Colourless oil, 75 % yield, e.r. = 50:50. **$^1$H NMR** (400 MHz, $CDCl_3$) $\delta$ = 7.36 – 7.22 (m, 13H), 7.22 – 7.16 (m, 1H), 7.16 – 7.10 (m, 2H), 5.04 (dddd, *J* = 47.9, 6.2, 4.4, 3.3 Hz, 1H), 4.64 – 4.42 (m, 4H), 3.86 – 3.59 (m, 4H), 3.00 (dddd, *J* = 26.9, 8.5, 5.4, 3.4 Hz, 1H), 2.88 – 2.76 (m, 4), **$^{19}$F NMR** (376.5 MHz, $CDCl_3$) $\delta$ = -194.5 (dddd, *J* = 47.8, 26.7, 23.6, 18.2 Hz), **$^{13}$C NMR** (100 MHz, $CDCl_3$) $\delta$ = 140.3, 138.0, 137.9, 128.6, 128.6, 128.6, 127.9, 127.9, 127.9, 127.8, 126.5, 91.9 (d, *J* = 175.3 Hz), 73.7, 73.4, 70.3, 70.2 d, *J*= 19.2 Hz), 46.9 (d, *J*= 19.8 Hz), 36.7,

33.7; **IR** (liquid film) ν 2980, 1496, 1454, 1362, 1260, 1098, 1027, 954, 803, 735, 696 $cm^{-1}$; **HPLC** Chiralpack Daicel IF-3 Heptane/iPrOH 99:1, 1ml/min, $t_1$: 7.8 min, $t_2$: 8.6 min.

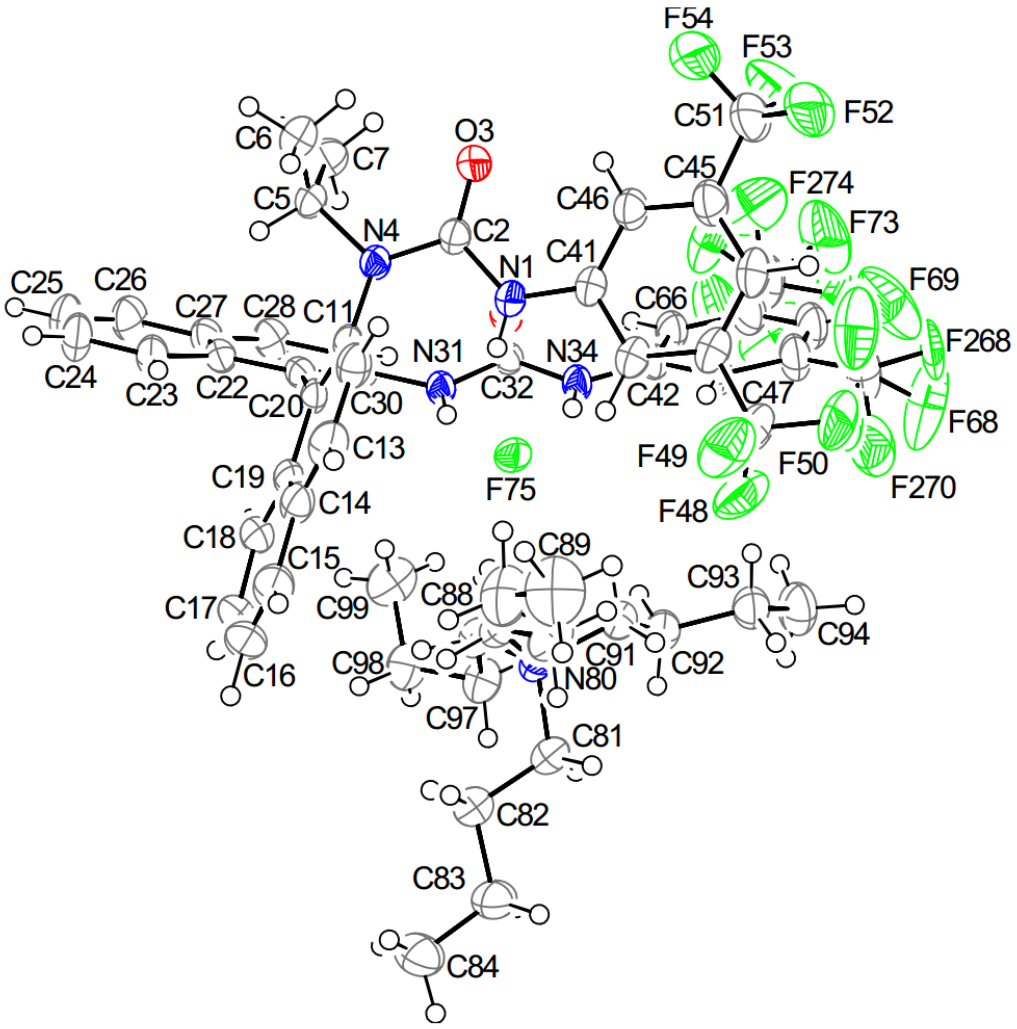
*4.2.4 X-ray Analysis*

Data were reduced using CrysAlisPro, solved using SuperFlip (97) and refined using CRYSTALS.[10,11] The Flack x parameter was refined in each case.[12,13] Bayesian analysis of the Bijvoet pairs was also carried out using all the data used in the refinement.[14] This gave the Hooft y parameter, the P2 probability (the likely-hood that the hand is correct given the crystal was enantiopure), and the P3 probability (the likely-hood that the hand is correct given the crystal was enantiopure or racemic).

Table 4.1: Crystal data and structure refinement for **4u**:TBAF.

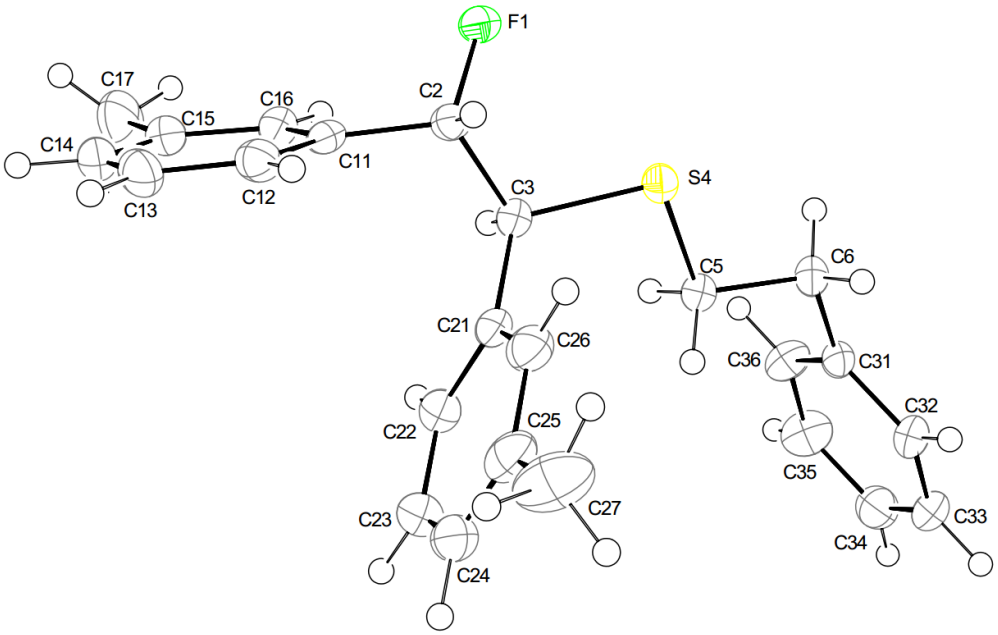
| Crystallographic Data for **4u**:TBAF complex | | |
|---|---|---|
| Empirical formula | C57 H64 F13 N5 O2 | |
| Formula weight | 1098.14 | |
| Temperature | 150 K | |
| Wavelength | 1.54184 Å | |
| Crystal system | Orthorhombic | |
| Space group | P 21 21 21 | |
| Unit cell dimensions | a = 10.22990(10) Å | $\alpha$= 90° |
| | b = 21.55920(10) Å | $\beta$= 90° |
| | c = 25.00480(10) Å | $\gamma$ = 90° |
| Volume | 5514.77(6) Å$^3$ | |
| Z | 4 | |
| Density (calculated) | 1.323 Mg/m$^3$ | |
| Absorption coefficient | 0.951 mm$^{-1}$ | |
| F(000) | 2296 | |
| Crystal size | 0.28 x 0.25 x 0.21 mm$^3$ | |
| Theta range for data collection | 4.088 to 76.391°. | |
| Index ranges | -12<=h<=12, -27<=k<=27, -31<=l<=31 | |
| Reflections collected | 164650 | |
| Independent reflections | 11531 [R(int) = 0.046] | |
| Completeness to theta = 76.391° | 99.9 % | |
| Absorption correction | Semi-empirical from equivalents | |
| Max. and min. transmission | 0.82 and 0.70 | |
| Refinement method | Full-matrix least-squares on F$^2$ | |
| Data / restraints / parameters | 11531 / 456 / 751 | |
| Goodness-of-fit on F$^2$ | 1.0039 | |
| Final R indices [I>2sigma(I)] | R1 = 0.0504, wR2 = 0.1438 | |
| R indices (all data) | R1 = 0.0511, wR2 = 0.1451 | |
| Absolute structure parameter | 0.000(16) | |
| Largest diff. peak and hole | 0.63 and -0.49 e.Å$^{-3}$ | |

Symmetry transformations used to generate equivalent atoms: #1 -x,y-1/2,-z+1/2


F54
F53
C51
F52
C6
C7
O3
C45
C5
C46
F274
F73
N4
C2
C41
N1
C25
C26
C27
C28
C11
C66
F69
F268
N31
N34
C24
C23
C22
C20
C30
C32
C42
C47
F68
C13
F49
F50
C19
F75
F270
C14
F48
C18
C15
C89
C93
C17
C99
C88
C94
C91
C92
C16
C98
N80
C97
C81
C82
C83
C84

| Crystallographic Data for **3d** | | |
|---|---|---|
| Empirical formula | C24 H25 F S | |
| Formula weight | 364.53 | |
| Temperature | 150 K | |
| Wavelength | 1.54184 Å | |
| Crystal system | Monoclinic | |
| Space group | P 21 | |
| Unit cell dimensions | a = 11.4021(3) Å | $\alpha$= 90°. |
| | b = 7.21710(10) Å | $\beta$= 108.519(3)°. |
| | c = 12.6576(3) Å | $\gamma$ = 90°. |
| Volume | 987.66(4) $Å^3$ | |
| Z | 2 | |
| Density (calculated) | 1.226 $Mg/m^3$ | |
| Absorption coefficient | 1.547 $mm^{-1}$ | |
| F(000) | 388 | |
| Crystal size | 0.28 x 0.22 x 0.15 $mm^3$ | |
| Theta range for data collection | 3.683 to 76.429°. | |
| Index ranges | -14<=h<=14, -9<=k<=9, -15<=l<=15 | |
| Reflections collected | 22206 | |
| Independent reflections | 4088 [R(int) = 0.033] | |
| Completeness to theta = 76.429° | 99.6 % | |
| Absorption correction | Semi-empirical from equivalents | |
| Max. and min. transmission | 0.79 and 0.66 | |
| Refinement method | Full-matrix least-squares on $F^2$ | |
| Data / restraints / parameters | 4088 / 1 / 236 | |
| Goodness-of-fit on $F^2$ | 1.0056 | |
| Final R indices [I>2sigma(I)] | R1 = 0.0317, wR2 = 0.0839 | |
| R indices (all data) | R1 = 0.0318, wR2 = 0.0841 | |
| Absolute structure parameter | 0.007(3) | |
| Largest diff. peak and hole | 0.35 and -0.20 $e.Å^{-3}$ | |

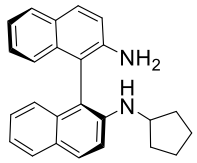
Table 4.2: Crystal data and structure refinement for **3d**.


F1
C17
C16
C2
C15
C14
C11
C3
S4
C13
C12
C5
C6
C21
C26
C36
C31
C32
C22
C25
C35
C27
C23
C33
C34
C24

## 4.3 Structure and Conformation of *bis*-Urea Catalysts for Hydrogen Bonding Phase-Transfer Catalysis: Insights from NMR Spectroscopy

### *4.3.1 Catalyst Synthesis and Characterisation*

(*S*)-*N*$^2$-(cyclopentyl)-[1,1'-binaphthalene]-2,2'-diamine (**5f**)

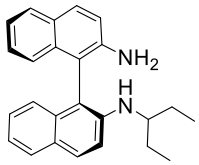


**5f**

In a round bottom flask equipped with a magnetic stirrer, cyclopentanone (240 µL, 2.7 mmol, 1.4 equiv.) was dissolved in THF (0.25 M) and a 20 % aqueous solution of $H_2SO_4$ was added (3.5 mL). After stirring for 30 minutes, (*S*)-1,1'-binaphthyl-2,2'-diamine (500 mg, 1.8 mmol, 1 equiv.) was added. After 5 min of stirring, the solution was cooled to 0 °C and $NaBH_4$ (700 mg, 18 mmol, 10 equiv.) was carefully added in portions. The mixture was stirred for 1 hour at room temperature, then quenched with 1 M KOH and diluted with EtOAc. The phases were separated, and the aqueous phase extracted three times with EtOAc. The combined organic phases were then washed with brine. After anhydrification with $MgSO_4$ and filtration, the solvents were evaporated under reduced pressure and the crude product was purified by column chromatography (hexane:EtOAc = 100:0 to 90:10, gradient) to afford the desired product as a white solid, 240 mg, 38 % yield. **$^1$H NMR** (500 MHz, $CDCl_3$) $\delta$ = 7.87 (d, *J* = 9.0 Hz, 1H), 7.82–7.75 (m, 3H), 7.31 (d, *J* = 9.0 Hz, 1H), 7.25–7.12 (m, 5H), 7.04 (d, *J* = 8.5 Hz, 1H), 6.98 (d, *J* = 8.5 Hz, 1H), 3.98 (dp, *J* = 7.9 Hz, *J* = 6.3 Hz 1H), 3.66 (s, 2H), 3.57 (d, *J* = 7.9 Hz, 1H), 1.98–1.82 (m, 2H), 1.50–1.34 (m, 4H), 1.28–1.16 (m, 2H), **$^{13}$C NMR** (126 MHz, $CDCl_3$) $\delta$ = 144.53, 143.04, 134.03, 133.74, 129.61, 129.53, 128.58, 128.23, 128.19, 127.71, 126.87, 126.78, 124.15, 123.88, 122.52, 121.96, 118.36, 115.49, 112.71, 112.49, 55.23, 33.72, 33.56, 23.77, 23.70; **IR** (solid) *v* = 3456, 3365, 3053, 2948, 2352, 2161, 2033, 1978, 1617, 1595, 1509, 1489, 1469, 1423, 1380, 1351, 1329, 1296, 1247, 1187, 1147, 1132, 1108, 1060, 1020, 941, 926, 883, 858, 817, 808, 772, 748, 685 cm$^{-1}$; **mp**

201–202 ˚C; **HRMS** (ESI+) m/z calculated for $C_{25}H_{25}N_2$ $(M+H)^+$ 353.20123, found 353.20119; $[\alpha]_D^{25}$ = -157.2 (c 0.5, $CHCl_3$).

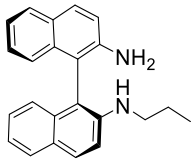
(*S*)-*N*$^2$-(pentan-3-yl)-[1,1'-binaphthalene]-2,2'-diamine (**5g**)



**5g**

In a round bottom flask equipped with a magnetic stirrer, 3-pentanone (5 mmol, 1.4 equiv.) was dissolved in THF (0.25 M) and a 20 % aqueous solution of $H_2SO_4$ was added (1 mL). After stirring for 30 minutes, (*S*)-1,1'-binaphthyl-2,2'-diamine (1.0 g, 3.52 mmol, equiv.) was added. After 5 minutes of stirring, the solution was cooled to 0 °C and $NaBH_4$ (1.3 g, 70.0 mmol, 10 equiv.) was carefully added in portions. The mixture was stirred for 1 hour at room temperature, then quenched with 1 M KOH and diluted with EtOAc. The phases were separated and the aqueous phase extracted three times with EtOAc. The combined organic phases were then washed with brine. After anhydrification with $MgSO_4$ and filtration, the solvents were evaporated under reduced pressure and the crude product was purified by column chromatography (hexane:EtOAc = 100:0 to 90:10, gradient) to afford the desired product as a white solid, 450 mg, 35 % yield. **$^1$H NMR** (500 MHz, $CDCl_3$) $\delta$ = 7.87 (d, *J* = 9.0 Hz, 1H), 7.83 (d, *J* = 9.1 Hz, 1H), 7.81–7.76 (m, 2H), 7.28–7.14 (m, 6H), 7.10 (d, *J* = 8.3 Hz, 1H), 7.02–6.97 (m, 1H), 3.70 (s, 2H), 3.56–3.29 (m, 2H), 1.54–1.20 (m, 4H), 0.84 (t, *J* = 7.4 Hz, 3H), 0.66 (t, *J* = 7.4 Hz, 3H), **$^{13}$C NMR** (126 MHz, $CDCl_3$) $\delta$ = 144.30, 142.98, 133.99, 133.86, 129.41, 128.44, 128.04, 127.98, 127.22, 126.64, 124.25, 123.58, 122.36, 121.49, 118.20, 114.45, 112.49, 111.62, 55.36, 27.21, 27.07, 10.04, 9.84; **IR** (solid) *v* = 3459, 3367, 3050, 2963, 2926, 2871, 2159, 1611, 1593, 1505, 1469, 1457, 1426, 1380, 1351, 1336, 1307, 1283, 1247, 1212, 1158, 1149, 1110, 1021, 958, 916, 860, 818, 809, 781, 746, 682, 622 $cm^{-1}$; **mp** 142–145 ˚C; **HRMS** (ESI+) m/z calculated for $C_{25}H_{27}N_2$ $(M+H)^+$ 355.21688, found 355.21680. Spectroscopic data are in agreement with those previously reported.[3]

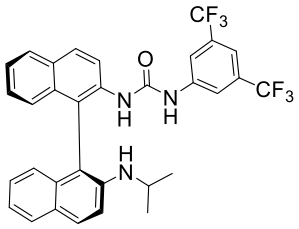
(*S*)-*N*$^2$-propyl-[1,1'-binaphthalene]-2,2'-diamine (**5h**)



**5h**

*N*-propylated aniline **5h** was synthesized according to the General Procedure A (*v. 4.2.1.2 Chiral Catalysts*) by employing 700 mg (1.47 mmol) of **5b** and 300 µL (1.7 mmol) of propyl iodide and stirring for 36 hours. **Purification** column chromatography, hexane:$Et_2O$ (90:10 to 80:20). White solid, 355 mg, 74 % yield. **$^1$H NMR** (400 MHz, $CDCl_3$) $\delta$ = 7.86 (d, *J* = 9.0, 1H), 7.83–7.71 (m, 3H), 7.25 (d, *J* = 9.0 Hz, 1H), 7.23–7.13 (m, 4H), 7.11 (d, *J* = 8.7 Hz, 1H), 7.07–6.95 (m, 2H), 3.66 (br s, 3H), 3.13 (t, *J* = 7.1 Hz, 2H), 1.42 (qd, *J* = 7.2, 3.2 Hz, 2H), 0.74 (t, *J* = 7.4 Hz, 3H), **$^{13}$C NMR** (101 MHz, $CDCl_3$) $\delta$ = 144.59, 143.07, 134.06, 133.76, 129.64, 129.59, 128.59, 128.24, 128.19, 127.68, 126.89, 126.81, 124.16, 123.81, 122.53, 121.90, 118.39, 114.34, 112.51, 112.28, 46.01, 23.03, 11.36.; **HRMS** (ESI+) m/z calculated for $C_{23}H_{23}N_2$ $(M+H)^+$ 327.18558, found 327.18530.

(*S*)-1-(3,5-bis(trifluoromethyl)phenyl)-3-(2'-(isopropylamino)-[1,1'-binaphthalen]-2-yl)urea (**5i**)



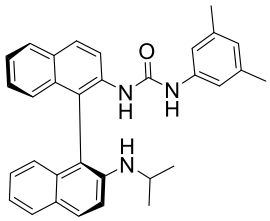
**5i**

In a flame-dried Schlenk under inert atmosphere, (*S*)-*N*$^2$-isopropyl-[1,1'-binaphthalene]-2,2'-diamine (**5e**) (500 mg, 1.5 mmol, 1 equiv.) was dissolved in dry DCM (0.5 M) and 3,5-bis(trifluoromethyl)phenyl isocyanate (1 equiv.) was added dropwise. The mixture was stirred 45 minutes at room temperature. After removal of the solvent under reduced pressure, the crude mixture was directly purified by column chromatography (hexane:EtOAc 100:0 to 80:20) to afford the desired products as a white solid, 720 mg, 83 % yield. **$^1$H NMR** (500 MHz, $CDCl_3$) $\delta$ = 8.42 (d, *J* = 9.0 Hz, 1H), 8.0 (d, *J* = 9.0 Hz, 1H), 7.95 (d, *J* = 8.2 Hz, 1H), 7.90 (t, *J* = 9.0 Hz, 1H), 7.77 (d, *J* = 8.0 Hz, 1H), 7.73 (s, 2H), 7.48 (s, 1H), 7.46 (t, *J* = 7.6 Hz, 1H), 7.28 (t, *J* = 8.0 Hz, 1H), 7.27 (d, *J* = 9.0 Hz, 1H), 7.21 (t, *J* =

7.5 Hz, 1H), 7.16 (t, *J* = 8.5 Hz, 1H), 7.14 (d, *J* = 8.5 Hz, 1H), 7.04 (s, 1H), 6.85 (d, *J* = 8.3, 1H), 6.56 (s, 1H), 3.79 (s, 1H), 3.34 (s, 1H), 1.03 (d, *J* = 6.3 Hz, 3H), 0.99 (d, *J* = 6.3 Hz, 3H), **$^{19}$F NMR** (471 MHz, $CDCl_3$) $\delta$ = -63.07 (s), **$^{13}$C NMR** (126 MHz, $CDCl_3$) $\delta$ = 152.31, 144.21, 140.05, 135.19, 133.98, 132.80, 132.24 (q, *J* = 33.3 Hz), 131.31, 130.46, 129.65, 128.39, 128.27, 127.48, 127.39, 127.10, 126.47 (q, *J* = 273 Hz), 125.42, 125.43–119.89 (m), 123.54, 122.48, 120.90, 120.72, 118.87 (d, *J* = 4.0 Hz), 116.76–115.92 (m), 115.13, 110.78, 44.71, 23.29, 23.04; **IR** (solid) *v* = 3342, 3971, 2963, 2160, 2031, 1676, 1619, 1598, 1572, 1503, 1474, 1426, 1385, 1334, 1275, 1174, 1129, 949, 881, 811, 773, 746, 723, 702, 681 $cm^{-1}$; **mp** 118–120 ˚C; **HRMS** (ESI+) m/z calculated for $C_{32}H_{26}N_3OF_6$ $(M+H)^+$ 582.19746, found 582.19698; $[\alpha]_D^{25}$ = -107.5 (c 0.5, $CHCl_3$).

(*S*)-1-(3,5-dimethylphenyl)-3-(2'-(isopropylamino)-[1,1'-binaphthalen]-2-yl)urea (**5j**)

In a flame-dried Schlenk under inert atmosphere, (*S*)-*N*$^2$-isopropyl-[1,1'-binaphthalene]-2,2'-diamine **5e** (127 mg, 0.4 mmol, 1 equiv.) was dissolved in dry DCE (0.4 M) and 3,5-dimethylphenyl isocyanate (1 equiv.) was added dropwise. The mixture was stirred overnight at room temperature. After removal of the solvent under reduced pressure, the crude mixture was directly purified by column chromatography (1$^{st}$ hexane:EtOAc 100:0 to 80:20; 2$^{nd}$ hexane:$Et_2O$ 100:0 to 80:20) to afford the desired products as a white solid in 83 % yield.

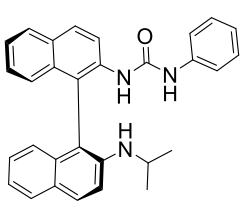


**5j**

**$^1$H NMR** (500 MHz, $CDCl_3$) $\delta$ = 8.60 (d, *J* = 9.1 Hz, 1H), 8.01 (d, *J* = 9.1 Hz, 1H), 7.91 (d, *J* = 8.1 Hz, 1H), 7.83 (d, *J* = 8.9 Hz, 1H), 7.75 (d, *J* = 8.7 Hz, 1H), 7.40 (t, *J* = 8.5, 7.4 Hz, 1H), 7.23 (t, *J* = 9.0, 8.2 Hz, 1H), 7.19 (t, *J* = 8.5, 7.4 Hz, 1H), 7.17 (d, *J* = 9.0 Hz, 1H), 7.14 (t, *J* = 8.7, 7.4, 1H), 7.10 (d, *J* = 8.4, 1H), 6.80 (d, *J* = 8.4, 1H), 6.66 (s, 1H), 6.57 (s, 2H), 6.49 (s, 1H), 6.10 (s, 1H), 3.70 (br s, 1H), 3.26 (br s, 1H), 2.13 (s, 6H), 1.00 (d, *J* = 6.2 Hz, 3H), 0.97 (d, *J* = 6.2 Hz, 3H), **$^{13}$C NMR** (126 MHz, $CDCl_3$) [overlapping signals]$\delta$ = 153.49, 143.80, 138.95, 136.64, 135.91,

133.69, 132.79, 130.76, 130.15, 129.24, 128.13, 128.05, 127.22, 127.02, 126.93, 126.65, 125.20, 124.63, 123.42, 122.05, 120.51, 119.35, 114.65, 110.54, 44.53, 23.14, 23.07, 21.20. **IR** (solid) *v* = 3338, 3054, 2963, 2918, 2507, 2160, 2034, 1658, 1617, 1596, 1564, 1499, 1424, 1272, 1248, 1213, 1173, 1147, 1017, 950, 808, 773, 744, 687 $cm^{-1}$; **mp** 114–115 °C; **HRMS** (ESI+) m/z calculated for $C_{32}H_{32}N_3O$ $(M+H)^+$ 474.25399, found 474.25365; $[\alpha]_D^{25}$ = -94.3 (c 0.5, $CHCl_3$).

(*S*)-1-(2'-(isopropylamino)-[1,1'-binaphthalen]-2-yl)-3-phenylurea (**5k**)

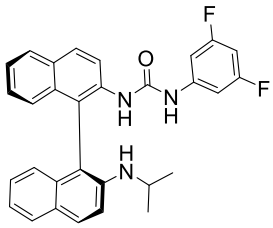


**5k**

In a flame-dried Schlenk under inert atmosphere, (*S*)-*N*$^2$-isopropyl-[1,1'-binaphthalene]-2,2'-diamine **5e** (80 mg, 0.25 mmol, 1 equiv.) was dissolved in dry DCM (0.5 M) and phenyl isocyanate (1 equiv.) was added dropwise. The mixture was stirred 4 hours at room temperature. After removal of the solvent under reduced pressure, the crude mixture was directly purified by column chromatography ($CHCl_3$:hexane:$Et_2O$ 1:1:0.04) to afford the desired products as a white solid, 100 mg, 92 % yield. **$^1$H NMR** (600 MHz, $CDCl_3$) $\delta$ = 8.60 (d, *J* = 8.9 Hz, 1H), 8.00 (d, *J* = 9.1 Hz, 1H), 7.90 (d, *J* = 8.2 Hz, 1H), 7.83 (d, *J* = 9.0 Hz, 1H), 7.77 (d, *J* = 8.1 Hz, 1H), 7.38 (t, *J* = 8.1, 1H), 7.25–7.17 (m, 2H), 7.16–7.12 (m, 2H), 7.09 (d, *J* = 8.7 Hz, 1H), 7.07–6.93 (m, 3H), 6.87–6.71 (m, 3H), 6.59 (s, 1H), 6.12 (s, 1H), 3.88–3.50 (m, 1H), 3.21 (s, 1H), 0.93 (d, *J* = 8.1 Hz, 3H), 0.92 (d, *J* = 8.1, 3H), **$^{13}$C NMR** (150 MHz, $CDCl_3$) [overlapping signals] $\delta$ = 153.25, 144.05, 137.05, 135.86, 133.91, 132.93, 130.95, 130.37, 129.46, 129.42, 128.29, 128.25, 127.57, 127.28, 126.86, 125.34, 124.95, 124.85, 123.55, 122.32, 120.51, 119.58, 115.03, 110.70, 44.65, 23.22, 23.17; **IR** (solid) *v* = 3301, 3052, 2970, 2969, 2161, 1647, 1618, 1598, 1544, 1496, 1441, 1424, 1385, 1358, 1335, 1309, 1298, 1242, 1176, 1149, 1086, 1023, 969, 902, 867, 832,

807, 771, 747, 735, 692, 629 $cm^{-1}$; **mp** 220–222 ˚C; **HRMS** (ESI+) m/z calculated for $C_{30}H_{28}N_3O$ $(M+H)^+$ 446.22269, found 446.22226; $[\alpha]_D^{25}$ = -104.2 (c 0.3, $CHCl_3$).

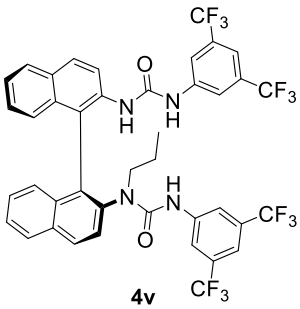
(*S*)-1-(3,5-difluorophenyl)-3-(2'-(isopropylamino)-[1,1'-binaphthalen]-2-yl)urea (**5l**)



**5l**

In a flame-dried Schlenk under inert atmosphere, (*S*)-$N^2$-isopropyl-[1,1'-binaphthalene]-2,2'-diamine **5e** (100 mg, 0.3 mmol, 1 equiv.) was dissolved in dry DCM (0.3 M) and 3,5-difluorophenyl isocyanate (1.0 equiv.) was added dropwise. The mixture was stirred 16 hours at room temperature. After removal of the solvent under reduced pressure, the crude mixture was directly purified by column chromatography (1st hexane:EtOAc 80:20; 2nd $CHCl_3$:hexane:$Et_2O$ 1:1:0.01) to afford the desired products as a white solid in 60 % yield. **$^1$H NMR** (500 MHz, $CDCl_3$) $\delta$ = 8.36 (d, *J* = 9.1 Hz, 1H), 8.01 (d, *J* = 9.2, 1H), 7.93 (d, *J* = 8.1 Hz, 1H), 7.88 (d, *J* = 9.0 Hz, 1H), 7.75 (d, *J* = 7.8, 1H), 7.43 (t, *J* = 8.6, 7.3 Hz, 1H), 7.29–7.23 (m, 2H), 7.20–7.10 (m, 3H), 6.83 (d, *J* = 8.0 Hz, 1H), 6.68 (s, 1H), 6.66–6.62 (m, 2H), 6.60 (s, 1H), 6.42 (tt, *J* = 8.9, 3.0 Hz, 1H), 3.82–3.72 (m, 1H), 3.31 (d, *J* = 8.5 Hz, 1H), 1.01 (d, *J* = 6.3 Hz, 3H), 0.97 (d, *J* = 6.3 Hz, 3H), **$^{19}$F NMR** (471 MHz, $CDCl_3$) $\delta$ = -108.69 (t, *J* = 8.4 Hz), **$^{13}$C NMR** (126 MHz, $CDCl_3$) $\delta$ = 163.2 (dd, *J* = 247.0, 14.8 Hz), 152.44, 144.08, (t, *J* = 13.7 Hz), 140.32 (t, *J* = 13.4 Hz), 135.28, 133.89, 132.83, 131.18, 130.46, 129.49, 128.31, 128.26, 127.39, 127.33, 126.98, 125.41, 125.19, 123.47, 122.33, 120.55, 115.04, 110.67, 103.18 (d, *J* = 29.8 Hz), 98.95 (t, *J* = 26.1 Hz), 44.63, 23.24, 23.04; **IR** (liquid film) *v* = 3330, 3115, 3056, 2966, 1693, 1662, 1614, 1597, 1569, 1479, 1425, 1383, 1350, 1295, 1264, 1233, 1208, 1171, 1114, 1006, 984, 957, 846, 835, 811, 780, 774, 717, 669, 646, 623 $cm^{-1}$; **mp** 233–235 °C; **HRMS** (ESI+) m/z calculated for $C_{30}H_{26}N_3OF_2$ $(M+H)^+$ 482.2038, found 482.2029; $[\alpha]_D^{25}$ = -118.1 (c 0.3, $CHCl_3$).

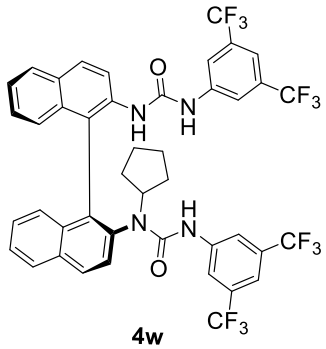
(S)-3-(3,5-bis(trifluoromethyl)phenyl)-1-(2'-(3-(3,5-bis(trifluoromethyl)phenyl)ureido)-[1,1'-binaphthalen]-2-yl)-1-propylurea (**4v**)



**4v**

In a flame-dried Schlenk under inert atmosphere, **5h** (1 equiv.) was dissolved in dry DCM (0.3 M) and 3,5-bis(trifluoromethyl)phenyl isocyanate (2 equiv.) was added dropwise. The mixture was stirred at reflux for 48 hours. After removal of the solvent under reduced pressure, the crude mixture was directly purified by column chromatography (pentane:$Et_2O$ 80:20) to afford the desired products as a white solid in 47 % yield. **$^1$H NMR** (500 MHz, DCM-$d_2$) $\delta$ = 8.49 (br s, 1H), 8.13 (d, *J* = 8.8 Hz, 1H), 8.05 (d, *J* = 9.1 Hz, 1H), 8.01 (d, *J* = 8.2 Hz, 1H), 7.96 (d, *J* = 8.2 Hz, 1H), 7.86 (s, 2H), 7.65 (s, 2H), 7.58 (d, *J* = 8.7 Hz, 1H), 7.56–7.49 (m, 2H), 7.46–7.36 (m, 2H), 7.35–7.16 (m, 2H), 7.12 (s, 1H), 7.08 (d, *J* = 8.6 Hz, 1H), 6.93 (d, *J* = 8.5 Hz, 1H), 6.85 (s, 1H), 3.10 (br m, 1H), 2.96 (br m, 1H), 1.56 (br m, 1H), 1.26 (br m, 1H), 0.58 (t, *J* = 7.3 Hz, 3H), **$^{19}$F NMR** (471 MHz, DCM-$d_2$) $\delta$ = -63.56 (s), -63.54 (s), **$^{13}$C NMR** (150 MHz, DCM-$d_2$) [overlapping signals] $\delta$ = 156.22, 152.05, 140.64, 140.09, 139.58, 135.91, 134.07, 133.72, 133.58, 132.38 (q, *J*= 33 Hz), 132.15 (q, *J*= 33 Hz), 131.68, 130.86, 130.81, 130.09, 128.92, 128.64, 128.50, 126.81, 125.36, 125.19, 123.67 (q, *J*= 272 Hz), 123.44 (q, *J*= 272 Hz), 120.80, 120.44, 118.52, 117.52, 116.10, 51.54, 21.91, 11.34; **IR** (liquid film) v = 3464, 3368, 2969, 1611, 1591, 1508, 1490, 1461, 1424, 1382, 1349, 1316, 1287, 1245, 1212, 1168, 1145, 1123, 1029, 958, 909, 821, 771, 747, 686, 621 cm$^{-1}$; **HRMS** (ESI+) m/z calculated for $C_{41}H_{29}N_4O_2F_{12}$ $(M+H)^+$ 837.20934, found 837.20751; $[\boldsymbol{\alpha}]_{\mathbf{D}}^{\mathbf{25}}$ = -71.4 (c 0.2, $CHCl_3$).

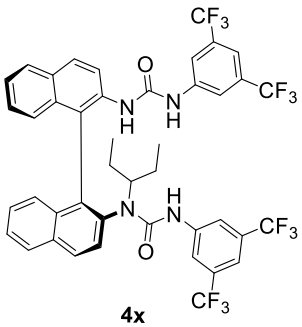
(*S*)-3-(3,5-bis(trifluoromethyl)phenyl)-1-(2'-(3-(3,5-bis(trifluoromethyl)phenyl)ureido)-[1,1'-binaphthalen]-2-yl)-1-(pentan-3-yl)urea (**4w**)



**4w**

In a flame-dried Schlenk under inert atmosphere, **5f** (1 equiv.) was dissolved in dry DCM (0.3 M) and 3,5-bis(trifluoromethyl)phenyl isocyanate (2 equiv.) was added dropwise. The mixture was stirred at reflux for 48 hours. After removal of the solvent under reduced pressure, the crude mixture was directly purified by column chromatography (1st hexane:EtOAc 90:10; 2nd $CHCl_3$ isocratic) to afford the desired products as a white solid in 90 % yield. **$^1$H NMR** (500 MHz, DCM-$d_2$) $\delta$ = 8.52 (d, *J* = 9.1 Hz, 1H), 8.14 (d, *J* = 8.7 Hz, 1H), 8.03 (d, *J* = 9.2 Hz, 1H), 8.02 (d, *J* = 8.3 Hz,1H), 7.93 (d, *J* = 8.1 Hz, 1H), 7.83 (s, 2H), 7.63 (br s, 1H), 7.60 (s, 2H), 7.55 (t, *J* = 8.1 Hz, 1H), 7.54 (t, *J* = 8.8 Hz, 1H), 7.50 (s, 1H), 7.39 (s, 1H), 7.38 (t, *J* = 8.8 Hz, 1H), 7.31 (ddd, *J* = 8.2, 6.8, 1.3 Hz, 1H), 7.21 (t, *J* = 7.8 Hz, 1H), 7.17 (d, *J* = 8.7 Hz 1H), 7.12 (s, 1H), 6.87 (d, *J* = 8.5 Hz, 1H), 6.80 (s, 1H), 3.83 (t, *J* = 8.5 Hz, 1H), 1.72 (m, 1H), 1.36 (s, 2H), 1.15 (s, 3H), 0.96–0.74 (m, 2H), **$^{19}$F NMR** (471 MHz, $CDCl_3$) $\delta$ = -63.52 (s), -63.54 (s), **$^{13}$C NMR** (126 MHz, DCM-$d_2$) [overlapping signals] $\delta$ = 156.26, 151.49, 140.20, 139.59, 139.37, 135.84, 133.64, 133.22, 133.13, 132.31, 132.00 (q, *J* = 33 Hz), 131.65 (q, *J* = 33 Hz), 130.51, 130.23, 129.59, 128.46, 128.42, 128.15, 127.29, 127.14, 126.81, 126.59, 125.49, 124.48, 123.20 (q, *J* = 273 Hz), 123.08 (q, *J* = 273 Hz) 120.37, 119.64, 117.95, 117.08, 115.56, 61.53, 30.46, 30.28, 23.88, 23.34; **IR** (liquid film) *v* = 3340, 3061, 2955, 2873, 1691, 1637, 1621, 1602, 1542, 1507, 1473, 1440, 1386, 1173, 1339, 1277, 1170, 1130, 950, 883, 846, 750, 682, 625 cm$^{-1}$; **mp** 130–131 °C; **HRMS** (ESI+) m/z calculated for $C_{43}H_{31}N_4O_2F_{12}$ $(M+H)^+$ 863.22499, found 863.22415; $[\alpha]_D^{25}$ **=** -15.7 (c 0.3, $CHCl_3$).

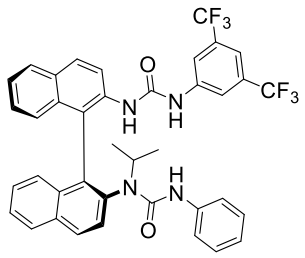
(*S*)-3-(3,5-bis(trifluoromethyl)phenyl)-1-(2'-(3-(3,5-bis(trifluoromethyl)phenyl)ureido)-[1,1'-binaphthalen]-2-yl)-1-(pentan-3-yl)urea (**4x**)



**4x**

In a flame-dried Schlenk under inert atmosphere, **5g** (1 equiv.) was dissolved in dry DCM (0.25 M) and 3,5-bis(trifluoromethyl)phenyl isocyanate (2 equiv.) was added dropwise. The mixture was stirred at reflux for 48 hours. After removal of the solvent under reduced pressure, the crude mixture was directly purified by column chromatography (1st hexane:EtOAc 100:5; 2nd $CHCl_3$ isocratic) to afford the desired products as a white solid in 41 % yield. **$^1$H NMR** (500 MHz, DCM-$d_2$) $\delta$ = 8.49 (d, *J* = 8.6 Hz, 1H), 8.11 (d, *J* = 8.7 Hz, 1H), 8.06 (d, *J* = 9.1 Hz, 1H), 7.99 (d, *J* = 8.2 Hz, 1H), 7.97 (d, *J* = 8.6 Hz, 1H), 7.84 (s, 2H), 7.72–7.59 (m, 4H), 7.53 (t, *J* = 8.4 Hz, 1H), 7.52 (s, 1H), 7.43 (t, *J* = 7.4 Hz, 1H), 7.40 (s, 1H), 7.29–7.26 (m, 2H), 7.12 (s, 1H), 7.10 (d, *J* = 8.5 Hz, 1H), 6.99 (d, *J* = 8.4 Hz, 1H), 6.87 (s, 1H), 3.08–2.92 (m, 1H), 1.87–1.70 (m, 1H), 1.70–1.59 (m, 1H), 1.54–1.35 (m, 1H), 0.95 (t, *J* = 7.4 Hz, 3H), 0.58–0.44 (m, 1H), -0.18 (t, *J* = 7.5 Hz, 3H), **$^{19}$F NMR** (471 MHz, DCM-$d_2$) $\delta$ = -63.53 (s), -63.54 (s), **$^{13}$C NMR** (151 MHz, DCM-$d_2$) [overlapping signals] $\delta$ = 156.31, 152.06, 142.50, 140.62, 140.02, 135.99, 134.06, 133.58, 133.42, 132.44 (q, *J* = 33.5 Hz), 132.10 (q, *J* = 33.5 Hz), 131.15, 131.02, 130.55, 130.21, 129.03, 128.90, 128.55, 127.63, 127.44, 127.06, 123.66 (q, *J* = 272.1), 123.46 (q, *J* = 273.3), 124.56, 124.38, 122.75, 122.57, 120.58, 118.46, 117.46, 116.04, 67.20, 28.73, 26.58, 12.88, 11.03; **IR** (liquid film) *v* = 3365, 3063, 2972, 2880, 1690, 1621, 1542, 1507, 1473, 1440, 1385, 1339, 1277, 1179, 1130, 882, 844, 822, 749, 725, 701, 682 cm$^{-1}$; **mp** 127–129 ˚C; **HRMS** (ESI+) m/z calculated for $C_{43}H_{33}N_4O_2F_{12}$ $(M+H)^+$ 865.24064, found 865.23976; $[\boldsymbol{\alpha}]_{\mathbf{D}}^{\mathbf{25}}$ = -59.7 (c 0.5, $CHCl_3$)

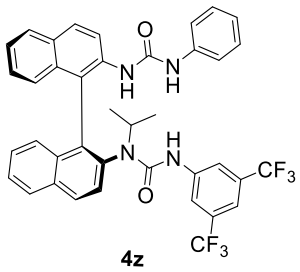
(*S*)-1-(2'-(3-(3,5-bis(trifluoromethyl)phenyl)ureido)-[1,1'-binaphthalen]-2-yl)-1-isopropyl-3-phenylurea (**4y**)



**4y**

In a flame-dried Schlenk under inert atmosphere, **5i** (1 equiv.) was dissolved in dry DCM (0.3 M) and phenyl isocyanate (1.5 equiv.) was added dropwise. The mixture was stirred at reflux for 16 hours. The crude was diluted with methanol (2 ml) and the solvent removed under reduced pressure, the crude mixture was directly purified by column chromatography (1st hexane:EtOAc 80:20; 2nd $CHCl_3$:hexane:$Et_2O$ 1:1:0.01) to afford the desired products as a white solid in 38 % yield. **$^1$H NMR** (500 MHz, DCM-$d_2$,) $\delta$ = 8.67 (d, *J* = 9.2 Hz, 1H), 8.11 (dd, *J* = 8.8, 0.8 Hz, 2H), 8.01 (d, *J* = 9.2 Hz, 2H), 7.97 (s, 1H), 7.92 (dd, *J* = 8.4, 1.1 Hz, 2H), 7.77 (s, 1H), 7.59 (d, *J* = 1.6 Hz, 2H), 7.58–7.50 (m, 2H), 7.41–7.17 (m, 6H), 7.12 (d, *J* = 8.6, 1H), 7.07–7.01 (m, 1H), 6.87 (dd, *J* = 8.5, 1.1 Hz, 1H), 6.63 (s, 1H), 3.74 (p, *J* = 6.9 Hz, 1H), 0.93 (d, *J* = 6.9 Hz, 3H), 0.74 (d, *J* = 6.9 Hz, 3H), **$^{19}$F NMR** (471 MHz, DCM-$d_2$) $\delta$ = -63.25 (s), **$^{13}$C NMR** (126 MHz, DCM-$d_2$) $\delta$ = 157.60, 152.03, 141.07, 140.68, 137.73, 136.88, 134.22, 133.84, 133.55, 132.36, 131.89 (q, *J* = 33.0 Hz), 130.50, 130.22, 129.90, 129.47, 129.39, 128.76, 128.45, 127.44, 127.23, 127.13, 125.77, 125.28, 124.42, 123.79 (q, *J* = 273.0 Hz), 122.37, 119.06, 118.85, 118.28, 115.80–114.99 (m), 52.52, 21.06, 21.00; **IR** (solid) *v* = 3327, 3061, 2358, 2160, 2016, 1717, 1618, 1594, 1560, 1527, 1506, 1473, 1442, 1386, 1338, 1275, 1236, 1174, 1128, 1059, 948, 928, 879, 820, 748, 732, 691, 680, 633 $cm^{-1}$; **mp** 136–139 ˚C; **HRMS** (ESI+) m/z calculated for $C_{39}H_{31}N_4O_2F_6$ $(M+H)^+$ 701.23457, found 701.23391; $[\alpha]_D^{25}$ = +9.2 (c 0.3, $CHCl_3$).

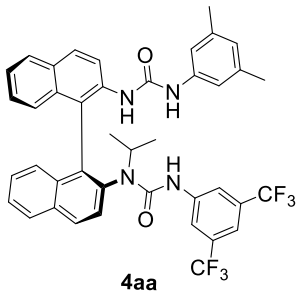
(*S*)-3-(3,5-bis(trifluoromethyl)phenyl)-1-isopropyl-1-(2'-(3-phenylureido)-[1,1'-binaphthalen]-2-yl)urea (**4z**)



**4z**

In a flame-dried Schlenk under inert atmosphere, **5k** (1 equiv.) was dissolved in dry DCM (0.3 M) 3,5bis-(trifluoromethyl)phenyl isocyanate (1.0 equiv.). The mixture was stirred at reflux for 24 hours. The crude was diluted with methanol (2 ml) and the solvent removed under reduced pressure, the crude mixture was directly purified by column chromatography (1st hexane:EtOAc 90:10; 2nd $CHCl_3$:hexane:$Et_2O$ 1:1:0.05) to afford the desired products as a white solid in 77% yield. **$^1$H NMR** (600 MHz, $CDCl_3$, 315 K) $\delta$ = 8.54 (d, *J* = 9.2 Hz, 1H), 8.10 (d, *J* = 8.8, 0.8 Hz, 2H), 8.00 (d, *J* = 9.2 Hz, 2H), 7.99 (d, *J* = 8.3 Hz, 1H), 7.89 (d, *J* = 8.2 Hz, 1H), 7.75 (br s, 2H), 7.56 (t, *J* = 7.5 Hz, 1H), 7.50 (d, *J* = 8.7 Hz, 1H), 7.44 (s, 1H), 7.37–7.29 (m, 2H), 7.23 (d, *J* = 8.7 Hz, 1H), 7.20–7.14 (m, 1H), 7.06–6.99 (m, 2H), 6.98–6.84 (br m, 4H), 6.60 (br s, 2H), 3.48 (br s, 1H), 1.05 (br s, 3H), 0.74 (br s, 3H), **$^{19}$F NMR** (471 MHz, $CDCl_3$, 315 K ) $\delta$ = -62.98 (s), **$^{13}$C NMR** (151 MHz, $CDCl_3$, 323 K) [overlapping signals] $\delta$ = 154.86, 152.77, 140.44, 140.07, 137.82, 136.21, 134.03, 133.35, 132.46 (q, *J* = 33.0 Hz), 132.29, 130.84, 130.77, 130.58, 129.95, 128.97, 128.74, 128.46, 127.92, 127.87, 127.48, 126.95, 125.06, 124.70, 123.76, 123.29 (q, *J* = 273.0 Hz), 120.75, 120.60, 120.27, 119.83, 116.85, 54.50, 20.68, 20.62; **IR** (liquid film) *v* = 3351, 3058, 2934, 2367, 1686, 1620, 1597, 1542, 1498, 1473, 1441, 1384, 1338, 1311, 1278, 1246, 1179, 1133, 1034, 934, 883, 842, 819, 750, 698, 682, 632, 617 $cm^{-1}$; **mp** 131–134 °C; **HRMS** (ESI+) m/z calculated for $C_{39}H_{31}N_4O_2F_6$ $(M+H)^+$ 701.23457, found 701.23419; $[\alpha]_D^{25}$ = -45.6 (c 0.3, $CHCl_3$).

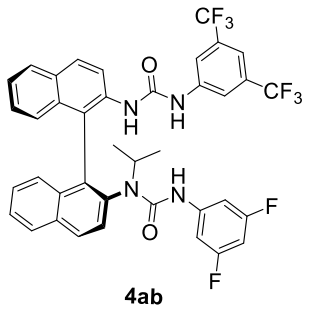
(*S*)-3-(3,5-bis(trifluoromethyl)phenyl)-1-(2'-(3-(3,5-dimethylphenyl)ureido)-[1,1'-binaphthalen]-2-yl)-1-isopropylurea (**4aa**)



**4aa**

In a flame-dried Schlenk under inert atmosphere, **5j** (1 equiv.) was dissolved in dry DCE (0.4 M) and 3,5-bis(trifluoromethyl)phenyl isocyanate (1.5 equiv.) was added dropwise. The mixture was stirred at 70 ˚C for 36 hours. After removal of the solvent under reduced pressure, the crude mixture was directly purified by column chromatography (DCM:$Et_2O$ 100:5) to afford the desired products as a white solid in 60 % yield. **$^1$H NMR** (500 MHz, $CDCl_3$, 323 K) $\delta$ = 8.50 (d, *J* = 9.2 Hz, 1H), 8.08 (d, *J* = 8.5 Hz, 1H), 8.00 (d, *J* = 9.4 Hz, 1H), 7.98 (d, *J* = 8.8 Hz, 1H), 7.89 (d, *J* = 8.3 Hz, 1H), 7.89 (d, *J* = 8.3 Hz, 1H), 7.74 (s, 2H), 7.55 (t, *J* = 7.6 Hz, 1H), 7.50 (d, *J* = 8.8 Hz, 1H), 7.44 (s, 1H), 7.32 (t, *J* = 7.5 Hz, 1H) 7.32 (t, *J* = 8.0 Hz, 1H), 7.22 (d, *J* = 8.3 Hz, 1H), 7.15 (br t, 1H), 6.87 (d, *J* = 8.6 Hz, 1H), 6.75 (br s, 1H), 6.56 (br s, 3H), 6.38 (br s, 1H), 3.46 (br s, 1H), 2.11 (s, 6H), 1.06 (d, *J* = 6.0 Hz, 3H), 0.80 (br s, 3H); **$^{19}$F NMR** (470 MHz, $CDCl_3$, 323 K) $\delta$ = -63.01 (s), **$^{13}$C NMR** (151 MHz, $CDCl_3$, 323 K) [overlapping signals] $\delta$ = 154.67 (br s), 152.88, 140.41, 140.16, 138.72, 136.20, 133.95, 133.30 (br s), 133.27, 132.43 (q, *J* = 32.9 Hz), 132.37, 132.31, 130.82, 130.63, 129.94, 128.76, 128.44, 127.87, 127.80, 127.46, 126.94, 126.89 (br s), 125.01, 124.71, 123.35 (q, *J* = 272.1 Hz), 121.03, 120.82, 119.72, 116.68, 54.64 (br s), 21.22, 20.60; **IR** (powder) ν = 3356, 3063, 2973, 2359, 1686, 1636, 1617, 1599, 1539, 1505, 1473, 1435, 1384, 1337, 1278, 1179, 113, 883, 841, 819, 749 cm$^{-1}$; **mp** 138–140 ˚C; **HRMS** (ESI+) m/z calculated for $C_{41}H_{35}N_4O_2F_6$ $(M+H)^+$ 729.26587, found 729.26527; $[\boldsymbol{\alpha}]_{\mathbf{D}}^{\mathbf{25}}$= -14.8 (c 0.3, $CHCl_3$).

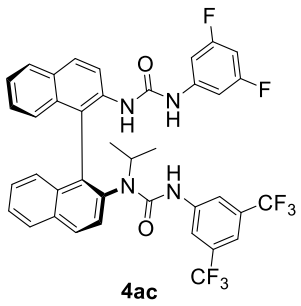
(*S*)-1-(2'-(3-(3,5-bis(trifluoromethyl)phenyl)ureido)-[1,1'-binaphthalen]-2-yl)-3-(3,5-difluorophenyl)-1-isopropylurea (**4ab**)



**4ab**

In a flame-dried Schlenk under inert atmosphere, **5i** (1 equiv.) was dissolved in dry DCM (0.14 M) and 3,5-bisfluorophenyl isocyanate (1.0 equiv.) was added dropwise. The mixture was stirred at reflux for 72 hours. The crude was diluted with methanol (2 ml) and the solvent removed under reduced pressure, the crude mixture was directly purified by column chromatography (1st hexane:EtOAc 80:20; 2nd hexane:$CHCl_3$ 30:70 to 0:100, 3rd $CHCl_3$:hexane:$Et_2O$ 1:1:0.05) to afford the desired products as a white solid in 30 % yield. **$^1$H NMR** (600 MHz, DCM-$d_2$) $\delta$ = 8.61 (d, *J* = 9.1 Hz, 1H), 8.12 (d, *J* = 8.8, 1H), 8.02 (d, *J* = 8.9 Hz, 1H), 8.01 (d, *J* = 7.4 Hz, 1H), 7.92 (d, *J* = 8.16, Hz, 1H), 7.69 (s, 2H), 7.64 (br s, 1H), 7.54 (d, *J* = 7.4 Hz, 1H), 7.53 (d, *J* = 8.8 Hz, 1H) 7.48 (br s, 1H), 7.41 (s, 1H), 7.46 (t, *J* = 7.4 Hz, 1H), 7.29 (t, *J* = 7.7 Hz, 1H), 7.2 (t, *J* = 7.7 Hz, 1H), 7.14 (d, *J* = 8.4, 1H), 6.96 (d, *J* = 7.3 Hz, 2H), 6.86 (d, *J* = 8.7 Hz, 1H), 6.65 (br s, 1 H), 6.45 (t, *J* = 8.8 Hz, 1H) 3.66 (p, *J* = 6.9 Hz, 1H), 0.95 (d, *J* = 6.9 Hz, 3H), 0.67 (br d, *J* = 6.9 Hz, 3H), **$^{19}$F NMR** (471 MHz, $CDCl_3$) $\delta$ = -63.47 (s), -109.50 ( br s), **$^{13}$C NMR** (150 MHz, DCM-$d_2$) $\delta$ = 163.50 (dd, *J* = 246.0, 14.9 Hz), 156.46, (br s) 152.00, 140.89, 140.59 (t, *J* = 13.5 Hz), 140.44, 136.51, 134.23, 133.73 , 133.60, 132.25, 132.15 (q, *J* = 33.0 Hz), 130.71, 130.49, 130.04, 129.05, 128.82, 128.54, 127.57, 127.28, 127.28, 125.67, 124.71, 123.74 (q, *J* = 273.0 Hz), 119.84 (br s), 119.54 , 118.33, 115.80 (br m), 104.02 (d, *J* = 29.9), 99.52 (t, *J* = 25.5 Hz), 53.19, 21.09, 20.88; **IR** (liquid film) *v* = 3341, 3060, 2969, 2930, 1717, 1688, 1620, 1604, 1534, 1507, 1475, 1439, 1386, 1338, 1277, 1237, 1177, 1134, 1060, 1019, 998, 976, 948, 929, 881, 844, 821, 750, 724 $cm^{-1}$; **mp** 126 – 127 ˚C; **HRMS** (ESI+) m/z calculated for $C_{39}H_{29}N_4O_2F_8$ $(M+H)^+$ 737.21573, found 737.21547; $[\alpha]_D^{25}$ = -16.5 (c 0.1, $CHCl_3$).

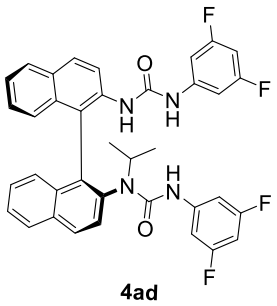
(*S*)-3-(3,5-bis(trifluoromethyl)phenyl)-1-(2'-(3-(3,5-difluorophenyl)ureido)-[1,1'-binaphthalen]-2-yl)-1-isopropylurea (**4ac**)



**4ac**

In a flame-dried Schlenk under inert atmosphere, **5l** (1 equiv.) was dissolved in dry DCM (0.3 M) and 3,5-bis(trifluoromethyl)phenyl isocyanate (1 equiv.) was added dropwise. The mixture was stirred at reflux for 48 hours. The crude was diluted with methanol (2 ml) and the solvent removed under reduced pressure, the crude mixture was directly purified by column chromatography (1$^{st}$ hexane:EtOAc 90:10; 2$^{nd}$ $CHCl_3$:hexane:$Et_2O$ 1:1:0.01) to afford the desired products as a white solid in 74% yield. **$^{1}$H NMR** (600 MHz, DCM-$d_2$) $\delta$ = 8.50 (d, *J* = 9.0 Hz, 1H), 8.14 (d, *J* = 8.8, 0.8 Hz, 1H), 8.02 (d, *J* = 9.2 Hz, 2H), 7.92 (d, *J* = 8.0 Hz, 1H), 7.83 (s, 2H), 7.56 (d, *J* = 8.5 Hz, 1H), 7.55 (t, *J* = 6.5 Hz, 1H), 7.51 (s, 1H), 7.39 (t, *J* = 7.4 Hz, 1H), 7.31 (t, *J* = 8.0 Hz, 1H) 7.22 (t, *J* = 7.7 Hz, 1H), 7.16 (d, *J* = 8.4 Hz, 1H), 6.99 (br s, 1H), 6.87 (d, *J* = 8.4 Hz, 1H), 6.78 (br s, 1H), 6.64 (d, *J* = 8.1 Hz, 2H), 6.33 (t, *J* = 8.6 Hz, 2H), 3.62 (br m, 1H), 1.00 (d, *J* = 6.3 Hz, 3H), 0.74 (br s, 3H), **$^{19}$F NMR** (565 MHz, DCM-$d_2$) $\delta$ = -63.37 (s), -110.62 (br s), **$^{13}$C NMR** (151 MHz, DCM-$d_2$) [overlapping peaks] $\delta$ = 163.4 (dd, *J* = 246.0, 15.3 Hz), 162.80 (d, *J* = 245.0), 155.64 (br s), 151.49, 140.94 (t, *J* = 13.7 Hz), 139.93, 139.63, 135.86, 133.77, 133.25, 133.20, 131.98 (q, *J* = 32.9 Hz), 131.85, 130.43, 130.21, 129.64, 128.42, 128.37, 128.18, 127.28, 127.15, 126.90, 126.77, 125.20, 124.43, 123.20 (q, *J* = 273.0 Hz), 120.32, 120.07 (br s), 119.78, 116.99, 101.08 (d, *J* = 26.8 Hz), 97.34 (t, *J* = 26.0 Hz), 20.56, 20.30; **IR** (solid) *v* = 3358, 2980, 2161, 2034, 1687, 1601, 1534, 1506, 1478, 1436, 1378, 1336, 1313, 1277, 1223, 1179, 1336, 1277, 1223, 1179, 1132, 1115, 1034, 957, 883, 840, 819, 784, 748, 699, 681, 626 cm$^{-1}$; **mp** 131–134 ˚C; **HRMS** (ESI+) m/z calculated for $C_{39}H_{29}N_4O_2F_8$ $(M+H)^+$ 737.21573, found 737.21545; $[\alpha]_D^{25}$ = -65.6 (c 0.3, $CHCl_3$).

(*S*)-3-(3,5-difluorophenyl)-1-(2'-(3-(3,5-difluorophenyl)ureido)-[1,1'-binaphthalen]-2-yl)-1-isopropylurea (**4ad**)



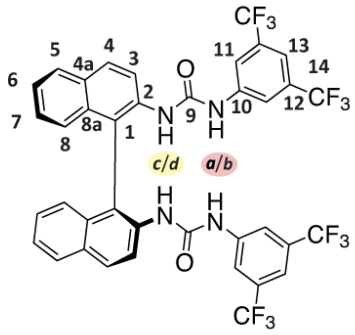
**4ad**

In a flame-dried Schlenk under inert atmosphere, (*S*)-$N^2$-isopropyl-[1,1'-binaphthalene]-2,2'-diamine **5e** (1 equiv.) was dissolved in dry DCM (0.3 M) and 3,5-difluorophenyl isocyanate (2 equiv.) was added dropwise. The mixture was stirred at reflux for 96 hours. The crude was diluted with methanol (2 ml) and the solvent removed under reduced pressure, the crude mixture was directly purified by column chromatography (1$^{st}$ hexane:EtOAc 80:20; 2$^{nd}$ $CHCl_3$:hexane:$Et_2O$ 1:1:0.05) to afford the desired products as a white solid in 41 % yield. **$^1$H NMR** (500 MHz, DCM-$d_2$) $\delta$ = 8.59 (d, *J* = 9.2 Hz, 1H), 8.12 (d, *J* = 8.7 Hz, 1H), 8.01 (d, *J* = 8.1, 1H), 8.00 (d, *J* = 9.1 Hz, 1H), 7.91 (d, *J* = 8.1 Hz, 1H), 7.57 (br s, 1H), 7.53 (t, *J* = 7.13 Hz, 1H), 7.52 (d, *J* = 8.7 Hz, 1H), 7.37 (ddd, *J* = 8.1, 6.8, 1.2 Hz, 1H), 7.30 (m, 2H), 7.21 (ddd, *J* = 8.3, 6.8, 1.3 Hz, 1H), 7.13 (d, *J* = 8.5 Hz, 1H), 6.99 (d, *J* = 8.1 Hz, 2H), 6.85 (d, *J* = 8.5 Hz, 1H), 6.83–6.76 (m, 2H), 6.64 (s, 1H), 6.58–6.44 (tt, *J* = 9.1, 2.4 Hz, 1H), 6.37 (tt, *J* = 9.1, 2.4 Hz, 1H), 3.64 (p, *J* = 6.9 Hz, 1H), 0.96 (d, *J* = 6.9 Hz, 3H), 0.66 (d, *J* = 6.9 Hz, 3H), **$^{19}$F NMR** (471 MHz, DCM-$d_2$) $\delta$ = -108.50 (br s), -109.94 (br s), **$^{13}$C NMR** (151 MHz, DCM-$d_2$) $\delta$ = 163.58 (dd, *J* = 246.0, 15.1 Hz), 163.48 (dd, *J* = 246.0, 15.1 Hz), 156.28, 152.01, 141.62 (t, *J* = 13.7 Hz), 140.72 (t, *J* = 13.4 Hz), 140.52, 136.62, 134.20, 133.72, 133.60, 132.28, 130.75, 130.42, 128.96, 128.80, 128.54, 127.56, 127.44, 127.21, 127.20, 125.63, 124.64, 119.70, 119.60, 103.85 (d, *J* = 26.5 Hz), 102.00 (d, *J* = 26.5 Hz), 99.37 (t, *J* = 25.7 Hz), 97.67 (t, *J* = 25.9 Hz), 53.21, 21.00, 20.87; **IR** (solid) *v* = 3350, 3061, 2918, 2031, 1686, 1604, 1536, 1507, 1480, 1435, 1337, 1312, 1282, 1224, 1201, 1189, 1163, 1115, 998, 984, 821, 750, 699, 670, 638 $^{-1}$; **mp** 135–137 ˚C; **HRMS** (ESI+) m/z calculated for $C_{37}H_{29}N_4O_2F_4$ $(M+H)^+$ 637.22212, found 637.22205; $[\alpha]_D^{25}$ = -56.6 (c 0.3, $CHCl_3$).

*4.3.2 NMR characterisation of BINAM Urea (**4a**) and iPr BINAM Urea (**4u**)*

NMR spectra of BINAM Urea (**4a**) and iPr BINAM Urea (**4u**) were recorded on an AVIII HD 500 or an AVIII HD 600 at room temperature, the samples were prepared at 25 mM concentration in DCM-$d_2$, unless otherwise stated.

*4.3.2.1 BINAM Urea (**4a**) – assignment and copy of NMR spectra*




Scheme 4.1: Structure and numbering of **4a**.

Table 4.3: Assignment chart of **4a** (500 MHz, DCM-$d_2$, 25 mM for $^{1}$H and $^{19}$F NMR, 40 mM for $^{13}$C and $^{15}$NMR 298K).

| $^{1}$H | δ [ppm] | Multiplicity $^{n}J_{HH}$ [Hz] | $^{13}$C | δ [ppm] | Multiplicity $^{n}J_{FC}$ [Hz] |
|---|---|---|---|---|---|
| NH (a/b) | 7.08 | s | 9 | 153.54 | s |
| NH (c/d) | 6.73 | s | 10 | 140.08 | s |
| 3 | 8.15 | d, $^{3}J$ = 9.0 | 2 | 134.95 | s |
| 4 | 8.04 | d, $^{3}J$ = 9.0 | 8a | 133.25 | s |
| 5 | 7.93 | d, $^{3}J$ = 8.2 | 12 | 132.23 | q, $^{2}J$ = 33.4 |
| 11 | 7.63 | s | 4a | 131.78 | s |
| 6 | 7.45 | t, overlap | 4 | 130.26 | s |
| 13 | 7.44 | s | 5 | 128.72 | s |
| 7 | 7.26 | t, $^{3}J$ = 7.8 | 7 | 127.65 | s |
| 8 | 7.01 | d, $^{3}J$ = 8.5 | 6 | 126.13 | s |
| $^{19}$F | δ [ppm] | Multiplicity $^{n}J_{FH}$ [Hz] | 8 | 125.62 | s |
| | -63.6 | s | 14 | 123.50 | q, $^{1}J$ = 273.0 |
| $^{15}$N | δ [ppm] | – | 3 | 123.14 | s |
| a/b | 107 | | 1 | 123.12 | br s |
| c/d | 105 | | 11 | 119.01 | s |
| | | | 13 | 116.70 | s |

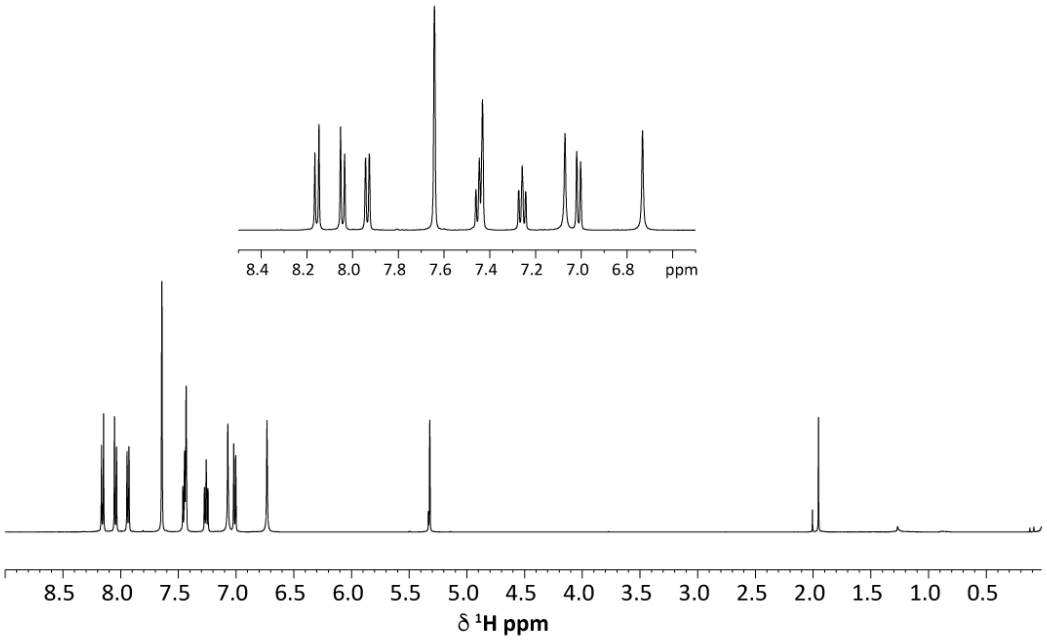



Figure 4.1: $^{1}$H NMR of **4a**.

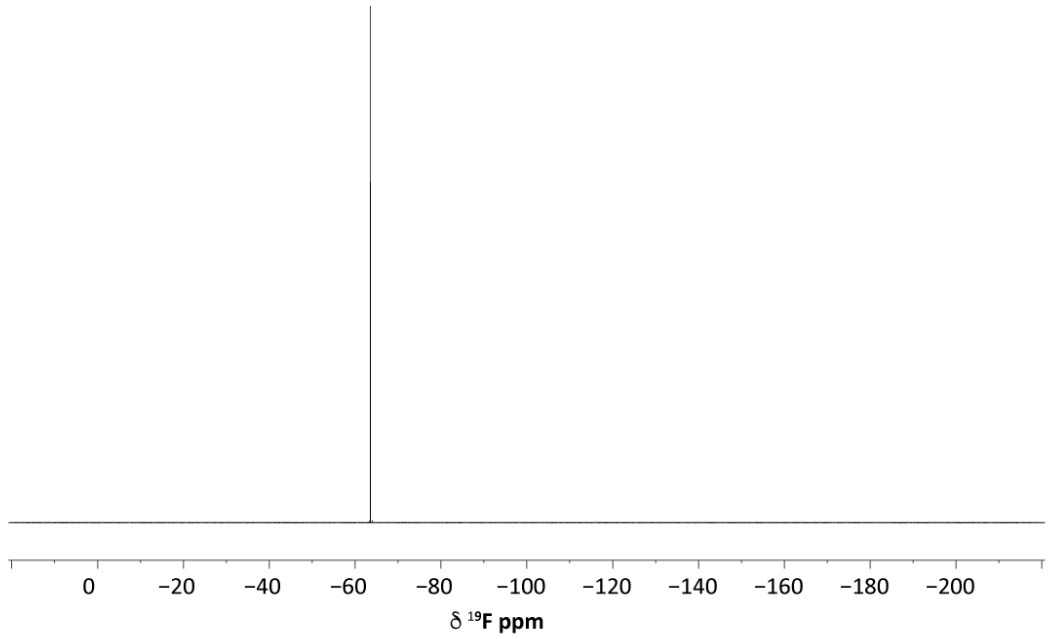



Figure 4.2: $^{19}$F NMR of **4a**.

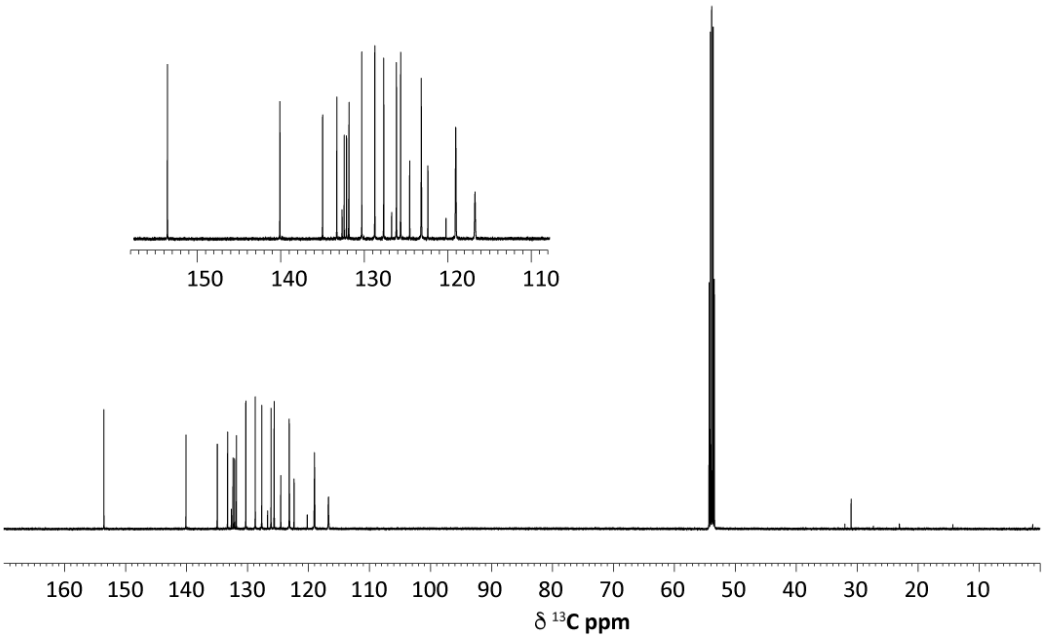



Figure 4.3: $^{13}C$ NMR of **4a**.

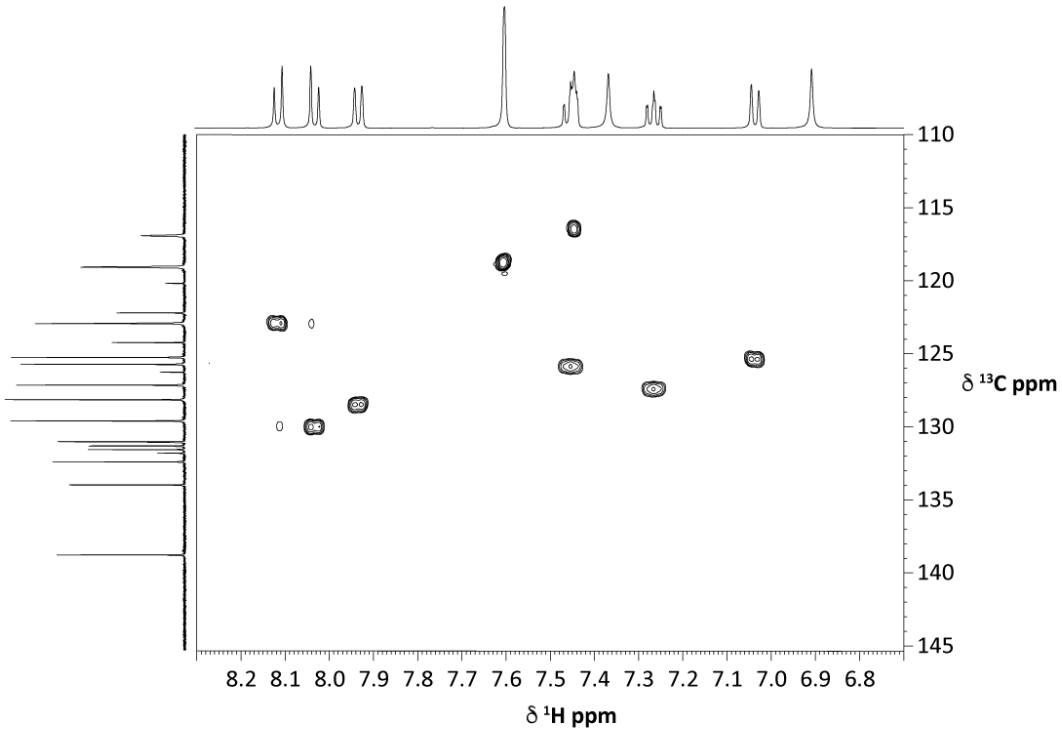



Figure 4.4: $^{1}H$-$^{13}C$ HSQC of **4a**.

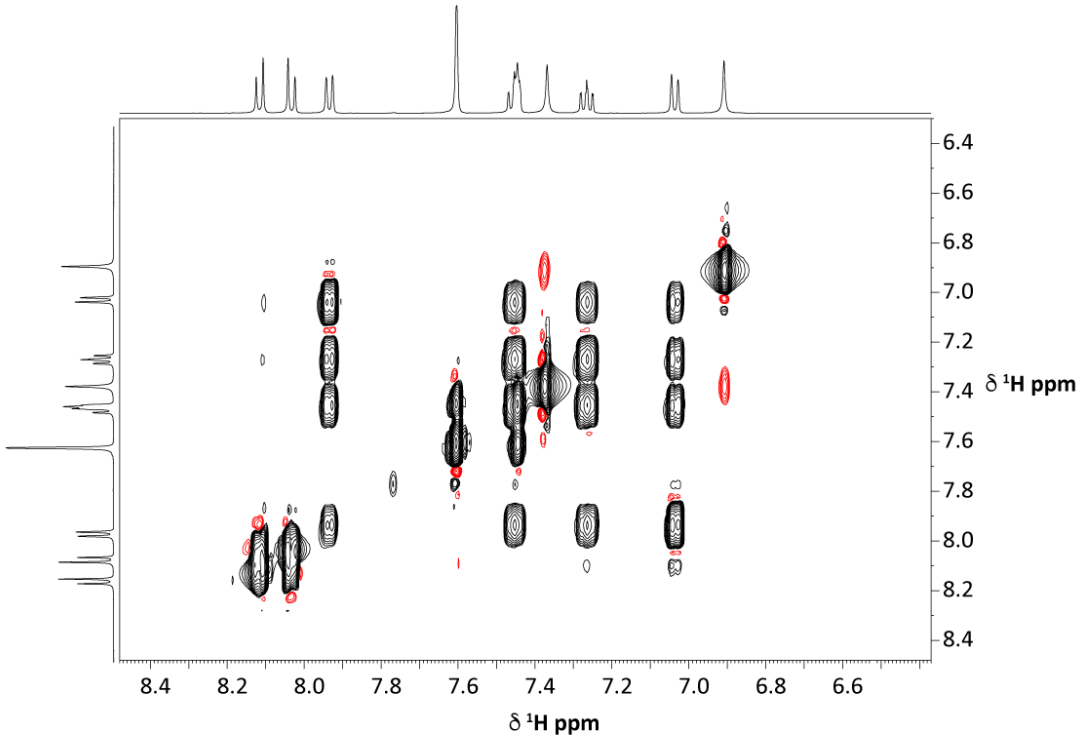



Figure 4.5: $^{1}$H TOCSY of **4a**.

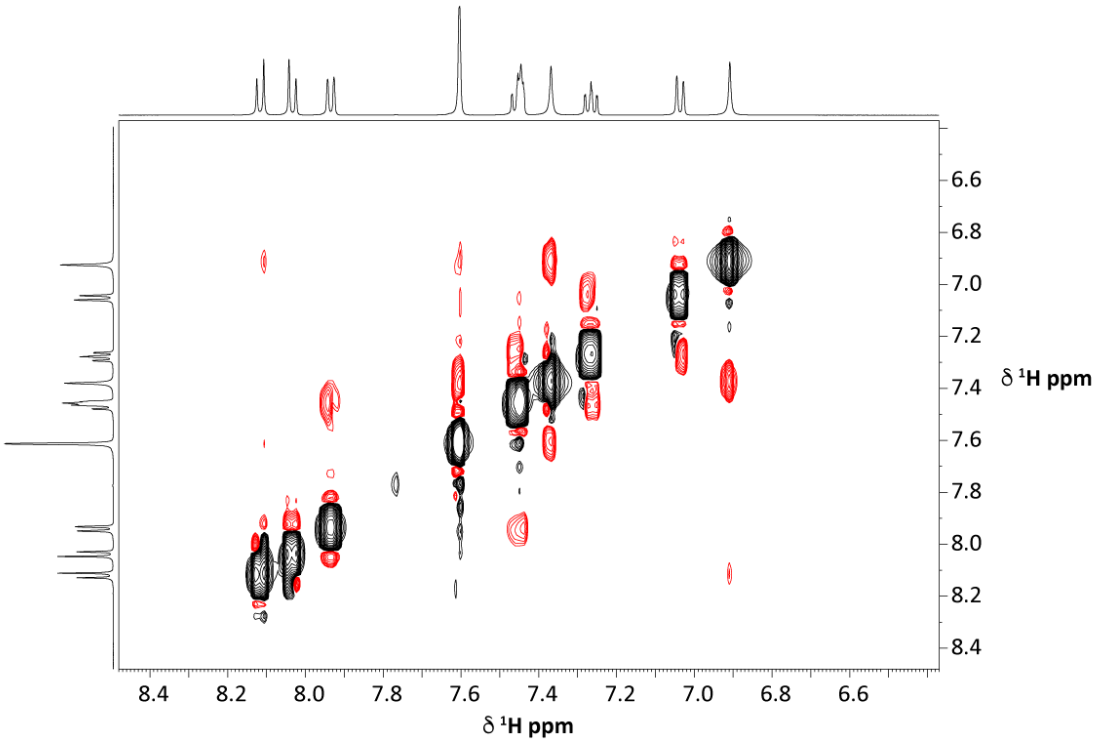



Figure 4.6: $^{1}$H NOESY of **4a**.

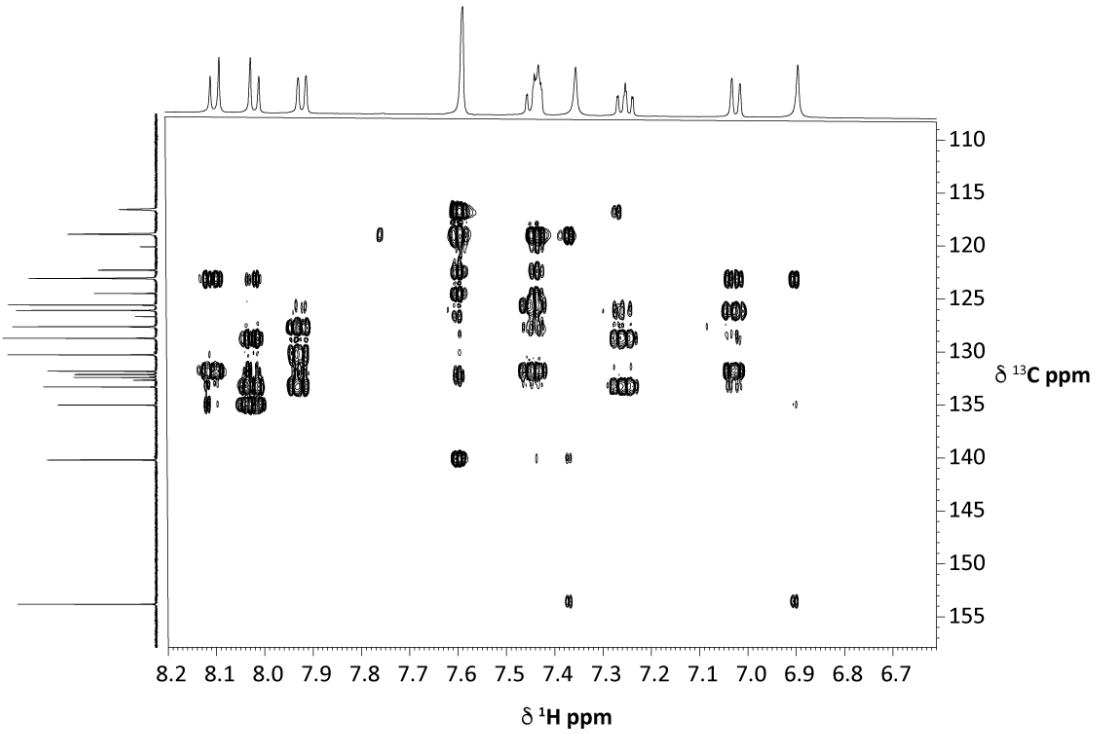



Figure 4.7: $^{1}H$-$^{13}C$ HMBC of **4a**.

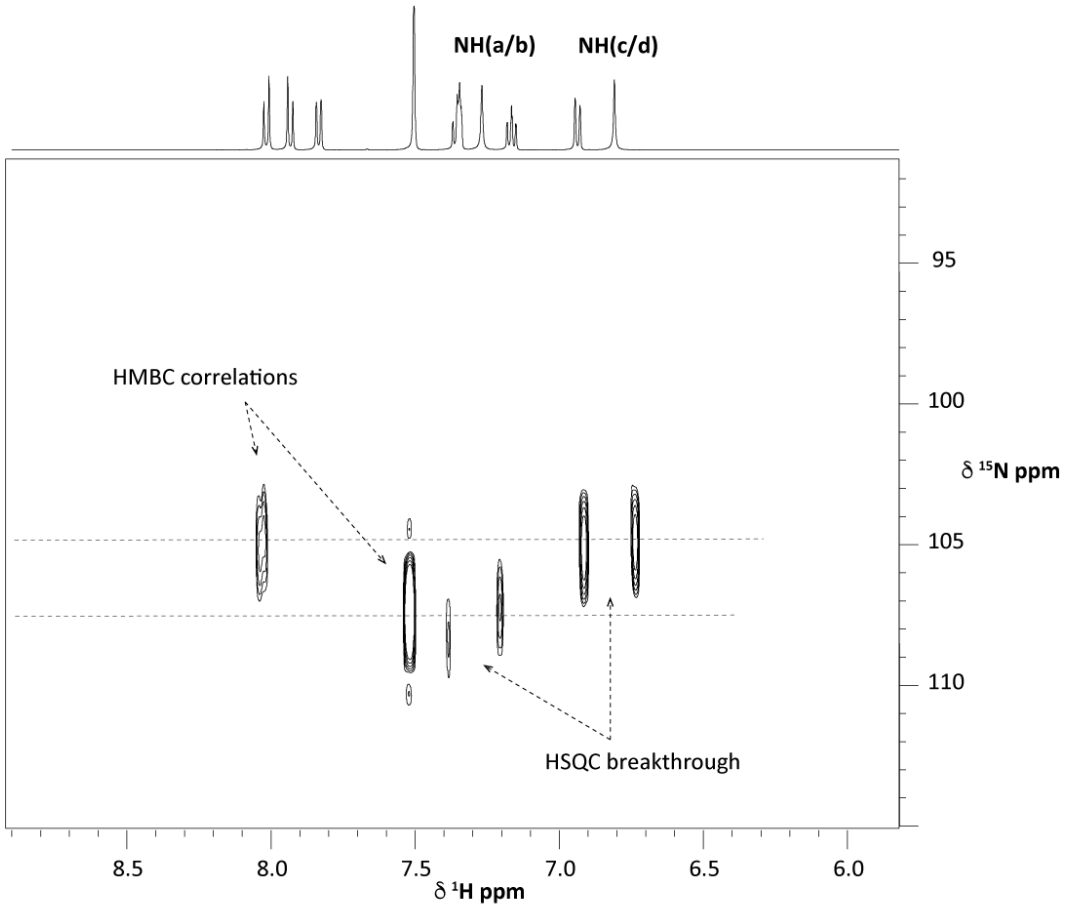
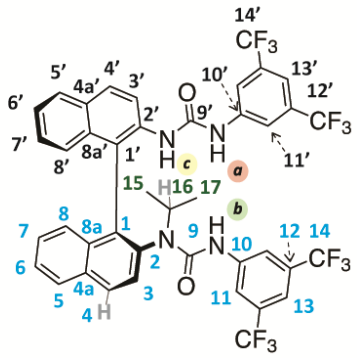



Figure 4.8: $^{1}H$-$^{15}N$ HMBC of **4a**.

*4.3.2.2 iPr BINAM Urea (**4u**) – assignment and copy of NMR spectra*



Scheme 4.2: Structure and numbering of **4u**.

Table 4.4: Assignment chart of **4u** (600 MHz, DCM-$d_2$, 25 mM, 298 K)

| $^{1}$H | δ [ppm] | $^{n}J_{HH}$ [Hz] | $^{13}$C | δ [ppm] | $^{n}J_{FC}$ [Hz] |
|---|---|---|---|---|---|
| NH (a) | 7.1 | br s | 9 | 156.17 | br s |
| NH (b) | 6.9 | br s | 9’ | 152.10 | s |
| NH (c) | 7.64 – 7.47 | br s | 10’ | 140.57 | s |
| 3’ | 8.47 | br d, $^{3}J$ = 8.5 | 2 | 140.39 | s |
| 4 | 8.14 | d, $^{3}J$ = 8.7 | 10 | 140.08 | s |
| 4’ | 8.05 | d, $^{3}J$ = 9.0 | 2’ | 136.00 | br s |
| 5 | 8.02 | d, $^{3}J$ = 8.2 | 8a | 134.17 | s |
| 5’ | 7.95 | d, $^{3}J$ = 8.2 | 8a’ | 133.74 | s |
| 11 | 7.85 | s | 4a | 133.63 | s |
| 11’ | 7.60 | s | 1 | 132.35 | s |
| 3 | 7.56 | d, $^{3}J$ = 8.7 | 12 | 132.41 | q, $^{2}J$ = 33.8 |
| 6 | 7.54 | t, overlap | 12’ | 132.12 | q, $^{2}J$ = 33.3 |
| 13 | 7.50 | s | 4 | 130.91 | s |
| 6’ | 7.42 | t, $^{3}J$ = 7.1 | 4a’ | 130.87 | s |
| 13’ | 7.40 | s | 4’ | 130.17 | s |
| 7 | 7.30 | t, $^{3}J$ = 7.1 | 5’ | 128.90 | s |
| 7’ | 7.25 | t, $^{3}J$ = 7.7 | 3 | 128.72 | s |
| 8 | 7.16 | d, $^{3}J$ = 8.5 | 5 | 128.64 | s |
| 8’ | 6.92 | d, $^{3}J$ = 8.4 | 7 | 127.74 | s |
| 16 | 3.64 | br m | 6 | 127.55 | s |
| 17 | 1.03 | d, $^{3}J$ = 6.9 | 7’ | 127.43 | s |
| 15 | 0.68 | br s | 8 | 127.17 | s |
| $^{19}$F | δ [ppm] | $^{n}J_{FH}$ [Hz] | 8’ | 125.78 | s |
| | -63.5 | s | 6’ | 125.12 | s |
| $^{15}$N | δ [ppm] | – | 14 | 123.65 | q, $^{1}J$ = 272.4 |
| N(a) | 108.0 | | 14’ | 123.48 | q, $^{1}J$ = 272.4 |
| N(b) | 106.8 | | 1’ | 121.40 | br s |
| N(c) | 107.6 | | 11 | 120.84 | s |
| N(iPr) | 119.0 | | 3’ | 120.58 | br s |
| | | | 11’ | 118.47 | s |
| | | | 13 | 117.49 | s |
| | | | 13’ | 116.09 | s |
| | | | 16 | 53.94 | s |
| | | | 15 | 20.97 | s |
| | | | 17 | 20.73 | s |

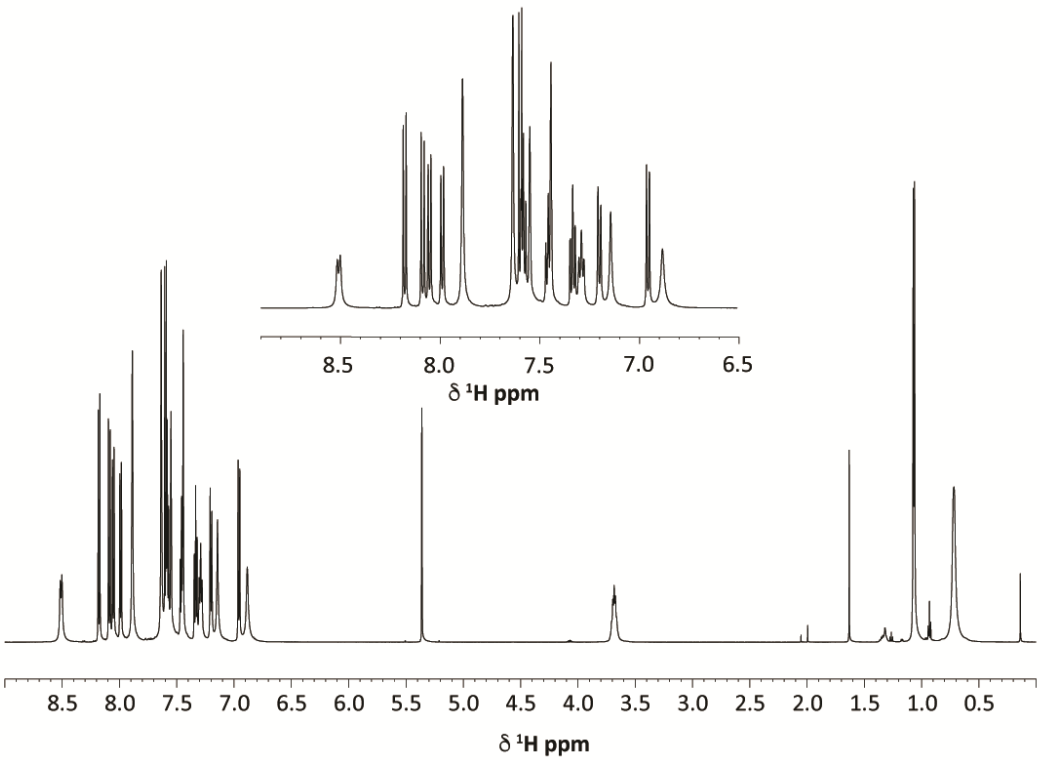



Figure 4.9: $^{1}H$ NMR of **4u**.

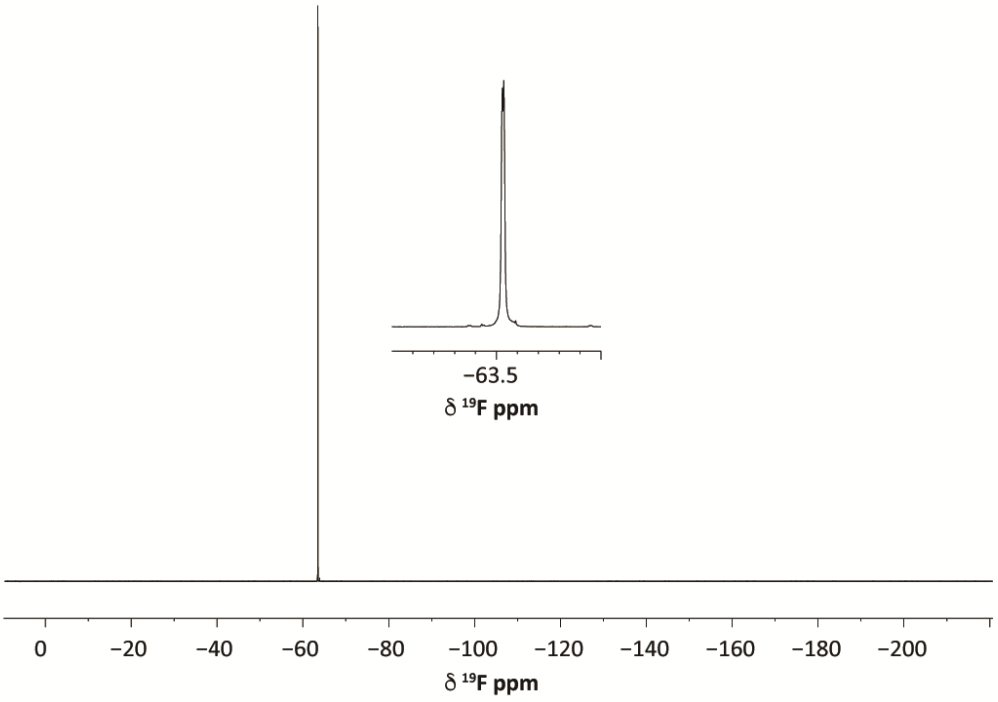



Figure 4.10: $^{19}F$ NMR of **4u**.

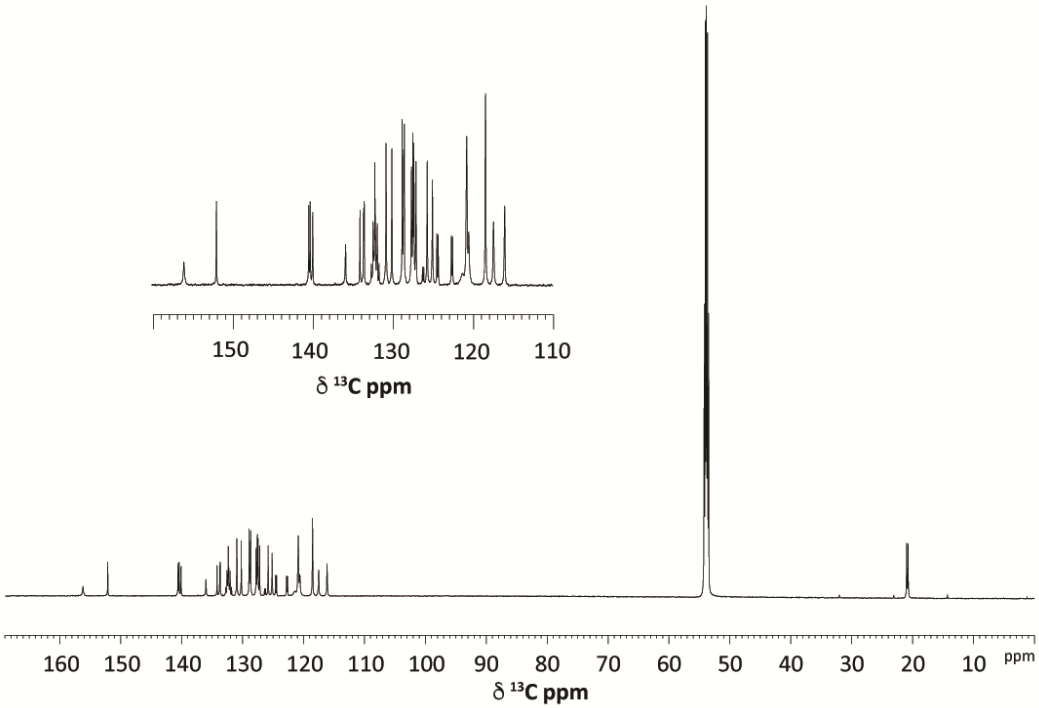



Figure 4.11: $^{13}C$ NMR of **4u**.

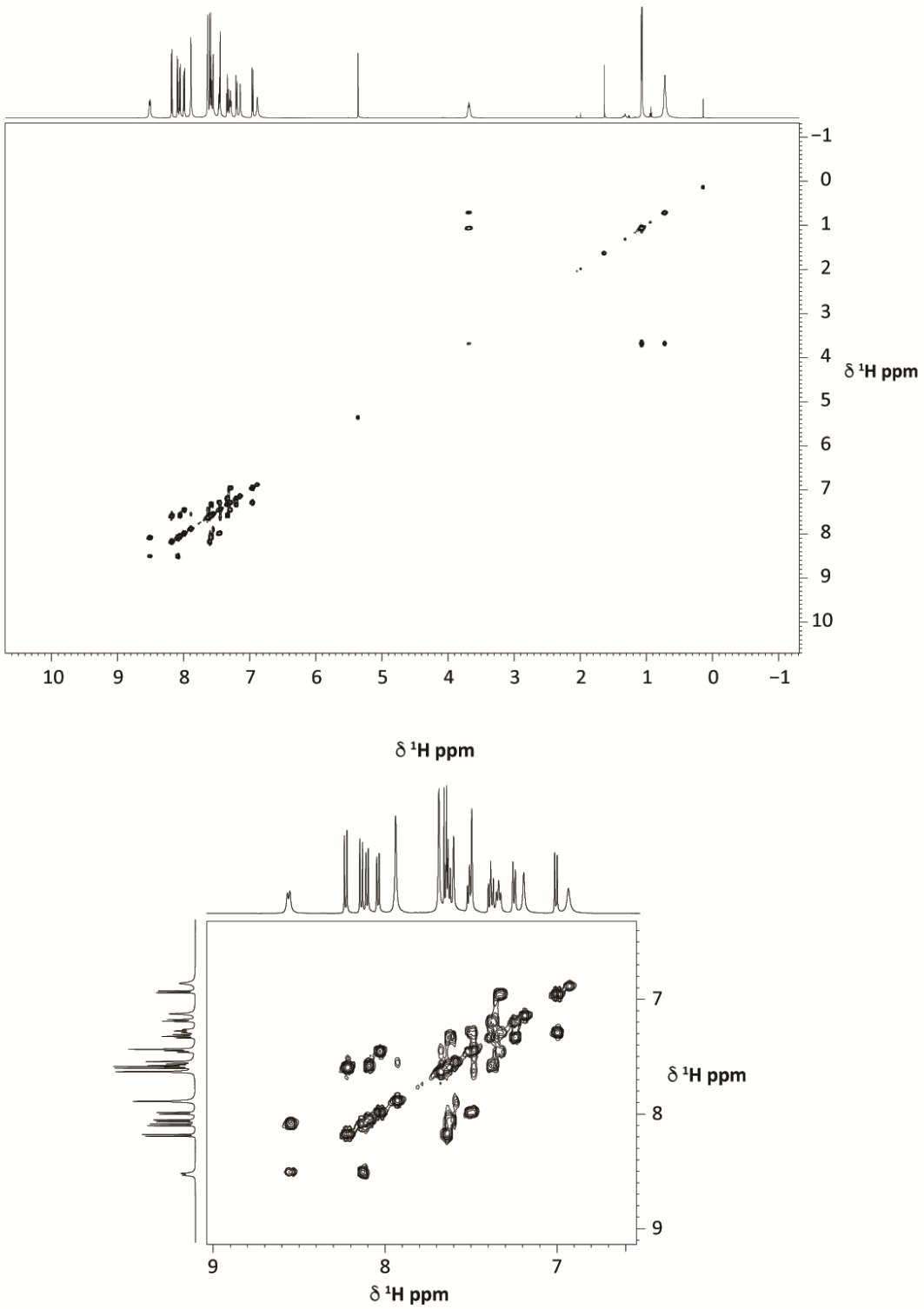
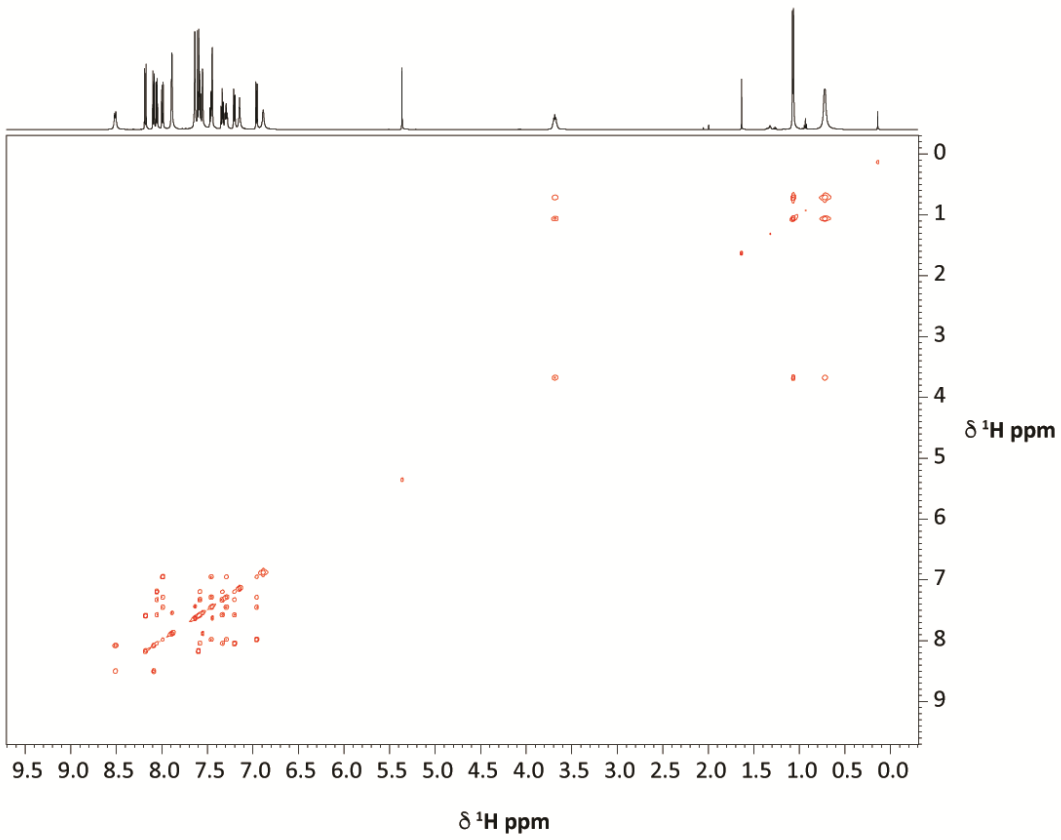



Figure 4.12: $^{1}$H COSY of **4u**.



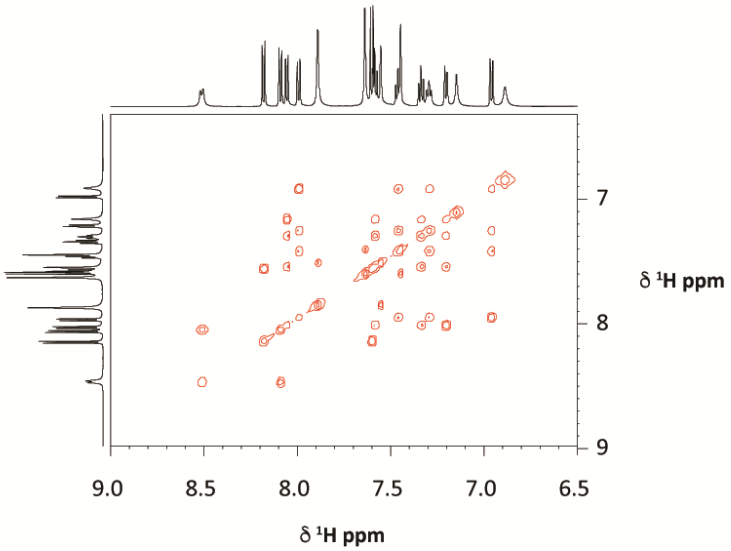




Figure 4.13: $^{1}$H TOCSY of **4u**.

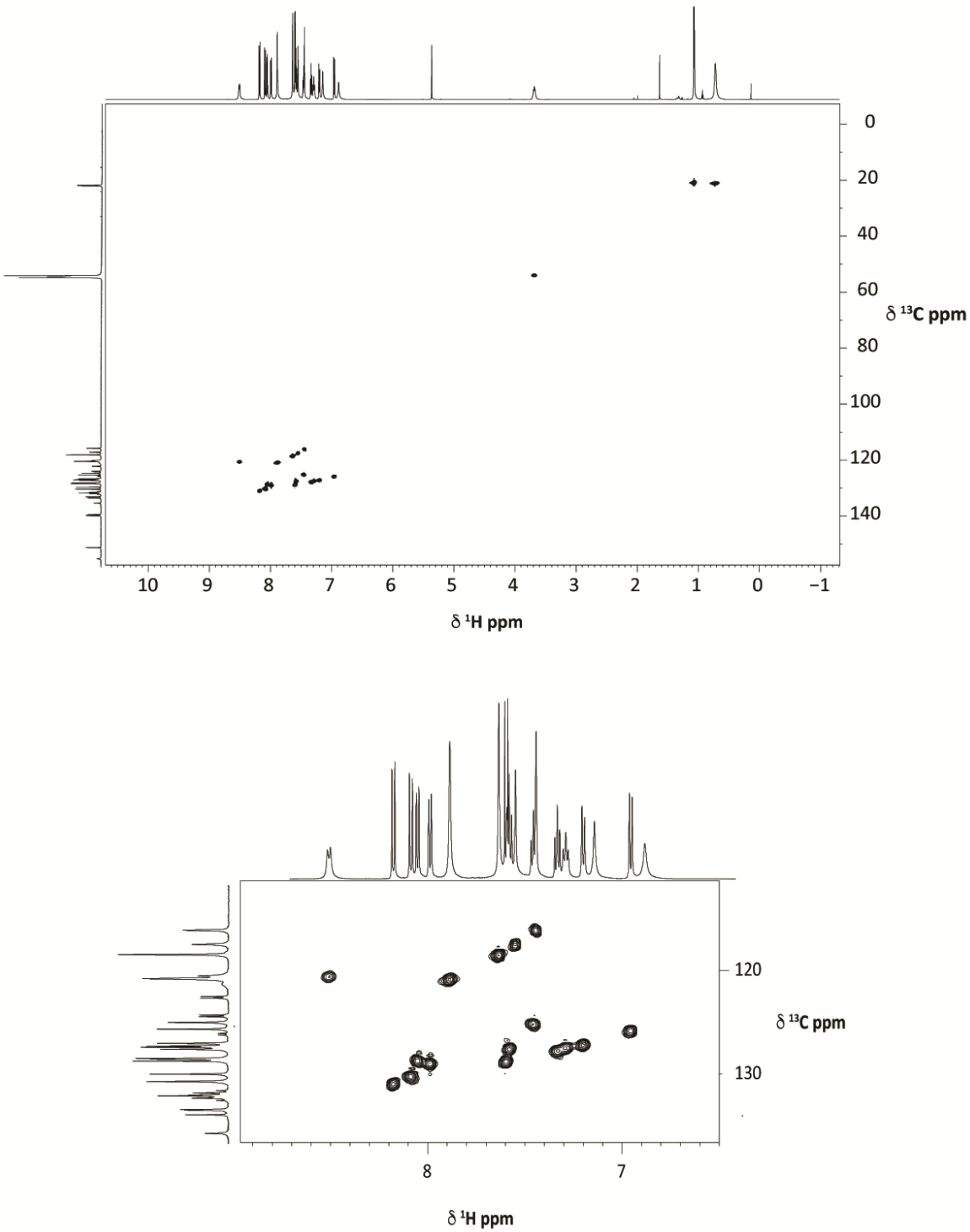



Figure 4.14: $^{1}H$-$^{13}C$ HSQC of **4u**.

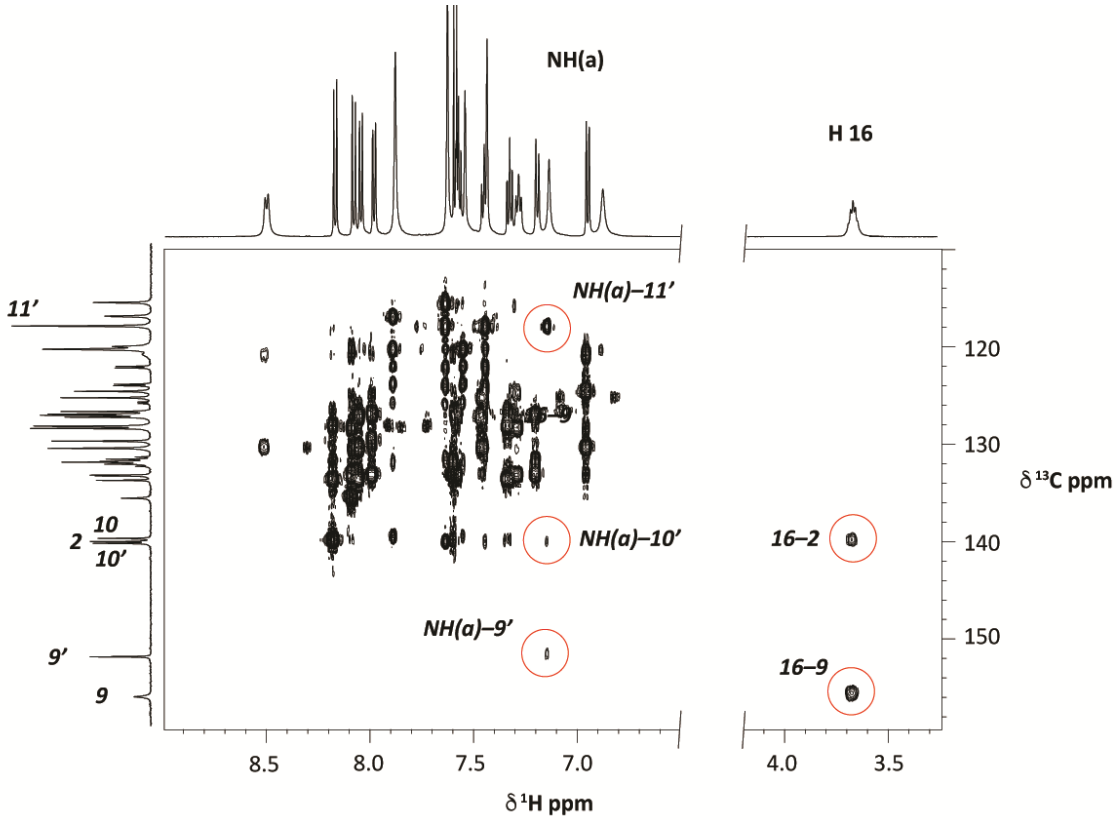



Figure 4.15: $^{1}H$-$^{13}C$ HMBC of **4u**.

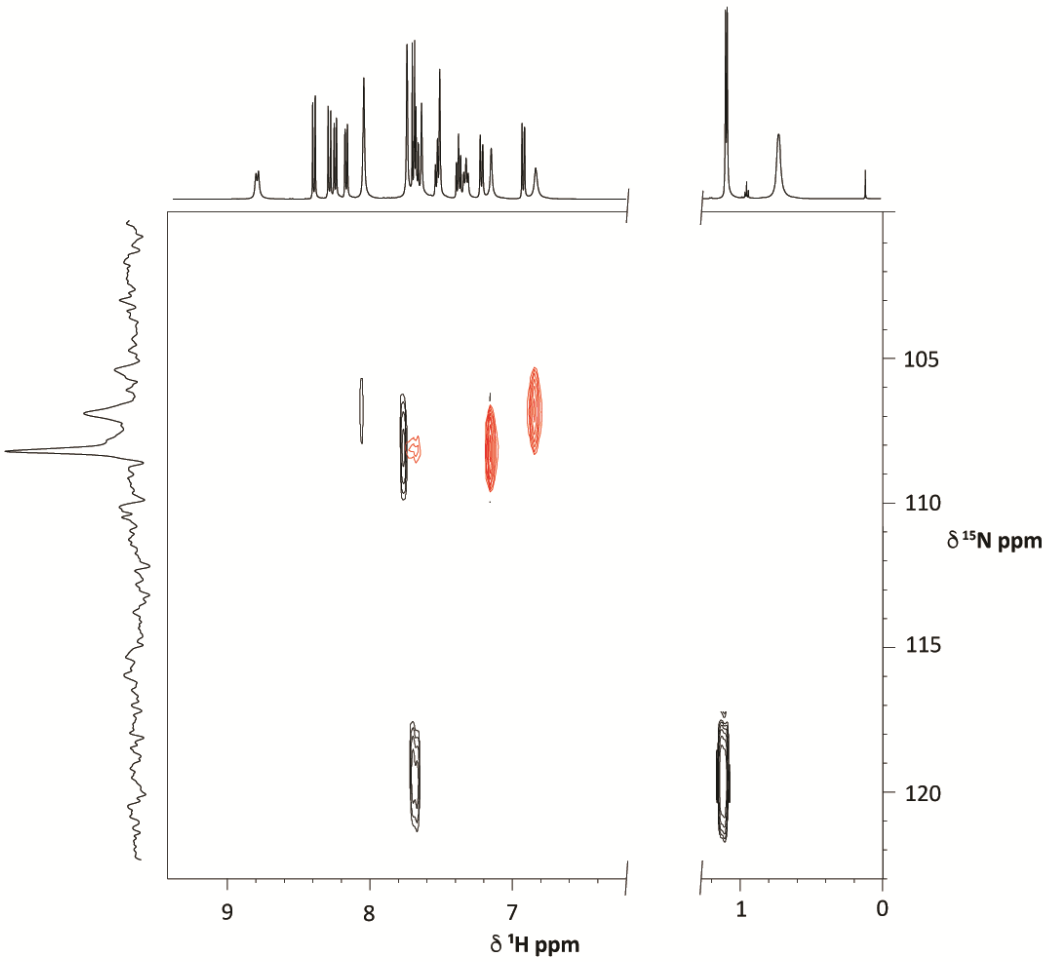



Figure 4.16: $^{1}H$-$^{15}N$ HSQC (red) and $^{1}H$-$^{15}N$ HMBC (black) of **4u**, in f1 dimension (vertical axis) an independently acquired $^{15}N$ NMR spectrum (*ineptrd*) is overlaid.

*4.3.2.3 iPr BINAM Urea (**4u**) – spectra in DMSO-$d_6$ and 1,2-DCB-$d_4$*

The samples were prepared at 25 mM concentration in DMSO-$d_6$ and recorded at room temperature.

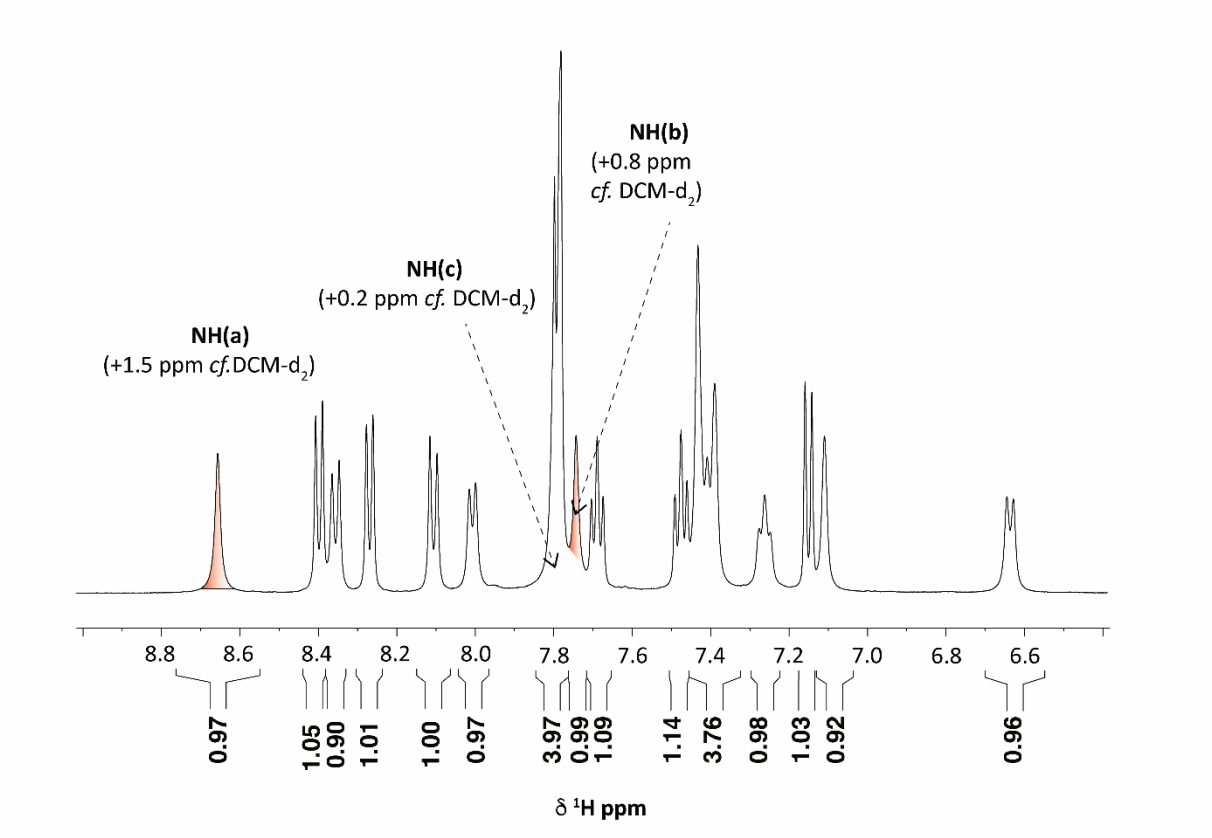



Figure 4.17: $^1$H NMR of **4u** in DMSO-$d_6$ (6–9 ppm), in brackets chemical shift differences compared with DCM-$d_2$.

The samples were prepared at 25 mM concentration in 1,2-dichlorobenzene-$d_4$ and recorded at room temperature (298 K) and 318 K.

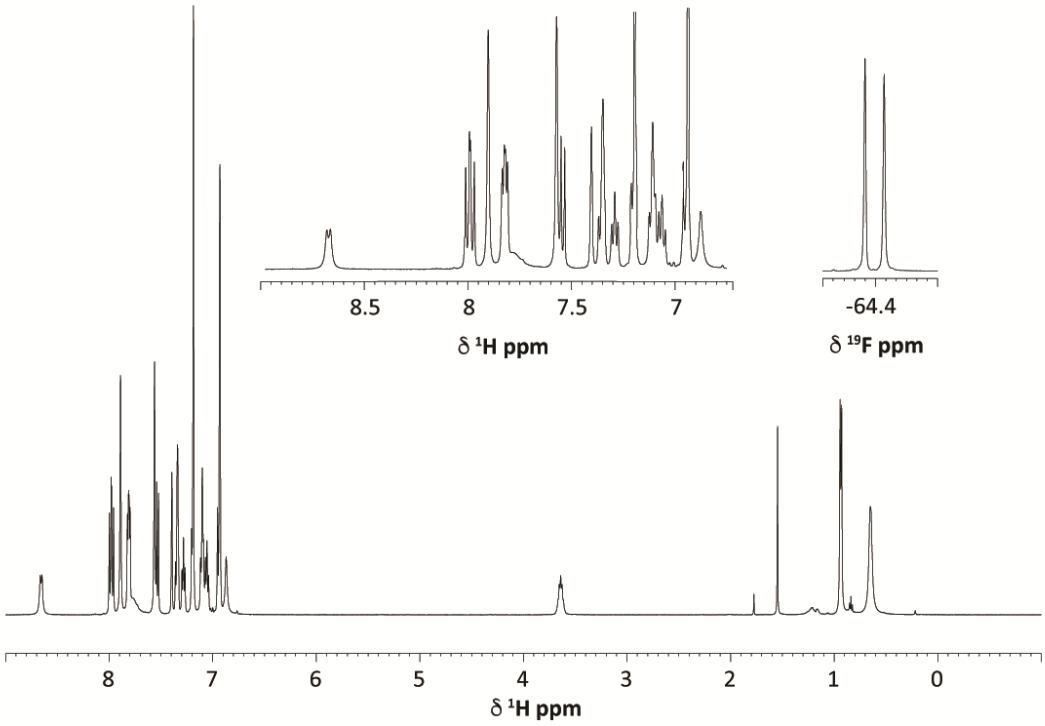



Figure 4.18: $^1$H NMR of **4u** in 1,2-dichlorobenzene-$d_4$ at 298 K full spectrum and 6–9 ppm detail (left inset) at 298 K, $^{19}$F NMR at 298 K (right inset).

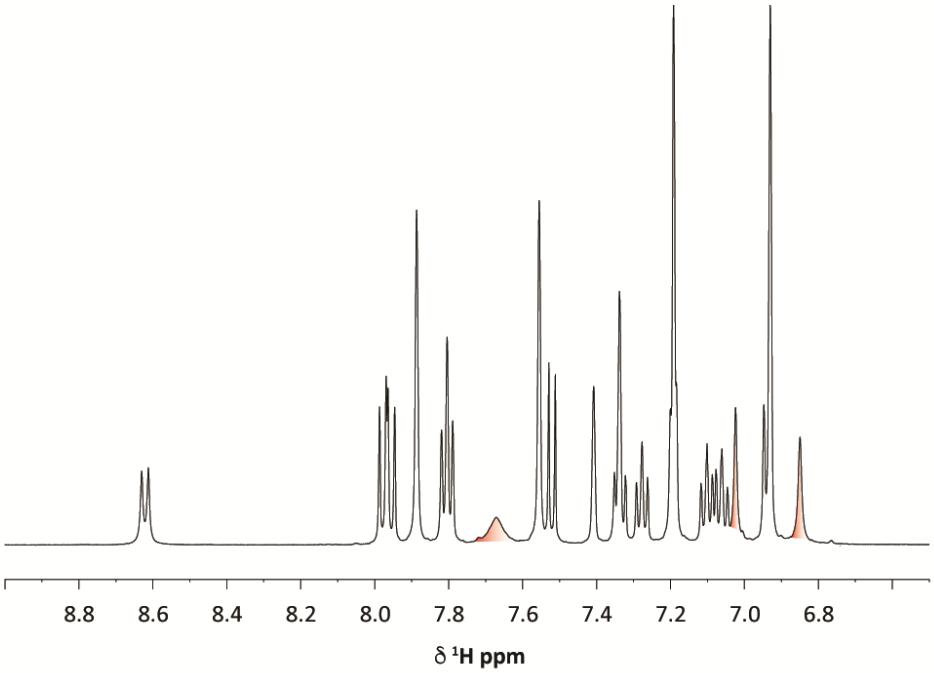



Figure 4.19: $^{1}$H NMR of **4u** in 1,2-dichlorobenzene-$d_4$ at 318 K (6–9 ppm).

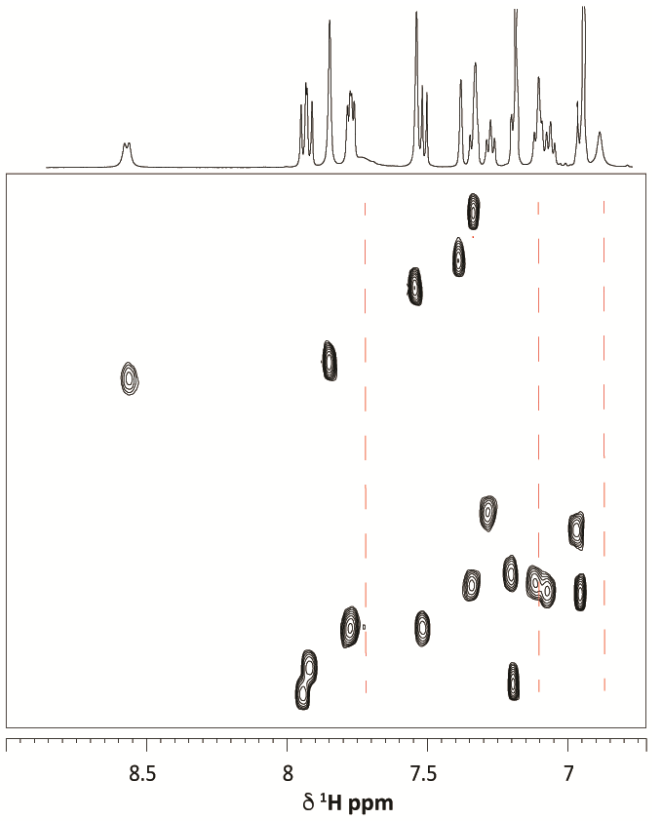



Figure 4.20: $^{1}$H-$^{13}$C HSQC of **4u** in 1,2-dichlorobenzene-$d_4$ at 298 K.

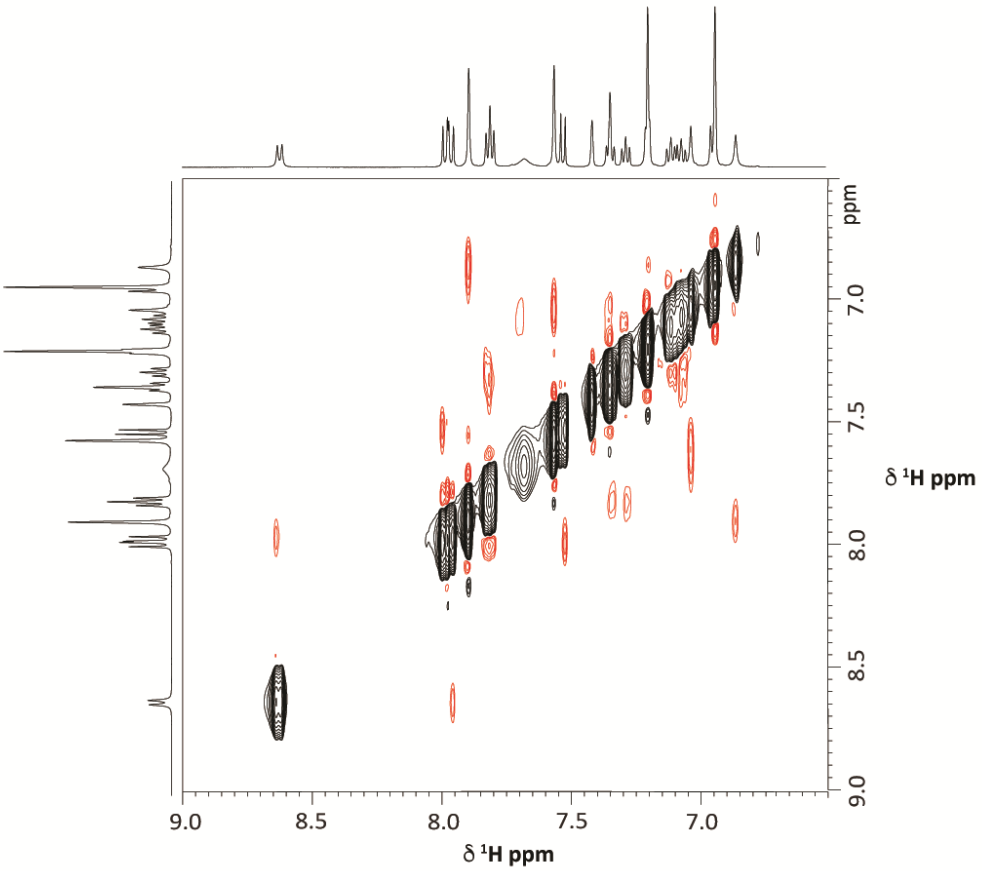



Figure 4.21: $^{1}$H NOESY spectra of **4u** in 1,2-dichlorobenzene-$d_4$ at 318 K (6–9 ppm).

*4.3.2.4 iPr BINAM Urea (**4u**) – NOESY*

NOESY spectra were acquired on a AVIII HD 600 using a previously developed pulse sequence (*noesygpph*)[15] and the parameters reported below.

| Parameter | Value |
|---|---|
| TD | 2048 (f1) x 256 (f2) pt |
| SW | 12 (f1) x 12 (f2) ppm |
| NS (DS) | 16 (8) |
| relaxation delay d1 | 2 s |
| mixing time d8 | 500 ms |

The intensity of NOESY cross-peak correlations was qualitatively assessed and listed in Table 4.5.

Table 4.5: nOe correlations of **4u** (600 MHz, DCM-$d_2$, 25 mM, 298 K)

| Proton | $\delta$ $^1$H [ppm] | nOe correlation |
|---|---|---|
| NH(a) | 7.1 | NH(c) (strong); 11’ (strong); 11 (weak); 3‘ (weak) |
| NH(b) | 6.9 | 11 (strong); 3 (weak); 15, 16, 17, (strong) |
| NH(c) | 7.64–7.47 | NH(a) (strong) |
| 3’ | 8.47 | 4’(strong); NH(a) (weak) |
| 4 | 8.14 | 3 (strong); 5 (strong) |
| 4’ | 8.05 | 3’ (strong); 5’ (strong) |
| 5 | 8.02 | 4 (strong); 6 (strong) |
| 5’ | 7.95 | 4’ (strong); 6’ (strong) |
| 11 | 7.85 | NH(b) (strong); NH(a) (weak) |
| 11’ | 7.60 | NH(a) (strong) |
| 3 | 7.56 | 4 (strong); NH(b) (strong); 16 (weak); 16, 17 (strong) |
| 6 | 7.54 | 5 (strong); 7 (strong) |
| 6’ | 7.42 | 5’ (strong); 7’ (strong) |
| 7 | 7.40 | 6 (strong); 8 (strong) |
| 7’ | 7.25 | 5‘ (strong); 8’ (strong) |
| 8 | 7.16 | 7 (strong) |
| 8’ | 6.92 | 16 (strong); 15 (strong); 17 (weak); 7’ (strong) |
| 16 | 3.64 | NH(b) (strong); 8’ (strong); 3 (weak) |
| 17 | 1.03 | 11 (weak); 3 (strong); 8’ (weak); NH(b) (strong) |
| 15 | 0.68 | 3 (strong); 8’ (strong); NH(b) (strong) |

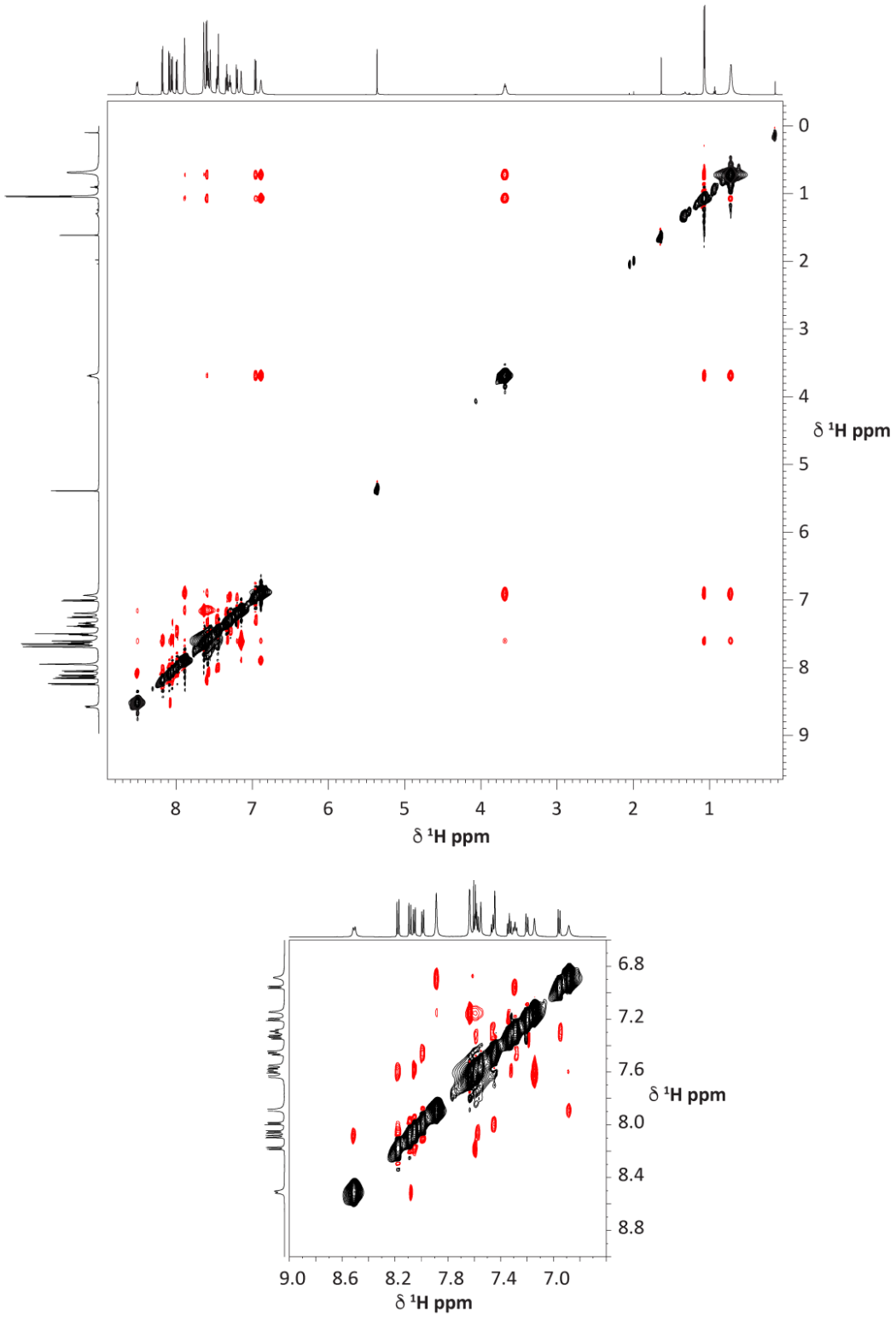



Figure 4.22: $^{1}$H NOESY spectra of **4u**.

*4.3.3 Binding studies*

*4.3.3.1 Uv-vis Titrations.*

A stock solution of *bis*-urea **4a** or **4u** (5 μM) in DCM (spectrophotometric grade) was prepared. A TBAF solution was prepared by weighing out around 30 mg of TBAF·$3H_2O$ (Merck, tetrabutylammonium fluoride hydrate 98%) in 1 ml of DCM (spectrophotometric grade) measured in a volumetric flask. An aliquot of exactly 200 μL of TBAF solution was transferred in an NRM tube, to which 4 μL of 4-fluoroanisole and 300 μL of DCM-$d_2$ were added. The exact concentration of fluoride was determined by $^{19}F$ NMR, integrating the $F^-$ peak (-118.9 ppm) and 4-fluoroanisole peak (-125 ppm, 0.07 M). The data were collected using a previously developed pulse sequence (*zgig*) and the following parameters:

| Parameter | Value |
|---|---|
| TD (SI) | 131072 (262144) pt |
| SW | 20 ppm |
| o1p | -122 ppm |
| NS (DS) | 16 (4) |
| relaxation delay d1 | 45 s |

The TBAF solution was subsequently diluted with the previously prepared stock solution of *bis*-urea to 0.2 mM. 800 μL of the stock solution of *bis*-urea were transferred in a quartz cuvette and a UV-vis spectrum was recorded before 10 equiv. of the TBAF solution were added in aliquots. After every addition a UV-vis absorption spectrum was recorded. The absorption at three wavelengths, chosen around $\lambda_{max}$, was plotted against the concentration of added fluoride. The association constant ($K_a$) was determined from the titration data points by non-linear least squares regression using Dynafit.[16] An example of input file for the determination of association constants for the formation of 1:1 complexes, $K_{a,\,1:1}$, is shown below.

```
[task]
  task = fit
  data = equilibria
 [mechanism]
  U + F <==> UF : Ka equilibrium
 [constants]
Ka = 100000 ?
 [concentrations]
U = 0.0000054
 [data]
variable F
plot titration
set UV.a | resp U = 50370, UF = 105740 ?
set UV.b | resp U = 46296, UF = 106296 ?
set UV.c | resp U = 42962, UF = 104814 ?

[set:UV.a]
0               0.272
7.4813E-07      0.307
1.49254E-06     0.336
2.23325E-06     0.366
2.9703E-06      0.393
3.7037E-06      0.421
4.4335E-06      0.447
5.15971E-06     0.471
5.88235E-06     0.49
6.60147E-06     0.502
7.31707E-06     0.511
9.09091E-06     0.522
1.08434E-05     0.531
1.25749E-05     0.536
1.42857E-05     0.543
1.76471E-05     0.552
2.09302E-05     0.555
2.72727E-05     0.56
3.33333E-05     0.563
4.73684E-05     0.567
0.00006 0.571

[set:UV.b]
0               0.25
7.4813E-07      0.288
1.49254E-06     0.318
2.23325E-06     0.349
2.9703E-06      0.379
3.7037E-06      0.41
4.4335E-06      0.438
5.15971E-06     0.463
5.88235E-06     0.484
6.60147E-06     0.496
7.31707E-06     0.507
9.09091E-06     0.519
1.08434E-05     0.529
1.25749E-05     0.536
1.42857E-05     0.543
1.76471E-05     0.554
2.09302E-05     0.556
```

```
2.72727E-05     0.562
3.33333E-05     0.565
4.73684E-05     0.569
0.00006 0.574

[set:UV.c]
0               0.232
7.4813E-07      0.27
1.49254E-06     0.3
2.23325E-06     0.333
2.9703E-06      0.364
3.7037E-06      0.394
4.4335E-06      0.423
5.15971E-06     0.449
5.88235E-06     0.471
6.60147E-06     0.485
7.31707E-06     0.495
9.09091E-06     0.51
1.08434E-05     0.52
1.25749E-05     0.527
1.42857E-05     0.535
1.76471E-05     0.547
2.09302E-05     0.55
2.72727E-05     0.555
3.33333E-05     0.558
4.73684E-05     0.563
0.00006 0.566
 [output]
  directory ./Output_Jan_20/iPrBINAM/75a
[end]
```

BINAM Urea **4a**

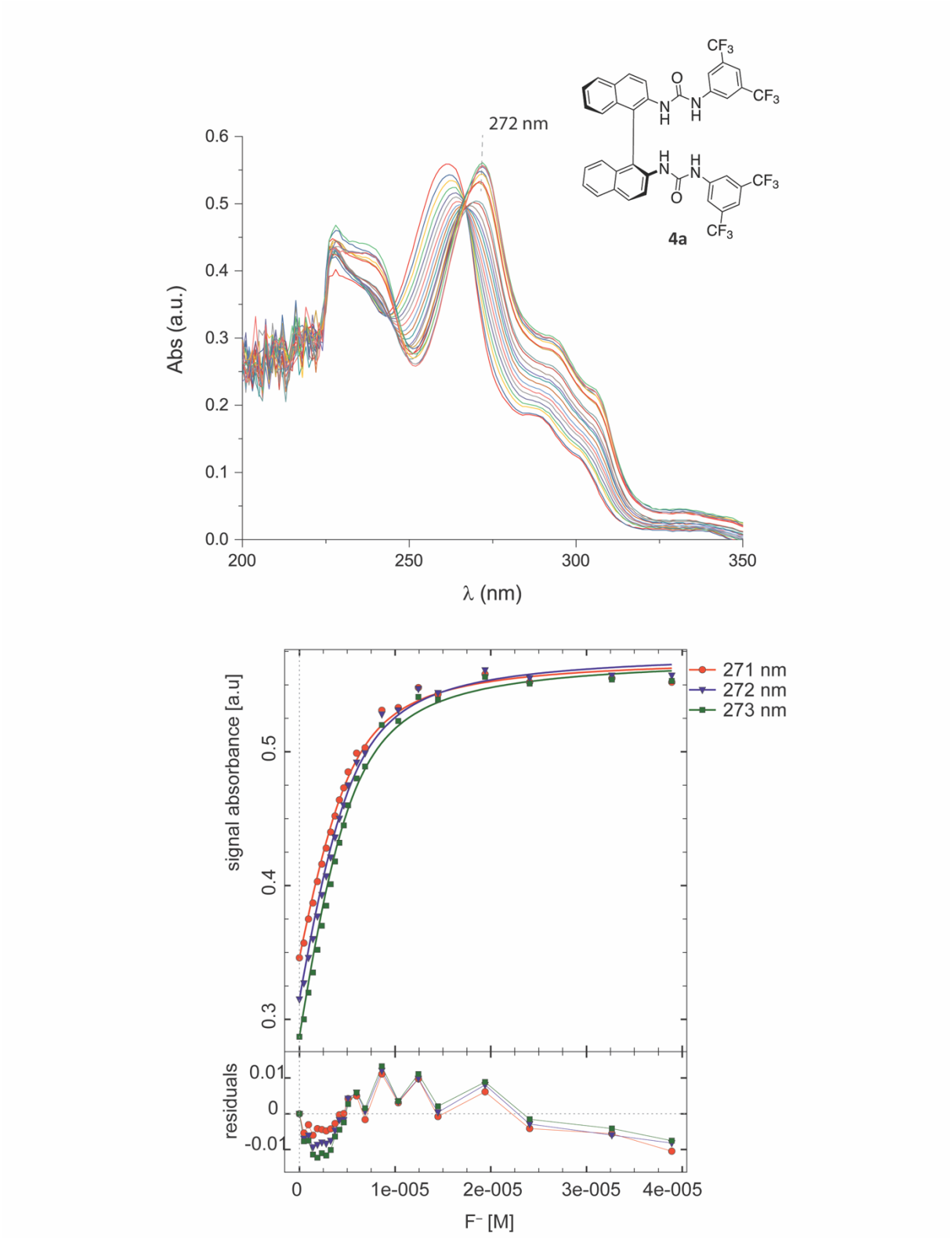



Figure 4.23: Stacked UV-vis spectra for the titration of **4a** with TBAF in DCM at 298K (top); titration profiles at 271, 272 and 273 nm, experimental (circles) and fitted function (lines). The corresponding residual plots are shown below the graphs.

iPr BINAM Urea **4u**

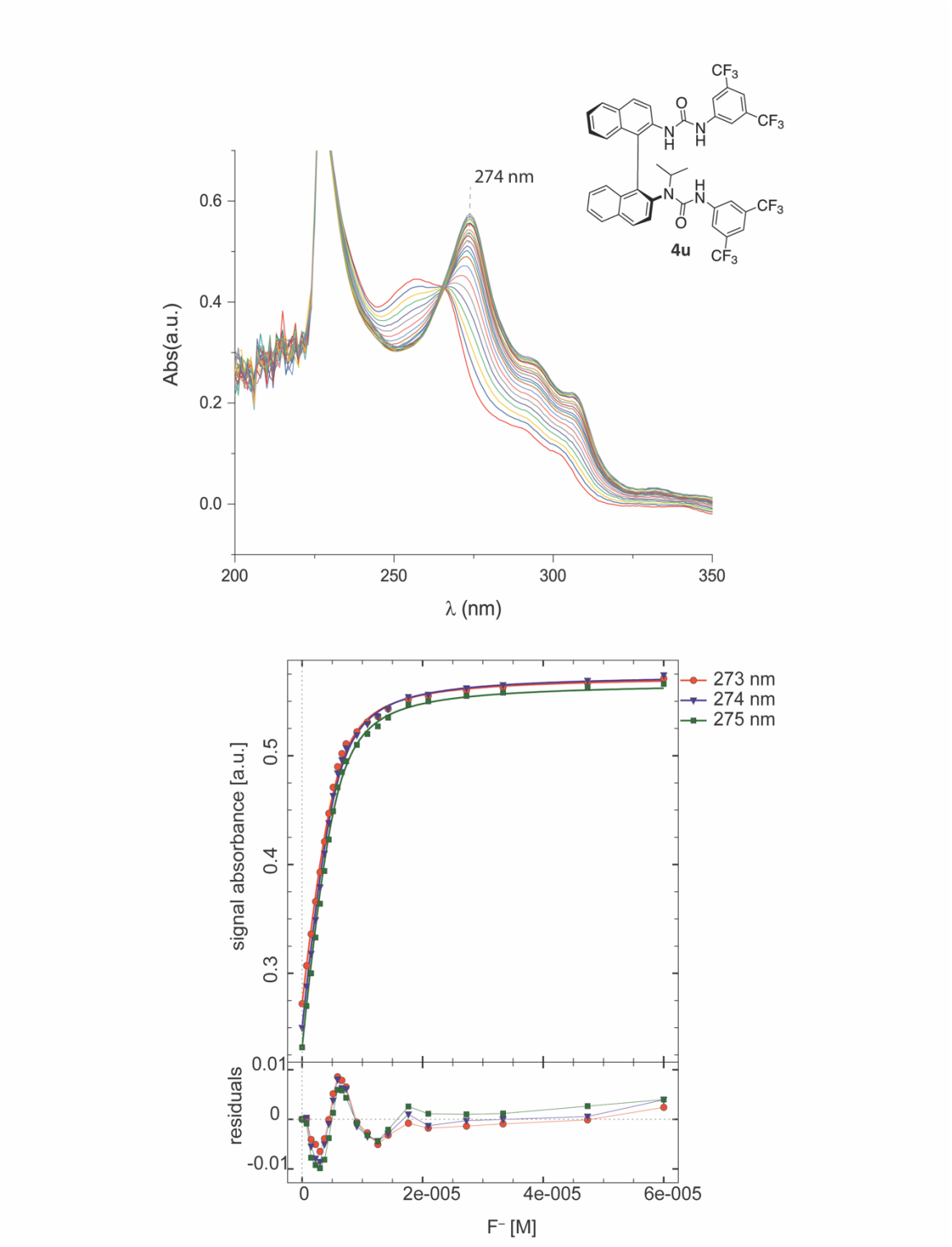



Figure 4.24: Stacked UV-vis spectra for the titration of **4u** with TBAF in DCM at 298K (top); titration profiles at 273, 274 and 275 nm, experimental (circles) and fitted function (lines). The corresponding residual plots are shown below the graphs.

*4.3.3.2 NMR Titrations.*

A known amount of *bis*-urea **4a** or **4u** (~ 1 mg) was weighted inside an NMR tube and dissolved in 0.5 mL of DCM-$d_2$ (~ 3 mM). A TBAF solution was prepared dissolving 10–50 mg of TBAF·$3H_2O$ (Merck, Tetrabutylammonium fluoride hydrate 98%) and 5 microliters of 4-fluoranisole in 1 ml of DCM-$d_2$ measured in a volumetric flask. The exact concentration of fluoride was determined by $^{19}F$ NMR, integrating the $F^-$ peak (-118.9 ppm) and 4-fluoroanisole peak (-125 ppm, 0.044 M). The data were collected using a previously developed pulse sequence (*zgig*) and the following parameters:

| Parameter | Value |
|---|---|
| TD (SI) | 131072 (262144) pt |
| SW | 20 ppm |
| o1p | -122 ppm |
| NS (DS) | 16 (4) |
| relaxation delay d1 | 45 s |

The TBAF solution was added in aliquot of 1-2 microliter (0.05–0.1 equiv.) from 0 to 7 equivalents. After each addition $^1H$ and $^{19}F$ NMR spectra were acquired on a Bruker AVIII HD 500. The chemical shifts of selected proton and fluorine signals were plotted against the amount of added TBAF. The association constants ($K_{a,\,2:1}$) were determined from the titration data points by non-linear least squares regression using Dynafit.[16] The following shows a typical input file for the determination of $K_{a,\,2:1}$ (K2 in input file) using the values of $K_{a,\,1:1}$ (K1 in input file) as obtained from the UV-vis titrations.

```
[task]
  task = fit
  data = equilibria
 [mechanism]
  U + F <==> UF : Ka equilibrium
 UF + U <==> U2F : Kb equilibrium
[constants]
Ka = 1048000
Kb = 1000 ?
[responses]
intensive
[data]
variable F, U
plot titration
set NMR.a | resp U = 8.518, U2F = 8.81 ?, UF = 9.099 ?
set NMR.b | resp U = -63.5245, U2F = -63.093 ?, UF = -63.087 ?
set NMR.c | resp U = 7.9846, U2F = 7.9207 ?, UF = 7.8872 ?

[set:NMR.c]
0           0.003014354       7.9846
0.000215139       0.003002345       7.9727
0.000428571       0.002990431       7.9609
0.000640316       0.002978611       7.949
0.000850394       0.002966884       7.9372
0.001058824       0.002955249       7.9295
0.001265625       0.002943705       7.9207
0.001470817       0.002932251       7.9151
0.001876448       0.002909608       7.9048
0.002076923       0.002898417       7.9001
0.002473282       0.002876292       7.8955
0.002863636       0.002854502       7.8955
0.003814126       0.002801444       7.8955
0.008081633       0.002563226       7.8934
0.014755814       0.002190664       7.8934
0.023594595       0.001697271       7.8903
0.031272727       0.001268668       7.8872

[set:NMR.a]
0           0.003014354       8.518
0.000215139       0.003002345       8.548
0.000428571       0.002990431       8.588
0.000640316       0.002978611       8.638
0.000850394       0.002966884       8.694
0.001058824       0.002955249       8.751
0.001265625       0.002943705       8.81
0.001470817       0.002932251       8.867
0.001876448       0.002909608       8.971
0.002076923       0.002898417       9.017
0.002473282       0.002876292       9.09
0.002863636       0.002854502       9.099
0.003814126       0.002801444       9.099
0.008081633       0.002563226       9.099
0.014755814       0.002190664       9.095
0.023594595       0.001697271       9.09
0.031272727       0.001268668       9.089
[set:NMR.b]
0           0.003014354       -63.5245
```

```
0.000215139     0.003002345     -63.5025
0.000428571     0.002990431     -63.4753
0.000640316     0.002978611     -63.4458
0.000850394     0.002966884     -63.4118
0.001058824     0.002955249     -63.3763
0.001265625     0.002943705     -63.3393
0.001470817     0.002932251     -63.2992
0.001876448     0.002909608     -63.2077
0.002473282     0.002876292     -63.093
0.002863636     0.002854502     -63.087
0.003814126     0.002801444     -63.087
0.008081633     0.002563226     -63.087
0.014755814     0.002190664     -63.083
0.031272727     0.001268668     -63.08
[output]
  directory ./output/FI-9-085_NMR
[end]
```

BINAM urea **4a**

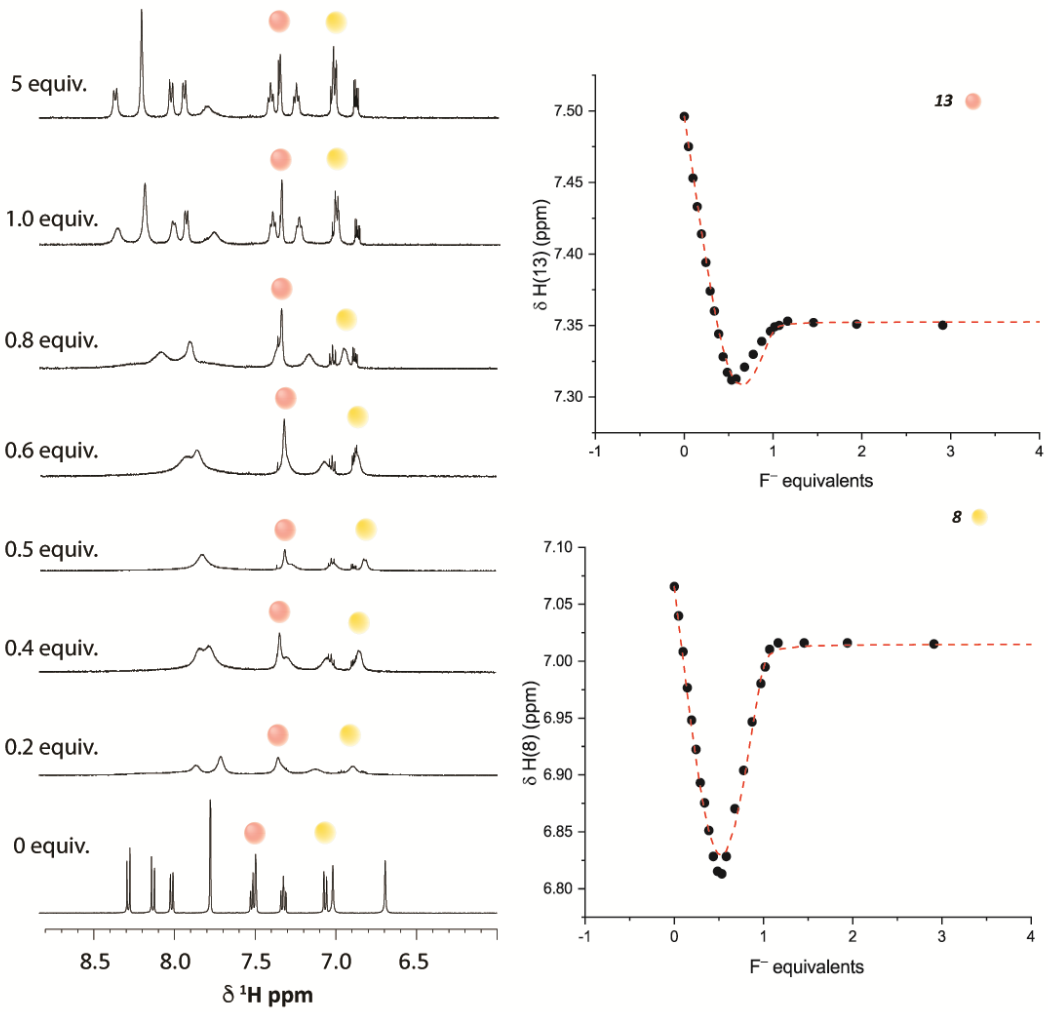



Figure 4.25: Stacked $^{1}$H NMR for the titration of **4a** with TBAF in DCM-$d_2$ at 298 K (left); titration profiles for H(13) and H(8) (right), experimental points (black circles) and fitted function (dashed lines).

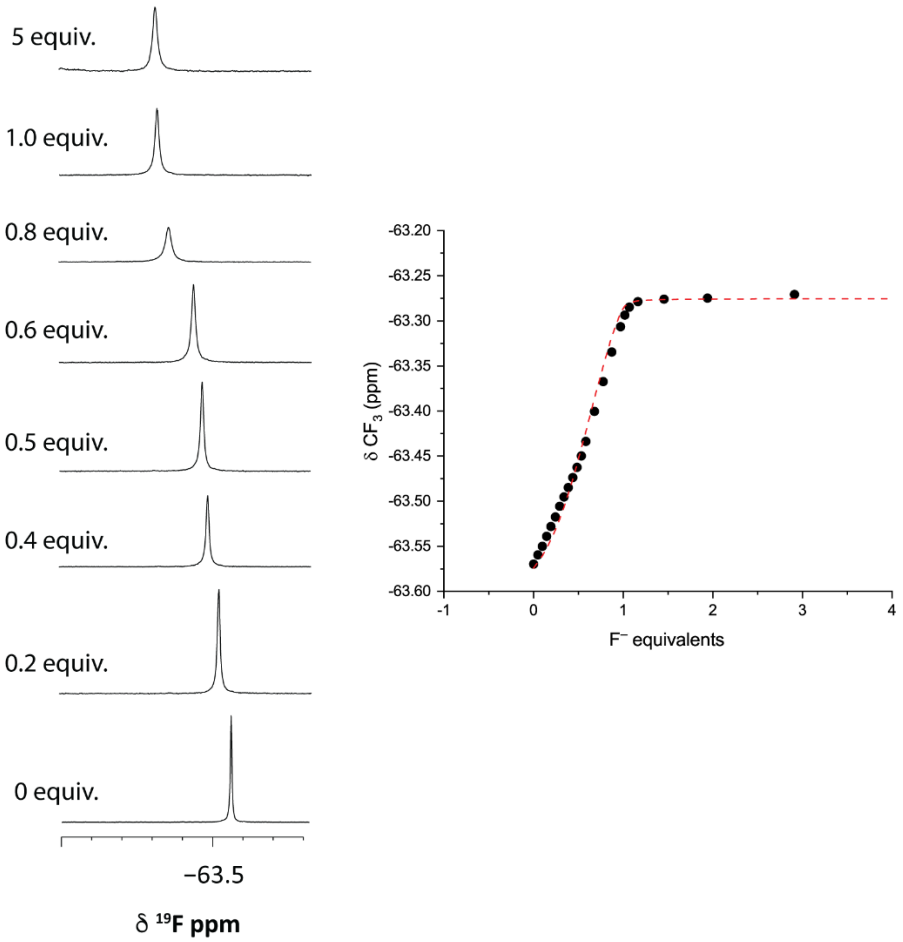



Figure 4.26: Stacked $^{19}F$ NMR for the titration of **4a** with TBAF in DCM-$d_2$ at 298 K (left); titration profiles (right), experimental points (black circles) and fitted function (dashed lines).

iPr BINAM urea **4u**

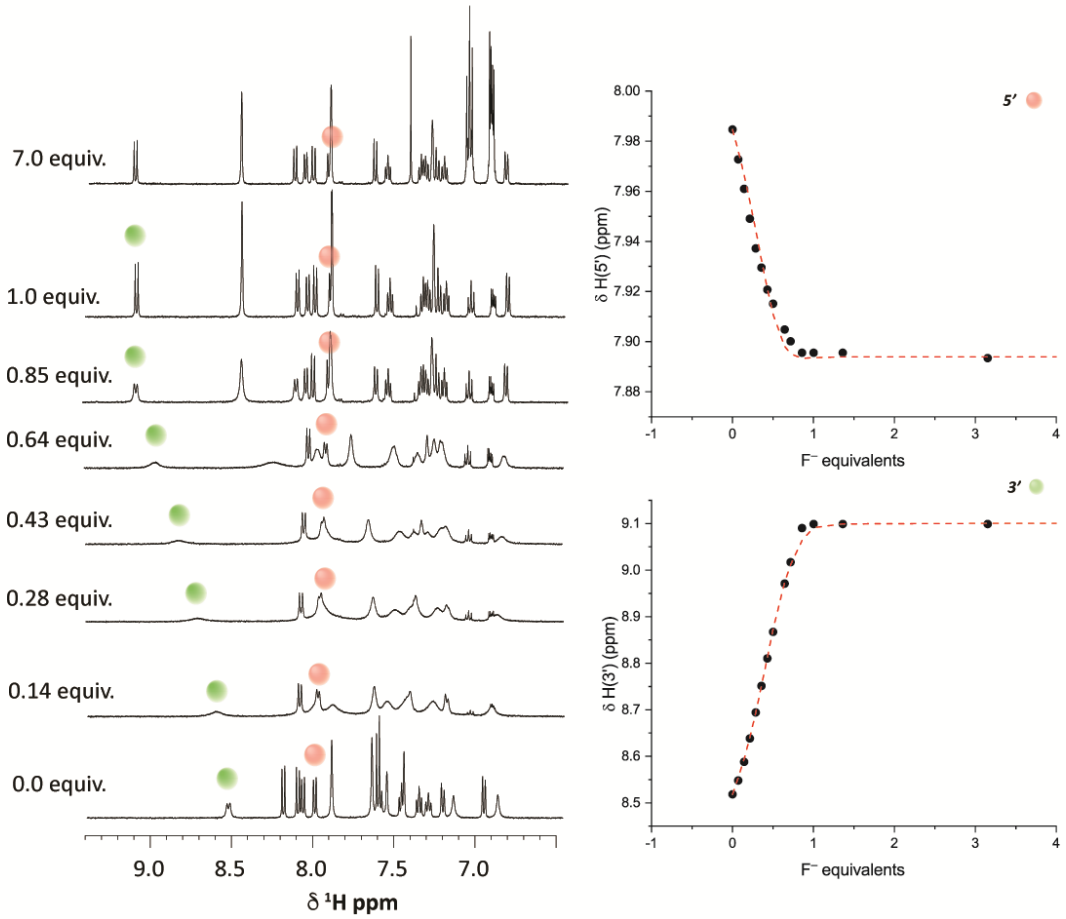



Figure 4.27: Stacked $^{1}$H NMR for the titration of **4u** with TBAF in DCM-$d_2$ at 298 K (left); titration profiles for H(5‘) and H(3‘) (right), experimental points (black circles) and fitted function (dashed lines).

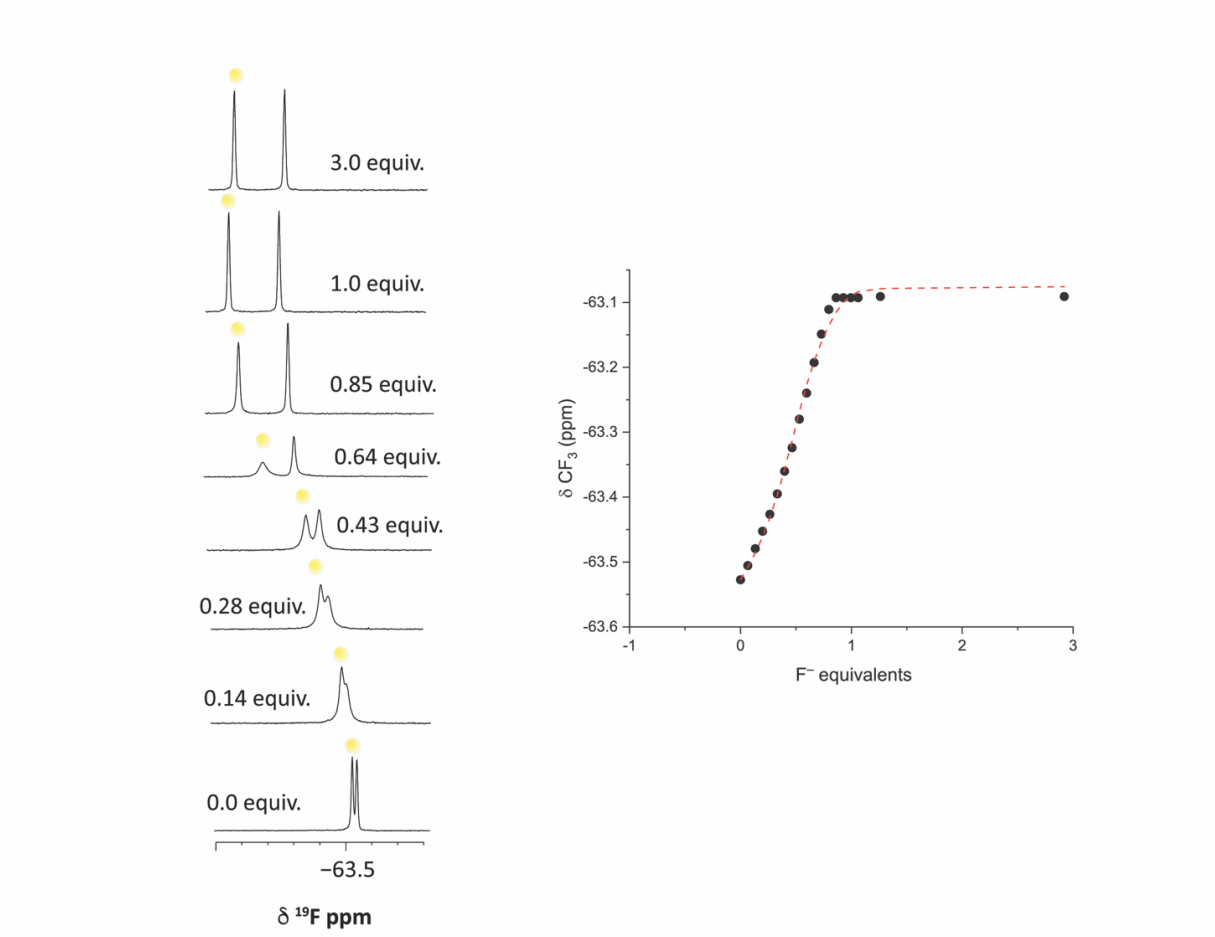



Figure 4.28: Stacked $^{19}F$ NMR for the titration of **4u** with TBAF in DCM-$d_2$ at 298 K (left); titration profiles (right), experimental points (black circles) and fitted function (dashed lines).

### *4.3.4 iPr BINAM Urea–TBAF Complex (**4u**:TBAF)*

#### *4.3.4.1 Sample Preparation*

An aliquot of **4u** was weighted inside a sealable NMR tube and dissolved in 0.5 ml of DCM-$d_2$. A solution of TBAF $3H_2O$ in DCM-$d_2$ at a known concentration was prepared according to the procedure previously described (*v. 4.3.3.2 NMR Titrations*). 1 equivalent of TBAF solution was then added to **4u** and the NMR tube sealed. The sample resulted stable for months stored at 253 K. NMR spectra of iPr BINAM Urea–TBAF complex (**4u**:TBAF) were recorded on an AVIII HD 500 or an AVIII HD 600 at room temperature, the samples were prepared at 3 mM concentration or at 10 mM for low sensitivity experiments. in DCM-$d_2$.

*4.3.4.2. Assignment and copy of NMR spectra*

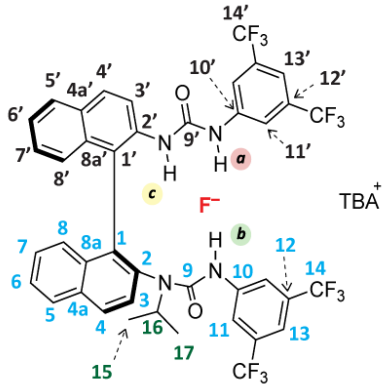



Figure 4.29: Structure and numbering of **4u**:TBAF.

Table 4.6: Assignment chart of **4u:**TBAF (500 MHz, DCM-$d_2$, 3 mM, 298 K); [a] 10 mM

| $^1$H | δ [ppm] | Multiplicity $^nJ$ [Hz] |
|---|---|---|
| NH(a) | 12.8 | d, $^{1h}J_{FH}$ = 61 |
| NH(b) | 12.2 | d, $^{1h}J_{FH}$ = 51 |
| NH(c) | 10.5 | d, $^{1h}J_{FH}$ = 34 |
| 3’ | 9.04 | d, $^3J_{HH}$ = 9.1 |
| 11 | 8.36 | s |
| 4 | 8.07 | d, $^3J_{HH}$ = 8.7 |
| 5 | 8.00 | d, $^3J_{HH}$ = 8.2 |
| 4’ | 7.95 | d, $^3J_{HH}$ = 9.2 |
| 5’ | 7.85 | d, $^3J_{HH}$ = 8.2 |
| 11’ | 7.81 | s |
| 3 | 7.56 | d, $^3J_{HH}$ = 8.8 |
| 6 | 7.49 | t, $^3J_{HH}$ = 7.5 |
| 6’, 7 | 7.28; 7.26 | t, overlap |
| 13, 13’ | 7.21 | s |
| 8 | 7.18 | d, $^3J_{HH}$ = 8.6 |
| 7’ | 7.14 | t, $^3J_{HH}$ = 7.5 |
| 8’ | 6.75 | d, $^3J_{HH}$ = 8.5 |
| 16 | 3.11 | sept, $^3J_{HH}$ = 6.6 |
| 17 | 1.25 | d, $^3J_{HH}$ = 6.8 |
| 15 | 0.33 | d, $^3J_{HH}$ = 6.8 |
| $^{19}$F | δ [ppm] | Multiplicity $^nJ_{FH}$ [Hz] |
| 14/14’ | -63.1 or -63.3 | s |
| F⁻ | -89.9 | ddd |

| $^{13}$C [a] | δ [ppm] | Multiplicity $^nJ_{CF}$ [Hz] |
|---|---|---|
| 9 or 9’ | 155.6 or 155.0 | s |
| 10 | 144.37 | s |
| 2 | 143.13 | s |
| 10’ | 143.12 | s |
| 2’ | 138.54 | s |
| 8a | 134.90 | s |
| 8a’ | 133.90 | s |
| 4a | 133.23 | s |
| 1 | 131.60 | s |
| 12, 12’ | 131.4 | q, $^2J$ = 30 |
| 4a’ | 129.90 | s |
| 1’ | 118.95 | s |
| 14 | 124.22 | q, $^1J$ = 273 |
| 14’ | 124.20 | q, $^1J$ = 273 |
| 4 | 130.37 | s |
| 3 | 129.07 | s |
| 4’ | 129.06 | s |
| 5 | 128.53 | s |
| 5’ | 128.30 | s |
| 8 | 126.86 | s |
| 7 | 126.72 | s |
| 7’ | 126.56 | s |
| 6 | 126.34 | s |
| 8’ | 125.21 | s |
| 6’ | 123.54 | s |
| 3’ | 120.01 | s |
| 11 | 119.84 | s |
| 11’ | 118.03 | s |
| 13, 13’ | 113.58 | s |
| 16 | 56.58 | s |
| 15 | 19.72 | s |
| 17 | 18.68 | s |

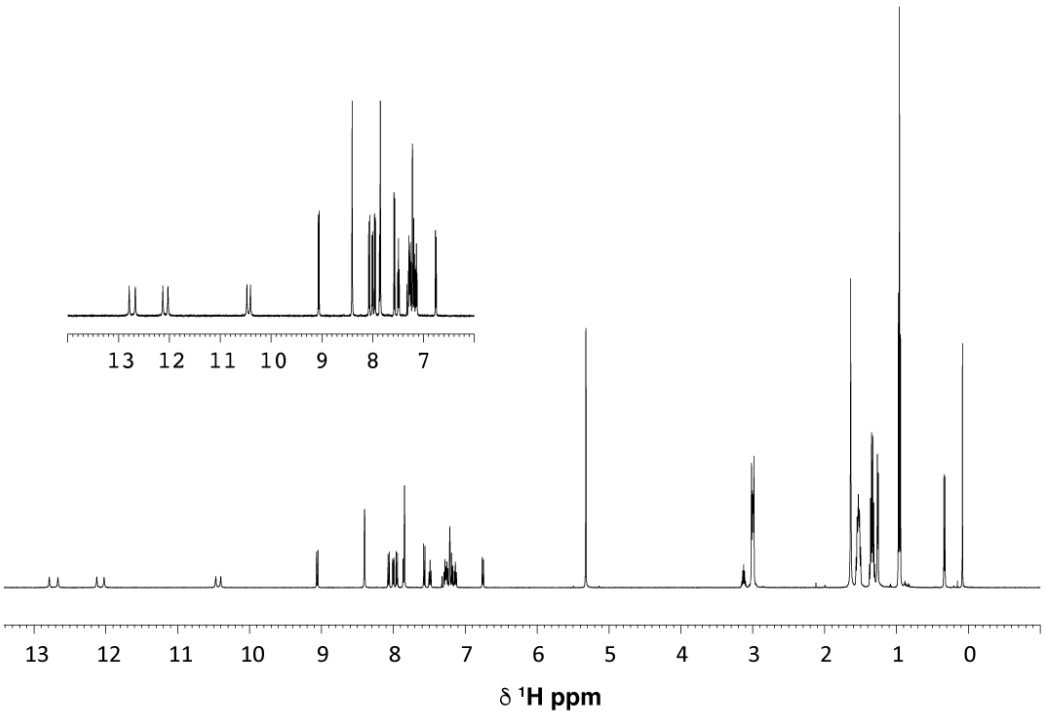



Figure 4.30: $^{1}$H NMR of **4u**:TBAF, (DCM-$d_2$, 3 mM, 298 K).

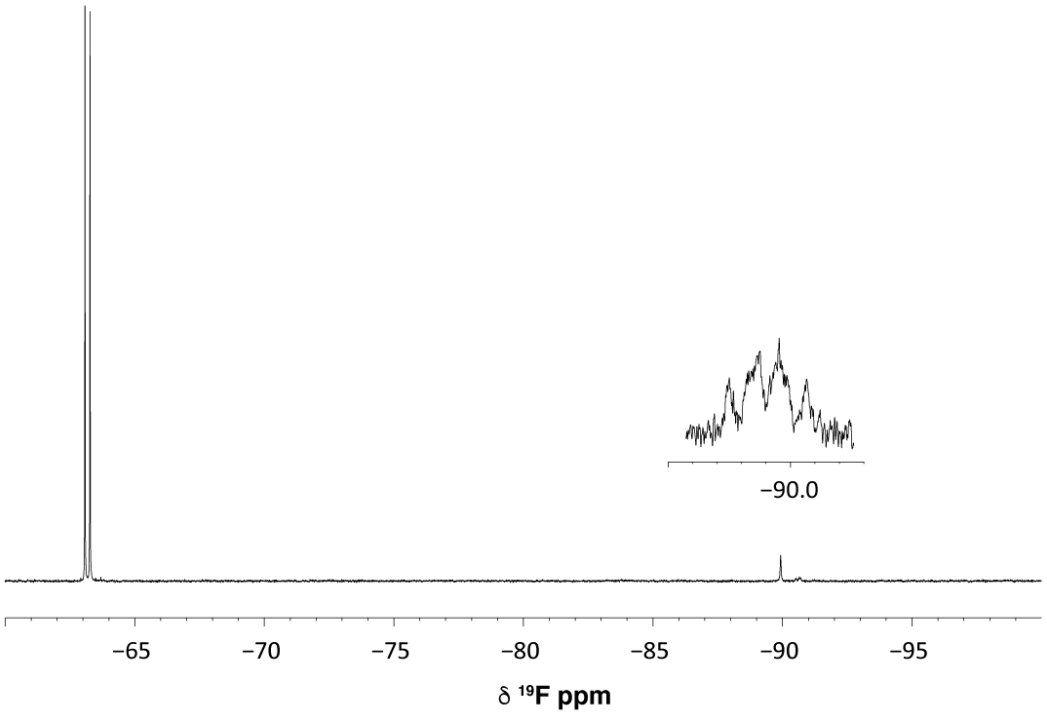



Figure 4.31: $^{19}$F{$^{1}$H} NMR of **4u**:TBAF, $^{19}$F NMR detail of fluoride splitting (inset), (DCM-$d_2$, 3 mM, 298 K).

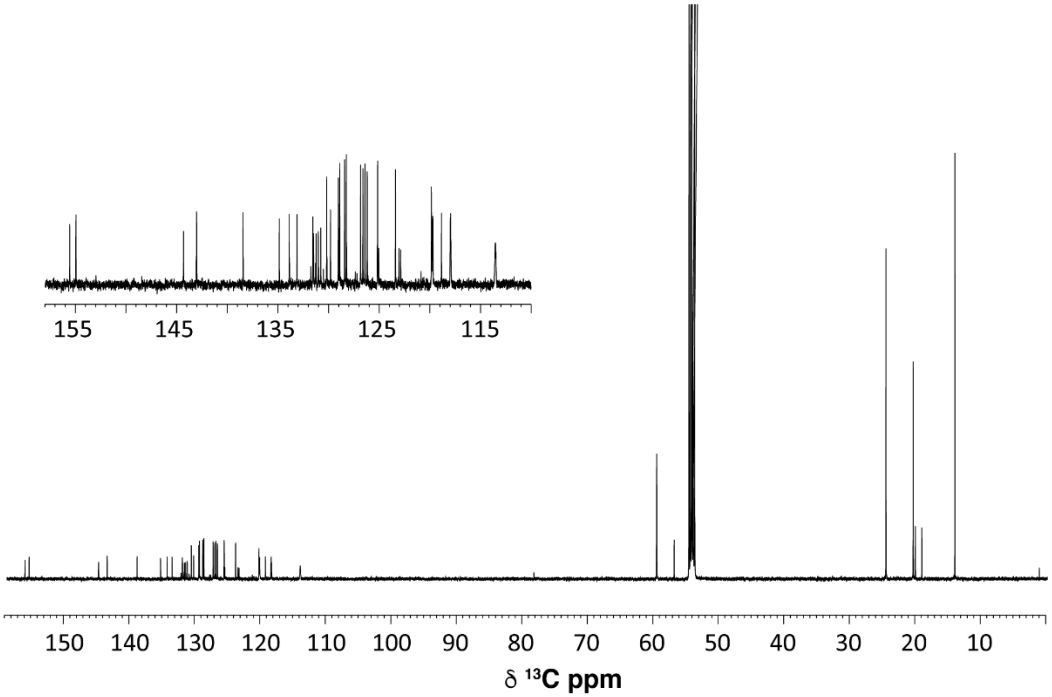



Figure 4.32: $^{13}C$ NMR of **4u**:TBAF, (DCM-$d_2$, 10 mM, 298 K).

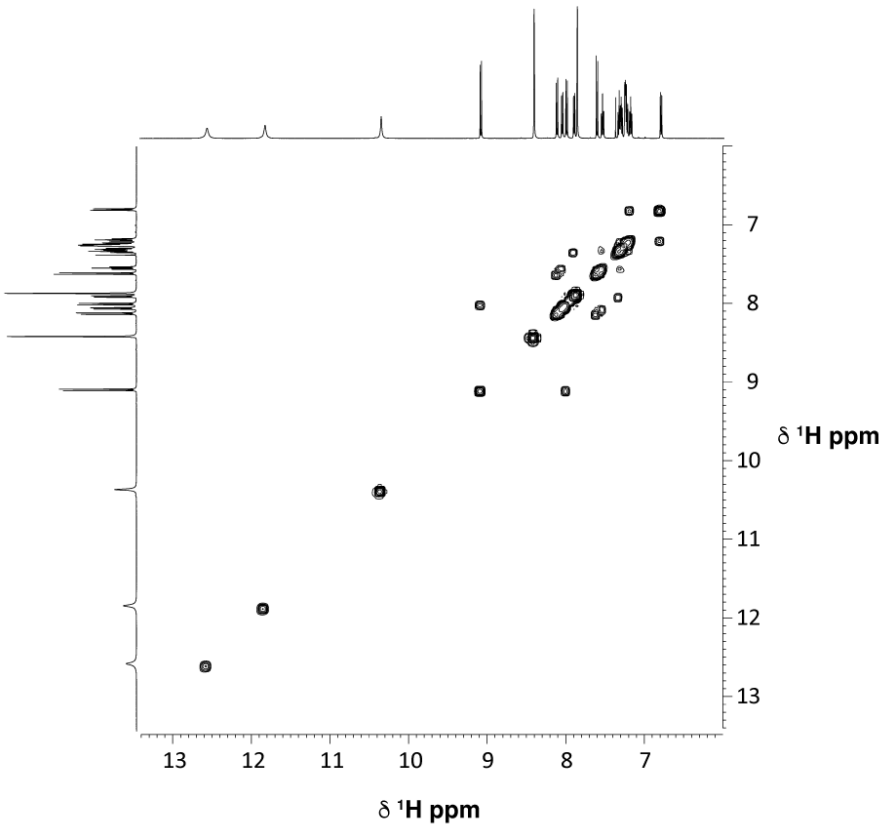



Figure 4.33: $^{1}$H COSY of **4u**:TBAF, (DCM-$d_2$, 10 mM, 298 K).

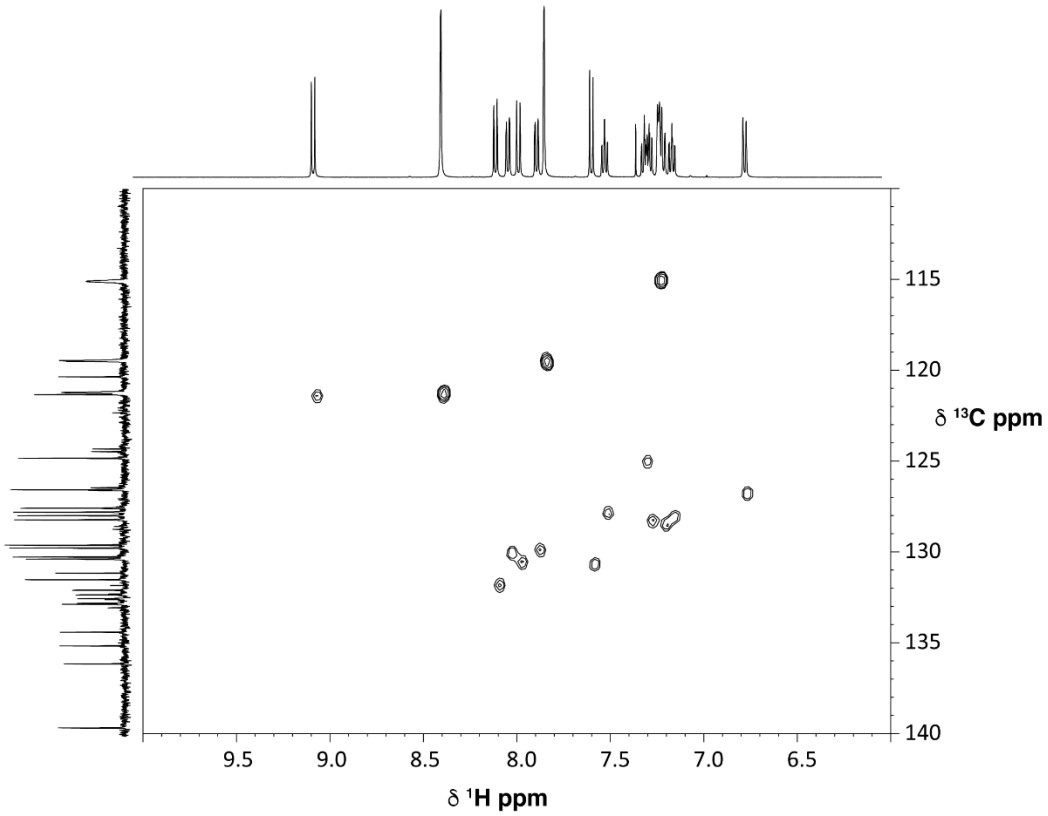



Figure 4.34: $^{1}H$-$^{13}C$ HSQC of **4u**:TBAF, (DCM-$d_2$, 10 mM, 298 K).

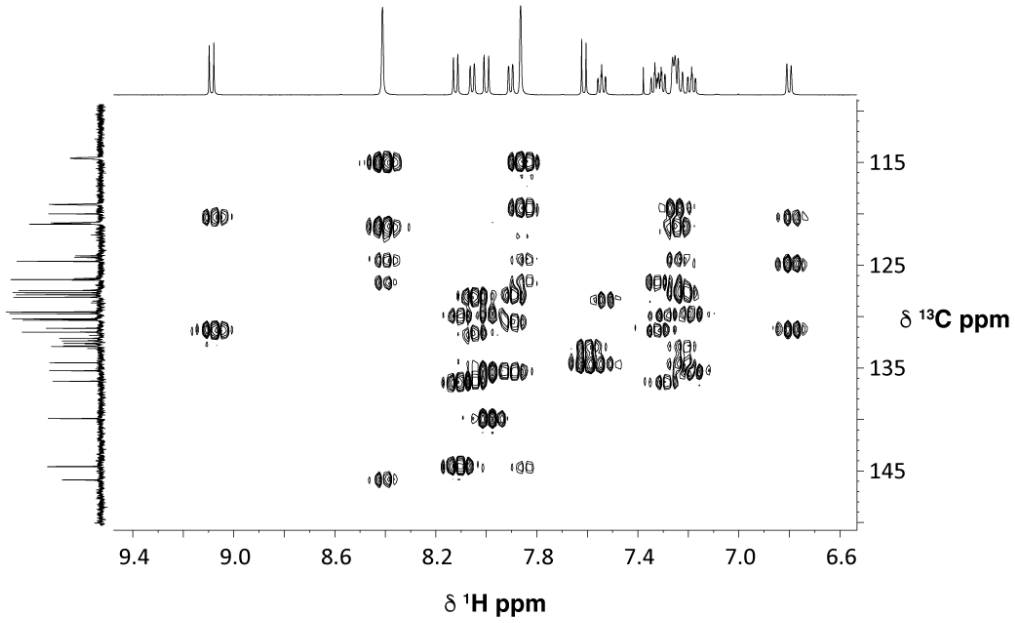



Figure 4.35: $^{1}H$-$^{13}C$ HMBC of **4u**:TBAF, (DCM-$d_2$, 10 mM, 298 K).

*4.3.4.3 Concentration and Variable Temperature Studies*

$^{1}H$ NMR and $^{19}F$ NMR spectra were recorded for samples of **4u**:TBAF at different concentrations 3, 10 and 25 mM, in DCM-$d_2$.

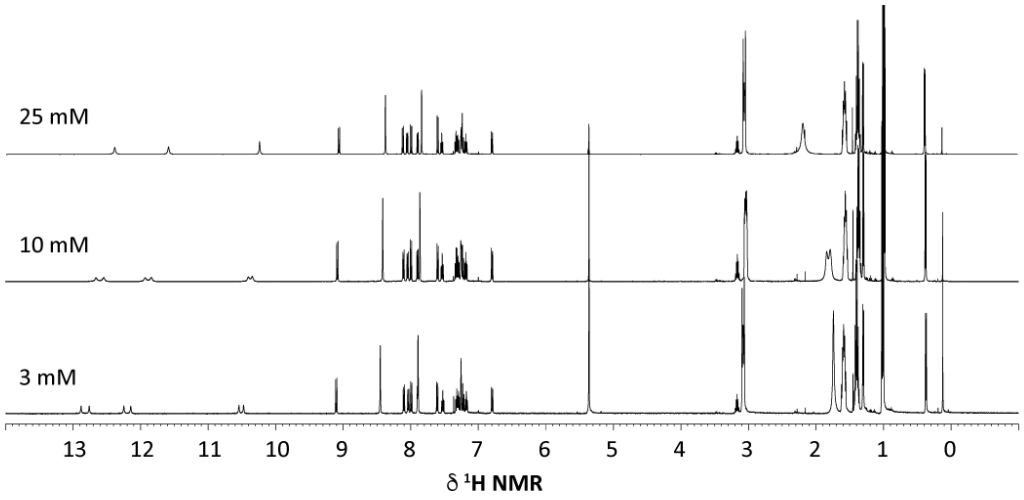



Figure 4.36: $^{1}H$ NMR spectra of **4u**:TBAF, 3–25 mM, 298 K.

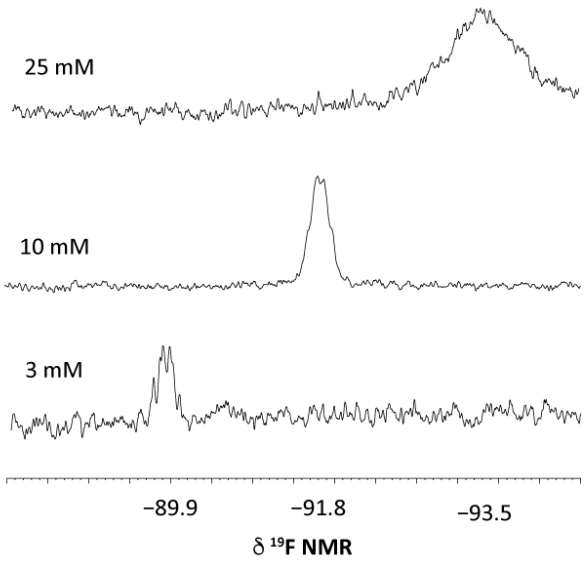



Figure 4.37: $^{1}H$ NMR spectra of **4u**:TBAF, 3–25 mM, 298 K.

$^1$H NMR **4u**:TBAF was recorded for a 25 mM sample at different temperatures, between 298 K and 233 K, in DCM-$d_2$.

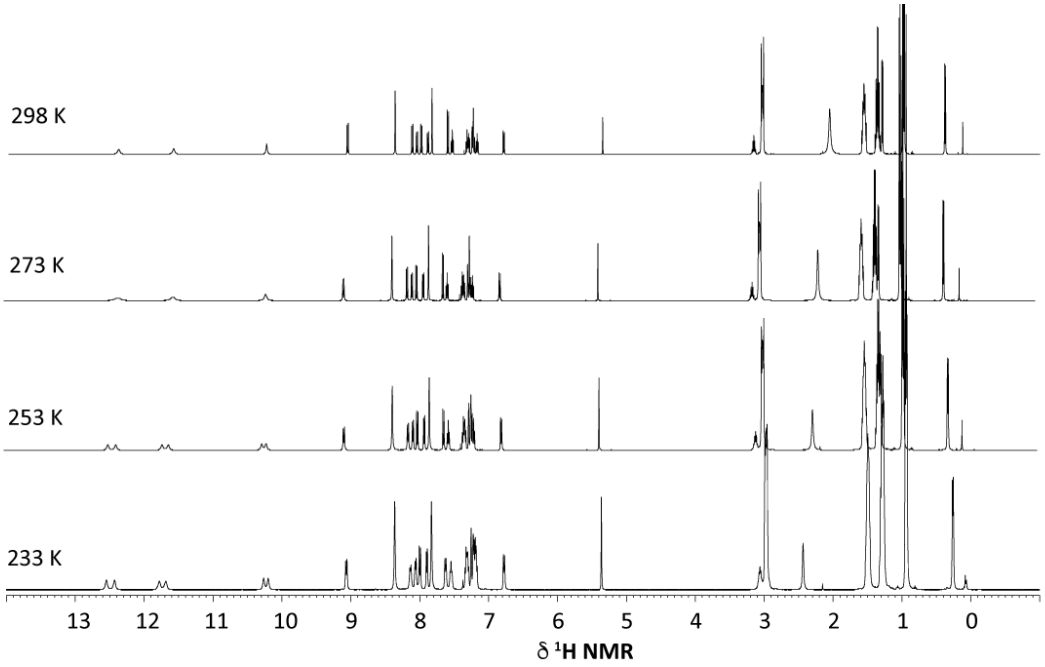



Figure 4.38: $^1$H NMR spectra of **4u**:TBAF, 25 mM, 298–253 K.

*3.4.4 1H-19F CLIP-HSQC*

$^{1}H$-$^{19}F$ CLIP-HSQC experiments were recorded on an AVIII HD 500 using a 3 mM sample (*v. 4.3.4.1 Sample Preparation*), at 298 K. The experiments were acquired using a modified sequence, from a previously developed one (*hsqcetgpclip*)[17] and the following parameters.

| Parameter | Value |
|---|---|
| TD | 2058 (f2) x 128 (f1) |
| SW | 10 (f2) x 60 (f1) |
| o1p/o2p | 10/-90 ppm |
| NS (DS) | 8 (4) |
| relaxation delay d1 | 2 s |
| delay for evolution of coupling CNST[2] | 48 Hz |

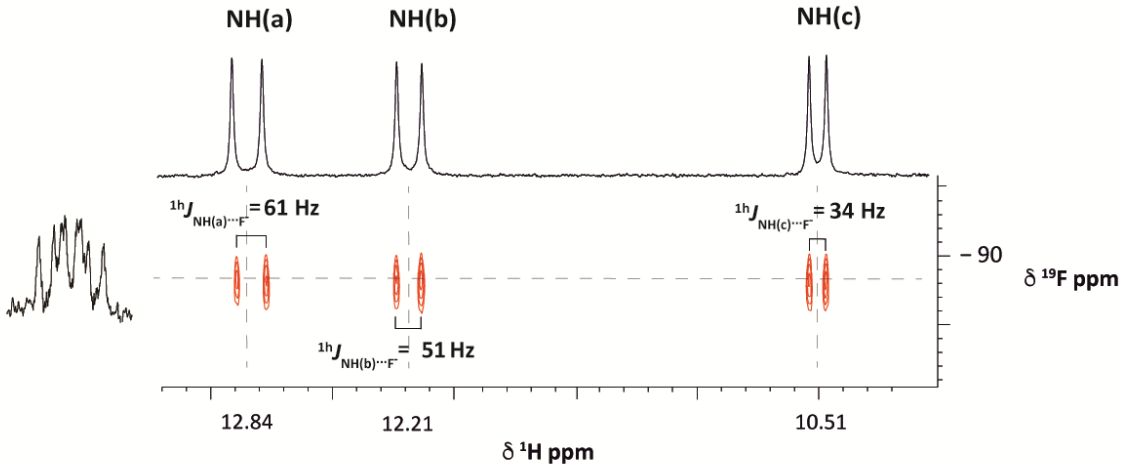



Figure 4.39: $^{1}H$-$^{19}F$ CLIP-HSQC of **4u**:TBAF, (500 MHz, DCM-$d_2$, 3 mM, 298 K).

*4.3.4.5 HOESY*

*For relative distance determination* – A 10 mM sample of **4u**:TBAF was prepared (*v.* 4.3.4.1 Sample preparation). 1D heteronuclear $^{1}H$-$^{19}F$ nOe experiments (HOESY) were acquired on a AVIII HD 500 using a previously developed pulse sequence (*hoesyfhgp1d*) and the parameters below.

| Parameter | Value |
|---|---|
| TD | 32768 pt |
| SW | 20 ppm |
| o1p/o2p | 5/-90 ppm |
| NS (DS) | 512 (16) |
| relaxation delay d1 | 3 s |
| mixing time d8 (n. experiments) | 10–600 ms (9) |

nOe build-up curves (Figure 4.40, Table 4.7) for the nOe developed between fluoride and NH protons were used to calculate the relative distances according to equation 4.1:

$$\eta_{NH}\{F^-\} \propto r_{NH-F}^{-6} \qquad (eq\ 4.1)$$

$\eta_{NH}\{F^-\}$ = NH···F⁻ nOe build-up rate
$r_{NH-F}$ = NH···F⁻ distance

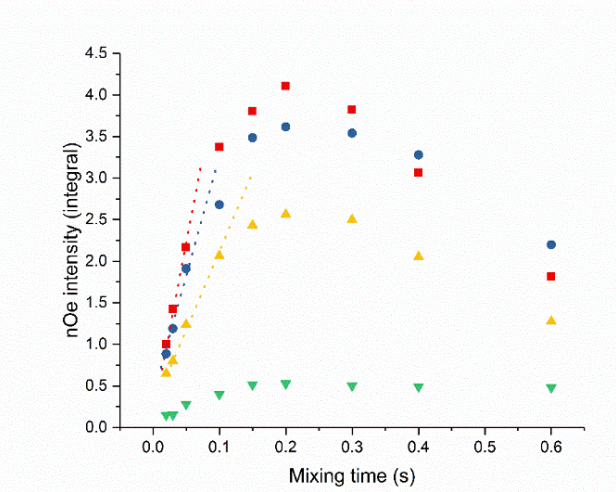



Figure 4.40: $^{1}H$-$^{19}F$ nOe build-up curves for NH-F and CH-F interactions of **4u**:TBAF, (DCM-$d_2$, 10 mM, 298 K).

Table 4.7: Determination of relative XH–F distances (NH(a) = 1.00) for **4u**:TBAF.

| nOe correlation | nOe build-up rate, η | $\sqrt[6]{\frac{1}{\eta}}$ | Distance, relative to H(a)–F = 1.0 |
|---|---|---|---|
| NH(a)–F | 38.579 | 0.544 | **1.00** |
| NH(b)–F | 34.373 | 0.555 | **1.02** |
| NH(c)–F | 19.868 | 0.608 | **1.12** |
| CH(11)–F | 2.880 | 0.838 | **1.54** |

*For absolute distance determination* – A 3 mM sample of **4ad**:TBAF was prepared (*v.* 4.3.4.1 Sample preparation, using **4ad** instead of **4u**). 1D heteronuclear $^{1}$H-$^{19}$F nOe experiments (HOESY) were acquired on an AVIII 500 using a previously developed pulse sequence (*hoesyfhgp1d*) and the parameters below.

| Parameter | Value |
|---|---|
| TD | 8192 pt |
| SW | 14 ppm |
| o1p/o2p (fluoride) | 7/-90.3 ppm |
| o1p/o2p (H-F reference) | 7/-112 |
| NS (DS) | 3379 (16) |
| relaxation delay d1 | 6 s |
| mixing time d8 | 30 ms |

Two experiments, irradiating $F^-$ (-90.3 ppm) and the F reference (-112 ppm), and using a mixing time (30 ms) known to lay within the linear-growth region of the nOe were used to calculate absolute NH–F distances (Table 4.8) according to equation 4.2.

$$r_{NH-F} = \sqrt[6]{\frac{I_{H-F\,ref.}}{I_{NH-F}}}\, r_{H-F\,ref.} \qquad (eq\ 4.2)$$

$r_{NH-F}$ = NH···$F^-$ distance
$r_{H-F\,ref.}$ = H-F reference distance = 2.60 Å
$I_{NH-F}$ = nOe intensity between NH···$F^-$
$I_{H-F\,ref.}$ = nOe intensity for the H-F reference

Table 4.8: Determination of absolute NH–F distances for **4ad**:TBAF.

| nOe correlation | $I_{H-F}$ | Absolute H···F distance [Å] | $^{1h}J_{NH-F}$ [Hz] |
|---|---|---|---|
| NH(a) | 1.00 | 1.83 | 60 |
| NH(b) | 0.77 | 1.91 | 48 |
| NH(c) | 0.5 | 2.05 | 35 |
| H(11)–F (ref.) | 0.12 | 2.60 | – |

*4.3.4.6 NOESY*

NOESY spectra were acquired on a AVIIIHD 600 using a previously developed pulse sequence (*noesygpphzs*)[18] with the parameters reported below.

| Parameter | Value |
|---|---|
| TD | 2048 (f1) x 256 (f2) pt |
| SW | 20 (f1) x 20 (f2) ppm |
| NS (DS) | 32 (16) |
| relaxation delay d1 | 3 s |
| mixing time d8 | 300 ms |

NOESY cross-peaks were integrated to quantify internuclear distances, taking as a reference H(3')–H(4') = 2.46 Å. Internuclear distances were determined using the equations 4.3 and 4.4 and reported in Table 4.9.[19]

$$r_{ij} = r_{ref} \sqrt[6]{\frac{z_{ref}}{z_{ij}}} \text{ (eq 4.3)} \quad z = \frac{2\, v_{raw}}{n_{diag2} v_{diag1} + n_{diag1} v_{diag2}} \text{ (eq. 4.4)}$$

$r_{i,J}$ = i,j distance [Å]
$r_{ref}$ = reference distance [Å]
$z_{ref}$ = cross-peak volume of the reference corrected according to equation 4.4
$z_{i,j}$ = cross-peak volume of the i, j correlation corrected according to equation 4.4
$v_{raw}$ = uncorrected volume of the cross peak
$v_{diag}$ = volume of the diagonal peak for each pair of interacting proton
$n_{diag}$ = number of nuclei of each signal

Table 4.9: Determination of absolute interproton distances for **4u**:TBAF.

| nOe cross peaks | z(i) | v(i) | (Zref/Z(i))^(1/6) | r ref | v ref | z ref | Distance [Å] |
|---|---|---|---|---|---|---|---|
| 16-8' | -0.016801 | -0.78 | 1.04228 | 2.46 | -1 | -0.022302 | 2.6 |
| NHa-NHc | -0.069323 | -1.47 | 0.827769 | 2.46 | -1 | -0.022302 | 2.0 |
| NHb-NHc | -0.018404 | -0.43 | 1.032536 | 2.46 | -1 | -0.022302 | 2.5 |
| Nha-11 | -0.003001 | -0.18 | 1.39696 | 2.46 | -1 | -0.022302 | 3.4 |
| Nha11' | -0.017299 | -0.62 | 1.082932 | 2.46 | -1 | -0.022302 | 2.7 |
| Nhb-11 | -0.012907 | -0.83 | 1.095427 | 2.46 | -1 | -0.022302 | 2.7 |
| Nhb-3 | -0.005844 | -0.19 | 1.250066 | 2.46 | -1 | -0.022302 | 3.1 |
| 3-16 | -0.001551 | -0.07 | 1.557699 | 2.46 | -1 | -0.022302 | 3.8 |

*4.3.4.7 T1 measurements*

The longitudinal relaxation time constants T1, were measured *via* $^{19}F$ inversion recovery experiments (*t1ir*) on an AVIII 500. T1 was calculated by non-linear fitting using Dynamic Center 2.3.3.

A 3 mM sample of **4u**:TBAF was used (*v. 4.3.4.1 Sample Preparation*), and a $^{19}F$ inversion recovery experiment was acquired with the following parameters.

| Parameter | Value |
|---|---|
| TD | 16384 |
| SW | 10 |
| o1p | -90 ppm |
| NS (DS) | 2 (0) |
| relaxation delay d1 | 30 s |
| variable delays (n. of points) | 0.01–5 s (10) |

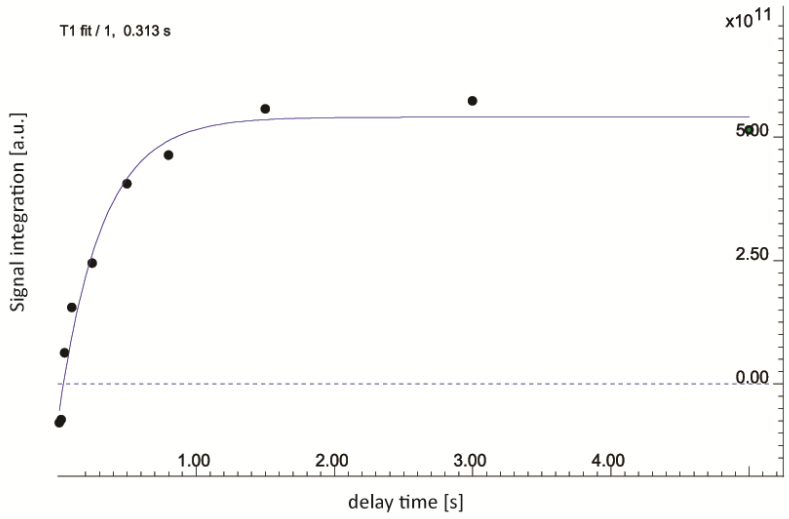



Figure 4.41: Inversion recovery plot of **4u**:TBAF, experimental data (dots) and fitted function (line). T1 = 0.313 s.

A 0.05 M sample of TBAF in DCM-$d_2$ was prepared by dissolving TBAF·3$H_2O$ (Merck, Tetrabutylammonium fluoride hydrate 98%) and 5 microliters of 4-fluoranisole in 1 ml of DCM-$d_2$ measured in a volumetric flask. The concentration of fluoride was determined by quantitative $^{19}$F NMR (*v. 4.3.3.2 NMR Titrations*). The $^{19}$F inversion recovery experiment was acquired with the following parameters.

| Parameter | Value |
|---|---|
| TD | 16384 |
| SW | 10 |
| o1p | -118 ppm |
| NS (DS) | 2 (0) |
| relaxation delay d1 | 30 s |
| variable delays (n. of points) | 0.005–10 s (10) |

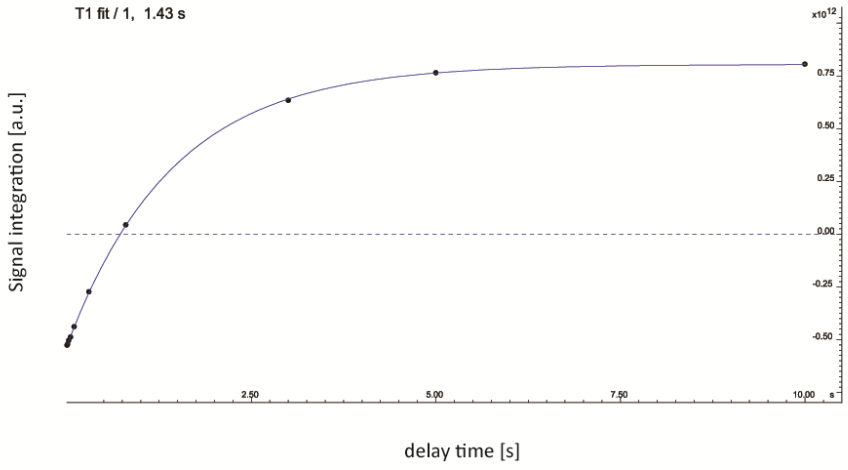



Figure 4.42: Inversion recovery plot of TBAF·3$H_2O$ in DCM-$d_2$, experimental data (dots) and fitted function (line). T1 = 1.43 s.

### *4.3.5 Hydrogen Bonding Coupling of bis-Urea–TBAF Complexes*

#### *4.3.5.1 Sample Preparation*

An aliquot of the selected *bis*-urea (~ 0.0015 mmol) was accurately weighted in an NMR tube and dissolved in 0.5 mL of DCM-$d_2$ (~ 3 mM final concentration). A solution of TBAF $3H_2O$ in DCM-$d_2$ at a known concentration was prepared according to the procedure at page 266 *(v. 4.3.1.2 NMR Titrations*). 1 equivalent of TBAF solution in DCM-$d_2$ was then added to the NMR tube. $^{1}$H NMR,$^{19}$F NMR, $^{1}$H NOESY and $^{1}$H-$^{19}$F CLIP-HSQC were recorded on an AVIII HD 500 at 273 K.

*4.3.5.2 Copy of NMR spectra*

*(S)-BINAM Urea–TBAF complex (**4a**:TBAF)*

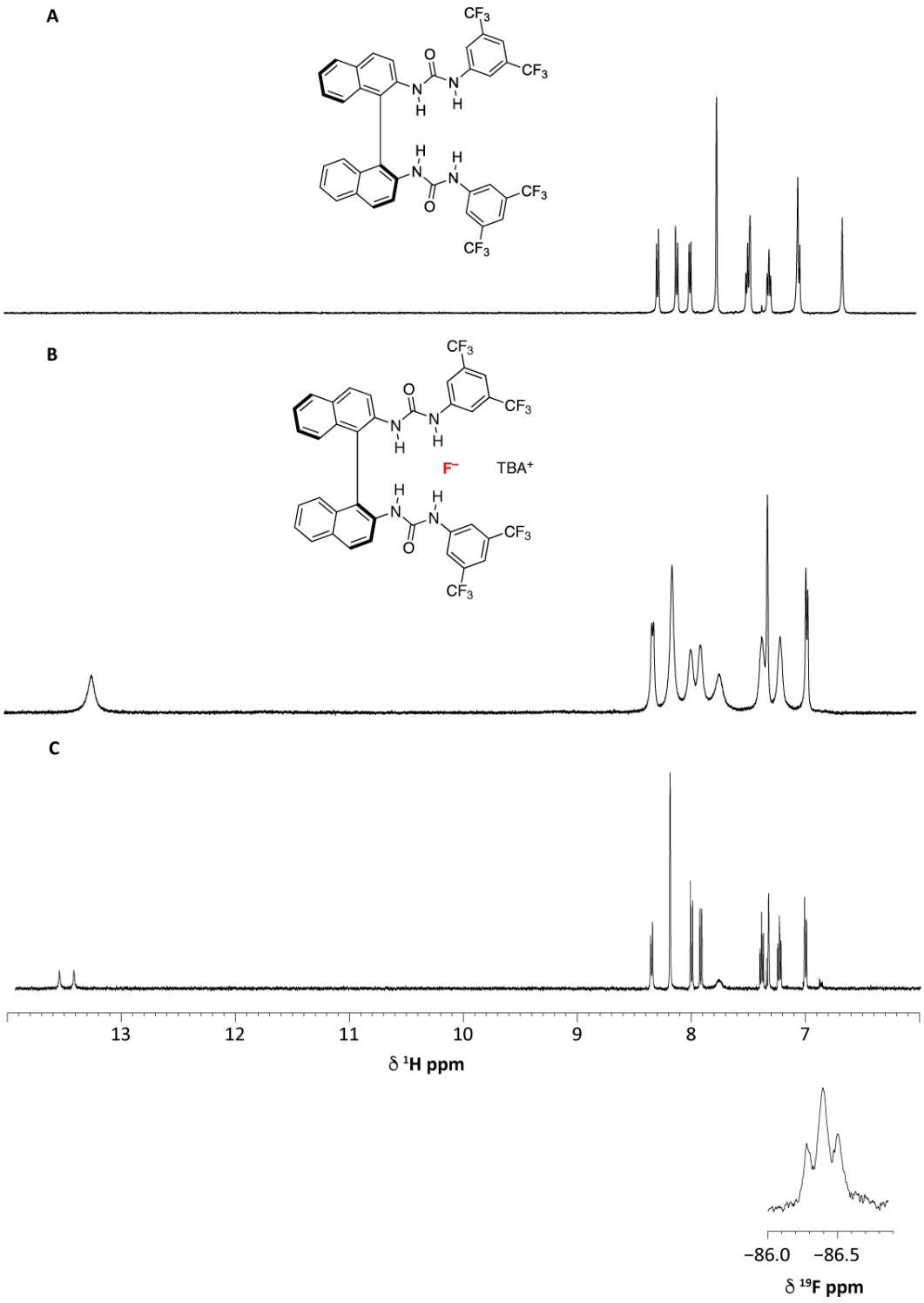



Figure 4.43: A) $^{1}$H NMR of **4a**, (DCM-$d_2$, 3 mM, 273 K); B) $^{1}$H NMR of **4a**:TBAF, (DCM-$d_2$, 3 mM, 273 K); $^{1}$H NMR of **4a**:TBAF, (DCM-$d_2$, 0.58 mM, 273 K); $^{19}$F NMR of **4a**:TBAF showing fluoride splitting, (DCM-$d_2$, 0.58 mM, 273 K)

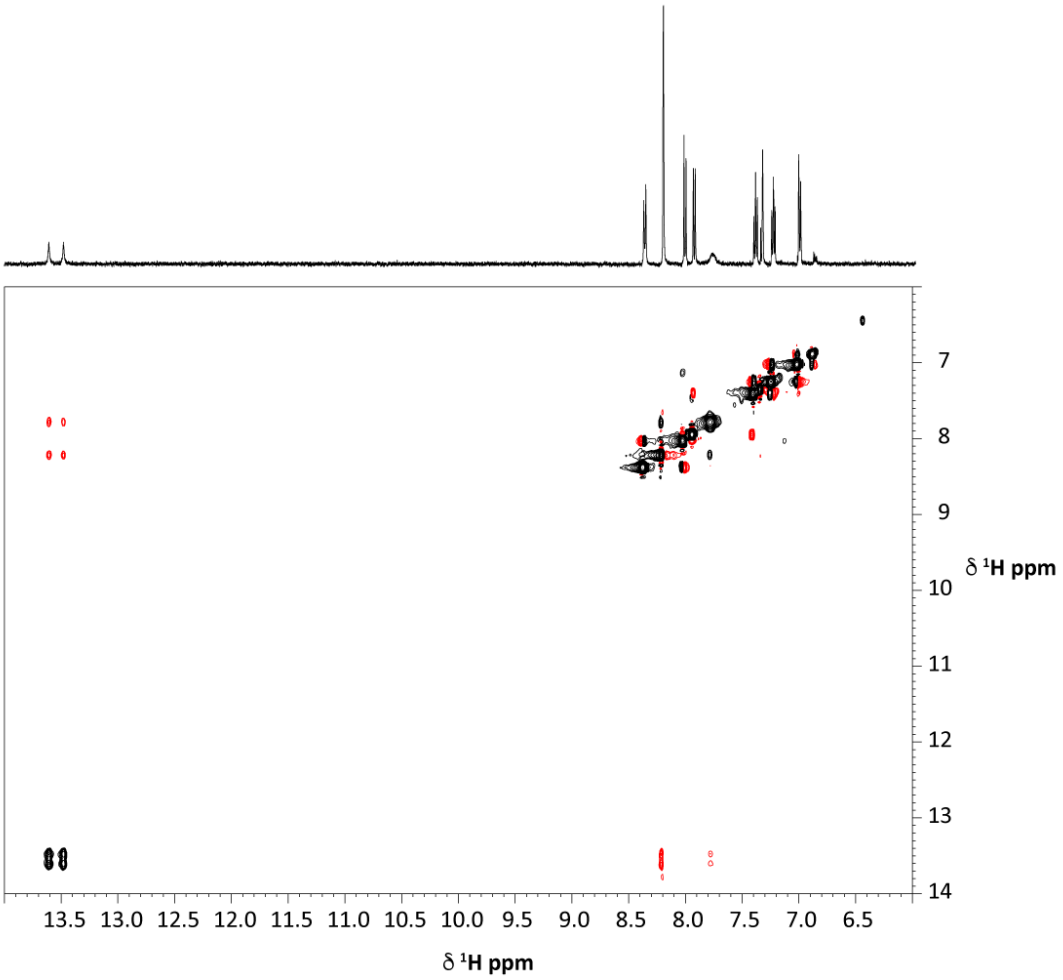



Figure 4.44: $^{1}$H NOESY of **4a**:TBAF (DCM-$d_2$, 0.58 mM, 298 K).

*(S)-Me BINAM Urea–TBAF complex (**4s**:TBAF)*

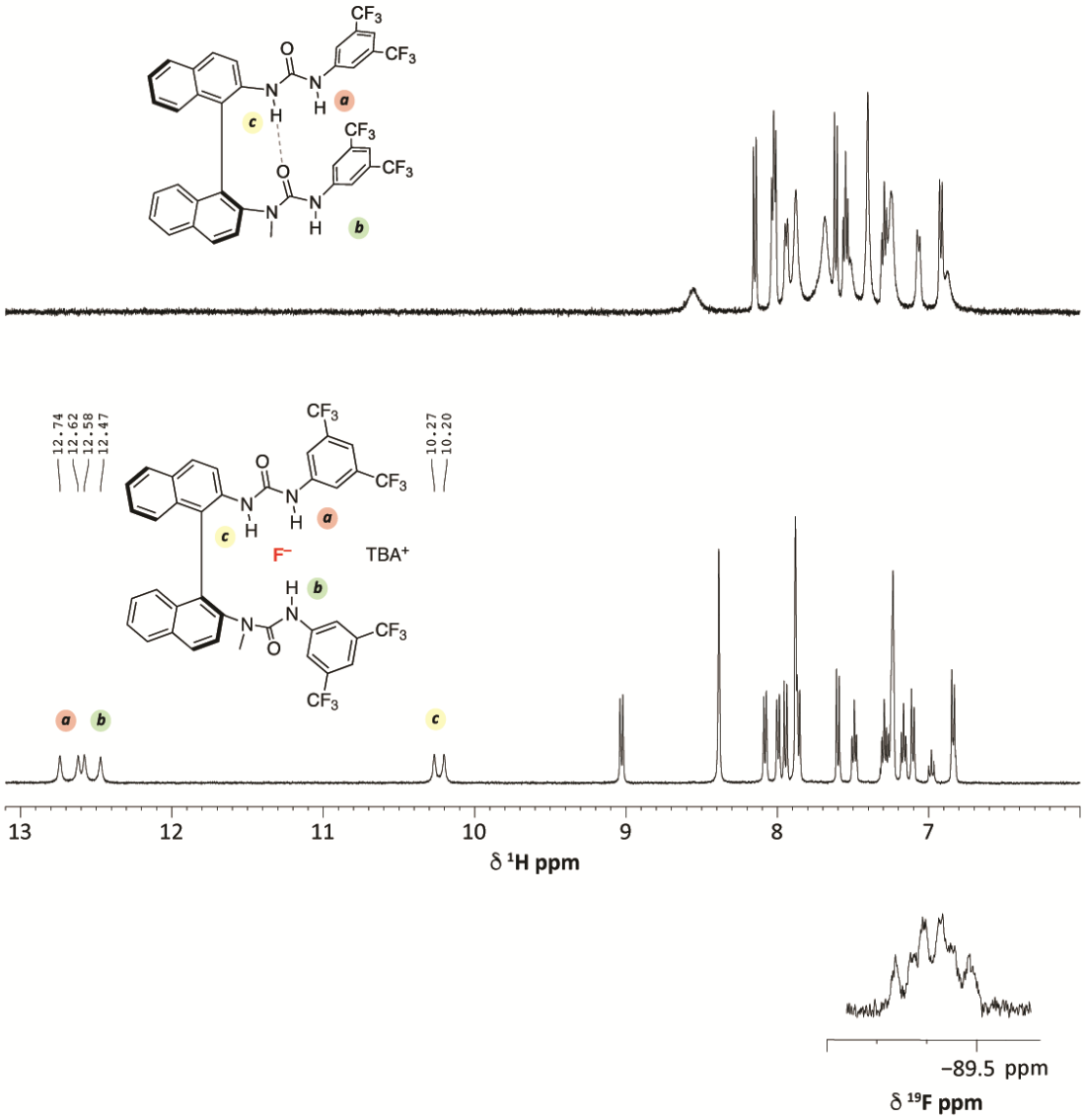



Figure 4.45: $^{1}H$ NMR of **4s** and **4s**:TBAF, $^{19}F$ NMR of showing fluoride splitting, (DCM-$d_2$, 3mM, 273 K).

*(S)-Et BINAM Urea–TBAF complex (**4t**:TBAF)*

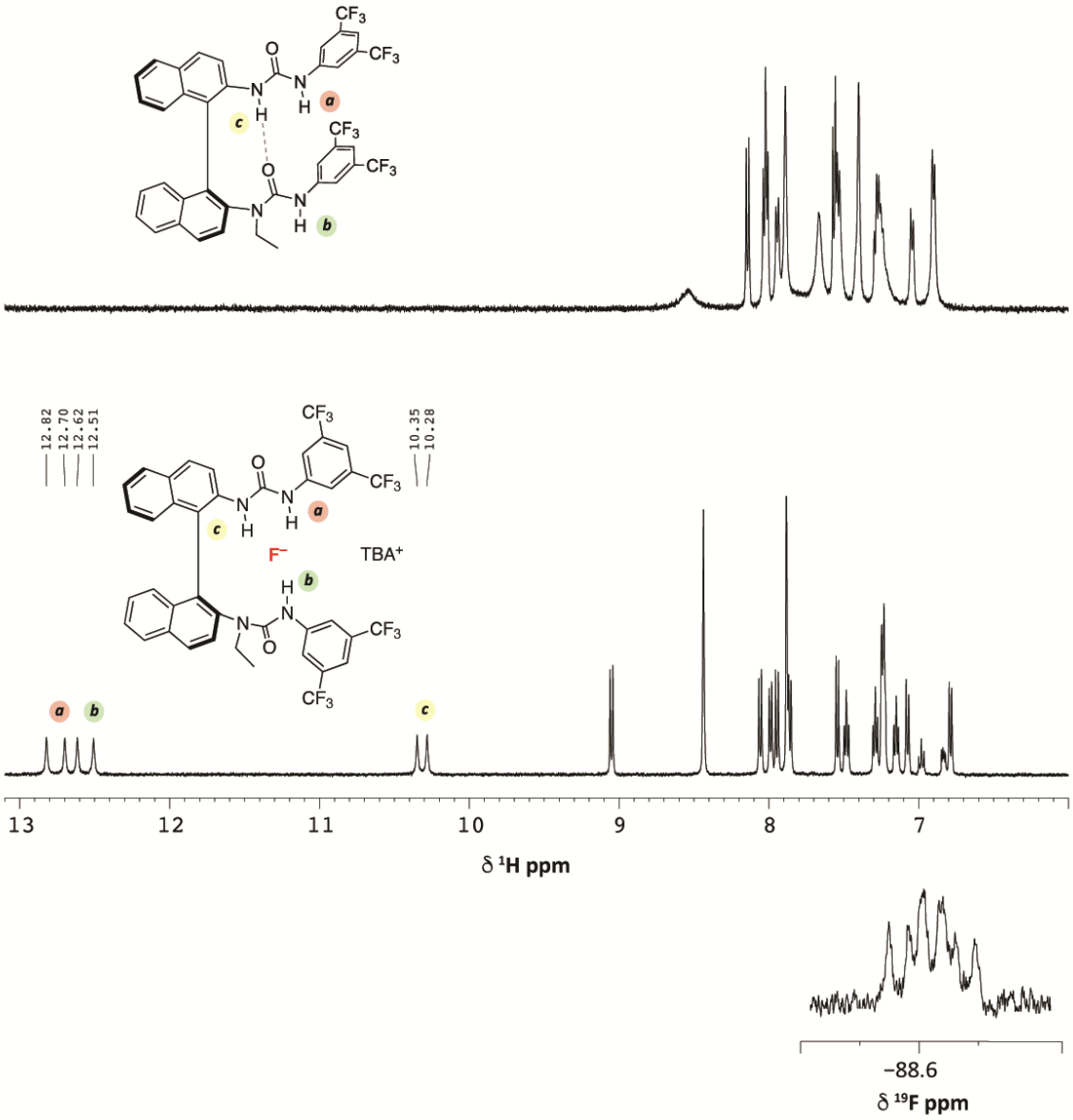



Figure 4.46: $^{1}$H NMR of **4t** and **4t**:TBAF, $^{19}$F NMR of showing fluoride splitting, (DCM-$d_2$, 3mM, 273 K).

*(S)-nPr BINAM Urea–TBAF complex (**4v**:TBAF)*

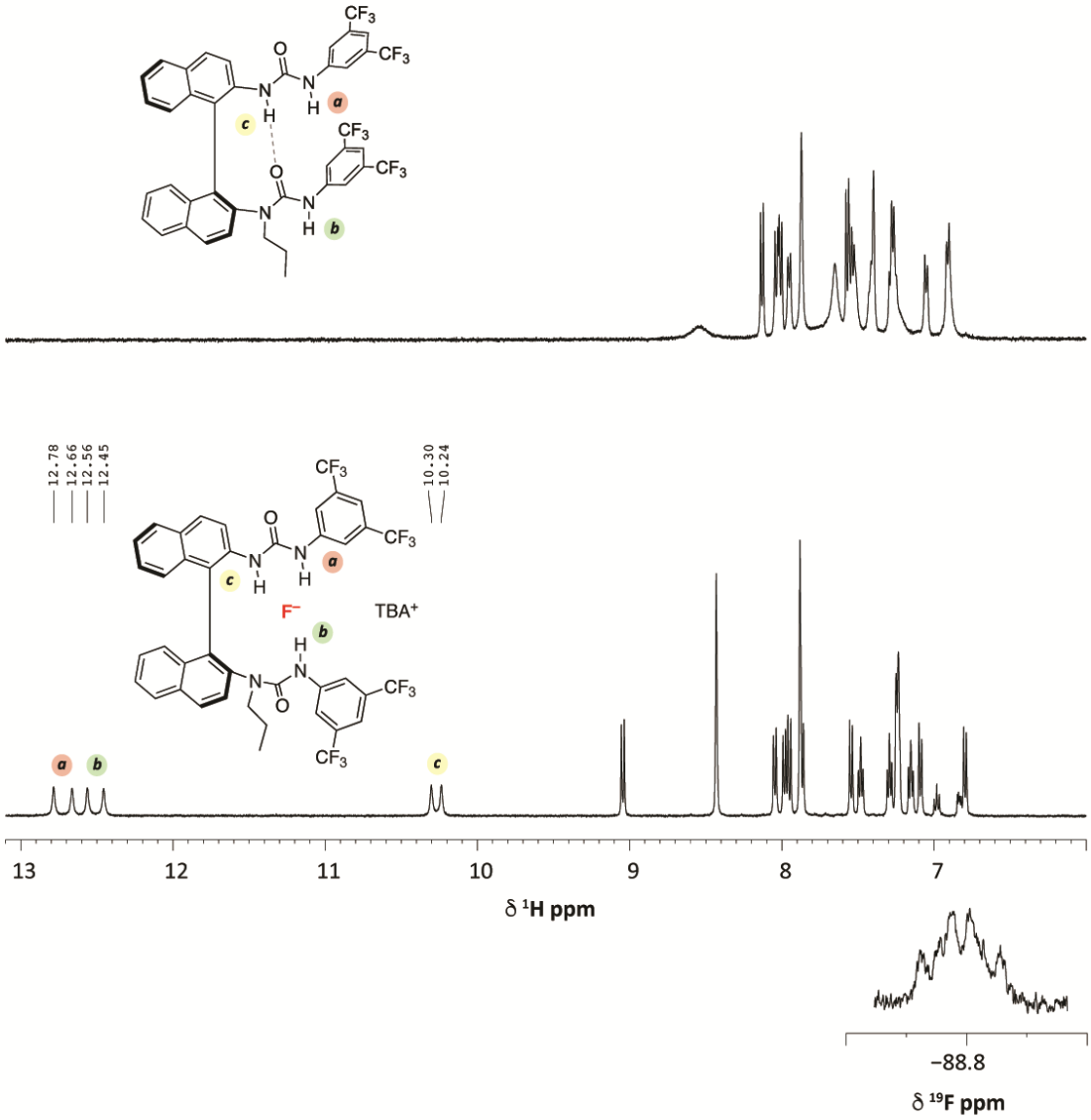



Figure 4.47: $^{1}$H NMR of **4v** and **4v**:TBAF, $^{19}$F NMR of showing fluoride splitting, (DCM-$d_2$, 3mM, 273 K).

*(S)-CyPen tBINAM Urea–TBAF complex (**4w**:TBAF)*

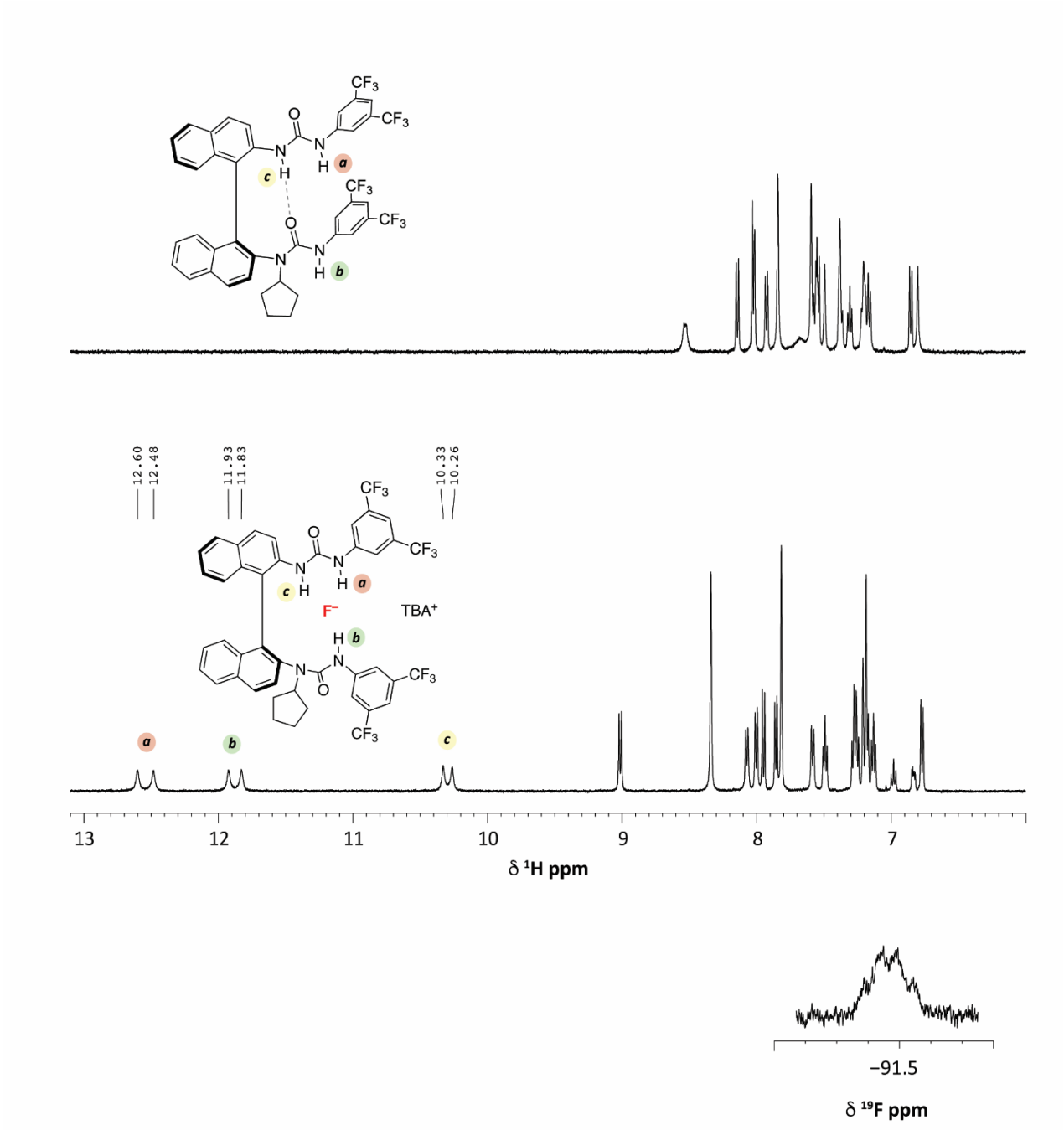



Figure 4.48: $^{1}$H NMR of **4w** and **4w**:TBAF, $^{19}$F NMR of showing fluoride splitting, (DCM-$d_2$, 3mM, 273 K).

*(S)-3-pent BINAM Urea–TBAF complex (**4x**:TBAF)*

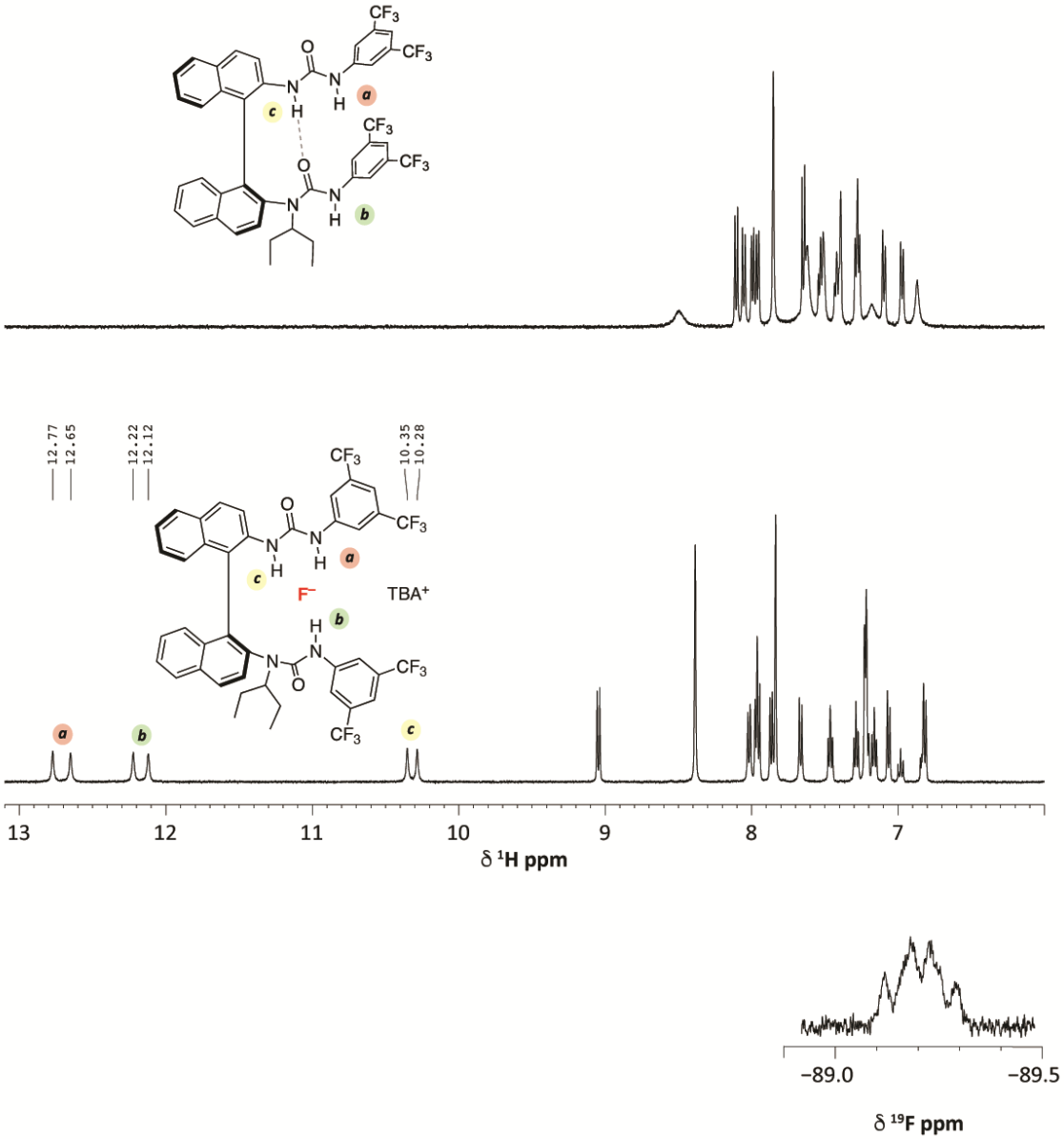



Figure 4.49: $^{1}$H NMR of **4x** and **4x**:TBAF, $^{19}$F NMR of showing fluoride splitting, (DCM-$d_2$, 3mM, 273 K).

(*S*)-iPr BINAM-*N*[a]-3,5-bis-(trifluoromethylphenyl)-*N*[b]-phenyl Urea–TBAF complex (**4y**:TBAF)

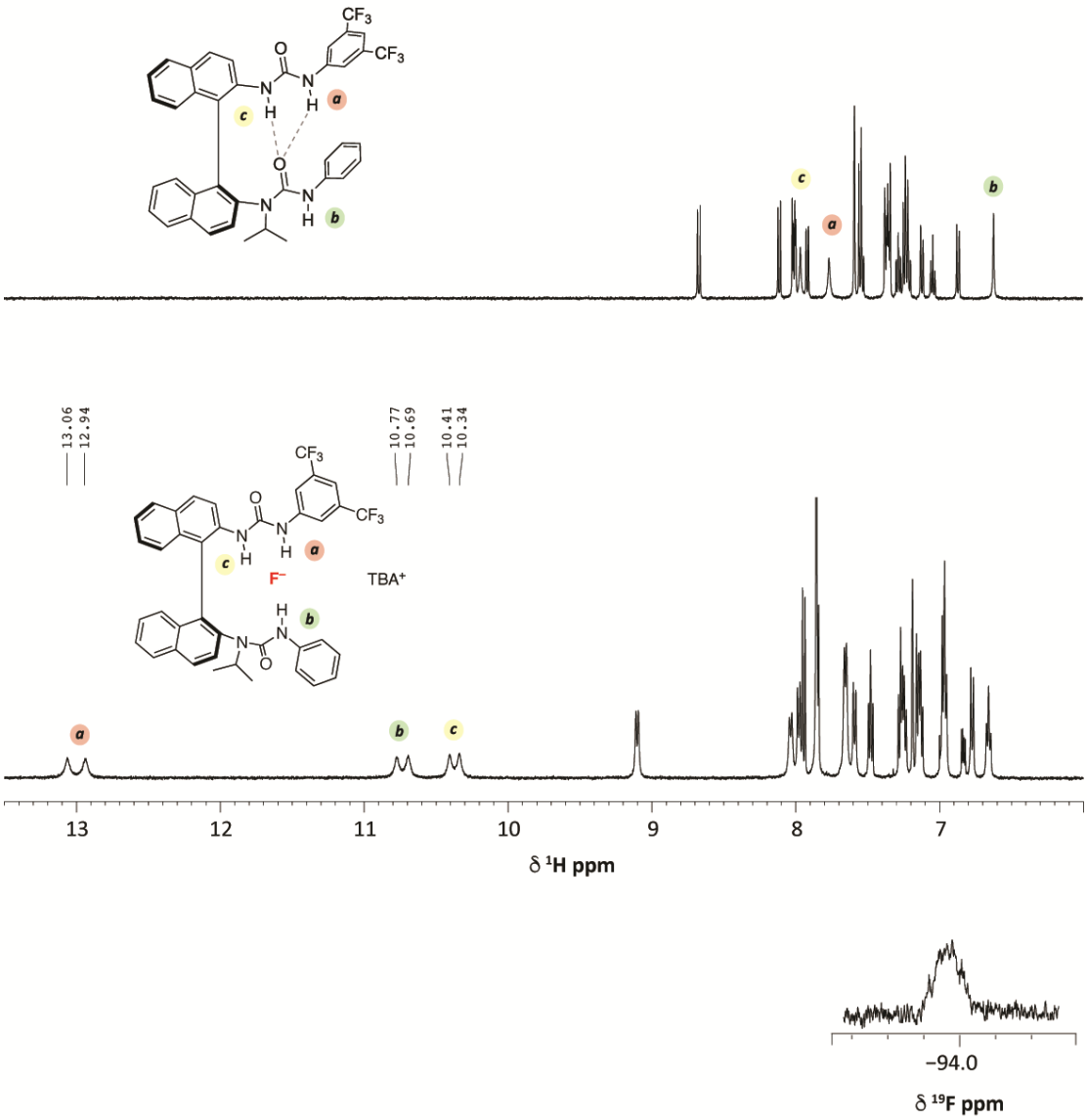



Figure 4.50: $^{1}$H NMR of **4y** and **4y**:TBAF, $^{19}$F NMR of showing fluoride splitting, (DCM-$d_2$, 3mM, 273 K).

(*S*)-iPr BINAM-*N*[a]-phenyl-*N*[b]-3,5-bis(trifluoromethylphenyl) Urea–TBAF complex (**4z**:TBAF)

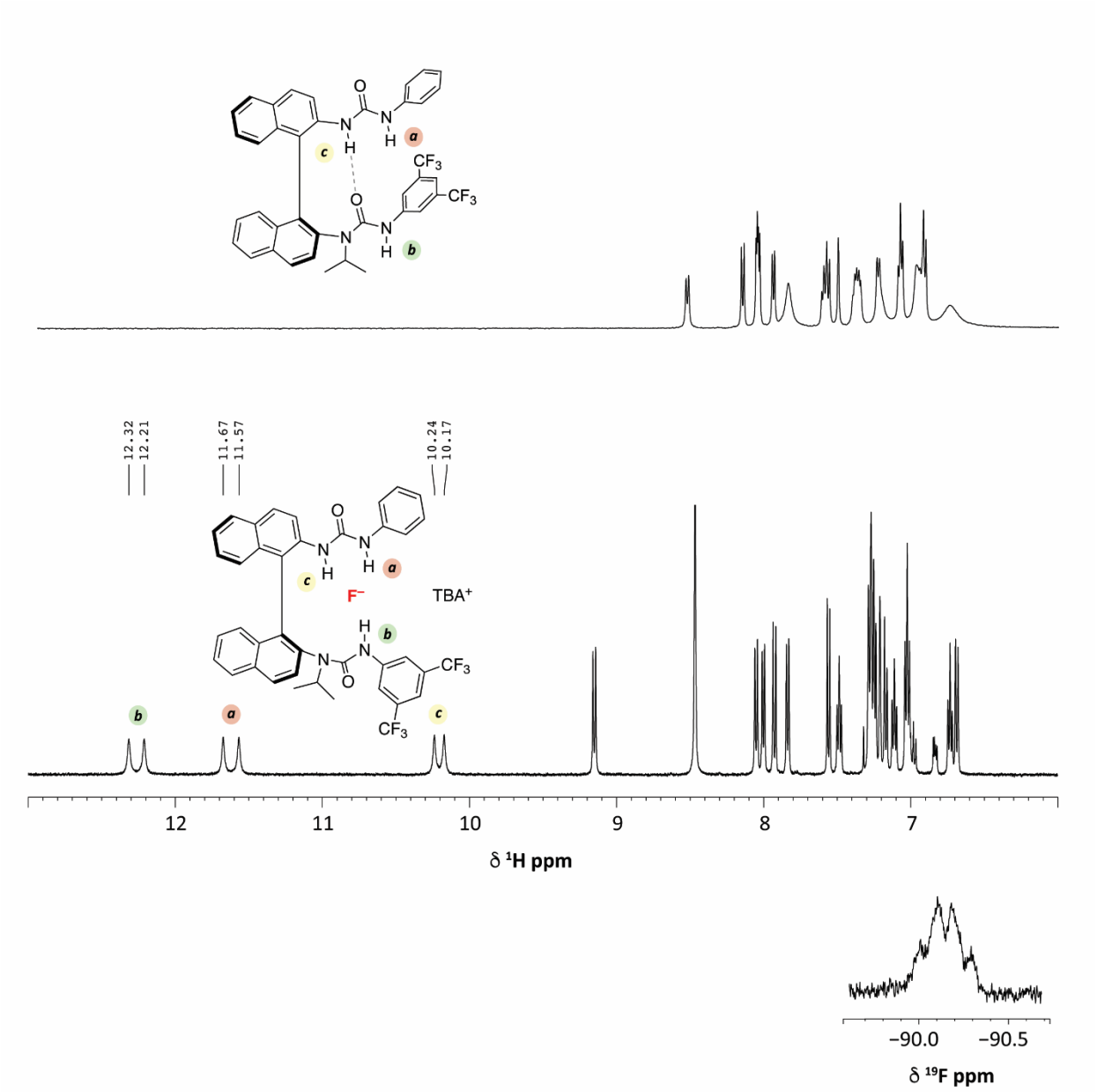



Figure 4.51: $^{1}$H NMR of **4z** and **4z**:TBAF, $^{19}$F NMR of **4z**:TBAF showing fluoride splitting (DCM-$d_2$, 3mM, 273 K).

(*S*)-iPr BINAM-*N*[a]-3,5-dimethylphenyl-*N*[b]-3,5-bis(trifluoromethylphenyl) Urea–TBAF complex (**4aa**:TBAF)

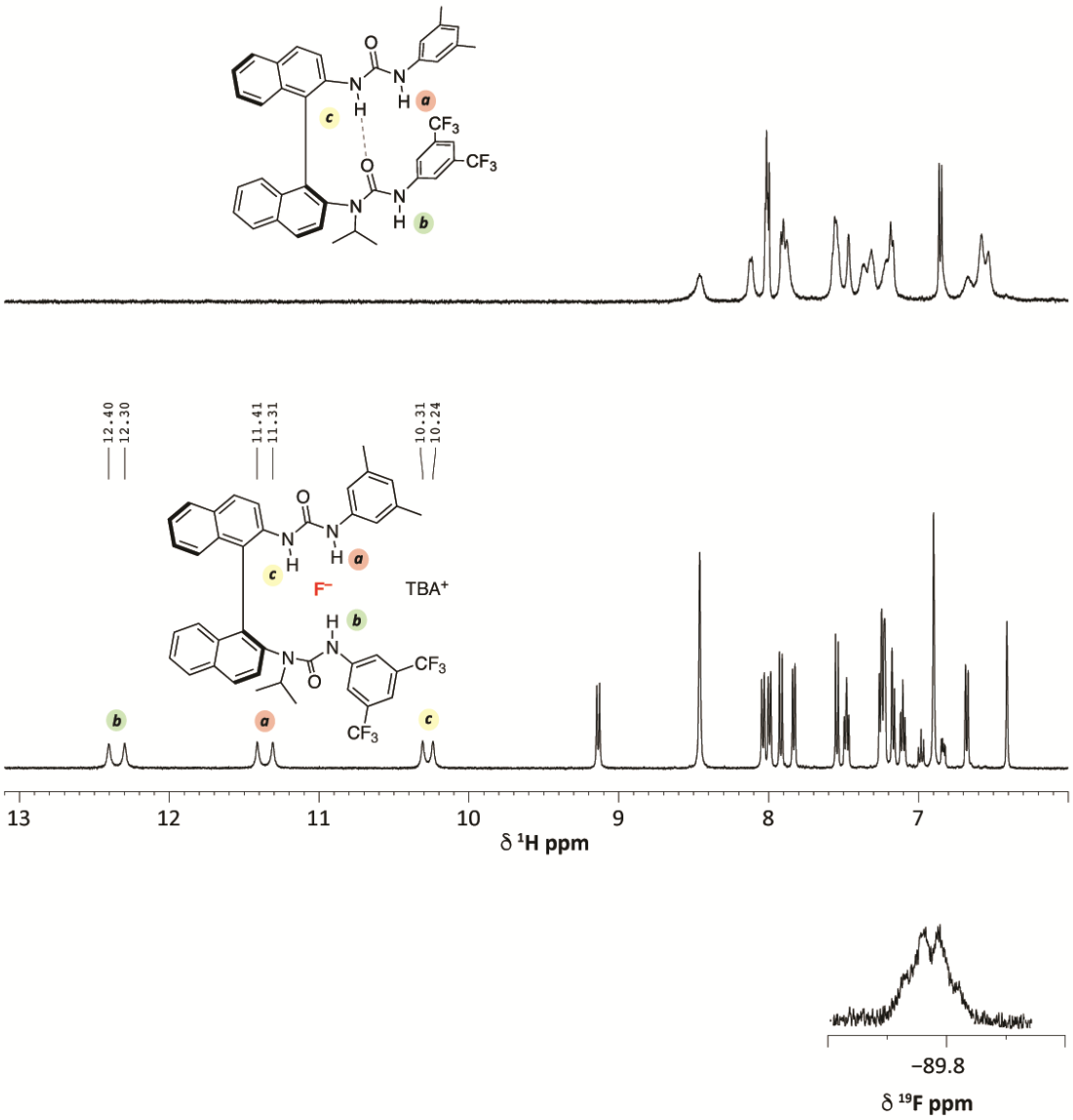



Figure 4.52: $^{1}$H NMR of **4aa** and **4aa**:TBAF, $^{19}$F NMR of **4aa**:TBAF showing fluoride splitting, (DCM-$d_2$, 3mM, 273 K).

(*S*)-iPr BINAM-*N*[a]-3,5-bis(trifluoromethyl)phenyl-*N*[b]-3,5-difluorophenyl Urea–TBAF complex (**4ab**:TBAF)

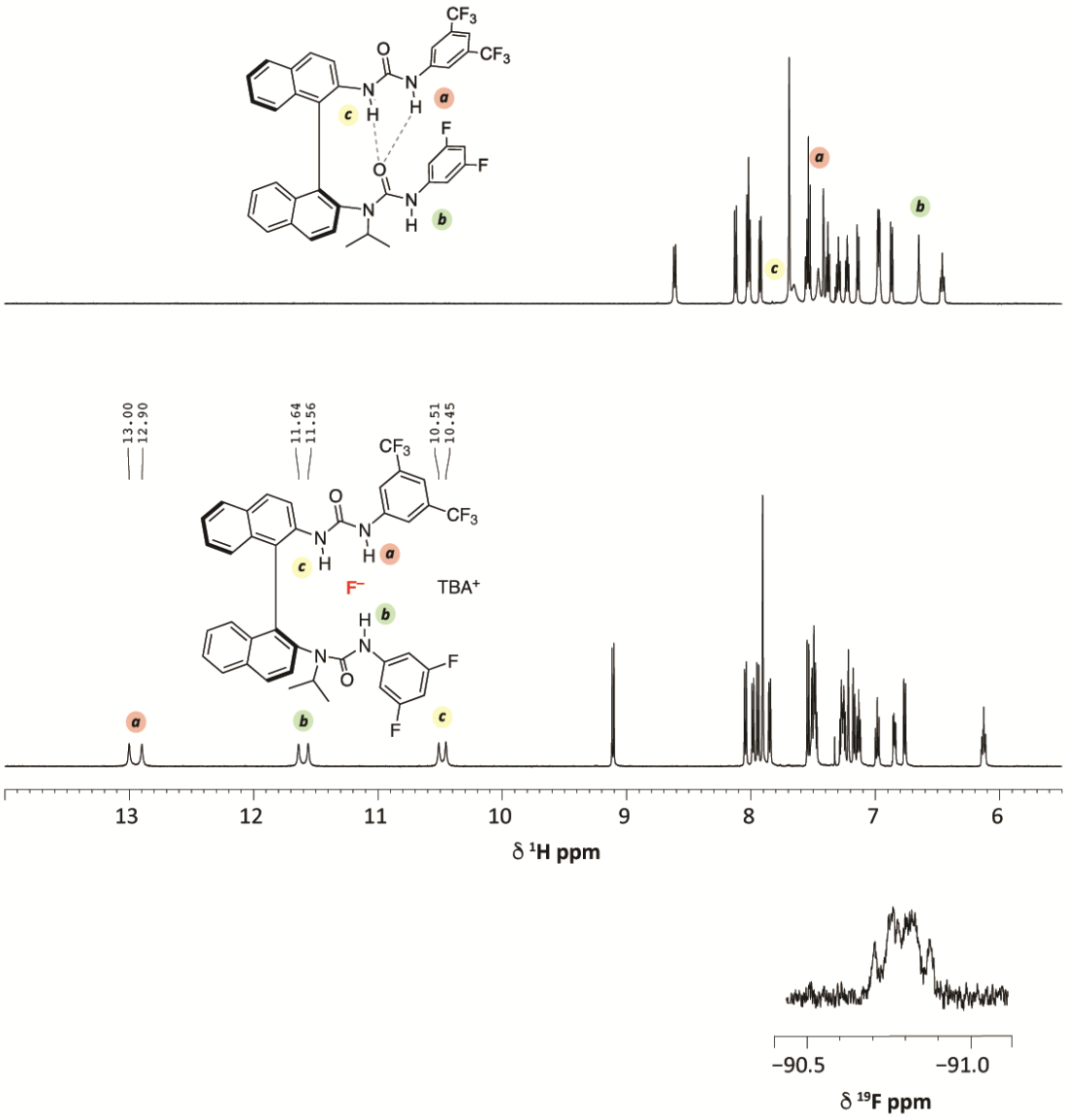



Figure 4. 53: $^{1}$H NMR of **4ab** and **4ab**:TBAF, $^{19}$F NMR of **4ab**:TBAF showing fluoride splitting, (DCM-$d_2$, 3mM, 273 K).

(*S*)-iPr BINAM-*N*[a]-3,5-difluorophenyl-*N*[b]-3,5-bis(trifluoromethyl)phenyl Urea–TBAF complex (**4ac**:TBAF)

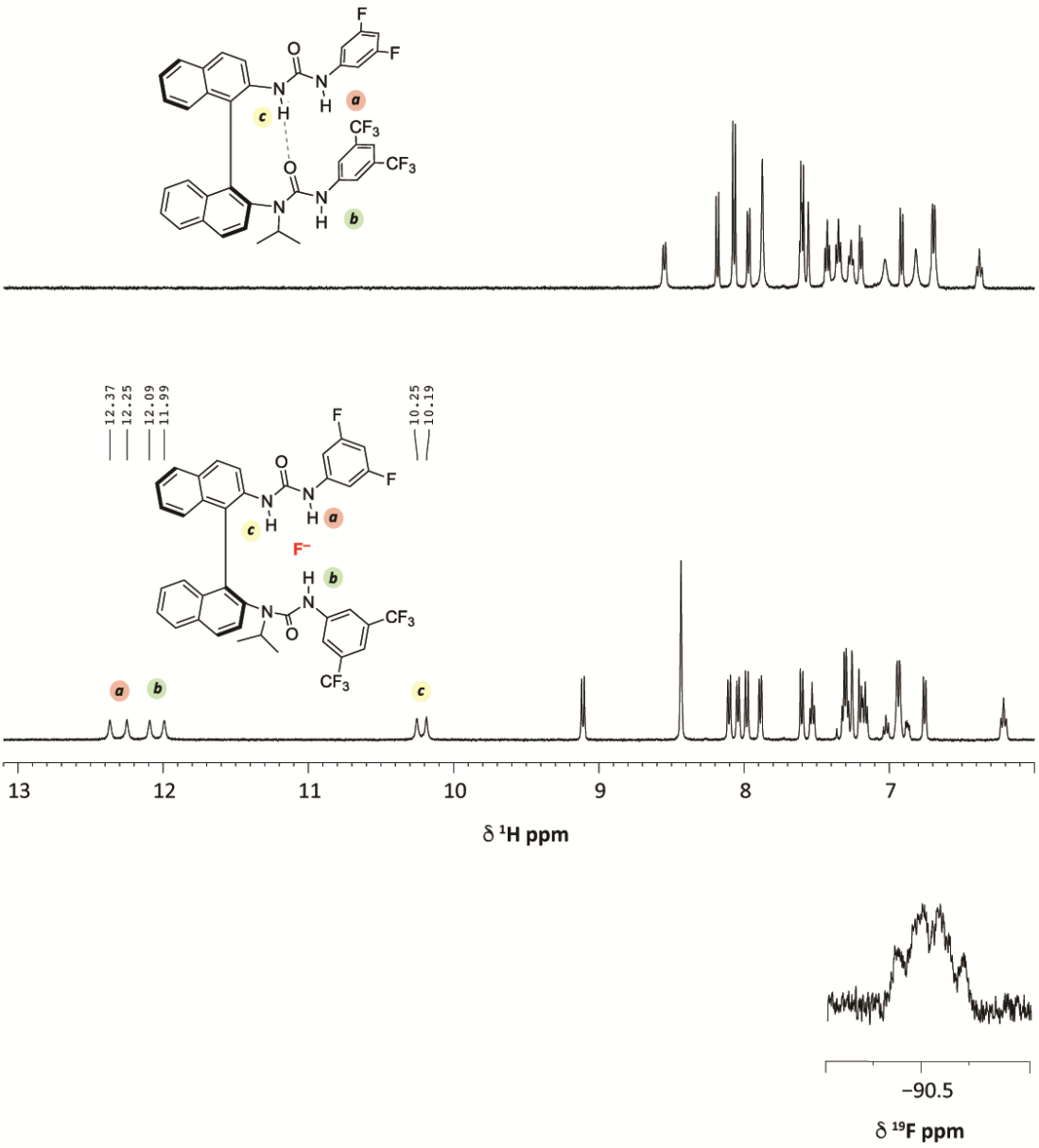



Figure 4.54: $^{1}$H NMR of **4ac** and **4ac**:TBAF, $^{19}$F NMR of **4ac**:TBAF showing fluoride splitting, (DCM-$d_2$, 3mM, 273 K).

(*S*)-iPrBINAM-$N^a$-$N^b$-3,5-difluorophenyl Urea:TBAF complex (**4ad**:TBAF)

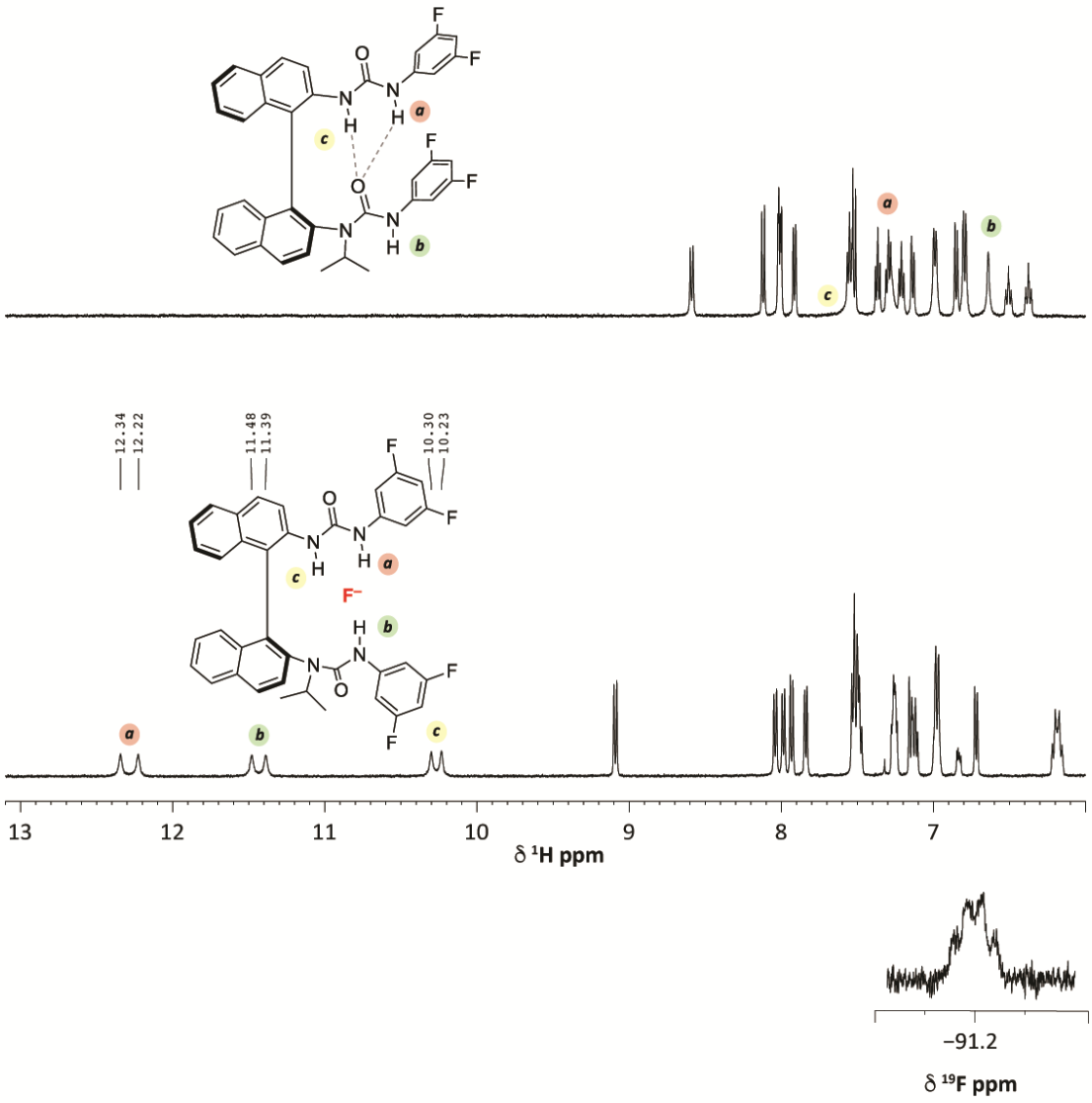



Figure 4.55: $^1$H NMR of **4ad** and **4ad**:TBAF, $^{19}$F NMR of **4ad**:TBAF showing fluoride splitting, (DCM-$d_2$, 3mM, 273 K).

*4.3.5.3 1H-19F CLIP-HSQC*

$^{1}$H-$^{19}$F CLIP-HSQC experiments were recorded on an AVIII 500 at 273 K, showing for every catalyst$^{19}$F chemical shift (f1 dimension), $^{1}$H chemical shift (f2 dimension), $^{1h}J_{NH\text{-}F^-}$ is derived measuring the cross-peaks' distance

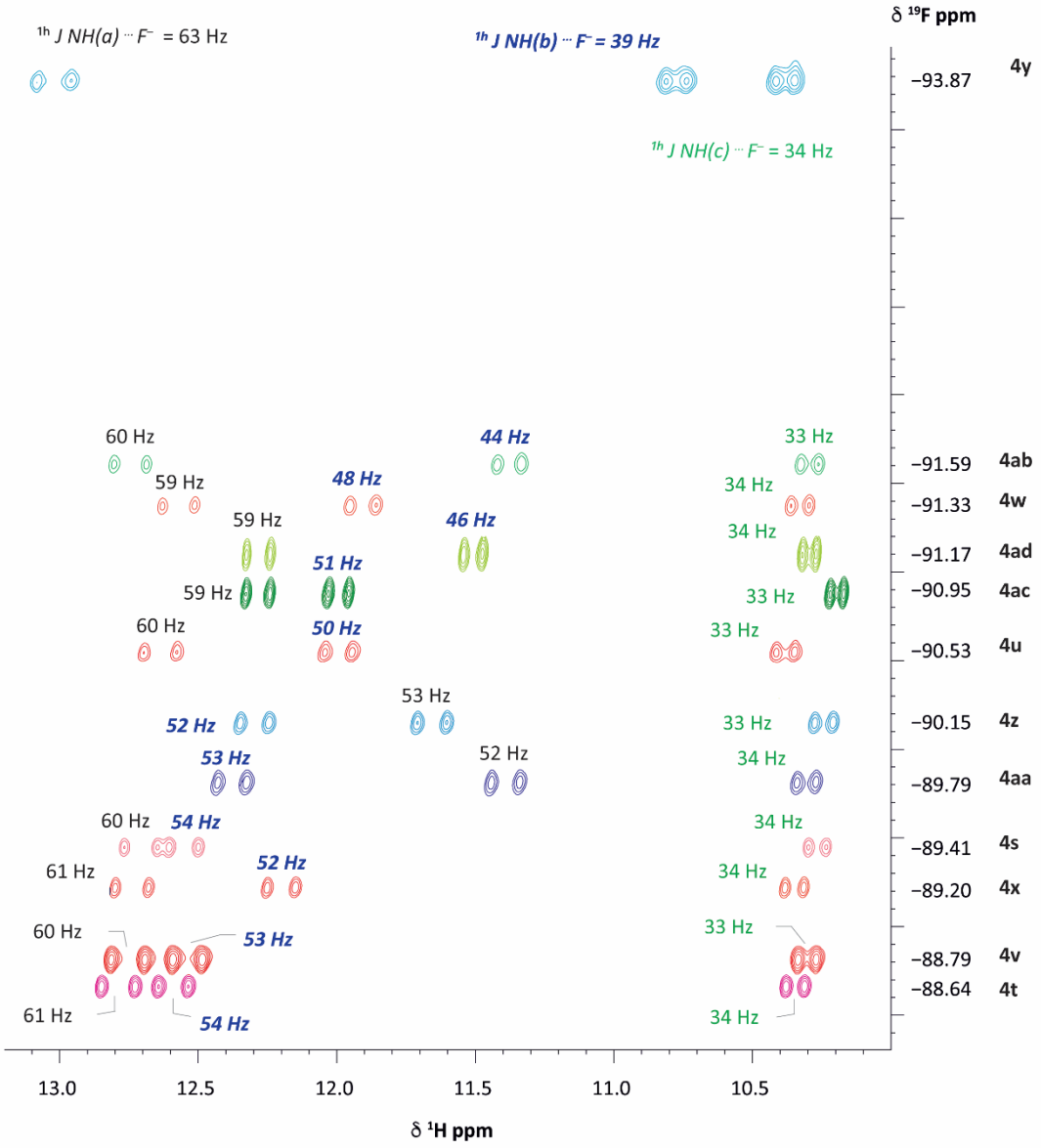
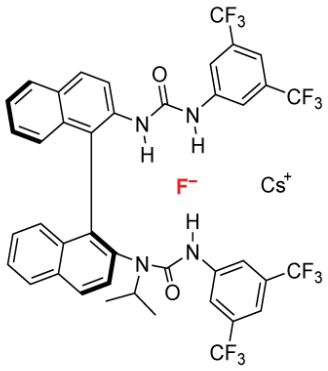



Figure 4.56: Stacked 1H-19F CLIP-HSCQ of catalyst **4s-4ad**, (500 MHz, DCM-$d_2$, 3 mM, 273 K).

*4.3.6 iPr BINAM Urea–CsF complex (**4u**:CsF)*

*4.3.6.1 Sample preparation*

(*S*)-iPrBINAM Urea **4u** (10.4 mg/0.0125 mmol), CsF (100 mg/0.66 mmol) and $PhF_6$ (2 µL) were dissolved in 0.5 mL of DCM-$d_2$ (25 mM) inside a sealed NMR tube. The sample was sonicated for 2 hours, after which it was directly taken to the NMR spectrometer. All the NMR spectra were recorded on an AVIII HD 500 equipped with a BCU II fridge unit, allowing variable temperature studies. The sample can be stored at room temperature without signs of degradation for months.




Scheme 4.3: Structure of **4u**:CsF.

*4.3.6.2 Variable temperature studies*

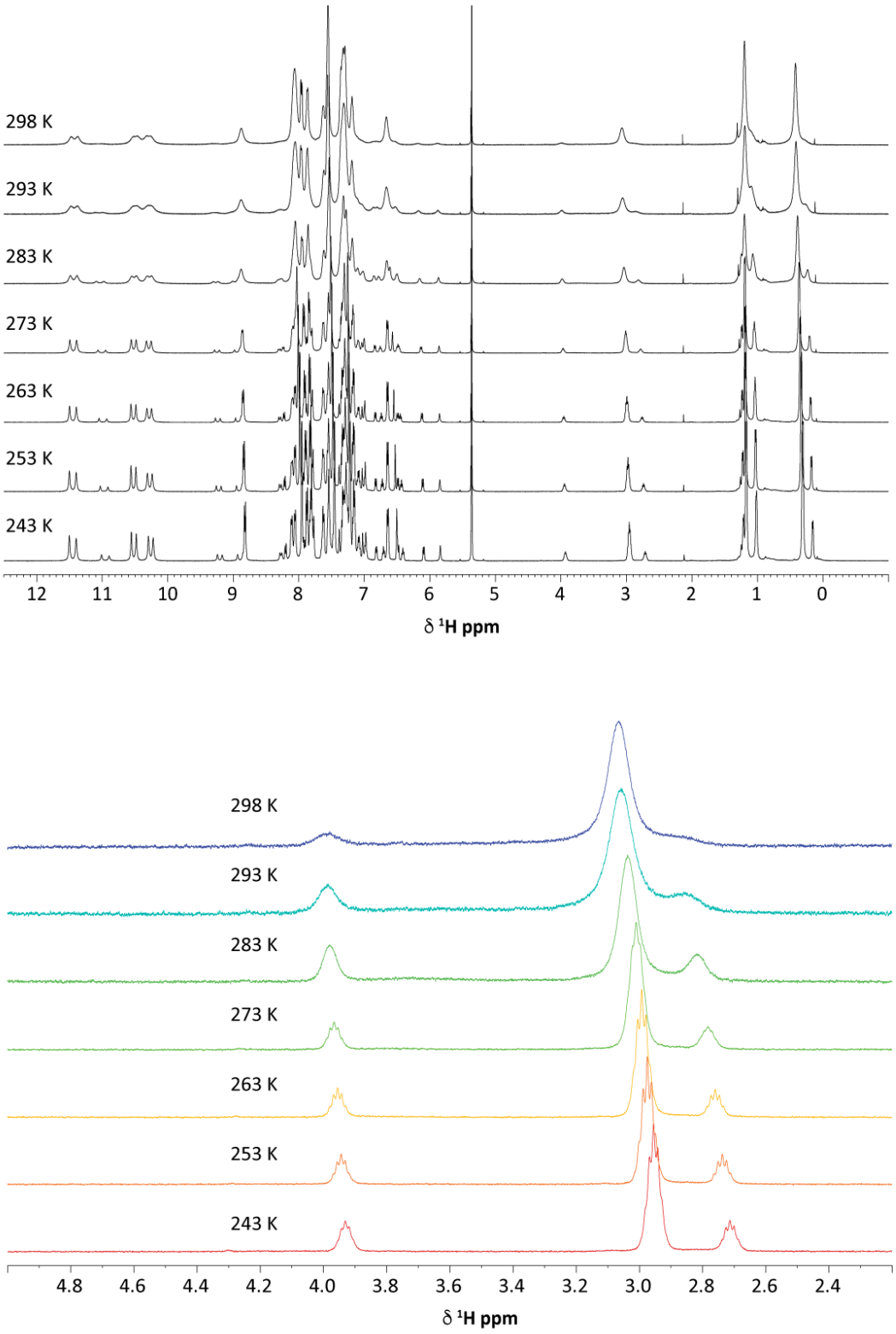



Figure 4.57: $^{1}$H NMR of **4u**:CsF 298–243 K, full spectra (top) and 2.3–4.9 ppm detail (bottom).

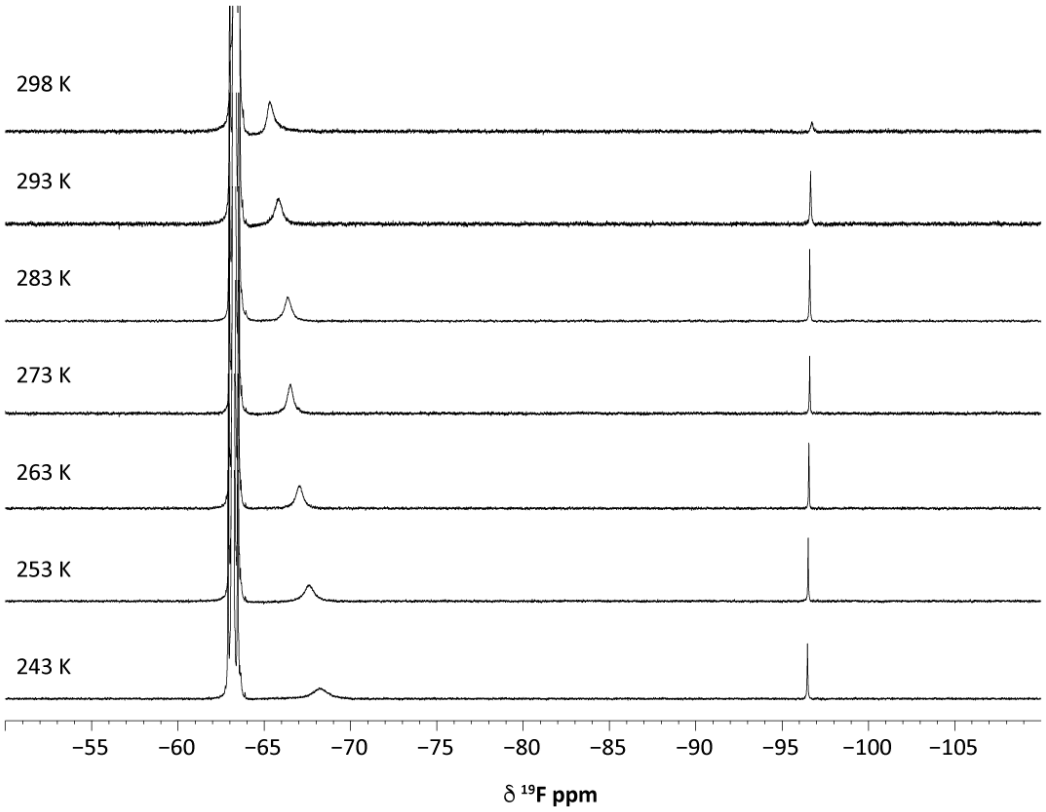



Figure 4.58: $^{19}$F NMR of **4u**:CsF 298–243 K.

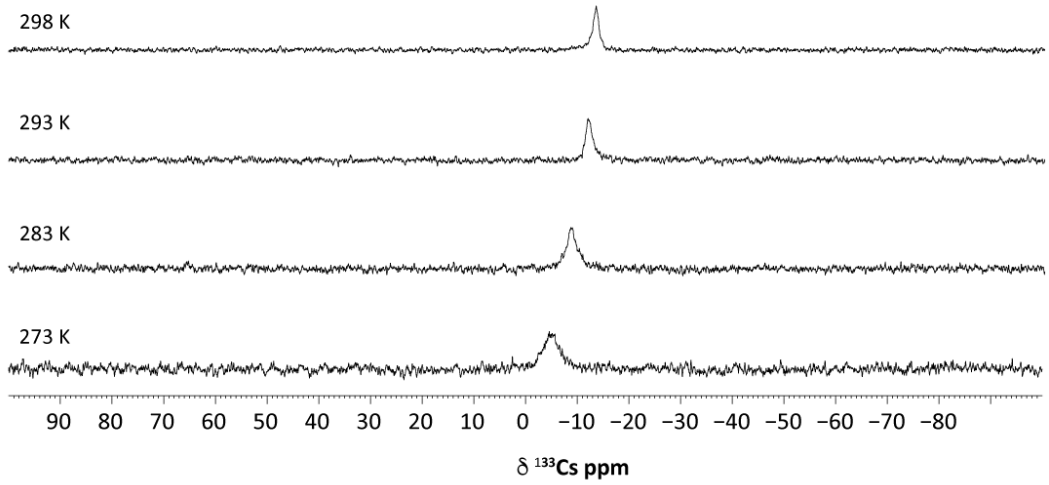



Figure 4.59: $^{133}$Cs NMR of **4u**:CsF 298–273 K.

*4.3.6.3 HSQC*

$^{1}H$-$^{13}C$ HSQC experiments were acquired using a previously developed pulse sequence (*hsqcedetgpsp.3*) at 273 K.

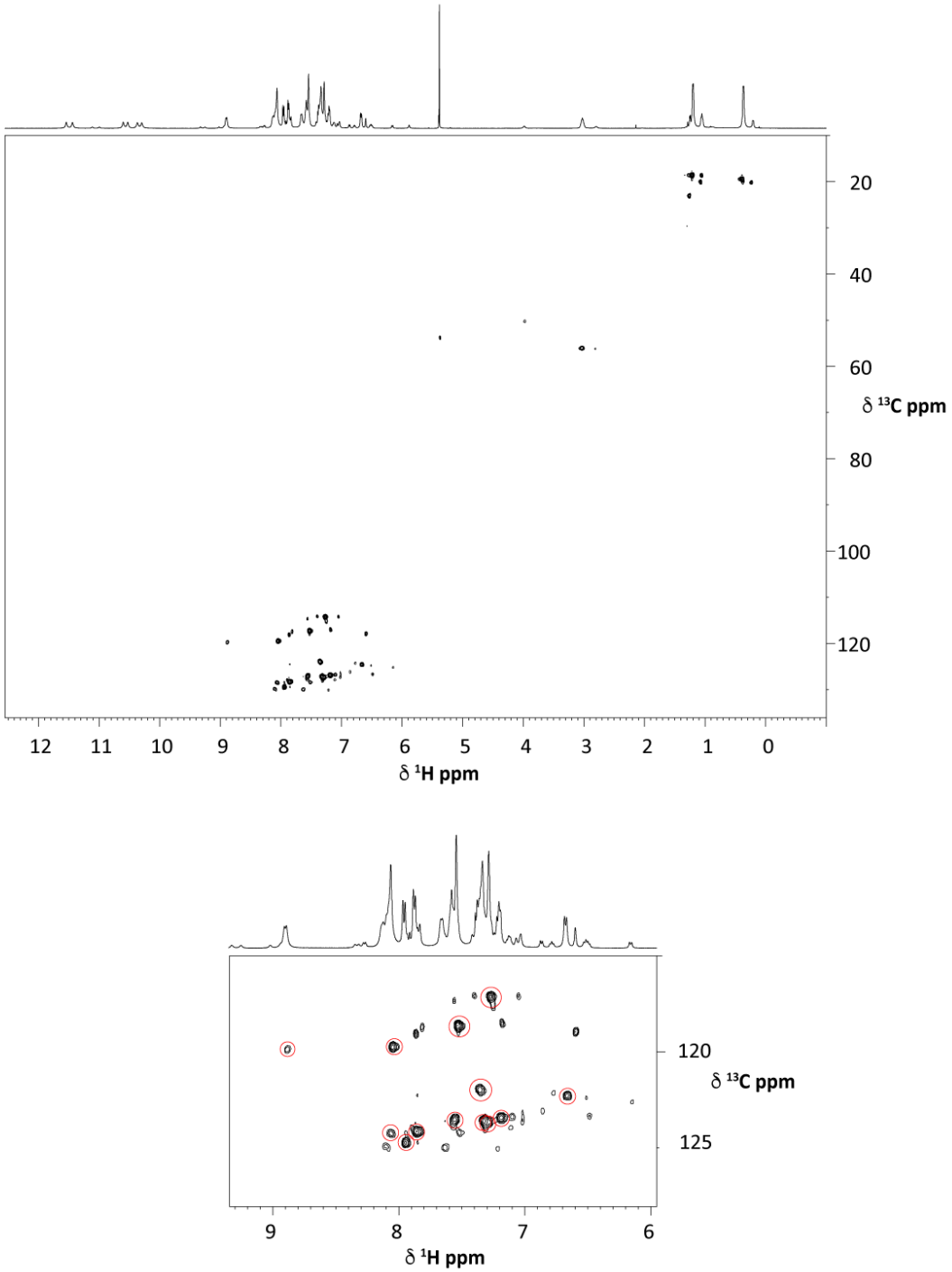



Figure 4.60: $^{1}H$-$^{13}C$ HSQC of **4u**:CsF at 273 K, full spectrum (top) and 6–9 ppm detail, correlations for the main species are circled in red (bottom).

$^{1}$H-$^{19}$F CLIP-HSQC experiments were acquired using a modified sequence from a previously developed one (*hsqcetgpclip*)[17] at 273 K and 243 K. The following parameters were used at both temperatures.

| Parameter | Value |
|---|---|
| TD | 2058 (f2) x 128 (f1) |
| SW | 10 (f2) x 60 (f1) |
| o1p/o2p | 10/-80 ppm |
| NS (DS) | 4 (4) |
| relaxation delay d1 | 2 s |
| delay for evolution of coupling CNST[2] | 40 Hz |

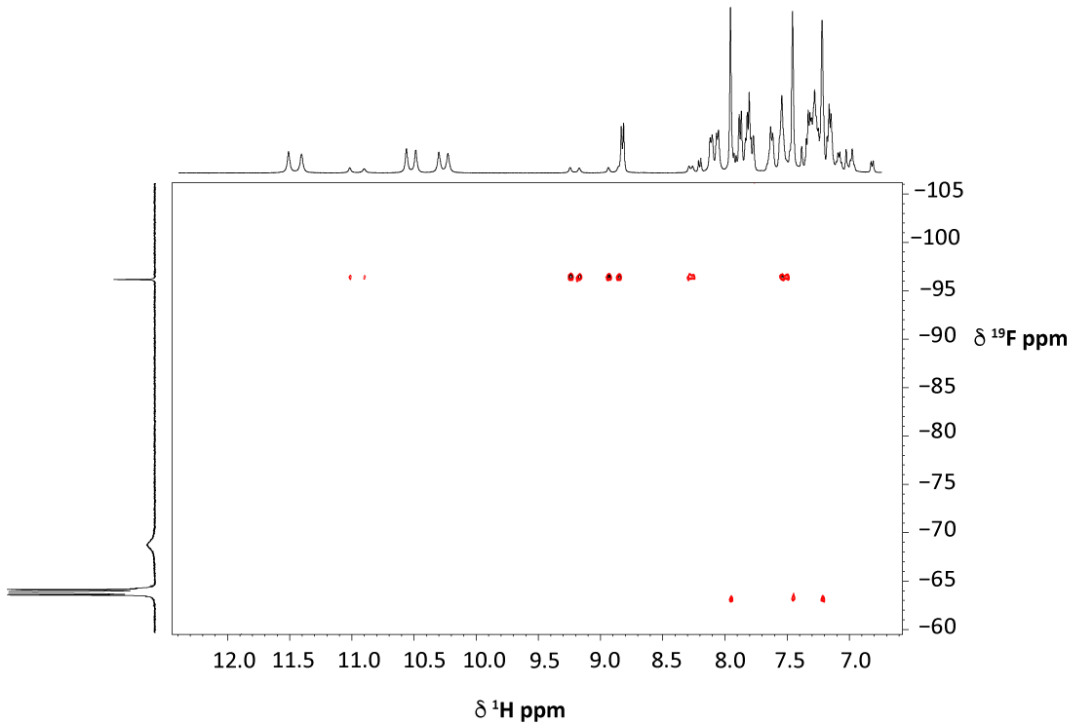



Figure 4.61: $^{1}$H-$^{19}$F CLIP-HSQC of **4u**:CsF at 243 K.

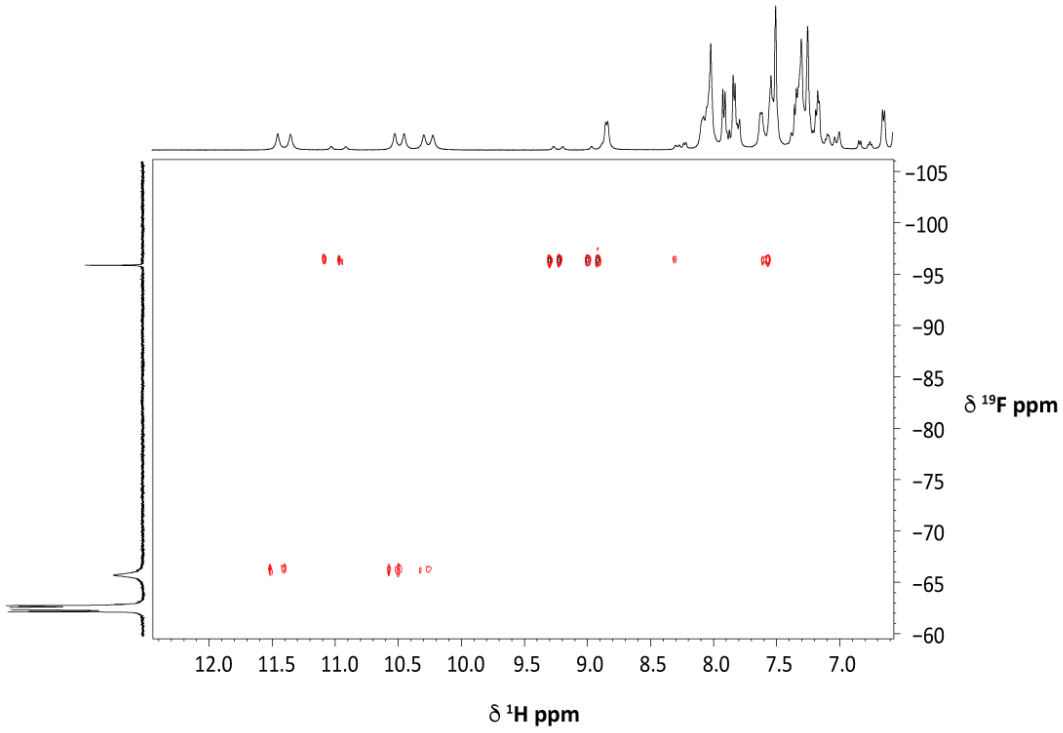



Figure 4.62: $^{1}H$-$^{19}F$ CLIP-HSQC of **4u**:CsF at 273 K.

*4.3.6.4 NOESY and ROESY*

NOESY experiments were acquired using a previously developed pulse sequence (*noesygpphzs*)[18] at 273 K, using the parameters listed below.

| Parameter | Value |
|---|---|
| TD | 2048 (f2) x 256 (f1) |
| SW | 20 (f2) x 20 (f1) |
| NS (DS) | 8 (32) |
| relaxation delay d1 | 2 s |
| mixing time d8 | 80 ms |

ROESY experiments were acquired using a previously developed pulse sequence (*roesyphpp.2*) at 243 K, using the parameters listed below.

| Parameter | Value |
|---|---|
| TD | 2048 (f2) x 256 (f1) |
| SW | 20 (f2) x 20 (f1) |
| NS (DS) | 8 (16) |
| relaxation delay d1 | 2 s |
| spin-lock pulse p15 | 100 ms |

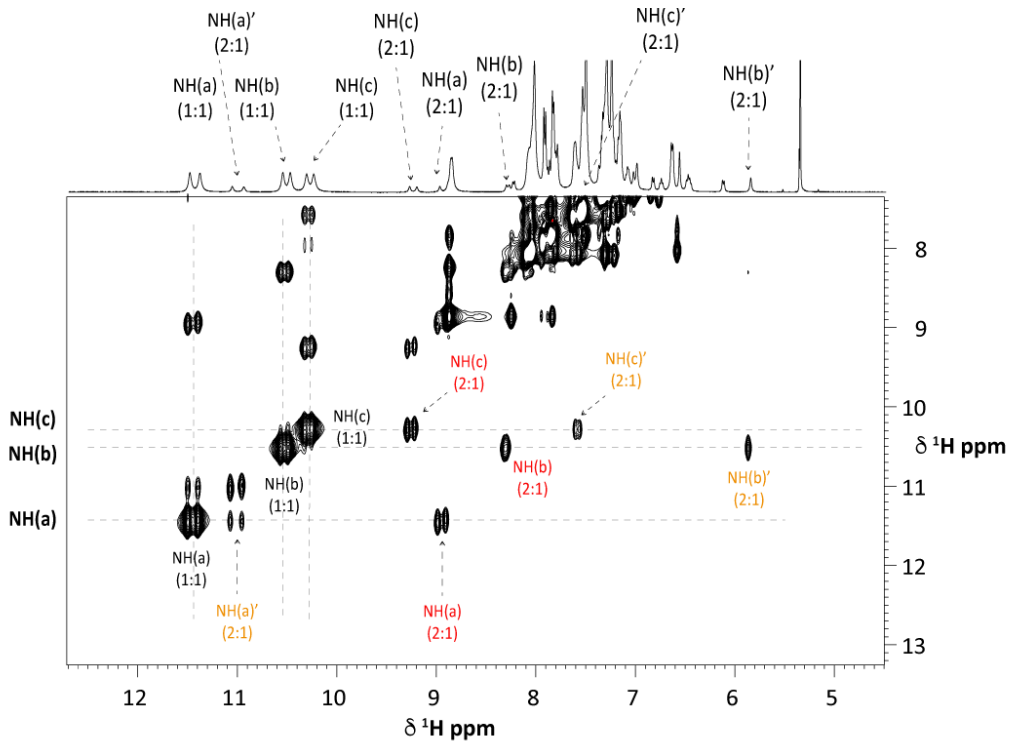



Figure 4.63: $^{1}$H NOESY of **4u**:CsF at 273 K, detail.

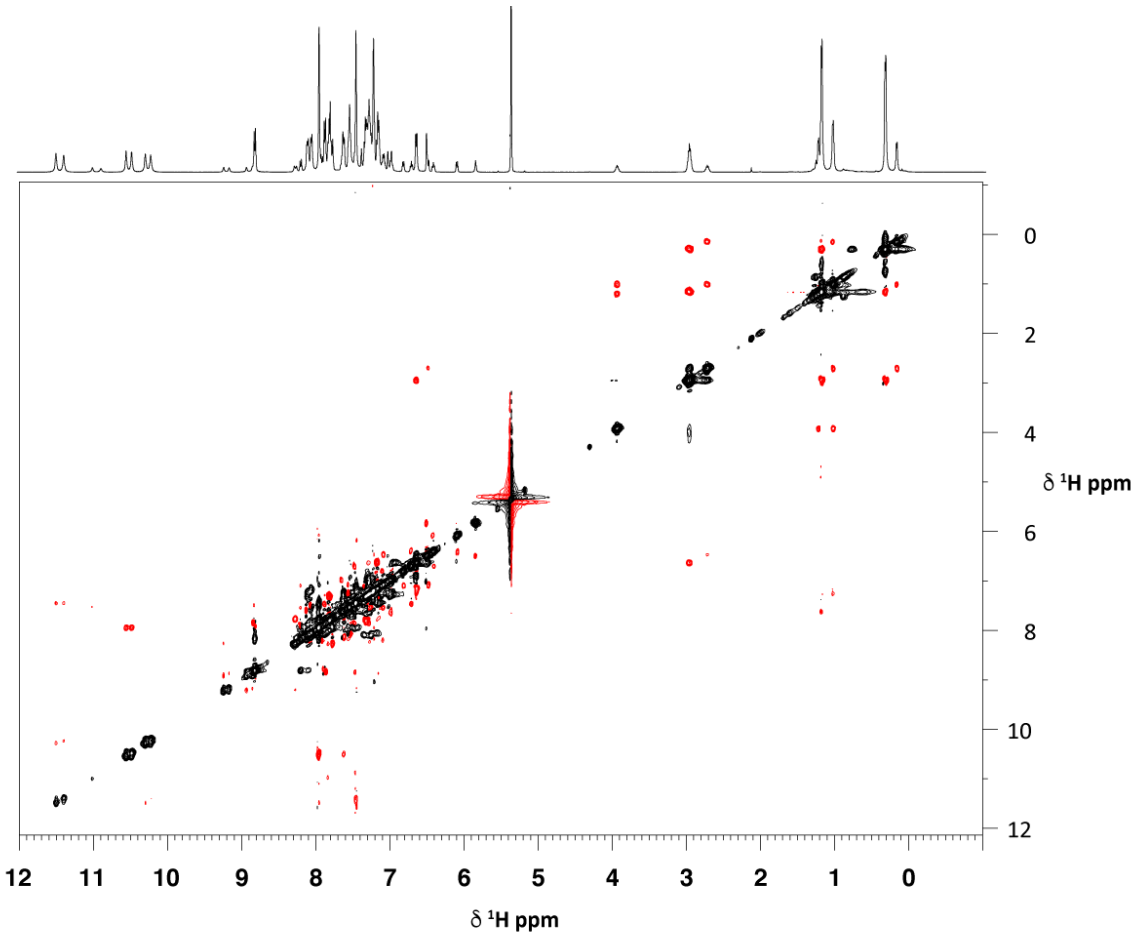



Figure 4.64: $^{1}$H ROESY of **4u**:CsF at 243 K, full spectrum.

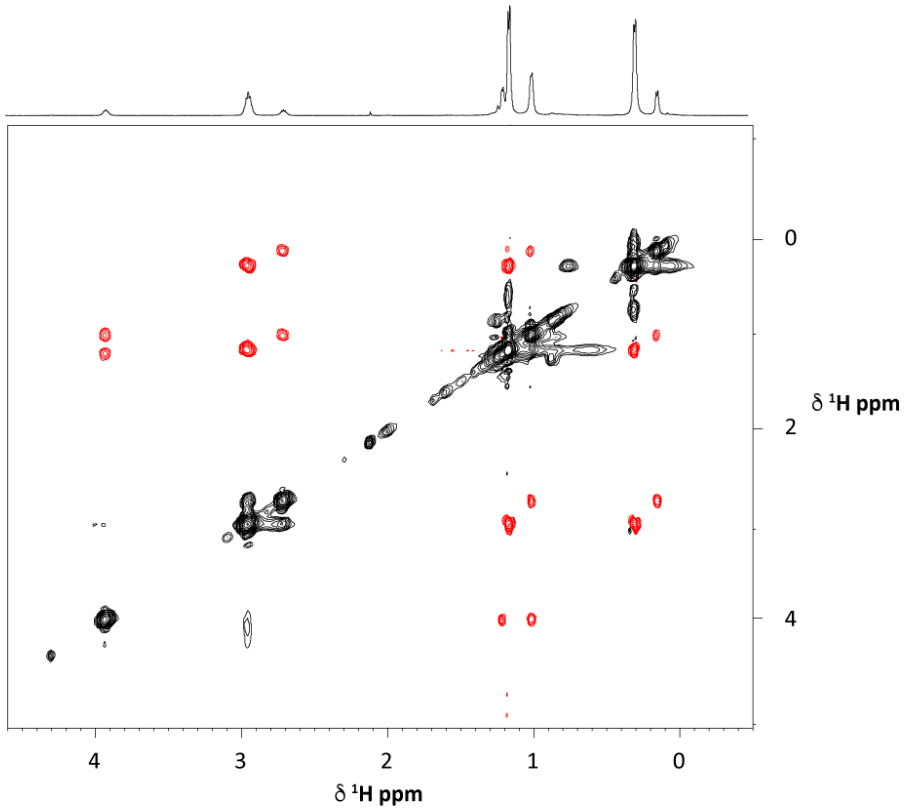



Figure 4.65:[1]H ROESY of **4u**:CsF at 243 K, -1–5 ppm.

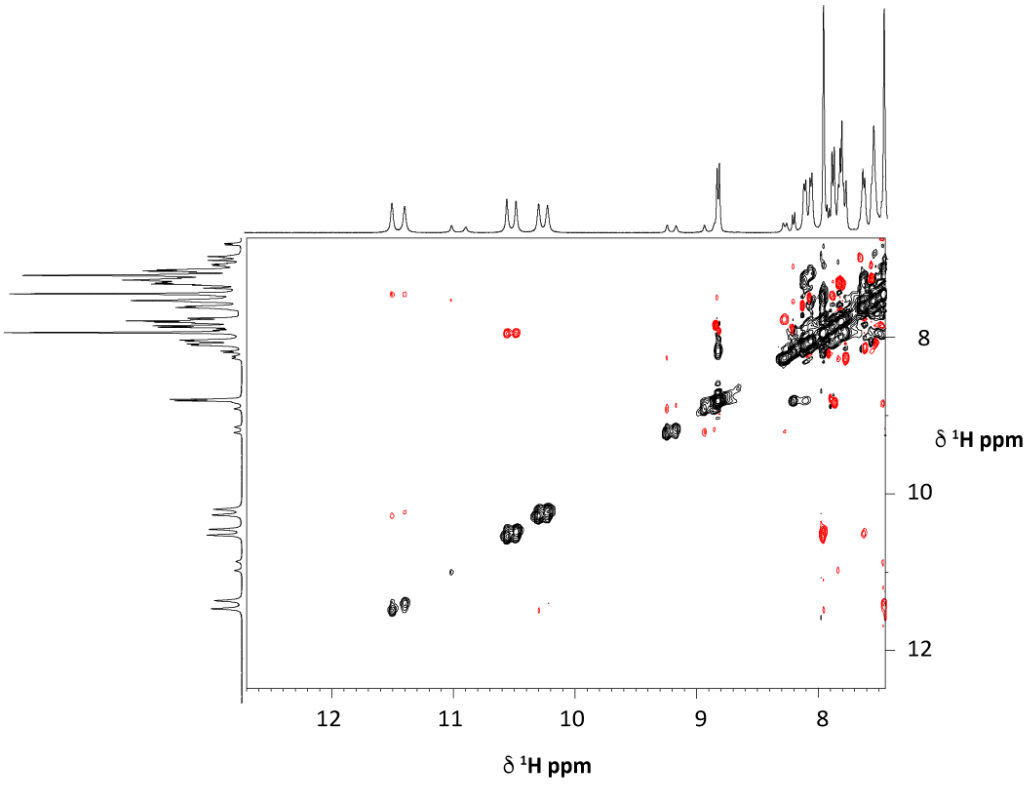



Figure 4.66:[1]H ROESY of **4u**:CsF at 243 K, 7–12.5 ppm.

*4.3.6.5 HOESY*

1D heteronuclear $^{1}H$-$^{19}F$ nOe experiments were acquired on an AVIII HD 500 using a previously developed sequence (*hoesyfhgh1d*) and the parameters reported below.

| Parameter | Value |
|---|---|
| TD | 65536 pt |
| SW | 20 |
| NS (DS) | 256 (16) |
| o2p | -96.5 ppm |
| relaxation delay d1 | 3 s |
| mixing time d8 | 80 ms |

A second set of experiments was performed using an modified sequence (*hoesyfhgh1d.cpd*), which included fluorine decoupling during acquisition, using the parameters reported below.

| Parameter | Value |
|---|---|
| TD | 131072 pt |
| SW | 20 |
| NS (DS) | 256 (16) |
| o2p | -96.5 ppm |
| relaxation delay d1 | 6 s |
| mixing time d8 | 80 ms |

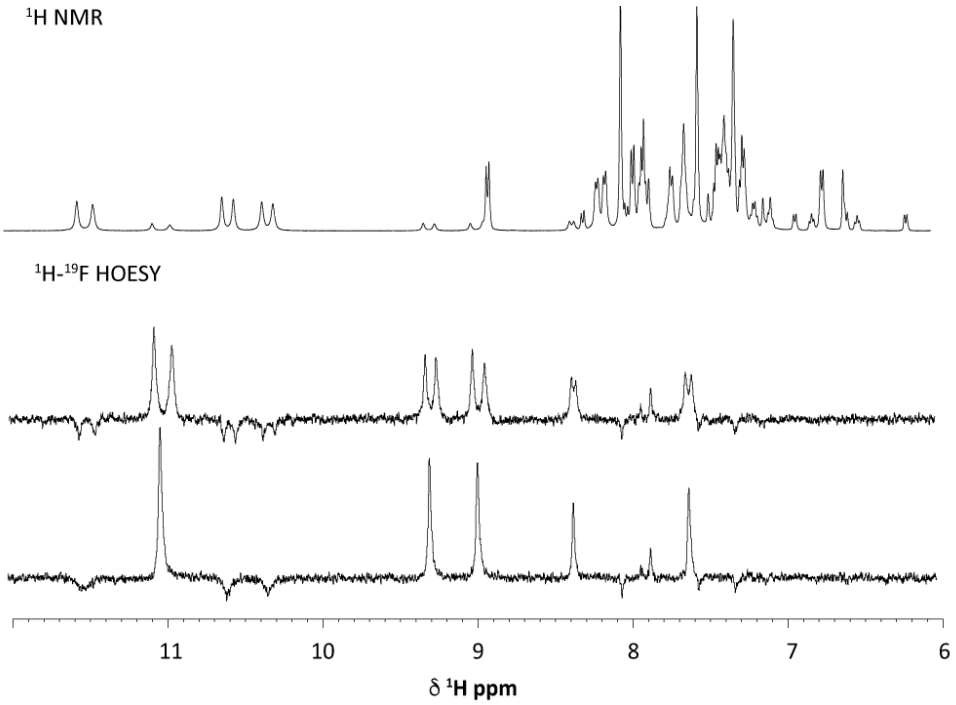



Figure 4.67: $^{1}H$ NMR and $^{1}H$-$^{19}F$ HOESY of **4u**:CsF at 243 K, 12.5–7 ppm.

*4.3.6.6 Diffusion studies*

Diffusion experiments were performed by measuring the diffusion coefficient (*D*) of selected resonances belonging to the two species, Cs[U:F] and Cs[$U_2$:F], U = **4u**. The diffusion coefficient was determined by means of $^1$H DOSY experiments acquired on an AVIII HD 500 at 243 K. The sample (*4.3.6.1 Sample preparation*) was cooled to 243 K inside the magnet and let equilibrate for an hour before the acquisition started. $^1$H DOSY were acquired using a previously developed pulse sequence (*dstebpgp3s,* diffusion measurement using double stimulated echo for convection compensation and LED using bipolar gradient pulses using 3 spoil gradients)[20] with the following relevant parameters.

| Parameter | Value |
|---|---|
| TD | 65536 pt |
| SW | 20 ppm |
| NS (DS) | 64 (4) |
| relaxation delay d1 | 5 s |
| $\Delta$ | 95 ms |
| $\delta$ | 3 ms |
| *Gradient,* $G_z$ (n. of 1D spectra) | 2–80 % (16) |

The diffusion coefficient of selected resonances was calculated by non-linear fitting using Dynamic Center 2.3.3. The data are presented as pseudo-2D spectrum in Figure 4.68, the diffusion coefficient of the two species was calculated as the average of the diffusion coefficients of the protons corresponding to each species.

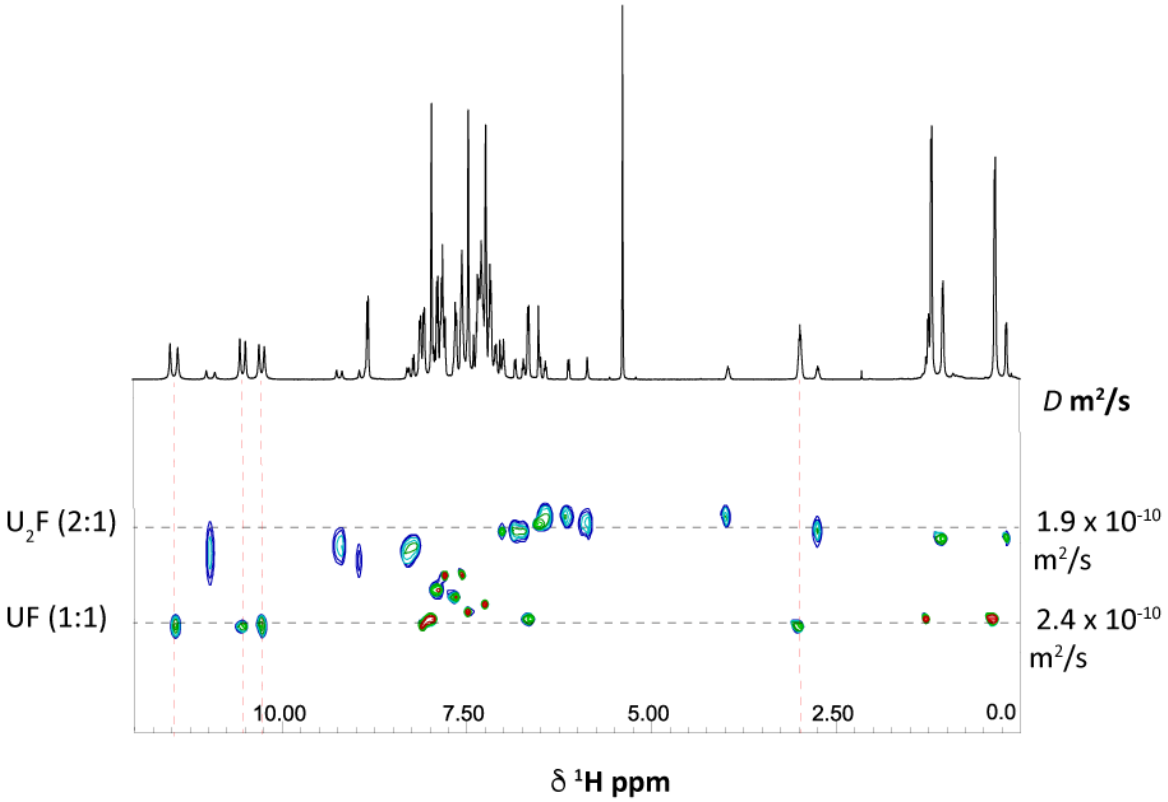



Figure 4.68: pseudo-2D $^{1}$H DOSY plot for **4u**:CsF

*4.3.6.7 T1 measurements*

The longitudinal relaxation time constant T1 was measured *via* $^{19}F$ inversion recovery experiments (*t1ir*) on an AVIII HD 500 at 298 K. Two set of experiments were performed, irradiating each time one of the two fluoride peaks corresponding to Cs[**4u**:F] and Cs[**4u**$_2$:F], using the parameters listed below. T1 was calculated by non-linear fitting using Dynamic Center 2.3.3.

Cs[**4u**:F]

| Parameter | Value |
|---|---|
| TD | 8192 |
| SW | 10 |
| o1p | -65 ppm |
| NS (DS) | 8(0) |
| relaxation delay d1 | 5 s |
| variable delays (n. of points) | 0.1–3000 ms (12) |

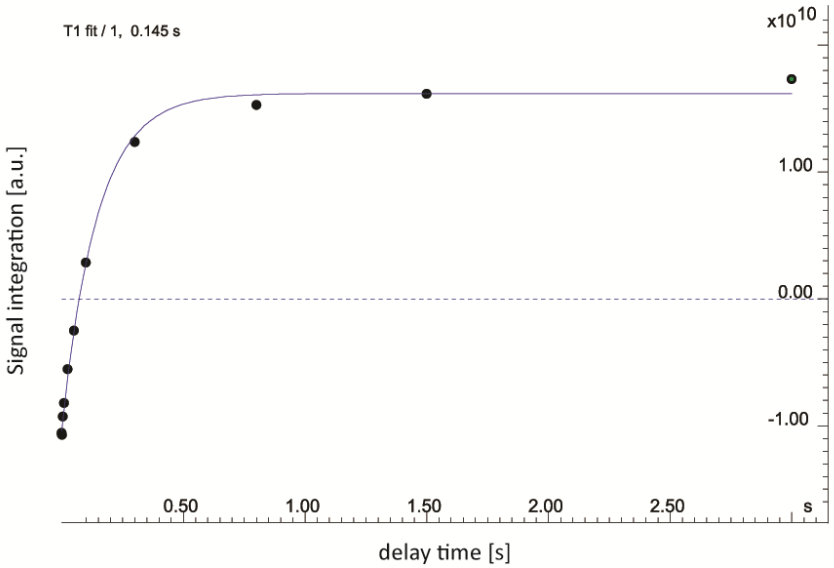



Figure 4.69: Inversion recovery plot of Cs[**4u**:F], experimental data (dots) and fitted function (line). T1 = 0.145 s.

Cs[**4u**$_2$:F]

| Parameter | Value |
|---|---|
| TD | 8192 |
| SW | 10 |
| o1p | -96.7 ppm |
| NS (DS) | 8(0) |
| relaxation delay d1 | 5 s |
| variable delays (n. of points) | 0.1–3000 ms (12) |

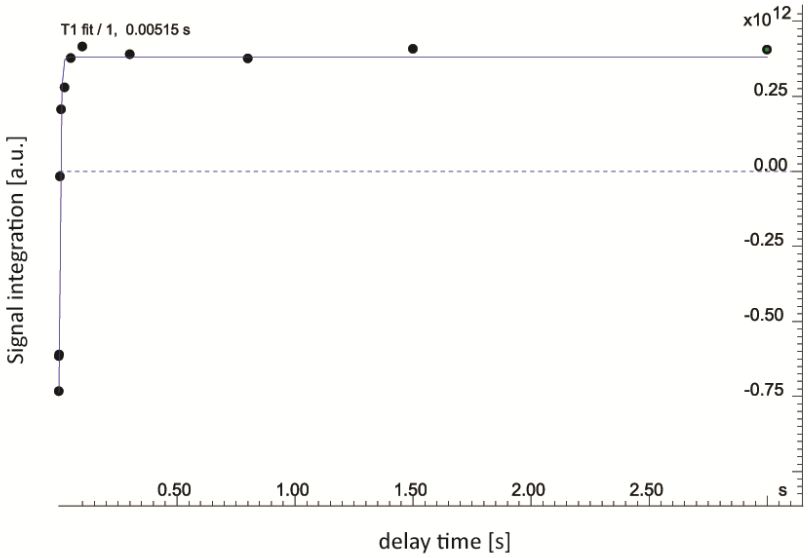
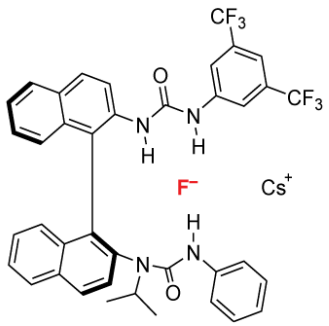



Figure 4.70: Inversion recovery plot of Cs[**4u**$_2$:F], experimental data (dots) and fitted function (line). T1 = 0.005 s.

*4.3.7 (S)-iPrBINAM-N$^a$-[3,5-bis(CF$_3$)phenyl]-N$^b$-phenyl bis-Urea–CsF Complex (**4y**:CsF)*

*4.3.7.1 Sample Preparation*

(*S*)-iPrBINAM-*N*$^a$-[3,5-bis(CF$_3$)phenyl]-*N*$^b$-phenyl bis-Urea **4y** (8.75 mg/0.0125 mmol), CsF (100 mg/0.66 mmol), PhF$_6$ (2 µL) and triphenyl methane (3 mg) were dissolved in 0.5 mL of DCM-d$_2$ (25 mM) inside a sealed NMR tube. The sample was sonicated for 2 hours, after which it was directly taken to the NMR spectrometer. All the NMR spectra were recorded on an AVIII HD 500 equipped with a BCU II fridge unit, allowing variable temperature studies. The sample can be stored at room temperature without signs of degradation for months.




Scheme 4.4: Structure of **4y**:CsF.

*4.3.7.2 Variable Temperature Studies*

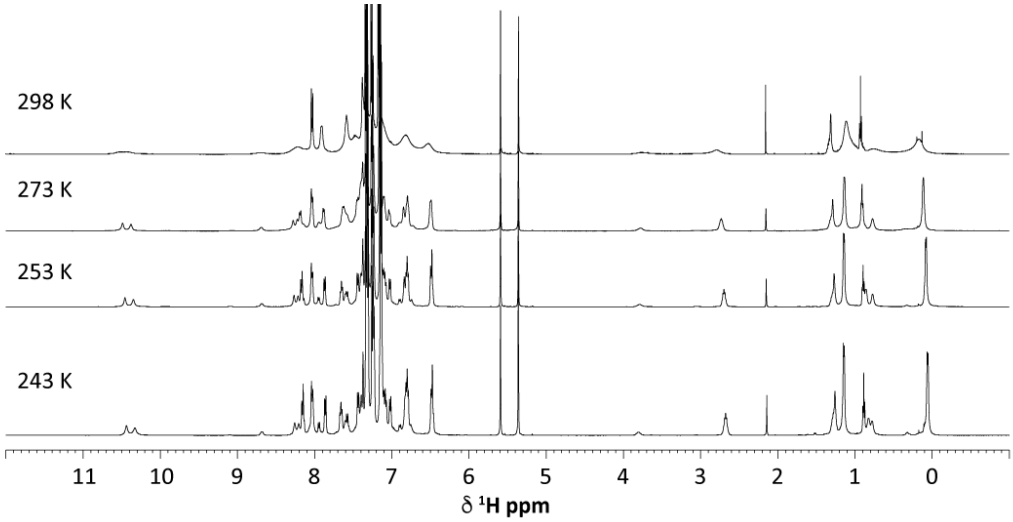



Figure 4.71: $^{1}$H NMR of **4y**:CsF, 298–243 K.

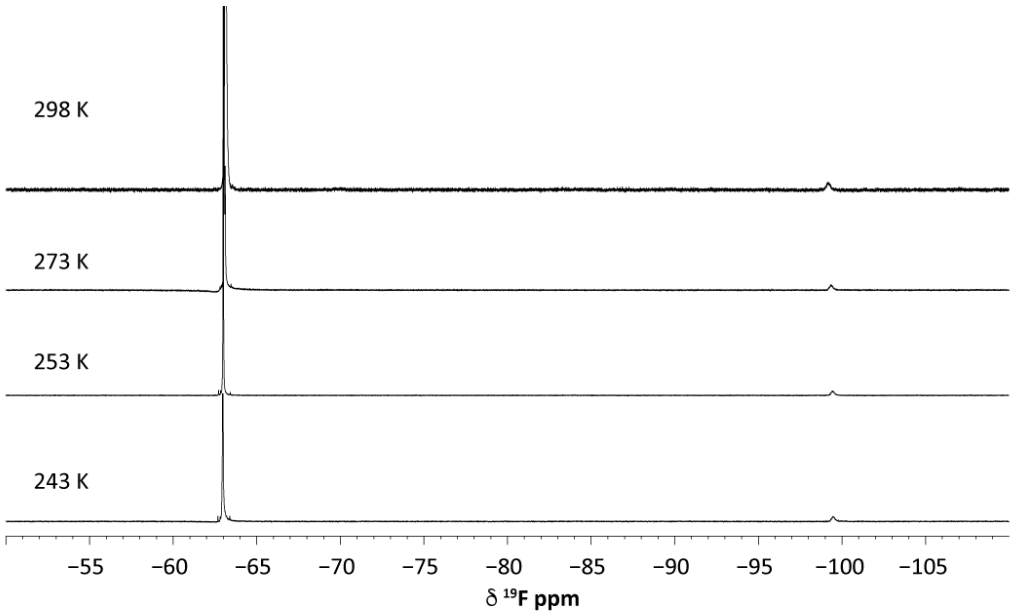



Figure 4.72: $^{19}$ F NMR of **4y**:CsF, 298–243 K.

*4.3.7.3 HSQC*

$^{1}H$-$^{13}C$ HSQC experiments were acquired using a previously developed sequence (*hsqcedetgpsp.3*) at 273 K.

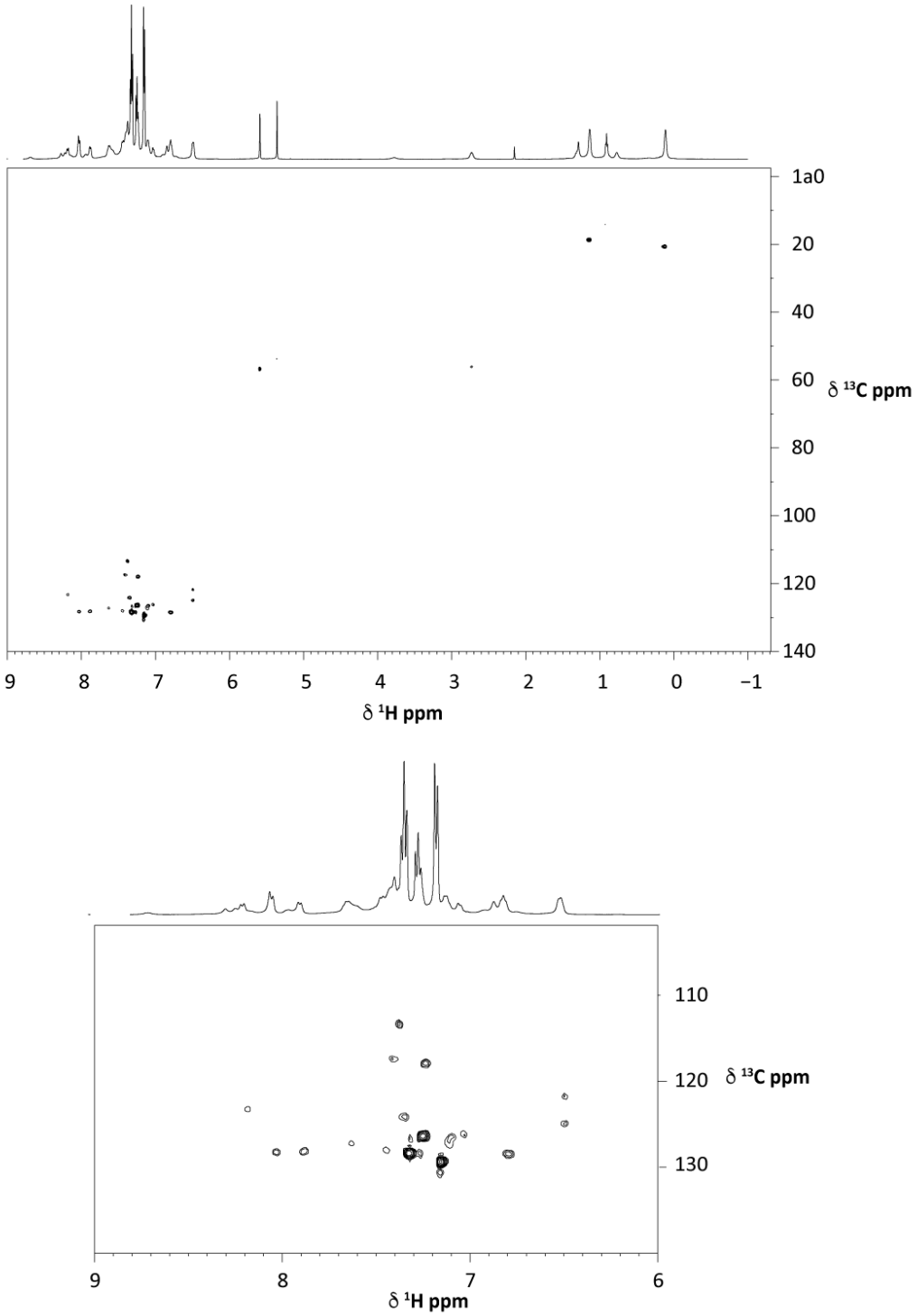



Figure 4.73: $^{1}H$-$^{13}C$ HSQC of **4y**:CsF, at 273 K.

$^{1}$H-$^{19}$F CLIP-HSQC experiments were acquired using a modified sequence from a previously developed one (*hsqcetgpclip*)[17] at 243 K.

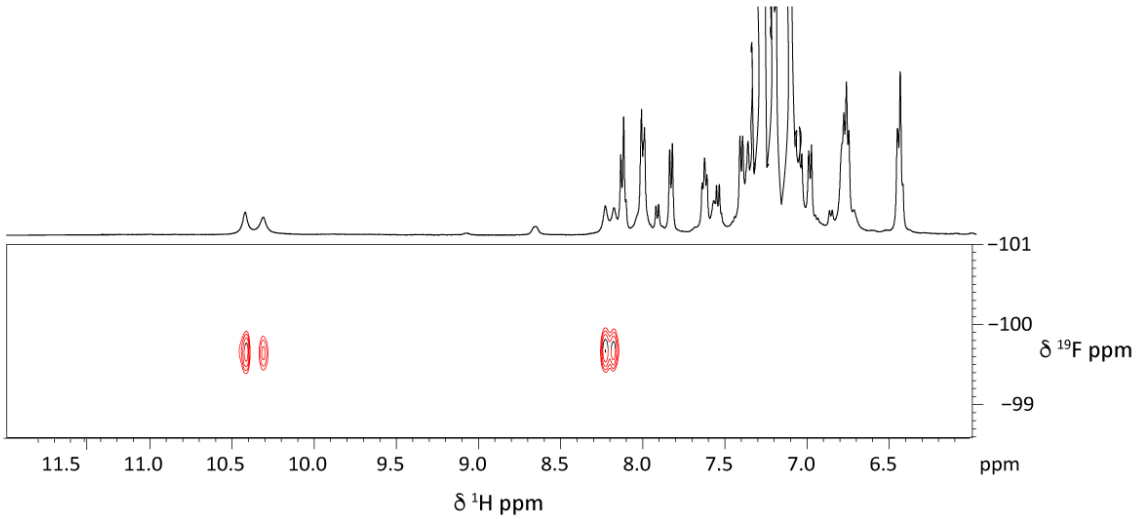



Figure 4.74: $^{1}$H-$^{19}$F CLIP-HSQC of **4y**:CsF, at 243 K.

$^{1}H$-$^{15}N$ HSQC experiments were acquired using a previously developed sequence (*hsqcedetgpsp.3*) at 248 K.

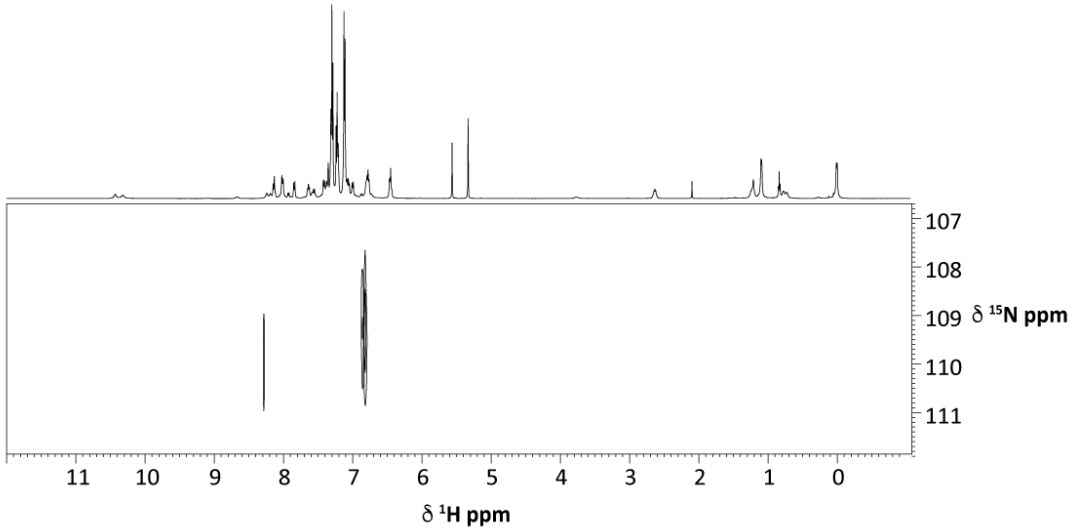



Figure 4.75: $^{1}H$-$^{15}N$ HSQC of **4y**:CsF, 248 K.

*4.3.7.4 ROESY*

ROESY experiments were acquired using a previously developed pulse sequence (*roesyphpp.2*) at 243 K, using the parameters listed below.

| Parameter | Value |
|---|---|
| TD | 2048 (f2) x 256 (f1) |
| SW | 20 (f2) x 20 (f1) |
| NS (DS) | 16 (32) |
| relaxation delay d1 | 2 s |
| spin-lock pulse p15 | 100 ms |

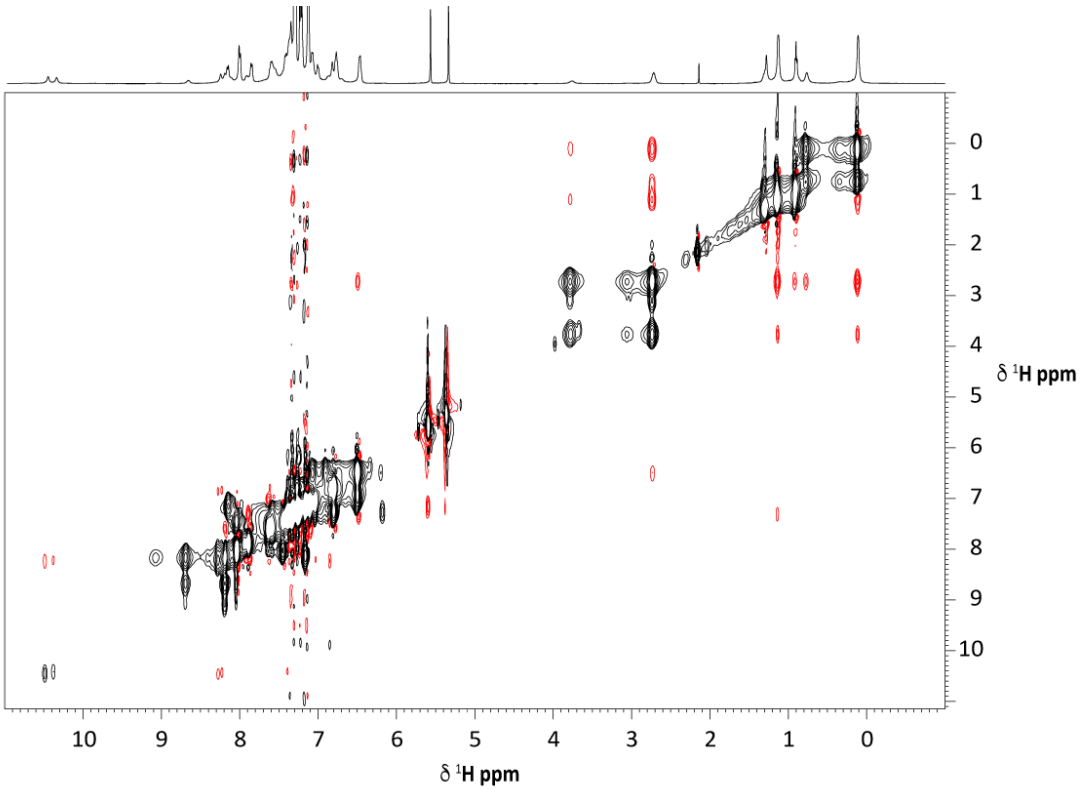



Figure 4.76: $^{1}$H ROESY of **4y**:CsF at 243 K, full spectrum.

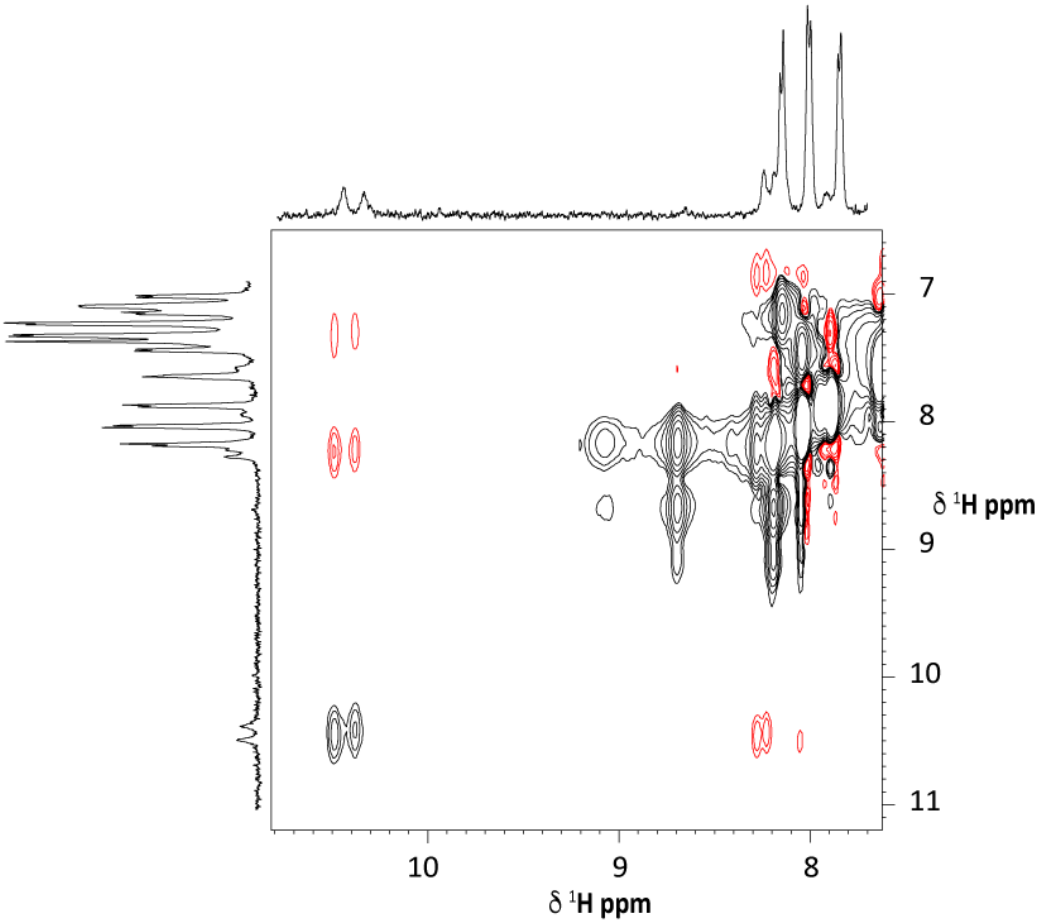



Figure 4.77: $^{1}$H ROESY of **4y**:CsF at 243 K, 7.5–11 ppm.

*4.3.7.5 HOESY*

1D heteronuclear $^{1}H$-$^{19}F$ nOe experiments were acquired on an AVIII HD 500 using a previously developed sequence (*hoesyfhgh1d*) and the parameters reported below.

| Parameter | Value |
|---|---|
| TD | 32768 pt |
| SW | 20 |
| NS (DS) | 128 (16) |
| o2p | -99.5 ppm |
| relaxation delay d1 | 3 s |
| mixing time d8 | 30 ms |

A second set of experiments was performed using a modified sequence (*hoesyfhgh1d.cpd*), which included fluorine decoupling during acquisition, using identical parameters to the ones reported above.

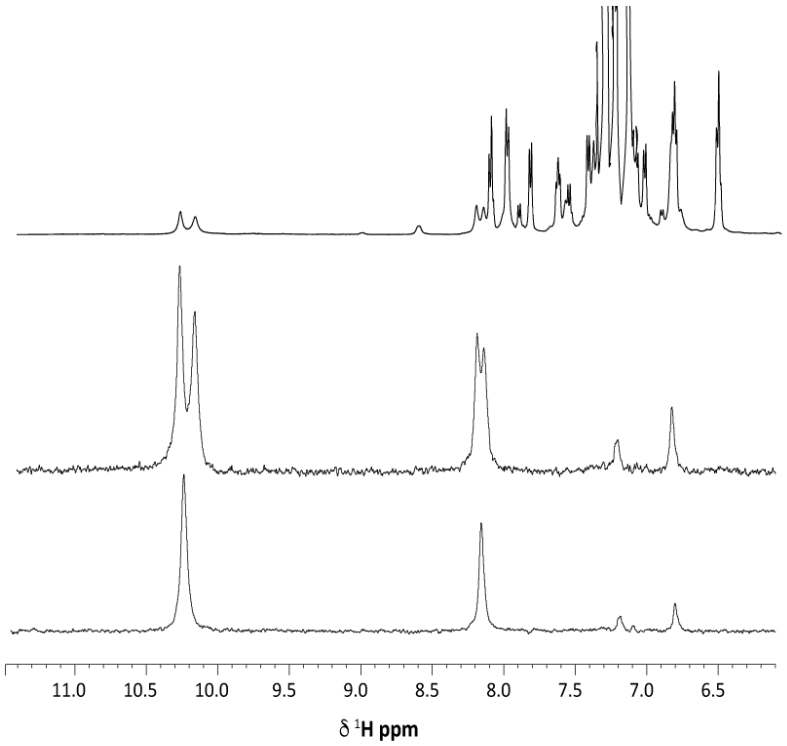



Figure 4.78: $^{1}H$ NMR and $^{1}H$-$^{19}F$ HOESY of **4y**:CsF at 243 K, 11.5–6 ppm.

*4.3.7.6 Diffusion measurements*

Diffusion experiments were performed by measuring the diffusion coefficient (*D*) of selected resonances belonging to the two species **4y** and **4y**:CsF. The diffusion coefficient was determined by means of $^{1}$H DOSY experiments acquired on an AVIII HD 500 at 243 K. The sample (*4.3.7.1 Sample preparation*) was cooled to 243 K inside the magnet and let equilibrate for an hour before the acquisition started. $^{1}$H DOSY were acquired using a previously developed pulse sequence (*dstebpgp3s,* diffusion measurement using double stimulated echo for convection compensation and LED using bipolar gradient pulses using 3 spoil gradients)[20] and the following relevant parameters.

| Parameter | Value |
|---|---|
| TD | 65536 pt |
| SW | 20 ppm |
| NS (DS) | 64 (4) |
| relaxation delay d1 | 5 s |
| $\Delta$ | 95 ms |
| $\delta$ | 3 ms |
| *Gradient,* $G_z$ (n. of 1D spectra) | 2–90 % (16) |

The diffusion coefficient of selected resonances was calculated by non-linear fitting using Dynamic Center 2.3.3. The diffusion coefficient of the two species was calculated as the average of the diffusion coefficients of the protons corresponding to each species. In view of the substantial difference in diffusion coefficients between the two species, the spectrum of **4y**:CsF can be obtained using a 1D $^{1}$H DOSY sequence (*dstebpgp3s1d*) setting $G_z$ = 90 % and otherwise identical parameters to the ones reported above.

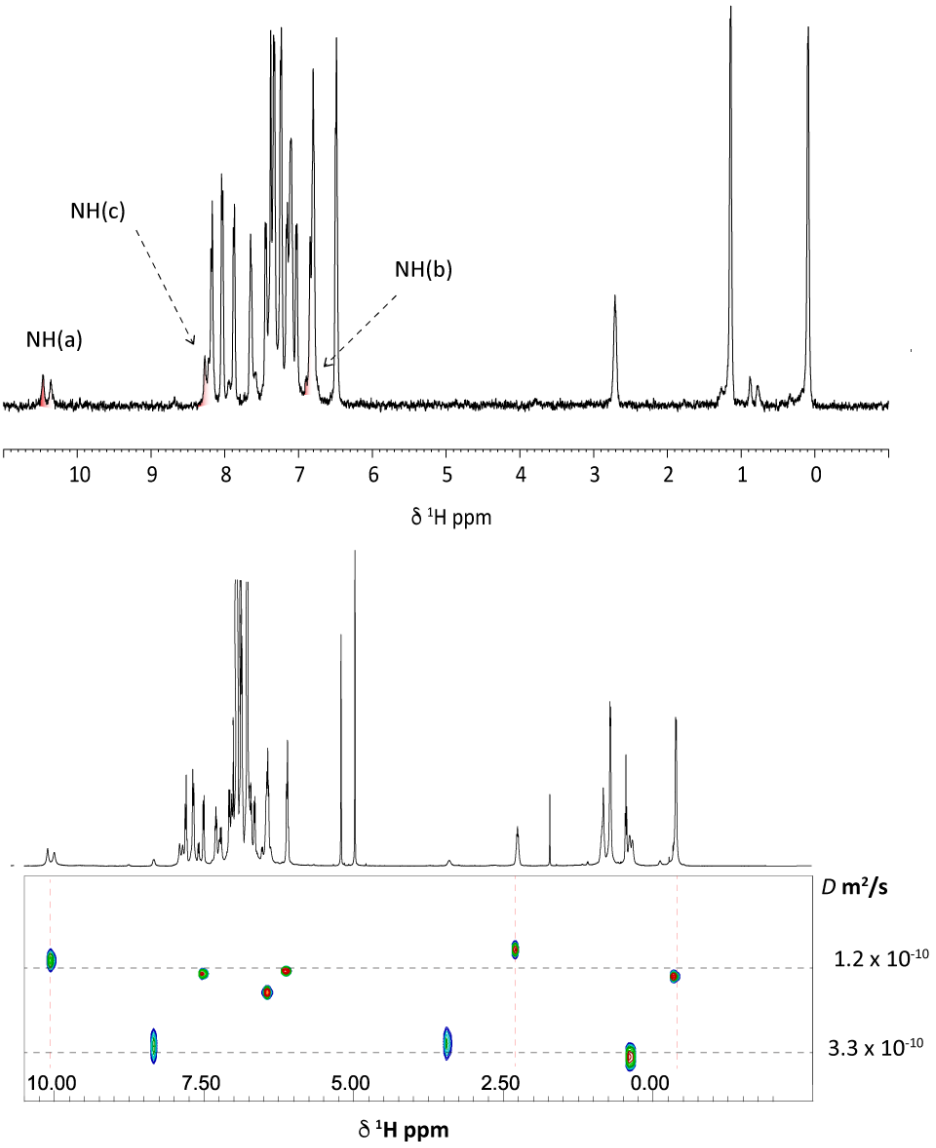



Figure 4.79: 1D DOSY (top) and pseudo-2D DOSY plot (bottom) of **4y**:CsF.

*4.3.8 X-ray Analysis*

Crystallographic data and structure refinement for **4ad**:CsF

| | | |
|---|---|---|
| Empirical formula | C37 H28 Cs1 F5 N4 O2 | |
| Formula weight | 1033.27 | |
| Temperature | 150 K | |
| Wavelength | 1.54184 Å | |
| Crystal system | Orthorombic | |
| Space group | P 21 21 21 | |
| Unit cell dimensions | a = 13.77790(10) Å | $\alpha$ = 90°. |
| | b = 15.42990(10) Å | $\beta$ = 90°. |
| | c = 16.92420(10) Å | $\gamma$ = 90°. |
| Volume | 3597.94(4) $Å^3$ | |
| Z | 4 | |
| Density (calculated) | 1.46 $Mg/m^3$ | |
| Absorption coefficient | 8.575 $mm^{-1}$ | |
| F(000) | 1576 | |
| Crystal size | 0.10 x 0.20 x 0.20 $mm^3$ | |
| Theta range for data collection | 3.683 to 76.1926°. | |
| Index ranges | -17<=h<=17, -19<=k<=18, -21<=l<=21 | |
| Reflections collected | 101161 | |
| Independent reflections | 7518 [R(int) = 0.0413] | |
| Completeness to theta = 76.429° | 99.6 % | |
| Absorption correction | Multi-scan | |
| Max. and min. transmission | 0.42 and 0.08 | |
| Refinement method | Full-matrix least-squares on $F^2$ | |
| Data / restraints / parameters | 7489 / 0 / 455 | |
| Goodness-of-fit on $F^2$ | 1.018 | |
| Final R indices [I>2sigma(I)] | R1 = 0.0317, wR2 = 0.0839 | |
| R indices (all data) | R1 = 0.058, wR2 = 0.154 | |
| Absolute structure parameter | -0.0010(15) | |
| Largest diff. peak and hole | 2.20 and -0.43 e.$Å^{-3}$ | |

## 4.4 References


(1) Jakab, G.; Hosseini, A.; Hausmann, H.; Schreiner, P. R. Mild and Selective Organocatalytic Iodination of Activated Aromatic Compounds. *Synth.* **2013**, *45* (12), 1635–1640.

(2) Tripathi, C. B.; Mukherjee, S. Lewis Base Catalysis by Thiourea: N -Bromosuccinimide-Mediated Oxidation of Alcohols. *J. Org. Chem.* **2012**, *77* (3), 1592–1598.

(3) Kim, K. H.; Lee, D. W.; Lee, Y. S.; Ko, D. H.; Ha, D. C. Enantioselective Oxidative Coupling of Methyl 3-Hydroxy-2-Naphthoate Using Mono-N-Alkylated Octahydrobinaphthyl-2,2′-Diamine Ligand. *Tetrahedron* **2004**, *60* (41), 9037–9042.

(4) Shi, M.; Liu, X. G. Asymmetric Morita-Baylis-Hillman Reaction of Arylaldehydes with 2-Cyclohexen-1-One Catalyzed by Chiral Bis(Thio)Urea and DABCO. *Org. Lett.* **2008**, *10* (6), 1043–1046.

(5) Holakovský, R.; März, M.; Cibulka, R. Urea Derivatives Based on a 1,1′-Binaphthalene Skeleton as Chiral Solvating Agents for Sulfoxides. *Tetrahedron Asymmetry* **2015**, *26* (23), 1328–1334.

(6) Pfeifer, L.; Engle, K. M.; Pidgeon, G. W.; Sparkes, H. A.; Thompson, A. L.; Brown, J. M.; Gouverneur, V. Hydrogen-Bonded Homoleptic Fluoride-Diarylurea Complexes: Structure, Reactivity, and Coordinating Power. *J. Am. Chem. Soc.* **2016**, *138* (40), 13314–13325.

(7) Ajvazi, N.; Stavber, S. Direct Halogenation of Alcohols with Halosilanes under Catalyst- and Organic Solvent-Free Reaction Conditions. *Tetrahedron Lett.* **2016**, *57* (22), 2430–2433.

(8) Helmkamp, G. K.; Pettitt, D. J. Mechanism of the Desulfurization of Episulfides with Methyl Iodide. *J. Org. Chem.* **1964**, *29* (11), 3258–3262.

(9) Denmark, S. E.; Vogler, T. Synthesis and Reactivity of Enantiomerically Enriched Thiiranium Ions. *Chem. Eur. J.* **2009**, *15* (43), 11737–11745.

(10) Palatinus, L.; Chapuis, G. SUPERFLIP - A Computer Program for the Solution of Crystal Structures by Charge Flipping in Arbitrary Dimensions. *J. Appl. Crystallogr.* **2007**, *40* (4), 786–790.

(11) Betteridge, P. W.; Carruthers, J. R.; Cooper, R. I.; Prout, K.; Watkin, D. J. CRYSTALS Version 12: Software for Guided Crystal Structure Analysis . *J. Appl. Crystallogr.* **2003**, *36* (6), 1487–1487.

(12) Flack, H. D. On Enantiomorph-polarity Estimation. *Acta Crystallogr. Sect. A* **1983**, *39* (6), 876–881.

(13) Cooper, R. I.; Thompson, A. L.; Watkin, D. J. CRYSTALS Enhancements: Dealing with Hydrogen Atoms in Refinement. *J. Appl. Crystallogr.* **2010**, *43* (5 PART 1), 1100–1107.

(14) Flack, H. D.; Bernardinelli, G. Reporting and Evaluating Absolute-Structure and Absolute-Configuration Determinations. *J. Appl. Crystallogr.* **2000**, *33* (4), 1143–1148.

(15) Wagner, R.; Berger, S. Gradient-Selected NOESY- A Fourfold Reduction of the Measurement Time for the Noesy Experiment. *J. Magn. Reson.* **1996**, *123* (1), 119–121.

(16) Kuzmič, P. Program DYNAFIT for the Analysis of Enzyme Kinetic Data: Application to HIV Proteinase. *Anal. Biochem.* **1996**, *237* (2), 260–273.

(17) Enthart, A.; Freudenberger, J. C.; Furrer, J.; Kessler, H.; Luy, B. The CLIP/CLAP-HSQC: Pure Absorptive Spectra for the Measurement of One-Bond Couplings. *J. Magn. Reson.* **2008**, *192* (2), 314–322.

(18) Thrippleton, M. J.; Keeler, J. Elimination of Zero-Quantum Interference in Two-Dimensional NMR Spectra. *Angew. Chem. Int. Ed.* **2003**, *42* (33), 3938–3941.

(19) Macur, S.; Farmer, B. T.; Brown, L. R. An Improved Method for the Determination of Cross-Relaxation Rates from NOE Data. *J. Magn. Reson.* **1986**, *70* (3), 493–499.

(20) Jerschow, A.; Müller, N. Suppression of Convection Artifacts in Stimulated-Echo Diffusion Experiments. Double-Stimulated-Echo Experiments. *J. Magn. Reson.* **1997**, *125* (2), 372–375.